THE UNIVERSITY
of EDINBURGH

On the Optimization of Offshore Wind Farm Layouts

Ajit Chitharanjan Pillai

A thesis submitted in partial fulfillment of the requirements

for the award of an Engineering Doctorate

The University of Edinburgh

2016

IDCORE

This thesis is submitted in partial fulfillment of the requirements for the award of an Engineering Doctorate, jointly awarded by The University of Edinburgh, The University of Exeter, and The University of Strathclyde. The work presented has been conducted under the industrial supervision of EDF Energy R&D UK Centre as a project within the Industrial Doctoral Centre for Offshore Renewable Energy (IDCORE).

THE UNIVERSITY
of EDINBURGH

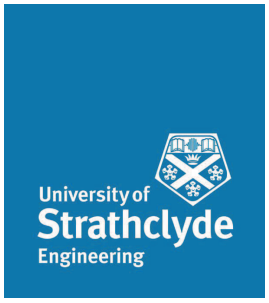

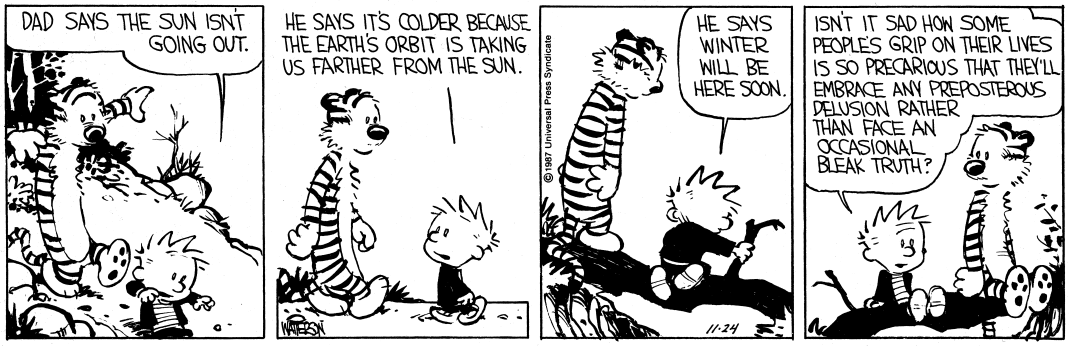

-Bill Watterson

Abstract

Layout optimization of offshore wind farms seeks to automate the design of the wind farm and the placement of wind turbines such that the proposed wind farm maximizes its potential. The optimization of an offshore wind farm layout therefore seeks to minimize the costs of the wind farm while maximizing the energy extraction while considering the effects of wakes on the resource; the electrical infrastructure required to collect the energy generated; the cost variation across the site; and all technical and consenting constraints that the wind farm developer must adhere to. As wakes, electrical losses, and costs are non-linear, this produces a complex optimization problem. This thesis describes the design, development, validation, and initial application of a new framework for the optimization of offshore wind farm layouts using either a genetic algorithm or a particle swarm optimizer.

The developed methodology and analysis tool have been developed such that individual components can either be used to analyze a particular wind farm layout or used in conjunction with the optimization algorithms to design and optimize wind farm layouts. To accomplish this, separate modules have been developed and validated for the design and optimization of the necessary electrical infrastructure, the assessment of the energy production considering energy losses, and the estimation of the project costs. By including site-dependent parameters and project specific constraints, the framework is capable of exploring the influence the wind farm layout has on the levelized cost of energy of the project.

Deploying the integrated framework using two common engineering metaheuristic algorithms to hypothetical, existing, and future wind farms highlights the advantages of this holistic layout optimization framework over the industry standard approaches commonly deployed in offshore wind farm design leading to a reduction in LCOE. Application of the tool to a UK Round 3 site recently under development has also highlighted how the use of this tool can aid in the development of future regulations by considering various constraints on the placement of wind turbines within the site and exploring how these impact the levelized cost of energy.

Acknowledgements

Acknowledgement, with gratitude, is due to the following:

Dr. John Chick, Professor Lars Johanning, and Dr. Mahdi Khorasanchi, under whose supervision this work was carried out. Without their continuous advice, support, and insight this work would not have been possible.

EDF Energy R&D UK Centre, who hosted the three year industrial element of this Engineering Doctorate and in particular the individuals who supervised this work over that three year period: Vincent de Laleu, Sebastien Pelissier, and Sami Barbouchi.

My friends and family who have offered advice and encouragement throughout this process.

Finally, funding from the Energy Technologies Institute (ETI) and the RCUK Energy Programme for the Industrial Doctoral Centre for Offshore Renewable Energy (Grant Number EP/J500847/1) is gratefully acknowledged.

Declaration

I declare that this thesis was composed by myself, that the work contained herein is my own except where explicitly stated otherwise in the text, and that this work has not been submitted for any other degree or professional qualification except as specified.

Parts of the work outlined in this thesis have been published:

- Chapter 4 is based on Ajit C. Pillai, John Chick, Lars Johanning, Mahdi Khorasanchi, and Vincent de Laleu. Offshore wind farm electrical cable layout optimization. *Engineering Optimization*, 47(12):1689—1708, 2015. ISSN 0305—215X. doi: 10.1080/0305215X.2014.992892.
- Section 5.5.1 is based on Ajit C. Pillai, John Chick, and Vincent de Laleu. Modelling Wind Turbine Wakes at Middelgrunden Wind Farm. In Proceedings of *European Wind Energy Conference & Exhibition 2014 Barcelona, Spain*, pages 1—10, 2014.
- Section 7.2.2 is based on Ajit C. Pillai, John Chick, Lars Johanning, Mahdi Khorasanchi, and Sami Barbouchi. Comparison of Offshore Wind Farm Layout Optimization Using a Genetic Algorithm and a Particle Swarm Optimizer. In *Proceedings of the ASME 2016 35th International Conference on Ocean, Offshore and Arctic Engineering (OMAE 2016) Busan, South Korea*, pages 1—11. ASME, 2016.
- Though not explicitly included in this thesis, the work of chapters 3-7 has formed the basis for Ajit C. Pillai, John Chick, Lars Johanning, Mahdi Khorasanchi, and Sebastien Pelissier. Optimisation of Offshore Wind Farms Using a Genetic Algorithm. In *Proceedings of the Twenty-fifth (2015) International Ocean and Polar Engineering Conference*, pages 644—652, 2015. ISBN 9781880653890.

All publications written as part of this work are appended in Appendix E.

Ajit Chitharanjan Pillai

Contents

List of Figures

List of Tables

Nomenclature

Acronyms

AEP	Annual Energy Production
AGA	Adaptive Genetic Algorithm
BODC	British Oceanographic Data Centre
BSUoS	Balancing Services Use of System
CAPEX	Capital Expenditure
CFD	Computational Fluid Dynamics
CMST	Capacitated Minimum Spanning Tree
COE	Cost of Energy
DAWM	Deep-Array Wake Model
DECEX	Decommissioning Expenditure
DWM	Dynamic Wake Meandering
FB	Financial Balance
GA	Genetic Algorithm
GBF	Gravity Based Foundation
GEBCO	General Bathymetric Chart of the Oceans
IBL	Internal Boundary Layer
LAT	Lowest Astronomical Tide
LCOE	Levelized Cost of Energy
LF	Load Factor
LP	Linear Programming
LPC	Levelized Production Cost
LWC	Large Wind Farm Correction
MILP	Mixed-Integer Linear Programming
MST	Minimum Spanning Tree
MTTR	Mean Time to Repair
NPV	Net Present Value
O&M	Operations and Maintenance
ODE	Ordinary Differential Equation
OECD	Organization for Economic Co-operation and Development
OHVS	Offshore High Voltage Substation
OPEX	Operational Expenditure
OWFLO	Offshore Wind Farm Layout Optimization
PBL	Planetary Boundary Layer

PSO	Particle Swarm Optimization	
RANS	Reynolds Averaged Navier-Stokes	
RNA	Rotor-Nacelle Assembly	
RPM	Revolutions Per Minute	
SAM	Storpark Analytic Model	
SCADA	Supervisory Control and Data Acquisition	
TEP	Total Energy Production	
TI	Turbulence Intensity	
TNUoS	Transmission Network Use of System	
TOE	Tons of Oil Equivalent	
TP	Transition Piece	
UWFLO	Unconstrained Wind Farm Layout Optimization	
UXO	Unexploded Ordnance	
WAsP	Wind Atlas Analysis and Application Program	
WD	Water depth	

Greek Symbols

α_{20}	Temperature coefficient of electrical resistivity at 20 °C	1/°C
β	Parameter of Frandsen wake model	
η	Best historical position of a particle's neighbourhood in a PSO	
λ_1	Screen power loss factor	
Ψ	Factor to account for the stepwise increase in wake diameter in the Frandsen wake model	
θ_1	Principal axis direction	$^\circ$
θ_2	Secondary axis direction	$^\circ$
ε	Eddy-viscosity term in Ainslie Eddy-Viscosity wake model	m^2/s
ε	Relative permittivity of the cable insulation	
ε_a	Ambient eddy-viscosity	m^2/s
ε_w	Generated eddy-viscosity	m^2/s

Roman Symbols

$\bar{f}$	Mean fitness value of the population	
A	The set of all traversable points within the configurational space (Chapter 4)	
A	Vessel Availability (Chapter 6)	
a	Axial induction factor	
A_i	Rotor swept area of turbine i	m^2
$A_{i,j}$	Area of intersection between the rotor plane of turbine i and the wake of turbine j	m^2
b	Selection bias in a GA	
B_t	Benefit of the development in year t	£

C	Cost	£
c	The distance between the conductor and the centre of the cable (Chapter 5)	
c_1	Larsen wake model parameter	
C_f	Foundation Cost (Chapter 2)	£
C_g	Electrical Grid Cost	£
C_M	Maintenance Cost	£
C_t	Cost of the development in year t	£
$C_{cable\ supply}$	Cost of cable supply	£
C_{CAPEX}	Capital Expenditure	£
$C_{DECEX,f}$	Cost of decommissioning a foundation	£
$C_{DECEX,t}$	Cost of decommissioning a turbine	£
C_{GBF}	Specific cost of a gravity based foundation	£/MW
C_{HV}	Cost of high voltage bays	£
C_{laying}	Cost of cable laying	£
$C_{monopile}$	Cost of monopile	£
C_{MV}	Cost of medium voltage switchgear	£
$C_{O\&M}$	Annual cost of operations and maintenance	£
C_{oe}	Cost of offshore export cable	£
C_{OHVS}	Cost of offshore high voltage substation	£
C_{OPEX}	Operational Expenditure	£
C_{perMW}	Wind turbine specific cost	£/MW
$C_{platform}$	Cost of offshore substation platform	£
$C_{pre-piling}$	Cost of pre-piling work during installation of jackets	£
$C_{t,install}$	Cost of turbine installation	£
C_{T_j}	Thrust coefficient experienced of turbine j	
$C_{trenching}$	Cost of cable trenching	£
C_{wt}	Wind turbine cost	£
C_X	Cost of transformers	£
d	Rotor diameter	m
d_a	Diameter of armour	mm
d_c	Conductor diameter	m
d_s	Mean diameter of sheath	mm
d_w	Wake diameter	m
d_{eff}	Effective rotor diameter (Larsen wake model)	m
$D_{i,j}$	Velocity deficit experienced by turbine i as a result of turbine j	
f'	The fitness value of the best parent of a given candidate solution	
f_i	Fitness value of individual i	
f_{max}	Fitness value of the best individual within the population	

g	Best historical position of the entire swarm in a PSO	
H	Hub height	m
I	Current	A
I_a	Ambient turbulence intensity	%
I_w	Mechanically generated turbine turbulence for use in the Ishihara wake model	%
k	Wake decay factor	
k_p	Proximity factor parameter defined by IEC 60287	
k_s	Skin factor parameter defined by IEC 60287	
L	The set of all cable types	
L	Length of vector defining layout (Chapter 3)	
l	Length of cable	m
L_2	Loss in turbine transformer at full load	kW
l_C	Length of cable	m
l_h	Horizontal length of cable	m
l_v	Vertical length of cable	m
$l_{\text{interference}}$	Length of cable to account for any interference	m
L_{armour}	Armour losses through AC subsea cables	W
L_{core}	Ohmic losses through the cable cores	W
l_{damage}	Length of cable to be included as a safety factor	m
$L_{dielectric}$	Dielectric losses through AC subsea cables	W
L_{genome}	The number of genes that make up an individual	
l_{LAT}	Length of cable needed at lowest astronomical tide	m
$L_{no\ load}$	Loss in turbine transformer at no load	kW
L_{screen}	Screen losses through AC subsea cables	W
$L_{transformer}$	Loss in turbine transformer	kW
LD	Mass of rotor nacelle blade assembly	kg
m_{jacket}	Mass of jacket foundation	kg
$m_{monopile}$	Mass of monopile	kg
n	Lifetime of wind farm	yr
N_L	Number of compounding periods per year	
n_s	Number of strings connected to the substation	
N_t	The set of turbines which can be connected to turbine t	
n_{export}	Number of export cables	
n_{passes}	Number of passes that must be done to cut the trench	
$n_{termination}$	Number of termination boxes needed in the cable network	
n_{trips}	Number of installation trips	
nG	Number of allowable turbine positions	
nT	Number of turbines	

P	Rated power	MW
p	A function of ambient and mechanically generated turbulence for use in the Ishihara wake model (Chapter 5)	
p	Best historical position of a particle in a PSO (Chapter 3)	
p_c	Probability that a pair of selected individuals are subjected to crossover	
P_e	Price of Electricity	£/MWh
p_m	Probability than mutation will occur	
$p_{m,gene}$	Probability than a gene within an individual solution will be subjected to mutation	
$p_{m,individual}$	Probability that an individual within the population will be subjected to mutation	
$P_{s,i}$	Probability of selecting individual i within a GA	
$P_{windfarm}$	Wind farm installed capacity	MW
q	Capacity	
R	Resistance	Ω/m
R	Vessel day rate (Chapter 6)	£/day
r	Effective Discount Rate	
R'	DC resistance maximum operating temperature	Ω/m
R_0	DC resistance at 20 °C	Ω/m
r_c	Cable lay rate	m/h
R_i	Rank of individual i in a GA (Chapter 3)	
r_i	Inflation rate	
r_l	Interest rate on any loans	
R_s	Sheath resistance at 20 °C	Ω
R_w	Radius of wake affected region	m
$R_{9.5}$	Wake radius at a location 9.5 rotor diameters downwind of the turbine	m
R_{ac}	AC resistance	Ω
$r_{install}$	Installation rate	days/unit
R_{nb}	Empirical relationship for the Larsen wake model	m
R_{s0}	Sheath resistance at 0 °C	Ω
$R_{support}$	Support vessel day rate	£/day
$r_{trenching}$	Trenching rate	m/h
S	The set of all substations	
s	Non-dimensional downwind distance	
sep_θ	Minimum separation between turbines along θ direction	m
T	The set of all turbines	
t	Time	yr
t	Turbine number (Chapter 4)	
t_{demob}	Time to demobilize the vessel	days

t_{load}	Time required to load the vessel	days
t_{mob}	Time to mobilize the vessel	days
$t_{transport}$	Time required for vessel to travel to turbine positions for installation operations	days
t_{trip}	Time for each installation trip	days
Th	A threshold value	
U	Velocity in x direction (Ainslie Eddy-Viscosity wake model)	m/s
U_∞	Undisturbed wind speed	m/s
U_i	Wind velocity experienced by turbine i	m/s
U_{OFTO}	Unrecoverable OFTO CAPEX	
V	The set of all turbine and substation positions, all vertices of the full graph, $V = T \cup S$ (Chapter 4)	
V	Velocity in r direction (Ainslie Eddy-Viscosity wake model)	m/s
V	Voltage	V
w_i	Inertia weight in a PSO	
X	Sheath reactance	Ω
x	Downwind distance (Chapter 5)	m
x	Vector representing layout (Chapter 3)	
x_0	Larsen wake model parameter	m
X_l	The set of cables that intersect cable arc l	
x_p	Argument of the Bessel function used to calculate the proximity effect	
x_s	Argument of the Bessel function used to calculate the skin effect	
X_{rating}	Transformer rating	MVA
y_p	Proximity effect parameter	
y_s	Skin effect parameter	
z_0	Roughness length	m
z_{02}	Increased roughness due to the presence of the wind farm	m

Chapter 1

Introduction

1.1 Current State and Trends of Offshore Wind Energy

With the mastery of fire 400,000 years ago, and the understanding of how to convert the stored chemical energy in wood fuels to both heat and light, homo erectus started the human race along a new path which would forever differentiate humans from the rest of the animal kingdom. Since this pivotal discovery, the human race has depended on the use of energy to propel further advancements and discoveries in all fields of study. Though energy has been a central element of human society since its discovery, it is the industrial revolution which marked the period after which this ability to harness and convert energy and its sources has defined our modern society. It was during this period that humans identified more energy dense fuels and found effective ways to control the release of energy to not only generate heat and light, but also to perform mechanical work. Today, energy in some form or another is integral in every field of study with many countries now considering the access to energy, both heat and electricity, to be a human right [1, 2].

The first forms of energy generation came as a result of combustion processes, and in fact to this day, combustion processes represent the principal means through which usable energy is generated. A major disadvantage of combustion processes is that these processes generate byproducts which include greenhouse gases. These emissions have been shown to negatively impact the environment and contribute towards anthropogenic climate change. Furthermore, there are concerns that these fuels are consumed more quickly than they are naturally formed leading to increased scarcity of these fuels. As a result of these factors, the energy sector and electricity generation in particular has recently focused on alternate energy sources which may offer a means to alleviate the environmental impacts of the energy sector while still fostering global economic growth and a growth of energy production.

Global energy use, and electricity in particular, is expected to increase further as global populations rise. At the same time, the energy sources used are shifting away from traditional energy cycles based on fossil fuels, thereby increasing the role for renewable

energy sources such as offshore wind (see Figure 1.1). Unlike fossil fuel resources, wind energy harnesses a natural energy flux thereby requiring no fuel to be mined or burned. By not making use of fuels, wind energy both reduces the dependency on fuel sources and offers to be an emissions-free, low-carbon, energy source.

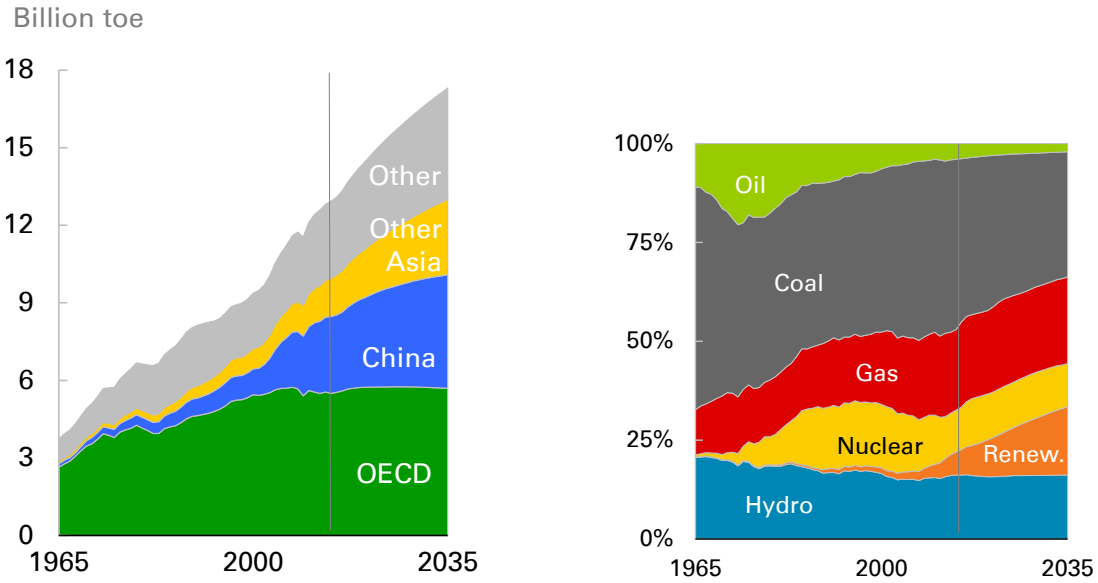

(a) Global energy consumption

(b) Primary inputs to power generation

Figure 1.1: Projected changes in energy landscape up to 2035 [3]

Since the introduction of global emissions targets and a global desire to decarbonize the energy sector, the global wind sector has grown and in recent years significant growth has been seen in the European offshore wind industry. This growth can be seen both in the size of turbines used, and the installed capacity of wind farms. So much so, that offshore wind turbines now represent the largest rotating machines that the human race builds and maintains.

The global installation of wind energy has accelerated rapidly in the past two decades, with the global installed wind energy capacity now exceeding 430 GW of which over 63 GW were installed in 2015 as shown in Figure 1.2 [4].

This growth in renewables is anticipated to continue partially in an effort to decarbonize the energy sector and partially driven by the need to maintain security of supply. Specifically in the years leading up to 2035 and 2050, it is anticipated that renewables, with a large contribution from offshore wind, will experience a growth in market share relative to other generation methods [3].

In the past decade, the offshore wind industry in Europe has rapidly grown from small demonstration projects to large wind farms exceeding several hundred megawatts

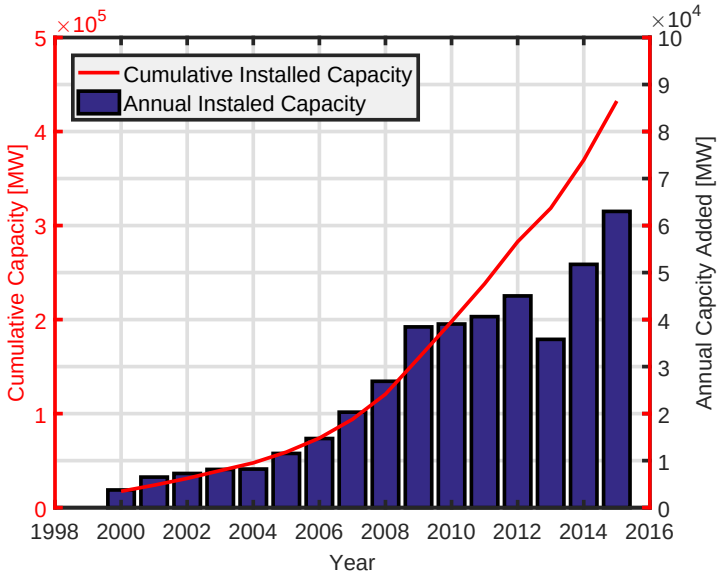

Figure 1.2: Annual and cumulative installed wind capacity [4].

in capacity and has seen a similar growth in both capacity installed annually and cumulative installed capacity. As of the end of 2015, the European offshore wind industry represents over 11 GW of installed capacity (see Figure 1.3) with an additional 60 GW of capacity at the planning stage [5].

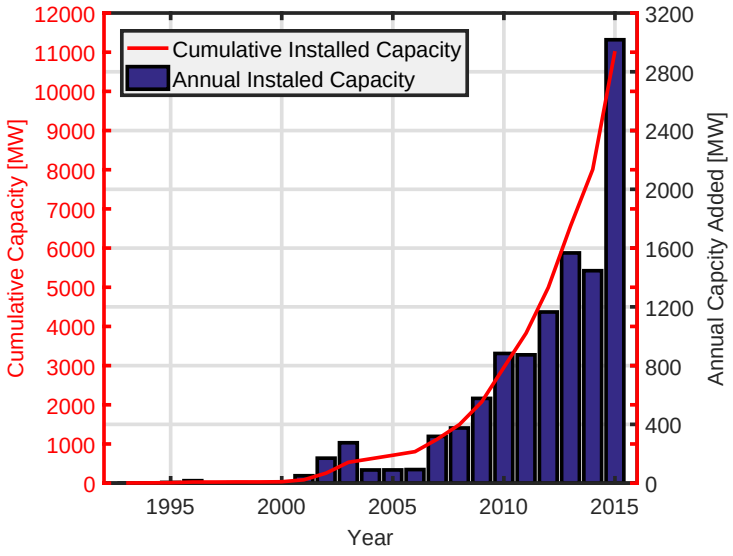

Figure 1.3: Annual and cumulative installed offshore wind capacity [5].

While the wind industry and specifically the offshore wind industry are reaching new heights with respect to installed capacity, the turbines used by these industries have also grown rapidly. In 2001, the typical offshore wind turbine had a rotor diameter of

112 m and generated approximately 3 MW. The present generation of turbines exceed 150 m in diameter and generate in excess of 8 MW (Figure 1.4) [6].

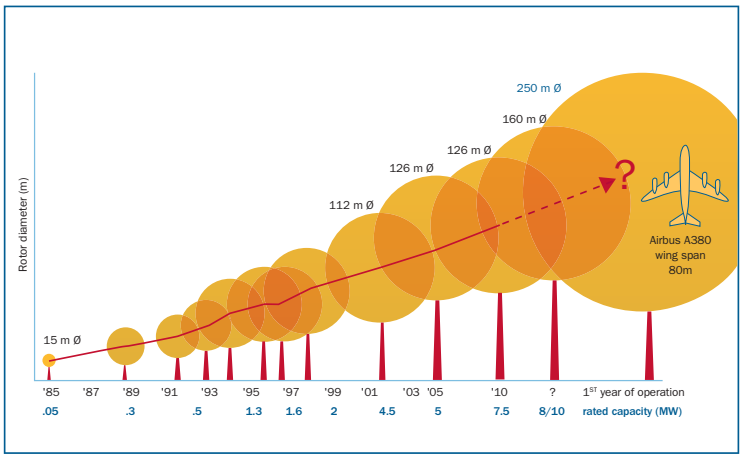

Figure 1.4: Growth of the size and capacity of wind turbines over the past 30 years [6].

As offshore wind has grown as a sector, the size of offshore wind farms has grown significantly and the distance from shore has also increased, placing the wind farms in deeper waters. The relationship between wind farm capacity, distance to shore, and average water depth is shown in Figure 1.5. As these factors have increased, the design of an offshore wind farm has also become a more complex problem for project developers to address.

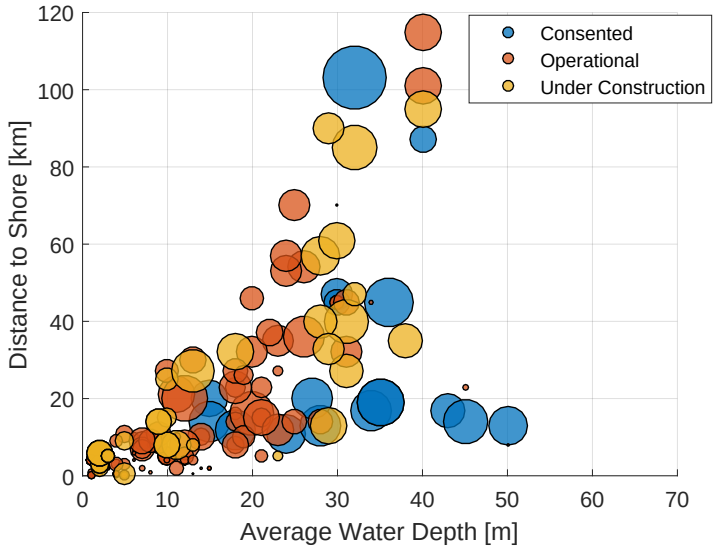

Figure 1.5: Offshore wind farms plotted as a function of their distance to shore and water depth. The size of the circles is proportional to the capacity of the wind farm [7].

1.2 The Wind Farm Layout Problem

As offshore wind farms become larger, both in terms of installed capacity and number of turbines; further from shore; and placed in deeper water, project developers have more decisions regarding the development which can impact the financial viability of the project. As wind farms have moved further offshore and become larger developments, licensing authorities have allowed developers greater flexibility in designing their wind farms thereby allowing developers to ensure that they extract as much energy as possible in as cost effective a way as possible. This increased flexibility has as a result increased the complexity of the wind farm design problem. In general, an offshore wind farm layout refers to the position of turbines, substations, and subsea cables within a specific wind farm area. Presently the UK licensing authority, The Crown Estate, leases an area of the seabed to offshore wind farm developers and it is then up to the developer to propose an arrangement of turbines within this given area.

In order to address this from the perspective of a wind farm developer, it is important to consider the impact that the layout of the wind farm has on the viability of the project. This therefore includes exploring how the layout of a wind farm impacts both the wind farm's yield and lifetime costs. Going beyond understanding the impact the layout has, the problem can be addressed as one where for a given project, the developer seeks to optimize the layout such that the most efficient wind farm layout with respect to energy production and cost is selected and built.

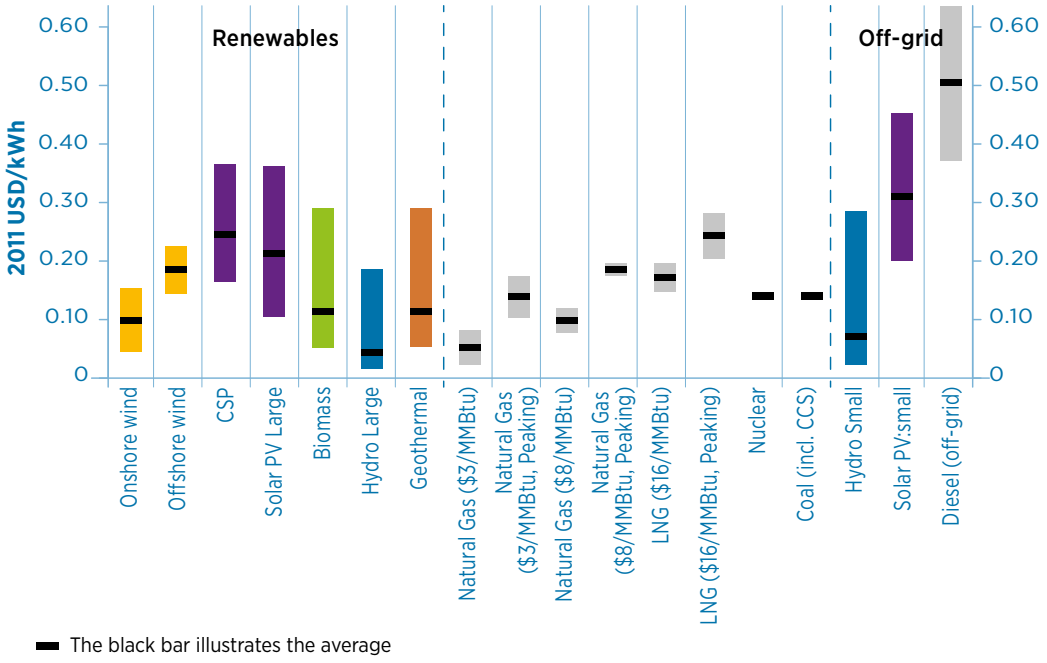

Figure 1.6: Cost of energy for different technologies among the OECD countries [8].

Additionally, although the offshore wind industry is established with over 11 GW of installed capacity, it is still a relatively young technology which is expensive compared to conventional thermal generation, as shown in Figure 1.6 [9]. To aid the offshore wind industry adequately compete with alternate energy sources, the field of layout optimization has become of increasing interest as through relatively small changes in the design of the wind farm, the cost of the project could potentially be improved making it more competitive and more investable. As wind farm layout optimization looks at the relative impact on the project as a result of changes in the layout, it is important that the relative error of the models, rather than the absolute error, are low.

1.3 Thesis Aim

The work presented as part of this thesis aims to develop a methodology and integrated tool for the optimization of an offshore wind farm's layout. The developed approach builds on the standard paradigm by incorporating the constraints faced by a project developer and seeks to aid developers in the offshore wind farm design process. In the development of the methodology, the objectives have been:

- develop and validate a detailed evaluation function for evaluating wind farm layouts
- identify the key parameters which affect the wind farm layout
- produce a framework by which different optimization algorithms can be compared using the same evaluation function
- compare the performance of this tool to existing approaches using both standard test cases and real wind farms
- offer insight into wind farm layout design approaches which can be used for future sites

Compared to existing offshore wind farm optimization tools, the presented methodology offers an increased degree of detail in assessing offshore wind farm layouts thereby increasing the ability with which the tool can differentiate between different layouts. The framework has been developed using a modular approach such that future work can easily expand and replace modules as desired giving a strong platform from which further studies can explore the importance of wind farm layouts. Furthermore, initial results from application of the tool show improvements over previously developed methodologies, while also highlighting the applicability of the tool to real sites such as Middelgrunden wind farm and a representative UK Round 3 site.

1.4 Layout of Thesis

This thesis consists of nine chapters:

Chapter 2 focuses on the existing work that has been done in the field of wind farm layout optimization highlighting the capabilities of existing approaches, their strengths, and their weaknesses. This chapter ultimately highlights the areas for improvement in future methodologies and tools. This chapter then also gives an overview of the methodology developed as part of the present work.

Chapter 3 introduces the idea of combinatorial optimization and the place it holds in addressing the offshore wind farm layout optimization problem. This chapter also explains the different constraints which need to be considered and the solution approach taken as part of the development of this framework for offshore wind farm layout optimization. The metaheuristic optimization algorithms implemented are also described in this chapter.

Chapter 4 introduces the electrical infrastructure optimization problem which is addressed as a sub-problem within the overall layout optimization framework. This work includes the optimization of the substation placement, intra-array cable paths, and export cable paths which have an impact on both the annual energy production and the cost of the layout. An application of this methodology to a representative UK Round 3 wind farm is also performed to show the capabilities of this sub-tool.

Chapter 5 presents the annual energy production module which for a given layout computes the energy produced by the wind farm including considerations for wind turbine wakes and electrical losses. Several wind turbine wake models are introduced and validated using data available from Middelgrunden, Horns Rev I, and Nysted wind farms. From this validation the implemented wake models are compared both in terms of performance and computational requirements indicating their suitability to be included in an optimization process.

Chapter 6 details the development and validation of a parametric cost model which includes the layout dependent costs. Where possible, the presented models are compared against actual wind farm data as well as published datasets.

Chapter 7 applies the full optimization methodology to three case studies. The first considers a fictional wind farm under three different resource conditions. The second study applies the methodology to Middelgrunden wind farm highlighting potential improvements that could have been made during the planning stages, and the third case study applies the methodology to a representative UK Round 3 wind farm area to highlight its capabilities for future wind farms.

Chapter 8 discusses the results and future extensions of this work before *Chapter 9* presents the final conclusions of this work. The relationships between these chapters is shown visually in Figure 1.7.

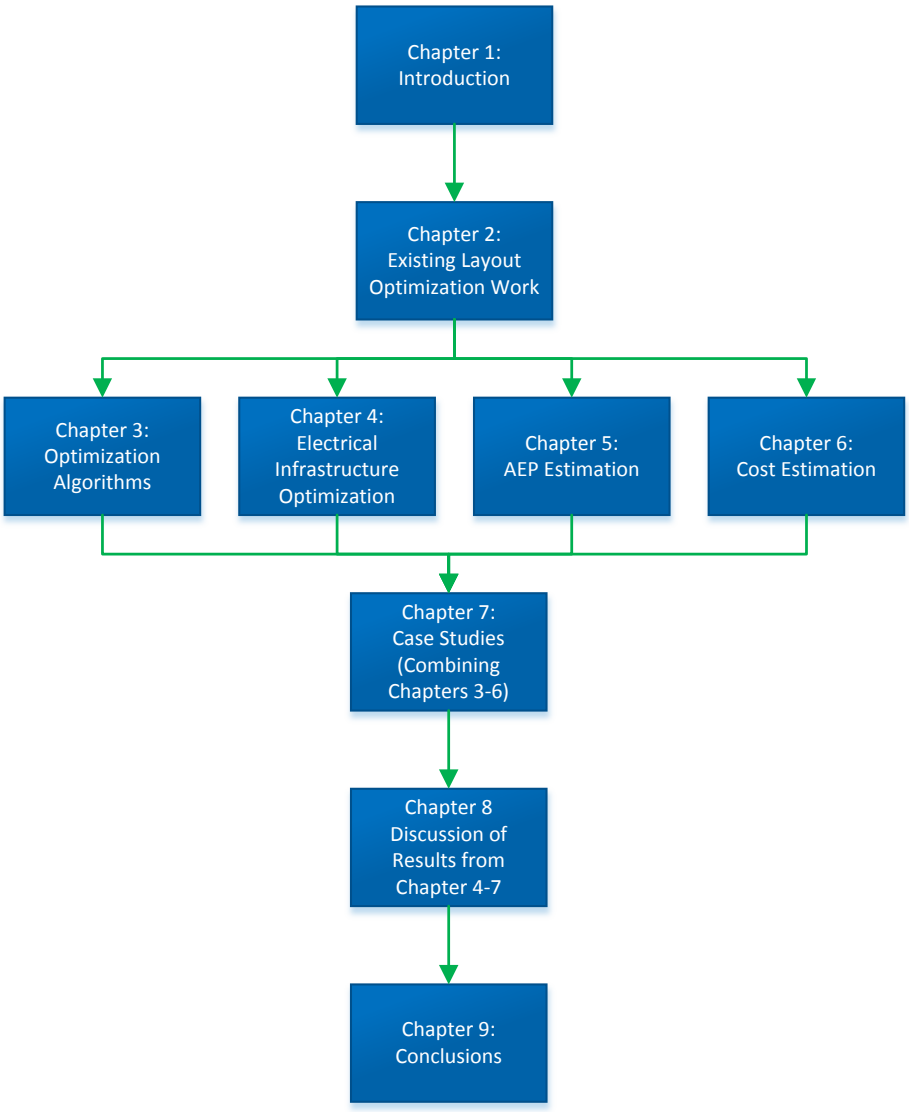

Figure 1.7: Relationship between thesis chapters

Chapter 2

State of the Art in Wind Farm Layout Optimization

2.1 Introduction

Layout optimization of both onshore and offshore wind farms seeks to automate the design of the wind farm layout and the placement of the wind turbines such that an objective function is either maximized or minimized. When considering the wind farm layout optimization problem there are a number of relevant metrics which can be used as an objective function. At their core, however, these measures attempt to minimize the effects of wind turbine wakes and turbine interactions within the wind farm area in order to ensure that the maximum energy is extracted from the available resource.

As research in this field is ongoing, it is important that future projects be aware of previous work in order to avoid repeated work. This chapter, therefore briefly reviews what has been done in the field of layout optimization of wind farms with specific emphasis on what areas future projects can and should focus on to avoid repeated effort.

This review is comprised of three principal sections: in Section 2.2 the structure of existing layout optimization tools are described and the necessary modules explained; in Section 2.3, previously developed tools are described in relation to the tool structure; and in Section 2.4 the existing approaches are summarized and compared, ultimately commenting on what scope there is for future offshore wind farm layout optimization tools. Chapter 3 describes the structure and components of optimization approaches in greater detail and describes fully the optimization algorithms deployed as part of the present tool.

Comprehensive reviews of wind farm layout optimization have previously been carried out by Tesauro et al. [10], Valverde et al. [11], Herbert-Acero et al. [12], and Rodrigues et al. [13]. Though these reviews have covered the work done both in academia and industry to tackle this problem, they have not highlighted in detail the specific areas

of improvement within this field that should be addressed by future projects, nor have they been completed with the consideration of real constraints.

2.2 Tool Structure in the Standard Paradigm

In general, optimization is the process of identifying the *best* solution to a problem within the set of all possible solutions given constraints (also known as solution space) [14]. One key concern with optimization in general is that as it is an iterative process, the more complex the solution space becomes as a result of detailed objective functions or constraints, the more time it takes for the solution to converge to an optimal solution. Tool developers must therefore strike a balance in the objective function between model accuracy and computational time in order for the tool to produce useful results in sensible time-scales.

In general, the standard paradigm within the wind farm layout optimization community is to link three principal components:

1. Annual Energy Production (AEP) Estimation/Wake Modelling;
2. Cost Model; and
3. Optimization Algorithm.

Although all three of these tools are not always present, at a minimum either the AEP estimation or cost models are required alongside an optimization module. As existing work has been structured in a similar way, they can be compared on how these principal modules have been implemented on a module-by-module basis.

2.2.1 Annual Energy Production Estimation

Widely regarded as the most important of the calculations in a layout optimization tool, the estimation of AEP uses data describing the wind resource data and the turbine performance curves to establish the energy generated, usually for a period of one year. Alternate terms used to express the energy production include the *total power production* and *total energy production*. Though these terms may sound as though they are different from the AEP, they are also measures of the energy output of the wind farm. AEP is, however, the most common term used to express this quantity within the wind industry [15].

The AEP calculation module is generally designed to take into account some or all of the system losses which can be expected for the wind farm. A significant source of energy loss within large arrays of wind turbines is the interactions between the turbines and the wakes of any upstream turbines. Wake modelling has therefore become increasingly

important in the field of layout optimization and all optimization tools include an AEP computation with some consideration of the wake effects [10–12, 16–18].

Advanced AEP models seek to compute as accurate an AEP as possible and therefore account not only for the aerodynamic losses, but also consider additional sources of loss such as the electrical losses in the intra-array and export cables. They may also seek to identify any degradation in the performance of the wind farm and accurately measure and predict the downtime of each individual turbine within the wind farm. These additional sources of loss are not included in most AEP computations, however, they do represent the principal manner in which AEP models can differ from one another.

In a situation such as layout optimization, where thousands of layouts may need to be assessed it is of prime importance that each step in the assessment of the layout take as little time as possible. As a result of this, AEP estimation for layout optimization seeks to balance the computational cost of the approach against the accuracy of the estimated AEP. In general therefore, computational fluid dynamics (CFD) are often not implemented in the modelling of turbine wakes, and analytic wake models are instead used. Analytic wake models have been found to require significantly less computational time when compared to fully-developed CFD approaches. Though CFD would be expected to model the flow in greater detail, the additional computational time required would render the optimizer too slow to be deployed in an optimization process for real sites. The implementation of analytic wake models as opposed to CFD models therefore represents a compromise that is made in layout optimization in order to reduce the computational time without significantly reducing the accuracy of the model. Common analytic wake models used in layout optimization include the Jensen/Park model developed in Jensen [19] and Katic et al. [20]; the Larsen model developed in Larsen [21, 22]; the Ishihara model developed in Ishihara et al. [23]; and the Frandsen model developed in Frandsen et al. [24]. The governing equations for these models are explored in greater depth in Section 5.4 with validation of the models explored in Section 5.5. The Fuga model developed in Ott et al. [25] and Ott and Nielsen [26] represents a linearized CFD model which is capable of modelling turbine wakes, wake superposition, and wake meander. Though this model represents significant speed improvements over traditional CFD models, it is still not as quick as many analytic approaches.

2.2.2 Cost Model

Although not considered in detail in the majority of existing layout optimization tools, cost estimation and financial accounting has been identified as an important component needed for future layout optimization tools [10, 17, 27]. Though some work has been done to develop accurate and site specific cost models, this still represents an area of high uncertainty due to the innate challenges in cost modelling. With these challenges in mind as well as with the desire to reduce the computational time, it is therefore common for layout optimization tools to use a cost function which is intentionally simplified in order to highlight only the layout dependent aspects while accepting limited accuracy in layout independent factors [18, 27–30].

Cost modelling has been approached in different ways across the various tools that have addressed this problem. Some tools have constructed a bottom-up approach where the costs are computed based on material and labour costs of the components [17, 31]; while others have used a top-down comparative approach based on industry averaged figures given in reports [16, 32, 33]; and some have even used a relative cost indicator based simply on the number of turbines in the wind farm [34, 35]. Where a cost model is included in the optimization process, the project costs are directly included in the objective function of the optimization.

Common metrics used to assess layouts have therefore been the *levelized production cost* (LPC) or *levelized cost of energy* (LCOE) which are both measures that combine the lifetime costs of the project and the lifetime energy production to give a single figure representing the unit value of the energy. The respective formulas for LPC and LCOE are [36, 37]:

$$\mathrm{LPC} = \frac{C_{CAPEX}}{a \times \mathrm{AEP}} + \frac{C_{OPEX}}{\mathrm{AEP}} \tag{2.1}$$

$$\mathrm{LCOE} = \frac{\sum_{t=0}^{n} \frac{C_t}{(1+r)^t}}{\sum_{t=0}^{n} \frac{\mathrm{AEP}_t}{(1+r)^t}} \tag{2.2}$$

where C_{CAPEX} is the capital expenditure (CAPEX), C_{OPEX} is the annual operations and maintenance costs or operational expenditure (OPEX), a is an annuity factor, AEP is the annual energy production, C_t is the total cost (both CAPEX and OPEX) incurred in year t, n is the project lifetime, and r is the discount rate. It is important to note that though these two measures look very similar, they discount the costs and energy production in slightly different manners leading to different final costs. The LPC gives the nominal annualized cost per unit energy produced for the project while the LCOE

gives the present value cost of the project over its lifetime relative to the present value energy output of the project over the lifetime of project.

An alternative metric that is used on occasion is the *net present value* (NPV) of the project. Unlike the LCOE and the LPC, the NPV is explicitly in currency units and represents the present value of the project accounting for the energy produced as a revenue stream. These models, which include some kind of revenue model, tend to use a simplified cost model, similar to those described above, while using an assumed price of electricity to determine the revenue over the project's lifetime. This electricity price is generally assumed constant over the lifetime of the project. Given these simplifications, the NPV tends to correlate to the LCOE.

$$\text{NPV} = \sum_{t=0}^{n} \frac{B_t - C_t}{(1+r)^t} \tag{2.3}$$

where B_t is the total benefit or revenue of the development in year t.

2.2.3 Optimization Algorithm

The final module to be included in a layout optimization tool is the optimization algorithm itself and the method by which new layouts are developed. Optimization algorithms in general search a solution space seeking the best possible valid solutions. Systems optimization is a growing field within operations research and engineering that works towards modelling real world problems and then optimizing these models. Layout optimization tools have therefore not developed new optimization algorithms, but have instead explored existing optimization algorithms seeking to identify which family of these optimization algorithms would best fit the problem at hand.

Given the complexity of the offshore wind farm layout optimization problem, an exhaustive search is impractical as no algorithms can reach proven optimality. Classical optimization techniques are limited to continuous, differentiable objective functions and therefore are often ill-suited for complex real world engineering problems [38]. As a result of this, a number of heuristics and metaheuristics have been applied to the problem [17, 29, 30, 34, 35, 39–48]. Of the algorithms that have been tried, the most common are the *genetic algorithm* and variations on the *greedy heuristic algorithm*. Less frequently used are the *particle swarm algorithm*, *linear programming*, *simulated annealing algorithm*, *ant colony optimization*, *viral based optimization*, *extended pattern search algorithm*, and *random search techniques* [10, 12, 13].

One of the distinguishing properties between layout optimization tools is therefore the selected optimization approach deployed. Optimization tools in general must balance finding high quality solutions with the time required to do so. In order to try and

characterize this problem better, several optimization algorithms have been applied in the literature exploring how the algorithms perform in terms of computational time and quality of solutions with some algorithms having been shown to consistently outperform others on either one or both of these metrics.

2.3 Previous Tools

This section explores specific previous projects that have explored the optimization of wind farm layouts. Projects making use of the same optimization algorithm or similar operating principles are wherever possible discussed together in order to avoid repetition. Each project is introduced and its design in regards to the three principal components identified earlier will be discussed.

To begin, the layout optimization tools mentioned previously are categorized into one of three categories depending on their level of complexity in modelling a real wind farm and their environment. The first group are what have been classified as *advanced tools* due to their inclusion of both an AEP model that accounts for numerous sources of energy loss and also include an economic model that estimates the cost of the project. The second group are what are referred to as *incomplete tools* as they either do not fully account for the various losses in the AEP module or they do not account for any costs. The final group represents *commercial software packages* which include a degree of layout optimization. Though these are not as well documented in the public domain, they are included as they represent tools that the industry presently relies on for the purpose of wind farm layout design and optimization.

2.3.1 Advanced Layout Optimization Tools

The most complete tools include an AEP module that uses validated wake models (discussed further in Chapter 5) as well as some model for the losses in the electrical subsystem. Advanced tools also include a cost assessment and therefore optimize over a metric that incorporates both the output of the wind farm (energy produced or revenue) and a financial measure of the project costs.

2.3.1.1 Offshore Wind Farm Layout Optimization (OWFLO) Project

The first tool to be discussed is the Offshore Wind Farm Layout Optimization project (OWFLO) by Christopher Elkinton [17, 39, 49–52]. This project is classified as an advanced tool as it includes a model for the energy loss due to both intra-array cables and export cables, includes a well known analytic wake model, and includes a bottom-up cost model which is partially validated.

AEP Model

The AEP model included as part of this tool accounts for several sources of energy loss. OWFLO models the electrical losses by taking into account the cable length and the rated capacity of the farm. The length of cable needed is found empirically from a relationship to the turbine density and area of the wind farm. This method of estimating the losses in cables is partially validated against another analytic study rather than any actual transmission data. This therefore introduces a source of uncertainty as it is unclear how accurate both this model and the reference analytic model is.

The AEP model implements the Jensen/Park wake model which is used in the flow modelling software WAsP. The Jensen model was originally developed for a single turbine on a flat terrain and a modification is required to account for the superposition of multiple wakes [19, 20]. In this case, Elkinton opted to use a root-sum-square method proposed by Katic et al. [20] and used in WAsP's implementation of the Park model [17, 33]. A major advantage of the Jensen wake model is that computationally, it is a very simple analytic model based on mass conservation; and therefore it requires neither significant computational power nor time to execute. At the same time, the Jensen wake model is considered to be the simplest analytic wake model; it is often used as a reference wake model as for many applications it is sufficiently accurate and given its simplicity it is quick to execute [53, 54]. The selection of this wake model is therefore justifiable and can be assumed to introduce an acceptable level of uncertainty to the AEP model.

Cost Model

The OWFLO project [17] also built one of the most comprehensive bottom-up engineering cost models included in a layout optimization tool. This cost model attributes the total cost to five main cost elements: the rotor-nacelle assembly (RNA), the support structure, the electrical interconnection, operations and maintenance, and the decommissioning costs. Of these, only the support structure costs and electrical infrastructure costs are impacted by the layout. As this model assumes that the installation costs contribute a constant percentage to each of the line items, the impact of changes in the wind farm layout on the installation costs are not captured by the model.

The RNA cost is based on a series of cost estimation projects including Opti-OWECS [55–60] and the DOWEC Cost Models [61]. Using these models, the cost of the RNA is described as a function of the rated capacity and the rotor diameter. Elkinton's validation of this cost model was limited due to the lack of available cost data at a sufficiently high resolution. Only Middelgrunden wind farm was found to have a cost analysis that included RNA costs, allowing the model to be validated. Comparing the RNA cost model to the actual spend at Middelgrunden revealed a model error of the order of 66% [51]. It should be noted that the Opti-OWECS project and DOWEC projects were both developing means of modelling future costs of turbines. The Opti-OWECS project focused on modelling future turbines between 1.5 MW and 3 MW in size, while the DOWEC Cost Model is based on a baseline 130 m rotor diameter, 6 MW turbine [55, 61]. This cost model therefore makes use of sub-models which have been based on scaling factors and have not been fully validated. This results in relatively high levels of uncertainty when deviating from the validated turbine sizes. The availability of additional cost data, however, would make it possible to tune this parametric cost model potentially reducing the uncertainty.

The support structure cost is based on a simplified geotechnical model constructed by Elkinton et al. [51]. This model uses the parameters of the turbine and the soil description to compute the necessary dimensions of either a gravity-based foundation, a monopile, or a tripod support structure. From this, the cost of manufacturing is based on the commodity prices of steel and concrete, as well as an additional factor for the labour required to manufacture the support structure. This bottom-up approach for the support structures was validated where possible against both existing wind farms and other models, though costs for real projects were only available for the gravity-based foundations and monopiles. Validation against these showed that the modelled masses had high error, but that the modelled costs were within $\pm 10\%$ of the data from real wind farms. As tripod costs were only validated against other models, it is difficult to judge the accuracy of this and uncertainty is introduced into the model. It should also be noted that the validation sites used were all constructed for similarly sized (2 MW

to 3 MW) turbines at about the same time. It therefore remains to be seen how this model scales to larger turbines or farms built at a time when commodity prices are different.

The electrical interconnection costs were divided into the medium voltage system and the high voltage system. The medium voltage system is used to connect the turbines to one another and the substation while the high voltage system is used to model the export cables from the substation to the grid. The medium voltage system cost is modelled by an equation given by Wright et al. [62] which uses the cable length and voltage level to estimate the cost. In this case, the total length of cable is estimated based on the turbine density of the layout. The high voltage system cost is modelled by a formula given by Ackermann and Negra [63] which uses the wind farm rated power, export cable lengths, and export cable voltage to estimate the number of export cables required, the cost of switchgear, the cost of transformers, the cost of the cables, and the cost of installation. Unfortunately upon validation against existing wind farms it was shown that models used in conjunction like this had high errors (up to 72% for some wind farms). The models did, however, give costs of the correct order of magnitude and it was therefore assumed that for a first-order LPC evaluation this would be acceptable [17]. This, however, further reduces the accuracy of the cost model as a whole and therefore the LPC has a high degree of uncertainty associated with it. At the same time, as the model does capture a degree of the impact of layouts, it might be sufficient for layout optimization purposes in which the relative LPC of layouts compared to one another is of importance.

Given that few offshore wind farms have been installed for significant periods of time, there is still high uncertainty and difficulty in accurately modelling the operations and maintenance (O&M) costs associated with future wind farms. This cost model therefore assumed that costs were constant over the lifetime of the project, choosing to ignore any potential inflation in costs or reduction due to learning. Specifically the costs were assumed to be 1.5-3% of the capital costs as recommended by the Opti-OWECS and DOWEC projects [58, 61]. This type of cost model therefore assumes that the OPEX scales consistently with the CAPEX which may not be a fair assumption. At the same time, models such as these are generally expected to be accurate in terms of order of magnitude. As with the other cost elements there is additional uncertainty introduced to the LPC estimate as a result of the assumptions made here.

The final cost term considered by this cost model is the decommissioning costs. As the first offshore wind farms are only now beginning to be decommissioned, the OWFLO project was unable to validate any of these costs. The OWFLO cost model, therefore, selected to base these costs on the methodology of a number of reports. These reports

made the decommissioning costs a function of the number of turbines, the installed capacity, labour cost of installing cables, and labour cost of installing turbines.

In all, the cost model used in this layout optimization tool is comprehensive in that it includes terms for all of the major cost parameters. However, upon validation it is shown that each of these terms has relatively high error ($30 - 150\%$ in some cases) and therefore significant uncertainty must be included when using this cost model. An important fact is that the LPC had not only high error, but a high range of error indicating that the LPC estimated by this model is largely indicative rather than an accurate estimate and might not be sufficiently accurate to compare layouts even on a relative basis. Given that this cost model may give such inaccurate LPC values, it may not be an appropriate model to use for layout optimization of real wind farms. Importantly though the individual model may not be accurate, the work has identified the key elements which must be included in the estimation of the costs of an offshore wind farm.

Optimization Module

The OWFLO project represents one of the few published comparisons of different optimization algorithms. For this tool, Elkinton implemented both a genetic algorithm (GA) and a greedy heuristic optimization algorithm in an LPC minimization problem. The project also did not only implement them to compare their results, but also executed the two together in order to take advantage of their respective strengths. These algorithms are fundamentally different and it is important to understand how they differ from one another.

The genetic algorithm is one of a family of optimization algorithms based on the behaviour of real biological systems. The genetic algorithm specifically is so named as it borrows its operating principles from genetics and natural selection. The genetic algorithm is therefore often classed as an *evolutionary algorithm* as the solution evolves over generations (iterations). In the OFWLO project, the wind farm area is reduced to a series of potential wind farm positions for which an array of ones and zeros can represent if a wind turbine is present or not. This array can be thought of as the *genetic code* of the layout. Generally, the wind farm area is discretized by producing a grid and allowing turbines to only be placed at the centre of each cell [10, 28, 35]. The method then begins by randomly generating a set of layouts for which the objective function, in this case the LPC, is computed. The layouts with the lowest LPC are kept while the rest are replaced through crossover and mutation. Crossover involves combining elements from two "parent" layouts into a "child" layout, while mutation involves randomly changing part of the genetic code (the layout). By including mutation a degree of randomness is

introduced allowing the solution to avoid local minima in search of the global minima. Chapter 3 explores the GA in greater depth.

The second optimization algorithm implemented by Elkinton is the greedy heuristic algorithm. This algorithm starts with a random layout from which three operations can be performed: add a single turbine, remove a single turbine, move a single turbine. After each operation the LPC is re-calculated and if an improvement has been made then the process repeats using this new layout as the base-case, if no improvement has been made then the algorithm reverts to the previous base-case and attempts an operation. A layout is deemed optimal if a predefined number of consecutive operations fail to improve the LPC [10, 17]. In general, a greedy heuristic will try to repeat a successful operation before trying one of the other two operations.

As the genetic algorithm is considered slow, but highly accurate in locating a global optima [17], and the greedy heuristic algorithm is relatively quick but less accurate this tool also attempted to run the two algorithms in series using the genetic algorithm to move towards the solution, and then refining it with greedy heuristic. For the cases considered in this tool, this two-step process was found to be more effective than using either of the optimization methodologies on their own [17, 51]. This can be described with regards to exploitation and exploration. In general, a genetic algorithm is effective at exploring the search space, while a greedy heuristic is a type of local search therefore excelling at the exploitation of existing solutions.

2.3.1.2 TOPFARM - Risø

TOPFARM was a project funded by the European Commission and led by Risø DTU National Laboratory for Sustainable Energy. This project looked at developing a methodology for the financial optimization of offshore wind farms taking into account a financial-balance as well as advanced wake models developed at Risø DTU. This project took advantage of a number of tools and resources of the partners involved in the project in order to develop the final tool which addresses the problem of layout optimization of wind farms. Unlike OWFLO, this project did not use the LPC as an objective function, but instead uses the *financial balance* of the project. This financial balance accounts for the energy output as a revenue term from which all lifetime costs are subtracted, effectively giving an NPV of the project in currency units [27, 64–67].

AEP Model

The TOPFARM AEP model is unique in that it links standard wake modelling techniques to aeroelastic codes in order to compute the turbine loads as a result of operation inside a wake. The computed loads are used to both give a measure of the energy yield as well as the fatigue on the turbines and thereby the degradation costs. The TOPFARM project is built upon existing Risø DTU flow models allowing it to accurately represent the flow environment throughout the wind farm. This includes a range of flow models ranging from analytic models through to CFD [64, 65].

The first work package of the TOPFARM project looked at a series of methodologies for modelling the wakes of turbines and the wind climate within a wind farm. This project looked at a number of models ranging from highly complex, computationally demanding CFD flow models to quicker analytic models. Ultimately a calibrated dynamic wake meandering (DWM) model was implemented. This model, developed by Risø DTU, has been shown to be a relatively quick computational method while still retaining significant accuracy [64, 68]. The DWM model is therefore used with the aeroelastic codes to include a more accurate description of the local wind climate for each turbine. This is then used to compute accurate turbine loads including thrust on the rotor which is then fed back to the flow model to compute the characteristics of the wake downwind of each turbine. In this way, the AEP computed for each turbine can be very accurate as the thrust is based on the output of aeroelastic codes rather than look-up tables.

Further losses such as the cable and electrical losses are, however, not considered in the computation of the AEP. This AEP value is therefore only layout dependent in the consideration of turbine wakes. Though the DWM is considered to be a quick model, it is not considered to be sufficiently fast to implement directly in the optimization tool. In order to accelerate the optimization and to reduce computational time in certain modes of the tool, the DWM model was pre-run for a number of cases to produce a series of look-up tables that the optimization routine could use [64]. It is not documented how the optimization routine makes use of these tables or if any interpolation is required. Depending on the mode selected for the tool, there are varying degrees of model accuracy; when running in a fast setting, using a number of look-up tables, it is important to incorporate a higher level of uncertainty.

Cost Model

The cost modelling methodology adopted by the TOPFARM project intentionally looks only at the costs that are layout dependent. To this end, constant costs such as wind farm planning and consenting, turbine supply, and the onshore electrical works are ignored entirely. The AEP of the wind farm is converted to a levelized revenue from which all the layout-dependent costs are subtracted. The financial balance objective function then gives a kind of relative, layout dependent NPV. The full financial balance formula used by the TOPFARM project is given by:

$$FB = P_e \cdot TEP - C_D - C_M - (C_f + C_g) \cdot \left(1 + \left(\frac{r_l - r_i}{N_L}\right)\right)^{n \cdot N_L} \tag{2.4}$$

where FB is the financial balance, P_e is the assumed price of electricity, TEP is the total energy production over the entire lifetime of the project, C_D is the degradation cost that represents the depreciation of the asset due to fatigue degradation, C_M is the maintenance cost, C_f represents the costs of foundations, C_g represents the cost of the electrical grid, N_L is the number of compounding periods per year, r_l is the interest rate on any loans, and r_i is the assumed inflation rate [64, 65].

The cost modelling methodology for this tool includes the layout dependent installation costs, the layout dependent degradation cost, and the maintenance costs. The unique feature of this tool is the inclusion of the degradation costs which are based on using each turbine's individual load conditions to estimate the wear and failure of individual components. In order to reduce the computational time, this is one place where the pre-run aeroelastic look-up tables can be used to look-up the turbine loads for a given set of conditions. These turbine loads are then combined with a failure rate database to determine the relative turbine reliabilities [65].

The computation of the cable costs incorporates its own heuristic optimization algorithm in order to determine the most cost-effective means of collecting the energy from the turbines. This algorithm also adds a penalty cost to account for the electrical system losses. In this way, although the electrical losses are not accounted for in the AEP model they are thought of as an additional cost in the financial balance model and they are therefore taken into account in the objective function. The AEP is levelized and converted to a present-day currency unit assuming a constant price of electricity [65].

Beyond this, little information regarding the actual means of computing the wind farm costs are given in the publicly available documentation. There is also no available discussion on the validity of a cost model constructed, nor is there a straightforward manner to independently validate it. Though the flow modelling and fatigue loads have been validated against site data and alternate models, it is unclear if the method by

which these are related to costs has been validated in any way. There is therefore uncertainty associated with the modelled costs, and there is also added uncertainty due to the assumption of a constant price of electricity.

Optimization Algorithm
TOPFARM like OWFLO uses a two-step optimization algorithm, but chooses to use a different implementation of the objective function for each of the optimization steps. The fully developed objective function is only used with the second step of the optimization algorithm to refine the solution, while a coarser financial balance is used with the first step. Unfortunately little is said in regards to the coarser model's accuracy or formulation. Like OWFLO this tool also chooses to use a genetic algorithm for the first step, but opts instead to use a sequential linear programming method for the second stage. Like the greedy heuristic algorithm this is an efficient search algorithm, however, it is sensitive to local minima [38]. Though a non-sequential linear programming formulation would avoid local minima, it was felt that using the genetic algorithm to accomplish this would prove more effective and less computationally intensive. The use of the two algorithms in conjunction therefore improves the tool's ability to reach a good solution [64]. The use of linear programming can also introduce additional uncertainties depending on the methods by which the non-linear elements of the objective function have been linearized.

The overall approach has been applied to a number of small existing wind farms to identify potential layout improvements. The work carried out as part of TOPFARM has indicated that the fatigue loads as a result of turbulent wakes have a significant impact on the financial balance due to a turbine's reliability decreasing when operating within a wake. The inclusion of the turbine reliability and the degradation cost in the financial balance has therefore allowed the tool to find layouts that would not have been possible if AEP alone was used as the objective function. This supports the use of an objective function that incorporates the AEP and the project lifetime costs while also identifying the importance of accounting for the turbine reliability [27]. However, the full cost methodology has not been validated leaving the specific results of this tool questionable. The specific cost functions, wake lookup tables, load lookup tables, and optimization algorithm are not widely available, so it is not possible to implement the same approach as the TOPFARM project and independently validate it.

2.3.1.3 Guillén PhD Thesis - TU Delft

The project by Guillén [16] sought to develop a design tool for the optimization of offshore wind farm layouts including specifically minimization of wake interactions, and the design of a minimal cost electrical infrastructure. Like OWFLO and TOPFARM, this was, therefore, considered to be an advanced layout optimization tool as it tried to account for as many of the system losses as possible and included cost in the optimization objective function. This tool intentionally implemented three different wake models, and a pair of electrical models in order to give flexibility to the tool and to benchmark newly created modules.

AEP Model

The AEP model by Guillén [16] includes a previously developed cable loss and cost model developed by Schoenmakers [69]. This model accounts for the cable losses by computing the cable losses for every possible wind speed between the the cut-in and cut-out wind speeds and applying the Weibull distribution in order to account for the probabilities of occurrence. At each possible wind speed, the total cable loss is a function of the current rating of the cable, the voltage rating of the cables, the thermal properties of the cable, the capacitive properties of the cable, the resistance of the cables, the dielectric loss factor, the frequency of AC transmission, the number of phases, the current distribution per phase for each wind speed, and the cable length. This electrical loss model is, however, not validated in this project nor did the original study validate it [16, 69] which does introduce uncertainty into this model. Having said that, the percentage loss predicted by the model for a number of typical Danish offshore wind farms is close to what is quoted by wind farm operators implying this might be an acceptable model for a first order approximation [69].

In terms of wake modelling, this tool implements the Jensen, Frandsen, and the Ainslie wake models. Each of the three have been previously validated and none of the models has been shown to be vastly superior to the others [53, 54]. These wake models along with other analytic wake models are discussed in greater detail in Chapter 5 along with the full formulations required to implement them.

Cost Model

Though this is classed as an advanced tool, the cost model employed is not as advanced as other projects such as OWFLO or TOPFARM. In fact, this is one of the simplest cost models in that the total cost of the wind is simplified to be only a function of the turbine retail price and the cable costs. The only layout dependent costs are therefore the cable costs.

Using the cost breakdown from the DOWEC cost model [61, 70] all costs other than the cable costs, including O&M costs, were expressed as a percentage value of the turbine costs. Unfortunately this introduces a significant level of uncertainty as the DOWEC cost model was based on projects that had been installed by 2002 and some estimation of how the industry learning curve would develop over subsequent years for a hypothetical future turbine [61]. It does therefore represent some level of averaging of early industry costs on relatively small projects and would be less applicable to large projects now without further tuning.

The cable costs are computed using a modified version of Schoenmakers' cable cost model. The original Schoenmakers model is not available as it was developed within Evelop Netherlands BV and remains their intellectual property. The model uses the cross-sectional area to compute the total amount of material needed for the cable and uses a constant factor to account for the material and labour cost per unit weight and length respectively [16, 69]. The model developed by Guillén's layout optimization tool builds on this idea and uses the layout to determine the current rating required for each string of turbines. This is then compared to available manufacturer data to correctly size the cable, and then compute the cost based on the material costs and a manufacturing/labour factor [16]. Verification of the cost models shows that the cost of cables is highly sensitive to the assumed price of raw copper. The price of copper has also been shown to vary significantly making it difficult for both the Schoenmakers [69] model and the Guillén [16] cable cost model to be fully validated as shown in Figure 2.1. This does introduce uncertainty to both the cost model and the LPC model.

Optimization Algorithm

In this tool, like the OWFLO project, the minimization of LPC is used as the objective function. Interestingly, however, the optimization routine for this tool changes only a single parameter, the spacing between turbines, which then affects the entire layout. This does therefore not allow for complex layouts, and the layout is in fact further constrained to a rectangular topology with regularly spaced strings of turbines. By changing the minimum separation distance for each iteration, the layout was changed and the LPC recomputed. Further simplifying this implementation, this tool opted not to write its own optimization algorithm, but instead chose to use the optimization

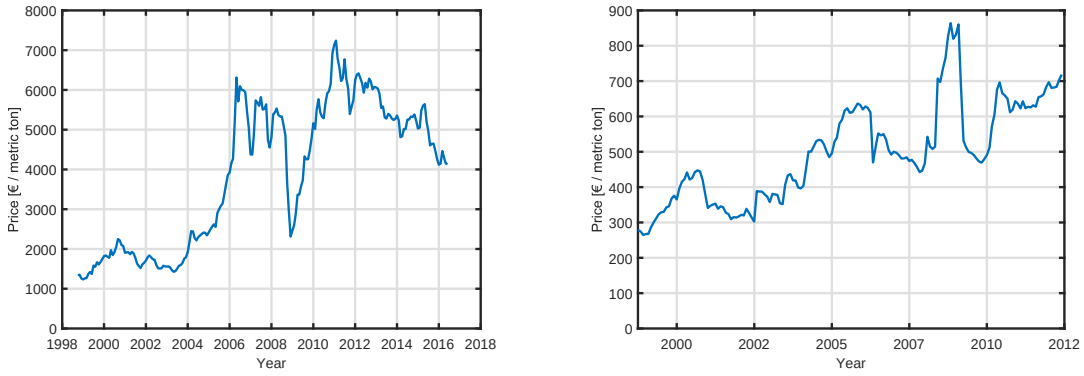

(a) Copper Price **(b)** Steel Price

Figure 2.1: Commodity prices from The World Bank [71].

toolbox in MATLAB. Within this toolbox a simple heuristic search algorithm, similar to the greedy heuristic algorithm described earlier, is used to find the separation distance for which the LPC is minimized. This search approach has been selected as it is computationally inexpensive [16]. No discussion is made to indicate the quality of solutions found by the toolbox compared to a bespoke implementation of optimization algorithms.

2.3.2 Incomplete Layout Optimization Tools

The following tools, classed as "incomplete" layout optimization tools, have been further sub-categorized based on the type of optimization algorithm used. Each of the tools and projects mentioned in this section include either a simplified AEP module or is lacking a cost model. A simplified AEP module is either one that does not take into account the wake effects, one that does so in a simplified manner, or a model that does not consider losses other than wakes. As previously described work [10, 12, 17, 27] has indicated the necessity of optimizing over a metric incorporating both AEP and cost considerations, the omission of a cost model made a tool incomplete in the eyes of this study.

2.3.2.1 Genetic Algorithm Optimization

The genetic algorithm represents one of the most common optimization algorithms applied to the wind farm layout optimization problem. In fact, the first work in the field of wind farm layout optimization, the seminal paper by Mosetti et al. [34] not only used a genetic algorithm to address the problem, but also defined three standard test cases which have frequently been used to benchmark different optimizers. These cases are described in greater detail in Section 7.2. In the survey of previously

constructed tools besides the advanced tools using the genetic algorithm, a number of incomplete tools were also found. Those of Mosetti et al. [34], Grady et al. [35], Emami and Noghreh [72], Mittal [28], O'Reilly [31], Zhang [44], Rašuo and Bengin [73], Ituarte-Villarreal and Espiritu [42], and Couto et al. [43] were all found to use the genetic algorithm in a similar implementation to what was described earlier. Kusiak and Song [74] and Rodrigues et al. [13], use modified versions of the genetic algorithm known as a multi-objective evolutionary strategy algorithm and Multi-Objective Gene-Pool Optimal Mixing Evolutionary Algorithm (MOGOMEA) respectively. These use a similar approach to the GA, however, allow for multiple objective functions to be simultaneously optimized. In their case, the AEP is maximized while the constraints are formulated in such a way that satisfying them would minimize the second objective. It is important to note that the objective function is therefore a weighted sum between the two objectives. It is important to note that a bi-objective optimization scheme is fundamentally different from using a single metric which accounts for the two objectives, as the bi-objective scheme requires that weights are used to identify the relative importance of the two objectives. The bi-objective objective function therefore represents an abstract combination between different parameters with the fitness values of solutions having little physical meaning.

With the exception of the model developed by Rašuo and Bengin [73], each of these models uses the Jensen wake model with either linear or sum of squares superposition. The model by Rašuo and Bengin [73], however, uses a simplified aerodynamic model to compute the wake through a series of equations that are iterated similar to blade-element momentum theory.

Shakoor et al. [48, 75, 76] uses a similar genetic algorithm to other tools, however, this work rotates the wind resource by 45° claiming significant improvements compared to other studies, however, given that the assumed resource is different, it is difficult to compare these results to any other studies. Given realistic boundary constraints it is also difficult to justify the rotation.

The models by Mittal [28] and O'Reilly [31] use a relative cost function in the optimization objective function; however, the cost function is not fully developed in either model. Both of these tools use a project cost formula which scales with the number of turbines originally conceived by Mosetti et al. [34] and which has been used by many projects in order to compare optimization algorithms applied to wind farm layout optimization. This cost function has not been validated against any real data and makes the assumption that the cost of a single turbine is one and for a large number of turbines, economies of scale will result in savings of one-third. It also makes the assumption that costs are not impacted by the layout of the turbines, but only the number of turbines to be installed in the wind farm. The function is:

$$C = nT\left(\frac{2}{3} + \frac{1}{3}e^{-0.0174nT^2}\right) \tag{2.5}$$

where C is the cost, and nT is the number of turbines in the wind farm.

These optimization tools combine the AEP and their relative cost function to produce a relative cost of energy metric. Both tools allow either this relative cost of energy or the AEP to be used as objective functions in the optimization process, however, given that the costs scale only with the number of turbines optimizing over the relative cost of energy results in AEP maximization. The remaining literature use the AEP explicitly as the objective function with the exception of the model by Zhang [44] which allows either the AEP or a noise propagation measure to be used as the objective function. Noise propagation is a common design metric for onshore wind farms where the noise of the wind farm is often a constraining factor. For offshore wind farms, however, this is generally not thought to be of concern.

None of these tools which implement a genetic algorithm include any further system losses. As their main purpose has been to demonstrate the capabilities of a genetic algorithm in solving a problem of this type, these tools have generally been applied to relatively small test cases, so it remains to be seen how quickly these implementations of the genetic algorithm would converge to a solution for a large wind farm. It also remains to be seen if the GA is the most appropriate heuristic when more detail is introduced to better represent the reality of the problem. Many of these projects identify the need to use a metric such as the cost of energy as optimizing only the AEP might not be the most sensible approach from the point of view of a developer [10, 28, 31]. Mosetti et al. [34] which is the earliest documented research into wind farm layout optimization used a weighted objective function in order to take both AEP and cost into account; however, the costs have no dependency on the layout and as a result the AEP term dominates the optimization process and in fact there is no benefit of including the costs in the objective function if the number of turbines is held constant.

2.3.2.2 Greedy Heuristic Optimization

Given the complexity of wind farm layout optimization, no optimization approach has been identified as being able to find a proven optimal solution without fully enumerating the possibilities. As a result, heuristic approaches such as the genetic algorithm or greedy heuristic algorithm have been deployed. These approaches sacrifice *proven optimality* in exchange for finding a *good, feasible solution*. The second most commonly implemented heuristic algorithm is that of the greedy heuristic algorithm. Of the incomplete tools surveyed, the greedy heuristic algorithm was used by Chen et al. [77], Ozturk and Norman [78], DuPont and Cagan [29, 79, 80], and Dilkina et al. [81].

A unique approach was that by DuPont and Cagan [29, 79, 80] in which an extended pattern search algorithm was used. This approach is a variation of the greedy heuristic algorithm and has the advantage of allowing multiple objectives to be simultaneously optimized and allows for a continuous solution space. A continuous solution space allows the turbines to be placed anywhere within the wind farm boundaries rather than at discrete predefined locations.

Like many of the publications, the tool by DuPont and Cagan [29, 79, 80] approximates the wind farm costs to a function of the number of turbines as Mosetti et al. [34] suggested (Equation 2.5). Of the other models, the models by Chen et al. [77] and Ozturk and Norman [78] use a profit based objective function using layout independent capital and O&M costs. These models therefore give a cost based only on the number of turbines, using Equation 2.5 like many other works. Both models also assume a price of electricity for the computation of the profit thereby requiring additional tuning in order to apply these for future projects. The patented approach by Dilkina et al. [81], however, uses an AEP objective function and does not consider any cost elements.

For the computation of the AEP, the models by Chen et al. [77], DuPont and Cagan [29, 79, 80], and Dilkina et al. [81] use a Jensen wake model. The Ozturk and Norman [78] model, however, uses a series of quadratic and linear interference equations to represent the wake interactions within the wind farm. All four models ignore further system losses such as electrical losses.

2.3.2.3 Mixed-Integer Linear Programming Optimization

Of the incomplete tools reviewed, the two tools by Fagerfjäll [32] and Archer et al. [82] used a mixed-integer linear programming (MILP) approach. MILP describes an optimization problem which is formulated as a linear programming (LP) problem involving both integer and non-integer decision variables. Linear programming in general describes a family of optimization problems where decision variables are combined in linear functions only. Linear programming often requires physical systems to be simplified or approximated as few systems are in reality linear. The tools developed by Fagerfjäll [32] and Archer et al. [82] therefore intentionally choose to simplify the problem to allow for a linear programming formulation. The tool by Fagerfjäll [32] optimizes for either the AEP or the profit using a validated wake model while the tool by Archer et al. [82] optimizes for only the AEP. Unfortunately neither model accounts for layout dependent system losses other than wake losses. By taking advantage of a graph theory formulation, the tool by Fagerfjäll [32] allows the MILP problem to be formulated such that the turbine layout can be optimized while the cables and collection network costs are minimized. However, the formulation does limit the possible positions of wind turbines to a discrete set of locations. The AEP model included in

both tools uses a linear wake superposition of the Jensen wake model to create a linear programming approximation of wind turbine wakes. This method is known to not be the most accurate; however, by making the simplifying assumptions that have been made, allows a MILP solution to be formulated reducing the computational complexity.

When profit maximizing, the tool by Fagerfjäll [32] uses average turbine costs for wind turbines and farms. This economic module also assumes a constant price of electricity in order to compute the revenue. The use of industry averaged costs from existing wind farms and the use of a constant price of electricity without any levelizing, introduce additional uncertainty in the economic model. An interesting conclusion from this tool is, however, the fact that road and cable costs were found to be sufficiently small relative to the revenue stream that they did not affect the overall layout.

When comparing this MILP implementation to available commercial software tools, it was found that an MILP approach was far more computationally intensive, requiring more time to converge on an optimal solution than heuristic approaches. In general, this is to be expected as the inclusion of both discrete integer decision variables and continuous decision variables is known to slow the optimization process [14]. However, for a series of test cases by Fagerfjäll [32] it was found by validation using the commercial packages that the layouts proposed by this new tool generated on average 40% more energy than the so-called optimal layouts proposed by WindPRO 2.6 by including approximately 50% more turbines. It should also be kept in mind that the analytic wake models used by this tool and its commercial counterparts tend to over-predict the velocity deficit as a result of the wind turbine wake therefore implying that a real wind farm would expect a higher power output than predicted by this tool.

2.3.2.4 Particle Swarm Optimization

Another optimization algorithm that is also based on an analogous process in the biological sciences is that of particle swarm optimization (PSO) algorithms. These algorithms are based on studies of the behaviour of swarms of birds and schools of fish [10, 14, 18, 83]. The Unconstrained Wind Farm Layout Optimization (UWFLO) project by Chowdhury et al. [18, 40] implements a particle swarm algorithm in their layout optimization problem.

The PSO treats possible layouts as particles in the swarm. By first initializing these particles to be random feasible layouts, the objective function is computed for each of these possible layouts. The particles then use knowledge of their current position in the search space, their previous best position within the search space, and the best positions of other members of the swarm in order to compute a *velocity vector* which dictates how they will move within the search space in the next iteration [14, 83]. For

each iteration, the objective function is computed for each of the particles and new velocities are assigned. In this way, the swarm explores the search space and converges on the best possible layout [10, 18].

In the UWFLO project by Chowdhury et al. [18, 40] the AEP and cost of energy are used as objective functions. To compute the AEP, the Jensen wake model is used to account for the wake losses. Unfortunately the UWFLO project does not take into account additional system losses such as the losses due to electrical cabling or turbine reliability. The costs in this model are based on quadratic response surfaces based on compiled data. In this way, the cost of a turbine was related to the rotor diameter and the cost of the wind farm was related to the number of turbines [18]. Though the quadratic response surfaces had been built based on existing wind farms, no validation of how this worked as a predictive model have been presented. It should be noted that based on what database of component costs is used to develop the quadratic cost relationships, it might be possible to improve the model by tuning it to the specific turbines or turbine-types under consideration.

This project went further than others and allowed the type of turbine to be varied as well, introducing additional decision variables and therefore degrees of freedom to the system [40]. This tool predicted that for a test case, the wind farm was the most productive when different turbine types were mixed into the wind farm. However, this did not include a consideration for how O&M costs may be affected by having to simultaneously maintain multiple turbine models within the same site.

The UWFLO project has further expanded this technique combining it with a series of systems to ensure that swarm diversity is maintained and the solution does not prematurely converge to a non-optimal solution. This development treats the continuous and discrete decision variables differently in what is referred to as a mixed-discrete particle swarm optimization algorithm [84].

2.3.2.5 Ant Colony Optimization

The final class of biologically inspired optimization algorithms is the ant colony optimization algorithm. In the literature, only Eroglu and Seçkiner [85] use such an optimization routine for the optimization of wind farm layouts. This project uses the AEP as an objective function, ignoring all wind farm costs. The wind turbine wakes are modelled using the Jensen wake model and represent the only loss of energy that is considered.

Like the PSO, this is classed as an algorithm making use of *swarm intelligence* and is analogous to the pheromone trails that ants rely on in order to identify the shortest path between their colony and a food source [14]. In nature, these pheromone trails

help the colony return to the food via the shortest path. In this case ants will initially randomly explore an area to find food leaving behind a chemical pheromone trail allowing them to find their way back to the colony. The quality or strength of the pheromone increases according to the quantity of food and its proximity. Future ants then use these pheromone trails to guide them to food. In this study an algorithmic implementation of this process is used to find the layouts which maximize the AEP. In this case, the pheromone strength is a measure of how unaffected by wake effects a layout is.

This study by Eroglu and Seçkiner [85] identified that the ant colony optimization algorithm converges on a solution more quickly than alternate metaheuristics, however, only a simple case was tested and there is therefore scope to explore the applicability of the ant colony optimizer for larger wind farms resembling real cases. This study was also conscious of the fact that maximizing AEP may not be the most realistic objective function to use and recommends potentially some kind of measure including the wind farm life based on the loading conditions to be used instead.

2.3.2.6 Stochastic Tools and Random Search

Another novel approach has been the implementation of a Monte Carlo simulation method and random search explored by Marmidis et al. [30] and Feng and Shen [86]. These methods also use the cost of energy as the objective function and the Jensen wake model. Like earlier studies, the cost is formulated using Mosetti's cost function (Equation 2.5) and system losses other than the wake effect are not taken into account.

Optimization algorithms based on Monte Carlo simulation or random search use repeated random sampling in order to develop the optimal layout. Increased numbers of samples results in increased accuracy of the algorithm. These approaches therefore effectively assume that the objective function is sufficiently complex that understanding the value at a given position within the search-space does not yield useful information on where to sample next. Compared to a genetic algorithm significant gains in the objective function can be noted, however, this comes at the cost of significant numbers of evaluation calls. Further study of the Monte Carlo simulation method is required to evaluate its suitability to the wind farm layout optimization problem.

2.3.2.7 Simulated Annealing

The final class of optimization algorithms are those which make use of a simulated annealing algorithm including the work by Bilbao and Alba [87] and Rivas et al. [88]. This algorithm is also a metaheuristic local search algorithm which the solution is thought of as a cooling material in a heat bath akin to an annealing process in metallurgy. This approach is very similar to a greedy heuristic algorithm, however, the algorithm allows inferior solutions to be accepted in intermediate iterations with the hope that these will eventually lead to improved solutions.

Both of these studies looked only at maximizing the AEP using the Jensen wake model and included no considerations for electrical losses or the project costs.

2.3.3 Commercial Layout Optimization Tools

Beyond the academic studies there are a number of commercial software packages which are used for the purpose of layout optimization. It should be noted that none of these packages are solely a layout optimization package but rather include layout optimization as a module. Principally most of these software packages are built upon wind-flow simulations and are designed to yield wind farm AEP estimates. Among the software packages, WindFarmer, WindPRO, WindFarm, WindSim, and openWind are commonly used by wind farm developers [10, 89, 90]. All the commercial software packages with the exception of WindSim use a flow model based on WAsP or linear flow modelling. This takes the wake effects and added turbulence into account.

openWind allows the user to select from three different wake models, the Jensen model, the modified Jensen/Park model, and their independently developed Deep-Array Wake Model. ReSoft's WindFarm software allows the user to either use an asymmetric wake model, or the Jensen/Park model. GL Garrad Hassan's WindFarmer uses a wake model based on the Ainslie Eddy-Viscosity model. EMD International's WindPRO allows users to choose between the Jensen, Ainslie Eddy-Viscosity model, or the Larsen model. WindSim, however, is not structured in the same way and is built instead on the repeated solving of the Navier-Stoke equations making it a full CFD approach. WindSim also accounts for wake effects using CFD. None of the software packages give much away in terms of their methodologies, making it difficult to establish exactly what is and is not included in their optimization routine.

Of the five, all offer optimization of the AEP, with WindFarm and openWind also allowing optimization to be done for the LCOE. WindPRO interestingly is the only one of the four to offer a layout optimization based on the noise levels. WindFarmer, WindPRO, and openWind are capable of taking electrical cable losses into account, however, WindFarmer and WindPRO require the purchase of an additional program

module in order to do so and do not design the intra-array cable network, but merely assess networks designed by the user.

In terms of optimization algorithm few of the program divulge their methodology. From what is available, it is known that openWind and WindFarmer both use a stochastic heuristic optimization process [10, 89, 90]. As both tools consider only a single layout at a time and look for improvements, they are sensitive to the initial layout as multiple add, remove, or move operations are not considered simultaneously. Table 2.1 compares the features of the available commercial tools.

Table 2.1: Comparison of Commercial Wind Farm Design Tools

	open-Wind	Wind-Farmer	Wind-Farm	Wind-Pro	Wind-Sim
Energy Yield Calculation	✓	✓	✓	✓	✓
Integration with WAsP	-	✓	-	✓	-
Analytic Wake Models	✓	✓	✓	✓	✓
ABL Interaction	✓	✓	-	✓	-
3D RANS Wind Flow Solver	-	-	-	-	✓
Cost Assessment	✓	✓	-	✓	-
Site Restrictions	✓	✓	✓	✓	✓
Layout Optimization (AEP)	✓	✓	✓	✓	✓
Layout Optimization (COE)	✓	-	✓	-	-
Electrical System Optimization	✓	-	-	-	-

2.4 Discussion and Conclusion

This survey of wind farm layout tools expands on previous reviews by Tesauro et al. [10], Herbert-Acero et al. [12], Pérez et al. [91]. The goal has been to survey the available layout optimization tools and identify where tool improvements can be made. As a first step in the development of a new tool it is important to identify what has been tried in the past so as to avoid any repeated research.

Based on the previous work in this field, it is important to note that the correct metric for optimization must be recognized. As a minimum, this metric needs to identify what elements of the wind farm are dependent on the layout, but more ideally try to be a holistic metric for assessing the layouts. In regards to the wind farm layout optimization problem it is clear that the energy capture or AEP of the wind farm is affected by the layout and must at some level be included in the metric along with the system losses which are affected by the layout: wake and electric cable losses. Another important factor that has been identified to be layout dependent is the cost of the

wind farm, some projects have gone a step further and looked only at costs which they believe to be layout dependent. However, a more detailed study should be carried out identifying which elements of both capital expenditure (CAPEX) and operations and maintenance expenditure (OPEX) are layout dependent. A fully developed layout tool should therefore consider a metric including the AEP accounting for all system losses, and both layout dependent CAPEX and OPEX.

Tools that have tried to do this have, however, suffered from overly simplified or approximated cost functions. Work therefore remains to identify to what extent simplifications can safely be made without adversely affecting the applicability of the tool. A fully developed wind farm layout optimization tool should attempt to include an accurate cost model that is parametrized on features which define the wind farm layout.

Much work has been done in the comparison of optimization algorithms, however, due to simplifications of many models the conclusions regarding algorithm suitability may be premature and a more complete survey of optimization algorithms should be carried out once development of a fully developed tool has been completed. It should, however, be noted that the idea of using two different optimization algorithms in conjunction with one another as proposed by Elkinton [17] and Réthoré et al. [27] will likely be a good approach as it takes advantage of the strengths of multiple algorithms and limits their weaknesses.

2.5 Structure of a New Layout Optimization Tool

Based on what has been done previously, there is scope to construct a tool following the standard paradigm of wake modelling, cost estimation, and optimization algorithm, but including greater detail in both the AEP and cost estimations. Few studies have looked at accurate representations of cable paths as a result of the layout and the impact that the electrical infrastructure, cable routing and substation placement, can have on the LCOE associated with the layout. As the electrical infrastructure will impact both the AEP and the cost, this could be an important addition to introduce to the standard approach in addition to greater detail in both the AEP and cost estimation methodologies.

The proposed methodology for the present tool therefore expands on the standard paradigm by introducing an additional evaluation step which optimizes and designs the necessary electrical infrastructure as shown in Figure 2.2. As the turbine positions are still the principal decision variables of the larger optimization problem, the electrical infrastructure would then be a function of the turbine positions. The AEP calculation, the next step in the evaluation of a layout, is then a function of the turbine positions,

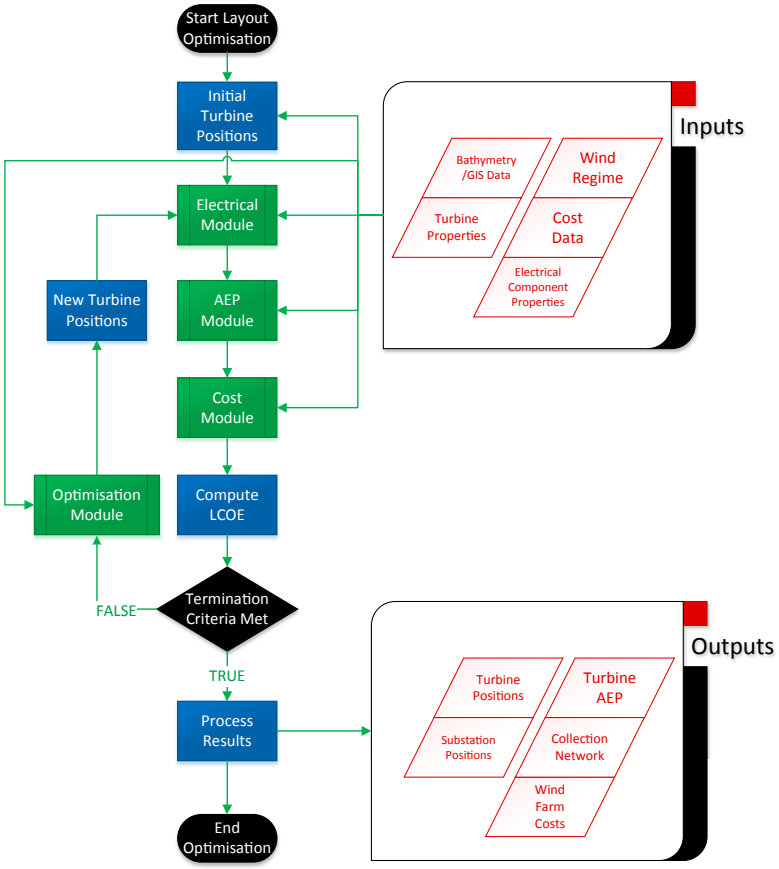

Figure 2.2: Structure of a new layout optimization tool.

the resource, and the now included electrical infrastructure. Likewise, the cost function must now also consider the electrical infrastructure in order to include the impact this has on the LCOE. As the tool ultimately seeks to differentiate between layout alternatives, both the cost and AEP assessment methodologies are used on a relative basis rather than an absolute basis.

Given that few existing tools have been applied to realistic large offshore wind farms, it is also important to explore including more realistic wake and cost functions that would be relevant to a developer in order to ensure that tools such as this can be of use.

Chapter 3

Optimization Algorithms

3.1 Introduction

The framework developed as part of this work seeks to optimize the layouts of offshore wind farms considering an accurate appraisal of the layouts as well as realistic constraints faced by a project developer. A key component of this is therefore the inclusion of an optimization module to alter and design the wind farm layouts.

Previous tools have used several different optimization strategies including: linear programming, greedy algorithms, genetic algorithms, and particle swarm optimizers to name a few. However, previous work has not given any indication as to which approach would be the best as has been described in Chapter 2. From the previous work in this field, there is little clarity as to what optimization strategy is most applicable to this problem, and how increasing the detail and complexity of the evaluation of wind farm layouts would affect the applicability of different optimization strategies. It is therefore important to develop the present framework in such a way that different optimization algorithms can easily be implemented without requiring the entire tool to be redeveloped. The approach taken, shown in Figure 2.2, is modular in its implementation to allow this flexibility. At the same time it is important given the increased detail introduced (this is described in Chapter 4, Chapter 5, and Chapter 6) to reevaluate the applicability of commonly used optimization algorithms.

The constructed tool has therefore been implemented with two separate optimization algorithms to address the problem. This chapter outlines the general principles behind optimization algorithms applied to offshore wind farm layout design as well as describing the optimizers implemented as part of this tool. In Section 3.2 the basics of systems optimization are introduced. Section 3.3 then explains the present formulation of the offshore wind farm layout optimization problem and describes the GA and PSO built as part of this project and the constraint sets which need be considered.

3.2 Combinatorial Optimization

Optimization as a term encompasses both a generic approach, as well as a mathematical field within operations research. A precise definition for optimization is given by Burke and Kendall [14]:

> ... **optimization** can be thought of as the process of **attempting to find the best possible solution** amongst all those available. Therefore, the task of optimization is to **model your problem in terms of some evaluation function** (which represents the quality of a given solution) and then **employ a search algorithm** to minimize (or maximize, depending on the problem) that objective function ... However, most of the problems are so large that is impossible to guarantee that the solution obtained is optimal. The term optimization can lead to confusion because it is sometimes also used to describe a process which returns the guaranteed optimal solution (which is, of course, subtly different from the process which just aims to find the best solution possible).

In its simplest form, an optimization problem consists of three key elements: *variables*, *constraints*, and an *objective function*. The objective function defines what the goal of the optimization process is, and what is defined as optimal. The variables are a representation of the decisions to be made as part of the problem in the pursuit of the objective, while the constraints represent the conditions or limits on these variables. The search space is thought to represent the domain of the function to be optimized and all valid solutions are located within this search space. The presence of constraints is said to limit the search space to a feasible region bounded by the constraints. If constraints are not included, then the optimization problem is described as unconstrained. Real problems, however, are rarely unconstrained [14, 92]. Figure 3.1 shows a simple search space corresponding to a minimization problem with two decision variables. In this simple case, no constraints are necessary, however, their inclusion can improve the performance by reducing the size of the search space [93].

The simplest mathematical representation of an optimization problem is shown in equations 3.1a-3.1c where x is a vector of decision variables; $f(x)$, $g(x)$, and $h(x)$ are general functions; b and c represent an inequality constraint and an equality constraint on x respectively.

$$\text{minimize} \quad f(x) \tag{3.1a}$$

$$\text{subject to} \quad g_i(x) \geq b_i \qquad \forall i \tag{3.1b}$$

$$h_j(x) = c_j \qquad \forall j \tag{3.1c}$$

Combinatorial optimization is a field of optimization which represents the study of the best selection, arrangement, sequence, etc. with respect to some objective function [14].

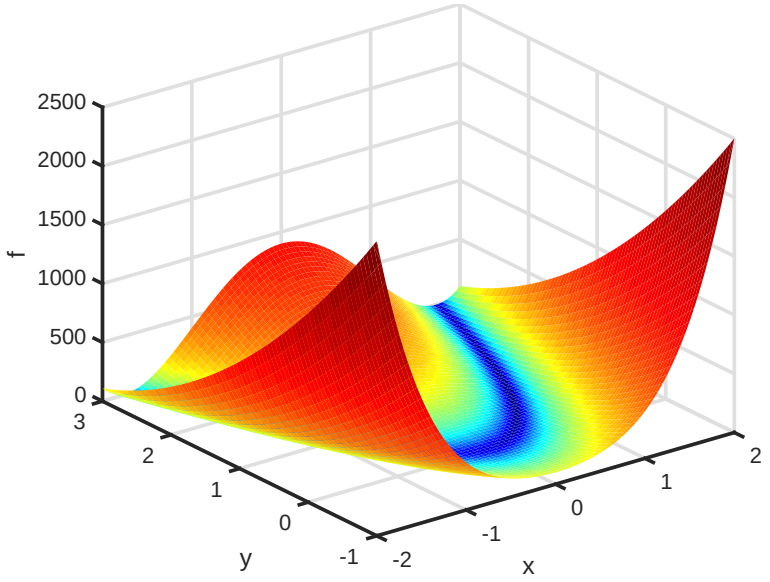

Figure 3.1: Example fitness function of two variables known as the Rosenbrock Function. The function is defined as $f(x, y) = (1 - x)^2 + 100(y - x^2)^2$ and has a global minima at $(x, y) = (1, 1)$ where $f(x, y) = 0$.

The wind farm layout optimization problem can therefore be classed as a combinatorial optimization problem as it seeks the best arrangement of turbines and ancillary equipment with respect to the cost of the wind farm.

In the case of wind farm layout optimization, the variables are a numerical representation of the wind farm layout and the constraints therefore represent the limiting factors on where turbines and infrastructure can be placed. These will include the wind farm boundary, exclusion areas, and any symmetry requirements. The objective function used would be the selected metric for evaluating the layouts many of which are explained in Chapter 2. Optimization problems often involve more than two decision variables making the multi-dimensional search space more challenging to visualize than the Rosenbrock function shown in Figure 3.1. Real world problems are often characterized by a high degree of dimensionality resulting in complex search spaces. Due to the high degree of complexity, exact analytic algorithms tend to not exist for real world problems and heuristics and metaheuristic algorithms must be applied instead. Figure 3.2 shows the relationship between the model complexity and the selection of a solution approach. Though heuristics and metaheuristics cannot guarantee that an optima is located or even that a feasible solution will be found, they do tend to find high quality solutions in acceptable time-scales. Metaheuristic therefore seek to balance the quality or accuracy of the solution with the time required to explore the search space. A realistic representation of the wind farm layout optimization problem would be characterized as one of these problems given the complexity of the development of

wakes and the discrete non-linearity of true cost functions; metaheuristic algorithms would therefore be relevant to this problem.

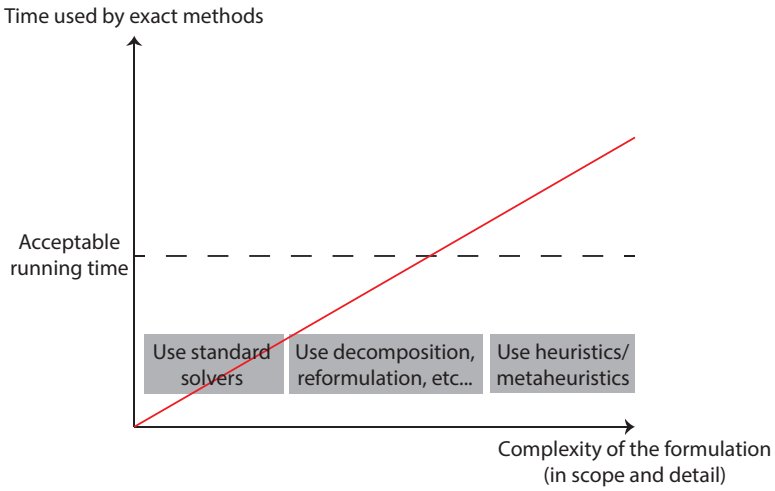

Figure 3.2: Depending on the complexity of the model at hand and the time required to execute the optimization method, different algorithm types are more appropriate.

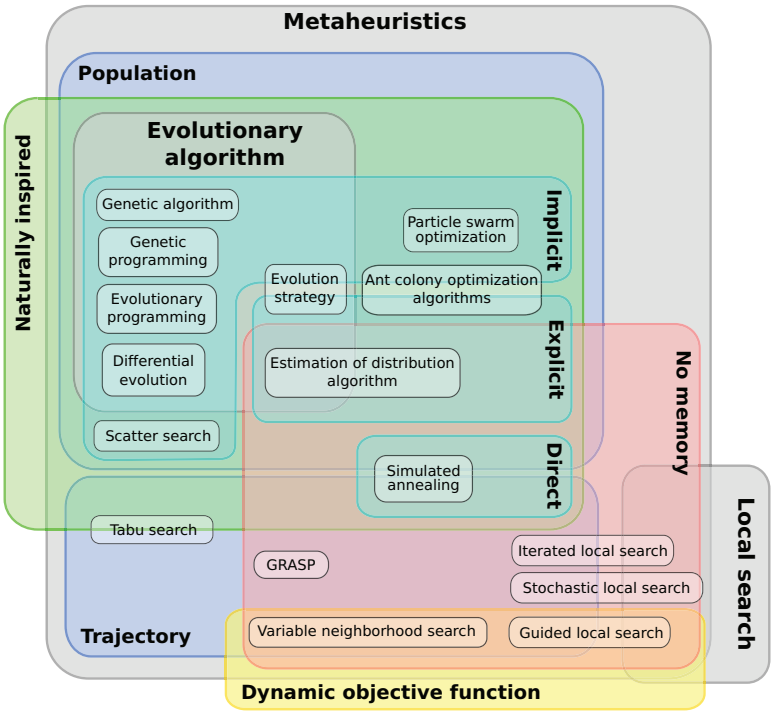

Figure 3.3: Classification of metaheuristic optimization algorithms [94].

Within heuristic or metaheuristic approaches there are a number of different properties along which they can be classified [95, 96]. One of these classifications often used within metaheuristic algorithms is the idea of *trajectory* versus *population-based* (see Figure 3.3). This classification highlights whether the algorithm considers a single

solution at each iteration or multiple and is a fundamental difference between many optimization algorithms. In a trajectory algorithm, the algorithm focuses on a single candidate solution and works to improve this solution while a population based metaheuristic considers a number of candidate solutions simultaneously and improve these using the knowledge of the entire population in order to guide the search. Trajectory algorithms therefore are sensitive to their initialization location within the search space and can have a tendency to converge upon local optima rather than identifying the global optima. Population based algorithms on the other hand do not suffer from this; however, as multiple solutions are considered simultaneously, the associated runtime for these algorithms is much higher. In general, population-based algorithms require more computational time than single solution trajectory algorithms, but are capable of finding better quality solutions [97]. A comprehensive review of population based metaheuristic algorithms is provided in Beheshti and Shamsuddin [96] and the application of optimization to renewable and sustainable energy is well described in Baños et al. [98].

3.3 Implemented Approach

3.3.1 Structure of Wind Farm Layout Optimization

The principal decision problem for the optimization of wind farm layouts is the decision of where to position the wind turbines. The necessary infrastructure such as substations and electrical cables needed for a given turbine layout can be thought of as a function of the turbine positions and therefore does not need to be incorporated into the encoding of a candidate solution.

The constraints for the wind farm layout optimization problem include at a minimum the boundary of the region within which turbines can be placed. Beyond this, physical constraints often defined by seabed constraints such as seabed slope, shipwrecks, or unexploded ordnance, identify specific regions within the wind farm area that turbines cannot be placed. Furthermore, a minimum separation between turbines is often worth considering to ensure that turbine blades do not clash and that there is sufficient space such that should a turbine fail catastrophically it does not negatively impact the other turbines of the farm. Finally, some regulators support limiting wind farms to have constant downwind and crosswind spacings between turbines thereby creating a symmetric layout with clear rows and columns.

To account for the potential symmetry constraints, the optimization algorithms implemented as part of this framework have been implemented using three different levels of constraint limiting the turbine positions. These represent a varying degree of freedom

that a site developer could be faced with depending on the specificities of the site in question. Depending on which of these constraint sets is used, the number and type of decision variables is altered, requiring three separate implementations of each optimizer. Existing tools generally make use of one of these three constraint sets, and no existing work has presented all three approaches within the same framework allowing them to be compared side by side.

In the first mode of operation, the variables of the optimization problem do not define the specific turbine coordinates, but rather the parameters of a regular rectilinear turbine layout. These parameters can in turn be combined to define a wind farm layout. In the second operational mode, also referred to as the binary decision case, nG possible turbine positions are pre-defined and the optimization algorithm must select which of these positions to use in the final layout. The third mode of operation, the continuous case, is one in which the variables of the optimization problem directly represent the coordinate locations of the wind turbines and there are no additional placement constraints. While the first and third modes of operation involve a real encoded optimizer in which the decision variables are reals, the second mode of operation involves a binary encoding as the decision variables are binary.

These three different modes of operation represent a varying degree of freedom within the turbine placement constraints.

Table 3.1: Description of Optimization Operational Modes

Operational Mode	Description	Number of Variables	Variable Type
1	Rectilinear Array Layout	6	Continuous
2	Binary Decision Problem	nG	Binary
3	Continuous Decision Problem	$2 \times nT$	Continuous

3.3.1.1 Rectilinear Array Layout Optimization (Operational Mode 1)

The first operational mode, Mode 1, represents a case in which the consenting constraints limit the developer to having a regularly spaced layout in which turbine positions have constant downwind and crosswind spacing. Based on discussions between stakeholders in the UK, offshore wind farm developers in the UK may be required to design their wind farms in this way in order to satisfy potential safety constraints imposed by Maritime and Coastguard Agency related to the use of radar by search and rescue helicopters flying over offshore wind farms [99]. Furthermore, in certain landscapes, a more orderly arrangement of wind turbines is sought in order to reduce the visual impact of the wind farm [100]. A regularly gridded layout also describes the

design principle taken by the majority of existing offshore wind farms. In this mode, each solution is defined by six variables which represent:

- the downwind spacing [m]
- the crosswind spacing [m]
- the principal axis direction [°]
- the secondary axis direction [°]
- grid translation along the principal axis direction [m]
- grid translation along the secondary axis direction [m]

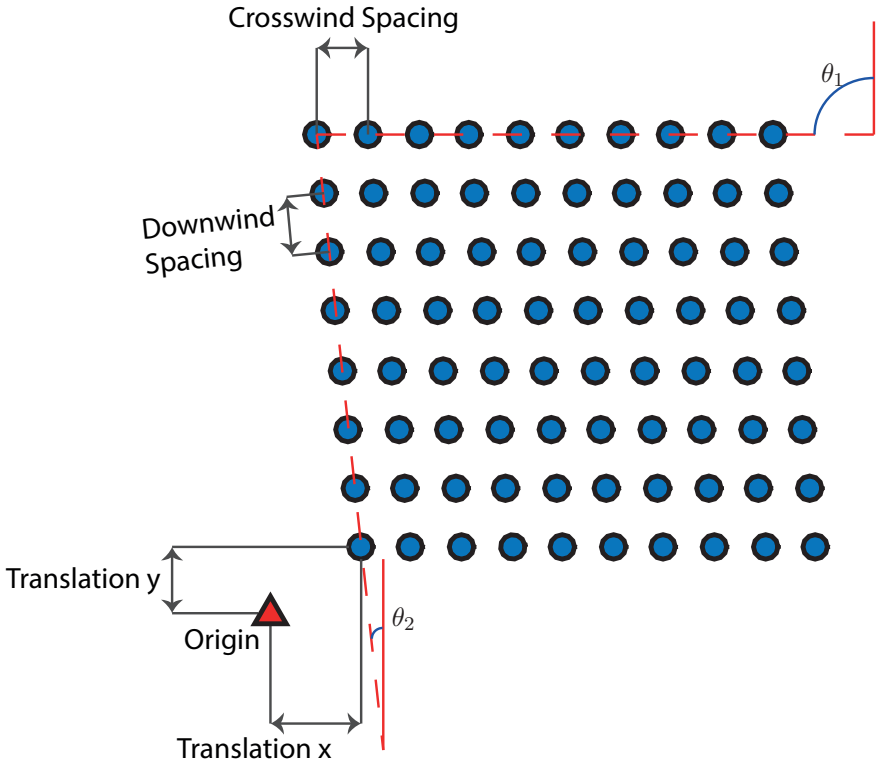

Figure 3.4: Diagram showing array parameters

These six parameters therefore define a unique grid on which the turbines are placed. These parameters represent the distance between the rows of turbines (downwind spacing), the distance between the columns of turbines (crosswind spacing), the definition of the orientation of the rows (principal axis direction), the definition of the orientation of the columns (secondary axis direction), and two translational parameters that define the "bottom left" coordinate of the grid from which the rest of the grid is generated. In the case that separate minimum separation distances are defined separately for the downwind and crosswind directions these are compared directly to the downwind and crosswind spacing variables thereby defining the lower bound of these variables. No upper bound is defined, however, as these variables increase in value fewer turbines will be placed in the domain and the number of turbine constraint will therefore imply

an upper bound on these. The axes directions are bounded by 0° and 360°. These six parameters are shown in Figure 3.4.

For this operational mode, the optimization problem can be presented mathematically as:

$$\begin{aligned}
&\text{minimize} && LCOE(x) && && (3.2a)\\
&\text{subject to} && x_1 \geq sep_{\theta_1} && && (3.2b)\\
&&& x_2 \geq sep_{\theta_2} && && (3.2c)\\
&&& x_3 \leq 360^\circ && && (3.2d)\\
&&& x_4 \leq 360^\circ && && (3.2e)\\
&&& x_5 \leq x_1 && && (3.2f)\\
&&& x_6 \leq x_2 && && (3.2g)\\
&&& countTurbines(x) \geq nT && && (3.2h)\\
&&& x_i \in \mathbb{R}_0^+ && \forall i = 1...6 && (3.2i)
\end{aligned}$$

In this case, the LCOE must be defined as a function of the optimization variables x. The first two constraints (equations 3.2b and 3.2c) ensure that any minimum separation constraints are satisfied where sep_{θ_1} and sep_{θ_2} are the minimum separation between turbines in the θ_1 and θ_2 directions respectively. Constraints 3.2d and 3.2e define the orientation of the axes of the grid. Constraints 3.2f and 3.2g define the translation of the generated grid in both the downwind and crosswind directions. Constraint 3.2h ensures that each layout has at least the required number of turbines given possible regions within the wind farm that turbines cannot be placed, $countTurbines(x)$ is a function which determines the maximum number of turbines in a given layout given the rectilinear array parameters, and the final constraint, constraint 3.2i defines all the decision variables of the optimization problem to be either positive real numbers or zero.

3.3.1.2 Binary Decision Problem (Operational Mode 2)

The second operational mode, Mode 2, represents the case where possible turbine locations are predefined and the optimizer must select which of these turbine positions to utilize as part of the layout. This case represents the most common way in which wind farm layout optimization has previously been addressed. In this implementation, each layout, solution, is represented by a binary string in which each bit or variable of the solution represents the presence of a turbine in a defined cell within the wind farm area.

The allowable turbine positions are either predefined or defined by discretizing a wind farm area. The discretization in this case is either done along a regular grid in which the cells are oriented along the dominant wind direction from the wind rose, or if it is important to utilize the space as best as possible, a triangulation algorithm can be used to "mesh" the wind farm area defining the vertices of such a mesh as the possible turbine locations. If a grid is generated with a consistent downwind and crosswind directions, then it is likely that this could still comply with the Maritime and Coastguard Agency's safety concerns, however, formal guidance has yet to be issued [101]. From the perspective of the optimization algorithm, it does not matter how the allowable turbine positions are defined, and as long as there are more possible turbine positions than turbines the optimization process can proceed.

$$\text{minimize} \quad LCOE(x) \tag{3.3a}$$

$$\text{subject to} \quad \sum_{i=1}^{L} x_i = nT \tag{3.3b}$$

$$minSep(x) \geq sep \tag{3.3c}$$

where x is the vector of decision variables for each solution.

In this implementation, the discretization of the wind farm area implicitly imposes the boundary and exclusion area constraints such that these constraints need not be explicitly included in the optimization problem. By integrating these constraints directly into the discretization algorithm, it allows these constraints to be checked only during the discretization step thereby accelerating the optimization phase. Therefore, only two explicit constraints are needed in the formulation of this optimization problem. The first constraint, constraint 3.3b ensures that the number of turbines (nT) sought is satisfied while constraint 3.3c ensures that all turbines maintain the minimum separation sep from one another by using a funciton $minSep(x)$ to identify the closest turbines in solution x and compute the distance between them.

3.3.1.3 Continuous Decision Problem (Operational Mode 3)

Operational Mode 3, the final implementation of the problem, represents the continuous problem in which the variables of the optimization problem are the coordinates of the turbines. This case therefore has no consideration for maintaining symmetry within the layout and would not be guaranteed to meet any of the rules that the Maritime Coastguard Agency is advocating [99, 102]. It should be noted that the solutions considered by Modes 1 and 2 could all be found when executing the Mode 3 version of

the problem as Mode 3 has fewer placement constraints than either Modes 1 or 2.

$$\text{minimize} \quad LCOE(x) \tag{3.4a}$$

$$\text{subject to} \quad \sum_{i=1}^{L} \frac{x_i}{2} = nT \tag{3.4b}$$

$$valid(x) = 1 \tag{3.4c}$$

In this formulation, a function *valid* is defined to ensure that the placement of turbines is valid given the relevant constraints. This therefore includes confirming that the turbine positions are within the overall boundaries, but outside any constraint regions, and that the minimum separation constraints between all turbines are maintained. In the previous two modes, the compliance with the boundary and obstacle regions did not need to be explicitly verified as they were included in the generation of the grid in Mode 1, and it is assumed that all the discretized turbine positions in Mode 2 are already compliant with the boundary and obstacle constraints.

The flexibility of including three sets of constraints will allow exploration into the direct impact of restricting the turbine placement in this way. Comparisons between Mode 1 and Mode 3 will give the impact on layouts of forcing symmetry while comparisons between Mode 2 and Mode 3 show the impact of using a discrete optimization algorithm over a continuous one, and finally comparisons between Mode 1 and Mode 2 in a case where Mode 2 has regularly spaced possible turbine positions shows the value of introducing holes in the interior of the wind farm or allowing "edge-weighting" in the design of the layout. While Mode 2 represents all the decision variables as binary requiring the use of a binary encoded optimizer, both Modes 1 and 3 have real value decision variables thereby requiring a real encoded optimizer.

The developed framework has implemented both a GA and a PSO for each of the three modes of operation. In addition, the framework will allow further optimization algorithms to be incorporated in the future. The GA and PSO were selected for the preliminary implementation as they are often applied to a wide range of engineering problems and have been shown to be relevant algorithms for complex real world problems [14, 96]. Although these algorithms have been applied to the offshore wind farm layout optimization problem in the past, they have not been applied to this problem with a detailed evaluation function nor have they been applied on the same framework allowing their performance to be directly compared. It is therefore of value to the wind farm design and analysis community to demonstrate that it is not necessary to simplify the evaluation function in order to apply these algorithms to this problem.

As discussed in Chapter 2, the GA is one of the most frequently used optimization algorithms for problems such as the offshore wind farm layout optimization problem and therefore represents a logical choice to use as a starting point. Several of the studies outlined in Chapter 2 have shown the genetic algorithm to outperform simpler optimization strategies such as hill climbing or greedy heuristics which is why these strategies have not been implemented in the framework at hand.

3.3.2 Genetic Algorithm (GA)

3.3.2.1 Operating Principle

As can be seen in Figure 3.3, the GA is classed as a population-based evolutionary algorithm. Furthermore, the GA is referred to as a biologically-inspired algorithm in that it borrows from evolutionary processes observed in nature. In line with this analogy, the GA therefore considers multiple candidate solutions at the same time with the aim at combining good solutions to create better solutions [103, 104].

The genetic algorithm is so named because its operating principles are based in biological evolution and has analogous steps to genetic principles. The general principle of natural evolution is succinctly described by Darwin [105]:

> As many more individuals of each species are born than can possibly survive; and as, consequently, there is a frequently recurring struggle for existence, it follows that any being, if it vary however slightly in any manner profitable to itself, under the complex and sometimes varying conditions of life, will have a better chance of surviving, and thus be naturally selected. From the strong principle of inheritance, any selected variety will tend to propagate its new and modified form.

Analogous to the evolutionary processes in biology, the genetic algorithm incorporates both the idea of inheritance as well as the exploration of slight variations to the individuals of the populations thereby taking advantage of the "survival of the fittest" concept commonly associated with evolutionary processes. In a GA, the representation of the solutions are thought of as genomes with each variable of the solution thought of as a gene. Each iteration of the algorithm is considered a generation in which part of the population is replaced by new candidate solutions generated by having existing solutions "reproduce." This reproductive step is where existing solutions are combined using the evolutionary processes to create new candidate solutions. The overall methodology is outlined in the flowchart shown in Figure 3.5 and described in Algorithm 3.1. The individual steps shown are explored in further detail in the sections that follow. Though the GA can be implemented in different ways, the general ideas of inheritance are common to all GAs and are well described in De Jong [106], Mitchell [107], and Haupt and Haupt [104].

As previously discussed, the different constraints require the GA to be implemented both using a binary encoding and a real encoding. The encoding refers to the method in which the decision variables are represented in the candidate solution. In a binary encoding, each of the decision variables is a binary variable and each gene of the solution represents one of these variables. In a real encoding, however, each gene of the solution, is represented by a real number which represents the value of a specific decision variable.

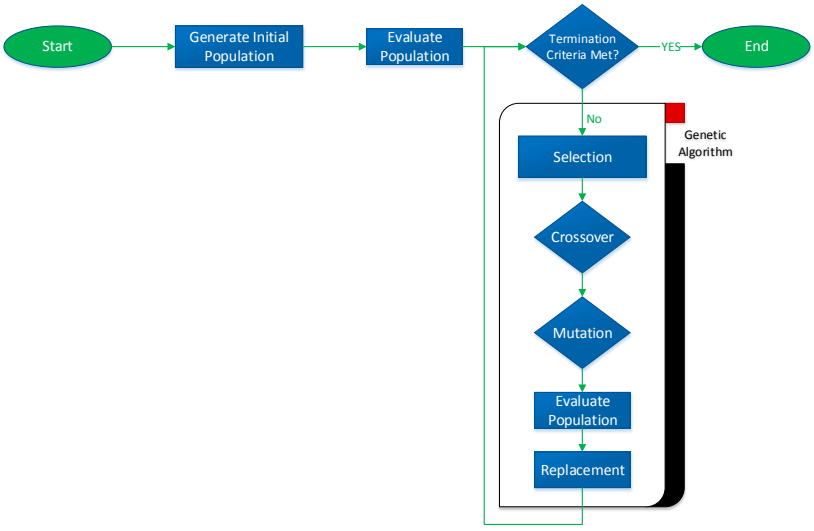

Figure 3.5: General flowchart for a genetic algorithm

3.3.2.2 Initialization

The first step of a population based metaheuristic, such as the GA, is the generation of initial solutions, or seeding the population. In this case, each of the three modes of operation uses a slightly different seeding approach in order to ensure that the decision variable values are within the defined constraints. In general, for each of the modes of operation, the seeding algorithm works to ensure that the initial values are randomized and the initial population is evenly distributed across the search space. The random seeding is done such that each of the candidate solutions in the population represents a feasible solution, and each is unique within the population. In addition, in this implementation the number of turbines is given to the optimizer and therefore each of the individuals within the population also has the same number of turbines. The general procedure is outlined in Algorithm 3.2.

Algorithm 3.1 Genetic Algorithm

Require: The number of turbines, the wind farm boundary, the wind farm obstacle regions, the minimum separation between turbines, the size of the population, the fitness function, the selection method.

```
initialize population
evaluate all individuals within the population
repeat
  repeat
    select two parents
    update crossover probability
    perform crossover
    for all generated children do
      evaluate child solution
      update mutation probability
      perform mutation on generated children
      evaluate child solution
      if child is better than worst member of population then
        remove worst member of population
        mark child for inclusion in population
      end if
    end for
  until population satisfies elitism requirement
  create next generation by combining remaining population with children marked for inclusion
until termination criteria met
return best individual
```

Algorithm 3.2 Initialization of Genetic Algorithm Population

Require: The number of turbines, the minimum separation between turbines, the wind farm boundary, any constraint regions where turbines cannot be placed

```
for all individuals in population do
  repeat
    for all genes do
      generate random valid value for gene
    end for
    check individual's compliance with constraints
    if individual is valid then
      check that individual is unique
    end if
  until individual is valid and unique
end for
return population
```

3.3.2.3 Selection

Within a genetic algorithm, selection describes the method by which individuals of the population are chosen to contribute genetic material to new candidate solutions. Continuing with the evolution analogy, two selected individuals in the population are chosen to be parents to two new children solutions. The typical approach for all selection methods is shown in Algorithm 3.3. In general, existing solutions should be more likely to contribute genetic material to the next generation, that is, to be selected, if they themselves represent good solutions relative to the other members of the population. This parental contribution to the child solutions represents both the inherited element and the competitive element of the genetic algorithm.

Algorithm 3.3 Genetic Algorithm: Selection

Require: Fitness values of all individuals, selection method
1: **for** all individuals **do**
2: compute probability of selection given selection method
3: **end for**
4: generate two random numbers
5: identify individuals corresponding to generated random numbers
6: **return** parent individuals

Given that the GA seeks to make progress towards the global solution, it is important that the correct level of *selective pressure* is applied to the problem at hand. Selective pressure reflects the extent to which the GA scales a solution's probability of being selected based on its fitness. With very high selective pressure, the best solution is always selected and there is a risk of the GA becoming trapped at a local solution. On the other side, exceedingly low selective pressure would equate to all individuals having an equal probability of being selected regardless of their fitness. Figure 3.6 illustrates the potential impact of both high and low selective pressure.

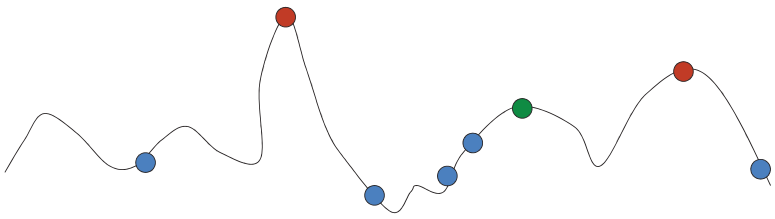

Figure 3.6: Visual representation of the impact of selective pressure; the black line represents the fitness function, while candidate solutions are shown as circles. Considering a population shown in blue, high selective pressure in which the best solution is always selected will result in a final solution near the green point. With modest selective pressure, the GA will likely converge to one of the red points, while with a low degree of selective pressure, the GA randomly explores the search space.

The selection method must therefore apply sufficient pressure such that the GA is making use of the evolutionary elements, while not applying too much pressure and risk converging to a local optima. The most common approaches for selecting individuals are roulette wheel selection, rank based selection, and tournament selection.

In roulette wheel selection (also referred to as fitness proportional selection), the probability that an individual is selected is related directly to the fitness of the individual in question relative to the fitness of the other individuals in the population [14, 104].

$$P_{s,i} = \frac{f_i}{\sum_i f_i} \tag{3.5}$$

where $P_{s,i}$ represents the probability of selecting individual i, and f_i represents the fitness of individual i in a maximization problem.

Equation 3.5 gives the transfer function for computing the probability of selection for an individual when using roulette wheel selection. This selection is equivalent to spinning a roulette wheel with sectors proportional in size to the fitness of the individuals. In this case, selective pressure is variable depending on the range of fitness values of the population. In a case with very similar solutions throughout the population, there is only a slight increase in probability that the best member gets selected compared to the worst, while if the range is very large then the best member will have a much larger probability of being selected compared to the worst solution. The fact that selective pressure cannot be directly controlled is one of the major drawbacks of a fitness proportional based selection.

The second approach is known as rank based selection. In this selection method, the individuals of the population are ranked from best to worst and assigned a probability based on a function of their rank score. Generally, the probability takes the form:

$$P_{s,i} = \frac{R_i^b}{\sum_i R_i^b} \tag{3.6}$$

where R_i represents the rank of individual i, and b is the bias that is used. The bias represents a quantification of the selective pressure with low bias values corresponding to a low selective pressure. Common values for b are 0.5 if low selective pressure is desired and 2 if high selective pressure is needed [108].

The final method commonly used for selection is what is referred to as tournament selection. In this selection method, members of the population are randomly selected and put in a tournament against one another. The individual with the best fitness

function emerges from the tournament and is selected. The tournament size acts as a proxy for the selective pressure with larger sizes resulting in higher selective pressure.

3.3.2.4 Crossover

Crossover is the principal genetic operator which is used to combine the selected parents to create children. In crossover, part of the genetic material from each parent is combined in such a way that new valid individuals are generated. The new individuals generated through the genetic operators, crossover and mutation, are considered for inclusion in the next generation of the population based on their fitness. Like selection, there are a number of common approaches for which crossover can occur.

The most basic form of crossover is single point crossover, shown in Figure 3.7. In single point crossover, a single location in the genome is identified and all genes preceding this location are taken from one parent while all genes following the crossover point are taken from the second parent.

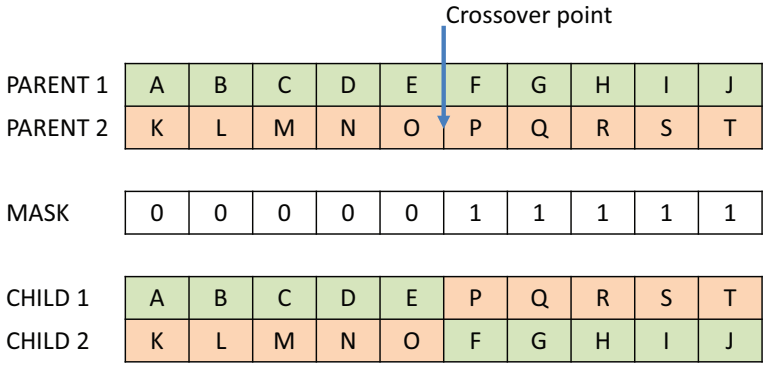

Figure 3.7: Single point crossover

A slightly more complex form of crossover is called two-point crossover and extended to k-point crossover. In these schemes, two or more locations are identified. The mechanism of inheriting genes is similar to the single point crossover with children inheriting genes from one parent until a crossover point is reached. When a crossover point is reached, the parent from which the child is inheriting is switched and inheriting continues until the next crossover point, or until the end of the genome is reached. The two-point crossover is shown visually in Figure 3.8.

The final approach commonly applied is a uniform crossover. This scheme describes a method in which a binary mask is defined. This mask defines for each gene if a gene is inherited from the first or the second parent. This is shown visually in Figure 3.9.

When speaking about solutions in an optimization problem, a *schema* is often thought of as a specific combination of variables. In general, single point crossover is considered

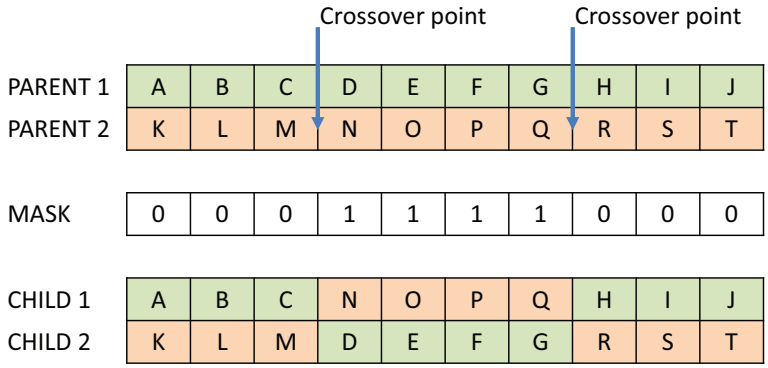

Figure 3.8: Two point crossover

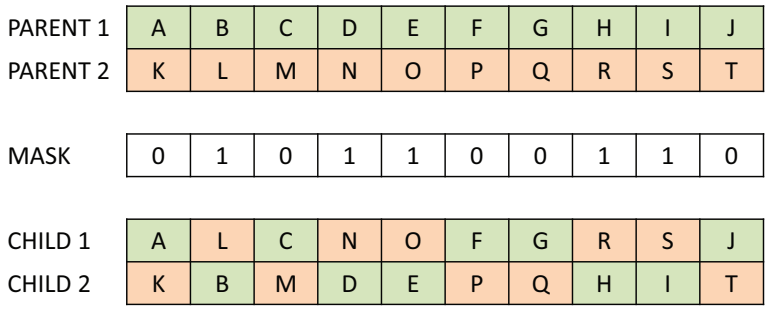

Figure 3.9: Uniform crossover

to be the most basic type of crossover as it will not be able to combine all schemata, and may therefore limit the crossover to progress quite slowly. In fact, both single point and two point crossover are thought to suffer from *positional bias* as they are highly sensitive to the position of the crossover operator. Positional bias refers to the risk of damaging schemata with long defining lengths. Uniform crossover, has therefore emerged as an effective means of eliminating positional bias. However, it still suffers from potential challenges as given its nature it is a highly disruptive approach and does not have a high probability of maintaining long schemata unless they are present in both parents [107, 109].

Since crossover is often considered to be the primary method by which the GA navigates the search space, it is generally assigned a relatively high probability on the order of 0.6 - 1.0 [97, 110]. In the event that crossover does not take place, children are generated by duplicating the parents.

3.3.2.5 Mutation

Where crossover seeks to explore the search space by causing large changes to the variables, mutation seeks to exploit the existing solutions causing small changes. Within the GA, the mutation operator is directly analogous to what Darwin [105] referred to as "the slight variation that might prove profitable" and is implemented as a degree of local search about the solution. In evolution, mutation is thought to be a probabilistic event which any gene in a genome is susceptible to. GAs therefore generally define a mutation operator which defines a probability that any given gene's value be changed to a random feasible value after which the feasibility of the overall solution must be checked. In the event that the solution is now infeasible, the mutation is undone, and the mutation process restarted. This process continues until a feasible solution is generated. Given the probabilistic nature of mutation, there is a non-zero probability that the solution will be unaltered during the mutation process.

As crossover is considered to be the main operating principle of the GA, mutation is generally assigned a much lower probability of occurring and is generally of the order of 0.001-0.05 [107, 111, 112]. Mutation helps ensure that no solutions within the search space have a zero probability of being evaluated, and therefore ensures that there is some degree of random search that is combined with the inheritance aspect of the GA. Mutation rates are often given as the probability that a candidate solution is mutated, or the probability that an individual gene is mutated. Depending on which definition is used, it is not uncommon for the mutation rates to be quoted as being an order of magnitude smaller than the range mentioned above. The probability of an individual gene mutating and the probability of an individual mutating are related by the length of the genome if all genes have the same probability of mutation.

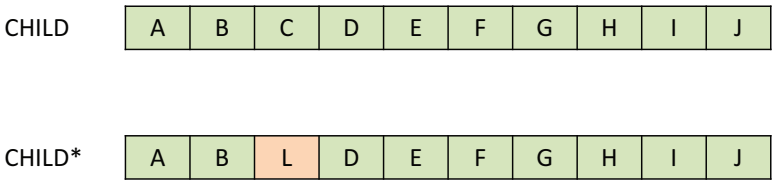

Figure 3.10: Mutation

3.3.2.6 Constraint Satisfaction

During initialization, crossover, and mutation it is important to ensure that the solutions under consideration are always valid solutions. In general, for the offshore wind farm layout optimization problem, four main constraints are considered:

- wind farm boundary;
- seabed obstacle constraint regions where turbines cannot be placed;
- minimum separation between turbines; and
- number of turbines.

For both Modes 1 and 2, the boundary and constraint regions are implicitly satisfied by the discretization of the wind farm area and therefore only the minimum separation and number of turbines constraints need to be checked. For Mode 3, however, all four validity constraints need to be checked. For each layout, it is therefore important to ensure that the layout is valid after each step in the process. Therefore, after each crossover operation, the validity of the children layouts are checked. If they are not valid, the crossover operation is considered to have failed, and crossover is redone using a new crossover mask. This process, generating a mask; crossing the parents; and checking the validity is repeated until feasible child solutions are produced. A similar process is done following mutation, to ensure that the children produced after the application of the genetic operators are valid. Unlike the initialization process, uniqueness is not required for the mutation operator and therefore a valid child is not checked against the existing population to check for uniqueness.

Considering mutation in Operational Mode 2, it is important to ensure that the number of 1's and 0's being flipped is equal to ensure that the number of turbines in the layout is maintained. The mutation process is therefore repeated until this condition is met.

3.3.2.7 Adaptive Crossover and Mutation

Crossover and mutation are often strongly linked to exploration and exploitation respectively, and the probabilities at which crossover and mutation occur therefore represent the balance between exploration of the search space and exploitation of existing solutions. In practice, constant values for these probabilities may not be the most logical approach as the balance between exploration and exploitation can be expected to shift depending on the solutions' location within the search space [14]. Work has therefore explored varying the probabilities adaptively responding to changes in fitness among the population. In this way, as the GA begins to converge to a local optima, it is important to increase both the crossover and mutation probabilities in order to try and scatter some of the individuals away from this local solution. Likewise, as the population becomes increasingly scattered across the search space it is important to

reduce the crossover and mutation probabilities in order to ensure that the population begins to converge. In the case of convergence to a local optima, the increased crossover and mutation rates will force additional evaluation calls, but this works to demonstrate that a global optima as opposed to a local optima has been located [111].

In order to take this into account, the simplest adaptive crossover and mutation strategies adjust the probabilities to be [111]:

$$p_c = \frac{k_1}{f_{max} - \bar{f}} \tag{3.7}$$

$$p_m = \frac{k_2}{f_{max} - \bar{f}} \tag{3.8}$$

where p_c is the probability of crossover, p_m is the probability of mutation, k_1 is the base probability of crossover, k_2 is the base probability of mutation, f_{max} is the fitness value of the best individual in the population, and $\bar{f}$ is the mean fitness value of the individuals in the population. Therefore, for both these expressions, as the population converges, the denominator will approach zero and the probabilities will increase.

Unfortunately, this strategy applies the same probabilities regardless of which individual within the population is considered. Both solutions of high and low fitness would therefore be subjected to the same rates of crossover and mutation and therefore there is no pressure to maintain good solutions within the population and cause greater disruption to the poor solutions. The probabilities can therefore be further adapted based on the individual's own fitness (f) relative to the population [111].

$$p_c = \begin{cases} \dfrac{k_1 (f_{max} - f')}{f_{max} - \bar{f}} & \text{for} f' \geq \bar{f} \\ k_3 & \text{for} f' < \bar{f} \end{cases} \tag{3.9}$$

$$p_m = \begin{cases} \dfrac{k_2 (f_{max} - f)}{f_{max} - \bar{f}} & \text{for} f \geq \bar{f} \\ k_4 & \text{for} f < \bar{f} \end{cases} \tag{3.10}$$

where k_1, k_2, k_3, and k_4 are constants. k_3 and k_4 are implemented to increase the crossover and mutation rates if the fitness of the best parent (f') or the fitness of the candidate solution is lower than the mean fitness value of the population regardless of the population's convergence. In this way solutions which are expected to be poor relative to the solutions already in the population are therefore assigned a higher likelihood of being disrupted. At the same time, by comparing either the fitness of the

best parent or the fitness of the individual under consideration to the best individual in the population helps ensure that the best individuals are preserved.

In general, it is suggested that the constants take the values: $k_1 = k_3 = 1$ and $k_2 = k_4 = \frac{1}{2}$.

Previous studies have found that the inclusion of adaptive parameters has led to increased diversity within a population and therefore can avoid premature convergence, converging to better solutions than fixed probabilities [111, 113, 114]. One drawback of the full adaptive implementation described in equations 3.9 and 3.10 is that the fitness value for each child solution needs to be established after crossover and before mutation in order to correctly determine what the probability of mutation should be for each individual. This therefore requires two evaluation calls per child solution as the children are evaluated prior to the mutation operation as well as a part of the replacement operation significantly increasing the computational time for each generation. Based on past studies into adaptive parameters it is generally held that the benefits introduced by using adaptive parameters outweighs the additional time required for each considered individual [111, 113, 114].

3.3.2.8 Replacement

The final step in the general GA is for the new child candidate solutions that have been created to be evaluated, and potentially included within the population. The replacement step therefore requires evaluating the new children solutions and comparing their fitness values to those of the existing members of the population. In general, children solutions are included in the population, if they have a better fitness functions than existing members of the population. In this way, the population's mean value will improve from generation to generation as new individuals are introduced to the population.

The traditional approach in which replacement operates is a *replace weakest first* strategy in which children as they are generated are compared to the worst members of the population and if they are superior, they are marked for inclusion in the next generation and the worst member is marked for removal. This is the processes taken in lines 13-16 of Algorithm 3.1. This process continues each time comparing the new child solutions against the worst member of the population which has not yet been marked for removal. The selection, crossover, and mutation operators are repeated until either a target number of children have been created, or a target proportion of the population has been replaced by new solutions. Many GA's define a target proportion by defining an elitism parameter which defines what proportion of the population is carried over to the next generation.

Generally, based on how GAs are defined, no individual will diminish in fitness and it would be expected that the population as a whole will either improve or stay the same from generation to generation. This is an important fact to note as the speed at which the GA progresses is highly dependent on the quality of individuals that have been generated and that are present in the population. The total number of evaluation calls (layouts evaluated) varies from generation to generation in order to ensure that the desired number of children are generated or the population has sufficient new members.

3.3.2.9 Convergence

In general convergence is defined as when the GA stops iterating as little or no improvement can be made from the position it is in and therefore it should stop operation. This can be defined as either a loss in diversity, or the GA having no improvements over a number of generations [104, 107]. Most GAs store the history of the best fitness score across all generations and the mean score. By comparing these, the GA can be said to have converged when:

$$\frac{f_{max}}{\bar{f}} \geq Th \tag{3.11}$$

where Th is a threshold used, commonly Th is set to 0.01 or less. Alternatively, the convergence criteria can be defined based on the number of unique individuals within the population or if the population has failed to find improvements in a given number of generations. Under this definition, as the diversity decreases beyond a threshold minimum number of unique individuals the GA can be considered to have converged. Likewise, if there is no improvement to the best individual after a given number of consecutive generations, then the GA can be considered to have converged.

3.3.3 Particle Swarm Optimization

3.3.3.1 Operating Principle

For each of the three instances of the problem described above, a second optimization algorithm, a particle swarm optimization (PSO) was also implemented.

Unlike the genetic algorithm in which individuals compete with one another to provide genetic material to the next generation of candidate solutions, the PSO creates a cooperative environment in which each individual (particle in this analogy) explores the search space while communicating to the rest of the population (swarm). In this way, it mimics the behaviour of shoaling fish or flocking birds who travel together, but each individual has their own velocity vector. The basis of the PSO is described by Kennedy and Eberhart [115]:

> As sociobiologist E.O. Wilson has written, in reference to fish schooling, "In theory at least, individual members of the school can profit from the discoveries and previous experience of all other members of the school during the search for food. This advantage can become decisive, outweighing the disadvantages of competition for food items, whenever the resource is unpredictably distributed in patches".

This cooperative behaviour implies that each individual's movement within the search space is governed by the particle's knowledge of their previously visited positions within the search space as well as the position of the other members within the swarm. A particle's velocity therefore becomes the principal way in which the optimization algorithm alters the candidate solutions from one iteration to the next. The general structure of a PSO is shown in Figure 3.11 and Algorithm 3.4.

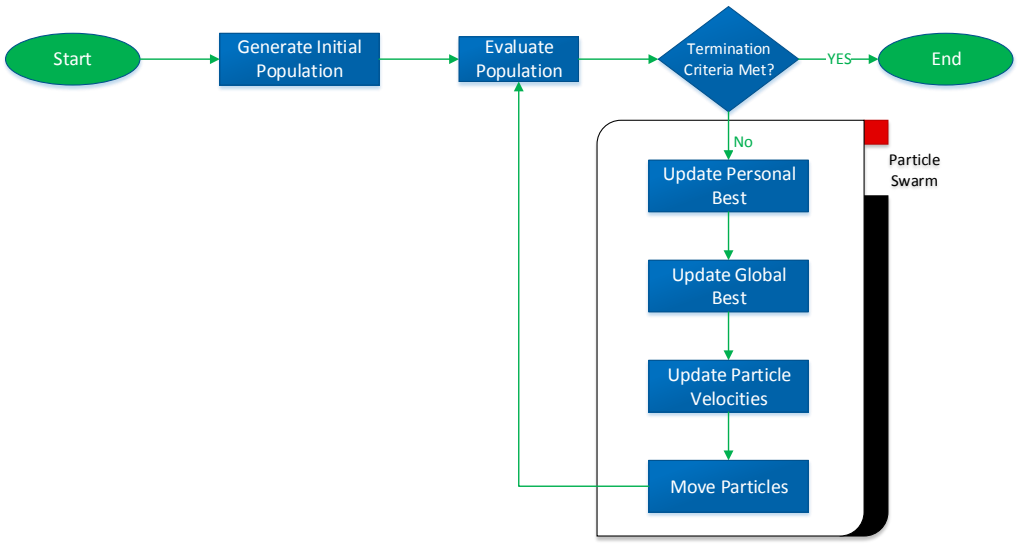

Figure 3.11: Flowchart of the particle swarm optimization algorithm

In general, this algorithm uses the best historical position of each particle along with the best historical position of the entire swarm to advise each particle's velocity. In each iteration, the personal and global best values are updated after evaluation of all the candidate solutions. This information is then used to update the velocities for each individual particle. Each particle is then moved in accordance with the velocity that it now has. For each individual it is the "move" operation that checks for compliance with the constraints and if it is not valid, then a new velocity is generated and the process repeated.

Algorithm 3.4 Particle Swarm Optimization

Require: The number of turbines, the minimum separation between turbines, the wind farm boundary, any constraint regions where turbines cannot be placed

```
initialize swarm positions and velocities
repeat
    evaluate all individuals within the swarm
    for all particles do
        if particle fitness is better than personal best then
            update particle's personal best
        end if
        if particle fitness is better than global best then
            update global best
        end if
    end for
    for all particles do
        update particle velocity
        update particle position
    end for
until termination criteria met
return global best
```

3.3.3.2 Particle Velocity

In each iteration of the PSO, all particles have their velocities updated, are moved, and are then evaluated. Regardless of whether the particles' fitness have improved, their new positions are kept and the process repeated iteratively. The particle velocity is partially random to avoid local minima, partially based on the particle's historical best position within the search space, partially based on the particle's neighbourhood, partially on the best position within the entire population, and partially inertial. In this way, by including the particle's previous best position, and the global best positions, the particle tries to exploit the knowledge of the swarm, while the random element helps the particle explore the search space. A major difference between the PSO and the GA is that the PSO allows particles to decline in fitness from generation to generation, recognizing that it may lead to better future positions. In this way, rather than only accepting velocities that lead to improvements in the particle, velocities are accepted as long as they satisfy the constraints regardless of how this may impact the particles fitness.

The velocity v_i is given by:

$$v_i = w_i v_{i-1} + C_1(p - x_{i-1}) + C_2(g - x_{i-1}) + C_3(\eta - x_{i-1}) + C_4 \times rand \qquad (3.12)$$

where C_1, C_2, C_3, and C_4 are coefficients (typically set to 2); w_i is the inertia weight, p is the best historical position of the particle in question, g is the best historical position of the swarm, η is the best historical position of the particle's neighbourhood, and $rand$ is a random number.

Based on Equation 3.12 it can be seen that a particle with a solution close to the best historical position of the swarm will also by definition have a solution close to its own historical best, thereby resulting in a small velocity. This therefore helps preserve good solutions, while solutions with poor fitness values will undergo greater change with a higher velocity. In a complex search space, however, good solutions may be "geographically" close to poor solutions and the velocity may need a scaling function in order to ensure that the solutions do not move too much. At the same time, to ensure that bad solutions do not extend beyond the search space or lead to excessively large velocities, the velocity is often constrained and scaled to fit within a finite range. This process is known as velocity clamping. For this problem, these velocity limits therefore represent very different things depending on the instance of the problem at hand and what the variables of the problem represent.

For Modes 1 and 3, which are real encoded, it was found through parameter tuning that the best results were found when the maximum velocity was not explicitly set, but allowed to change dynamically based on where the particle was relative to the edges of the search space as well as what the natural velocity would be. In this way, if a velocity were to take the particle beyond the boundaries of the search space then the particle would be limited to a location along the boundary thereby remaining within the search space. Mode 2, the binary PSO, represents a unique case where the velocity handling needed to be addressed differently given the discrete values that each variable can occupy. This is discussed further in Section 3.3.3.5.

3.3.3.3 Neighbourhoods

The original form of the PSO only considered a particle to be affected by its own history and the global best position within the swarm. This, however, is generally no longer used [83]. As the PSO is based on social behaviour, it is common to define *social neighbourhoods* which have spheres of influence over one another. In this way, a particle's velocity is also impacted by the fitness and location of its neighbours within the search space.

The simplest of neighbourhood topologies is one in which every individual is connected to all others and the global best position within the swarm impacts the velocity. This represents the canonical PSO and is often referred to as a *gbest* topology [116]. This topology represents the situation in which all particles are in communication with each

other, and the improvement of the entire swarm is communicated to the rest of the swarm. The individuals of the swarm are, however, only aware of the improvement that the swarm as a whole has made and not the specific improvements found by every other individual in the swarm.

By including smaller neighbourhoods within the swarm, the PSO can take advantage of cooperative local search around each of the neighbourhoods which is especially useful when complex evaluation functions are used and good solutions could potentially be scattered throughout the search space.

More complex neighbourhood designs include the *wheel*, *circular*, *random*, and *dynamic neighbourhoods* as shown in Figure 3.12. In a wheel neighbourhood design all individuals are connected to a single particle. In this way, all information transfer through the swarm must go through a specific individual thereby introducing a filter or inertia to the system. The focal individual effectively acts as a buffer for the swarm compared to the gbest topology. This topology is often referred to as a hub and spoke topology.

The circular topology is one in which each individual is connected to its n closest neighbours in such a way that the entire swarm is interconnected. This topology ensures that particles that are distant from one another are also relatively independent as information must be carried through the intermediate particles in order to transfer throughout the swarm. However, as all particles are connected to one another improvements found by any individual particle will filter through to the entire swarm.

Also commonly used are random neighbourhoods in which particles are randomly assigned to neighbourhoods These random neighbourhoods are only connected to one another through the best particle, and only through influencing the position of the best individual does information transfer out of a neighbourhood into the entire swarm.

More recent work has looked at dynamic neighbourhoods In this scheme, neighbourhoods are redefined every iteration based on either similarity or some random system. Much work has explored the performance of different neighbourhood topologies; however, no strong conclusions have been reached regarding the performance of the different topologies [83, 116–119]. As such, the present framework has implemented the principal types of neighbourhood topologies discussed in the literature. In general, for the implemented problem instances, the dynamic random neighbourhood was found to work well.

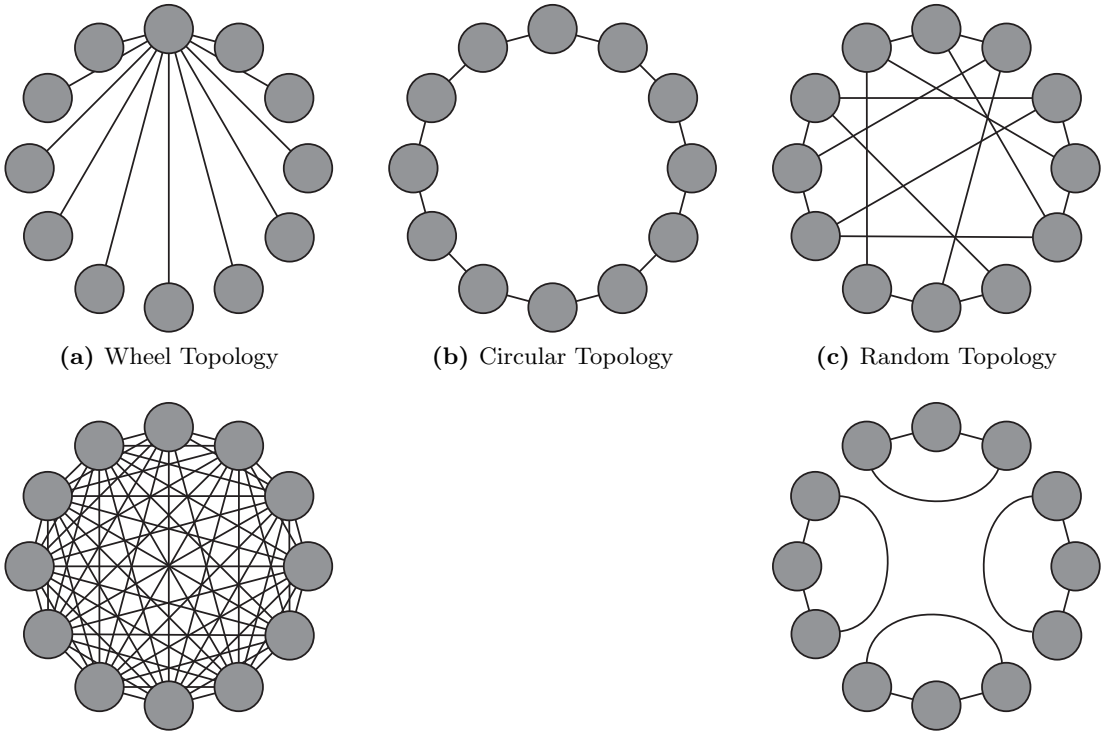

(a) Wheel Topology **(b)** Circular Topology **(c)** Random Topology

(d) Fully-Connected Topology **(e)** Clustered Topology

Figure 3.12: Neighbourhood topologies commonly used in a PSO.

3.3.3.4 Move Particle

In the PSO, each particle's position at any given iteration is related to its past position by:

$$x_i = x_{i-1} + v_{i-1} \tag{3.13}$$

where a given particle has a solution defined as x_i and the velocity is given by v_i for iteration i.

After x_i is defined, the constraints are checked against the solution defined by x_i. If a solution which violates the constraints is proposed, v_{i-1} and therefore x_i are recomputed. As there is a stochastic element in the particle velocity, this will eventually produce a valid position. For the binary particle swarm case, the constraints are enforced more implicitly by the discretization of the search space. To ensure, however, that the number of turbines is kept constant in the binary PSO, the velocity vector is checked to ensure that the number of existing 1's being flipped to a 0 is the same as the number of existing 0's being flipped to a 1. This is a similar process to how feasibility was insured during the mutation step of the GA.

3.3.3.5 Binary PSO

Like the GA, the PSO was implemented to function with a binary encoding of the decision variables. This complicates matters slightly as the position for each bit must be either 0 or 1. The continuous velocity, must therefore be adjusted such that it corresponds to the bit in question being either a 0 or a 1. To do so, Equation 3.12 must be processed in order to ensure that the move operation defines each bit as either 0 or 1. To solve this, a sigmoid transfer function is commonly used to convert the velocity for a given bit to a probability of the given bit being a 1 [120–122].

Using this standard transfer function, however, introduced a challenge in satisfying the number of turbines constraint. In order to easily check and satisfy this constraint, the transfer function was redefined such that it represented the probability that a bit is flipped. This then allowed the algorithm to ensure that equal numbers of ones and zeros were flipped thereby preserving the number of turbines within the wind farm. This, however, required a change in the transfer function as both highly negative and highly positive velocities should correspond to a high probability of the bit flipping. The s-shaped Sigmoid function was therefore replaced with a v-shaped function. The use of a v-shaped transfer function has also been proposed by Mirjalili and Lewis [122]. Figure 3.13 shows typical s-shaped (sigmoid) and v-shaped transfer functions.

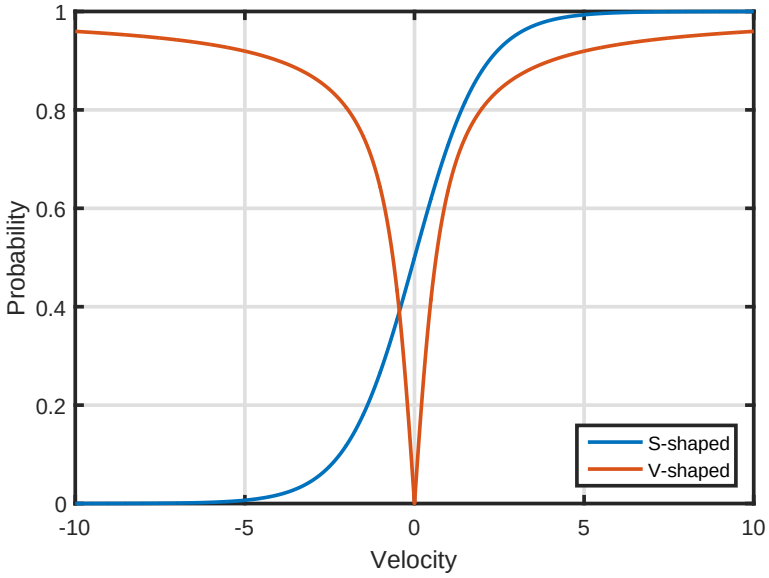

Figure 3.13: Transfer functions for binary particle swarm optimization

3.3.3.6 Convergence

The final step of the PSO is testing for convergence of the solution. Like the GA, this is done when the solutions within the swarm are sufficiently similar that there is little progress being made. For the present implementation a similar threshold based convergence criteria was defined, however, unlike the GA, particle solutions were not directly considered, but instead the best historical values of each particle.

The convergence is therefore given as true if:

$$\frac{f_{max}}{\bar{f}_p} \geq Th \tag{3.14}$$

where f_{max} is the fitness value of the best individual in the swarm, f_p represents the fitness value of each individual's best historical position, and $\bar{f}_p$ is the average of these best historical positions. Defining the convergence in this way ensures that the best positions that particles have occupied rather than their present locations are used to check the converge as it is from this set, the set of particle bests, from which the best overall solution will reside.

The PSO is also stopped if, like the GA, a given number of iterations pass without any improvement to the best particle or a maximum number of iterations is reached.

3.4 Chapter Summary

This chapter has provided an introduction to the optimization principles relevant to the offshore wind farm layout optimization problem. From here, three different implementations of the optimization problem given different sets of constraints has been described. These three interpretations all depend on how the turbine positions are constrained, in the first mode of operation turbines positions are defined by generating a fixed grid of points based on a regular downwind and crosswind spacing; in the second mode of operation, allowable turbine positions have been predefined and the optimization routine selects which of these positions to use; and in the third mode of operation the coordinates of each turbine are directly determined by the optimizer. Given that these three different interpretations have different ways in which the turbine layout is defined, the variables of the decision problem vary between each of these modes of operation. All of these modes of operation, however, represent valuable ways in which layouts can be explored.

For each of these three interpretations, the implementation of two separate optimization algorithms, the genetic algorithm and the particle swarm optimizer, have been

described. The subsequent three chapters describe the methodology and validation of the separate components that are involved in evaluation of a given layout. These approaches are relevant regardless of the interpretation of the constraints used in the overall optimization problem. Chapter 7 details the application of the optimization algorithms and the evaluation function as an integrated offshore wind farm layout optimization framework.

Chapter 4

Electrical Infrastructure Optimization

4.1 Introduction

The electrical infrastructure impacts both the energy yield and the costs of an offshore wind farm and therefore plays an important role in the optimization of offshore wind farm layouts. Both the capital costs of the cables and the energy losses that occur when transmitting are directly a function of the positions of wind turbines. Similarly the lengths of cable depend on where the substations are placed relative to both the onshore connection point and the turbines. The optimization of the collection network, the cables (intra-array and export) and substations, therefore form an important component of the overall optimization of an offshore wind farm layout.

Considering the future UK Round 3 and large European offshore wind projects as a point of context, the electrical infrastructure problem has been approached including as many realistic constraints as possible and formulated using a combination of heuristics and mixed-integer linear programming (MILP). As heuristics are used, this method may not reach proven optimality, but rather reaches a good feasible solution in an acceptable run time.

This optimization problem includes the determination of the substation positions given the realistic constraints faced by a developer, the determination of the intra-array cable layout given this substation position, and the selection of the export cable route from each substation.

Previous work in this field has either looked at small wind farms, or has omitted some of the necessary constraints needed for the application of the approach to a real wind farm. Most have elected to work only on a single construction phase of a wind farm with a single offshore high voltage substation (OHVS), as subsequent phases and additional OHVS would follow the same procedure.

Fagerfjäll [32] implemented an MILP based approach for the electrical cable layout, assuming that all the turbines were connected to a single substation. This approach used a variation on the minimum spanning tree (MST) problem (see Figure 4.1a), a minimum Steiner tree, in order to solve for the electrical cabling. A minimum Steiner tree is similar to an MST, in that both trees attempt to connect a set of nodes in the lowest cost manner. While in an MST the arcs may branch only at nodes, the arcs of a Steiner tree may branch anywhere along an arc and not only at nodes (see Figure 4.1b). By approximating the problem to that of the minimum Steiner tree, the cable length is therefore further reduced compared to the equivalent MST. Similar work has also been undertaken by Lindahl et al. [123] and Svendsen [124] using a MILP implementation to solve for a capacitated minimum spanning tree, that is an MST where there are capacity constraints on the arcs connecting nodes. Both of these studies, however, correctly identified that the computational time for these problems grows very quickly with the number of turbines. In fact, the capacitated minimum spanning tree (CMST) problem is NP-hard and therefore an optimal solution is not found in polynomial time. For the CMST specifically, common approaches identify solutions in exponential time [125]. The problem therefore becomes exponentially more complex as more turbines are added and more possible cable arcs must be considered.

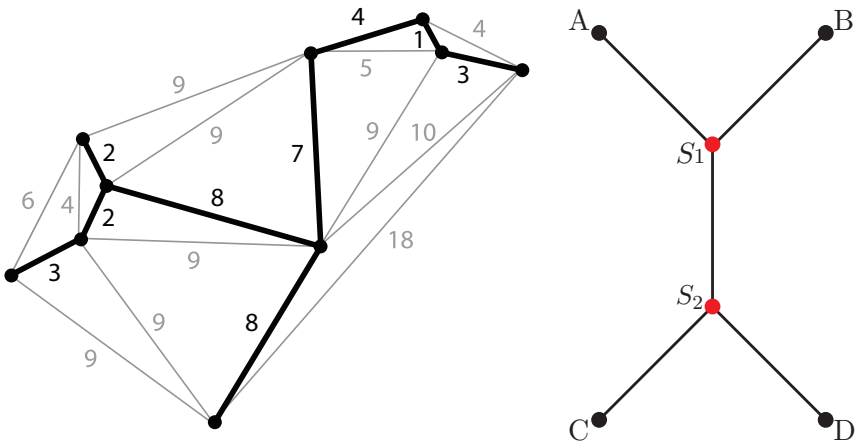

(a) Minimum Spanning Tree **(b)** Steiner Tree

Figure 4.1: Examples of a minimum spanning tree and a Steiner tree

Due to the complexity, past work has often opted to use heuristic algorithms such as genetic algorithms in order to optimize the electrical cable layout [126–132]. These studies have therefore sacrificed finding the proven optimal solution in favour of a good feasible solution in acceptable time-scales. Bauer and Lysgaard [133] simplified the problem to only allowing strings of turbines without any branching, allowing a variation on a vehicle routing problem algorithm to be applied. This does find solutions in

reasonable time-scales; however, not allowing branching reduces the problem complexity significantly, and eliminates many feasible solutions unnecessarily including potentially the optimal solution.

Studies carried out by Dutta and Overbye [126, 134, 135] have looked at using a minimum spanning tree and applying the capacity constraints by running the MST on clustered turbines representing the capacity constraints of the largest cross-section of cable. This work has also modified the MST to represent a minimum Steiner tree. Dutta and Overbye [135] also include an algorithm to account for exclusion areas where cables may not be placed, by constructing convex hulls from the obstacle and turbine positions to derive a shortest path.

Given the desire to apply the methodology to real sites, the electrical intra-array cable optimization problem has been approached pragmatically, dividing the overall problem into three separate sub-problems:

1. the placement of the substations;
2. the determination of the intra-array cable layout; and
3. the design of the export cables.

The present work opts to continue on from the work of Fagerfjäll [32], Svendsen [124], and Lindahl et al. [123] using a MILP formulation for the electrical cable layout problem and introduce additional constraints to represent the realistic case of UK Round 3 sites. The new constraints introduced in this work take into account complex geographical information systems (GIS) shapes as constraints and the fact that cables may not cross in the offshore environment. Additional constraints have also been explored to aid in reducing the computational time. The overall structure of the electrical infrastructure optimization module and the relationship between the three sub-problems defined above are shown in Figure 4.2.

4.2 Process Overview

The design of offshore wind farms and the decision regarding the number of substations to build is largely driven by the capital expenditure (CAPEX) associated with building a substation along with the necessary foundation works. Projects tend therefore to minimize the number of substations such that substations are efficiently designed with a minimum surplus capacity. The total number of substations is therefore often predetermined based on the number of construction phases or the total wind farm capacity and the maximum capacity of substations.

As a result of this, the decision of where to place the substations is effectively a process of selecting the substation positions which will result in the minimum total collection

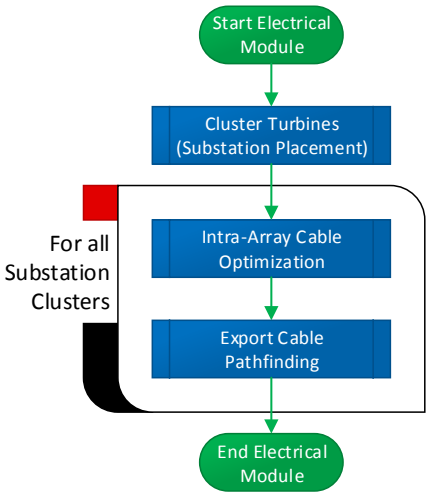

Figure 4.2: Flow overview of the electrical module

network cable as this will minimize both costs and losses of the collection system. It has previously been shown that given the significant length of cable required for the export cable when compared to the in-field cables and the high voltage levels used, the costs associated with the export cable are minimally impacted by changes in the substation positions [32]. In order to address this problem it was therefore decided to divide the problem into three sub-problems: first the determination of the substation positions; secondly the construction of a CMST representing the cabling for each substation and its assigned turbines; and lastly the design of the export cables for each substation.

In the offshore environment cable junctions require additional switchgear and power electronics, the installation of which will require some sort of physical structure to house them. Presently all junction boxes and circuit breakers designed for the offshore wind sector are designed to be housed in a turbine or placed on a substation platform [136]. This limitation in the offshore environment results in wind farm collection networks only branching at either turbines or substations. Though a minimum Steiner tree or a CMST with Steiner points would reduce the length of cable needed to connect a wind farm as proposed by Fagerfjäll [32], and Dutta and Overbye [134, 135], it is not feasible to implement a Steiner tree in the offshore environment due to this branching constraint. A CMST without Steiner points was therefore selected for use in this study as this better represents the physical constraints of offshore wind farms.

The CMST formulation requires costs for each potential cable connection under consideration. In order to assess this, it was first necessary to determine the length of cable required to connect two turbines, and then apply a per metre cost for that cable type. As the costs of cables including the installation costs scale with cable length it is necessary to determine the lengths of potential cables prior to running the CMST. This

effectively introduces yet another sub-problem. Given the complex GIS constraints, this was addressed through the implementation of a pathfinding algorithm in order to ensure that the cables would not pass through the constrained regions. Additional constraints were also introduced in order to reflect that cables may not cross one another. The overall module approach is outlined in Algorithm 4.1.

Algorithm 4.1 Offshore Wind Farm Electrical Infrastructure Optimization

Require: The turbine positions, the GIS obstacles, and the number of substations
1: Given the number of substations assign each turbine to a substation and compute the substation positions using the *Capacitated kmeans++ Clustering*
2: **for** all substations **do**
3: **for** all turbines assigned to substation **do**
4: Identify the 10 closest turbines
5: Identify the constrained shortest path between the turbine and substation using *Delaunay Triangulation Based Navigational Mesh Pathfinding*.
6: **for** 10 closest turbines **do**
7: Identify the constrained shortest path between turbine pair using *Delaunay Triangulation Based Navigational Mesh Pathfinding*.
8: **end for**
9: **end for**
10: Formulate MILP for substation and its assigned turbines given the 11 possible arcs for each turbine computed above
11: **repeat**
12: Solve *MILP*
13: **if** any cables in MILP solution cross **then**
14: Add individual crossing constraints
15: **end if**
16: **until** No cables cross
17: **end for**
18: **for** all substations **do**
19: Find shortest cable path from substation to landfall
20: **end for**
21: **return** substation positions, cable paths, cable flows, cable types, export cable paths, and export cable lengths

As shown in Algorithm 4.1, there are in fact three optimization sub-problems as part of this optimization module:

1. Capacitated Clustering Problem/Facility Location;
2. Constrained Shortest Path/Pathfinding; and
3. Construction of Constrained Capacitated Minimum Spanning Tree.

The *Constrained Shortest Path* problem is executed for each turbine finding the possible connections between it, the ten closest turbines to it, and the substation. This data is used for the MILP CMST problem which is executed for each of the substations. The number of turbines to pathfind to is a parameter, and ten was empirically selected as

turbines were found to always be connected either to one of their six closest neighbours or the substation in all tests conducted. Ten was therefore selected to give additional flexibility, however, the framework is designed to accept any valid integer for this parameter. Once the intra-array network has been created the pathfinding and shortest path algorithms are executed again to determine the optimal path of the export cable from each substation.

4.3 Substation Placement

4.3.1 Problem Description

The substation placement problem can be described that for nT turbines, k substations must be placed optimally. As the overall problem seeks to design the intra-array cable paths the logical approach is to try and reduce these path lengths from the outset by efficiently placing the substations. The substation placement problem has therefore been addressed as a *Capacitated Centred Clustering problem (CCCP)* and facility location problem. Based on the turbine positions and the number of substations desired, the turbines are divided into clusters each within the capacity of the substations.

4.3.2 Problem Formulation

Mathematically, the problem can be expressed as:

$$\text{minimize} \quad \sum_{t\in T}\sum_{s\in S}\left(x_t - x_s\right)^2 z_{t,s} \tag{4.1a}$$

$$\text{subject to} \quad \sum_{s\in S} z_{t,s} = 1 \qquad \forall t \in T, \tag{4.1b}$$

$$\sum_{t\in T} z_{t,s} = n_s \qquad \forall s \in S, \tag{4.1c}$$

$$\sum_{t\in T} x_t z_{t,s} = n_s x_s \qquad \forall s \in S, \tag{4.1d}$$

$$\sum_{t\in T} z_{t,s} \leq Q_s \qquad \forall s \in S, \tag{4.1e}$$

$$z_{t,s} \in \{0,1\} \tag{4.1f}$$

$$x_t \in \mathbb{R}^n \quad x_s \in \mathbb{R}^n \quad n_s \in \mathbb{N} \quad \forall t \in T \quad \forall s \in S \tag{4.1g}$$

where T is the set of turbines and S is the set of substations.

In the above formulation, Equation 4.1a states the objective function of the optimization process which is to minimize the square of the Euclidean distance between the position

x_s of each substation, s, and the individual turbine positions x_t if the turbine t is assigned to substation s denoted by the state of $z_{t,s}$. The variable $z_{t,s}$ is defined as 1 if the turbine t is assigned to substation s, it is 0 otherwise. Equation 4.1b limits each turbine to being connected to exactly one substation. Equation 4.1c defines the number of turbines assigned to substation s to be given by n_s. Equation 4.1d defines the geometric centroid of the turbines assigned to substation s to be the position of the substation, and Equation 4.1e ensures that each substation satisfies the capacity constraints Q_s.

4.3.3 Solution Approach

The CCCP as formulated, is NP-hard and has previously been studied by Negreiros and Palhano [137], Geetha et al. [138], and Chaves and Lorena [139]. These studies have identified heuristic algorithms as well suited for solving this problem. Based on the comparative study by Negreiros and Palhano [137] which compared heuristic approaches for the CCCP, it was decided to build a two-phase heuristic for this problem. The first stage would identify the ideal cluster centres ignoring the capacity and obstacle constraints, and the second phase would apply first the capacity constraints finding a good solution starting from the solution of the first stage, and finally once the capacity constraints were satisfied, the obstacle constraints would be applied to refine the solution. It is recognized that the implementation of a heuristic algorithm cannot ensure an optimal solution, and the substation positions generated by this algorithm represent only a feasible solution.

For the first phase, a *kmeans++* algorithm was selected. This is a variation on the commonly deployed *kmeans* clustering methodology which intelligently selects the initial cluster centre positions in order to improve performance [140, 141]. Both *kmeans* and *kmeans++* work by iteratively computing the cluster centre (geometric centroid) based on what turbines are assigned to the cluster, then based on the new geometric centroid, the turbines are each reassigned to the closest cluster centre. This process is repeated until the cluster centres converge. In general, both *kmeans* and *kmeans++* have been shown to be effective clustering techniques [137].

Using the approach outlined in Algorithm 4.2, it was possible to successfully partition a wind farm to ensure that substations were in good, feasible positions if not in the optimal position. This process also ensured that the substation capacities and any GIS obstacles were correctly implemented as constraints for the substation positions.

The proposed method also explored swapping turbine assignments in order to ensure that the identified substation positions accurately minimize the distance to turbines, and each turbine is therefore assigned to the closest substation unless capacity con-

Algorithm 4.2 Capacitated kmeans++

Require: Set of turbines T to be clustered into k clusters while obeying O obstacles

1: Perform kmeans++
2: Balance clusters based on capacity
3: Update cluster centres based on assigned turbines
4: Look for elements which can be moved to improve total distance while maintaining capacity constraints.
5: Update cluster centres based on assigned turbines
6: Identify pairs of turbines which can have their substation assignments swapped to yield improved total distance between turbines and substations.
7: Update cluster centres based on assigned turbines
8: Shift substations (cluster centres) to nearest allowable position based on obstacles
9: **return** Substation positions and turbine assignments

straints are active in which case the turbines with the lowest global impact to the cost are assigned to a substation farther away. It should be noted that the result of introducing the GIS and capacity constraints has a major impact on the computational time of the clustering, but a very minor effect on the value of the objective function.

4.4 Cable Path Creation Based on Pathfinding

4.4.1 Problem Description

Before constructing the capacitated minimum spanning tree it is necessary to compute the costs of putting a cable between two turbine locations. In order to do this while considering the GIS obstacle constraints, it was necessary to compute a constrained shortest path between the positions. Given the constraints, the construction of the graph of possible cable paths is an NP-hard problem. Dutta and Overbye [135] addressed exclusion areas by defining a bypassing algorithm. This bypassing algorithm constructs a convex hull of the obstruction and the turbines to be connected. The edge of this convex hull can then be traversed to find the shortest path. This approach, however, is not guaranteed to find the shortest path, and in fact will incorrectly mark areas as impassable if the obstacle is not convex. This bypassing algorithm is therefore only well suited if the exclusion areas can be described as simple convex shapes. As the tool developed here seeks to account for realistic seabed constraints that may take on concave shapes it was decided that a convex hull based bypassing algorithm would not be the most efficient approach. As a result, a pathfinding approach was taken. The pathfinding approach was found to correctly account for concave obstacle regions.

Pathfinding can theoretically, depending on the algorithm applied, guarantee a shortest path between two points in a constrained configurational space regardless of whether

the obstacles are convex or not. Pathfinding problems frequently arise in video games and robot motion problems as it is necessary for a *robot* to move from an origin location to a destination location taking into account obstacles which it cannot pass through. In the case of cable paths, turbines are either connected by a cable to another turbine or the substation and therefore there is a finite set of origin-destination pairs for which a path must be found.

4.4.2 Problem Formulation

In general, pathfinding can be described as a specific case of a shortest path tree traversal. The shortest path of a graph can be mathematically formulated as:

$$\text{minimize} \sum_{i \in A} \sum_{j \in A} d_{i,j} \cdot u_{i,j} \tag{4.2a}$$

$$\text{subject to} \sum_{i:(i,k) \in V} u_{i,k} - \sum_{j:(k,j) \in A} u_{k,j} = \begin{cases} -1, & \text{if } k = p_1 \\ 1, & \text{if } k = p_2 \\ 0, & \text{if } (k \in A : k \notin \{p_1, p_2\}) \end{cases} \tag{4.2b}$$

$$u_{i,j} \in 0, 1 \qquad \forall (i,j) \in A \tag{4.2c}$$

where $u_{i,j}$ is a binary variable describing the connectivity between points i and j in space A in the shortest path. This variable is 1 if i and j are connected in the shortest path and 0 otherwise. The points p_1 and p_2 represent the source and termination points respectively and are also with the space A. The cost of connecting points i and j (the length of the edge connecting i and j) is given by $d_{i,j}$. V is the set of all turbine and substation positions and represents all the vertices of the full graph; $V = T \cup S$.

This general formulation, however, represents the optimization problem once a graph representing the configurational space, the traversable space in which cables can be laid, has been constructed. There are a number of different methods to construct this graph depending on what kind of pathfinding algorithm is deployed. For this study both a grid based pathfinding algorithm and a navigational mesh were implemented. The navigational mesh ultimately proved to be the more appropriate algorithm to implement.

4.4.3 Solution Approach

For problems such as this, there are two main approaches for finding the shortest path, one is to reduce the obstacle data to a *walkability grid* representing on a regular grid where cables can and cannot be placed. The shortest path can then be found using a standard grid search algorithm such as *A* Pathfinding* or *Dijkstra's algorithm*. However, this simplifies all the constraints to consisting of regular rectangles and given the complexity of real offshore wind sites this was found to often eliminate possible paths as can be observed in Figure 4.3. Though this could be avoided by using a finer grid size, other challenges still remained. For example, by creating a grid, the cable paths were limited in having only 8 options of where to go from any given grid position (Figure 4.4), often causing problems with paths overlapping cables near substations and no simple means of avoiding this. Paths based on the grid were also longer than necessary due to being fixed to the grid.

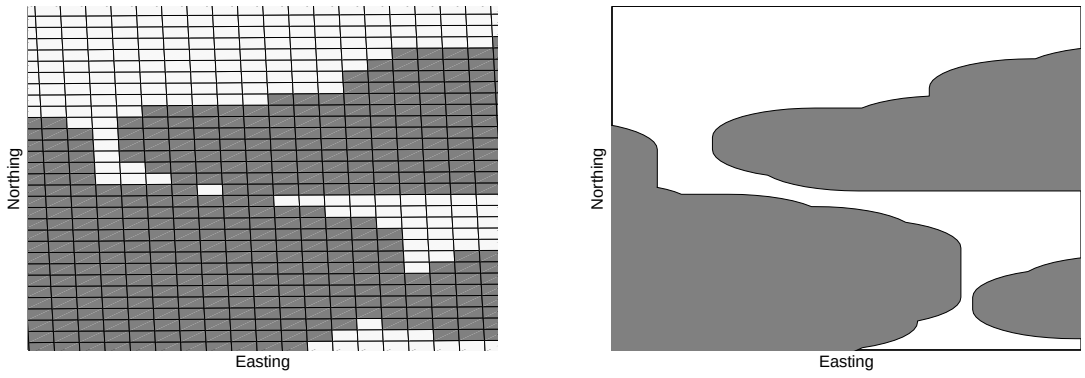

(a) Grid Based Pathfinding Obstacles **(b)** Navigational Mesh Pathfinding Obstacles

Figure 4.3: Comparison of obstacle representation in grid based and navigational mesh based pathfinding.

The alternative method uses what is known as a visibility graph and navigational mesh, and is capable of avoiding all of the above problems, but at a significant cost in complexity [142]. The visibility graph is a graph for which an arc exists between any two vertices if they are 'visible' to one another. Visibility is defined as true if the two points can be connected by an arc without the arc passing through an obstacle. It is important to note that in terms of a visibility graph, points along the obstacle edges are considered to be an open set, and valid arcs can pass along the obstacle edges. The optimal path is in fact the shortest path between vertices on such a graph. The difficulty in working with visibility graphs is that algorithms for testing visibility are computationally complex. The most efficient algorithms still operate in $O(n\ log\ n + k)$ where n is the number of vertices and k is the number of edges [143]. Given that the

GIS constraints for a typical offshore wind farm can constitute several thousand vertices this was thought to be too computationally complex.

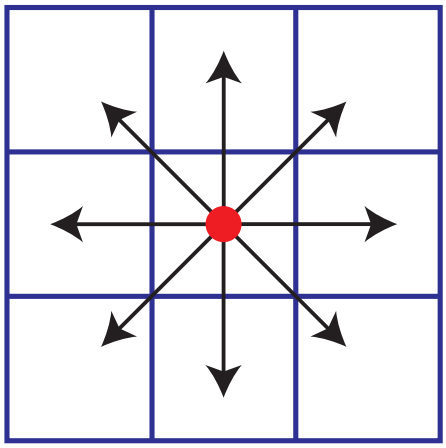

Figure 4.4: Grid based system allows a path to go only to one of the 8 adjacent squares surrounding it.

The proposed methodology, therefore uses a heuristic algorithm which can create a close approximation of the visibility graph in a fraction of the computational time. This approach, shown in Algorithm 4.3, is known as a navigational mesh based pathfinding algorithm and creates a traversable graph which obeys the obstacle constraints. One such algorithm, proposed by Jan et al. [144, 145] was adopted for this project. This approximation method uses the edges of a constrained Delaunay Triangulation to define the graph. A Delaunay Triangulation is defined as a triangulation in which no vertex is within the circumcircle of any triangle of the triangulation, and a constrained Delaunay Triangulation is given the obstacle edges as a constraint such that no triangulation edges cross the obstacles. By triangulating the obstacle vertices along with the origin and destination positions it is possible to create a graph representing the traversable area. In order to improve the performance of the graph and better approach the full visibility graph solution, this method includes the Fermat points of the triangles and connects these to the graph. A Fermat point is defined for triangles for which the largest angle is less than 120° to be the position internal to the triangle that minimizes the distance to the triangle vertices. For a triangle in which the largest angle is greater than or equal to 120° the Fermat point is located at one of the vertices. Once these Fermat points are found, they are then added to the graph and connected to their respective triangle vertices and any adjacent Fermat points (Figures 4.5d and 4.5e).

As this produces a potentially sub-optimal path, Jan et al. [145] proposed a *path shortening* method which removes redundant Fermat points or vertices from the solution paths therefore reducing the total length to on average within 2% of the optimal path, but in a fraction of the time. The original path shortening algorithm was enhanced

by checking all possible short-cuts, constructing a graph, and then running Dijkstra's shortest path algorithm (see Algorithm 4.4).

Algorithm 4.3 Delaunay Triangulation Based Navigational Mesh Shortest Path

Require: Polygon obstacles, origin point, destination point, and site boundary
1: Construct the configurational space given the obstacle polygons
2: For the configurational map construct a constrained Delaunay triangulation for the vertices making up the obstacles, the origin point, and the destination point. The edges of the obstacles serve as the constraints for the triangulation.
3: Create a graph of all vertices and triangle edges of the triangulation
4: Insert Fermat points in triangles that have angles less than 120°
5: Connect the Fermat points to the vertices of their triangles and any adjacent Fermat points
6: Find the shortest path in the graph using Dijkstra's algorithm.
7: Apply the path shortening procedure
8: **return** cable path

Algorithm 4.4 Path Shortening

Require: Polygon obstacles, cable path
1: Compute the length of each segment of the path
2: Compute the length for all possible short-cuts
3: **for** all possible shortcuts **do**
4: **if** shortcut does not intersects an obstacle **then**
5: Add short-cut length to graph adjacency matrix
6: **end if**
7: **end for**
8: Find shortest path along graph using Dijkstra's algorithm
9: **return** cable path

Figure 4.5 shows a visual representation of the pathfinding process. Comparing the resulting paths in Figures 4.5e and 4.5f shows the need for including the path shortening subroutine. It is important to note that inclusion of the path-shortening algorithm with the improvement suggested still does not ensure optimality, however, it can lead to significantly reduced path lengths. It should be noted that generally, however, this method does find the optimal path between two points.

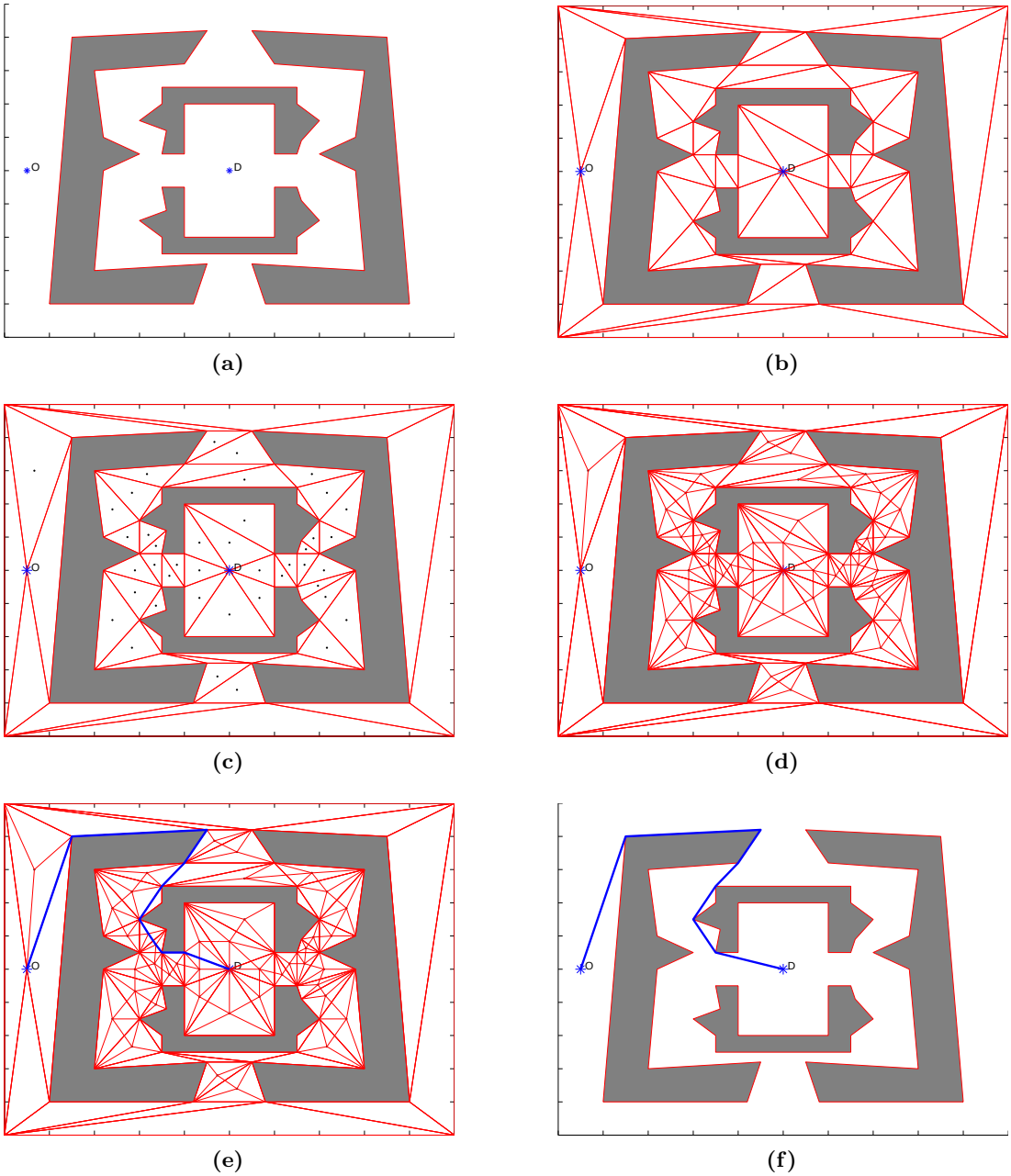

Figure 4.5: A simplified example of the pathfinding approach. Figure 4.5a shows the problem formulation with the origin 'O', and destination 'D' points marked and obstacles shown in grey. Figure 4.5b shows the result after performing a constrained Delaunay triangulation on the configurational space. Figure 4.5c shows the Delaunay Triangulation with the Fermat points added for the appropriate triangles. Figure 4.5d shows the graph formed by the triangle edges and Fermat points connected to the appropriate triangle vertices and adjacent Fermat points. Figure 4.5e shows the results from a Dijkstra's shortest path algorithm on the constructed graph and Figure 4.5f shows the results after applying the path shortening function.

4.5 Intra-Array Cable Optimization

4.5.1 Problem Description

Through the preceding sub-problems the substations have been placed and a graph of possible cable connections has been constructed with the path and length of each cable computed. The remaining task is to select which of these cables to use to minimize the total cost of the intra-array cable infrastructure and what cable cross-section each cable should be. Given the arc costs between turbines and the constraints described in Equation 4.3, this problem could be described as a CMST problem with additional constraints. The MST seeks to find the sub-graph of a connected graph which connects all vertices at minimum total cost (Figure 4.1a). The CMST variation on this problem introduces additional constraints to account for maximum capacities on the arcs. The CMST is an NP-hard problem and exact methods are often avoided though easily formulated. Similar to previous studies, the CMST was here implemented as an MILP problem and solved using the Gurobi solver through MATLAB [146].

The CMST is not a new problem and the formulation used in this work is based on that of Gouveia [147, 148]. This work has generalized this formulation to allow for multiple arc types and a simultaneous selection of not only the cable paths, but the cable cross-sectional area.

4.5.2 Problem Formulation

Mathematically, the CMST can be formulated as:

$$\text{minimize} \quad \sum_{i\in V}\sum_{j\in N}\sum_{l\in L}\left[(c_l \cdot d_{i,j} \cdot y_{i,j,l}) + \left(f_{i,j} \cdot y_{i,j,l} \cdot d_{i,j} \cdot \frac{R}{A_l} \cdot c_f \cdot I^2\right)\right] \tag{4.3a}$$

$$\text{subject to} \quad \sum_{i\in V}\sum_{l\in L} y_{j,i,l} \leq 1 \qquad \forall j \in V, \tag{4.3b}$$

$$\sum_{i\in V}\sum_{l\in L} f_{j,i} \cdot y_{j,i,l} - \sum_{i\in N}\sum_{l\in L} f_{i,j} \cdot y_{i,j,l} = g_j \qquad \forall j \in V, \tag{4.3c}$$

$$f_{i,j} - \sum_{l\in L} Q_l \cdot y_{i,j,l} \leq 0 \qquad \forall (i,j) \in V, \forall l \in L, \tag{4.3d}$$

$$\sum_{l\in L} y_{i,j,l} \leq 1 \qquad \forall (i,j) \in V, \tag{4.3e}$$

$$\sum_{l\in L} y_{i,j,l} + y_{q,r,l} \leq 1 \qquad \forall (i,j,q,r) \in X, \tag{4.3f}$$

$$\sum_{i\in V}\sum_{l\in L} y_{i,j,l} + y_{j,i,l} \leq Q_{connection} \qquad \forall j \in T, \tag{4.3g}$$

$$f_{i,j} \geq 0 \qquad \forall (i,j) \in V, \tag{4.3h}$$

$$y_{i,j,l} \in \{0,1\} \qquad \forall (i,j) \in V, \forall l \in L \tag{4.3i}$$

The above formulation represents the minimum constraints to represent a CMST with multiple arc types each with a different capacity rating. In this formulation there are two decision variables: $f_{i,j}$ represents the the power flow between nodes i and j and $y_{i,j,l}$ is a binary variable representing the presence of a cable between nodes i and j of cable-type l. Both i and j are turbine or substation elements of the set V and l is a cable-type of the set L. The quantity $Q_{connection}$ represents the physical constraint on the number of connections at each turbine position.

The objective function is made up of two terms, the first represents the fixed capital cost of the cable and its installation where c_l is the per-length cost of cable-type l, $d_{i,j}$ is the length of cable needed between nodes i and j. The second term represents a factor to account for the peak losses in the cable. In this regard, the CMST is bi-objective and minimizes both the CAPEX costs of the cable and the losses in the cable. The losses are monetized by applying a cost of electricity c_f to represent the forgone revenue due to the loss. The losses are computed using: R is the resistivity of the cable, A_l is the cross-sectional area of cable type l, and I is the current level at peak. The cable length, and the flow in the cable is also used in the calculation of the peak loss. This bi-objective approach ensures that not only is the cable length minimized, but solutions with lower flow levels in cables are preferred in order to reduce the peak Ohmic losses.

The seven constraints listed represent the minimum necessary for this problem including the fact that cables cannot cross one another. General CMST formulations and past wind farm planning tools do not include the constraints given by equations 4.3e, 4.3f, and 4.3g [32, 124, 147, 149, 150]. Equation 4.3b stipulates that each node, or turbine can have at most one cable exporting power. Equation 4.3c imposes the flow balance constraints such that the difference between all flow out of each node and the flow into each node must be equal to the flow supplied at each node (the power generated by the turbine) denoted by g_j. Equation 4.3d imposes the capacity constraint where Q_l is the capacity of cable-type l. Equation 4.3e ensures that every cable can be of only a single cable-type. Equation 4.3f accounts for the fact that for an offshore wind farm intra-array cables may not cross. In order to impose this, X is the set of cable pairs that cross. Constraint 4.3g constrains the number of cables connected to a turbine to $Q_{connection}$ to account for the physical space for circuit breakers in a turbine tower. Finally Equations 4.3h and 4.3i constrain x_{ij} to be a positive flow, and y_{ijl} to be a binary variable as explained earlier.

4.5.3 Solution Approach

Although previous work formulated the problem similarly, they identified that a heuristic algorithm would be appropriate given that the problem is NP-hard [123, 124, 129]. For this reason it was decided to use Gurobi, a commercial MILP solver which combines simplex solving techniques with bespoke cutting plane generation algorithms, and heuristic algorithms. Using Gurobi, the MIP gap, the relative difference between the upper and lower bounds, is used as a measure of optimality and a termination criteria. Generally Gurobi attempts to find a true global optimum which has an MIP gap approaching 0. In order to improve the performance the MIP gap was relaxed to 0.01. This means that once the upper and lower bound of the solutions are within a 1% difference the solution is considered optimal. This means in the worst case, the solution found is 1% away from optimality for the given path lengths.

As stated earlier, the crossing constraints were imposed, however, it was found during the development of the methodology that imposing the full set of crossing constraints for all pairs of cables resulted in many inactive constraints. The formulation of these inactive constraints resulted in unnecessary computations and produced a more complex search space reducing the optimizer efficiency. It was therefore decided to take an approach similar to the implementation of cutting planes and instead solve the MILP, check if any of the paths in the solution crossed, and if so impose those individual constraints and then solve the updated MILP problem. In this way the MILP solver is called iteratively, slowly increasing the number of constraints, until the solution is found. By doing this, the inactive constraints are not unnecessarily formulated and less memory is required. Even in small cases this row generation approach was shown to perform better than the full implementation. Table 4.1 shows a comparison of the performance using the full constraints and using the row generation approach. The comparison here shows that relative to the full constraint set, the use of the row generation approach results in a significant reduction in the number of constraints which need to be formulated thereby reducing the relative time needed to solve the problem. Due to the way in which the cable routes were found using the pathfinding algorithm described in Section 4.4 it was not necessary to impose further constraints representing the regions where cables could not be placed.

Based on previous work by Fagerfjäll [32] it was decided to explore the introduction of additional constraints in order to improve performance. Two additional constraints were therefore introduced:

$$f_{i,j} - \sum_{l \in L} y_{i,j,l} \geq 0 \qquad \forall i, j \in T, \qquad (4.4a)$$

Table 4.1: Comparison of full crossing constraint implementation to row generation method

		Number of Crossing Constraints		Time to Solve CMST [s]	
	Turbines	Full	Row Generation	Full	Row Generation
	52	790804	104	701.47	1867.68
	62	844914	2	847.94	13.79
	61	405862	0	1340.13	36.43
Total	175	2041580	106	2889.54	1917.90

$$\sum_{i \in T} \sum_{l \in L} y_{i,j,l} + y_{j,i,l} \geq 1 \qquad \forall j \in T \qquad (4.4b)$$

Equation 4.4a relates the flow and activity of an arc, while Equation 4.4b stipulates that there must be at least one active edge connected to each node. Neither of these constraints is necessary in order to solve the problem, however, performance improvements were noted when they were included.

4.5.4 Intra-Array Cable Network With Reliability Requirements

The intra-array cable optimization formulation as discussed above was developed for radial cable topologies. Though the majority of existing wind farms have been built with radial topologies, it is important to consider ring topologies which include redundancy and satisfy a reliability criterion through a combination of excess capacity in the collector network and multiple paths from each turbine to the substations [151–153]. The intra-array cable network optimization with reliability requirements can therefore be seen as seeking to design a minimum cost collection network that in the event of a single cable fault ensures that at a minimum every turbine is still grid connected and at a maximum requiring the power to be exported from all turbines. The degree to which the turbines can export in a single cable fault is dependent on the level of reliability sought by the wind farm operators.

Wind farms have generally been designed with one of three cable network topologies shown in Figure 4.6. These topologies are:

- **Radial Topology:** a cable topology in which turbine are connected in strings emanating from the substation. There is no level of redundancy in this topology, and in the event of a cable failure, one or more turbines will be rendered disconnected from the substation and the grid.
- **Double-Sided Ring Topology:** a cable topology with basic redundancy achieved by connecting the terminal ends of two radial strings. This form of redundancy

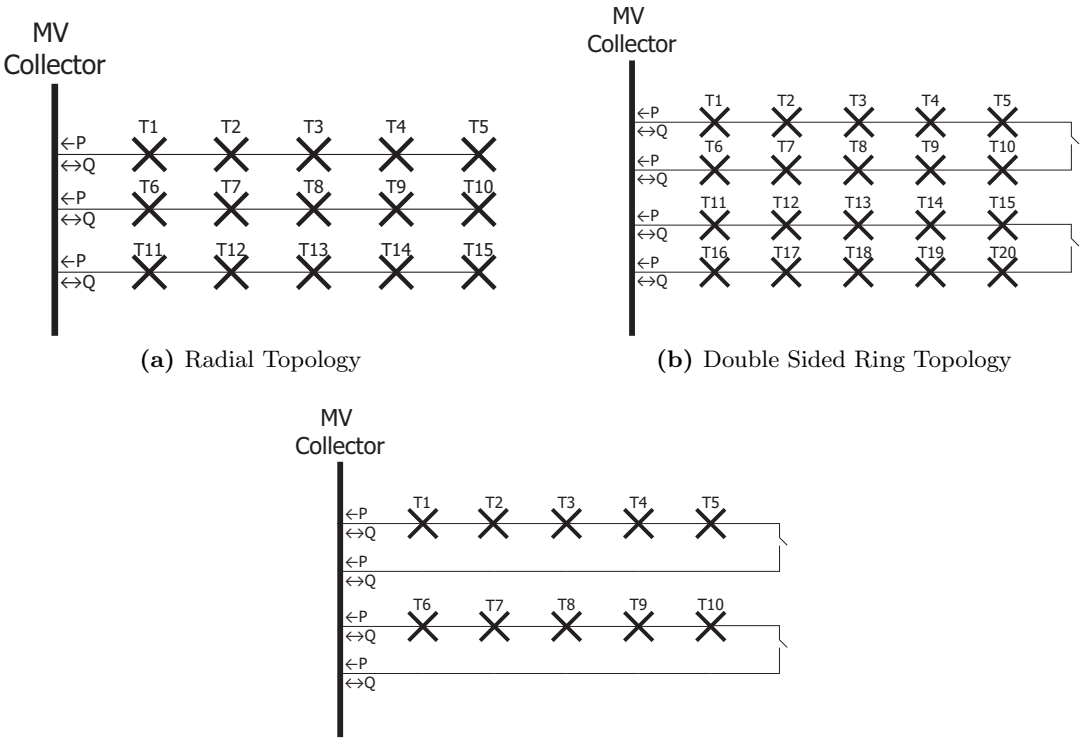

(a) Radial Topology

(b) Double Sided Ring Topology

(c) Single Sided Ring Topology

Figure 4.6: Principal network topologies

does not ensure that the power can be exported from all turbines during a fault, however, all turbines can remain grid connected and therefore the grid can supply power to them to keep the power electronics in working order.

- **Single-Sided Ring Topology:** this cable topology is similar to the double-sided ring, however, the number of turbines per ring is reduced such that all power from the turbines can be exported in the event of failure. In this topology, the cross-sectional area of all cables in the ring are generally the same in order to allow the power to flow either way around the ring given a single fault anywhere in the ring.

The ring layouts were assumed to represent a modification and a special case of the approach developed for the radial layouts. In this implementation, scenarios involving rings were assumed to use a single cable cross-section, and the assumption was made that turbines could be connected to only two other turbines rather than the three which was allowed in the radial design.

The MILP formulation was therefore amended by changing constraint Equation 4.3b and Equation 4.3g as follows:

$$\sum_{i \in V} \sum_{l \in L} y_{j,i,l} \leq 2 \qquad \forall j \in V, \ (4.5a)$$

$$\sum_{i \in V} \sum_{l \in L} y_{i,j,l} + y_{j,i,l} = 2 \qquad \forall j \in T \ (4.5b)$$

Furthermore, constraints 4.4a and 4.4b, the constraints originally included to improve the performance, must now be omitted as the ring topology would be infeasible with these constraints enforced. In the ring topologies, one arc for each ring is assumed to be normally open, that is to say that in normal operation, there should be no flow through this arc, and it is only used in the event of a cable fault elsewhere on the loop.

In order to ensure that the correct type of ring topology is adopted, the capacity of the cables is scaled according to the following factors presented in Table 4.2.

Table 4.2: Cable Reliability: Capacity Multipliers

Topology	Redundancy	Capacity Multiplier
Radial	0%	1.00
Double-Sided Ring	50%	1.00
Single-Sided Ring	100%	0.50

With these modifications, the MILP formulation can be used to design either radial or ring intra-array cable topologies. Given the size of the problem both with and without the reliability criteria, it was felt that introducing this as a further decision in the optimization approach would lead to diminished performance and significantly longer run-times. The reliability criteria has therefore been implemented as a user input under which the electrical network is designed.

4.6 Export Cable Path Optimization

4.6.1 Problem Description

The final step of the electrical infrastructure optimization module is the design of the export cable path. Each substation will have one or two export cables which transmit the power that is collected at the substations to the grid located onshore. The optimization of the export cable therefore seeks to connect the substations to a 'landfall' location while minimizing the costs. This has been approached as a separate problem to the substation positioning and intra-array cable design as the export cable path has a less

significant impact on the LCOE than the intra-array cabling [32]. Like the intra-array cables addressed in Section 4.5, the export cable may not cross the GIS obstacle regions, nor may the export cables cross the intra-array cables. These constraints therefore must be included in the export cable design. As every substation must be connected to the landfall location, this problem does not involve the design of a network, but merely the locating of the shortest route between the substation and the landfall position given the constraint regions.

Given that the export cable must connect the substations and the landfall location there are no options of what connections to make, but merely the path this connection takes. The export cable cannot, therefore, be considered simultaneously as the intra-array cables as a single path would be generated which could risk making it impossible to connect some turbines in the wind farm. It was therefore decided to treat the export cable as a separate problem to follow the intra-array cables and to be constrained by the intra-array cables.

4.6.2 Problem Formulation

As this operation seeks to minimize the cost of the export cable for each substation, the problem reduces to finding the shortest path between the offshore substations and the landfall position. This therefore can be formulated according to the same general formulation as that given in Equation 4.2. Given the problem formulation, it was decided to apply the same pathfinding algorithm that was developed and deployed for the intra-array cabling problem.

As was the case when the Delaunay Triangulation based Pathfinding Algorithm was applied for the intra-array cable problem, a graph representing the traversable space must first be constructed. Unlike the intra-array problem where the MILP formulation ensured that cables did not intersect by considering all the cables at the same time, this application of the pathfinder will be used for the placement of a single cable, and therefore the traversable space should take into account any cables that are already within the space. Once these obstacles are added to the GIS obstacles, Algorithm 4.3 can be executed to yield the cable path in a similar manner to which it was used in the intra-array network.

4.6.3 Solution Approach

In order to construct the visibility graph approximation taking into account the cables within the intra-array collection network it was necessary to convert those cable paths to polygon exclusion areas and include them as part of the constraint regions. Using a buffering algorithm, the polylines describing the paths of the intra-array cables were converted to polygons including a buffer regions about each of the polylines (P_i). To simplify the polygon shapes, a union operation was performed reducing each of the buffer polygons to the minimum number of points describing these constraints (B). This approach is detailed in Algorithm 4.5 statements 1-4.

In order to account for the combination of polygon constraints it was necessary to use boolean polygon operations. The three principal boolean operations that can be performed on areas are: *union*, *intersection*, and *difference*. To perform boolean operations, it is assumed that the polygons are each defined by a set of points and to perform the operations, the faces of the polygon overlay satisfying the given requirements are extracted. Given two polygons $\mathcal{P}_1$ and $\mathcal{P}_2$ it is possible to describe the operations as shown in Figure 4.7. To perform a *union*, $\mathcal{P}_1 \cup \mathcal{P}_2$, the faces that are labelled either $\mathcal{P}_1$ or $\mathcal{P}_2$ are extracted, while to perform the intersection, $\mathcal{P}_1 \cap \mathcal{P}_2$, only the faces that are labelled both $\mathcal{P}_1$ and $\mathcal{P}_2$ are extracted. The difference, $\mathcal{P}_1 \backslash \mathcal{P}_2$, is defined as the faces in the polygon overlay that are labelled with $\mathcal{P}_1$, but not labelled with $\mathcal{P}_2$ [143].

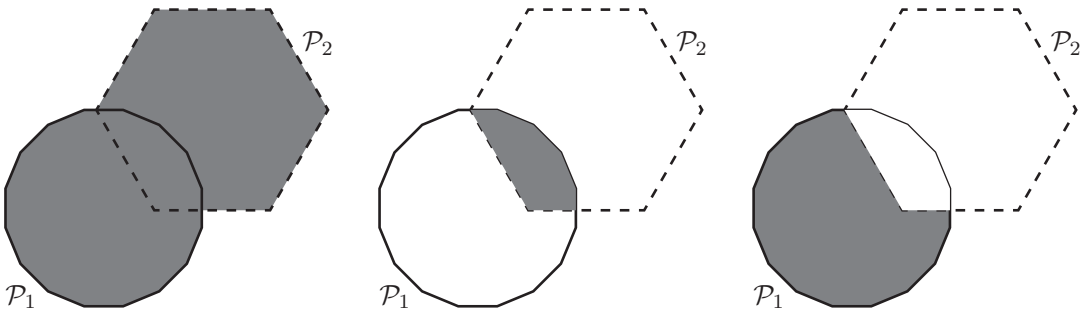

(a) Union **(b)** Intersection **(c)** Difference

Figure 4.7: Boolean operations on two overlapping polygon areas

As these polygon constraints include the substation position, it is necessary to define the substation and the area immediately surrounding the substation as not being within the intra-array cable buffer constraints. This is done in order to ensure that the export cable can reach the substation. To do this, a circle was defined around the substation of radius 200 m (S). A set subtraction is then performed between the buffer polygon and the newly created circle to create a set representing the added constraints due to the intra-array cables. To include this in the overall optimization scheme, a set subtraction operation is performed between the existing traversable space which already includes

the polygon obstacle constraints (A) and the set subtraction previous performed to create the updated traversable points (A_{export}).

The Delaunay Triangulation Based Pathfinding algorithm is then run with A_{export} as the traversable space to produce the export cable path for a given substation. In order for subsequent substations to take this export cable into account when their own export cables are designed, this export cable P_{export} is added to the intra-array cable path polygon constraints.

Algorithm 4.5 Export Cable Path Optimization

Require: Substation positions, landfall position, site boundary, traversable points (A), and intra-array cable paths

for all intra-array cable paths **do**
  Add a separation buffer to cable path polyline to create a polygon, P_i
  Compute the *union* of all cable path polygons: $B = B \cup P_i$
end for
for all substations **do**
  Construct a circle polygon around substation, S
  Compute $A_{export} = A \backslash (B \backslash S)$
  Execute Delaunay Triangulation Based Navigational Mesh Pathfinding given the substation position, landfall position, and updated polygon obstacles (G_2)
  Update cable path constraints to include the export cable: $B = B \cup P_{export}$
end for
return Export cable paths

4.7 Application

4.7.1 Study Description

In order to assess the performance of this approach compared to other MILP and simple estimation methodologies it was applied to a real offshore wind farm. This study considers a UK Round 3 site off the south coast of England which was planned to have between 121 and 194 turbines. The site interestingly has a number of GIS constraints that would need to be taken into account during both the siting of turbines and the design of the intra-array cable network. These GIS constraints include unexploded World War II ordnance, ship wrecks, and areas where the seabed characteristics are unsuitable for turbines or cables.

As no decision had been made on the layout of the turbines or the size of the turbine, a realistic turbine layout was designed using DNV GL WindFarmer 5.3. This layout considers only the overall site boundary and the GIS constraints and has been generated for the explicit purpose of testing this optimization tool; it does not represent a real

layout designed by the project developer. The layout studied here consists of 175 6 MW turbines representing 1050 MW installed. This layout is larger than the 968 MW maximum allowed capacity for the wind farm and has been generated for the explicit purpose of demonstrating the capabilities of this optimization tool. To demonstrate the capabilities of this tool, a radial network topology has been selected.

For this layout, the results using this tool are compared to running a simple design tool ignoring the GIS constraints, as well as estimating the total cable length only using the separation distance between turbines in the crosswind direction. The latter two represent methodologies often employed in layout optimization tools and cost models. The estimation based on the turbine separation considers neither the GIS constraints nor the capacity of cables and therefore represents a theoretical lower bound on the length of cable albeit an unrealistic lower bound.

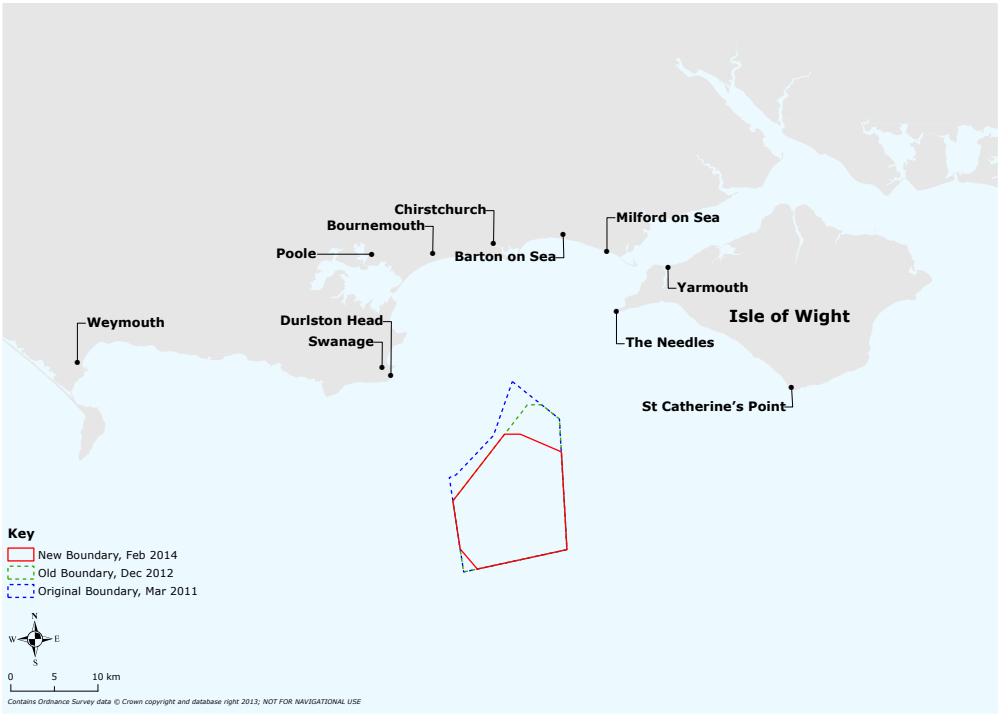

Figure 4.8: Illustrative map showing the UK Round 3 Site project site courtesy of Navitus Bay Development Ltd.

Based on the most recent boundaries shown in Figure 4.8 (red boundary) along with the GIS data provided by the developer of the site it was possible to generate turbine layouts using DNV GL WindFarmer 5.3. These turbine positions were then input to the intra-array cable optimization tool.

All MILP optimization problems were run using a gap of 0.01. A solution is also shown using the grid based pathfinding, however, this method required the relaxation of the crossing constraint and the solutions produced by this method therefore do not represent realistic solutions that could be built.

4.7.2 Substation Placement

Running first the substation placement component of the tool allowed the new constrained capacitated kmeans++ (CC-kmeans++) algorithm to be benchmarked against more common clustering approaches such as kmeans and kmeans++. It should be noted that neither of these algorithms are designed to include capacity constraints nor GIS based constraints limiting the area where it is permissible to place the cluster centre.

Comparing the performance for a range of wind farm sizes within the wind farm area it was found that the clustering was relatively inelastic to the number of turbines, and more strongly governed by the number of clusters that the turbines were to be partitioned into. Importantly, the constrained capacitated kmeans++ approach proved to be far slower than traditional clustering approaches, however, even given this it was deemed to have an acceptable performance.

As can be seen in Figure 4.9 though the performance of the new clustering algorithm is much slower than kmeans++, it gives similar results in terms of total distance between the turbines and the centre location while at the same time adhering to the GIS and substation capacity constraints. Though the increase in computational time is relatively high, it is not sufficiently increased to affect the full optimization of the electrical infrastructure.

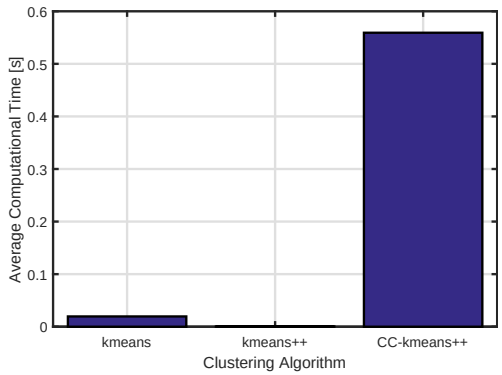

(a) Average time to partition wind farm into two clusters.

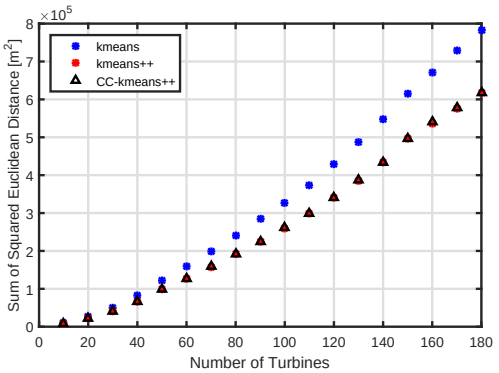

(b) Sum of distance between turbines and substation.

Figure 4.9: Comparison of the clustering algorithms. In both graphs lower values indicate better performance.

4.7.3 Optimized Intra-Array Cable Layout

The full implementation of both the substation placement and the intra-array cable optimization for a wind farm of 175 turbines within the wind farm site area gave the cable results shown in figures 4.10 and 4.11 (with and without the GIS constraints imposed respectively). Table 4.3 shows the results compared to the solutions of simpler MILP programs which ignore GIS constraints. From this comparison, it was found that the total cable length increased by almost 9 km representing an added capital cost of approximately £3.9 million and when compared to using an estimation based on the intra-turbine spacing, the total amount of cable is increased by approximately 13 km representing approximately £5.7 million.

Table 4.3: Cable Length Comparison

Method	Cable Length [km]	Delta [km]	Capital Cost [£m]
Turbine Spacing Based	148.75	-	64.56
CMST no GIS	157.66	8.91	68.42
CMST with GIS	161.84	13.09	70.24

From the results, a number of differences can be observed; ignoring the GIS constraints leads to a number of cables crossing the obstacle regions as would be expected. Interestingly, however, running either the A* grid based pathfinding (Figure 4.12) or the navigational mesh both produce fundamentally different solutions to the cable layout problem from the base case. This can be attributed to the optimal solution being more than just re-routing the cables that violate the obstacle constraint.

Looking at the A* solution shown in Figure 4.12, it can be observed that the grid based pathfinding is unable to find feasible solutions due to the limitations mentioned previously and in fact was unable to produce solutions without cables crossing. The proposed full methodology does, however, successfully place the substations at acceptable locations and designs an infield cable layout that does not violate any of the constraints including the GIS based constraints. This is shown in Figure 4.11.

4.7.4 Export Cable Optimization

The final step of the electrical infrastructure optimization tool is to design the offshore export cable paths for each substation. No landfall position had been identified by the project and therefore an assumption was made. The cable path is found using the Delaunay triangulation base pathfinding algorithm previously described. The resulting paths for the case under consideration are shown in Figure 4.13. Like the intra-array cable solution, the identified cable path adheres to the constraints imposed in that the

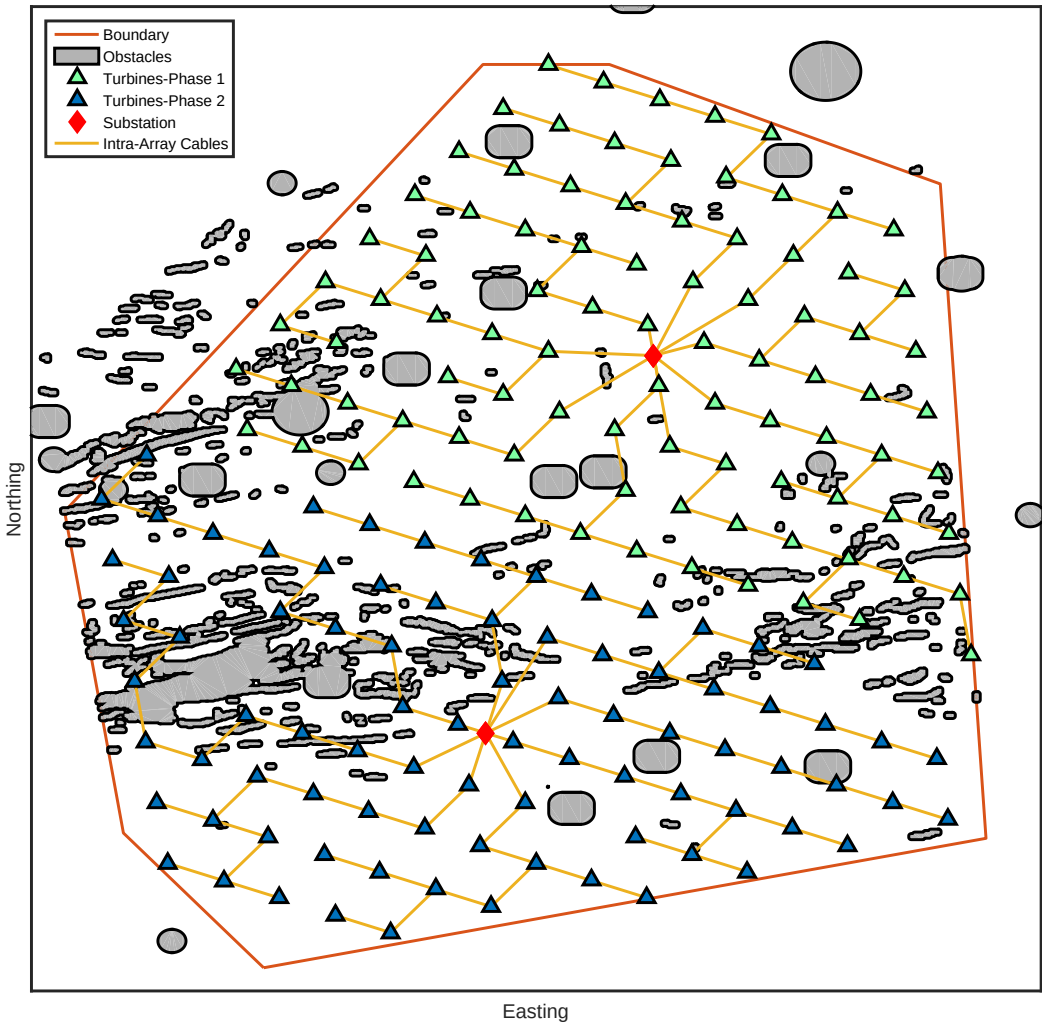

Figure 4.10: Cable layout, no GIS constraints

export cable does not go through any of the constraint regions nor does it intersect any of the existing cables. The path lengths identified are indicated in Table 4.4.

4.7.5 Intra-Array Cable Optimization with Redundancy

Though this case has explored a radial cable network, the most common type of offshore collection network topology, it is useful to assess the value of introducing redundancy into the system. To do this, a lifetime cost analysis has greater relevance than the CAPEX considerations that have been made. In order to explore the lifetime cost it was therefore necessary to include the failure rates of these components and the mean time to repair (MTTR). These statistics can then be used to estimate the lost production due to cable failures. As each of the topologies has fundamentally different degrees of redundancy it is anticipated that the lost production will vary across these. Quantifying

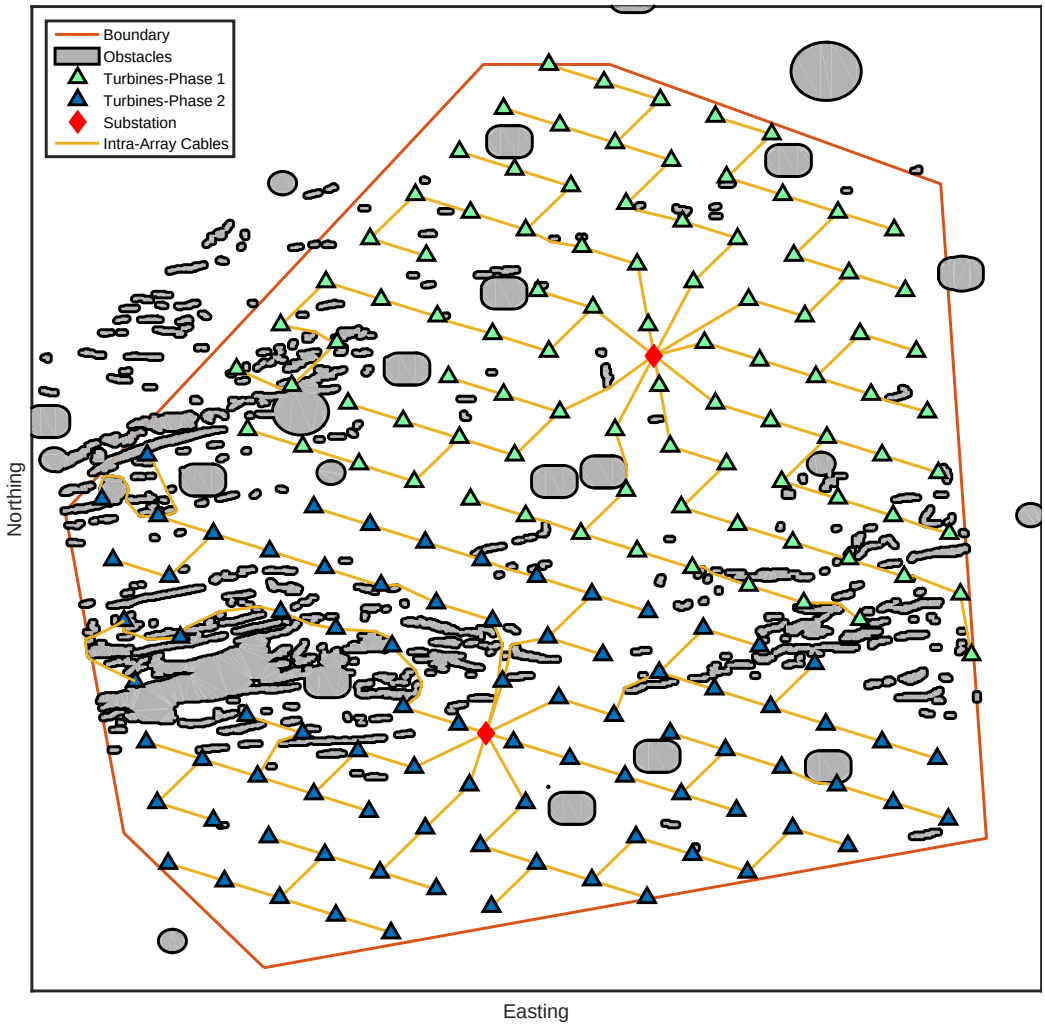

Figure 4.11: Cable layout, full optimization method

these differences in lost production in monetary terms will allow the different intra-array topologies to be compared. To do this, two studies were planned, the first uses a simplistic analysis to estimate the downtime based on available failure statistics, while the second was to take a more rigorous approach using a simulation based stochastic model to take into account not only the probabilistic nature of the failures, but also of the wind and wave conditions which govern the weather access periods. Unfortunately due to time constraints, the second study has not been performed and future work should explore the cost of including redundancy in the intra-array network to greater detail.

Using the statistics published by Sannino et al. [154] based on a cable manufacturer's experience with offshore wind farm cables (Table 4.5), it is possible to estimate the expected value in downtime over the course of the year based on the length of each

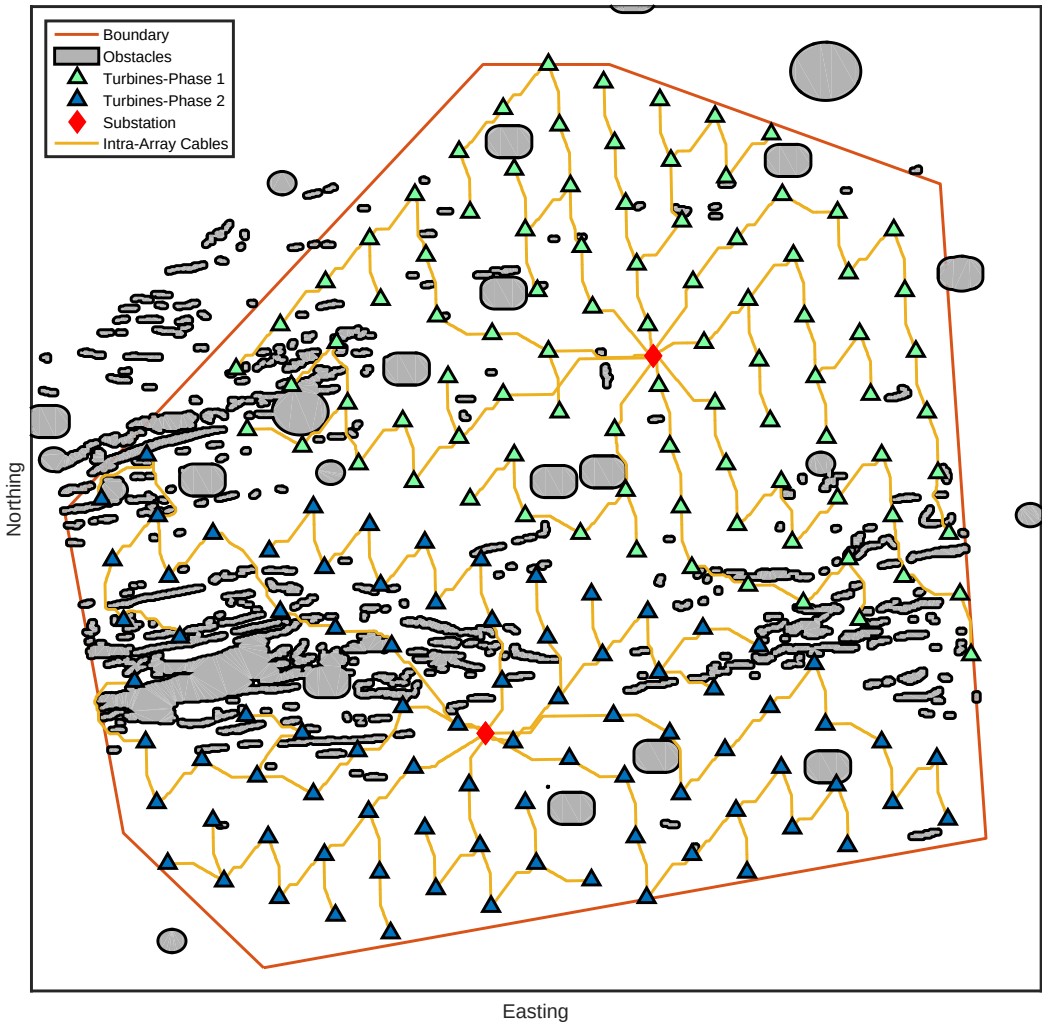

Figure 4.12: Grid based pathfinding using an A* search algorithm

cable section, the failure rate per unit length, and the MTTR. From this expected value, the lost production is computed given the capacity factor of the site. In the case of this analysis, the capacity factor of 39% was taken from the output of the approach identified in Chapter 5.

Considering just a single phase of the project at hand for illustrative purposes, the lifetime costs of the electrical infrastructure can be computed for each of the optimized designs. As is indicated in Table 4.6, when redundancy is included in the system, the total length of cable increases. It should be noted that the present tool does not allow tapered rings, that is rings with varying cross-sectional areas. This therefore further increases the costs as savings cannot be made in the ring configurations by shifting to smaller cross-sections for specific cable segments. This effect on cost is shown in Table 4.7.

Table 4.4: Export Cable Summary

Phase	Distance to Landfall [km]	Cable Length [km]
Phase 1 (North)	27.9	28.2
Phase 2 (South)	34.7	39.9

Table 4.5: Offshore Wind Farm Cable Failure Statistics [154]

Failure Rate $\left[km^{-1} \cdot year^{-1}\right]$	0.015
MTTR [h]	1440

Table 4.6: Comparison of Intra-Array Cable Network Lengths with Redundancy

	Cable Length [km]			
Configuration	3x630 mm	3x300 mm	3x150 mm	Total
Radial	38.4	19.3	14.4	72.1
Double Sided Ring	83.2	0.0	0.0	83.2
Single Sided Ring	116.9	0.0	0.0	116.9

Table 4.7: Comparison of Intra-Array Cable Network Costs with Redundancy

Configuration	CAPEX Cost[1]	Lost Production Cost[2]	Total Cost[3]
Radial	£21,658,029	£24,485,698	£46,143,726
Double Sided Ring	£31,471,966	£17,799,426	£49,271,392
Single Sided Ring	£44,216,672	£1,502,877	£45,719,549

[1] See Section 6.2.5 for CAPEX cost methodology

[2] A present value strike price of £140/MWh was assumed to monetize the lost production

[3] Direct OPEX costs due to cable failures are not included here

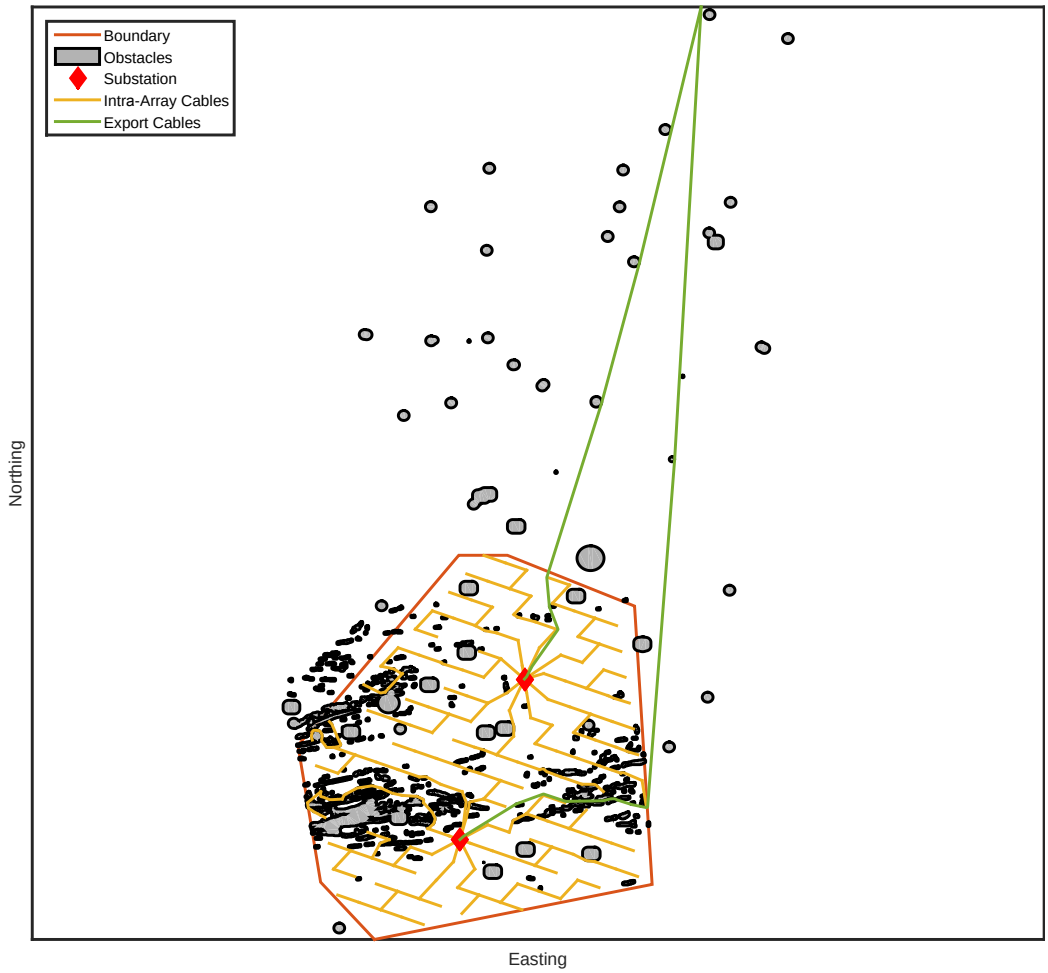

Figure 4.13: Full electrical infrastructure optimization with export cable path optimization

As can be seen in Table 4.7, at the assumed failure parameters, given turbine positions, and considering only the effects of the electrical infrastructure, the total cost variation over the lifetime of the project for the three network topologies is within a narrow band of less than £5 million. In order to explore the importance of the failure data and the strike price, a one-factor-at-a-time approach sensitivity analysis has been performed. Though this ignores the interactions between the factors, it does highlight the need for accurate data when assessing the various cable topologies [155].

Figures 4.14a-4.14c show that a slight change in either the failure rate, the MTTR, or the strike price can change which of the network topologies is most optimal. The results obtained using a one at a time sensitivity analysis showed that the lifetime cost of both the radial and double-sided ring topologies are sensitive to any one of the parameters, while the single-sided ring is relatively insensitive to any of the parameters due to its

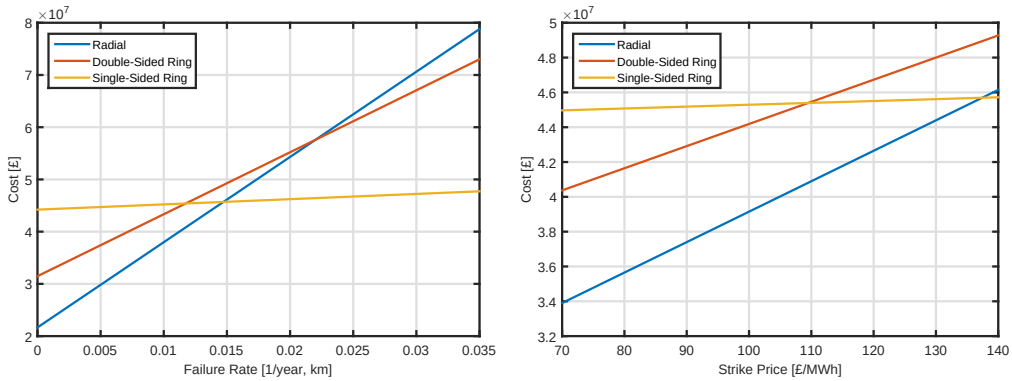

(a) Failure Rate **(b)** Strike Price

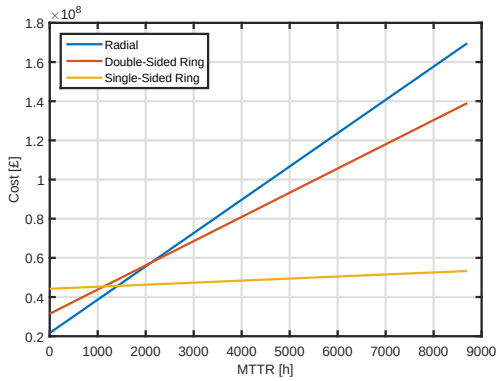

(c) MTTR

Figure 4.14: Sensitivity of lifetime intra-array cable costs

high degree of redundancy. This indicates that before deciding which network topology to deploy it is important to have reliable failure rate data. This analysis has also ignored any change in the operations and maintenance costs which would be incurred as a result of changing the cable topology. A more rigorous analysis would need to include these costs as well in order to ensure that the reduction in lost production can balance the change in CAPEX and OPEX. Having said that, the work done here shows that for the case considered the increased CAPEX of the single-sided ring is outweighed by reduction in lost production in the event of a failure making it the most cost effective option.

4.8 Chapter Summary

This chapter has outlined a solution approach for the electrical infrastructure design problem for an offshore wind farm by means of dividing it into several sub-problems and solving these using heuristics. These sub-problems have included a location-constrained capacitated clustering approach for placing the substations; a navigational mesh based pathfinding algorithm to determine possible cable connections; an MILP formulation to construct a CMST and select which cable connections should be installed; and use of the navigational mesh based pathfinding algorithm to determine the export cable paths.

The CCCP compares well in performance against traditional clustering methods such as kmeans and kmeans++, although consistently slower than both, it has consistently better cluster centres than kmeans, and very similar results to kmeans++ while adhering to the GIS and capacity constraints. This implementation represents a novel approach to the positioning of an offshore substation and is one of the first automated approaches used for this application.

To address the determination of possible cable connections it was decided to implement a navigational mesh pathfinding algorithm based on constructing an approximation of a visibility graph to describe the configurational space where cables can be placed. From the resulting graph that is constructed a standard shortest path algorithm with a bespoke path shortening heuristic is applied in order to produce good feasible solutions which approach optimality. The lengths of these paths are then scaled by the unit cable costs to define the edge costs in the MILP implementation of a CMST. Separate cables along the same path are entered into the MILP formulation to represent the range of cable cross-sections available.

The results of this approach applied to a real offshore wind farm previously under development have yielded promising results indicating that this approach is not only valid but shows improvements over commonly used approaches based on the turbine separation distance. There are, still improvements that can be made, but this approach represents a strong step forward to the efficient automation of the layout design of an offshore wind farm and optimizing all aspects of the layout. This tool has also been capable of including reliability criteria in the construction of the intra-array cable network, allowing the developer to develop realistic collection networks and compare different network topologies.

As part of the evaluation function for the overall wind farm optimization problem this step will allow accurate cable losses and costs of the electrical infrastructure to be incorporated. By including these, it is believed that for large offshore wind farms more accurate layout optimization can be done while including an increased level of

detail over previously developed methods. At the same time, as heuristics are used, this approach may not reach proven optimality, however, it does find high quality solutions in acceptable time scales.

Chapter 5

Annual Energy Production Estimation

5.1 Introduction

With regards to layout optimization, one of the main areas in which layouts can differ from one another is in the variation in annual energy production (AEP). As the principal purpose of constructing a wind farm is to generate electricity, it is important for this layout optimization tool to accurately model the energy production of a wind farm using the relevant site information while capturing the impact that the turbines have on one another. In order to estimate the AEP it is necessary to model the wind regime in which the wind farm will operate based on either atmospheric models or wind measurement campaigns as well as model the way in which the individual turbines affect the wind resource. In addition to this, it is also necessary to evaluate the losses due to the electrical subsystem (described in Chapter 4).

The principal source of energy loss which is dependent on the layout of the wind farm and the relative positions of the turbines comes as a result of operating wind turbines within the *wake* of upwind turbines. Wind turbines convert the wind energy to useful energy in two processes completed in sequence. In the first process, the kinetic energy of the wind is converted to mechanical energy at the rotor, and in the second this mechanical energy is converted to electrical energy at the generator [136, 156]. Due to the mechanical extraction of energy, conservation of both energy and momentum dictate that directly behind the rotor-plane, downwind of the rotor, the wind is less energetic. The *wake* is a term used to describe this region downwind of an operating turbine in which the wind resource is characterized by reduced wind velocities and increased turbulence intensities as a result of the energy extraction [136]. As the effect of wakes within wind farms can result in up to a 10-20% reduction of wind farm energy yield, under specific operational conditions, significant research effort has focused on means to reduce the impact of wakes within large wind farms [157].

The present chapter includes a description of the available methodologies for the estimation of the AEP as well as the validation of analytic wake models using available data from operational offshore wind farms. The second section of this chapter explores the general approach for estimating the AEP from the given wind resource. The third section then explores the physical description and aerodynamics of wind turbine wakes. The fourth section then describes both kinematic models which have been developed for wind turbines and more advanced field models. Section 5.5 validates the implemented kinematic wake models using data available from Middelgrunden, Horns Rev I, and Nysted wind farms in order to rate the relative accuracy and computational time of the kinematic models and identify which models would be relevant for inclusion in the optimization framework. Finally a number of proposed strategies for the mitigation of wind turbine wake effects is also summarized as these could potentially be implemented into the layout optimization tool. The final section, Section 5.6, describes an approach implemented for assessing the electrical losses which affect the AEP. From this, two principal sources of layout dependent energy losses are included in the AEP computation allowing the LCOE to both have increased accuracy and greater ability to compute LCOEs which consider the impact of the turbine layout.

5.2 Annual Energy Production (AEP)

Determination of the AEP of a wind farm by using a site wind rose, the turbine power curve, the turbine positions, and a wake model is a common procedure as part of wind farm design, and a statistical approach is generally taken [17, 32, 89, 91, 158].

As offshore wind farm sites tend to be characterized by very low turbulence and low spatial variation especially at distances exceeding 5 km from shore, a single wind rose can be used to represent the site [136, 159]. Using this wind rose, each wind speed and direction pair can be stepped through and applied to the wind farm with wake losses computed for each turbine as a function of the production of the upwind turbines. The total energy produced for each wind speed and direction pair is then scaled based on the joint-probability of occurrence for that wind speed and direction combination. For each wind speed and direction combination, the sum of the individual turbine yields is then adjusted to account for the electrical losses for that wind speed/direction combination. The sum of the net generation over all the wind speed and direction combinations results in the net AEP. Generally, the gross AEP is considered to be the annual energy production not accounting for any sources of energy loss, while the net AEP is the annual energy production taking into account both wakes and additional sources of energy loss such as the electrical collection network. This approach is shown diagrammatically in Figure 5.1 highlighting that the calculation is done for each turbine

for each wind speed and direction combination. Compared to the traditional AEP calculation method, a step has been added here to account for the electrical losses. This considers the designed electrical collection network required for the given turbine positions and computes the losses for each wind speed and direction combination through the entire network.

Given accurate models characterizing the degradation and damage of components as a function of the loads experienced due to operation within a wake, it would in principle be possible to include similar corrections to include losses due to component degradation and failure. By doing so, a more accurate turbine availability could be computed. Presently, the relationship between wake effects, fatigue loading, component degradation, and turbine availability is still actively being studied [27, 160, 161].

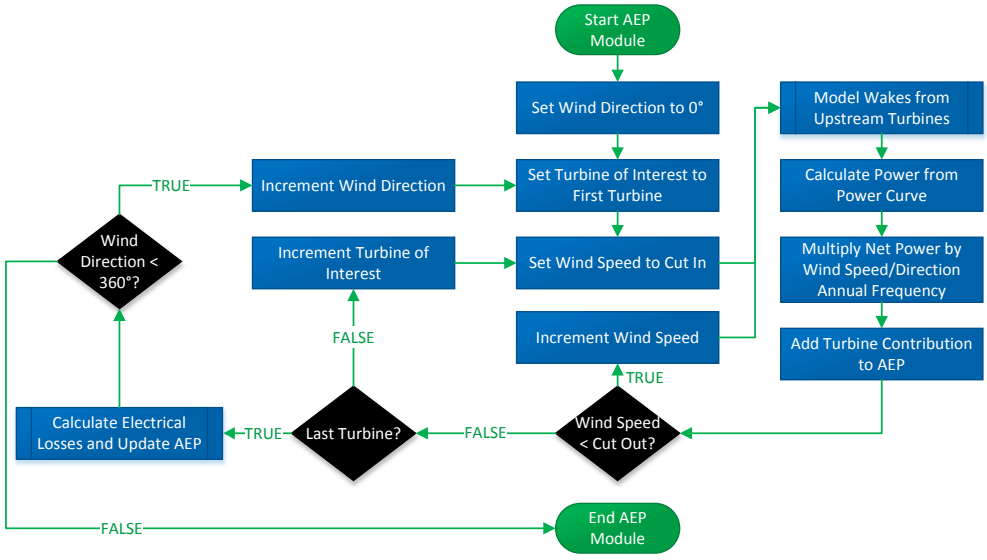

Figure 5.1: General flow of AEP calculation

As a key component of the net AEP evaluation is updating the incident wind speed to account for the wakes created by upwind turbines, it is important to both understand the dynamics of wind turbine wakes and methods to model them.

Algorithm 5.1 Offshore Wind Farm AEP Estimation

Require: The turbine positions, the free-stream wind data, the desired wake model, the number of direction steps, the number of wind speed steps, turbine power and thrust curves, global system efficiency, availability

```
for all wind directions do
    Order the turbines based on the wind direction
    for all wind speeds do
        Update free-stream wind data to include Large Wind Farm Correction if using Large Wind Farm Correction
        for all wind turbines do
            Compute combined wake deficit from upstream turbines
            Update free-stream wind data to include wake
            Compute power from turbine power curve
        end for
        Multiply power by annual frequency of wind speed and direction
        Calculate losses in the intra-array cables and turbine transformers
        Add to total energy yield
    end for
end for
Apply global system efficiencies and availability
```

5.3 Behaviour of Wind Turbine Wakes

The wake of a wind turbine refers to the flow of air directly behind operating wind turbines. The disruption caused as a result of the extraction of energy from the wind by a rotating machine leads the wake to be characterized by two principal physical phenomena: a reduction in wind velocity within the wake, and an increased level of turbulence intensity in the flow. These physical phenomena have respectively been widely attributed to result in reduced power production on a downwind turbine and unsteady loading on a downwind wind turbine [162, 163]. Figure 5.2 shows a unique set of atmospheric conditions under which water vapour condensed in such a way that the wakes at Horns Rev I could be seen clearly.

Ott et al. [25] describes wind turbine wakes as having the following characteristics:

1. an expanding conical shape downwind of an operating turbine;
2. within this volume of air, a velocity deficit is experienced;
3. an increased level of turbulence is experienced within this volume of air;
4. at any given downwind distance, the maximum momentum (velocity) deficit is observed along the centreline of this volume;
5. this centreline may meander, and may not always be at the centre of the wake's cross-section; and
6. air mixes across the boundary of this volume allowing the wake to recover downwind.

(a) Seen from the south **(b)** Seen from the southeast

Figure 5.2: Photographs from Horns Rev I from February 12, 2008. The atmospheric conditions at the time resulted in sea surface water forming a fog in the wake of the turbines making it possible to visualize the wake region within an offshore wind farm [164]. Courtesy: Vattenfall. Photographs taken by Christian Steiness.

As one moves further downwind from a wind turbine, the waked flow has more opportunity to mix with the undisturbed flow which surrounds the wake. This slowly dissipates the wake and allows the wind to recover to the undisturbed wind conditions. The modelling of wind turbine wakes and the velocity deficit as a result of operation within the wake of an upwind turbine represents an important step in the calculation of the AEP of a wind farm. Given that the turbine responds differently to the wind depending on the wind speed, and the affected region downwind is impacted by the wind direction, the wake behind each turbine must be computed for every turbine and for every wind speed and wind direction combination as shown in Figure 5.1 and described in Algorithm 5.1.

5.4 Modelling Wind Turbine Wakes

Modelling of wind turbine wakes can be divided into two main systems of modelling: *explicit* and *implicit* models. Explicit models, also known as kinematic models, use only momentum and mass balance through the rotor disk to compute the velocity deficit and occasionally the added turbulence intensity. Implicit models, also known as field models, use a Reynolds-Averaged Navier-Stokes (RANS) solver to evaluate the flow [165, 166]. For both model types, different models using different parametrization exist. In previous layout optimization tools both kinematic and implicit models have been applied.

For all types of wake models, a distinction is generally made between the near wake region, the region directly behind the wind turbine, and the far wake. In the near wake, the wake is dominated by the shape of the flow field, the pressure gradient across the

turbine rotor, the rotor shape, and the properties of the individual blades [163, 165]. The far field is less heavily dependent on the rotor shape and represents sufficient distance from the rotor that mixing within the wake has occurred. In the far wake, the wake shape is assumed to be axisymmetric, self-similar, and Gaussian [167]. In general the near wake extends from the rotor plane up to approximately two or three rotor diameters downwind of the turbine, and the far wake represents any region beyond this [162, 168, 169]. Most wind turbines are spaced at separations beyond two to three rotor diameters, and are therefore generally assumed to be operating in the far wake. Though still of interest for the understanding the aerodynamics of wind turbine wakes, the modelling of near wakes is generally omitted when considering the impact wind turbine wakes have on downwind turbines within a wind farm.

Explicit wake models make a number of assumptions regarding the flow characteristics which allow the wakes to be parametrized by a series of simplified momentum balance equations. The various explicit models differ from one another based on assumptions regarding the wake, and what elements of the flow they choose to parametrize the wake on.

An important point to note is that the majority of explicit wake models have been developed as single wake models. That is to say they describe the wake behind a single turbine rotor and are not truly applicable to cases where there are multiple wakes interacting with one another. However, they are often applied to situations where wakes merge and overlap through simple analytic techniques to account for the superposition and merging of wakes.

This section discusses four analytic wake models which have been frequently applied, the Jensen [19], Larsen [21, 22], Frandsen [24], and Ishihara [23] models. In addition to these, the Ainslie Eddy-Viscosity model [170], a commonly used implicit model is also discussed as this represents the model that is most frequently used for wind farm AEP studies in commercial software packages [158, 171, 172].

5.4.1 N.O. Jensen/Park Model

A frequently used kinematic wake model is the Jensen wake model, sometimes also referred to the Park wake model when applied in 3D to an entire wind farm, developed at Risø DTU. Risø DTU has been a leading institution in wind turbine research and has contributed a number of kinematic wake models [173]. Risø DTU has also taken advantage of a close working relationship with a number of wind farm operators and turbine manufacturers allowing them access data with which to both develop and validate these models.

The Jensen model is one of the earliest analytic wake models and was originally developed in 1983 based only on mass conservation. Despite its age, it remains commonly used and has been, until the most recent version, the wake model used in the WAsP flow modelling software package. This wake model describes the wake downwind of a single turbine and assumes a linear expansion of the wake as shown in Figure 5.3 [19, 53, 167].

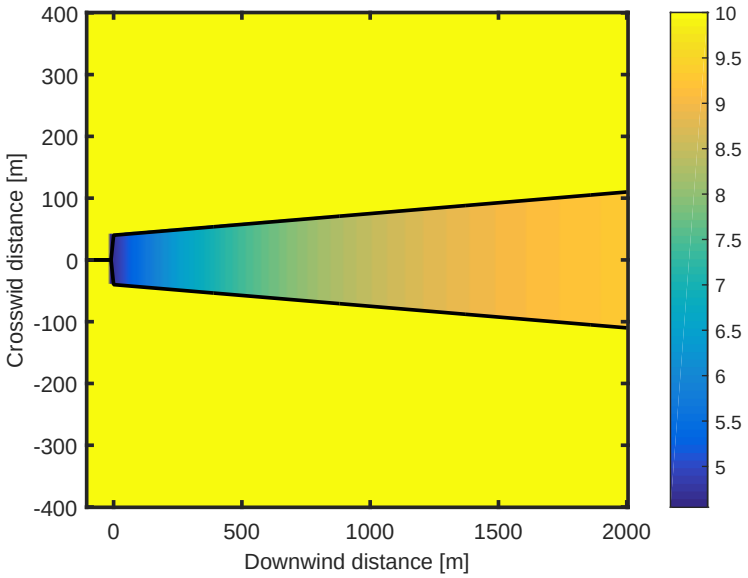

Figure 5.3: N.O. Jensen single wake. Free-stream wind velocity is 10 m/s from the west.

As the wake is assumed to expand linearly downwind of the turbine, the diameter of the wake, d_w, is given as a function of the downwind distance:

$$d_w = d \times (1 + 2ks) \tag{5.1}$$

where d is the rotor diameter, k is the wake decay factor, and s is the non-dimensional distance downwind of the turbine ($s = \frac{x}{d}$, where x is the distance downwind of the turbine) [16, 91, 165].

The wake decay factor, k, describes the relative persistence of the wake and the speed at which mixing across the wake boundary layer is occurring. Higher wake decay factors correspond to a wake that decays more quickly and is therefore less persistent, however, will at the same time expand more quickly in the radial direction. A high wake decay factor therefore is associated with a high degree of mixing and therefore high ambient turbulence intensity. The wake decay constant is often given to be 0.04 or 0.05 for offshore sites where the ambient turbulence is relatively low and 0.075 for onshore sites where there is typically higher ambient turbulence intensity. More generally it can be

related to the characteristic roughness length of the site, z_0, and the turbine hub height, H, as given in Equation 5.2 [91, 161].

$$k = \frac{1}{2 \cdot ln\left(\frac{H}{z_0}\right)} \tag{5.2}$$

The ambient turbulence intensity, I_a, can also be related to the site roughness and the hub height often being approximated by Equation 5.3 [161].

$$I_a \approx \frac{1}{ln\left(\frac{H}{z_0}\right)} \tag{5.3}$$

Combining Equations 5.2 and 5.3 allows the wake decay constant to be expressed in terms of the ambient turbulence intensity:

$$k \approx \frac{1}{2} I_a \tag{5.4}$$

Using this approximation, it is possible to determine a more accurate wake decay constant for the site based on the available site data.

The model then defines three scenarios for a downwind rotor. First, the rotor plane can be located fully within the wake of an upwind turbine and the turbine would therefore experience a maximum possible velocity deficit. Secondly, only part of the rotor plane can be located within the waked region and therefore will experience a velocity deficit less than the maximum. Alternatively, all of the rotor plane area can be outside of the waked region and therefore there will be no velocity deficit due to the wake of the upwind turbine [19, 91]. The maximum velocity deficit is therefore scaled by the proportion of the rotor plane area within the wake.

The velocity deficit, $D_{i,j}$, experienced by turbine i due to the wake of turbine j, relative to the upwind free flow velocity, U_∞ is given by:

$$D_{i,j} = \frac{1 - \sqrt{(1 - C_{T_j})}}{(1 + 2ks)^2} \cdot \frac{A_{i,j}}{A_i} \tag{5.5}$$

where C_{T_j} is the thrust coefficient of the upwind turbine j defined by the turbine's thrust curve provided by the manufacturer, $A_{i,j}$ is the area of intersection between the downwind turbine's rotor plane and the wake of the upwind turbine, and A_i is the rotor swept area of the downwind turbine i. It is important to note that this model assumes that the thrust coefficient C_T does not exceed 1.

The wind velocity experienced by the downwind turbine, U_i, is therefore given by:

$$U_i = U_\infty \cdot (1 - D_{i,j}) \tag{5.6}$$

The original Jensen wake model as described above only accounts for the wake behind a single wind turbine. In real wind farms it can be expected that a downwind turbine could be affected by multiple wakes. Further development of this model by Katic et al. [20] led to a means of superposing multiple single wakes to compute the total velocity deficit experienced by a turbine due to the combined effect of multiple upwind turbines.

Using this updated formulation, the total velocity deficit factor experienced by turbine i, D_i, is given empirically by the sum of squares of the individual velocity deficit factors:

$$D_i = \sqrt{\sum_j (D_{i,j})^2} \tag{5.7}$$

Alternate approaches for including the superposition of wakes are briefly covered in Section 5.4.5.

Similarly, the velocity formulation using this updated deficit factor becomes:

$$U_i = U_\infty \cdot (1 - D_i) \tag{5.8}$$

A further modification to the Jensen/Park model is known as the Modified Jensen/Park model uses a simplification for determining the overlapping areas between the rotor plane and the wake [166]. The version developed for DNV GL's WindFarmer for example, uses the horizontal overlap relative to the ground and to scale the deficit [89].

5.4.2 G.C. Larsen Model

A subsequent model also developed at Risø DTU was the model by G.C. Larsen. This model is also an explicit kinematic model, however, it parametrizes the wake on a different set of parameters compared to the Jensen model. The Larsen wake model is a closed form expression of the RANS equations using the Prandtl turbulent boundary layer equations [21, 22]. Unlike the Jensen wake model, a linear expansion of the wake is not assumed and rather than using the intersection area between the rotor and the wake, the radial distance between the upwind and downwind turbines is used in the parametrization. This model requires the hub height, and the ambient turbulence intensity to describe the wake rather than a proxy such as the wake decay coefficient. As is often the case when using kinematic models, both the Larsen and Jensen models

do not estimate the amount of added turbulence due to the wind turbines extracting energy.

Following the same form as Equation 5.6, the velocity within the wake is defined relative to the undisturbed free wind speed by the wake deficit factor. For the Larsen wake model, this deficit factor is given by:

$$D_{i,j} = \frac{1}{9}\left(C_{T_j}A_i(x+x_0)^{-2}\right)^{\frac{1}{3}}\left(r^{\frac{3}{2}}\left(3c_1^2C_{T_j}A_i(x+x_0)\right)^{-\frac{1}{2}} - \left(\frac{35}{2\pi}\right)^{\frac{3}{10}}\left(3c_1^2\right)^{-\frac{1}{5}}\right)^2 \quad (5.9)$$

The radius of the wake affected region, R_w, is given by:

$$R_w = \left(\frac{35}{2\pi}\right)^{\frac{1}{5}}\left(3c_1^2\right)^{\frac{1}{5}}\left(C_tAx\right)^{\frac{1}{3}} \quad (5.10)$$

where x is the distance between the turbines in the downwind direction, x_0 is a constant based on the rotor position relative to the coordinate system, r is the distance between the turbines in the crosswind direction, and c_1 is a parameter related to the Prandtl mixing length.

The parameters x_0 and c_1 are specific to this wake model and are defined by:

$$x_0 = \frac{9.5d}{\left(\frac{2R_{9.5}}{d_{\text{eff}}}\right)^3 - 1} \quad (5.11)$$

$$c_1 = \left(\frac{d_{\text{eff}}}{2}\right)^{\frac{5}{2}}\left(\frac{105}{2\pi}\right)^{-\frac{1}{2}}\left(C_{T_j}A_ix_0\right)^{-\frac{5}{6}} \quad (5.12)$$

where d_{eff} is the effective rotor diameter, and $R_{9.5}$ is the wake radius at a distance of 9.5 rotor diameters downwind of the turbine.

$$d_{\text{eff}} = d\sqrt{\frac{1+\sqrt{1-C_{T_j}}}{2\sqrt{1-C_{T_j}}}} \quad (5.13)$$

$$R_{9.5} = 0.5(R_{nb} + min[H, R_{nb}] \quad (5.14)$$

where H is the hub height, and R_{nb} is an empirical relationship related to the ambient turbulence:

$$R_{nb} = max\left[1.08d,\ 1.08d + 21.7d(I_a - 0.05)\right] \quad (5.15)$$

The formulation of Equation 5.14 takes into account what is known as the blockage effect. This effect describes the situation in which the wake radius exceeds the hub

height. In this case, a correction is made to ensure that the ground effect is taken into account.

What is presented above is known as the first order Larsen wake model. A second order model also exists which introduces an additional term to the velocity deficit to better describe the behaviour in the near wake [21]. As turbines will generally not be placed within the near wake of another turbine as it represents a potential safety risk, it was decided that the first order Larsen model would be sufficient for implementation in this tool.

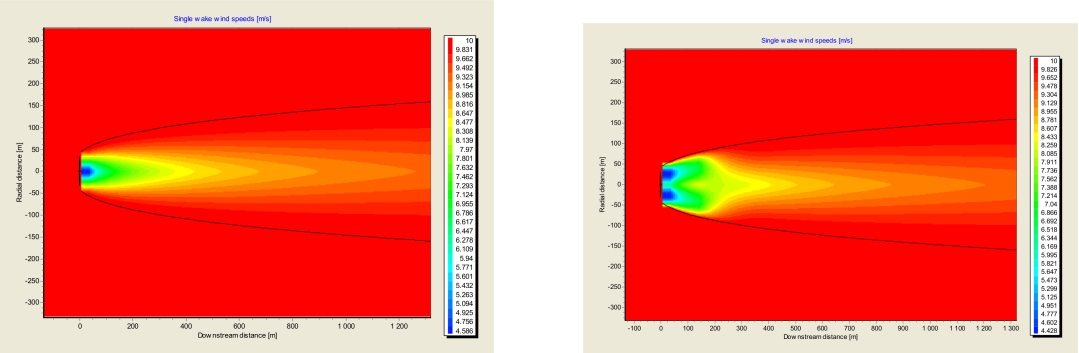

(a) G.C. Larsen First Order **(b)** G.C. Larsen Second Order

Figure 5.4: G.C. Larsen single wake. Generated using WindPRO [172].

As can be seen in Figures 5.4a and 5.4b, the near wake profile of the second order Larsen wake model is significantly different from the first order, with a double dip profile rather than the Gaussian profile of the first order. The shape of the far wake is, however, still Gaussian in the second order model.

No agreed upon method exists for superposing the single wakes modelled by the Larsen wake model, however, either linear superposition or sum of squares superposition tend to be used [53, 165]. Both of these approaches are discussed in greater detail in Section 5.4.5.

It should be noted that the Larsen model is sometimes a challenging model to implement as a number of versions exist each of which offers slight variations on the formulations above. Common variations that are seen in the literature include the following three equations which are often seen in some combination [21, 53, 165, 172, 174, 175]:

$$R_w = \left(\frac{35}{2\pi}\right)^{\frac{1}{5}} \left(3c_1^2\right)^{\frac{1}{5}} \left(C_t A \left(x + x_0\right)\right)^{\frac{1}{3}} \tag{5.16}$$

$$x_0 = \frac{9.5d}{\left(\frac{2R_{9.5}}{d}\right)^3 - 1} \tag{5.17}$$

$$c_1 = \left(\frac{d}{2}\right)^{\frac{5}{2}} (C_t A x_0)^{\frac{-5}{6}} \tag{5.18}$$

This present work, however, opted to use the formulations given earlier in this section as they were found to have the strongest agreement with observed values even if they did not correspond to the formulation used by similar studies.

5.4.3 Frandsen Model

Yet another analytic wake model developed at Risø DTU is the Frandsen wake model. This model was originally developed as part of the Storpark Analytic Model (SAM) with the goal of identifying not only the optimal distances between turbines within a wind farm, but also the optimal distance between large wind farms [165]. Unlike the previously described explicit wake models, the Frandsen model is unique in that it has an advanced method of superposing the wakes with some consideration for the interaction between the wind farm and the planetary boundary layer (PBL). The Frandsen wake model describes three possible wake regimes in a wind farm accounting for multiple wakes in addition to a basic single wake formulation.

The Frandsen wake model was originally developed for large wind farms of rectangular geometries with regular spacing in both the downwind and crosswind directions. As a result of this, it therefore describes the single wake, or superposition of wakes within a large symmetrical wind farm. Though this wake model is rarely used as it was originally formulated, it has played a vital role in modelling the interactions between wind farms and the PBL [24].

Like other explicit models, the Frandsen single wake model is based on the actuator-disk theory and in fact, like the Jensen model, the extent of the velocity deficit is dependent on the proportion of the rotor swept area that is within wake affected flow. The expansion of the wake, however, differs significantly from the Jensen model, with the three different regimes of the model defined depending on how wakes have merged.

The three regimes are highlighted in Figure 5.5. The first regime describes where multiple wakes overlap merge in a single row, and step increases in the wake diameter are observed directly following a turbine. Regime two represents where the wakes from neighbouring rows meet and no further lateral wake expansion occurs. In regime two, however, there is still vertical expansion of the wake in order to satisfy the momentum equations. In the third regime, the wind farm is thought to be in balance with the planetary boundary layer. This regime occurs downwind of large wind farm. It is proposed that within a wind farm regimes one and two will occur, while regime three should be used to describe the wake interactions between large wind farms adjacent to one another [16, 24]. This model was one of the first models to consider the interaction

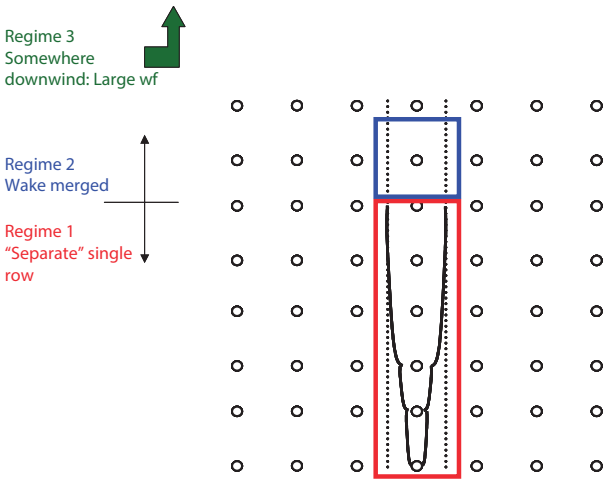

Figure 5.5: Visual description of wake regimes; wind from the south, parallel to turbine rows. Figure from Frandsen et al. [24].

between the wind farm and the PBL. This interaction is one that would be expected in especially large wind farms like those planned for offshore sites.

The wake diameter in the Frandsen model is given by:

$$d_w = d \times max\left[\beta, \alpha s\right]^{\frac{1}{2}} \Psi \tag{5.19}$$

where α is 0.7, Ψ is a factor to account for the stepwise increase in wake diameter directly behind a rotor, and β is given by:

$$\beta = \frac{1 + \sqrt{1 - C_{T_j}}}{2\sqrt{1 - C_{T_j}}} \tag{5.20}$$

In a single wake, the velocity is given by:

$$U = \begin{cases} \frac{U_\infty}{2}\left(1 + \sqrt{1 - 2\frac{A_i}{A_w}C_T}\right), & \text{if } a \leq 0.5 \\ \frac{U_\infty}{2}\left(1 - \sqrt{1 - 2\frac{A_i}{A_w}C_T}\right), & \text{if } a > 0.5 \end{cases} \tag{5.21}$$

where a is the axial induction factor.

$$a = 1 - \frac{U}{U_\infty} \tag{5.22}$$

where U is the wind velocity at the rotor plane.

The theory that Frandsen introduced in his model also includes the interaction between the wake and the planetary boundary layer which are potentially of great importance when considering large offshore wind farms (this is discussed further in Section 5.4.8). As a result of this, though a "single wake" can be described, this considers a single wake of a turbine within a large wind farm. The wake profile behind a single turbine is shown in Figure 5.6.

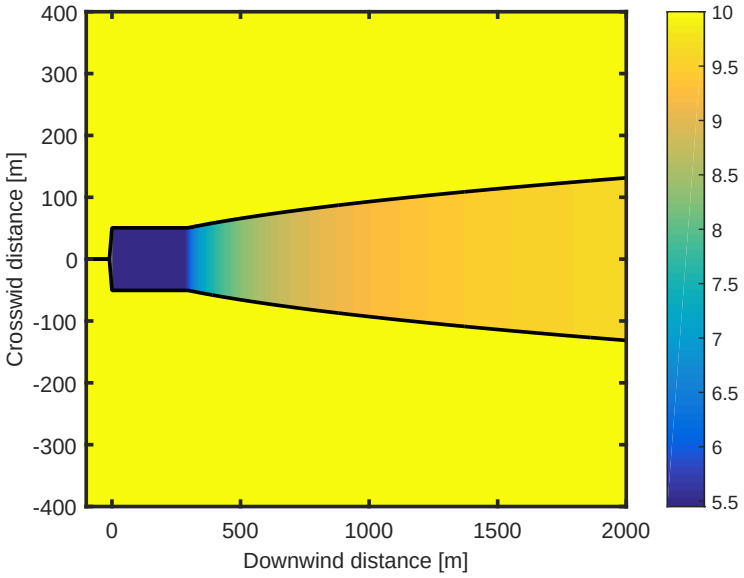

Figure 5.6: Frandsen single wake model. Free-stream wind velocity is 10 m/s from the west.

5.4.4 Ishihara/University of Tokyo Model

The last of the kinematic models discussed here is the Ishihara model developed at the University of Tokyo [23]. This model is unique among the explicit models considered in that it accounts explicitly for both the ambient turbulence as well as the mechanical generated turbulence in the wake recovery zone. This model was originally developed based on wind tunnel experiments, and therefore includes a number of empirical constants. Unfortunately, little work has been done to validate or adjust this model to represent real wind farms at full scale [167, 176]. Like the other models described, this is a single wake model which uses a sum of squares method for superposing the single wakes.

In this model, the wake diameter is given by:

$$d_w = \frac{k_1 \left(C_{T_j}\right)^{\frac{1}{4}}}{0.833} d^{\left(1-\frac{p}{2}\right)} x^{\frac{p}{2}} + d \tag{5.23}$$

where p is a function of the ambient turbulence, I_a, and the mechanically generated turbulence, I_w.

$$p = k_2 \left(I_a + I_w \right) \tag{5.24}$$

The mechanically generated turbine turbulence is given by:

$$I_w = \frac{k_3 C_T}{max\left[I_a, 0.03 \right]} \left(1 - e^{\left[-4 \left(\frac{x}{10d} \right)^2 \right]} \right) \tag{5.25}$$

For a single wake, the velocity experienced by a downwind turbine is given by:

$$U_i = U_\infty \cdot \frac{\sqrt{C_T}}{32} \left(\frac{1.666}{k_1} \right)^2 \left(\frac{x}{d} \right)^{-p} e^{-\frac{r^2}{d_w^2}} \tag{5.26}$$

From the original experiments, the k parameters were found to be:

$$k_1 = 0.27 \tag{5.27}$$

$$k_2 = 6.00 \tag{5.28}$$

$$k_3 = 0.004 \tag{5.29}$$

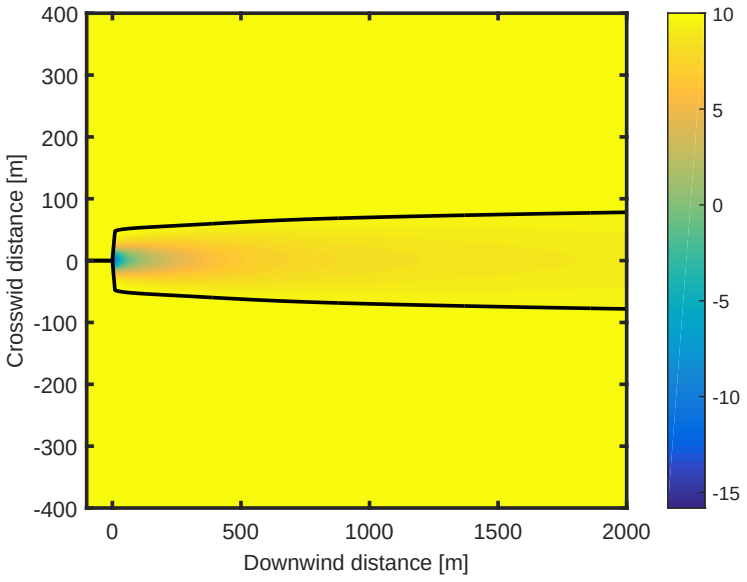

Figure 5.7: Ishihara single wake model. Free-stream wind velocity is 10 m/s from the west.

As can be seen in Figure 5.7, the Ishihara wake model poorly describes the near wake with velocities directly behind the rotor reaching speeds approaching -15 m/s in this example case. Though there is a velocity reduction in the wind directly behind the rotor in all wake models, this is the only model of those implemented here that

predicts a reversal in wind direction directly behind the rotor. The reversal of flow is unrealistic as it would reverse the pressure gradient across the rotor plane representing an impossible situation. This indicates that the near wake region is poorly defined using the Ishihara wake model and the results up to approximately three rotor diameters should be ignored. Further uncertainty can be expected as the model has been tuned using wind tunnel data at model scale rather than data at full scale. It can be expected that further tuning will be necessary in order to make use of this wake model for real sites.

5.4.5 Wake Superposition

In general, analytic wake models have been developed to describe the wake behind a single turbine. However, in large offshore wind farms, a turbine will often be operating within the wake of a number of upwind turbines. Some superposition formulae is therefore necessary in order to superpose the single turbine wakes in order to effectively model the wind speed that a turbine will experience when operating within the bounds of multiple wind turbine wakes.

As the analytic wake models do not represent the physics of the merging and superposition of wakes, a mathematical approach has been taken. The methods employed for approximating the superposition of wakes therefore includes:

1. geometric sum;
2. linear superposition;
3. energy balance;
4. sum of squares; and
5. maximum deficit.

Each of these approaches takes a slightly different mathematical approach to estimate the wind speed experienced by a turbine operating within the wake of multiple upwind turbines. Respectively, each of these superposition methods are given by:

$$\frac{U_i}{U_\infty} = \prod_j \frac{U_{ij}}{U_j} \tag{5.30}$$

$$\left(1 - \frac{U_i}{U_\infty}\right) = \sum_j \left(1 - \frac{U_{ij}}{U_j}\right) \tag{5.31}$$

$$U_\infty^2 - U_i^2 = \sum_j \left(U_j^2 - U_{ij}^2\right) \tag{5.32}$$

$$\left(1 - \frac{U_i}{U_\infty}\right)^2 = \sum_j \left(1 - \frac{U_{ij}}{U_j}\right)^2 \tag{5.33}$$

$$U_i = U_\infty \left(1 - max\left[\frac{U_{ij}}{U_j}\right]\right) \qquad \forall j \in T \tag{5.34}$$

In general, the sum of squares (Equation 5.33) is recommended for use and has been found to provide the best agreement with data [165].

5.4.6 Ainslie Eddy-Viscosity Model

The second family of wake models is the implicit wake models also referred to as field models. These are based on either full or simplified CFD and as a result are computationally more intensive than the kinematic models. Field models come in a range of resolutions and computational times ranging from the simplest which do not differ significantly in terms of precision or computational time from kinematic models, to more advanced large eddy simulations which can take over several weeks to reach a solution for a single set of conditions. Direct numerical simulations are still considered to be too expensive computationally to be used for more than individual cases [25].

Of the field models, the most commonly employed model is the Ainslie or Eddy-Viscosity Wake Model. This wake model is one of the available wake models in the commercial wind farm design packages, WindFarmer, WindPro, and openWind [89, 158, 172]. The Ainslie Eddy-Viscosity model is a two-dimensional field model solving an axisymmetric set of time averaged Navier-Stokes equations using an eddy-viscosity closure [170, 172]. A closure problem arises due to the inclusion of a non-linear Reynolds stress term in the RANS formulation. This is 'closed' by using the eddy-viscosity formulations which relate the turbulence stresses to the mean flow. This is a similar simplification of the flow is to that of the Larsen model and the Ainslie Eddy-Viscosity model is therefore not a full field model. A pictorial description of this model is shown in Figure 5.8.

In cylindrical coordinates the continuity equation is given by:

$$\frac{1}{r}\frac{\partial rV}{\partial r} + \frac{\partial U}{\partial x} = 0 \tag{5.35}$$

where U and V are respectively the velocities in the x and r directions.

The RANS formulation gives the Navier-Stokes equation to be approximated to:

$$U\frac{\partial U}{\partial x} + V\frac{\partial uU}{\partial r} = -\frac{1}{r}\frac{\partial\left(r\overline{UV}\right)}{\partial r} \tag{5.36}$$

The Reynolds Stress term ($\overline{UV}$) is closed using the eddy-viscosity ($\varepsilon(x)$):

$$-\overline{UV} = \varepsilon(x)\frac{\partial U}{\partial r} \tag{5.37}$$

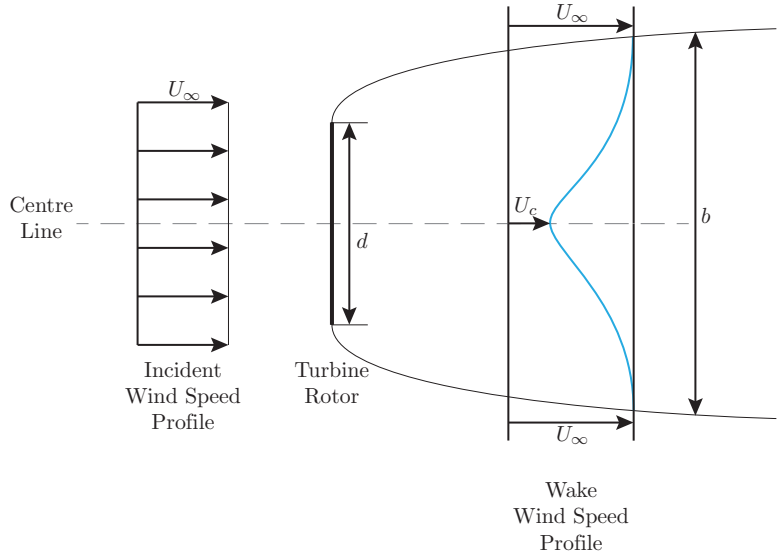

Figure 5.8: Wake profile used in the Ainslie Eddy-Viscosity model. Figure inspired by DNV GL - Energy [158].

The eddy-viscosity is given by two terms, the ambient eddy-viscosity (ε_a) and the eddy-viscosity generated due to the wind shear in the wake of a turbine (ε_w):

$$\varepsilon(x) = \varepsilon_a + \varepsilon_w(x) \tag{5.38}$$

The eddy-viscosity generated due to the wake is given by:

$$\varepsilon_w(x) = kb(U_\infty - U_c(x)) \tag{5.39}$$

where k in this case is an empirical constant found to be 0.015 [165]. The parameter b is the wake width which is given by:

$$b = \sqrt{\frac{3.56C_T}{8D_m(1 - 0.5D_m)}} \tag{5.40}$$

where D_m is the velocity deficit along the centreline of the wake:

$$D_m = 1 - \frac{U_c}{U_\infty} \tag{5.41}$$

The wake deficit is initialized using the following empirical equation such that the wake deficit at a distance of two rotor diameters downwind of the the turbine is given by:

$$D_{m_i} = C_T - 0.05 - (16 \cdot C_T - 0.5)\,\frac{I_a}{10} \tag{5.42}$$

Ainslie assumed a Gaussian profile of the wake and therefore the velocity in the wake is given by:

$$1 - \frac{U}{U_\infty} = (U_\infty - U_c)\, exp\left(-3.56\left(\frac{r}{b}\right)^2\right) \tag{5.43}$$

Some variants of the Ainslie Eddy-Viscosity model exist applying correction terms to the boundary condition to improve the description of the near wake. In order to avoid accurate accounting of the pressure gradients in the wake, an assumption was made by Ainslie that at a distance of two rotor diameters downwind of the turbine, the velocity profile is Gaussian distributed [165, 170, 172]. Using the initial conditions shown above, the two-dimensional flow field can be solved using a numerical method such as the Crank-Nicolson method [89, 177, 178].

5.4.6.1 Simplified Ainslie Eddy-Viscosity

Based on the full solution of the eddy-viscosity model it was found that the initial Gaussian shape profile is preserved further downwind. Therefore the wake can be parametrized by the centreline velocity profile behind the rotor and the wake width. These assumptions, supported by the full solution to the Navier-Stokes equations, simplify the above equations to a single ordinary differential equation (ODE) with the same wake initialization parameters at a distance of two rotor diameters behind the turbine [177]. The simplified ODE can therefore be given to be (see Appendix A for the derivation of this ODE):

$$\frac{dU_c}{dx} = \frac{16\varepsilon\left(U_c^3 - U_c^2 - U_c + 1\right)}{U_c C_T} \tag{5.44}$$

As this is a first-order differential equation, a numerical integration scheme using a 4th order Runge-Kutta method can be implemented to solve for the velocity deficit within the wake. It should be noted that in this methodology, all parameters including U_c, U_∞, b, x, and r are non-dimensionalized using the free-stream wind velocity U_∞ and the rotor diameter d as appropriate. Validation by Anderson [177] in Figure 5.9 shows that the simplified model closely matches the original Ainslie Eddy-Viscosity model with regards to the velocity deficit while resulting in reduced computational time. The single wake profile of this model is shown in Figure 5.10.

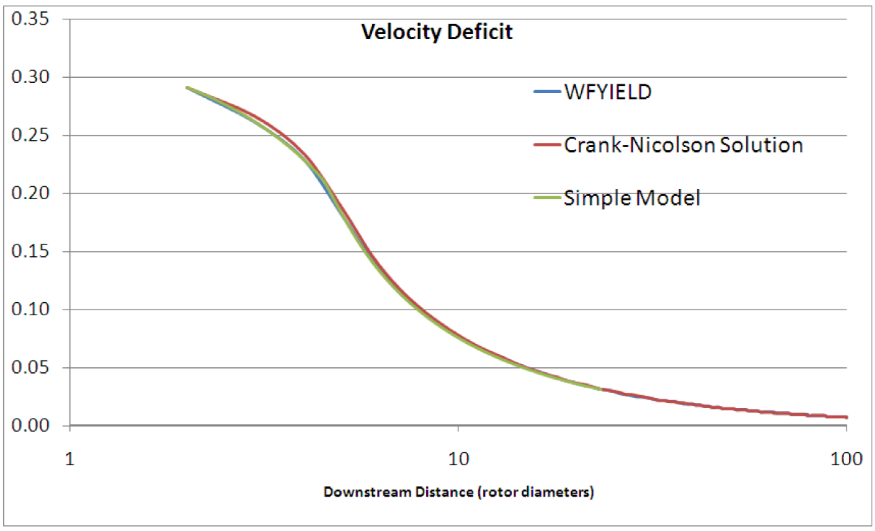

Figure 5.9: Validation of the simplified eddy-viscosity model performed by Anderson [177].

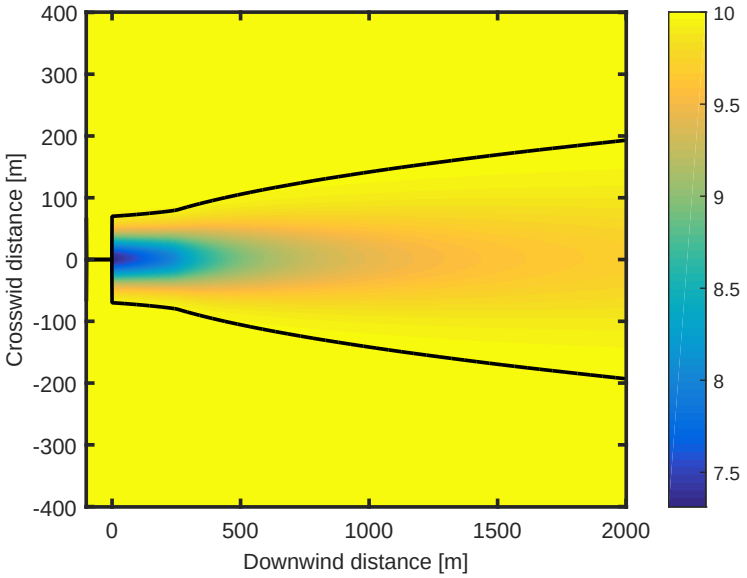

Figure 5.10: Simplified Ainslie Eddy-Viscosity single wake model. $C_T = 0.4$, $I_a = 10\%$.

5.4.7 Further Field Models

Increasing in complexity, implicit models include three-dimensional field models which are either full CFD or parabolized Navier-Stokes equations. Of these, the full CFD models tend to better describe the near wake behaviour [179].

Of the three dimensional field models, the most well known is WAKEFARM which was developed by ECN as part of the European EfficieNt Development of Offshore WindFarms (ENDOW) project. WAKEFARM is a 3D parabolized RANS code using

an eddy-viscosity turbulence closure. Boundary conditions are applied at 2.25 rotor diameters where the far wake is considered to begin and correction factors are used to describe the near wake. Modifications to the WAKEFARM tool have also allowed both anisotropic and isotropic turbulence models to be used with better results coming from the move to an isotropic model. WAKEFARM has been in development for a number of years now, and ECN continues to identify improvements to the code, such as changing the initial velocity deficit profile from Gaussian to double-dip in the near wake similar to the second order Larsen analytical model [165, 180].

Another family of field models is that of elliptic field models using generalized actuator discs or actuator lines [163, 165, 181]. These model types are widely used to achieve a better description of the near wake. However, they come at the price of increased computational time and are generally only considered for a single cases.

Three-dimensional field models are widely considered to be too computationally intensive for use in a layout optimization tool as single solutions often take many hours [17, 165]. Even two-dimensional field models are not recommended for an optimization process with both WindPro and WindFarmer recommending the use of the Jensen/Park wake model when optimizing a layout [158, 172]. Though the explicit models are considered to have reduced accuracy when compared to field models, they are thought to be sufficiently accurate and are significantly quicker leading to their use in optimization tools [17, 53, 182].

5.4.8 Interaction of Wakes with the Planetary Boundary Layer

It has been recognized that wind turbines and wind farms are not passive elements in the wind, and in fact there is an interaction between the wind farms and the PBL. As a result of the omission of this interaction in kinematic wake models, these models will under-predict the wake deficit in the interior of a large wind farm, a wind farm containing more than five rows of turbines, resulting in over estimation of wind farm AEP [24, 183].

In order to improve the accuracy of analytic wake models, semi-empirical corrections have been developed based on the observations made at existing large wind farms such as Horns Rev I and Nysted. These semi-empirical corrections extend the existing analytic wake models improving the model performance and suitability of these models for large wind farms [158, 183, 184]. This is done by modelling the interaction between the wind farm and the PBL similar to how a forest or change in surface roughness is modelled in wind flow models. These models develop an internal boundary layer (IBL) as a result of a change in surface roughness, the development of which results in a change in the wind speed [185].

The common approach for introducing the large wind farm correction (LWC) with an analytic wake model is to use the development of the IBLs to update the free stream wind speed, and then apply any standard analytic wake model. In this regard, the LWC is an independent step before the application of the wake model.

The LWC is dominated by the boundary layer modification which is a result of the development of an IBL behind each wind turbine. The height of this IBL grows with the following relationship given by Garratt [185] as a function of the fetch x and the higher of the two roughness values at the change z_{02}:

$$\frac{dh}{dx} \propto \frac{1}{ln\left(\frac{h}{z_0}\right)} \tag{5.45}$$

DNV GL - Energy [158] give a modified version of the IBL growth based on their validation studies performed in wind tunnels, onshore wind farms, and offshore wind farms [171]:

$$\frac{dh}{dx} = \frac{9}{10} \cdot \frac{1}{ln\frac{h}{z_{02}}} \tag{5.46}$$

When applying the LWC it is modelled that there are two IBLs produced, one at the top of the rotor plane, and one at the bottom. The velocity deficit therefore becomes a function of where the downwind rotor is relative to both of these IBLs [158, 183, 184]. The development of two IBLs is shown in Figure 5.11.

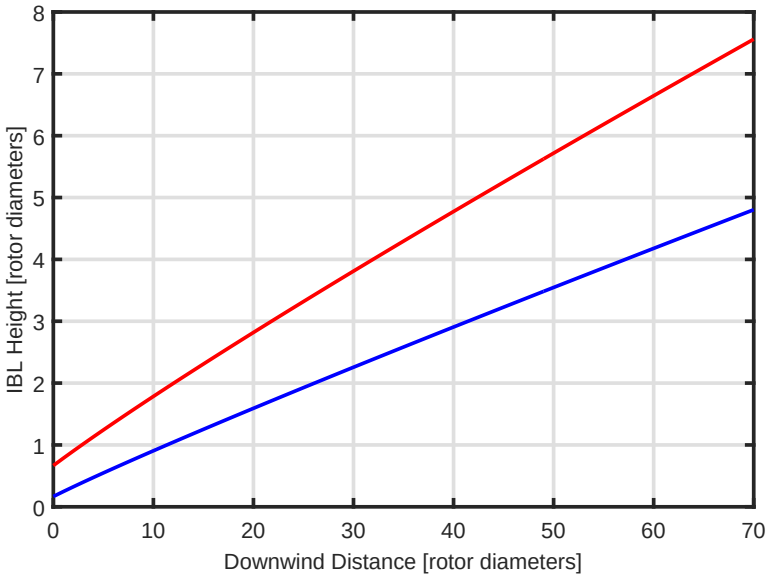

Figure 5.11: IBL development as a result of a turbine.

Alternatively, models such as the deep-array wake model (DAWM) opt to define the wake as only being a result of the IBL development [184]. This approach uses either a traditional analytic wake model or the velocity deficit due to the IBL growth depending on the applicability criteria defined in the model. Unlike the LWC approach, the DAWM therefore does not use the IBL growth in conjunction with an analytic model, but simply applies one or the other depending various application criteria defined as part of the model [175].

5.5 Validation of Wind Turbine Wake Models

Previous studies have looked at the expansion and applicability of these single wake models to wind farms and the fields involving the superposition and interaction between multiple wakes. These have been summarized and outlined by Jansen [175].

Additional studies have also looked at applying different wake models to available time series data from offshore wind farms such as Horns Rev I, Nysted, Vindeby, Lillgrund, and Middelgrunden [53, 167, 186–188].

Looking specifically at the application of kinematic, explicit models for integration into a layout optimization tool, the study by Tong et al. [176] compared the Jensen/Park, Larsen (first order), Frandsen, and Ishihara wake models behind a single turbine. Similarly, Gaumond et al. [53] considered a single row of the Horns Rev wind farm and showed that the modelled power deficit as predicted by the Jensen, Larsen, and FUGA wake models are validated by the observed power deficits.

As published studies have considered single turbines or a single row of turbines rather than an entire wind farm, it is worth exploring the applicability of the wake models to entire wind farms. This section therefore applies the different kinematic wake models, the simplified Ainslie Eddy-Viscosity model, and the LWC where applicable to full wind farms in order to assess their overall suitability for inclusion in the wind farm layout optimization framework.

5.5.1 Middelgrunden Wind Farm

In order to assess the wake models it was decided to use data available for Middelgrunden wind farm in Denmark to compare four existing wake models. The analytic models of N.O. Jensen, G.C. Larsen, and Ishihara were compared in terms of accuracy and computational time to one another and to a simplified representation of the Ainslie Eddy-Viscosity field model. The Middelgrunden site poses a unique opportunity as the turbines are spaced at only 2.4D. Though this close spacing is in a non-dominant wind

direction, looking specifically at the time periods when the wind is in this direction allows us to establish how these wake models compare for closely spaced turbines.

An advantage of Middelgrunden wind farm is that 10-minute averaged SCADA data for four years (2001-2004) is available courtesy of the Virtual Wakes Laboratory and Middelgrunden Wind Cooperative [189]. Given that the dominant wind direction at Middelgrunden is perpendicular to the single row of turbines, the site is not the best suited for a general wake study. Though the reduction in AEP due to the wake effect is minimal, within specific wind sectors the impact is quite apparent given the close spacing along these sectors. The wind rose describing the site resource over this period is shown in Figure 5.13.

The wake modelling done at Middelgrunden as part of this study can therefore be further subdivided into two major steps: the selection of relevant data to explore and the application of the wake models to the selected data periods.

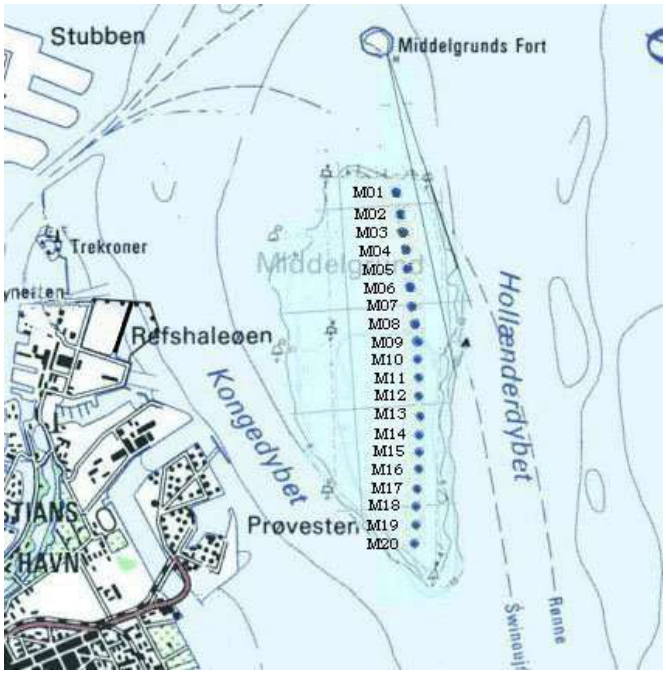

Figure 5.12: Turbine positions at Middelgrunden wind farm. Courtesy Middelgrunden Wind Cooperative [190].

Given that previous studies had already explored the flow conditions at Middelgrunden wind farm, it was decided to use a similar methodology for the selection of the relevant data [187, 191]. Middelgrunden wind farm is comprised of twenty Bonus B-76/2000 turbines placed along a single arc in a roughly North-South orientation as shown in Figure 5.12. Wakes are therefore only expected when the wind direction is parallel to the direction of this arc (357°). As wakes are the focus of this study, it was important

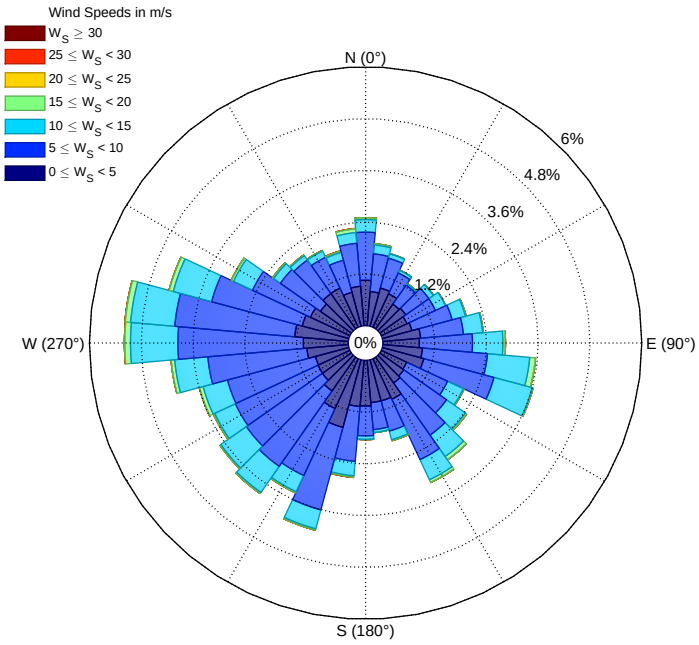

Figure 5.13: Wind rose for Middelgrunden wind farm based on time-series data from 2001-2004. Data used courtesy of The Middelgrunden Wind Cooperative [189].

to filter out the data periods during which the wind was perpendicular to the arc of the turbines resulting in no power loss due to wakes. Although winds from the South would be expected to result in measurable wake losses it is not considered in this study as due to the proximity to shore and as a result of the shorter fetch a more significant speed-up is observed [191]. Given Middelgrunden's proximity to shore it was important to ensure that the selected data period represented offshore conditions where possible.

In order to not bias the results, it was also important to use time periods where data was available for all twenty turbines, all twenty were grid connected, and all were generating power. In order to do this, the data-set was filtered based on the mean active power for each interval to ensure that they were generating, and based on the generator RPM in order to ensure that they were grid-connected. Any time intervals where any one wind turbine was not operating or was in an error-state was immediately filtered out.

Based on these filtering criteria, a number of different sector sizes were considered to observe how this affected the accuracy of the wake models. For each case, the same 357° azimuth was considered. It was also later decided to relax the direction criteria such that turbine 1, the northernmost turbine, was only checked against the incoming wind direction rather than all the turbines. This is similar to the methodology used in studies at Horns Rev wind farm [53, 167].

Table 5.1: Middelgrunden Data Selection Scenarios

Sector Size	Turbines Checked	Time Periods
±30°	All	1646
±15°	All	25
±30°	Turbine 1	4701
±15°	Turbine 1	2299
±10°	Turbine 1	1609
±5°	Turbine 1	930
±1°	Turbine 1	248

For the seven cases outlined in Table 5.1 the Jensen, G.C. Larsen, Ishihara, and Simplified Eddy-Viscosity wake models described were run. Given the size of the wind farm, the Frandsen model and the LWC correction were not applied to this site, as the wind farm was thought to be too small for these models to be applicable. The total normalized production value for each of the twenty turbines was then computed across the entire data-set while the computational time was measured. The analysis was also repeated for individual wind speed bins to observe the model performance at specific wind speed ranges. As would be expected, the computational time for each of the wake models was roughly linear with the number of time periods for which the wakes needed to be computed.

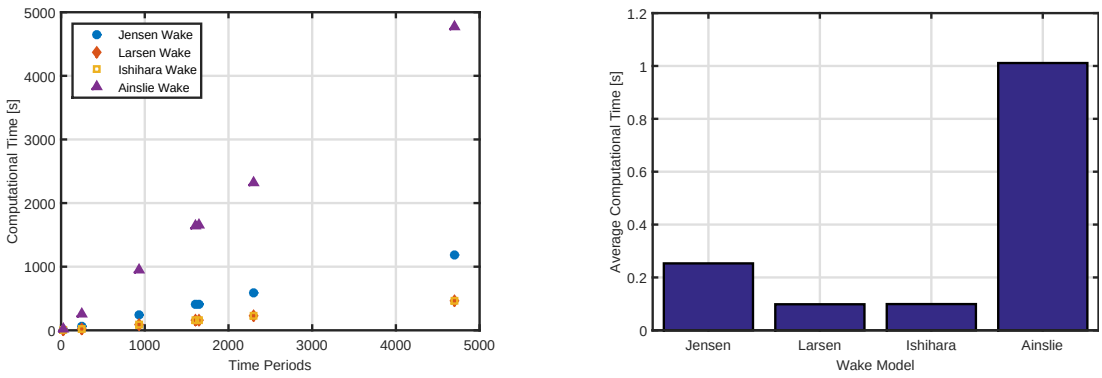

(a) **(b)**

Figure 5.14: Computational time for each wake model and filtering criteria is shown in (a) with the average computational time normalized by the number of data points is shown in (b).

As can be seen from Figure 5.14, for each case the Larsen and Ishihara models were consistently the quickest with very little difference between them, while the Simplified Eddy-Viscosity model was consistently the slowest. This is not unexpected as field models such as the Eddy-Viscosity model in general tend to be more computationally intensive than kinematic models such as the Jensen, Larsen, and Ishihara models.

To begin with, the wind direction criteria was applied to all turbines. Applying the direction constraint in this manner lead to few valid time periods as is indicated in Table 5.1 as the wind direction needed to be within the identified sector for all turbines in the given time period. In fact, reducing the sector size to $\pm 10^\circ$ about the azimuth led to no valid time periods in the data-set. Therefore the application of the wind direction constraint to all the turbines is limited to only considering $\pm 30^\circ$ and $\pm 15^\circ$ sectors about the azimuth.

Figure 5.15 shows the normalized average power produced from each turbine under the two scenarios in which the wind direction requirement was applied to all turbines. From this it can be observed that all the wake models correctly predict a decrease in the power produced relative to the first turbine in the arc. For the two scenarios considered, the Larsen model was found to be the most accurate for the larger sector size (12.48% RMS error), while the Jensen model was the most accurate for the smaller sector (8.09% RMS error). The smaller sector size was found to have lower RMS error for each of the models compared to the larger sector size indicating the models are generally more suitable for the smaller sector size (see Table 5.2). The Jensen and Ishihara models showed the greatest improvement with their RMS error decreasing 10.62 percentage points and 8.15 percentage points respectively. The Larsen and Simplified Eddy-Viscosity models, however, only showed a 1.28 percentage point and 3.04 percentage point decrease respectively.

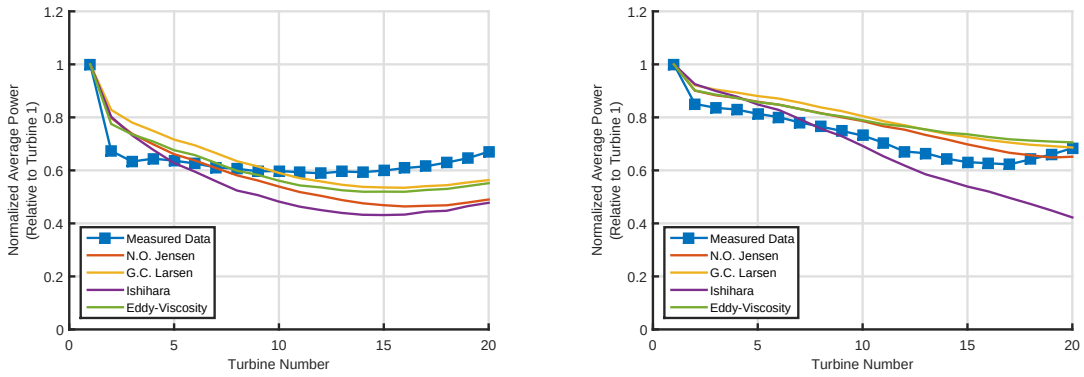

(a) 357°±30° **(b)** 357°±15°

Figure 5.15: Wake deficit - wind direction criteria applied to all turbines

Table 5.2: RMS Error, Directional Criteria Applied to All Turbines

Sector	Jensen	Larsen	Ishihara	Eddy-Viscosity
±15°	**8.09%**	11.19%	15.10%	10.08%
±30°	18.71%	**12.48%**	23.25%	13.13%

Relaxation of the directional criteria as described earlier was similar to the methodology used by Gaumond et al. [53, 186] and Crasto and Castellani [167] in their analyses of wakes at Horns Rev. With the relaxed wind direction sector, the wind direction criteria was only applied to the upwind turbine, turbine 1. By relaxing this directional criteria smaller sector sizes could be investigated. Figure 5.16 show the normalized power output from each of the turbines for the ±15° and ±30° sectors respectively. From these figures it can be observed that as in the previous scenarios a decrease in power output is observed down the line of turbines as would be expected. However, unlike the previous scenarios where the move from a ±30° sector to a ±15° sector resulted in improvements in the wake models, the application of the directional criteria to only the first turbine appears to increase in error as the directional sectors decrease in size (see Table 5.3). Best performance was in fact observed for all the wake models when the largest sector size was considered. For this method of data selection, the Larsen model proved to be the most accurate for all but the smallest of the sector sizes when the Simplified Eddy-Viscosity gave marginally better results.

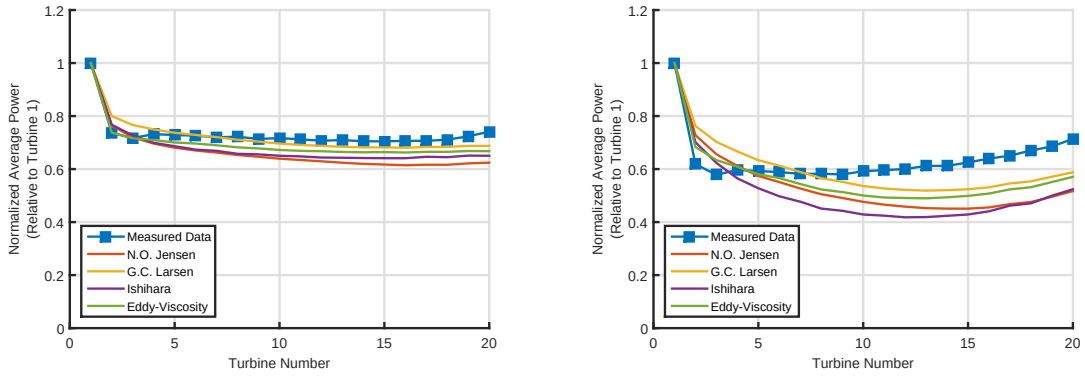

(a) 357°±30° **(b)** 357°±15°

Figure 5.16: Wake deficit - direction sector applied to turbine 1

Table 5.3: RMS Error, Directional Criteria Applied to Turbine 1

Sector	Jensen	Larsen	Ishihara	Eddy-Viscosity
±1°	45.91%	41.76%	61.20%	**41.09%**
±5°	38.73%	**33.40%**	53.58%	34.19%
±10°	30.97%	**23.77%**	40.20%	26.15%
±15°	23.84%	**15.88%**	27.44%	18.67%
±30°	15.59%	**8.34%**	13.52%	11.23%

As would be expected, the behaviour of the wakes vary with the wind speed and the wake models are therefore more accurate when applied at specific wind speeds at this site. Figure 5.17 shows the model behaviour at specific wind speeds. As can be seen in

this series of figures, the wake models all perform best around 8 m/s. High errors can be observed at both low and high wind speeds.

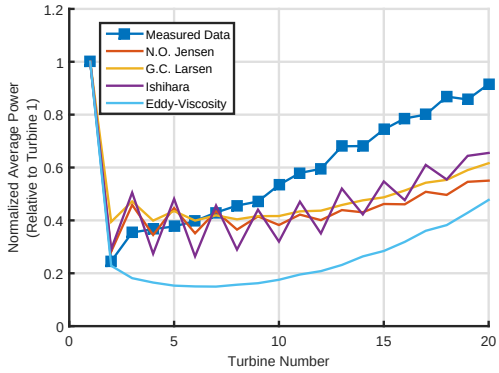

(a) 5 m/s Free Wind

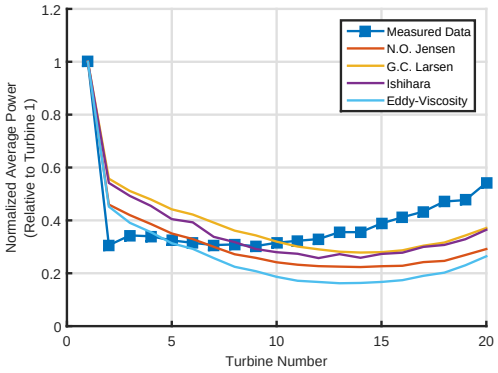

(b) 8 m/s Free Wind

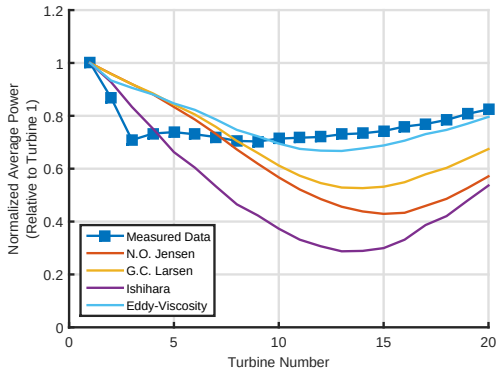

(c) 15 m/s Free Wind

Figure 5.17: Turbine waked wind velocities

Similar studies applied to Horns Rev found that the Larsen model best described the power deficit at Horns Rev [53, 167, 186]. These studies also found that decreasing the sector size beyond ±15° led to higher levels of error. Smaller sectors such as ±5° or ±1° therefore led to an over-estimation of the wake effect and the power deficits down a single line of turbines at Horns Rev. Similarly in the present study, smaller sectors such as ±10° or ±5° lead to higher levels of RMS error. This result did, however, not hold for the analysis in which all turbines were compared against the direction criteria.

Checking all the turbines against the direction criteria lead to difficult results due in part to the lack of data that satisfied the requirements. In fact, the smaller sector size under consideration, ±15°, had only 25 valid time periods thereby implying high levels of uncertainty due to the dearth of data. Though this scenario did result in lower RMS error than the case where the direction criteria was only applied to turbine 1, this needs to be further explored with larger data-sets.

Furthermore, checking all the turbines against the direction criteria resulted in lower levels of RMS error for similarly sized sectors. This is in fact as we would expect as comparing all turbines against the directional sector ensures that there is little variation in wind direction through the wind farm. It can be expected that the methodology which is similar to that of studies at Horns Rev, considering the direction only at one turbine, would be more applicable of the end-use in a layout optimization tool.

Interestingly, the simplified field model was not significantly more accurate than a simpler analytic model and in fact only outperformed the analytic models on one occasion. The Simplified Ainslie Eddy-Viscosity model was, however, consistently the slowest as expected due to the iterative nature required in solving it. The Jensen model, though the simplest in principle requires a relatively complex computation to determine the ratio of the rotor plane area that is within a wake and therefore suffers as a result of this. The Larsen and Ishihara models likely have similar computational times as they are both relatively simple and require the same order of computations in order to compute the waked velocities.

It is important to note that none of the wake models implemented include any consideration of wake drift or wake meandering. This omission does increase the uncertainty of these wake models, however, it is unclear to what degree [25, 68, 192].

The Bonus turbines in question are also have anemometers which are known to report erroneously low wind speeds [191]. The use of these anemometer readings therefore introduces some uncertainty and it is worth exploring a similar study where better data might be available.

The average wind speed measured by the anemometer on turbine 1 over the data period was 6.6 m/s indicating that the optimal region of the models may in fact be very close to the average condition at the site leading to the low levels of RMS error observed. Had the site had an average condition further from the accurate region of the models we could expect increased levels of error.

5.5.2 Horns Rev I

As part of the UpWind Project, a European FP6 project which ran from 2006 to 2011, Dong Energy A/S and Vattenfall Wind Power A/S allowed aggregated normalized data from Horns Rev I wind farm to made publicly available [193, 194]. Horns Rev I is located in the North Sea approximately 18 km off the west coast of Denmark and has been operational since 2002. The wind farm includes 80 Vestas V80-2.0 turbines with a total installed capacity of 160 MW arranged in an oblique rectangle (Figure 5.18). Given the regular orientation of the turbines at Horns Rev it gives a unique opportunity to compare the wake models for a full wind farm for a range of incoming wind directions.

Horns Rev I is often used as a test site for comparing wake models as the wind turbines are regularly spaced and there are a number of upwind met masts from which free stream wind data can be obtained. Often, full time-series data has been used for a comparison, however, the aggregated normalized data that is freely available can also be used. In this study, only the aggregated normalized data was available, and therefore no time-series data has been used.

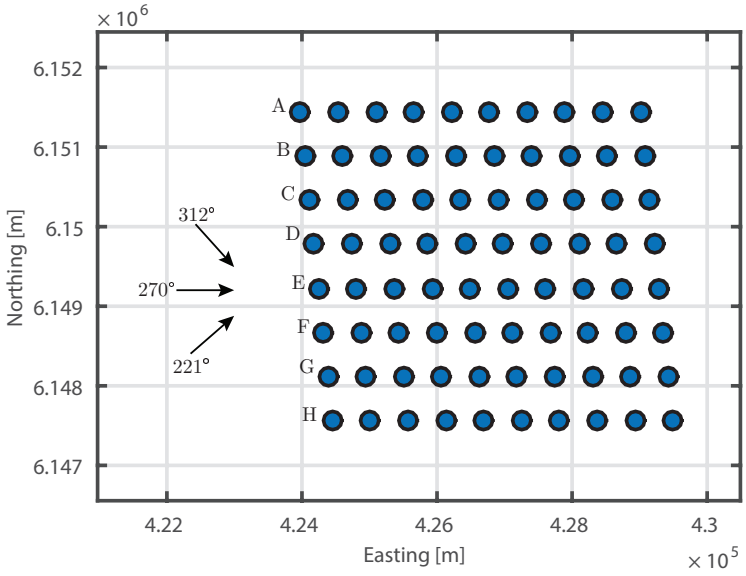

Figure 5.18: Layout of Horns Rev Offshore Wind Farm

The publicly available data consists of normalized power outputs for three incoming wind speeds (6 m/s, 8 m/s, and 10 m/s) and three wind directions (221°, 270°, and 312°) as measured by met masts positioned upwind of the wind turbines along each of these directions. For each of the three wind directions, a range of direction sector sizes have been aggregated. As this data has already been filtered and corrected, and there are met masts on site, many of challenges faced with the Middelgrunden data are avoided. As various sizes of direction sectors are provided as part of the Horns Rev I data-set, a similar study to what was done with Middelgrunden wind farm can be undertaken. This can not only compare the performance of the wake models, but the relative performance of the wake models for varying direction bin sizes.

Like Middelgrunden wind farm, the effect of wakes is clearly visible at Horns Rev for each the wind speeds under consideration as can be seen in Figure 5.19. Furthermore, Horns Rev is a sufficiently large wind farm that one would expect to observe the PBL interactions [171, 184]. The application of the LWC would therefore seem to be relevant. Previous work has used Horns Rev I to characterize the interaction between wind turbine wakes and the PBL, even going so far as having tuned these correction terms based on the results at Horns Rev [158, 184]. The present study has therefore tested

each wake model both with and without the large wind farm correction. The models under consideration are those previously described in Section 5.4:

1. N.O. Jensen;
2. G.C. Larsen;
3. Frandsen;
4. Ishihara; and
5. Simplified Ainslie Eddy-Viscosity.

Given the available data, a range of cases were selected to test the applicability of the models for a range of wind direction sector sizes and for both winds in-line with the turbine rows and misaligned winds. These 'off-axis' cases allow the wake models to be tested in cases in which multiple wakes which are not inline with one another affect one another. All the cases considered are shown in Table B.1 in Appendix B. Compared to the Middelgrunden cases considered in Section 5.5.1 comparison of the wake models at Horns Rev, shows not only the applicability of the wake models to a large wind farm with more wake interactions, but the applicability of the models for cases where there are wake interactions not only along the principal axis of the wind farm. Validation of the wake models at a number of sites is necessary in order to show that the wake models are applicable regardless of the geographic location of the wind farm and the atmospheric conditions specific to an individual wind farm site. For the application in the generic layout optimization framework it is important to ensure that the AEP module is not regionally biased.

The in-line case (Figures 5.19-5.23), shows that for all three wind speeds provided in the UpWind data set, there is a clear wind speed deficit as a result of the interaction between turbines and wind turbine wakes.

As was the case with the Middelgrunden cases studied, the performance of the wake models for the inline wind direction is greatly impacted by the size of wind direction sector under consideration (Figures 5.20 and 5.21).

For all the 27 cases, Table 5.4 show the average RMS error for each of the wake models based on the size of the direction sector. Table 5.5 shows the same results, but for the cases where the LWC is applied in addition to the standard wake models. As can be seen in these tables, at large direction sectors ($\pm 15^\circ$ and $\pm 10^\circ$) all the models behave accurately with a maximum RMS error of 6.61%. Interestingly, however, not all the models respond in the same way to the inclusion of the LWC. The N.O. Jensen and G.C. Larsen models show an improvement at $\pm 15^\circ$ with the LWC, however, they perform better for all the smaller sectors without the LWC. The Frandsen and Simplified Eddy-Viscosity models show improvements for both the $\pm 15^\circ$ and $\pm 10^\circ$ sector sizes with the LWC, but again for smaller sector sizes the models performs better without the LWC.

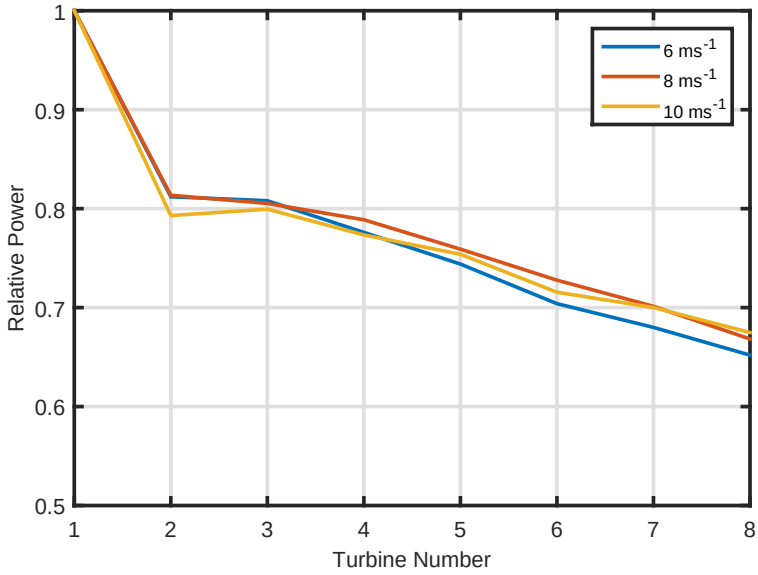

Figure 5.19: Power production along row E of Horns Rev I for winds with a direction of $270° \pm 15°$

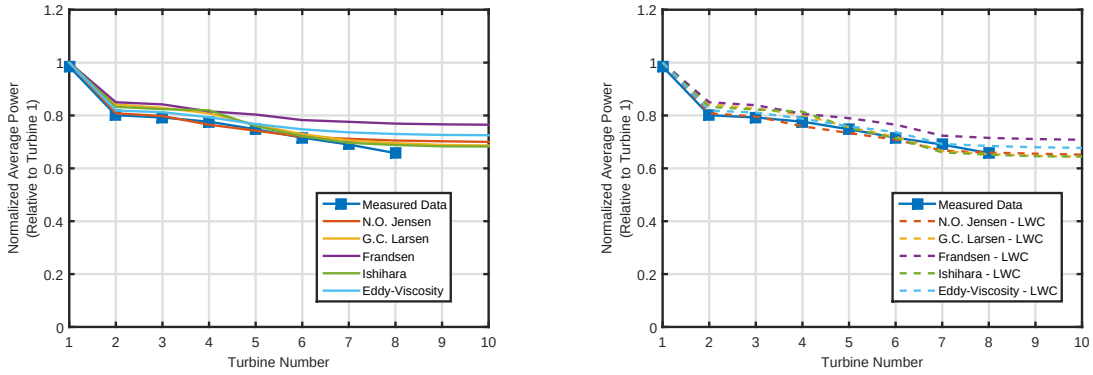

(a) Without LWC **(b)** With LWC

Figure 5.20: Horns Rev, Row E, 8 m/s, $270° \pm 15°$ with and without the LWC

The Ishihara model on the other hand is improved at the smallest sector size ($\pm 1°$) and the largest sector size ($\pm 15°$) while for all the sector sizes in between, the inclusion of the LWC increases the RMS error. From these results it is therefore unclear if the inclusion of the LWC at Horns Rev is justifiable.

Sorensen and Nielsen [195] had previously found when exploring the applicability of the LWC at Horns Rev that, "While an internal roughness seems to be a good idea at other locations it is apparently not appropriate on this location." This supports that Horns Rev I may in fact not be a relevant site for application of the LWC. Having said that, for wind direction sectors of $\pm 10°$ and $\pm 15°$ many of the models were capable of

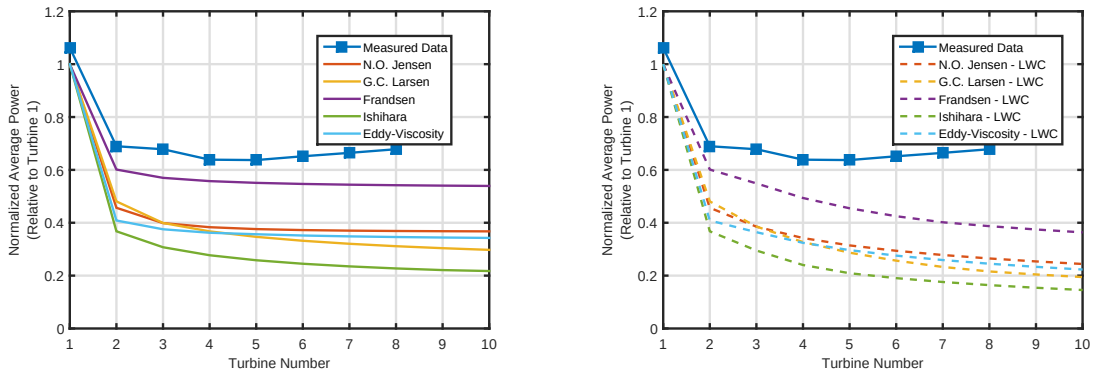

(a) Without LWC **(b)** With LWC

Figure 5.21: Horns Rev, Row E, 8 m/s, 270° ± 1° with and without the LWC

estimating the power output with an RMS error of less than 5% with the LWC only having a small impact on the performance.

Table 5.4: Horns Rev Wake Modelling - RMS Error by Sector Size

Sector Size	N.O. Jensen	G.C. Larsen	Frandsen	Ishihara	Eddy-Viscosity
±15°	**4.52%**	4.70%	6.61%	4.82%	5.09%
±10°	2.87%	2.90%	5.07%	2.95%	**2.75%**
±5°	12.86%	7.28%	**4.87%**	9.00%	9.31%
±2.5°	16.07%	20.41%	**5.29%**	27.54%	20.16%
±1°	24.59%	25.98%	**12.11%**	29.53%	23.87%
Average	13.24%	13.63%	**7.93%**	15.84%	13.23%

Table 5.5: Horns Rev Wake Modelling - RMS Error by Sector Size (With LWC)

Sector Size	N.O. Jensen	G.C. Larsen	Frandsen	Ishihara	Eddy-Viscosity
±15°	**4.61%**	4.69%	5.78%	4.80%	4.62%
±10°	3.95%	3.46%	3.37%	3.47%	**2.64%**
±5°	14.70%	9.22%	**6.78%**	10.34%	10.77%
±2.5°	23.42%	27.46%	**14.07%**	32.82%	26.23%
±1°	24.56%	27.45%	**14.14%**	29.24%	23.39%
Average	14.40%	15.17%	**9.33%**	16.53%	13.74%

Analysing the data from the perspective of wind speed shows that each of the models performs better at 8 m/s than they do at either 6 m/s or 10 m/s in the cases where the LWC is not applied (see Table 5.6 and Figures 5.22 and 5.23). With the LWC applied (see Table 5.7), the behaviour is a little more erratic with some models still performing

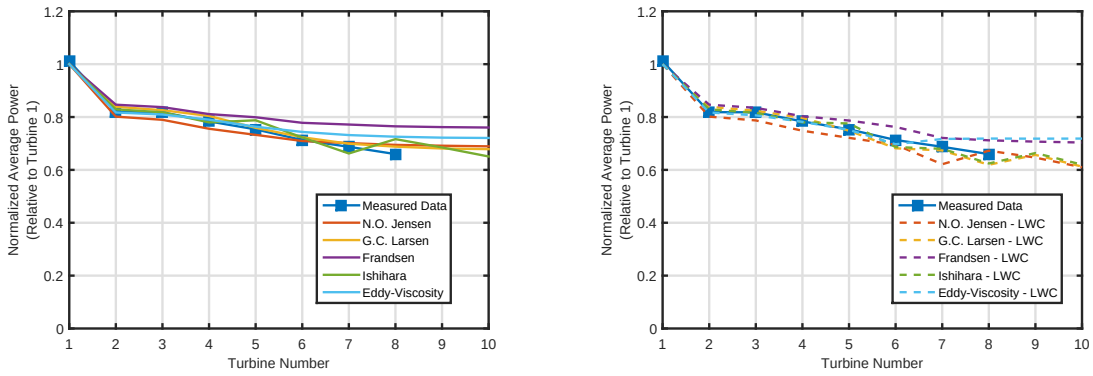

(a) Without LWC **(b)** With LWC

Figure 5.22: Horns Rev, Row E, 6 m/s, $270^\circ \pm 15^\circ$ with and without the LWC

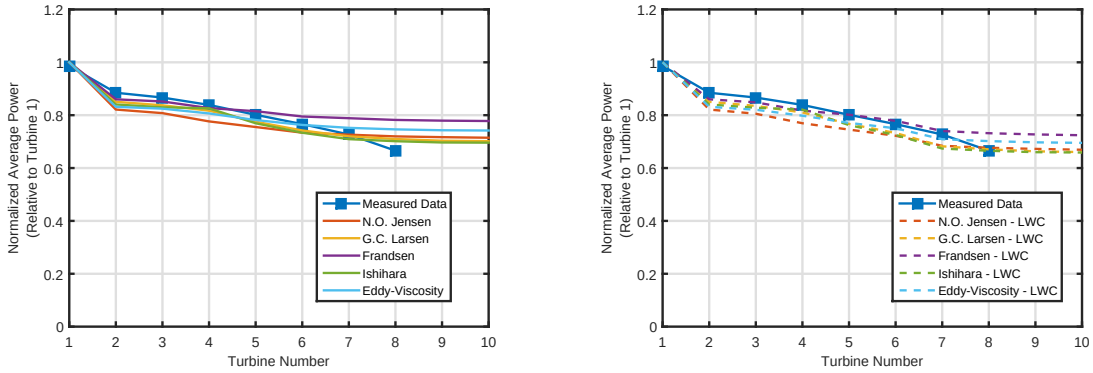

(a) Without LWC **(b)** With LWC

Figure 5.23: Horns Rev, Row E, 10 m/s, $270^\circ \pm 15^\circ$ with and without the LWC

best at 8 m/s (G.C. Larsen and Frandsen) while all the others appear to perform with lower RMS error at 10 m/s.

Table 5.6: Horns Rev Wake Modelling - RMS Error by Wind Speed

Wind Speed [m/s]	N.O. Jensen	G.C. Larsen	Frandsen	Ishihara	Eddy-Viscosity
6	14.64%	14.37%	**8.78%**	17.20%	14.18%
8	11.66%	11.87%	**6.90%**	14.69%	11.87%
10	13.42%	14.64%	**8.11%**	15.62%	13.65%

Finally, comparing the off-axis directions (Figures 5.24 and 5.25) to the inline direction (Figure 5.20) allows us to see that for Horns Rev, the models in question perform better for the inline direction, regardless of whether the LWC is implemented or not (see Tables 5.8 and 5.9). Although the models perform best for the inline direction, the

Table 5.7: Horns Rev Wake Modelling - RMS Error by Wind Speed (With LWC)

Wind Speed [m/s]	N.O. Jensen	G.C. Larsen	Frandsen	Ishihara	Eddy-Viscosity
6	17.04%	17.06%	**10.39%**	18.94%	15.27%
8	13.28%	13.24%	**8.44%**	15.86%	13.06%
10	12.87%	15.21%	**9.17%**	14.78%	12.89%

performance for these off-axis cases results in only a marginal increase in error for the $\pm 15^\circ$ case.

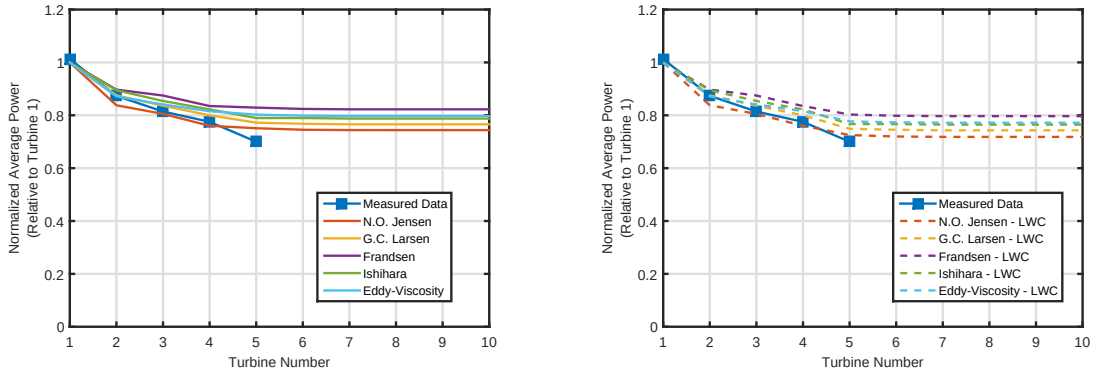

(a) Without LWC **(b)** With LWC

Figure 5.24: Horns Rev, Row E, 8 m/s, $221^\circ \pm 15^\circ$ with and without the LWC

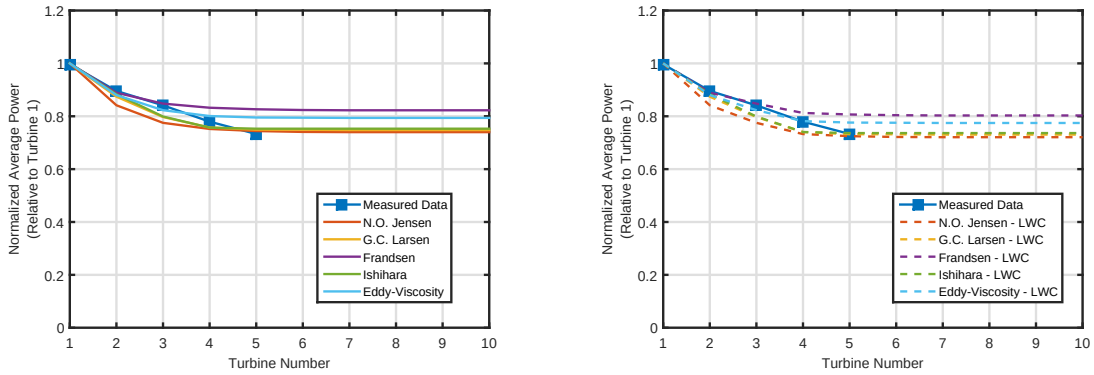

(a) Without LWC **(b)** With LWC

Figure 5.25: Horns Rev, Row E, 8 m/s, $312^\circ \pm 15^\circ$ with and without the LWC

These results have shown that for larger sector sizes of $\pm 10^\circ$ and $\pm 15^\circ$, these wake models all show accurate results. However, as the wind direction sector becomes narrower approaching 1°, the error increases significantly. This is consistent with what was observed at Middelgrunden indicating that in general these analytic models will perform best with wind direction sectors at least 20° or 30° wide. Furthermore, these

Table 5.8: Horns Rev Wake Modelling - RMS Error by Wind Direction

Wind Direction	N.O. Jensen	G.C. Larsen	Frandsen	Ishihara	Eddy-Viscosity
$221° \pm 15°$	**5.25%**	5.72%	7.64%	6.18%	6.23%
$270° \pm 15°$	**2.54%**	2.80%	5.17%	2.70%	3.07%
$312° \pm 15°$	5.78%	**5.57%**	7.01%	5.59%	5.98%

Table 5.9: Horns Rev Wake Modelling - RMS Error by Wind Direction (With LWC)

Wind Direction	N.O. Jensen	G.C. Larsen	Frandsen	Ishihara	Eddy-Viscosity
$221° \pm 15°$	**5.17%**	5.60%	7.26%	6.08%	5.90%
$270° \pm 15°$	2.64%	2.77%	3.70%	2.66%	**2.33%**
$312° \pm 15°$	6.01%	5.69%	6.38%	5.65%	**5.64%**

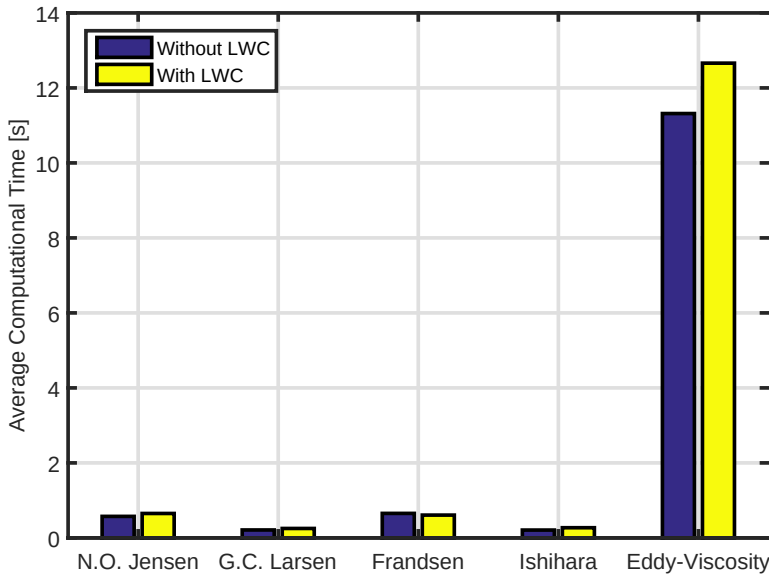

Figure 5.26: Computational time for each wake model both with and without the LWC when applied to Horns Rev I

results show that the LWC offers minimal improvements for a site where the theory says it should be applied. Given that the LWC requires additional calculations in addition to a traditional analytic wake model, the results here from Horns Rev indicate that this may not represent good value for the optimization framework as minimal improvements are observed for a significant increase in computational time. A comparison of the average computational time for each model both with and without the LWC is shown in Figure 5.26.

Based on the results of this comparison, it appears that using either the N.O. Jensen, G.C. Larsen, or Eddy-Viscosity model for large wind direction sectors would be appro-

priate, however, as the sectors become narrower, it becomes prudent to shift instead to the Frandsen Wake Model. It is important to keep in mind though, that unlike the other models, the Frandsen Wake Model has only been designed for use with large symmetric wind farms, and therefore is not be applicable to either small wind farms or large wind farms that do not have regularly spaced turbines [24, 165].

5.5.3 Nysted

Through the UpWind project, data is also available for Nysted wind farm. Like Horns Rev this is aggregated data that has already been filtered, binned, and normalized. Nysted wind farm (also known as Rødsand I) consists of 72 2.3 MW Siemens turbines. Like Horns Rev, Nysted wind farm is sufficiently large that the large wind farm correction should be explored.

As is the case with the turbines at Horns Rev, the turbines at Nysted are deployed along an oblique rectangle as indicated in Figure 5.27. This therefore allows a similar study to be carried out, testing the applicability of these wake models at yet another site. However, at Nysted only wind direction sectors of 5° width were provided in the data-set. As the models performed poorly at these sizes for both Horns Rev and Middelgrunden, a very limited validation has been completed. The Nysted dataset consists of normalized power output for inflow speeds of 6 m/s, 8 m/s, and 10 m/s at 263°, 268°, 273°, 278°, 283°, 288°, and 293°. For this site 278° represents the inline case [189]. The full set of available cases is presented in Table B.2 in Appendix B.

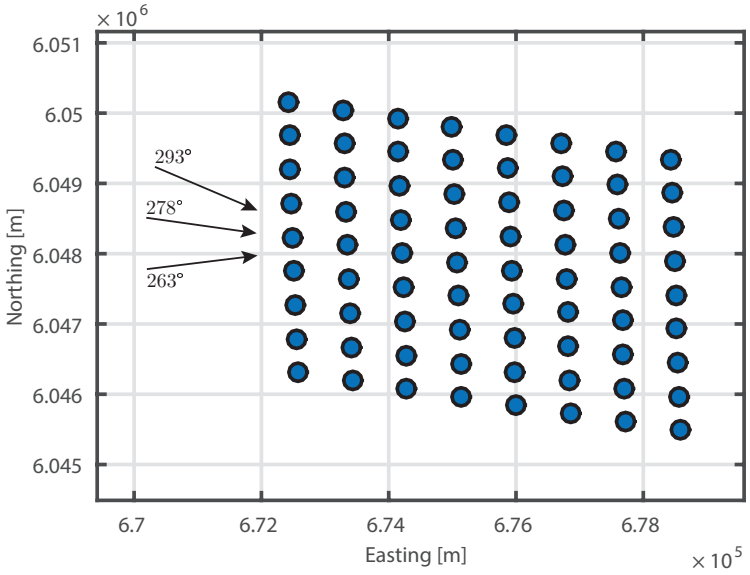

Figure 5.27: Layout of Nysted Offshore Wind Farm

As was the case for both Middelgrunden and Horns Rev I, a variation in the model performance as a function of wind speed can be observed. Consistent with the other sites, it appears as though the models in general perform best somewhere in the 8 m/s to 10 m/s range.

Tables 5.10 and 5.11 show the average RMS error for each of the models. Interestingly, for Nysted, the LWC does not appear to improve the models with the RMS errors in fact increasing. Although the Frandsen model proved to be an accurate model for Horns Rev, it has much higher error than any of the alternate models for the Nysted data. This indicates that something about the arrangement of turbines at Nysted wind farm does not suit the assumptions of this model.

Table 5.10: Nysted Wake Modelling - RMS Error by Wind Speed

Wind Speed [m/s]	N.O. Jensen	G.C. Larsen	Frandsen	Ishihara	Eddy-Viscosity
6	14.47%	**13.93%**	45.63%	15.48%	14.58%
8	10.10%	**10.09%**	17.63%	12.74%	10.29%
10	**8.25%**	8.58%	46.04%	11.15%	9.03%

Table 5.11: Nysted Wake Modelling - RMS Error by Wind Speed (With LWC)

Wind Speed [m/s]	N.O. Jensen	G.C. Larsen	Frandsen	Ishihara	Eddy-Viscosity
6	**13.02%**	13.82%	45.63%	15.86%	14.10%
8	11.32%	12.44%	18.26%	14.13%	**10.79%**
10	**8.71%**	10.32%	46.04%	12.96%	9.21%

Comparing the wind direction results indicates that all the models other than the Frandsen model perform well for the off-axis cases with the results consistently within the error of the data (Figures 5.28 and 5.29). The inline case (Figure 5.30), however, shows marginally higher error with many of the models now having over predicted wake deficits.

Table 5.12: Nysted Wake Modelling - RMS Error by Wind Direction

Wind Direction	N.O. Jensen	G.C. Larsen	Frandsen	Ishihara	Eddy-Viscosity
$263° \pm 2.5°$	6.49%	6.01%	36.79%	**5.99%**	7.36%
$268° \pm 2.5°$	6.28%	**6.18%**	33.06%	6.32%	8.84%
$273° \pm 2.5°$	**10.44%**	14.16%	31.81%	23.85%	14.82%
$278° \pm 2.5°$	22.25%	22.20%	50.20%	22.12%	**11.96%**
$283° \pm 2.5°$	**11.47%**	11.87%	33.71%	17.11%	13.19%
$288° \pm 2.5°$	12.19%	8.50%	32.62%	**8.49%**	13.92%
$283° \pm 2.5°$	7.47%	**7.15%**	36.87%	7.99%	9.00%

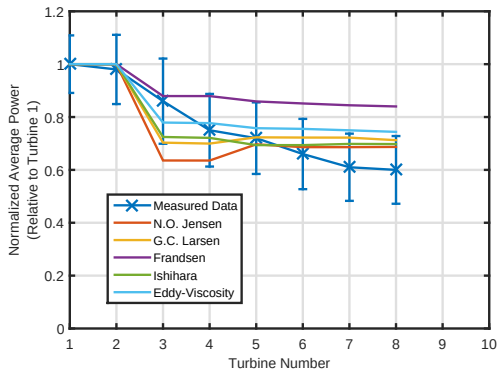

(a) Without LWC

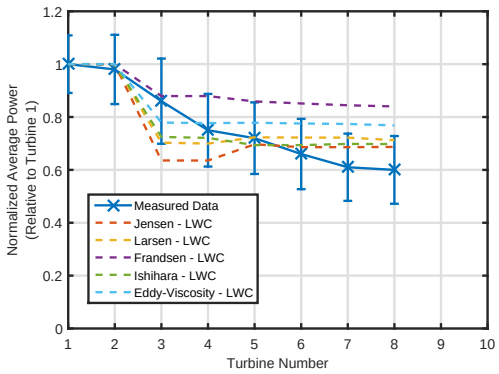

(b) With LWC

Figure 5.28: Nysted, Row 5, 8 m/s, 263° ± 2.5° with and without the LWC

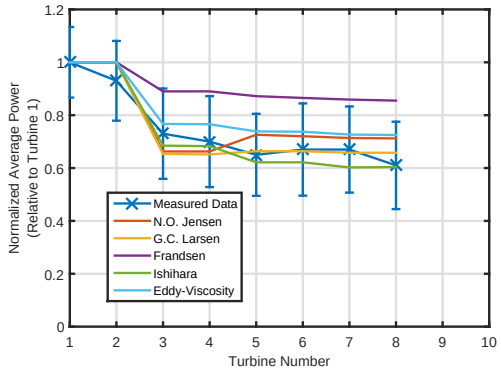

(a) Without LWC

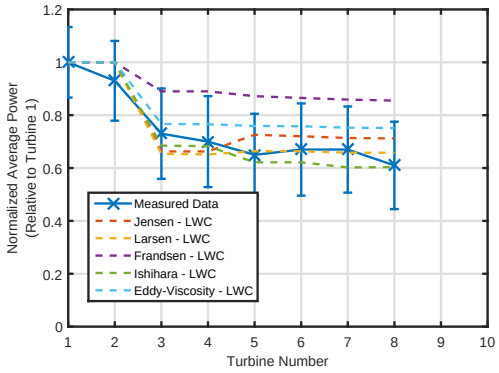

(b) With LWC

Figure 5.29: Nysted, Row 5, 8 m/s, 293° ± 2.5° with and without the LWC

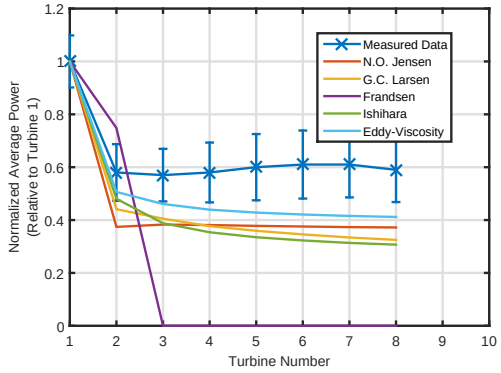

(a) Without LWC

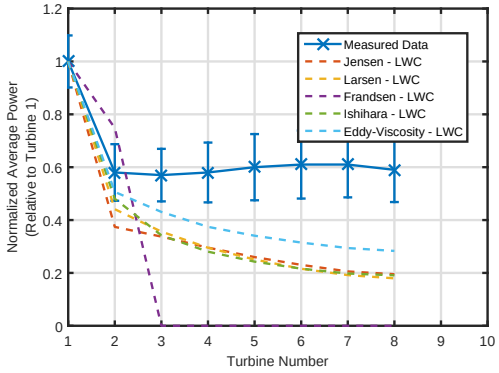

(b) With LWC

Figure 5.30: Nysted, Row 5, 8 m/s, 278° ± 2.5° with and without the LWC

Tables 5.12-5.14 show that though the inclusion of the LWC appears to improve the results at Nysted for specific wind sectors, it is found that when considering all the

Table 5.13: Nysted Wake Modelling - RMS Error by Wind Direction (With LWC)

Wind Direction	N.O. Jensen	G.C. Larsen	Frandsen	Ishihara	Eddy-Viscosity
$263° \pm 2.5°$	6.49%	6.01%	36.79%	**5.99%**	7.48%
$268° \pm 2.5°$	6.28%	**6.18%**	33.06%	6.32%	8.87%
$273° \pm 2.5°$	**9.62%**	13.63%	31.32%	22.57%	13.25%
$278° \pm 2.5°$	28.27%	28.67%	50.20%	29.44%	**22.28%**
$283° \pm 2.5°$	**9.43%**	11.62%	35.61%	15.86%	10.29%
$288° \pm 2.5°$	9.55%	12.09%	32.67%	12.04%	**8.30%**
$293° \pm 2.5°$	7.47%	**7.15%**	36.87%	7.99%	9.10%

Table 5.14: Nysted Wake Modelling - RMS Error by Wake Model

	N.O. Jensen	G.C. Larsen	Frandsen	Ishihara	Eddy-Viscosity
Without LWC	10.94%	**10.87%**	36.44%	13.12%	11.30%
With LWC	**11.02%**	12.19%	36.64%	14.32%	11.37%

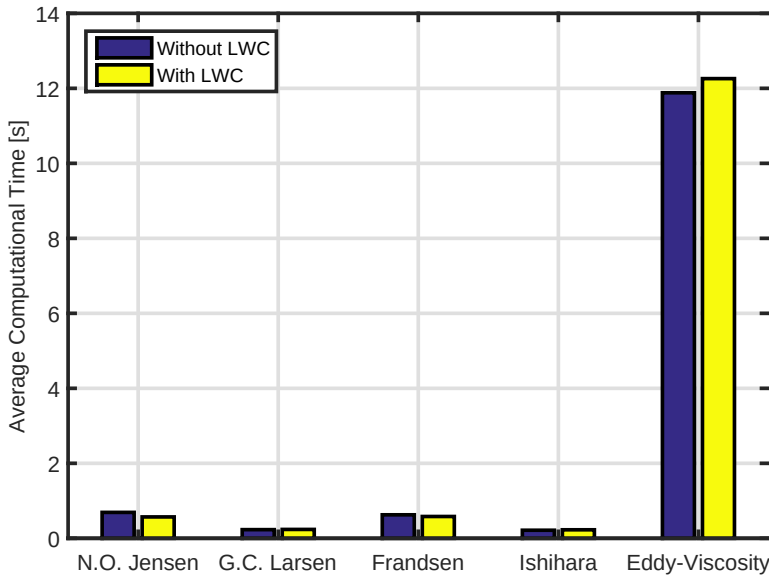

Figure 5.31: Computational time for each wake model both with and without the LWC when applied to Nysted

available data the RMS error increases. Furthermore because of the uncertainty on the measured data, the implemented models both with and without the LWC are within the measurement uncertainty of the measured data. This therefore emphasizes that the LWC may not give sufficient improvements to justify the increased computational time. Given that the results are within the measurement uncertainty, it is necessary for further data with lower measurement uncertainty is needed in order to evaluate the impact of including the LWC.

An interesting point to note is that for this wind farm, the Frandsen model (both with and without the LWC) offers erratic results for the inline case. The Frandsen model has not previously been validated in the literature [165], and as such very limited tuning of several of the parameters has been undertaken. This model is also limited in that, a more complex method has been developed to account for the combination of wakes and the variation in wind speed across the rotor plane. This has, however, not been implemented here as it has not been fully described in the literature. The present study therefore makes use of a sum of squares analytic method to account for the superposition of wakes. It is acknowledged that this is not how the authors of the model had designed its use, however, for Horns Rev this functioned well.

The high errors observed here for all models can be attributed to the small sector sizes which were found to yield high error for the other two sites as well. The computational time plot shown in Figure 5.31 shows that similar to both Middelgrunden and Horns Rev I, the G.C. Larsen and Ishihara wake models are consistently the fastest at Nysted wind farm. Even with the inclusion of the LWC which increases the computational time, these models are still quicker than the alternatives.

Overall, across all the sites explored in this study, the G.C. Larsen model is shown to be consistently one of the fastest models while at the same time yielding relatively low error compared to the other models. As such, this model would be well suited for inclusion in the optimization process. Further validation studies should, however, be completed in order to fully characterize the performance of these models for a range of wind farm sizes and shapes.

5.6 Modelling Electrical Losses

The final step within the estimation of the annual energy production is the estimation of the electrical losses within the wind farm. The need to include this arises from the fact that these losses are a function of each turbine's individual production and the electrical cable infrastructure. As such these losses are affected by the layout of the wind farm and should be included in order to accurately assess the layouts. Presently, most layout optimization tools either use a constant loss assumption for the electrical infrastructure, or they use more simplistic loss functions which do not adequately account for the impact of the layout [12, 17]. As the electrical losses can represent up to 5% of the total AEP, this can be an important component of the AEP estimation especially when comparing layouts.

Based on *IEC 60228: Conductors of insulated cables* [196], *IEC 60287: Calculation of the current rating* [197], and the *Cigre TB-490* [198], this approach uses parameters

provided by the cable manufacturers, the flow of power through each cable segment, and some assumptions on the cable design based on discussions with industry experts in order to estimate the losses in the cables and the turbine transformers.

5.6.1 Turbine Transformer Losses

Offshore wind farms traditionally consist of turbines with generators at a nominal voltage of 690 V. In order to bring this up to the collection network voltage most turbines therefore have a transformer placed either in the nacelle or inside the turbine tower. This transformer is designed to transform the power generated at 690 V to the collection network voltage (typically 33 kV or 66 kV). It should be noted that very modern turbines do use higher generator voltages sometimes forgoing a turbine transformer.

Fassbinder [199], Schoenmakers [69], and Lundberg [200] had previously demonstrated that the transformer losses were quadratic and increased with the load level. As a result, they can be modelled as:

$$L_{transformer} = L_{\text{no load}} + L_2 \cdot \text{load ratio}^2 \tag{5.47}$$

where $L_{\text{no load}}$ represents the no-load losses. Given that load ratio ≤ 1, $L_{\text{no load}} + L_2$ represents the full-load losses. As a result of this, in order to assess the losses for any given load level, it is necessary to know the no-load and full-load losses associated with the given transformer. In discussion with transformer manufacturers, Schevensteen et al. [201], was able to give the ratings for a 6 MVA transformer (Table 5.15) from which the load curves could be derived (see Figure 5.32).

Table 5.15: Turbine Transformer Loss Specifications [201]

Voltage [kV]	Transformer Rating [MVA]	No-load Losses [kW]	Full-Load Losses [kW]
33	6	5.50	43
66	6	6.50	45

Following the modelling of the wakes, each turbine's production could then be updated to include these transformer losses prior to estimation of the losses in the intra-array cables.

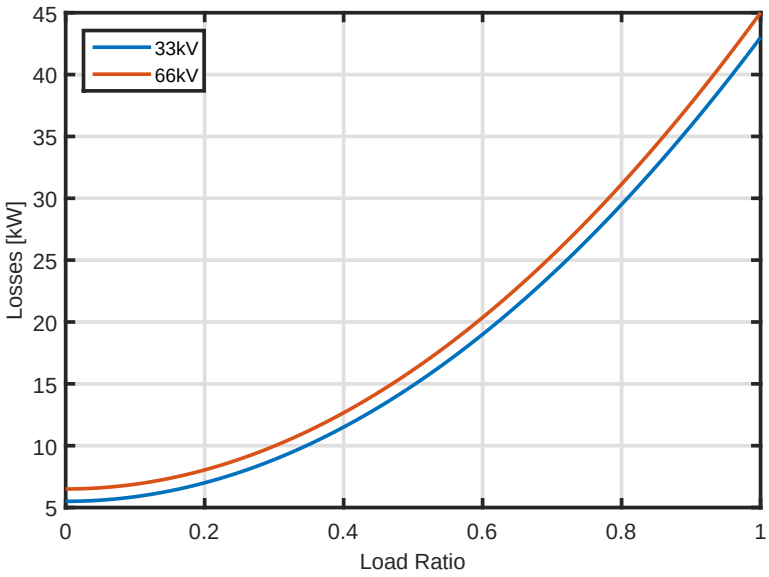

Figure 5.32: Transformer losses

5.6.2 Intra-Array Cable Losses

The intra-array cable losses are based on the relevant standards and the documentation provided by the cable manufacturers. Besides basic material properties, the specifications given in Table 5.16 are required for the model to compute the intra-array cable losses [196, 197].

In general, for a typical three-core subsea cable, as pictured in Figure 5.33, the cable losses can be modelled as being made up of four constituents:

1. **Core losses:** These are the thermal losses that occur in the conductor core and are the traditional ohmic losses of a metal conductor;
2. **Dielectric losses:** These are the losses as a result of the charging currents required to energize the cable;
3. **Sheath/Screen losses:** These are the losses as a result of eddy-currents in the screen; and
4. **Armour losses:** These are the losses as a result of the eddy-currents in the armour.

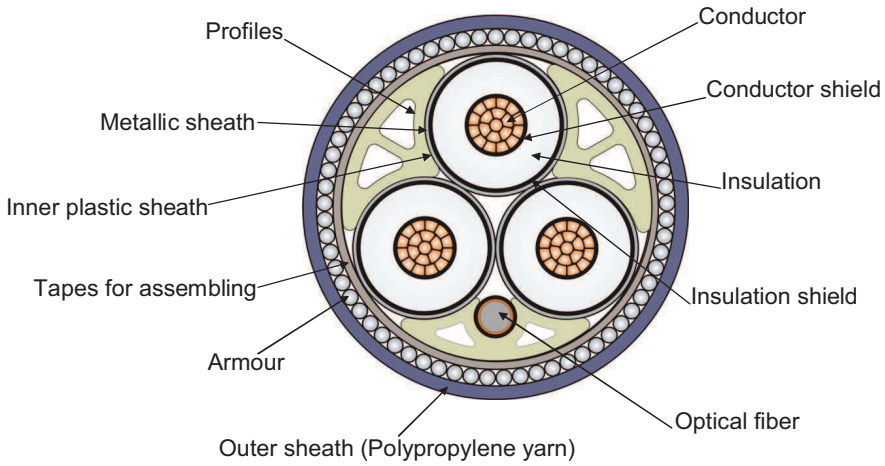

Figure 5.33: Example of a three-core cable design [198].

Table 5.16: Cable specifications required for loss calculation

Description	Units
Conductor Cross-Sectional Area	m^2
Resistance per Unit Length	Ω/m
Conductor Diameter	mm
Diameter over Insulation	mm
Outer Diameter of Cable	mm
Insulation Loss Factor	-
Insulation Thickness	mm
Screen Cross-Sectional Area	mm^2
Sheath Thickness	mm
Screen Resistance per Unit Length	Ω/m
Distance Between Conductor Axes	mm
Relative Permittivity of Insulation	F/m

5.6.2.1 Core Losses

According to IEC [197], the core losses are defined as:

$$L_{core} = 3R_{ac} \cdot I^2 \cdot l \tag{5.48}$$

where R_{ac} represents the effective AC resistance for each conductor and I is the current in each of the 3-cores of a 3-core power cable and l is the length of the cable.

The effective resistance R_{ac} is given by:

$$R_{ac} = R'(1 + y_s + y_p) \tag{5.49}$$

where R' is the DC resistance of the conductor when operating at the maximum temperature. This is given by:

$$R' = R_0(1 + \alpha_{20} \cdot \Delta T) \tag{5.50}$$

where R_0 is the DC resistance of the conductor at 20 °C, α_{20} is the temperature coefficient of electrical resistivity at 20 °C, and ΔT is the maximum allowable temperature rise of the conductor. R_0 is a property that is provided by the cable manufacturer and α_{20} is a property of the material from which the conductor is extruded. ΔT is defined to be 70 °C in IEC 60287 [197].

The parameters y_s and y_p are the skin effect and the proximity effect factors respectively and are given by [197]:

$$y_s = \frac{x_s^4}{192 + 0.8 \cdot x_s^4} \tag{5.51}$$

$$y_p = \frac{x_p^4}{192 + 0.8 \cdot x_p^4} \left(\frac{d_c}{s}\right)^2 \cdot 2.9 \tag{5.52}$$

where d_c is the conductor diameter and s is the distance between the conductor axes. The parameters x_s and x_p are arguments of a Bessel function used to calculate the skin and proximity effects respectively. These are given by:

$$x_s^2 = \frac{8\pi f}{R'} 10^{-7} k_s \tag{5.53}$$

$$x_p^2 = \frac{8\pi f}{R'} 10^{-7} k_p \tag{5.54}$$

where f is the supply frequency, and the parameters k_s and k_p are factors for which the IEC 60287 standard provides values depending on the type of conductor.

5.6.2.2 Dielectric Losses

The dielectric losses are dependent only on the cable geometry and voltage level and is given by IEC [197]:

$$L_{dielectric} = 2 \cdot \pi \cdot f \cdot C \cdot U_0^2 \cdot \tan\delta \tag{5.55}$$

where C is the per unit length capacitance, U_0 is the RMS voltage, and $\tan\delta$ is the insulation loss factor given by the manufacturer.

The cable capacitance is given by:

$$C = \frac{\varepsilon}{18ln\left(\frac{D_i}{d_c}\right)} \cdot 10^{-9} \tag{5.56}$$

where ε is the relative permittivity of the insulation, and D_i is the diameter of the insulation.

5.6.2.3 Sheath/Screen Losses

According to the IEC [197], the screen losses scale with the core losses and are given by:

$$L_{screen} = \lambda_1 \cdot L_{core} \tag{5.57}$$

where λ_1 is the screen power loss factor given by the equation:

$$\lambda_1 = \frac{R_s}{R_{ac}} \cdot \frac{1.5}{\left(1 + \left(\frac{R_s}{X}\right)^2\right)} \tag{5.58}$$

where R_s represents the screen resistance at maximum operating temperature and X is the reactance of the sheath.

R_s is computed from the resistance of the sheath at 20 °C and material properties of the sheath. The maximum operating temperature rise, ΔT, is taken to be 55 °C.

$$R_s = R_{s0} \cdot (1 + \alpha_{20}\Delta T) \tag{5.59}$$

The sheath reactance, X, is defined in Equation 5.60 where d_s is the mean diameter of the sheath.

$$2\pi f \cdot 10^{-7} \cdot ln\left(\frac{2s}{d_s}\right) \tag{5.60}$$

5.6.2.4 Armour Losses

Like the sheath losses, the armour losses also scale with the core losses and are given by [197]:

$$L_{\text{armour}} = \lambda_2 \cdot L_{core} \tag{5.61}$$

The armour power loss factor, λ_2, is dependent on the shape and material of the armouring. For a steel wire armour around round conductors, the power loss factor

is given to be:

$$\lambda_2 = 1.23\frac{R_{\text{armor}}}{R_{ac}} \cdot \left(\frac{2c}{d_a}\right)^2 \frac{1}{\left(\frac{2.77R_a 10^6}{2\pi f}\right)^2 + 1} \tag{5.62}$$

In this case, R_{armour}, is the resistance of the armour and is given by the geometry of the armour. The parameter c is the distance between the conductor and the centre of the cable.

Given discussions with cable manufacturers, it has been possible to collect representative data to use this model. As subsea cables are bespoke, the exact dimensions of the insulation layers and therefore properties of the cables will vary from site to site [202]. The values used in this model are representative values provided by cable manufacturers. It should be noted that as this model assumes that the cable is operating at the maximum allowable temperature rise, it represents the maximum loss in the cable. Furthermore, as the design standards have been developed to ensure that the conductors and insulation are conservatively sized, there are safety factors within the IEC calculation steps which will result in this method consistently overestimating the losses. Computing the real temperature rise and thereby the real losses was felt to be too complex a problem for a very small increase in overall accuracy.

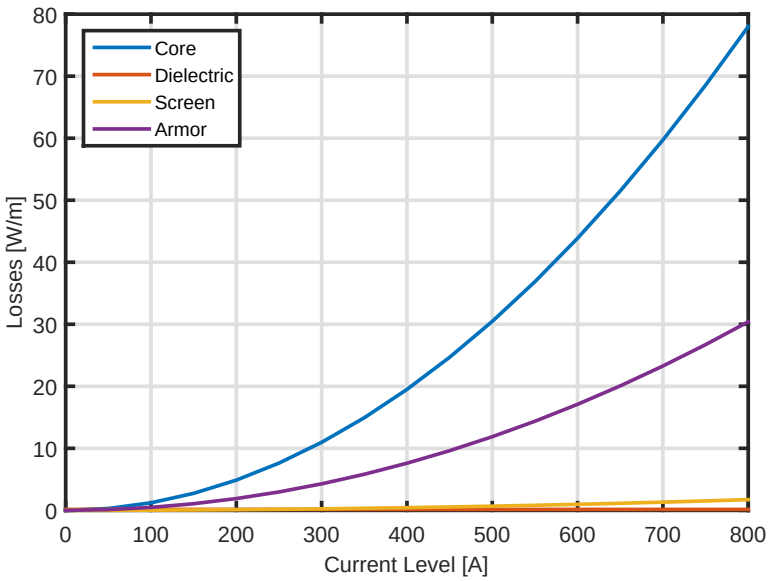

Figure 5.34: Cable losses per unit length of cable for a 33 kV 630 mm cable. As the voltage is constant, the dielectric losses (pictured in red) are constant regardless of the current level, while the core, screen, and armour losses increase quadratically with the current level.

As can be seen in Figure 5.34, though the core losses dominate at all current levels, as the current level increases the armour losses also represent a significant portion of the total cable losses and should therefore not be ignored.

5.7 Chapter Summary

Within the goal of producing a layout optimization framework for offshore wind farms, this chapter has explored the estimation of the annual energy production of the wind farm and a vital component in the determination of a layout's LCOE. The AEP represents the output of the wind farm, and is directly related to the lifetime energy production of the project and the eventual profit. As such, this chapter has outlined an approach for the estimation of the AEP for offshore wind farms given information regarding the resource at the site, the wind farm layout (including electrical infrastructure), and the wind turbine specifications.

The overall strategy for computing the AEP has been outlined and includes the modelling of wind turbine wakes. As there are numerous kinematic wake models which have been developed in the literature, the key models have been introduced, explained, and validated using real data available from Middelgrunden, Horns Rev I, and Nysted wind farms. From this, it was demonstrated that the G.C. Larsen model represents a good balance between accuracy and speed and would be well suited for use in the optimization routine. In addition to this, the LWC, a semi-empirical method for accounting for a wind farm's interaction with the PBL did not show consistent improvements and therefore further work must explore the conditions under which the LWC should be applied.

Finally, an approach for the estimation of electrical losses has been outlined. This approach includes both the transformer losses in each turbine as well as the cable losses which would be expected. In the full optimization routine, as the electrical infrastructure would have been designed prior to execution of the AEP module, it is anticipated that a full cable network is known and therefore the accurate losses will help asses the layouts.

It is believed that the AEP estimation methodology proposed using the G.C. Larsen wake model, transformer losses, and collection network losses will represent a good balance between accuracy and computational complexity and is therefore well suited for the inclusion in the layout optimization framework.

Chapter 6

Cost Modelling

6.1 Introduction

From the perspective of an offshore wind farm developer, for an offshore wind farm to be successful it needs to generate as much energy as possible for the lowest possible cost. As a result of this, work in layout optimization has identified that the inclusion of costs in the objective function is important in order to accurately represent the interests of a project developer [10, 12, 17, 27, 32, 40]. With this in mind, the cost model has been designed such that the definition of the wind farm layout is central in each of the sub-models in order to capture the impact that the placement of turbines, cables, and substations has on the costs and thereby the levelized cost of energy. This allows the tool to either be used to simply assess the costs of a given turbine layout, or when implemented as part of the objective function in the optimizer allows the minimization of the lifetime costs, as a developer would realistically seek to do when planning the wind farm.

As was the case with the electrical infrastructure module (see Chapter 4), projects similar to the UK Round 3 projects are considered as a point of context. Where relevant, scaling laws have been developed allowing data from smaller wind turbines and wind farms to be applied to future wind farms with larger wind turbines. Overall, this tool is therefore best suited for projects similar to UK Round 3 projects with individual project phases not exceeding 1 GW. Although the cost estimation methods presented here should be valid beyond 1 GW phases, there will likely be further cost savings as the capacity increases that the presented model does not capture. These cost savings, would, however, likely have a low dependence on the layout and therefore the effect of the wind farm layout on the costs would still be captured.

In order to capture the impact the wind farm layout has on the project costs, the tool has been designed to operate at several different levels of detail depending on the available site and project data. The minimum required inputs are the positions of the turbines and the necessary ports, while more detailed approaches consider the bathymetry throughout the site. Representative costs, vessel parameters, and operational durations

have been assumed based on discussions with members of the industry. However, given the parametric approach of the model these can easily be changed to better represent a specific project's conditions. As the tool is ultimately used to differentiate between layouts under consideration, the cost model is used on a relative rather than an absolute basis.

As it is believed that this tool would be particularly relevant to early planning stages, the implemented cost correlations have been based on and validated against historical data where possible rather than based on a full bottom-up engineering approach. In general, it is the belief that detailed engineering design of the wind farm, and the tender process would happen after the initial deployment of this tool, and therefore the costs in this model remain high-level while still capturing the impact the layout has on these costs. Having said that, the presented approach does go beyond assuming a constant cost per turbine, or a cost that is only affected by the number of turbines, such as the approach taken by previous layout optimization studies [16, 28, 29, 34, 35, 40, 43–48].

A recurring challenge in modelling costs for large infrastructure projects, such as large offshore wind farms, is that the incurred costs have an element of project-specificity and as a result it is difficult to both validate empirical models and predict future costs based on costs incurred on previous projects. The present cost model therefore strives to ensure that the key element captured by the model is the impact that the layout of the offshore wind farm might have on each of the cost elements. With this in mind, the actual cost may vary from what is presented here, but it is believed that the relative cost of different layouts will remain largely unchanged with respect to one another. Therefore given accurate inputs for a specific project it should be possible to capture the true costs of the project and specifically the impact that the wind farm layout might have on these costs.

Specific project costs are affected by the regulatory frameworks in place. For example the UK has a unique approach to the offshore transmission assets when compared to other countries and this affects the way in which the costs of building the offshore substations and export cables are accounted for. The present model is therefore best suited for application to sites in the UK waters, however, each of the cost components could be updated to consider geographic specific elements. For the most part, it would be expected that although these regional differences may impact the financial viability of a project, they would not impact the layout. In order to standardize all the costs, values have been converted to 2011-GBP.

6.2 Model Components

In order to estimate the costs associated with the wind farm, eight independent sub-models are executed in series:

1. Turbine Supply;
2. Turbine Installation;
3. Foundation Supply;
4. Foundation Installation;
5. Intra-Array Cables (Supply and Installation);
6. Decommissioning;
7. Operations and Maintenance (O&M); and
8. Offshore Transmission Assets.

Each of these cost elements also has a different contribution to both the capital expenditure (CAPEX) and the operational expenditure (OPEX) as well as having different sensitivity to the wind farm layout as Table 6.1 shows.

Table 6.1: Cost Contribution to CAPEX and OPEX

Cost Element	CAPEX	OPEX	Sensitivity to Layout
Turbine Supply	✓	-	Low
Turbine Installation	✓	-	Medium
Foundation Supply	✓	-	Medium
Foundation Installation	✓	-	Medium
Intra-Array Cables	✓	-	High
Decommissioning	✓[1]	-	Medium
Operations and Maintenance	-	✓	Medium
Offshore Transmission Assets	✓	✓	Low

[1] Though listed as a CAPEX term, these costs are incurred at the end of life

In the following section the operating principles of each of these sub-models is outlined and the default values based on industry estimates are provided. The applicability of each of the models is also discussed in order to clearly define the cases for which this tool can be applied accurately. The sensitivity of each cost centre to the layout is also discussed in order to identify which of the sub-models are priorities for the layout optimization framework.

Validation of cost models have often struggled due to inconsistent and unclear terminology for the cost breakdown [203]. In the sections that follow, each of these eight cost centres are explained highlighting what is and is not included in each.

6.2.1 Turbine Supply

Turbine supply can be defined as the price that the turbine manufacturer is charging the developer to supply the desired numbers of turbines (including towers, nacelles, and blades) to the construction port. It does not include any transportation costs beyond the construction port nor does it include the foundations and transition piece (TP).

Turbines are frequently parametrized based either on their rated power (P) or the rotor diameter (d). As the turbine power production is directly dependent on the rotor area, and therefore a function of the rotor diameter, both of these parameters can be said to represent the size of the wind turbine.

Estimating the manufacturer price of wind turbines has been done in many existing studies and has generally applied empirical correlations as the precise cost incurred by a project developer will be based not only on the cost of the turbine, but existing relationships between the developer and turbine manufacturer. The same developer may in fact be given different prices for different projects [204]. Previous cost modelling methodologies have therefore generally used the turbine size to scale the mass of the turbine components, and then assess the nominal cost based on empirical relationships between the mass of the components and their cost [17, 205–207].

Rather than mass scaling, a recent study focusing on the costs of 2 MW to 5 MW turbines, has found an empirical relationship for the supply cost of turbines based only on the total installed capacity of the wind farm [208]. A difficulty in using empirical relationships to estimate the costs of future projects, is that as offshore wind turbines have moved from onshore turbines simply placed offshore, to turbines specially designed for the offshore environment, the costs of these offshore turbines have therefore developed independently of their onshore counterparts leading to empirical relationships which validate poorly [209]. It can be expected that the next generation of offshore wind turbines, the 5 MW to 8 MW class, will take advantage of significant improvements in design and manufacturing processes learned through the previous generations making it more difficult to apply the existing models to estimate these future costs without introducing additional uncertainty. It should also be noted that bottom-up approaches have in the past been shown to have varying degrees of accuracy [17].

In order to accurately consider projects utilizing the larger 5 MW to 8 MW turbines which are approaching commercial deployment it was decided that the costs would instead be based on budget quotes provided by turbine manufacturers. These costs have been supplied courtesy of a UK Round 3 development team and include an average cost per MW installed (C_{perMW}) for turbines in the range of 5 MW to 8 MW assuming that these enter serial production prior to 2017 and are delivered in 2018 or 2019 [204]. From this, the total supply cost is therefore simply a function of the installed capacity

($P_{windfarm}$), and within this range is relatively independent of the specific turbine that is used:

$$C_{wt} = C_{perMW} \times P_{windfarm} \tag{6.1}$$

Ultimately, the turbine supply is not influenced by the turbine layout, but rather the number of turbines. Therefore, only if layouts with different turbine models and different installed capacities are under consideration would one expect this to have an impact on the costs. For a set of layouts, however, with the same installed capacity and the same turbine model, the placement of the turbines has no bearing on the turbine supply costs as defined this model.

In discussions with a wind farm development team, it was also found that turbines in the 5 MW to 8 MW range for a 500 MW to 1000 MW wind farm had approximately the same price per installed capacity highlighting that in fact, the turbine supply costs for these turbines is relatively independent of the turbine model [204]. This value is broadly similar to that quoted by market studies such as that by Mone et al. [210]:

$$C_{perMW} = \frac{£1,200,000}{MW} \tag{6.2}$$

This represents the average cost for a development between 500 MW and 1 GW [204]. The uncertainty of this cost would therefore be expected to increase as the wind farm deviates from this size and the installation date deviates from 2018. It would be expected that as more turbines would be ordered, the developer would be able to secure a lower unit price for the individual turbines. This is therefore an important factor to account for when considering layouts with different installed capacities. Given that this model hinges on the data provided from the turbine manufacturers, it is important to have accurate updated values for these that represent the project at hand.

6.2.2 Turbine Installation

The turbine installation cost estimation is based on transporting the turbines supplied above from the construction port to the wind farm and installation of these at the turbine positions. It does not include the foundation transport to site nor the foundation installation costs. Unlike the turbine supply term, the installation term is impacted by the turbine layout as this influences the distances that the installation vessel must travel. This model is based on a commonly applied methodology in which the total installation time required is estimated, and from this a cost is derived [211–215].

For this model, the installation strategy assumed is a self-transport scheme in which the same vessel transports the turbines from the construction port to the installation

location and installs the turbine, this would be similar to the use of a jack-up vessel or a self-propelled installation vessel. Previous models have also included a *barge* strategy in which feeder barges are used to transport the units from shore to the installation vessel [211]. More recently, however, this installation strategy has been abandoned for turbine installation operations due to the risk involved with the offshore lifts required when using a feeder vessel [213].

For the self-transport strategy, the model computes the total time that the vessel must be hired for in order to install all the turbines. The computation is therefore sensitive to not only the coordinates of the turbines and the construction port, but also the parameters of the vessel. Based on various industry sources the base values which have been assumed for a jack-up vessel are given in Table 6.2.

Table 6.2: Turbine Installation - Default Vessel Parameters

Parameter	Symbol	Value	Source
Average Vessel Speed	v	6 kn	[213]
Vessel Capacity	q	5 units	[213]
Load Time	t_{load}	1.4 days	[204, 214]
Install Rate	$r_{install}$	3 $\frac{days}{turbine}$	[204, 214]
Mobilization	t_{mob}	14 days	[211]
Demobilization	t_{demob}	7 days	[211]
Availability	A	0.75	[211]
Day Rate	R	£160,000	[211]

Given the coordinates of the wind turbines and the construction port, the turbines are clustered using the vessel capacity limit to act as a cluster capacity. This therefore identifies clusters of turbines that can be installed in a single trip. A CMST (similar to that used in Chapter 4) is then constructed to minimize the total distance that the vessel needs to travel in order to install the turbines and return to the installation port. This approach utilizes the same Delaunay Triangulation Based Pathfinding Algorithm to ensure that valid vessel paths are designed taking into account the land masses as constraint regions that the vessels cannot pass through. From this, the total distance to be covered by the installation vessel is known, and from the vessel speed, the total transportation time, $t_{transport}$ can be found.

For each trip, the total time is therefore given by:

$$t_{trip} = (t_{load} + t_{transport} + r_{install} \times q) \times \frac{1}{A} \tag{6.3}$$

The total cost is therefore given by:

$$C_{t,install} = R \times \left(t_{mob} + t_{demob} + \sum_{i=1}^{n_{trips}} t_{trip,i} \right) \tag{6.4}$$

where n_{trips} is the total number of trips from the construction port that the vessel must take. This is computed based on the number of turbines to be installed and the capacity of the vessel. R is the day rate for the relevant vessel, crew, and any necessary specialist equipment.

The $t_{transport}$ term is affected by the turbine coordinates as well as the port coordinates due to the model computing the route the vessel must take in order to install the turbines. Having said that, in general for wind farms explored using this model, the dominant term tends to be the $t_{installation}$ term, and therefore the total turbine installation cost, although affected by the turbine positions, is not significantly affected by changes to the layout within the same wind farm boundaries. For larger wind farms though, with greater distances between turbines and a greater distance from the shore, the $t_{transport}$ term would be expected to have a more significant impact on the overall cost, and the result of optimizing the vessel movements will have a greater impact on the costs warranting the inclusion of this calculation step.

6.2.3 Foundation Supply

The foundation supply term includes all costs in procuring both the transition pieces and foundations. One would think that the turbine positions here would have a limited impact on the foundation supply costs as they had a limited impact on the turbine supply costs, however, this is not the case. The foundation design and therefore its cost includes a consideration of the site conditions where the foundation is to be installed. Specifically, this considers the water depth at the individual turbine positions. The engineering design of the foundation would consider the soil conditions that the foundation would be expected to be installed in, and therefore these should be incorporated into the cost estimation of the foundation supply. However, it is believed that the present layout optimization tool would be deployed prior to completing detailed geotechnical and geophysical surveys of the site and therefore it is important that the cost models implemented do not depend on this data.

Furthermore foundation designs are also dependent on the mass that they will need to support (the mass of the turbines) and therefore this must also be taken into account in order to estimate the cost. Like the turbine supply costs, it would not be entirely correct to assume that costs of foundations for smaller turbines in shallower waters could easily be scaled to represent the needs of the larger turbines and deeper waters. It should be

noted that like the turbines, the best approach would be to receive budget quotes from foundation suppliers; however, this might make it more difficult to accurately describe the impact of water depth and geophysical conditions.

Though there are a number of offshore wind turbine foundations, the main foundation types that have be considered are: gravity based foundations (GBF), monopile foundations, and jacket foundations. These are shown in Figure 6.1. These represent the types of foundations that are most commonly used in the offshore wind sector and are expected to be used moving forward [17, 136, 216]. More innovative foundations such as suction buckets and floating foundations are under development, although as these are not presently in serial production it is difficult to estimate realistic costs and characterize how these costs change based on the wind farm layout. When deployed in arrays, floating foundations are believed to be capable of taking advantage of common anchor points thereby having foundation costs depending on not only the site conditions at each individual turbine location, but also based on the relative position of the turbine within the wind farm [217, 218]. This, however, remains hypothetical and until such designs are implemented, it would be premature to speculate on the impact that the wind farm layout might have on these costs.

Existing foundation cost models have used several different approaches to parametrize the cost. These approaches have included everything from assuming a constant price per foundation type (ignoring water depth, turbine loads, and geotechnical site characteristics) to including a complete bottom-up engineering approach based on detailed turbine characteristics and soil parameters [17, 34, 35, 91]. The more detailed models have proven very difficult to validate and have often tended to significantly overestimate the foundation costs. Given this, and that this optimization tool would be used prior to completing detailed geotechnical surveys at the site, it was decided that including detailed soil conditions would represent an unrealistic degree of detail in the inputs; the foundation costs were therefore parametrized on only the mass of the turbine and the water depth.

6.2.3.1 Gravity Based Foundation (GBF)

Gravity based foundations are wide structures generally made out of concrete and filled with some ballast. These structures are effective in keeping the structure in place due to their mass and overcome overturning moments due to the width of the structure [136, 220].

Given that the next generation of gravity based foundations can be installed without a heavy-lift vessel using a float and sink installation strategy, it is believed that it might prove to be cost-effective to use gravity based foundations. In order to facilitate this,

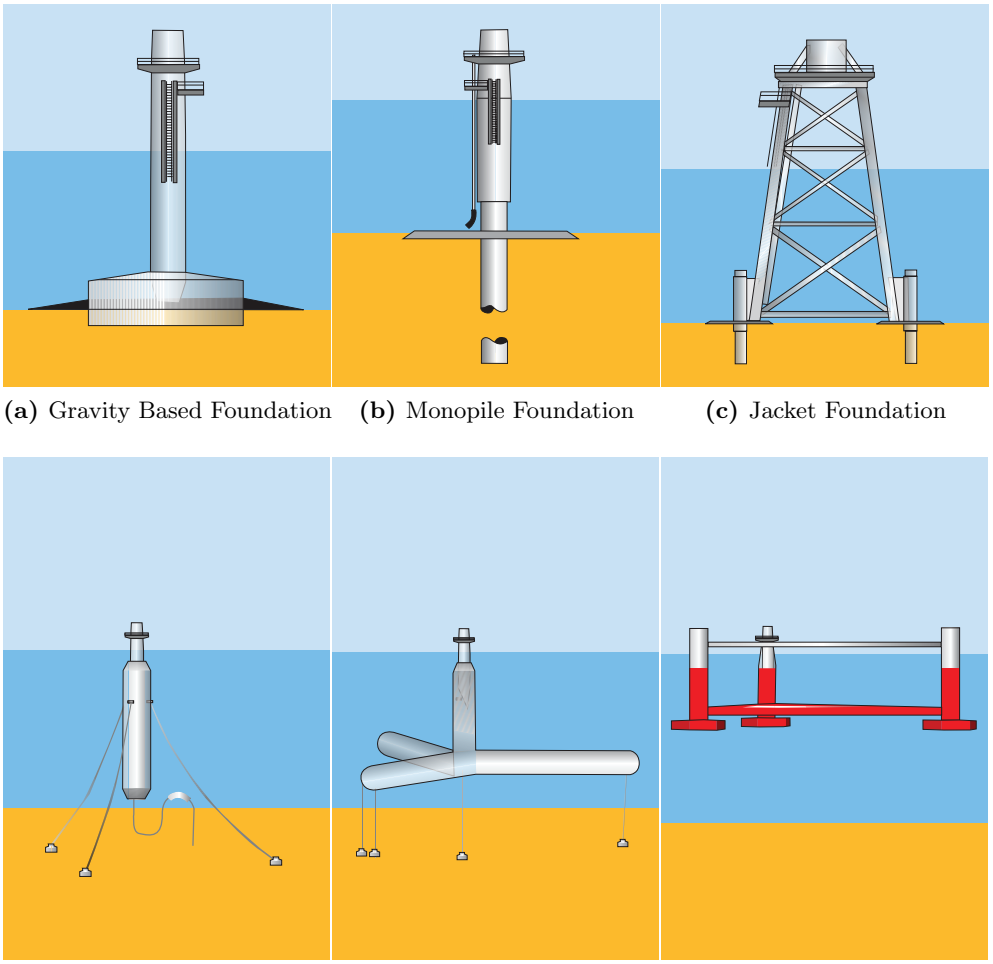

(a) Gravity Based Foundation **(b)** Monopile Foundation **(c)** Jacket Foundation

(d) Spar Floating Foundation **(e)** TLP Floating Foundation **(f)** Semi-Submersible Floating Foundation

Figure 6.1: Foundation types EWEA [219].

this tool considered a number of potential approaches to model the cost of gravity-based foundations. Although a bottom up approach would include a full consideration of the geotechnical site characteristics, these models tend to not to validate well with errors of up to 22% in mass estimation and up to 16% in cost estimation [17]. It would be expected that as the available validation data represents small first generation foundations, the error will be more significant for the types of GBF foundations to be deployed for future turbines. Other resources have looked instead at the GBF costs being dependent only on the turbine parameters and water depth creating semi-empirical relationships [221–223].

As can be seen in Table 6.3 and Figure 6.2 the three reports all agree that the costs increase linearly with depth. However, the three sources differ in costs estimated for the foundation types. This is due to the differences in model assumptions and the

Table 6.3: GBF Costs per MW

Depth [m]	Bloomberg 2011 [221]	Bloomberg 2013 [222]	Market Study [223]
5	£561,000	£472,600	-
10	-	£491,300	-
11	-	-	£315,800
15	-	£510,000	-
20	-	£528,700	£410,430
24	-	-	£422,470
25	£701,250	£547,400	-
28	-	-	£434,370
30	-	-	-
32	-	-	£460,430
35	-	-	-
40	-	-	-
45	£828,750	-	-

data from which the models are derived. The correlation presented by Bloomberg New Energy Finance [221] represents the costs anticipated for traditional first generation gravity based foundations designs for a 5 MW turbine assuming that they enter serial production in 2017. This is therefore based on a combination of historical costs for smaller GBFs and further design optimization and industrial learning. The correlation presented by Bloomberg New Energy Finance [222] is prepared in a similar manner, however, with more recent foundation designs taken as a base accounting for the slightly lower normalized costs. This correlation is, however, not developed with a specific turbine class in mind. The final correlation presented by a foundation manufacturer [223] for the GE 150-6MW turbine highlights the savings that can be made through second generation GBF designs which allow for a float and sink installation concept requiring no heavy lift operations during installation. Not only are these designs cheaper to install due to the avoidance of a heavy lift vessel, but more efficient material use further reduces the cost as indicated. In order to increase the applicability of this data to depths beyond 32 m and values between the data points available, a linear depth-dependent relationship was built from the provided values.

$$C_{GBF} = 6.605 \times 10^{-3} \cdot WD + 2.570 \times 10^{-2} \qquad \left[\frac{£m}{MW}\right] \tag{6.5}$$

where WD is the water depth.

As no data was found for larger turbines to validate this model, this cost element has higher uncertainty if applied to larger turbines. It would be expected that that GBF mass and therefore cost is not only a function of the water depth, but also the mass

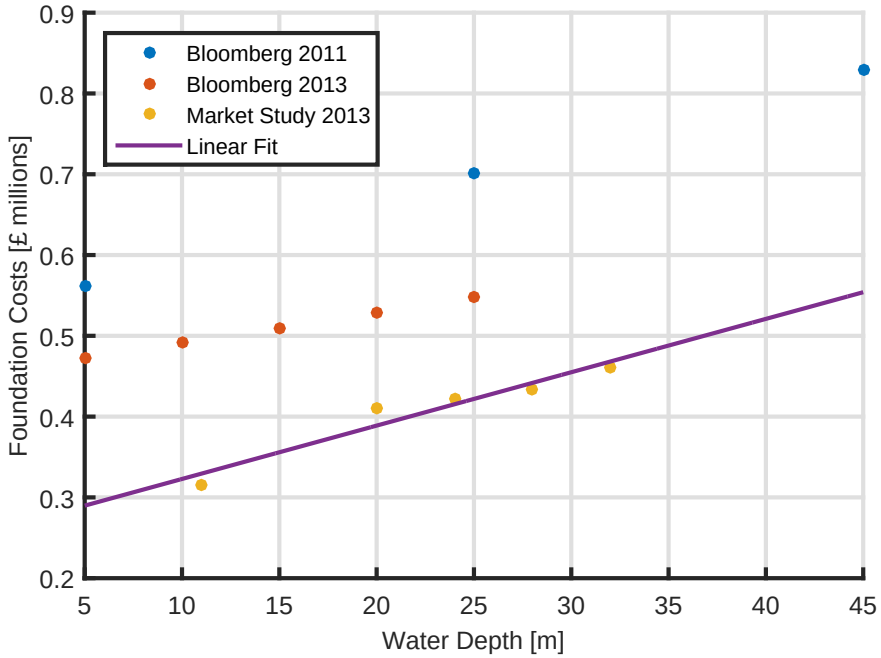

Figure 6.2: Normalized GBF costs per installed MW [221–223].

of the turbine that it must support. This mass, however, is not directly proportional to the power rating of the turbine [214]. Increasing the power rating of the turbine, would be expected to result in a less than proportional increase in turbine mass (see Figures 6.3 and 6.4). The approach taken where the cost of the foundation is normalized by the turbine rating, would therefore be expected to over-predict foundation costs for larger turbines, and under-predict the foundation costs for turbine sizes smaller than the base. To confirm this, however, similar GBF costs would need to be collected for a range of turbine types.

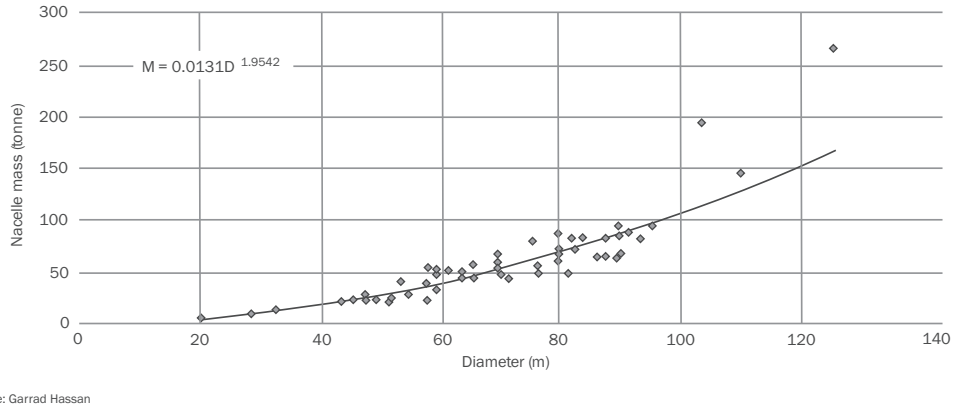

Figure 6.3: Scaling of wind turbine nacelle system mass for rotors of less than 80 m diameter [206].

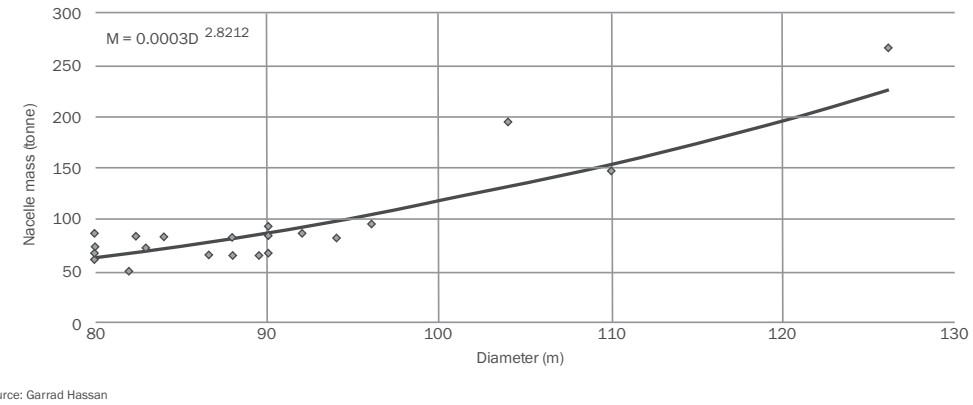

Figure 6.4: Scaling of wind turbine nacelle system mass for rotors of greater than 80 m diameter [206].

6.2.3.2 Monopile Foundation

Monopile foundations represent one of the most frequently used foundation types in offshore wind. Monopiles are generally a single cylindrical welded tube that is either driven or drilled into the seabed [136]. Like gravity based foundations, a number of empirical correlations have been built to describe the costs of monopile foundations. Elkinton [17] took a bottom up approach and based the monopile cost on the mass required given the loading conditions of the turbine and the soil parameters. This approach, however, reported errors of up to 49% for the pile embedment length, and up to 39% for the pile mass when applied to Horns Rev I [17]. This study attributes the error to the high sensitivity of the length, mass, and cost of the monopile to the soil parameters. In order to reduce the dependency on high quality soil data which likely would not be available when this tool would be deployed, simpler empirical relationships were sought, similar to the GBF foundation costs. Dicorato et al. [208] included a comparison of three empirical monopile cost functions identifying a function dependent on both the hub height and the rotor diameter as being the most accurate.

These correlations, unfortunately, only included small turbines with rated powers less than 3.6 MW, and therefore it remains unclear how accurate this relationship will be for larger turbines [208].

An alternate approach models the necessary mass of the monopile based on the RNA load and then converts this monopile mass to a cost based on the unit cost of materials. The present generation of 5 MW to 8 MW turbines are similar to one another with rotors of approximately 100 tonnes in mass, and nacelles ranging from 244 tonnes to 390 tonnes depending on the drive train configuration [214]. The total RNA mass for these turbines therefore ranges from approximately 350 tonnes to 500 tonnes. Table 6.4

indicates the monopile masses that can be expected for various depths for turbines with RNA masses of 340 t and 475 t RNA mass [224].

Table 6.4: Impact of Tower Head Mass on Monopile Mass [224].

	Monopile Mass [t]	
Water Depth [m]	475 t head mass	340 t head mass
20	500	520
25	700	650
30	950	800
35	1100	950
40	1325	1075

From the mass of a monopile, the cost can be estimated given a cost of finished steel for monopiles. This value was taken to be £2000 per metric tonne based on past work in this field [225].

$$C_{monopile} = £2000 \times m_{monopile} \tag{6.6}$$

Like the gravity based foundations, Bloomberg New Energy Finance [221, 222] have provided estimates for monopile costs at different depths. Comparing the various methods outlined above, the following comparison can be made:

Table 6.5: Monopile Foundation Costs for a 6 MW Turbine in £m

Depth [m]	Bloomberg [221]	Bloomberg [222]	Dicorato [208]	470 t Seidel [224]	340 t Seidel [224]
5	2.78	2.81	2.10	-	-
10	2.90	-	2.33	-	-
15	3.01	-	2.55	-	-
20	3.12	-	2.77	1.06	1.11
25	-	3.84	3.00	1.49	1.38
30	-	-	3.22	2.02	1.70
35	-	-	3.44	2.34	2.02
40	-	-	3.67	2.82	2.28
45	-	4.61	3.89	-	-

From Table 6.5 and Figure 6.5 it can be observed that the existing models all have costs which are linear with the water depth. The models by Bloomberg New Energy Finance [221], von Waldow et al. [222], and Dicorato et al. [208] also give the cost normalized by the power rating of the wind turbine implying a linear relationship between cost and turbine capacity. The models given by Seidel [224] also show a linear relationship with the water depth, but highlight that the curves have different slopes depending on the RNA mass.

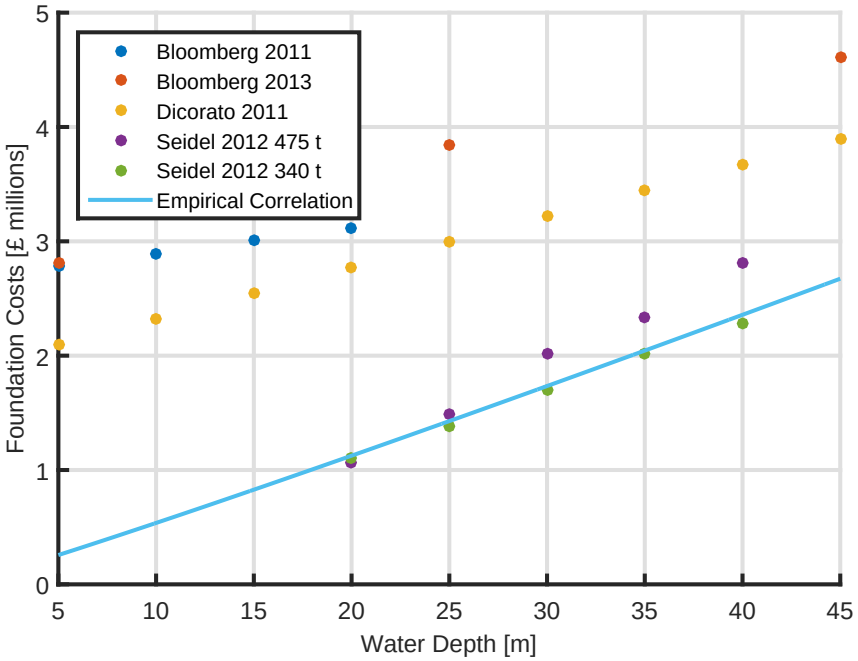

Figure 6.5: Monopile Cost for 6 MW Turbine in £m[208, 221, 222, 224].

As was the case with the GBF costs, the correlations presented by Bloomberg New Energy Finance [221, 222] assume that monopiles continue to be manufactured along the same lines as existing monopiles. This therefore, does not account for any design optimization over time and learning that has been ongoing. The model by Dicorato et al. [208] is based entirely on fitting the cost information for existing turbines. This work, therefore, seeks to explain the costs for current turbines while the Bloomberg New Energy Finance studies are projecting costs. The models by Seidel [224] represent a turbine manufacturer's estimate of the costs of foundations for one of their future turbines. This therefore does take into account the advances in monopile designs.

Given that the monopile mass would be expected to scale with both the water depth and the size of the turbine, it was decided to try and build an empirical correlation based on available data (data used for constructing the empirical correlation is listed in Appendix C). Rather than using the RNA mass, it was decided to use the *load factor*, (LF), a factor relating to the dimensions of the wind turbine first introduced by Dicorato et al. [208] for use in scaling the monopile costs. This is similar in the approach taken by Dicorato et al. [208], however, more turbines and especially larger turbines could be included thereby making the correlation more applicable to the next generation of turbines. This load factor is a term introduced by Dicorato et al. [208] and is a measure of the dimensions of the turbine; it is not equivalent to the capacity factor.

$$LF = H\left(\frac{d}{2}\right)^2 \tag{6.7}$$

where H is the hub height and d is the rotor diameter of the turbine.

This correlation found the mass of the monopiles to be given by a function of both the water depth (WD) and the load factor:

$$m_{monopile} = 26.7903 \cdot WD^{1.1967} \cdot LF^{0.4719} \tag{6.8}$$

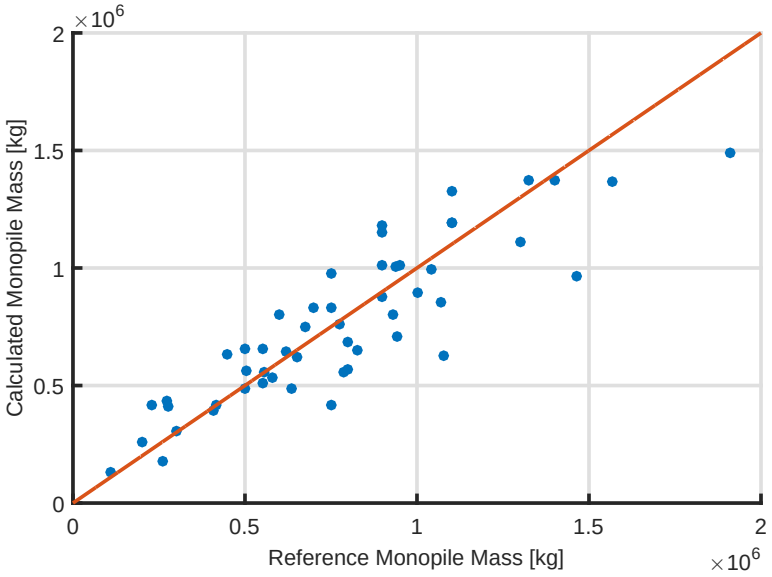

Figure 6.6: Empirical correlation fit to the available monopile mass data

The cost could then be determined using Equation 6.6. Overall, for the available data, this empirical correlation for the monopile masses (see Figure 6.6) has an RMS error of 23.4%. No available data for the costs of monopiles could be located, and as such it cannot be said how well this correlation works for the overall cost of monopiles. The spread observed in the data relative to the empirical correlation and relatively high error are likely due to the omission of the soil conditions which are known to have an impact on the foundation design and cost [17, 226]. From this mass correlation, it can be observed, that based on existing wind turbine monopiles, the assumption of a linear water depth dependency made by other empirical models fits the collected data well. However, the present correlation also considers a dependency on the size of the turbine a factor that many models choose to omit as they are specific to a particular turbine or turbine type.

As can be seen in Figure 6.5, the empirical correlation identified by surveying existing offshore wind turbine monopiles gives a relationship very similar to those given by Seidel

[224]. Interestingly the relationship by Seidel [224] is based on a bottom-up approach while the present correlation is based on surveying existing monopiles. The models by Bloomberg New Energy Finance [221], Bloomberg New Energy Finance [222], and Dicorato et al. [208] sit somewhere between these extremes in methodology and are based on a combination of surveying existing monopiles and a bottom-up engineering approach.

Existing cost functions which are based on the costs incurred by actual projects make use of data for small wind turbines thereby biasing the cost function towards these smaller turbines which do not use optimized monopile designs. More modern designs such as those proposed by Seidel [224] and those used to construct the present empirical relationship show that through the design optimization process undertaken by the industry, the mass of steel has reduced compared to what was initially identified, reducing the cost of monopiles as the majority of their cost is based on the cost of the raw materials.

6.2.3.3 Jacket Foundation

Previous studies looking specifically at offshore wind turbine foundation masses found an empirical relationship between the mass of a jacket (m_{jacket}) foundation and the water depth that it is installed and the nacelle mass (LD) similar in form to the monopile relationship that we have identified [227]. From this source, the mass of a jacket foundation is given by:

$$m_{jacket} = 16.0 \times WD^{0.19} \times LD^{0.48} \tag{6.9}$$

The unit cost of the finished steel for a wind turbine jacket is assumed to be $£4000/ton$ leading to the following cost relationship for jacket foundations:

$$C_{jacket} = £4000 \times m_{jacket} \tag{6.10}$$

The assumed steel price here is higher than that used for monopiles to account for the manufacturing complexity associated with jacket foundations [227].

The costs found using this methodology were originally validated against offshore substations, however, comparing the formula against correlations proposed by Bloomberg New Energy Finance (BNEF) based on data from a number of manufacturers show that the formula under-predicts the cost of smaller jackets which would be used for turbines [221].

Compiling a larger data set of jackets used both in offshore wind and in offshore oil and gas has allowed the relationship given by Kaiser and Snyder [227] to be updated taking into account not only jackets used for substations and large platforms, but smaller jackets designed for individual turbines (see Appendix C for the data used to create this empirical correlation). Doing so, gives the mass of the foundations to be given by Equation 6.11. This mass can then be converted to a cost using Equation 6.10.

$$m_{jacket} = 8.1734 \times WD^{0.7955} \times LD^{0.0917} \tag{6.11}$$

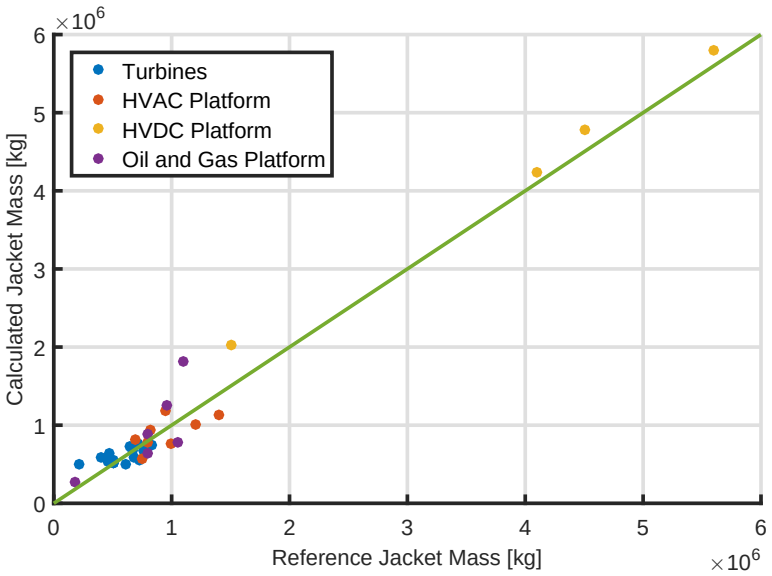

Figure 6.7: Empirical correlation fit to the available jacket mass data.

The jacket mass correlation built (see Figure 6.7) had an error of 27.9% when compared to the published masses of the structures. Like the monopile correlation, this error is due to the omission of soil conditions at the site, and the differences in the designs across different sites. Given the range of jackets used for this model, however, it is possible to estimate masses for a range of jacket sizes including individual turbines, HVAC platforms, and HVDC platforms.

Figure 6.8 shows the different jacket cost relationships considered. As can be seen, the empirical correlation built from existing jackets was found to have a similar shape as the other correlations and predicts similar results with regards to cost indicating that the mass relationship is at least consistent with the approaches taken by others.

As jacket foundations require pin-piles to secure the structure to the seabed, it is important that this is also considered in the full cost of foundation. van Wijnagaarden [228] previously developed a model to design these pin-piles and gave the pin-pile weights for a jacket foundation requiring four pin-piles.

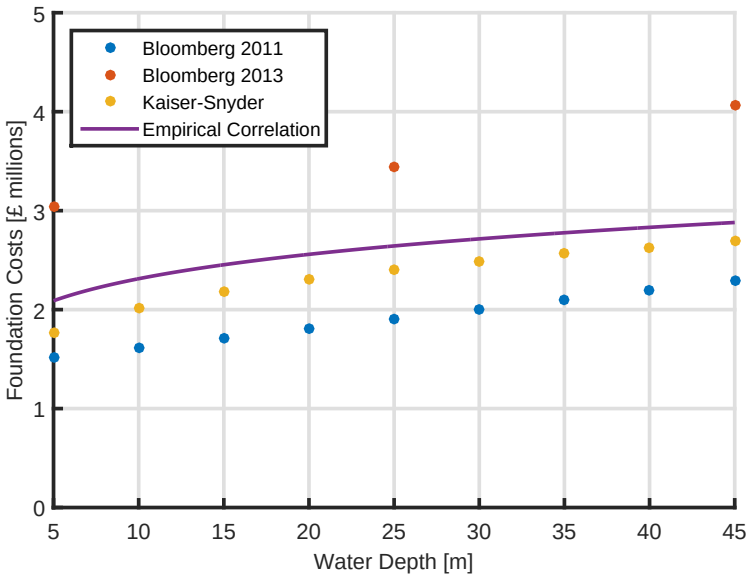

Figure 6.8: Costs of jacket foundations [221, 222, 227].

Table 6.6: Pin-Pile Mass [228]

Water Depth [m]	3.6 MW	6 MW	8 MW
20	558	1380	1800
40	339	793	1097
60	500	946	1244

The pin-piles used for a jacket foundation would be similar in design to a monopile, but as there would be four for each foundation, each pile would be significantly smaller in diameter and shorter. Their mass-cost relationship, however, would be expected to be similar to a monopile and therefore Equation 6.6 would apply to convert the mass of the pin-piles to costs.

6.2.4 Foundation Installation

Like the turbine installation sub-model, the foundation installation covers all costs of transportation of the foundations and TPs from the construction port to the turbine positions, and installation of these. It is therefore built in a similar manner as the turbine installation model; however, in addition to the installation process for the foundations and TPs a second operation is assumed to be required in order to complete the necessary site preparation prior to installation. The vessel used for this phase has a transport time which is computed in a similar manner as that described in the turbine installation module; however, there is no need for it to return to the construction port before completion of the preparatory work as no vessel capacity need be considered.

Additionally, as jacket foundations look to be the preferred foundation type for the larger offshore wind farms in deeper water, a specific model for jacket installation has been developed for use with jacket foundations only [214].

6.2.4.1 Self-Installation

A general approach for modelling the foundation installation costs is to use the same module as the turbine installation, but altering the vessel parameters to correctly represent the specifications of the foundation installation vessel. This time-based approach is taken by Kaiser and Snyder [211, 213, 227]. This methodology is based on estimating the time required to load, transport, and install the foundations and converting this to a cost by use of the vessel day rate. For the foundation model, the same equations apply as in the turbine installation models (Equations 6.3 and 6.4), however, the vessel parameters shown in Table 6.7 were used instead to represent the differences between the turbine and foundation installation processes.

Table 6.7: Foundation Installation - Default Vessel Parameters

Parameter	Symbol	Value	Source
Vessel Speed	v	6 kn	[213]
Vessel Capacity	q	3 units	[213]
Load Time	t_{load}	0.75 days	[204, 214]
Install Rate	$r_{install}$	3 $\frac{days}{foundation}$	[204, 214]
Mobilization	t_{mob}	14 days	[211]
Demobilization	t_{demob}	7 days	[211]
Availability	A	0.75	[211]
Day Rate	R	£160,000	[211]

Compared to the turbine installation, the jacket foundation installation is characterized by a decreased vessel capacity due to the greater deck space required for each foundation compared to the nacelle and blades. In principle, depending on the foundation type and size, the installation rate ($r_{install}$) would also vary, however, as a baseline 3 days per foundation is used. The vessel capacity is highly specific to the foundation design and the vessel that is being used for the project.

In order for these cost estimates to be accurate, accurate data regarding the project parameters and vessels to be used is necessary. It is therefore important for this framework to be of value, that valid parameters are used. Although some suggested values are provided, these will vary from project to project and site to site.

This approach does not model each component of the installation time, and therefore assumes that all installation processes are completed by the same vessel. Realistically, it is likely that some seabed preparatory work will need to be completed at each foundation

position prior to beginning the installation work. This work would require a different vessel, and a more detailed model might be better suited for capturing this. The way this model is built, however, it would be possible to include a position based time multiplier to account for slower drilling rates at specific turbine positions due to soil conditions. Again, at present as the soil conditions are omitted, this cost differential is not captured by the model. For each trip, the total time is therefore given by Equation 6.3.

Like the turbine installation, the transportation time, $t_{transport}$, is estimated by grouping the installation positions into clusters based on the vessel capacity, and then finding the shortest path between the port, and the turbines of each cluster. From this, the total distance to be covered by the installation vessel is known, and from the vessel speed (v), the total transportation time, $t_{transport}$ can be found.

The total cost is therefore given by:

$$C_{f,\ install} = R \times \left(t_{mob} + t_{demob} + \sum_{i=1}^{n_{trips}} (t_{trip,i}) \right) \tag{6.12}$$

where n_{trips} is the total number of trips from the construction port that the vessel must take. This is computed based on the number of turbines to be installed and the capacity of the vessel (q).

6.2.4.2 Barge Based Installation

The alternative to a self-installation model is a barge based approach. This installation method assumes that the installation vessel is supplied with foundations and TPs from supply barges and therefore the primary installation vessel need not return to port until all foundations have been installed. This effectively means that the capacity of the installation vessel is unlimited as it never needs to return to the construction port in order to resupply. This will result in a quicker total installation time, however, as supply barges are needed to support the installation vessels additional costs are accrued daily.

The barge based installation method is therefore modelled in the same manner as the self-installation; however, with the installation vessel capacity increased to infinity, and the vessel day rate changed to represent the cost of the additional vessels. In addition the time taken to load the barges is assumed to not affect the overall installation time as it is assumed that the supply barges are managed such that there is always an available foundation when needed by the installation vessel. Therefore, the load time does not need to be included in t_{trip} and as the capacity is infinite, there will always be a single trip for the installation vessel. Table 6.8 summarizes the necessary changes for the barge based installation strategy.

Table 6.8: Foundation Installation (Barge Strategy) - Default Vessel Parameters

Parameter	Symbol	Value	Source
Vessel Capacity	q	∞ units	[213]
Install Rate	$r_{install}$	3 $\frac{days}{foundation}$	[204, 214]
Mobilization	t_{mob}	14 days	[211]
Demobilization	t_{demob}	7 days	[211]
Day Rate	R	£210,000	[204, 211]

6.2.4.3 Jacket Installation - Specific Model

Rather than using the general approach outlined above, a more specific installation model to represent jacket foundations has been built. The cost of installing jacket foundations can be divided between two installation stages, the cost of the pre-piling phase and the cost of installing the jackets at the pre-piled positions.

Pre-Piling

Jacket foundations are characterized by having several small piles or pins that secure them in place to the seabed. In order to facilitate this, they are frequently pre-piled, that is, the positions are surveyed and drilled before the jackets are placed at the position in order to reduce the time that the heavy-lift vessel is required. The pre-piling stage therefore requires specialist equipment, however, the specialist vessel will not need to return to shore prior to completion of all the pre-piling as there is nothing that is being transported and placed at the wind farm site at this stage.

The pre-piling cost is therefore based on the vessel and equipment parameters given in Table 6.9.

The total cost of pre-piling can therefore be computed as:

$$C_{pre-piling} = (t_{mob,p} + t_{demob,p}) \times R_p + (C_{mob,d} + C_{mob,equip} + C_{overhead}) + (n_t \times C_{drill}) + (R_{crew,p} + R_{crew,d} + R_s + R_{cleaning} + R_p) \times \frac{n_t \times r_{pre} + t_{transport}}{A} \tag{6.13}$$

where n_t is the number of turbine foundations to be installed. The $C_{overhead}$ term includes the fixed costs of sea-fastening all equipment, any surveys that need to be completed, the fabrication of any drilling templates, and any remaining costs that will be incurred only once for the pre-piling process. The majority of the pre-piling costs are layout independent as they must be incurred for each foundation position, however, the layout directly affects the transportation time from the port and to the foundation positions, thereby affecting the overall pre-piling costs. Table 6.9 gives the cost parameters for the installation of the jacket pre-piles.

Table 6.9: Jacket Installation - Pre-Piling Cost Parameters

Parameter	Symbol	Value	Source
Vessel Speed	v	6 kn	[211]
Pre-piling Vessel - day rate	R_p	£120,000	[211]
Mob/Demob of Pre-piling Vessel	$C_{mob,d}$	£1,500,000	[204]
Overhead Costs	$C_{overhead}$	£2,400,000	[204]
Pile Cleaning - day rate	$R_{cleaning}$	£2,000	[204]
Pre-piling rate	r_{pre}	2 days/foundation	[204]
Mob/Demob Drilling Equip.	$C_{mob,equip}$	£750,000	[204]
Drilling gear/crew - day rate	$R_{crew,d}$	£20,000/day	[204]
Drilling cost per position	C_{drill}	£50,000	[204]
Mob. Pre-piling Vessel	$t_{mob,p}$	14 days	[204]
Demob. Pre-piling Vessel	$t_{demob,p}$	7 days	[204]
Availability	A	0.75	[211]
Pre-pile Crew	$R_{crew,p}$	£30,000/day	[204]
Spread day rate	R_s	£10,000/day	[213]

Jacket Installation

The second stage of the installation of the jacket foundations following the pre-piling work is to transport the jackets from the construction port to the turbine positions and to install them there. This process is done in a manner similar to the generalized foundation installation calculation (Equations 6.3 and 6.12), looking at the time required to complete the installation process and then converting this time to a cost based on the vessel costs. Given the jacket installation parameters outlined below, the cost of installing all the jackets assuming a single installation vessel are given by Table 6.10.

Table 6.10: Jacket Installation - Jacket Installation Cost Parameters

Parameter	Symbol	Value	Source
Vessel Speed	v	6 kn	[213]
Vessel Capacity	q	3 units	[213]
Load Time	t_{load}	0.75 days	[204, 214]
Install Rate	$r_{install}$	1.5 $\frac{days}{foundation}$	[204, 214]
Mobilization (days)	t_{mob}	14 days	[211]
Demobilization (days)	t_{demob}	7 days	[211]
Availability	A	0.75	[211]
Day Rate	R	£160000	[211]

6.2.4.4 Scour Protection

The final piece for many foundation installation processes is the deployment of scour protection to aid in reducing the erosion around the foundation structure. This is modelled in a similar manner to the barge installation strategy, however, with a reduced installation time compared to the foundation installation, and decreased vessel day rate as no heavy lift vessel will be needed.

6.2.5 Intra-Array Cables

The intra-array cables cost model considers all the necessary cabling works necessary to connect the turbines to the substations and models the cost for both the delivery of the extruded cables to the construction port, and the cost of using a specialist cable burial vessel to trench the cable. The costs are broken down into two further models: the supply of the cables, and the installation of the cables.

6.2.5.1 Cable Supply

Using the intra-array cable optimization tool developed as part of this project (Chapter 4), it has been possible to design optimized intra-array cable configurations given a set of turbine positions and cable parameters. From this optimized layout, the tool provides the horizontal cable lengths required along with the cross-section. The total cable to be supplied includes this horizontal length, an additional vertical length, some spare cable, and the costs associated with a termination. These termination costs include not only the cost of the physical termination, but also of sealing all hang-offs, including communications cables, and the cost of a cable bending restriction. Based on industry standard estimation methods, the vertical length (l_v) of cable is defined to be:

$$l_v = 2 \times (l_{LAT} + l_{\text{interference}} + l_{damage}) \tag{6.14}$$

where l_{LAT} is the water depth at lowest astronomical tide (LAT), while $l_{\text{interference}}$, and l_{damage} are two surplus lengths introduced to account for any interference variation and to give some surplus in the event of damage.

The total number of termination boxes is twice the number of cable segments as one termination box is needed at each end of the cables.

The total length of cable is therefore given by:

$$l_C = (1 + spare) \times l_h + (l_v \times n_{termination}) \tag{6.15}$$

where *spare* is a predefined surplus amount of cable to account for any variations in bathymetry, generally taken to be 2.5% of the total horizontal length of cable.

The total cost for the supply is therefore the total length for each conductor size multiplied by the unit cost of the cables (see Table 6.11).

$$C_{cable\ supply} = \sum_{i=1}^{N_c} r_i \times l_{C,i} \tag{6.16}$$

Table 6.11: AC Three-Phase Cable Costs Per Metre (r_i) for Copper Conductors [229]

Conductor Diameter [mm]	33 kV	66 kV
95	£140	£170
120	£153	£183
150	£157	£191
185	£179	£213
240	£204	£247
300	£238	£289
400	£272	£327
500	£319	£383
630	£361	£434
800	£442	£531

In general 66 kV cables are more expensive than their 33 kV counterparts (for same size of conductors) as the construction for 66 kV "wet" designs requires greater insulation and as a result of this must be run through an extruder a slower speed. In addition the larger overall cable diameter due to the increased insulation results in a lower capacity on the same sized drum requiring more splices [202].

6.2.5.2 Cable Installation

The installation of the intra-array cables like the installation of foundations is made up of a number of processes each of which can be modelled independently. For the purposes of this model, it is assumed that all cables are trenched and laid separately. The costs can therefore be attributed to trenching, and then laying the subsea cables.

Cable Trenching

The first step of the cable installation, the cutting of the trenches, is modelled based on a series of vessel parameters outlined in Table 6.12 and the total horizontal length for which trenches need to be dug.

From this, the trenching cost is based on estimating the total amount of time needed to trench the cables, and multiplying this time by the vessel day rate. The total cost of trenching is therefore given by:

$$C_{trenching} = (R_{vessel} + R_{support}) \times \left(\frac{l_h \times n_{passes}}{A \times r_{trenching}} + t_{mob} + t_{demob} \right) \tag{6.17}$$

Table 6.12: Cable Trenching - Default Vessel Parameters

Parameter	Symbol	Value	Source
Vessel Day Rate	R_{vessel}	£55,000	[211]
Support Vessel Day Rate	$R_{support}$	£20,000	[204]
Mobilization	t_{mob}	14 days	[211]
Demobilization	t_{demob}	7 days	[211]
Trenching Speed	$r_{trenching}$	200 m/h	[204]
Number of passes	n_{passes}	2	[204]
Availability	A	0.75	[211]

Cable Laying

The next step is to model the costs associated with laying the cables. This is done in a similar process based on the vessel parameters and the rate at which cables can be laid (Table 6.13). Like other processes, this is based on a time conversion, and a monetization of this time-based on the vessel costs of both the main cable vessel as well as any additional support vessels. In this case, it is expected that two support vessels are needed.

$$C_{laying} = (R_{vessel} + R_{support}) \times \left(\frac{l_h}{r_c \times A} + t_{mob} + t_{demob} \right) \tag{6.18}$$

Table 6.13: Cable Laying - Default Vessel Parameters

Parameter	Symbol	Value	Source
Vessel Day Rate	R_{vessel}	£115,000	[211]
Support Vessels Day Rate	$R_{support}$	£60,000	[204]
Mobilization	t_{mob}	14 days	[211]
Demobilization	t_{demob}	7 days	[211]
Cable Laying Rate	r_c	2 km/h	[204]
Availability	A	0.75	[211]

6.2.6 Decommissioning

The decommissioning costs of an offshore wind farm remain highly uncertain as no large offshore wind farms have yet been decommissioned. Presently, only Vindeby and Yttre Stengrund wind farms, 5 MW and 10 MW wind farms respectively, have started the decommissioning process [7]. Furthermore, foundations may act as artificial reefs promoting growth of marine species. As the wind farm is decommissioned, it may therefore be deemed better environmentally to leave the foundations in place than to remove them and disrupt the marine species that have grown on the structure [230]. The decommissioning cost model is based on removing all turbines and foundations and therefore represents the maximum cost to be incurred by the project. This model also does not consider potentials for recycling the materials for cost recovery. This therefore mimics the installation modules for both the foundations and turbines and is based on the time for which boats must be hired. Like the installation processes it is assumed that the foundations and turbines are decommissioned in separate steps.

The decommissioning costs for the turbines are therefore given by the parameters in Table 6.14.

Table 6.14: Turbine Decommissioning - Default Vessel Parameters

Parameter	Symbol	Value	Source
Average Vessel Speed	v_t	6 kn	[213]
Vessel Capacity	q_t	5 units	[213]
Vessel Unload Time	$t_{unload,t}$	5.5 days	[204, 214]
Vessel Rate	$r_{decommission,t}$	3 $\frac{days}{turbine}$	[204, 214]
Mobilization	$t_{mob,t}$	14 days	[211]
Demobilization	$t_{demob,t}$	7 days	[211]
Availability	A_t	0.75	[211]
Day Rate	R_t	£110,000	[211]

The total time for a single trip which the decommissioning vessel must be hired is given by:

$$t_{trip,t} = (t_{unload} + t_{transport} + q_t \times r_{decommission,t}) \times \frac{1}{A_t} \tag{6.19}$$

where $t_{transport}$ is the time spent transiting from the port to all of the turbines. This is the only element of the decommissioning costs that is layout dependent and like the installation processes this is estimated using the clustering and pathfinding approach.

The total decommissioning cost is therefore given by:

$$C_{DECEX,t} = R_t \times \left(t_{mob,t} + t_{demob,t} + \sum_{i=1}^{n_{trips,t}} (t_{trip,t,i}) \right) \tag{6.20}$$

In the same manner, the decommissioning costs for the foundations are defined by the vessel parameters in Table 6.15.

Table 6.15: Foundation Decommissioning - Default Vessel Parameters

Parameter	Symbol	Value	Source
Average Vessel Speed	v_f	6 kn	Kaiser and Snyder [213]
Vessel Capacity	q_f	4 units	Kaiser and Snyder [213]
Vessel Unload Time	$t_{unload,f}$	5.5 days	Douglas Westwood [214], Hui et al. [204]
Vessel Rate	$r_{decommission,f}$	0.5 $\frac{days}{turbine}$	Douglas Westwood [214], Hui et al. [204]
Mobilization	$t_{mob,f}$	14 days	Kaiser and Snyder [211]
Demobilization	$t_{demob,f}$	7 days	Kaiser and Snyder [211]
Availability	A_f	0.75	Kaiser and Snyder [211]
Day Rate	R_f	£110,000	Kaiser and Snyder [211]

$$t_{trip,f} = (t_{unload,f} + t_{transport,f} + q_f \times r_{decommission,f}) \times \frac{1}{A_f} \tag{6.21}$$

The total cost is therefore given by:

$$C_{DECEX,f} = R_f \times \left(t_{mob,f} + t_{demob,f} + \sum_{i=1}^{n_{trips,f}} (t_{trip,f,i}) \right) \tag{6.22}$$

Though there is a layout dependent element to the decommissioning costs it should be noted that due to all costs being discounted and decommissioning occurring at the end of the wind farm's life, these costs when discounted have a small contribution to the LCOE and therefore, a very small impact on the overall layout optimization.

6.2.7 Operations and Maintenance (O&M)

Like the decommissioning process there is significant uncertainty over the lifetime operations and maintenance costs of a large offshore wind farm. In order to capture the main drivers of the operations and maintenance costs, it was decided to base the model on the installed capacity and the turbine positions. In this way, turbine reliability statistics are *not* incorporated, and the model will not accurately consider the differences in reliability between different turbine models. At the same time, given the difficulty in characterizing the impact that operating in a wake can have on the fatigue damage, this effect is also not considered in estimating the O&M costs.

In order to model the O&M costs, an estimate made by a developer for both a 500 MW and a 1000 MW offshore wind farm were used to define the cost variability with capacity [231]. As this source gives an itemized breakdown of the O&M costs for two different sized wind farms, it is possible to design a simplistic relationship between the capacity of an offshore wind farm and the O&M cost using a Cobb-Douglas function [232].

The Cobb-Douglas function applied to the line-item costs as a function of the installed capacity gives:

$$C_p = C_{baseline} \times \left(\frac{\text{Driver}_p}{\text{Driver}_{baseline}} \right)^b \tag{6.23}$$

where C_p and $C_{baseline}$ are the project O&M costs and the baseline O&M costs respectively, and Driver_p and $\text{Driver}_{baseline}$ are the cost driver of the project at hand and the baseline case respectively. In this case the cost driver is either installed capacity or distance to shore. The parameter b is defined as the elasticity parameter and is given for each line item cost as:

$$b = \frac{ln(1+x)}{ln(2)} \tag{6.24}$$

where x is a measure of how that specific line item cost scales with the driver, in this case capacity. These parameters are derived from work by Chu et al. [232] using the same base O&M cost data.

Table 6.16 shows the O&M costs for both 500 MW and 1000 MW wind farms along with the x measures.

Using the Cobb-Douglas function again, the same approach was taken to establish the variation of the cost items with the distance from the operations and maintenance port.

As this model only looks at the effect on costs that the capacity (Q) and distance (D) from shore have, the combined Cobb-Douglas function can be written as:

$$C_p = C_{baseline} \times \left(\frac{Q_p}{Q_{baseline}} \right)^{b_1} \times \left(\frac{D_p}{D_{baseline}} \right)^{b_2} \tag{6.25}$$

Table 6.16: Annual Operations and Maintenance Cost Variability with Capacity and Distance [231, 232]

Item	500 MW	1000 MW	$x_{capacity}$	$x_{distance}$
SPV Management Costs				
SPV Costs	£1,500,000	£2,250,000	0.50	0.00
Insurance	£7,556,000	£15,112,000	1.00	0.00
SPV Contingency	£400,000	£600,000	0.50	0.00
Fixed O&M				
Onshore Service and maintenance	£500,000	£750,000	0.50	0.00
Service Base	£200,000	£300,000	0.50	0.00
Asset Management	£2,079,000	£3,258,000	0.57	0.00
Environmental Monitoring	£800,000	£1,400,000	0.75	0.20
Training Facilities	£500,000	£500,000	0.00	0.00
Electricity	£250,000	£500,000	1.00	0.00
Emergency Capability	£500,000	£1,000,000	1.00	0.20
HSE Costs	£500,000	£1,000,000	1.00	0.00
Cable and Electrical monitoring	£200,000	£400,000	1.00	0.50
Offshore Platform Servicing	£300,000	£600,000	1.00	0.50
Boat Maintenance	£600,000	£1,200,000	1.00	0.00
Maintenance Costs				
First Maintenance Costs	£12,190,000	£23,565,000	0.93	0.33
Second Line Maintenance Costs	£2,411,000	£4,512,000	0.87	0.90
Third Line Maintenance Costs	£15,000,000	£29,112,500	0.94	0.50

The total annual operations and maintenance cost using this approach is then given by:

$$C_{O\&M} = \sum_{i=1}^{\text{line items}} \left(C_{baseline,i} \times \left(\frac{Q_{p,i}}{Q_{baseline,i}} \right)^{b_{1,i}} \times \left(\frac{D_{p,i}}{D_{baseline,i}} \right)^{b_{2,i}} \right) \tag{6.26}$$

6.2.8 Offshore Transmission

The final cost element to be included is the offshore transmission asset and fees to be paid to the offshore transmission operator (OFTO). In the UK, it is required by the regulator (Ofgem) that the offshore transmission assets are owned by a company separate to the wind farm operator. This therefore means that part of the CAPEX for the construction of the transmission assets is not incurred by the wind farm project, instead an annual fee is paid to the OFTO. Generally, wind farm operators select to build the offshore transmission assets and then transfer these to an OFTO in order to ensure that the design is compliant and represents the best value for the wind farm

project. As the wind farm developer generally builds these assets, part of the CAPEX is incurred by the project while the rest is transferred to the OFTO when the offshore transmission assets are transferred [233, 234].

The offshore transmission asset is therefore made up of two terms, one CAPEX term representing the non-recoverable OFTO CAPEX, and an annual fee that is to be paid to the OFTO which is included as an OPEX term. Both of these terms are based on the initial CAPEX required to build the offshore transmission asset, and therefore the first step in including all the OFTO cost elements is to understand the CAPEX associated with the construction of the offshore substation, the export cables, the onshore substation, and any onshore export cables.

In general, the offshore transmission asset costs will be relatively inelastic to the layout. The size of the substation and the costs associated with this will be fixed dependent on the size of the wind farm. The only element of the offshore transmission costs that will have some layout dependency is the cost of the export cable as this is dependent on where the substation is located relative to the intra-array cables and the landfall location.

6.2.8.1 Offshore Substation

The main cost for an offshore substation is the MV/HV transformers which are needed to step-up the collection network voltage to the export level. Based on the capacity of the wind farm phase, the transformer cost can be determined based on the following empirical relationship given by Dicorato et al. [208] for transformers with rating, X_{rating}, greater than 150 MVA:

$$C_X = 36.2848 \times 10^6 \times X_{rating}^{0.7513} \times n_X \qquad [£] \tag{6.27}$$

As this tool is being designed with UK Round 3 wind farms in mind, it was decided on discussion with the development team of a Round 3 site to design the substations to have 2 export cables and therefore 2 transformers (n_X), each sized to have surplus capacity [234]. This surplus capacity shown in Equation 6.28 is only indicative, and the precise value used will depend on the level of redundancy that the wind farm developer wishes to include. Given this level of excess capacity, each of the transformer ratings (X_{rating}) would be given by:

$$X_{rating} = \frac{P_{wind\ farm}}{n_X} \times \frac{3}{2} \quad [\text{MVA}] \tag{6.28}$$

For a 500 MW substation, this therefore requires two transformers each rated at 375 MVA.

The medium voltage (MV) switchgear is also given by Dicorato et al. [208] and is based on the voltage level of the collection network (V) and the number of strings connected to the substation (n_s):

$$C_{MV} = 3.44 \times 10^4 + 6.46 \times 10^2 \times V n_s \qquad [£] \tag{6.29}$$

The substation also needs to have high voltage (HV) bays to accommodate the export cable. These costs are determined based on guidance from National Grid [235] provided by National Grid.

$$C_{HV} = 3160000 \times n_{export} \qquad [£] \tag{6.30}$$

The final element of the offshore high voltage substation (OHVS) cost is the cost of the platform itself including all installation costs. This cost is estimated based on an empirical relationship proposed by Dicorato et al. [208] based on surveying the costs of existing OHVS platforms. This empirical relationship has also been shown to be in close agreement with values quoted in the COIN Document [235].

$$C_{platform} = 2.153 \times 10^6 + 7.54 \times 10^4 \times P_{wind\ farm} \qquad [£] \tag{6.31}$$

The total cost of the offshore substation is therefore given by:

$$C_{OHVS} = C_X + C_{MV} + C_{HV} + C_{platform} \qquad [£] \tag{6.32}$$

6.2.8.2 Offshore Export Cable Supply

The next step of the OFTO calculation is the cost of the offshore export cables. For the purposes of this tool, the number of export cables is taken as an input and it is assumed that there is 25% additional capacity across these export cables in order to give some degree of redundancy in the event of a cable failure. The 25% value was selected based on discussions with experts in the field [234].

The export cable cost, is therefore based on selecting the appropriate cross-section to accommodate the power that is to be exported and the length of cable needed:

$$C_{oe} = r_i \times l_c \times n_{export} \tag{6.33}$$

where r_i is the unit cost of the export cable given by cross-section in Table 6.17 and the cable limits are given in Table 6.18.

Table 6.17: AC Export Cable Costs [229]

Area [mm]	132 kV	150 kV	220 kV
630	£520	£532	£595
800	£637	£652	£729
1000	£759	£782	£875
1200	£881	£901	£1008
1600	£1126	£1152	£1288
2000	£1372	£1403	£1569
2500	£1678	£1716	£1919

Table 6.18: AC Export Cable Current Ratings [229]

Area [mm]	132 kV	150 kV	220 kV
630	778 A	774 A	765 A
800	858 A	855 A	843 A
1000	947 A	940 A	921 A
1200	990 A	981 A	960 A
1600	1061 A	1051 A	1025 A
2000	1299 A	1187 A	1181 A
2500	1375 A	1258 A	1248 A

6.2.8.3 Offshore Export Cable Installation

The export cable installation methodology is based on a similar methodology as the intra-array cables; however, it is not explicitly broken down into different vessels for the trenching and laying steps. Compared to the intra-array cable, it is anticipated that the export cable will represent a more significant single length of cable and therefore a simultaneous lay and bury installation approach will likely be deployed [236]. The cost parameters for the export cable installation are given in Table 6.19.

Table 6.19: Offshore Export Cable Installation - Parameters [237]

Item	Symbol	Rate
Pre-lay speed	$R_{pre-lay}$	800 m/hr
Post-installation survey speed	$R_{post\ survey}$	500 m/hr
Trenching speed	$R_{trenching}$	75 m/hr
Average backfill speed	$R_{backfill}$	500 m/hr
Weather allowance	W	0.70
Day Rate	r_{vessel}	£115,000

Like other installation processes, these parameters are used to compute the time required to install the component at hand, in this case, the offshore export cables. The vessel day rate, r_{vessel} is then used to convert this time to a cost. The total cost is

therefore given by:

$$C_{\text{offshore export installation}} = n_{export} \times r_{vessel} \times \left[\frac{1}{W} \times l_c \times \frac{1}{24}\left(\frac{1}{R_{pre-lay}} \times \frac{1}{R_{post\ survey}} \times \frac{1}{R_{trenching}} \times \frac{1}{R_{backfill}}\right)\right] \tag{6.34}$$

6.2.8.4 Onshore Works

The final component of the OFTO CAPEX is the estimation of the costs of some of the onshore works. The onshore elements of the OFTO include the cost of grid connection, the cost of landfall, the onshore export cable, the onshore substation, enabling costs representing the costs incurred by the first phase of the wind farm in a project of multiple substations, and a general 'other' category.

Each of these is estimated based on discussions with National Grid [235] and are given in Table 6.20.

Table 6.20: OFTO Onshore Works - Parameters [235]

Item	Symbol	Rate
Grid Connection	r_{grid}	£4,880,000
Landfall	$r_{landfall}$	£840,000
Onshore Cable Cost	$r_{cable,onshore}$	£467,500/km
Onshore Cable Installation	$r_{install,onshore}$	£386857.14/km
Onshore Substation	$C_{onshore\ substation}$	£87,200,000
Enabling Works	$C_{enabling\ works}$	£10,170,000
Other	C_{other}	£26,000,000
OFTO Non-Recoverable CAPEX	U_{OFTO}	0.08

The onshore substation enabling works are designed to allow later project phases to be connected to the same substation, and the 'other' costs are only realized for the first substation. All subsequent project phases do not require these costs and therefore have lower CAPEX than the first project phase. The formulae below give the estimation for the cost of the first OFTO and later OFTOs respectively.

$$\begin{aligned} C_{\text{onshore,first}} = {} & n_{export}(r_{grid} + r_{landfall} + l_{c,onshore} \times r_{cable,onshore}) \\ & + l_{c,onshore} \times r_{install,onshore} + C_{onshore\ substation} \\ & + C_{enabling\ works} + C_{other} \end{aligned} \tag{6.35a}$$

$$\begin{aligned} C_{\text{onshore,others}} = {} & n_{export}(r_{grid} + r_{landfall} + l_{c,onshore} \times r_{cable,onshore}) \\ & + l_{c,onshore} \times r_{install,onshore} \end{aligned} \tag{6.35b}$$

6.2.8.5 Calculation of Transmission Fee

The final step of the offshore transmission asset costs is specific to the regulatory requirements in the UK. In the UK, as the transmission asset must be sold to an OFTO and an annual fee paid to the OFTO, the LCOE contribution from the offshore transmission assets comes in the form of the annual fee paid to the OFTO. This annual fee is based on three components, one of which is based on the CAPEX of the transmission assets. The above approach therefore estimates this CAPEX term which is used to compute the transmission fee correctly.

The transmission fee is defined by a structure created by National Grid and the regulator OFGEM. This transmission fee is made up of three terms [234].

1. Transmission Network Use of System Charges - Local (TNUoS-Local);
2. Transmission Network Use of System Charges - Zonal (TNUoS-Zonal); and
3. Balancing Services Use of System Charges (BSUoS).

The TNUoS-Local component represents the local charges for the cost of installing and maintaining the transmission system and is based on a correlation given by National Grid [234].

$$TNUoS_{local} = 0.80\,(3.76 + 0.0706 \times (1 - U_{OFTO}) \cdot C_{CAPEX} + 0.5) \tag{6.36}$$

where U_{OFTO} is the unrecoverable OFTO CAPEX proportion.

The TNUoS-Zonal and BSUoS charges, however, are not dependent on the CAPEX, but rather the rated capacity of the transmission asset, where the wind farm is located geographically, and the annual generation. Based on where the wind farm is located, National Grid has defined tariffs for generators which would be applied. The TNUoS-Zonal charge is therefore defined by three components: a shared year-round tariff (r_s) which is scaled by the annual capacity factor of the generator; a non-shared year-round tariff (r_{ns}); and a residual tariff (r_{res}) which is payable by all generators. These tariffs are all regionally specific and can vary significantly depending on the location of the wind farm. The total TNUoS-Zonal charge is therefore given by the product of these rates and the installed capacity of the wind farm as shown in Equation 6.37 [238].

$$TNUoS_{zonal} = (r_s \times f_{load} + r_{ns} + r_res) \times P_{wind\ farm} \tag{6.37}$$

The BSUoS charge, is also given based on a regionally specific tariff; however, it is dependent on the AEP of the wind farm and not the installed capacity [239]:

$$BSUoS = r_{BSUoS} \times AEP \tag{6.38}$$

The annual fee to be paid is then given by:

$$C_{OFTO} = TNUoS_{local} + TNUoS_{zonal} + BSUoS \tag{6.39}$$

As this is an annual fee, it is implemented in the LCOE calculation as an OPEX term that is incurred in each year of operation.

6.2.9 Levelization of Costs

As this tool has been developed with the levelized cost of energy (LCOE) in mind, it is important to identify when the different costs are incurred. For the purpose of this model, this was seen as an input, as the construction duration would be a factor of the size of the wind farm and the CAPEX spend profile that the developer was comfortable with. In general, it is assumed that the CAPEX spend is equally spread across the construction duration and then OPEX is incurred in each year of operation. The decommissioning terms must be set to be incurred during the decommissioning period at the end of life in order for the levelization of the cost to be done correctly.

The LCOE was therefore calculated based on the net costs incurred in each year on an annual basis. which was taken as an input. The lifetime costs are levelized using the following formulae:

$$C_{levelized} = \sum_{t=1}^{n} \frac{C_t}{(1+r)^t} \tag{6.40}$$

From this, the LCOE can be computed as per the definition given by Tegen et al. [36] and Foster et al. [37]:

$$\text{LCOE} = \frac{C_{levelized}}{\sum_{t=1}^{n} \frac{\text{AEP}_t}{(1+r)^t}} \tag{6.41}$$

where r is the real discount factor that is assumed over the life time of the project and n is the years in the project life. The discount factor represents the time value of money and is generally on the order of 8-12% for commercial power projects in the UK [14].

6.3 Chapter Summary

This chapter has outlined the cost estimation methodology which has been implemented as part of the offshore wind farm layout optimization framework. The constructed cost model has focused on identifying and capturing the layout-dependent cost elements. Therefore, though the absolute cost may not be the most accurate, it is believed that for the purposes of layout optimization the relative cost will be sufficiently accurate to aid in the differentiation between different layouts. By linking this model for a wind farm's lifetime cost to the previously described assessment steps allows an offshore wind farm layout to be evaluated by calculation of the LCOE.

The parametric cost model is based around eight principal cost centres has been developed which can estimate the lifetime costs of an offshore wind project. For these cost centres, a range of cost models have been implemented in order to describe various design options available to the project developer. The end user of the wind farm layout optimization framework can therefore select the most appropriate models for the particular site in order to accurately assess the project costs. Where possible, these different approaches have been validated against available published data and benchmarked against one another. Each of the methods implemented have, however, been developed with a large project exceeding 500 MW in mind, and the regulatory framework of the UK is considered. The present models should therefore only be applied to projects of this size in the UK. Full deployment of the optimization framework is detailed in Chapter 7.

Chapter 7

Deployment of the Layout Optimization Framework

7.1 Introduction

The preceding chapters have discussed the various components of the constructed layout optimization tool; however, these chapters have not explored the application of the integrated framework. Once the electrical infrastructure optimization, annual energy production, and cost estimation have been independently validated, integrated with one another, and linked through the implementation of the optimization algorithms, a complete layout optimization tool has been developed which is capable of minimizing the levelized cost of energy of an offshore wind farm through the consideration of different layout alternatives.

This chapter explores the application of the tool to standard "benchmark" tests used in the wind farm layout optimization community, a real existing wind farm site, and a proposed offshore wind farm based on a UK Round 3 site. Through these case studies it should be possible to observe:

- improvements the present framework offers over existing layout optimization tools;
- improvements that could have been made to an existing wind farm had layout optimization been considered during the planning stage; and
- the applicability of such a tool for large future offshore wind farms.

As described in the preceding chapters, the constructed framework follows the traditional paradigm for this problem in including a wake model, a cost function, and an optimization algorithm. However, the principal extensions of the traditional paradigm made in this work are:

- the use of more advanced wake models than the Jensen/Park models;
- the inclusion of the substation positions and intra-array cabling considering constraint regions;
- the inclusion of layout impacted cable losses;

- the integration of a parametric cost model; and
- the implementation of three different levels of turbine placement constraints.

These additions to the current paradigm will increase the ability for the optimization process to discern between different layouts and better identify good layouts through a more accurate estimation of the wind farm LCOE; this is demonstrated in the cases considered in this chapter. For each of the cases studied, the GA and PSO were executed considering all three modes of operation described in Chapter 3. For the cases given by Mosetti et al. [34], a grid of allowable turbine positions was defined as part of the case definition and was therefore used when the binary decision version of the problem was addressed.

For all studies, a population size of 100 individuals was used, and convergence was said to occur if either the diversity of the population fell below 10% or there was no improvement in the best solution over 50 generations or iterations. Table 7.1 gives an overview of all the cases explored in this chapter, while Tables 7.2 and 7.3 describe the parameters of the GA and PSO respectively.

Table 7.1: Summary of Executed Case Studies

Case	Number of Turbines	Turbine Capacity [MW]	Total Installed Capacity [MW]	Number of Offshore Substations	Area [km^2]
Mosetti Case 1	26	0.659	17	1	4.0
Mosetti Case 1	30	0.659	20	1	4.0
Mosetti Case 2	19	0.659	13	1	4.0
Mosetti Case 2	39	0.659	26	1	4.0
Mosetti Case 3	15	0.659	10	1	4.0
Mosetti Case 3	39	0.659	26	1	4.0
Middelgrunden	20	2.00	40	0	5.7
UK Round 3	175	6.00	1050	3	152.6

Table 7.2: Genetic Algorithm Parameters

Parameter	Description
Population Size	100
Maximum Generations	1000
Probability of Crossover	Adaptive
Probability of Mutation	Adaptive
Elitism	20%
Stop Criteria	Diversity $< 10\%$
	$\frac{\text{Mean Score}-\text{Best Score}}{\text{Best Score}} \leq 0.001$
	Maximum generations reached
	No improvement over 50 generations

Table 7.3: Particle Swarm Parameters

Parameter	Description
Swarm Size	100
Maximum Generations	1000
Velocity Clamping	Dynamic
Velocity Transfer Function (Binary Encoding)	$T(x) = \left\lvert \frac{2}{\pi} \times arctan\left(x \cdot \frac{\pi}{2}\right) \right\rvert$
Neighbourhood Topology	Global (gBest)
Stop Criteria	Diversity $< 10\%$
	Maximum generations reached
	No improvement over 50 generations

7.2 Mosetti et al. Cases

In the first work to explore the optimization of wind farm layouts, Mosetti et al. [34] laid out three fictional case studies which have been used since to benchmark the performance of wind farm layout optimization tools. Each of these cases considers a square shaped wind farm area of (2 km by 2 km) discretized into one hundred possible turbine positions (see Figure 7.1). Given the discretization of the wind farm area originally proposed, the optimization problem is generally implemented as a binary decision problem in which the variables of the decision problem represent the presence of a turbine in a specific cell.

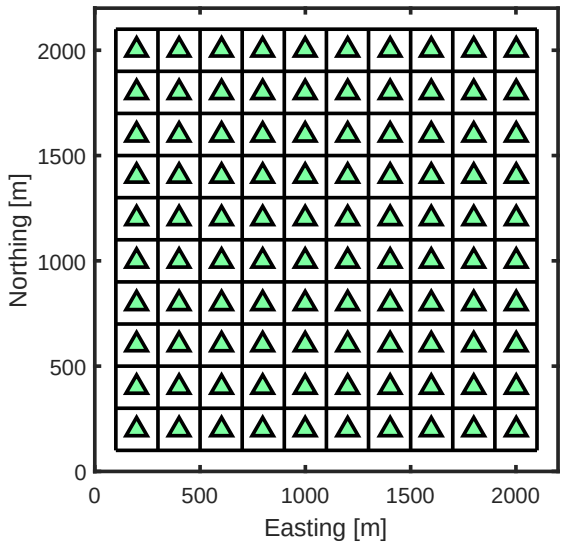

Figure 7.1: Discretized wind farm area showing possible turbine positions for Mosetti et al. [34] cases.

The original case study used an implementation of the Jensen/Park wake model and defined the wind farm annual cost as a constant function of the number of turbines

given in Equation 2.5 and sought to minimize the cost while maximizing the AEP as shown in Equation 7.1. Although this is not explicitly an LCOE or LPC computation, it does consider both the energy production of the wind farm and the annual cost of the project. The objective employed was:

$$\text{Objective} = \frac{1}{AEP} w_1 + \frac{C}{AEP} w_2 \tag{7.1}$$

where w_1 and w_2 are arbitrarily chosen weights. In the original study, w_1 was kept small relative to w_2 in order to keep the emphasis on identifying the lowest cost per energy produced.

The original study also defined a fictional wind turbine, a 40 m rotor diameter turbine, at a hub height of 60 m with a rated capacity of 659.1 kW with a constant thrust coefficient of $C_t = 0.88$ in the range of wind speeds considered.

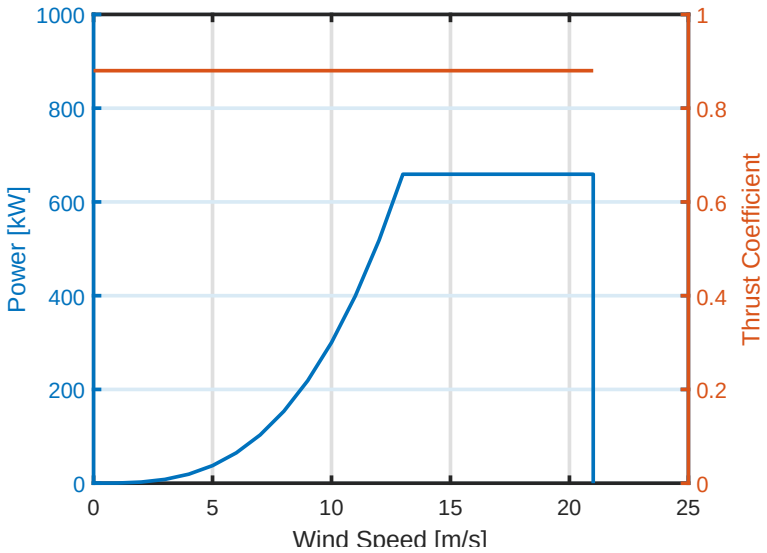

Figure 7.2: Fictional power and thrust curves given by Mosetti et al. [34].

Given the single parameter cost function defined by Mosetti et al. [34], the original definition of the cases did not require the water depth or the location of ports and these were therefore omitted from the definition of the cases. In addition to this, no exclusion areas, defining regions where turbines, substations, or cables could not be placed, were included in the original case. However, all are used by the present evaluation function in the determination of a layout's LCOE. In order to keep the case considered by this work as close as possible to the original definition while using the more detailed evaluation function developed in our present work, a constant water depth across the wind farm area was assumed, the port was assumed to be very far away relative to the size of the wind farm, and it was assumed that no constraint regions existed within the wind farm

area thereby allowing turbines, substations, and cables to be placed anywhere within the wind farm area. The port was placed in the North East relative to the wind farm.

It should be noted that though these case studies are commonly referred to by the community, only two studies following the original have applied their optimizer to all three original cases using the same discretized grid and present their results in full [35, 240]. Unfortunately, however, these studies do not consistently use the same number of turbines as the original study and as a result there is some difficulty in accurately interpreting the identified improvements and comparing the results directly. The focus of these studies has also been on illustrating the capabilities of different optimization algorithms rather than the development of a framework applicable to real wind farm problems.

Beyond these two studies and the original, other frameworks which have used these resource cases have either not used the same discretization of the wind farm area, the same number of turbines, or have not addressed all three cases making it challenging to make direct comparisons on the capabilities of the frameworks [28–30, 41–47, 241–244]. The recent work by Shakoor et al. [48, 75, 76] looks at similar cases; however, rotates the domain by 45° thereby defining a sufficiently different wind resource that these results cannot fairly be compared to the past studies.

Although many tools have allowed the number of turbines to be a decision variable of the optimization process, the present work decided instead to keep the number of turbines constant throughout the optimization process. As this project uses the number of turbines as an input factor, it was decided to use wind farms with the same size as Mosetti et al. [34] and Grady et al. [35] as these are the two sets of results most commonly used as benchmarks. By using the same sized wind farms as those used in these studies it will be possible to directly compare the performance of the optimizers and the changes in LCOE highlighted by the methodology.

In order to compare the layouts fairly, the original layouts produced in previous studies have been re-evaluated using the present evaluation function. This ensures that all AEP, cost, and LCOE values have been computed using the same methodology and reference data. The differences between the present results and those previously published therefore represent either a difference as a result of the evaluation function, the optimization algorithm, or a combination of both. The work presented here demonstrates that a more detailed, complex evaluation function than what has been previously considered is still suitable for the wind farm layout optimization problem. Through the application of three different sets of constraints on the turbine placement as described in Chapter 3 it will also be possible to see the cost associated with different types of constraints and

how these constraints will limit the types of solutions found. The three sets of constraint explored in this chapter are:

- **Mode 1:** rectilinear array layout where the layout is defined by six variables;
- **Mode 2:** binary decision problem where the optimizer selects from a pre-defined set of allowable positions; and
- **Mode 3:** continuous decision problem where the optimizer directly selects the coordinates of each turbine.

7.2.1 Constant Wind Speed, Constant Direction

7.2.1.1 Case Description

The first of the three cases described by Mosetti et al. [34] proposes a scenario in which the wind farm experiences a constant 12 m/s wind from a single direction. For all three cases, the wind direction is discretized into 36 sectors each of a 10° width. For the purposes of this first case, the wind is assumed to always be from the sector centred on 0° as shown in Figure 7.3.

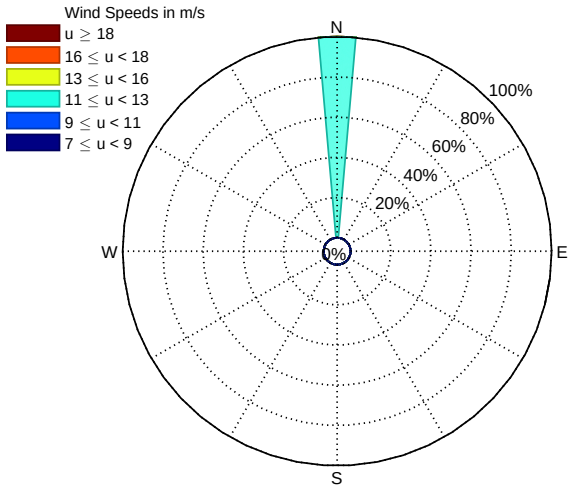

Figure 7.3: Wind Rose for the first case defined by Mosetti et al. [34].

This simple case does not represent a realistic site as the wind conditions are constant and unchanging; however, it is sufficiently simple that the result should be easily interpreted. As the wind is consistently from one direction it is expected that a preferential orientation exists and the wind farm should be preferentially facing this direction and maximize the spacing along this direction while reducing the spacing between turbines in the perpendicular (crosswind) direction.

7.2.1.2 Results

The results presented in Table 7.4 show the outputs from re-evaluating the original layouts proposed in the previous studies [34, 35] as well as the outputs from execution of the GA and the PSO for this case. As the developed method keeps the number of turbines constant throughout the optimization run, it was necessary to execute each of the optimizers and constraint sets for two different wind farm sizes corresponding to the studies originally performed by Mosetti et al. [34] and Grady et al. [35] respectively. Figure 7.4 shows the original layouts proposed by Mosetti et al. [34] and Grady et al. [35]. The layouts proposed by the present tool are shown in Figures 7.5 and 7.6.

Table 7.4: Layout Optimization Results: Constant Wind Speed, Constant Direction

Study	Number of Turbines	Constraint Mode	Lifetime Cost [£]	AEP [MWh]	LCOE [£/MWh]
Mosetti et al. [34]	26	Binary	4.42×10^8	9.90×10^4	522.87
GA	26	Array	4.40×10^8	1.18×10^5	435.97
PSO	26	Array	4.39×10^8	1.18×10^5	434.87
GA	26	Binary	4.41×10^8	1.01×10^5	510.46
PSO	26	Binary	4.41×10^8	1.01×10^5	510.46
GA	26	Continuous	4.41×10^8	1.18×10^5	438.40
PSO	26	Continuous	4.42×10^8	1.16×10^5	447.18
Grady et al. [35]	30	Binary	4.77×10^8	1.13×10^5	496.29
GA	30	Array	4.76×10^8	1.33×10^5	419.75
PSO	30	Array	4.76×10^8	1.33×10^5	419.61
GA	30	Binary	4.77×10^8	1.13×10^5	496.29
PSO	30	Binary	4.77×10^8	1.13×10^5	496.29
GA	30	Continuous	4.77×10^8	1.35×10^5	412.16
PSO	30	Continuous	4.78×10^8	1.33×10^5	421.64

From the results presented in Table 7.4 it can be observed that for both wind farm sizes, the proposed optimizers either find improvements or the same solution proposed by the references cases. As is highlighted in the table, in both cases, the costs are similar as the micrositing within the $4\,\mathrm{km}^2$ wind farm area results in very minimal changes in the installation costs.

From the results shown in Table 7.4 it can be seen that the layouts identified by the present tool using the same discrete grid as the original studies show either small improvements or no improvement compared to the original studies. The relaxation of the positioning constraint, however, allowing the layout to diverge from the fixed grid allows the optimizer to identify significant improvements with respect to the LCOE. Somewhat surprisingly, the array optimizer was capable of finding solutions of similar quality as the continuous mode of operation highlighting that further tuning can likely be done

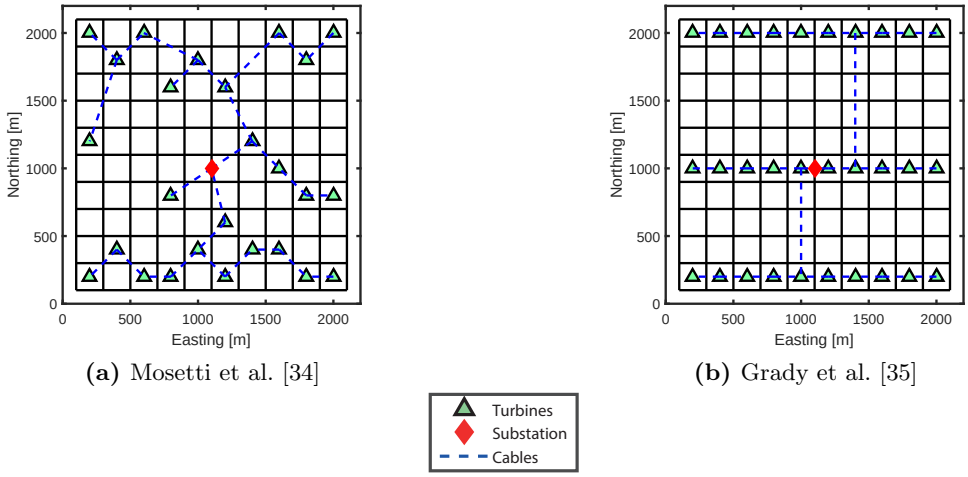

(a) Mosetti et al. [34] **(b)** Grady et al. [35]

Figure 7.4: Original optimized layout for the case of a constant wind speed and constant direction

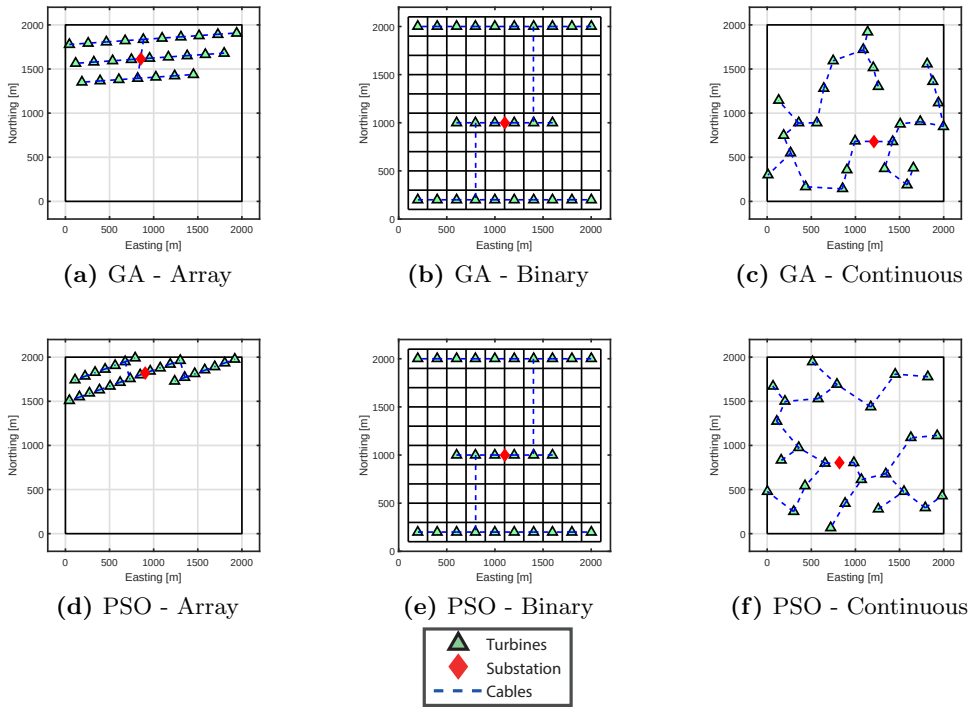

(a) GA - Array **(b)** GA - Binary **(c)** GA - Continuous

(d) PSO - Array **(e)** PSO - Binary **(f)** PSO - Continuous

Figure 7.5: Optimized layouts for the case of a constant wind speed and constant direction with 26 turbines using both optimization algorithms and all three constraint sets. Results correspond to the top half of Table 7.4 (cf. Mosetti et al. [34]).

for the continuous optimizers. This is further discussed in Section 8.6. Given that the binary optimizer consistently underperformed its array and continuous counterparts it

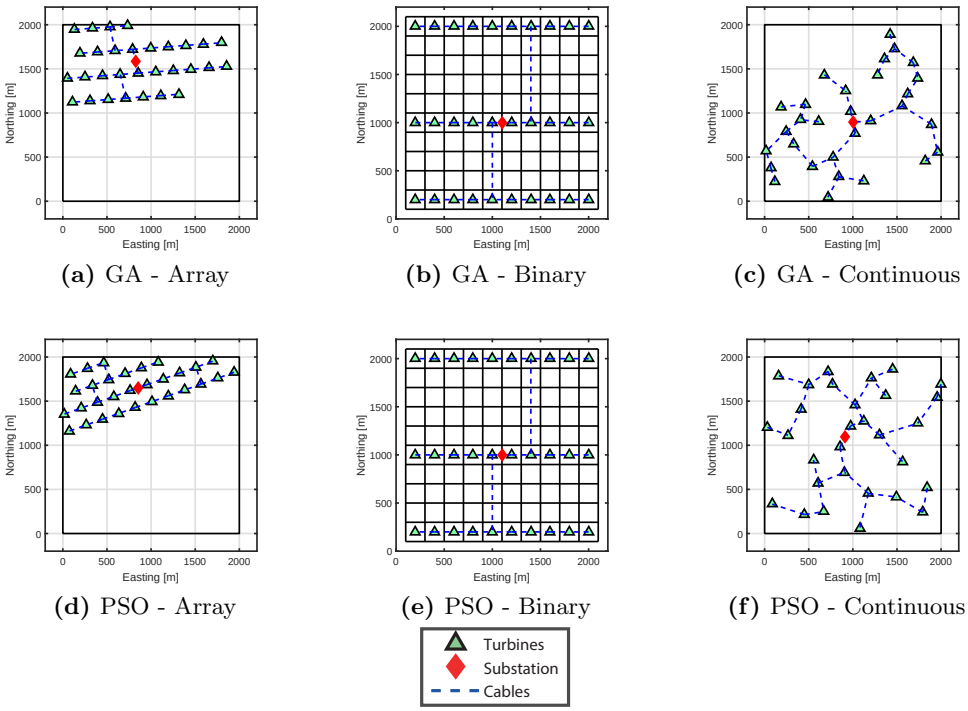

(a) GA - Array (b) GA - Binary (c) GA - Continuous

(d) PSO - Array (e) PSO - Binary (f) PSO - Continuous

Figure 7.6: Optimized layouts for the case of a constant wind speed and constant direction with 30 turbines using both optimization algorithms and all three constraint sets. Results correspond to the bottom half of Table 7.4 (cf. Grady et al. [35]).

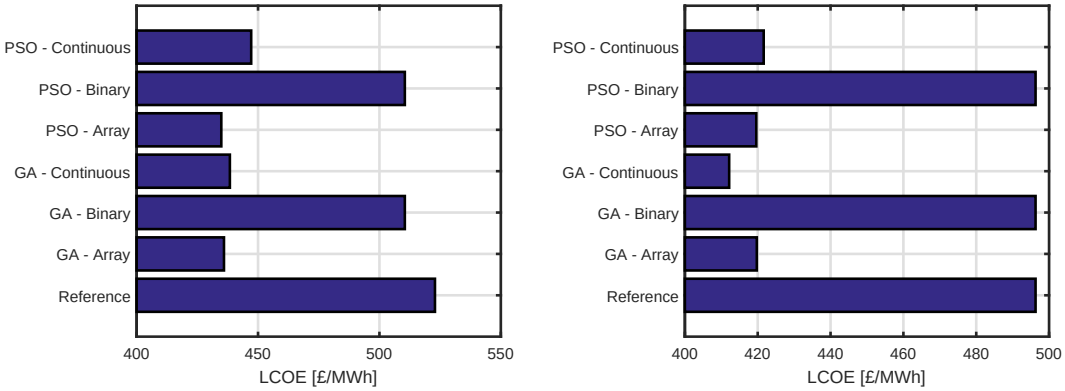

(a) Small Wind Farm - 26 Turbines (b) Large Wind Farm - 30 Turbines

Figure 7.7: LCOE for the designed layouts

is unclear how much of this is due to tuning or the discretization of the wind farm area. Having said that, there is still room to further tune the binary optimizer in order to improve the performance.

An interesting point to note was that in the 30 turbine case suggested by Grady et al. [35], both the GA and PSO when operating in the binary decision problem mode were unable to offer improvements, and converged on the same layout proposed by Grady et al. [35].

From Figure 7.7 it can be seen that all the cases show high costs relative to the £100/MWh target for offshore wind. This is a result of the installation port being considered to be far away relative to the size of the wind farm. This was done in order to reduce the bias related to the location of the port, however, introduces high fixed costs for all the considered layouts. Additionally, the costs are very high as a full offshore substation is assumed for a wind farm of less than 30 MW. More realistically, a wind farm of this size would only be built very close to shore and would not use an offshore substation. Since the substation costs are unaffected by layout the inclusion of these does not affect the results on a relative basis. Furthermore, the choice of vessels and the costs associated with these are based on what would be used for larger turbine in a large wind farm. These vessels are likely therefore over-sized and more expensive than a project of this size would realistically use further increasing the costs. These cost elements affect all the considered layouts in a similar manner and therefore do not impact the layout optimization step as this is done on a relative basis.

7.2.2 Constant Wind Speed, Variable Direction

7.2.2.1 Case Description

The second case considers a "case of multiple wind direction with constant intensity" [34]. This wind regime is defined as having a constant wind speed of 12 m/s with an equal probability that the wind will blow from any direction. The corresponding wind rose is shown in Figure 7.8.

Similar to the first case, this does not represent a realistic site, however, it highlights the impact that wind direction can have on the layout and the results of increased complexity of the wind resource. In this case, however, as the wind is uniformly distributed from all directions there is no preferential orientation with which the turbines can be expected to be aligned. Unlike Case 1 where only the downwind spacing impacted the AEP, in this case both the downwind and crosswind spacing will affect the AEP.

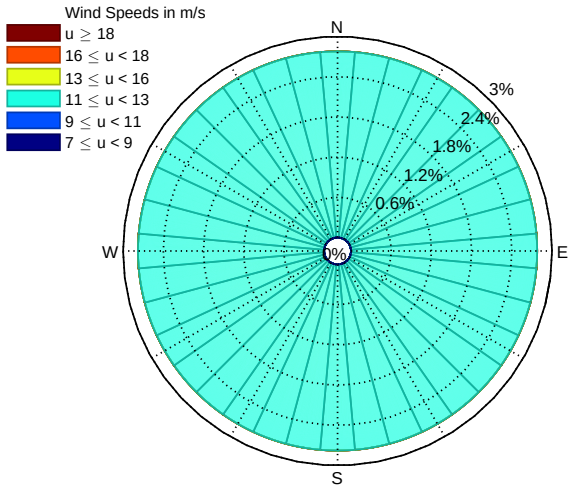

Figure 7.8: Wind Rose for the second case defined by Mosetti et al. [34].

7.2.2.2 Results

Figure 7.9 shows the original results for this case from the work by Mosetti et al. [34] and Grady et al. [35] which have been used as a reference case. Similar to the results for Case 1, these two sets of results differ in the number of turbines they used. Mosetti et al. [34] used 19 turbines, while Grady et al. [35] used 39. Both sizes of wind farms have been explored using the newly developed framework in order to easily compare the new results to the original reference cases. The original layouts proposed by Mosetti et al. [34] and Grady et al. [35] for this case are shown in Figure 7.9.

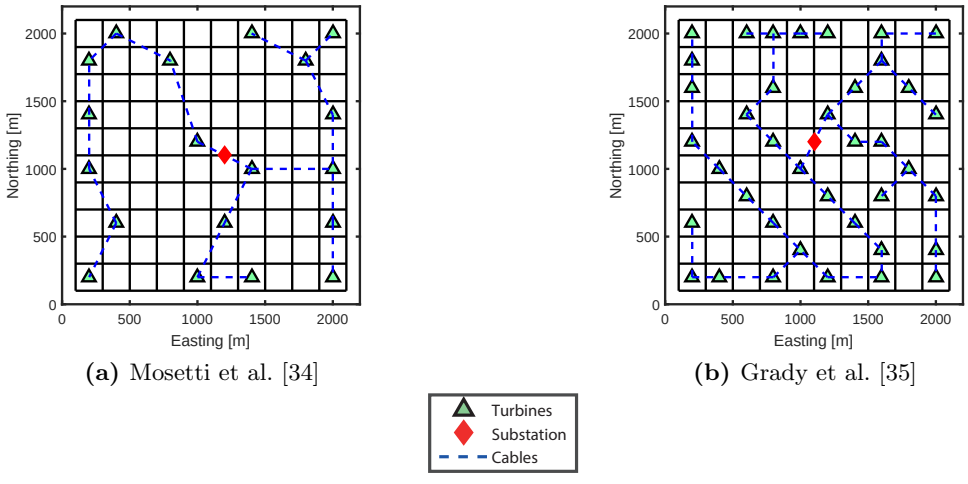

(a) Mosetti et al. [34]

(b) Grady et al. [35]

Figure 7.9: Original optimized layout for the case of a constant wind speed and variable direction

The results of the present framework for this resource case are shown in Table 7.5. From this table it can be seen that similar to the results from Case 1, the newly developed layout optimization framework for offshore wind farms is capable of identifying improvements using either the GA or the PSO optimizer regardless of the constraint set used. The results for the 19 turbine wind farm are shown in Figure 7.10 and for the 39 turbine wind farm in Figure 7.11. Figure 7.12 shows the LCOE for each of the final layouts.

Table 7.5: Layout Optimization Results: Constant Wind Speed, Variable Direction

Study	Number of Turbines	Constraint Mode	Lifetime Cost [£]	AEP [MWh]	LCOE [£/MWh]
Mosetti et al. [34]	19	Binary	3.77×10^8	8.17×10^4	540.25
GA	19	Array	3.76×10^8	8.24×10^4	534.65
PSO	19	Array	3.77×10^8	8.32×10^4	530.79
GA	19	Binary	3.77×10^8	8.18×10^4	539.88
PSO	19	Binary	3.77×10^8	8.21×10^4	537.49
GA	19	Continuous	3.77×10^8	8.29×10^4	532.37
PSO	19	Continuous	3.77×10^8	8.19×10^4	538.29
Grady et al. [35]	39	Binary	5.62×10^8	1.57×10^5	419.13
GA	39	Array	5.62×10^8	1.59×10^5	413.67
PSO	39	Array	5.61×10^8	1.61×10^5	408.07
GA	39	Binary	5.61×10^8	1.59×10^5	412.25
PSO	39	Binary	5.61×10^8	1.59×10^5	413.00
GA	39	Continuous	5.62×10^8	1.61×10^5	409.33
PSO	39	Continuous	5.62×10^8	1.58×10^5	417.29

Unlike the first resource case, in this case, the binary optimizers implemented as part of this work were capable of identifying improvements when compared to the original studies. Likewise, the optimizers running with either the array or continuous constraint sets were able to find significant improvements over the discretized case. As was seen in Case 1, the array optimization was still able to find superior layouts to the continuous constraint set, implying that the continuous constraint set has prematurely converged in this case and further improvements should be possible through improved parameter tuning.

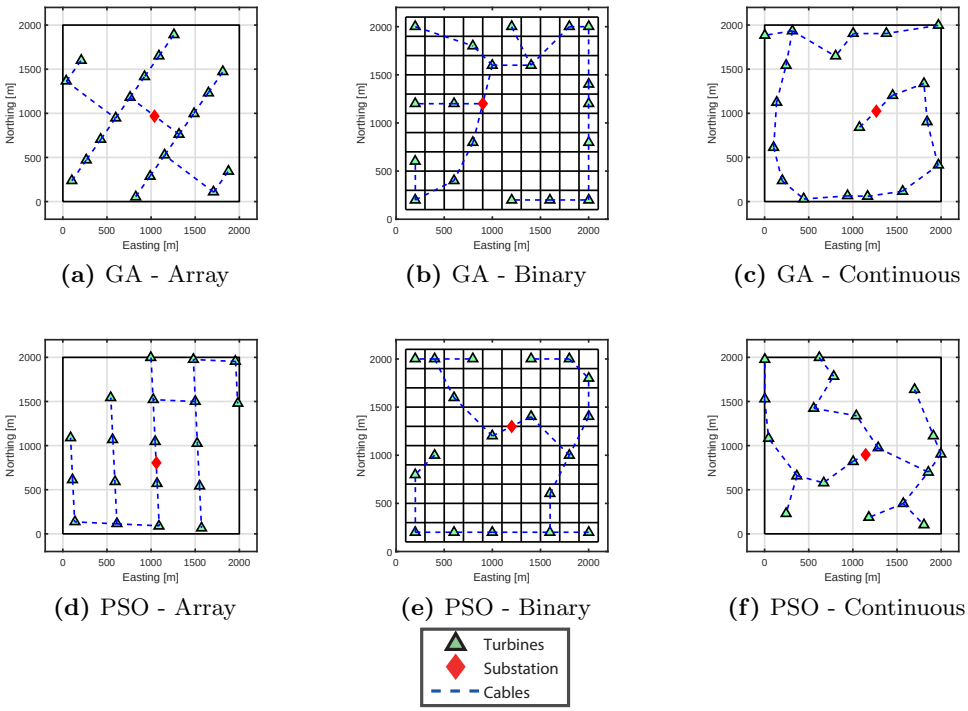

(a) GA - Array **(b)** GA - Binary **(c)** GA - Continuous

(d) PSO - Array **(e)** PSO - Binary **(f)** PSO - Continuous

Figure 7.10: Optimized layout for the case of a constant wind speed and variable direction with 19 turbines using both optimization algorithms and all three constraint sets. Results correspond to the top half of Table 7.5 (cf. Mosetti et al. [34]).

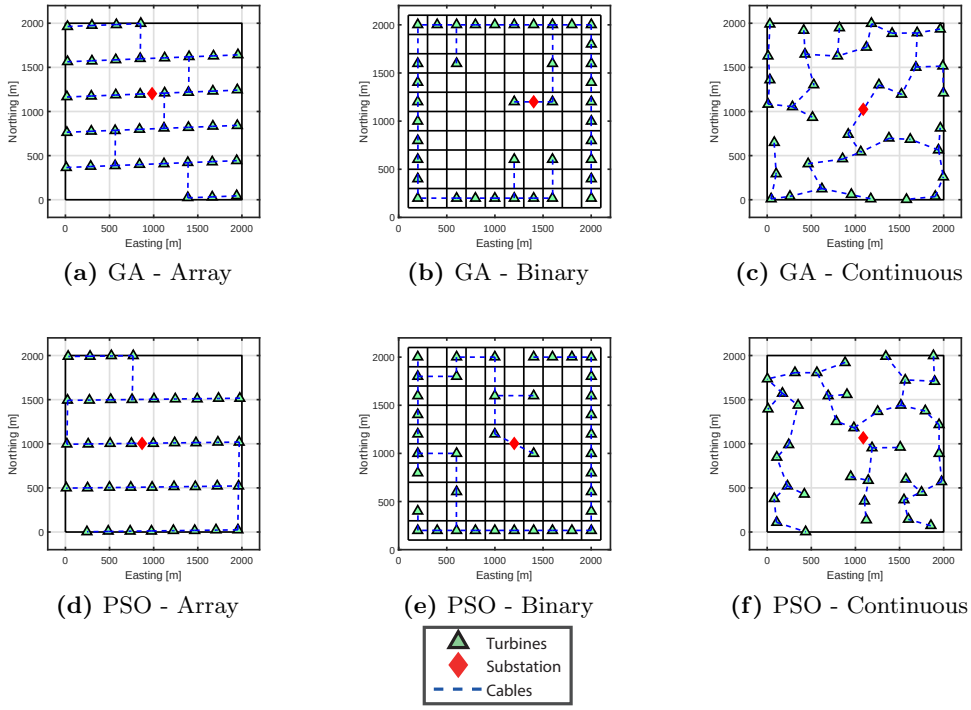

(a) GA - Array **(b)** GA - Binary **(c)** GA - Continuous

(d) PSO - Array **(e)** PSO - Binary **(f)** PSO - Continuous

Figure 7.11: Optimized layout for the case of a constant wind speed and variable direction with 39 turbines using both optimization algorithms and all three constraint sets. Results correspond to the bottom half of table 7.5 (cf. Grady et al. [35]).

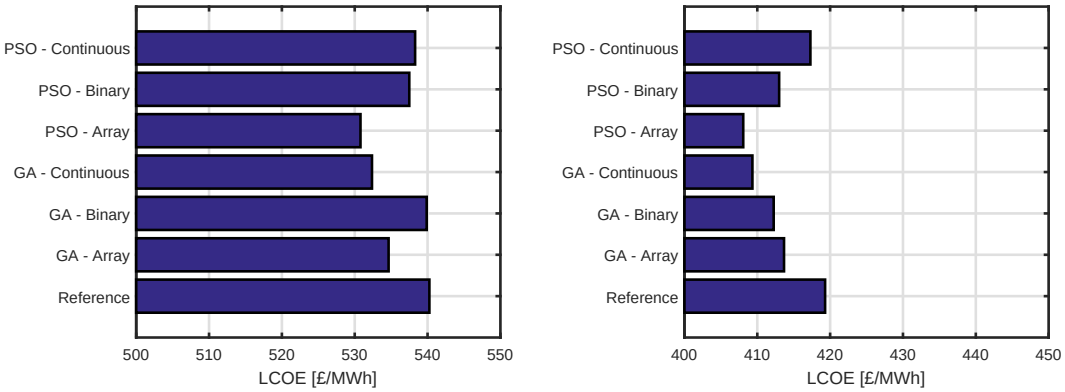

(a) Small Wind Farm - 19 Turbines **(b)** Large Wind Farm - 39 Turbines

Figure 7.12: LCOE for the designed layouts

7.2.3 Variable Wind Speed, Variable Direction

7.2.3.1 Case Description

The final case proposed by Mosetti et al. [34] was one of "multiple wind direction and intensity". In this case, the wind can either be 8 m/s, 12 m/s, or 17 m/s with varying probabilities for different directions. The probability of each wind speed and direction occurring is shown in Figure 7.13.

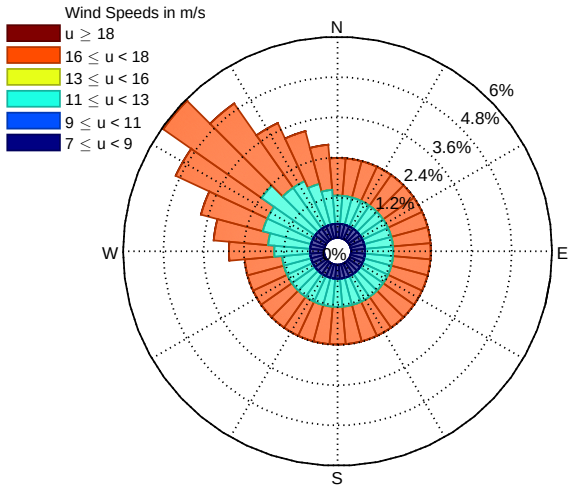

Figure 7.13: Wind Rose for the third case defined by Mosetti et al. [34].

Unlike the earlier cases, this case begins to resemble a real wind farm size with both varying wind speeds and direction. However, it is still not quite realistic in that the wind speed takes only one of three discrete values. Like Case 2, there is no clear preferential orientation from the wind rose as there was with Case 1, however, there is a clear dominant wind direction which one would expect to be exploited effectively in the placement of the turbines.

7.2.3.2 Results

Like the other cases, Mosetti et al. [34] and Grady et al. [35] used wind farms of different sizes requiring each optimizer to be run twice for each set of constraints in order for comparisons to be made against both of the original reference cases. The layouts are presented in Figure 7.14.

The results of executing the current framework with both the GA and the PSO are found in Table 7.6 with the corresponding layouts plotted in Figure 7.15 for the smaller wind farm and Figure 7.16 for the larger wind farm.

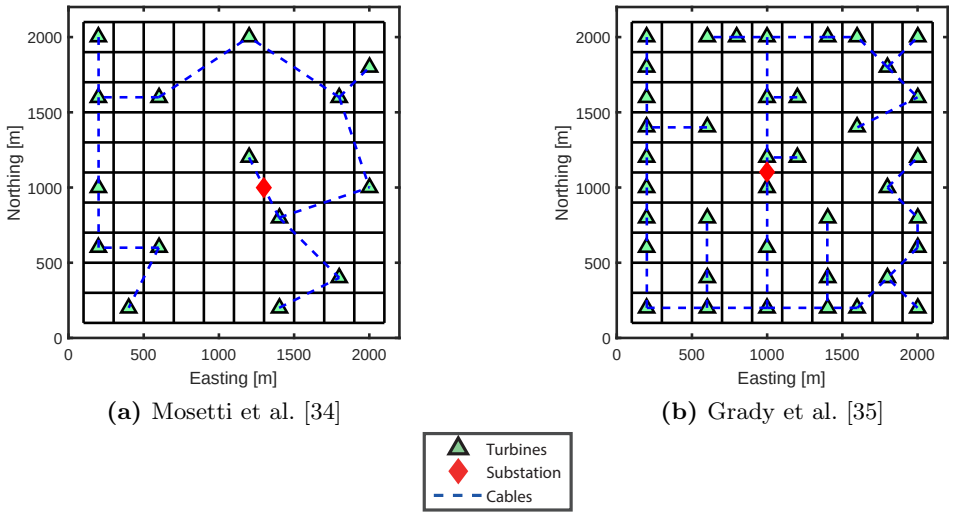

(a) Mosetti et al. [34]

(b) Grady et al. [35]

Figure 7.14: Original optimized layout for the case of a variable wind speed and variable direction

Table 7.6: Layout Optimization Results: Variable Wind Speed, Variable Direction

Study	Number of Turbines	Constraint Mode	Lifetime Cost [£]	AEP [MWh]	LCOE [£/MWh]
Mosetti et al. [34]	15	Binary	3.40×10^8	6.89×10^4	576.94
GA	15	Array	3.38×10^8	6.92×10^4	572.51
PSO	15	Array	3.39×10^8	6.93×10^4	571.51
GA	15	Binary	3.39×10^8	6.92×10^4	573.10
PSO	15	Binary	3.39×10^8	6.91×10^4	573.87
GA	15	Continuous	3.39×10^8	6.91×10^4	573.92
PSO	15	Continuous	3.39×10^8	6.91×10^4	574.22
Grady et al. [35]	39	Binary	5.62×10^8	1.74×10^5	377.14
GA	39	Array	5.61×10^8	1.75×10^5	376.40
PSO	39	Array	5.63×10^8	1.75×10^5	375.50
GA	39	Binary	5.62×10^8	1.74×10^5	377.27
PSO	39	Binary	5.62×10^8	1.75×10^5	376.72
GA	39	Continuous	5.62×10^8	1.75×10^5	375.50
PSO	39	Continuous	5.62×10^8	1.76×10^5	376.72

From Figure 7.17 it can be seen that the present framework identified improvements over the reference cases for all three constraint sets including the binary decision problem, though for the larger wind farm only one of the two optimization algorithms was capable of identifying the improvement. This behaviour is similar to what was seen in Case 1. Furthermore, the array optimizer was able to find superior layouts compared to the other constraint sets similar to the other cases. This highlights the need for further

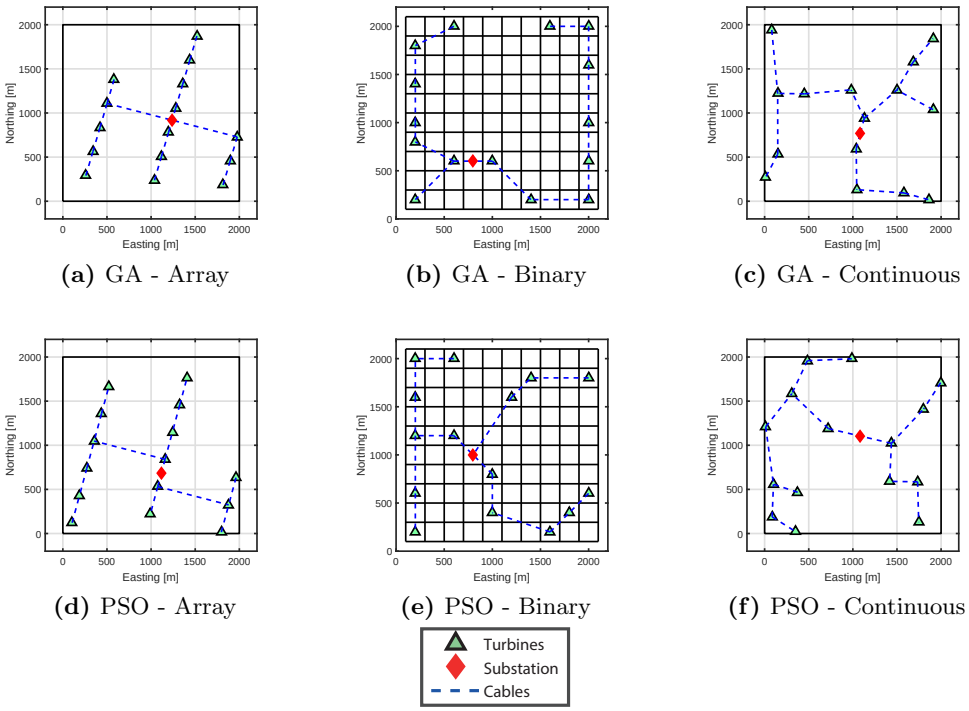

(a) GA - Array **(b)** GA - Binary **(c)** GA - Continuous

(d) PSO - Array **(e)** PSO - Binary **(f)** PSO - Continuous

Figure 7.15: Optimized layout for the case of a variable wind speed and variable direction with 15 turbines using both optimization algorithms and all three constraint sets. Results correspond to the top half of Table 7.6 (cf. Mosetti et al. [34]).

tuning, as it would be expected that some of the constraint sets would be able to offer superior layouts to the array optimizer.

7.2.3.3 Sensitivity to the Number of Turbines

As the developed framework uses the number of turbines as input to the optimization process, it can be used to aid in deciding the optimal size of a wind farm.

Continuing with the third Mosetti et al. [34] case, the number of turbines was increased from 5 to 80 in discrete steps, and the PSO optimizer executed with the array constraints. Doing so, produced the results shown in Figure 7.18 in which the LCOE is seen to decrease at first and then increase. The minima of this curve would represent the optimal size of the wind farm with the corresponding layout representing the optimal layout for this scenario. From this analysis, given the array constraints, the PSO identified 55 turbines as being the optimal size.

Using this approach, this framework can easily be used to perform sensitivity studies on the impact of altering the size of the wind farm as well as determining the optimal size of the wind farm.

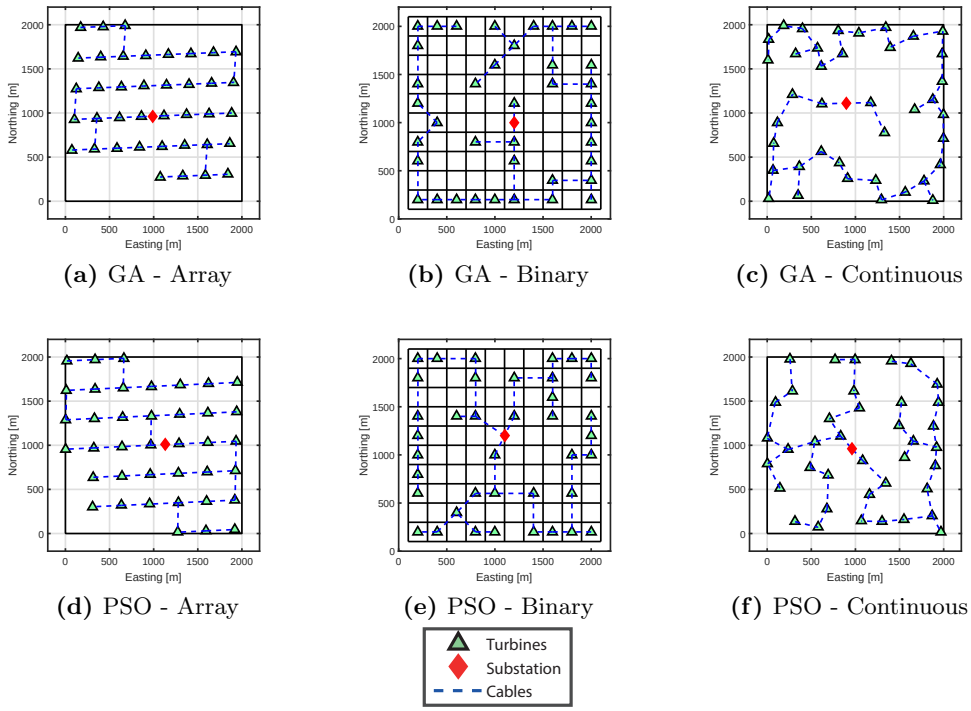

(a) GA - Array **(b)** GA - Binary **(c)** GA - Continuous

(d) PSO - Array **(e)** PSO - Binary **(f)** PSO - Continuous

Figure 7.16: Optimized layouts for the case of a variable wind speed and variable direction with 39 turbines using both optimization algorithms and all three constraint sets. Results correspond to the bottom half of Table 7.6 (cf. Grady et al. [35]).

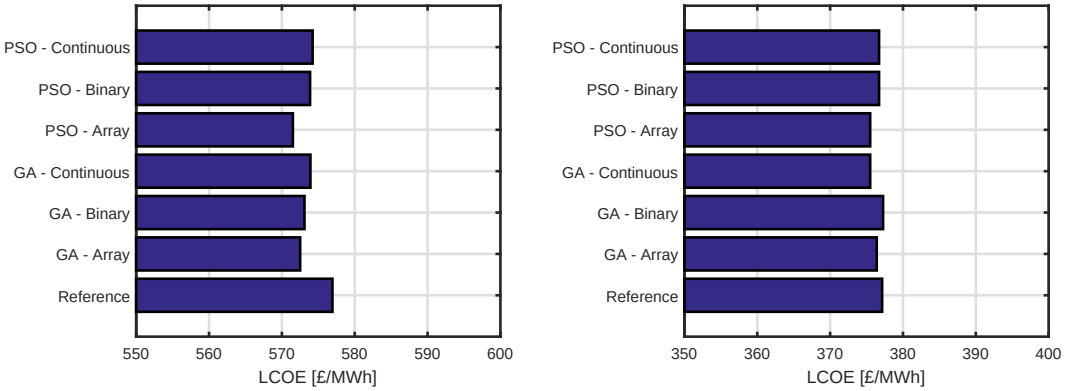

(a) Small Wind Farm - 15 Turbines **(b)** Large Wind Farm - 39 Turbines

Figure 7.17: LCOE for the designed layouts

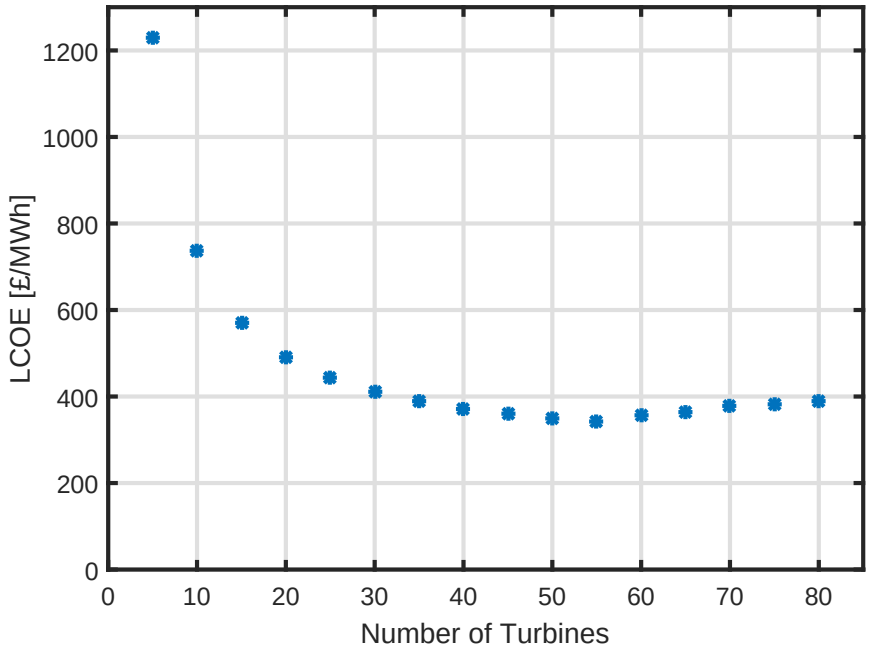

Figure 7.18: LCOE sensitivity to the number of turbines

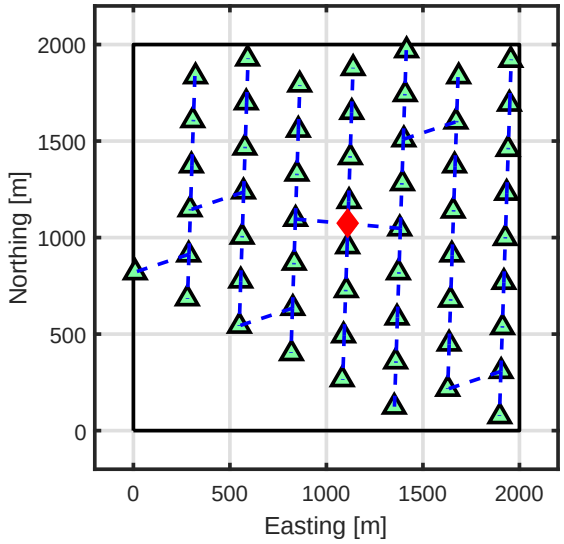

Figure 7.19: Optimal layout for 55 turbines in case of variable wind speed and variable direction. Layout found using PSO and array constraints.

7.3 Middelgrunden Wind Farm

7.3.1 Case Description

As introduced in Section 5.5.1, Middelgrunden wind farm near Copenhagen offers a good application of this methodology as the necessary data regarding the site are available. This wind farm is composed of twenty Bonus 2 MW turbines located at a distance of approximately 5 km from shore. Though this is a small offshore wind farm with no offshore substation it still provides an interesting test case for this optimization methodology.

The public data set includes not only production data from 2001-2004, but also a high level CAPEX breakdown. Complimenting this, data from the British Oceanographic Data Centre (BODC) and the General Bathymetric Chart of the Oceans (GEBCO) can be used for academic purposes to provide bathymetric data at a 30″ resolution [245]. This combination of data provides sufficient information for the evaluation function and therefore for the full optimization methodology to be applied for this real site. Table 7.7 gives an overview of the relevant data for the Middelgrunden case study.

Using the publicly available resource, cost, and production data from Middelgrunden wind farm this work first validates the full evaluation function and tries to understand if the differences in AEP, cost, or LCOE would impact on the layout. From this, the second part of the study applies the full optimization framework to identify any improvements to the layout that can be identified by this tool. Throughout the optimization process, a minimum separation of 175 m between turbines is imposed. The wind rose, using the same data as the analysis in Section 5.5.1 is shown in Figure 7.20 and the relevant turbine performance curves are shown in Figure 7.21.

Table 7.7: Data Overview

Data	Description	Source
Wind	Turbine SCADA data from 2001-2004	[189]
Turbine	Bonus B76-2000 Power and Thrust Curves	[189]
Layout	Turbine coordinates for existing layout	[189]
Bathymetry	30″ global bathymetry	[245]
Boundary	Coordinates defining the boundary	[27]
Costs	CAPEX and OPEX cost breakdown	[190, 246]

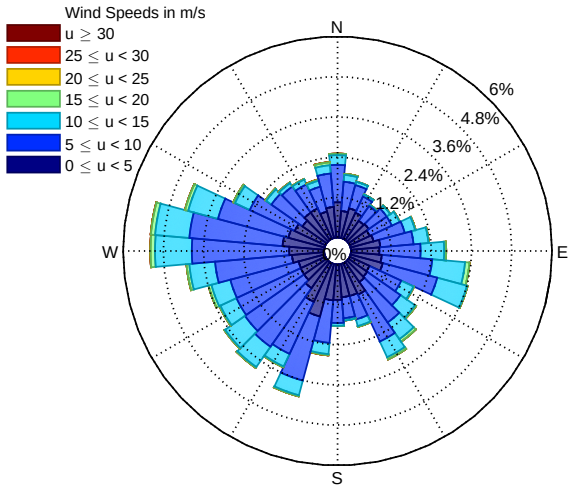

Figure 7.20: Wind rose for Middelgrunden wind farm based on time-series data from 2001-2004. Data used courtesy of The Middelgrunden Wind Cooperative.

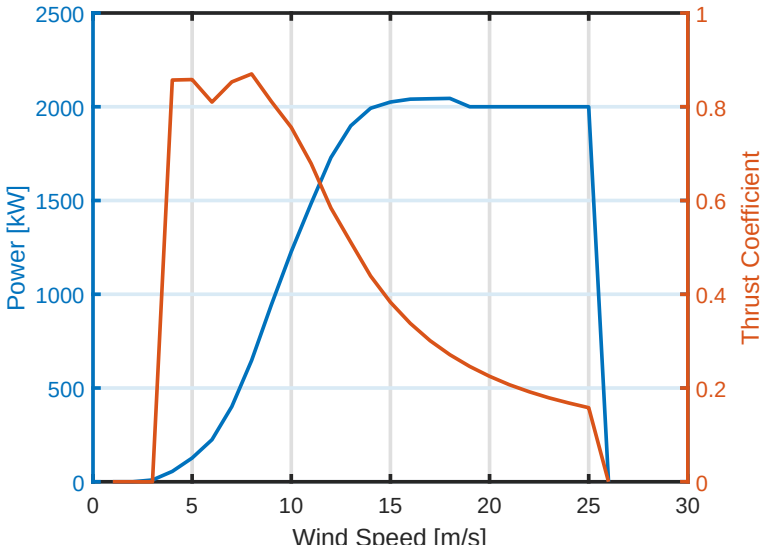

Figure 7.21: Power and thrust curve for Bonus B76-2000 turbines at Middelgrunden wind farm [189].

7.3.2 Results

7.3.2.1 Validation of Evaluation Function

Given the actual turbine positions and the site data, execution of the evaluation function for the actual layout gave an AEP of 95.41 GWh and an LCOE of £92.82 MWh. The full costs with a comparison to those published by the project is shown in Table 7.8

based on data provided by Larsen et al. [246] and Middelgrundens Vindmøllelaug I/S [190].

Table 7.8: Middelgrunden - Cost Validation (£k)

	Modelled				
	CAPEX	DECEX	OPEX	Published	Error
Turbine	£35,224			£27,054	30.20%
Turbine Supply	£27,826				
Turbine Installation	£7,398				
Foundation	£13,457			£13,121	2.56%
Foundation Supply	£2,365				
Foundation Installation	£11,092				
Array Cable	£5,319			£4,573	16.30%
Array Cable Supply	£2,188				
Array Cable Installation	£3,131				
Decommissioning		£13,925			
Turbine		£7,218			
Foundation		6,707			
Project Management	£3,949				
Contingency	£9,791				
O&M			£2,424	£798	203.67%

From this evaluation, it can be observed that the main areas in which the cost estimate differ are the turbine costs and the operations and maintenance costs. The models used for estimating these costs are generic and therefore high error is not unexpected. These differences in cost are discussed further in Chapter 8.

Using the Larsen wake model as described in Chapter 5 and the resource data available from 2001-2004, it was possible to compute the AEP and compare this to the reported AEP over the first four years and two months of operation [246]. Over this period, the wind farm maintained a 93% average availability which was used when estimating the AEP [17, 246]. Table 7.9 shows the computed and reported AEP (including the wind farm availability) and shows that the AEP for Middelgrunden is quite accurate with only 0.61% error over the 50 month period.

Table 7.9: Middelgrunden - AEP Validation

	Computed [GWh]	Reported [GWh]	Error
AEP	95.41	96.00	-0.61%

Combining these figures, the evaluation of the existing wind farm layout at Middelgrunden wind farm therefore estimates the LCOE of the wind farm to be £92.74/MWh.

7.3.2.2 Optimization of Middelgrunden Layout

After having applied the evaluation function to the site, it was felt that it would be applicable to apply the full optimization methodology to Middelgrunden as the necessary input data was available. During the optimization stage, 100% availability was assumed as the present methodology does not consider how the availability of a wind farm may be impacted by the layout. The AEP and LCOE figures reported during this optimization are therefore noticeably higher and lower respectively compared to the validation case considered in Section 7.3.2.1.

As no existing grid of allowable turbine positions had been defined, a triangulation was performed on the wind farm area with a target distance between vertices of 100 m. This generated 658 allowable turbine positions within the wind farm site as shown in Figure 7.22.

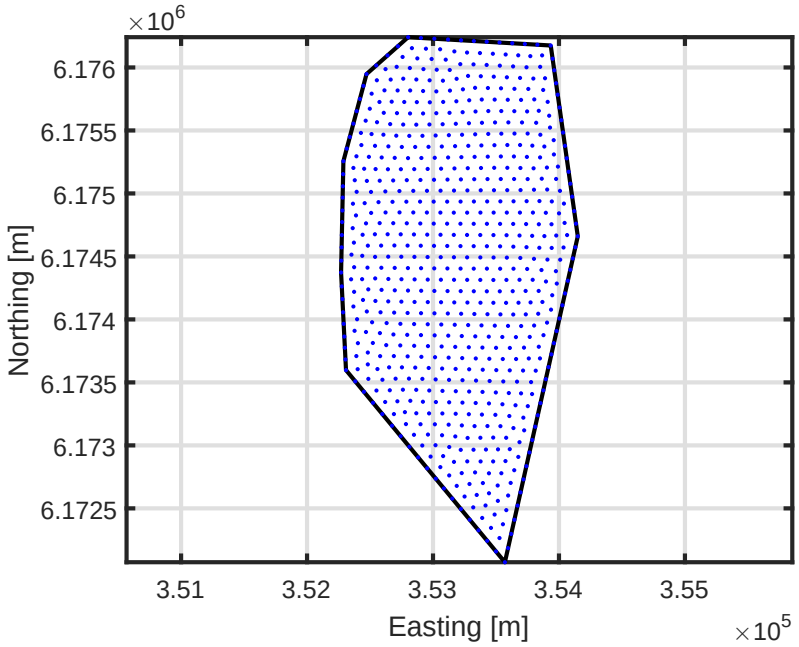

Figure 7.22: Allowable turbine positions for Middelgrunden wind farm when executing the optimization with the binary constraints

As was seen in the Mosetti cases, the optimization algorithms executed with either the array or continuous constraints consistently led to better results than the binary constraint set. This is the expected result as the binary constraint set is the most restrictive with regards to turbine placement. In this case, the continuous optimization was capable of finding improvements in LCOE of 1.4% or 1.7%, while the more constrained array constraints allowed improvements of up to 3.5%. An interesting point is that in all the cases identified, the improvement in LCOE comes through both an increased AEP and an increase in project cost.

Table 7.10: Layout Optimization of Middelgrunden Wind Farm

Case	Number of Turbines	Constraint Mode	Lifetime Cost [£]	AEP [MWh]	LCOE [£/MWh]	Improvement
Existing	20	-	9.15×10^7	1.02×10^5	86.63	-
GA	20	Array	9.25×10^7	1.07×10^5	83.69	3.4%
GA	20	Binary	9.26×10^7	1.05×10^5	85.40	1.4%
GA	20	Continuous	9.23×10^7	1.05×10^5	85.01	1.9%
PSO	20	Array	9.22×10^7	1.07×10^5	83.59	3.5%
PSO	20	Binary	9.24×10^7	1.05×10^5	85.13	1.7%
PSO	20	Continuous	9.24×10^7	1.04×10^5	85.59	1.2%

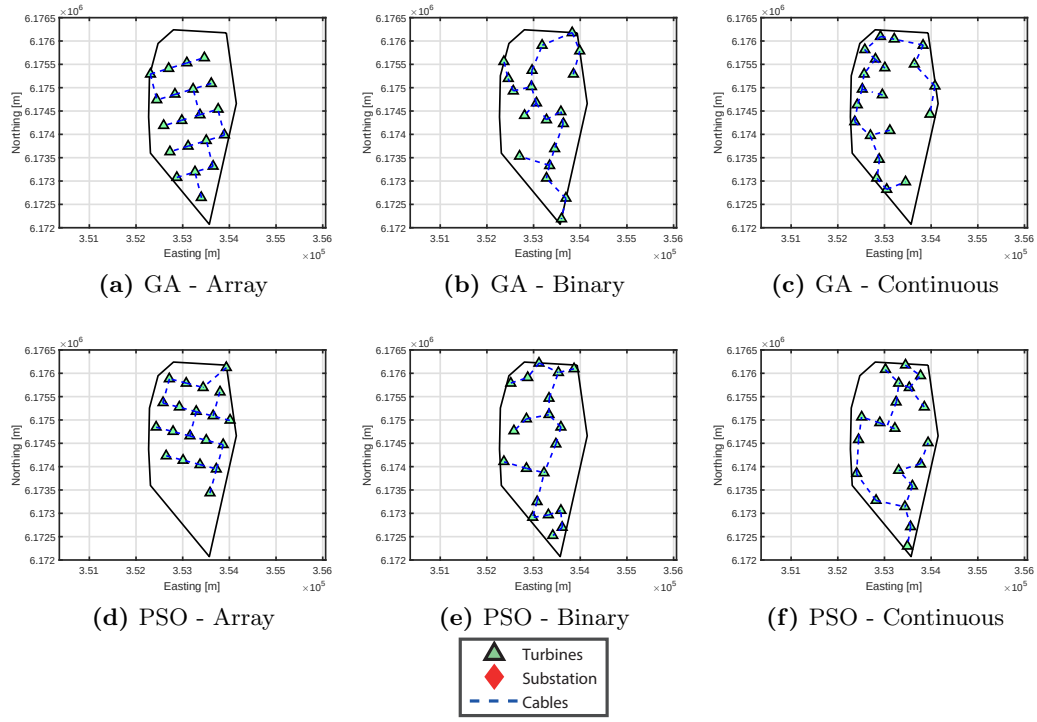

(a) GA - Array **(b)** GA - Binary **(c)** GA - Continuous

(d) PSO - Array **(e)** PSO - Binary **(f)** PSO - Continuous

Figure 7.23: Optimized layouts for Middelgrunden wind farm using both optimization algorithms and all three constraint sets.

The relative change in discounted expenditure (cost) and AEP combined with information regarding the electricity sale price in each year allows the change in LCOE to be converted to an NPV. This is desirable as the TOPFARM project Larsen et al. [64] reported *financial balance* improvements for Middelgrunden wind farm as a result of optimization of the wind farm layout. The improvements in financial balance correspond to the NPV improvement when including the consideration of the wake induced fatigue loads and how these impact the O&M costs. NPVs can therefore be more fairly compared to the financial balance than the LCOE can. The TOPFARM

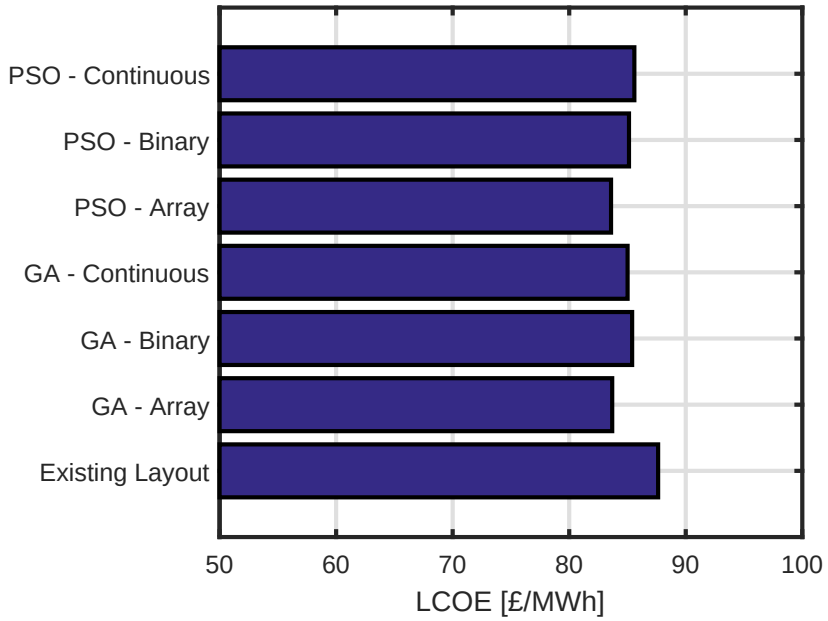

Figure 7.24: LCOE for optimized layouts at Middelgrunden wind farm

project reported total financial balance improvements on the order of €2.1 million as a result of improvements to the layout. This would principally be realized due to reductions in the wake interactions. Using the documented electricity sale prices [190], the proposed layouts correspond to NPV improvements between €1.0 million and €3.5 million if considering the costs over the lifetime of the project, but revenues from only the first fifteen years. Projecting the electricity sale price for the remaining ten years of operation by assuming it remains constant at 2015 values results in a lifetime NPV improvement between €1.5 million and €4.7 million depending on which of the six layouts is considered.

The financial balance term from the TOPFARM project includes both the direct increases in NPV as well as an assessment of the reduced maintenance costs due to the reduced fatigue loading as a result of increased wake efficiency. As the wake efficiency of the layouts proposed by the present tool are also increased compared to the installed layout, further savings can be made due to reduced maintenance costs. The present model, however, has no means of capturing the layout's impact on maintenance costs and therefore only the direct NPV increases are reported. If a TOPFARM style financial balance was to be calculated for these layouts, these values would exceed the NPV improvements identified.

7.4 UK Round 3 Site

7.4.1 Case Description

This section describes the application of the full layout optimization methodology to a site identified by The Crown Estate as suitable for renewable energy development and specifically offshore wind. This Round 3 site, located in the English Channel, is the same area considered in Section 4.7. For the purposes of this study, wind farms made up of 175 6 MW turbines are considered to show the applicability of the methodology to large wind farms similar to planned future developments. Throughout the optimization process, a minimum separation of 450 m between turbines is imposed.

As mentioned in Section 4.7 the site area is defined by a number of deep pockets, shipwrecks, and unexploded ordnance (UXOs) which limit where turbines and the supporting infrastructure can be placed. The bathymetry data used is supplied by SeaZone Solutions Ltd. through the EDINA Marine Digimap Service [247] while the site boundary, shipwrecks, and UXOs are provided by Navitus Bay Ltd. through The Crown Estate Marine Data Exchange Program [248, 249]. Key sources of data are shown in Table 7.11.

Table 7.11: UK Round 3 - Data Sources

Data	Description	Source
Wind	2011 Zone 7 Navitus Bay, Met Office Zone Wind Analysis	[248]
Turbine	Alstom Haliade 150-6MW Power and Thrust Data	[250]
Bathymetry	6″ Gridded Bathymetry Data	[247]
Seabed Slope	2011 Zone 7 Navitus Bay West Isle of Wight, FUGRO Geophysical Survey	[249]
UXO and Wrecks	2011 Zone 7 Navitus Bay West Isle of Wight, FUGRO Geophysical Survey	[249]
Boundary	Navitus Bay Wind Park Project Boundaries	[251]

The wind rose presented in Figure 7.25 shows the wind regime that is used for this study. On average, wind speeds at the site are 8.74 m/s and roughly from the South-southwest.

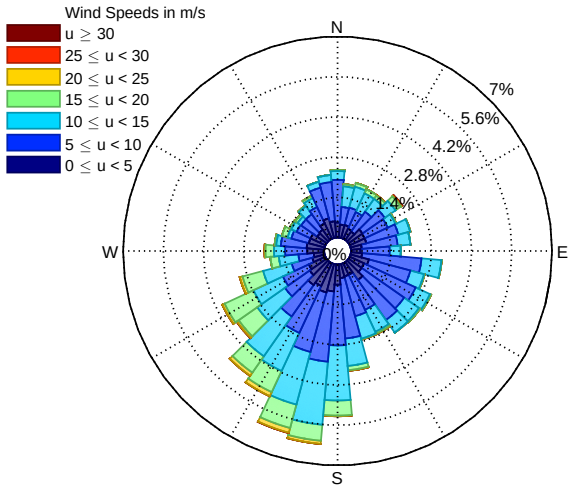

Figure 7.25: Wind Rose for the UK Round 3 site

7.4.2 Results

For this case study, each of the six optimizers were executed once with the corresponding results reported in Table 7.12. Figures 7.27-7.32 show the layouts produced by the tool excluding the export cables.

For the binary case, a set of allowable points were generated by triangulating the wind farm area such that the triangle vertices were approximately 500 m apart. The quality of layouts produced in this mode of operation will be intrinsically linked to the resolution at which the allowable points are produced, however, the runtime is also directly related to this. In order to highlight the capabilities of the approach, a 500 m resolution was selected, as shown in Figure 7.26.

Table 7.12: Layout Optimization of UK Round 3 Wind Farm

Case	Number of Turbines	Constraint Mode	Lifetime Cost [£]	AEP [MWh]	LCOE [£/MWh]
GA	175	Array	4.40×10^9	5.49×10^6	77.65
GA	175	Binary	4.40×10^9	4.87×10^6	87.55
GA	175	Continuous	4.40×10^9	5.40×10^6	78.83
PSO	175	Array	4.40×10^9	5.66×10^6	75.26
PSO	175	Binary	4.40×10^9	5.04×10^6	84.54
PSO	175	Continuous	4.39×10^9	5.24×10^6	81.04

The GA executed using the array constraints produces the layout shown in Figure 7.27. This layout orients the wind farm such that the spacing between turbines is increased along these directions. The developed layout, uses the full wind farm area placing the

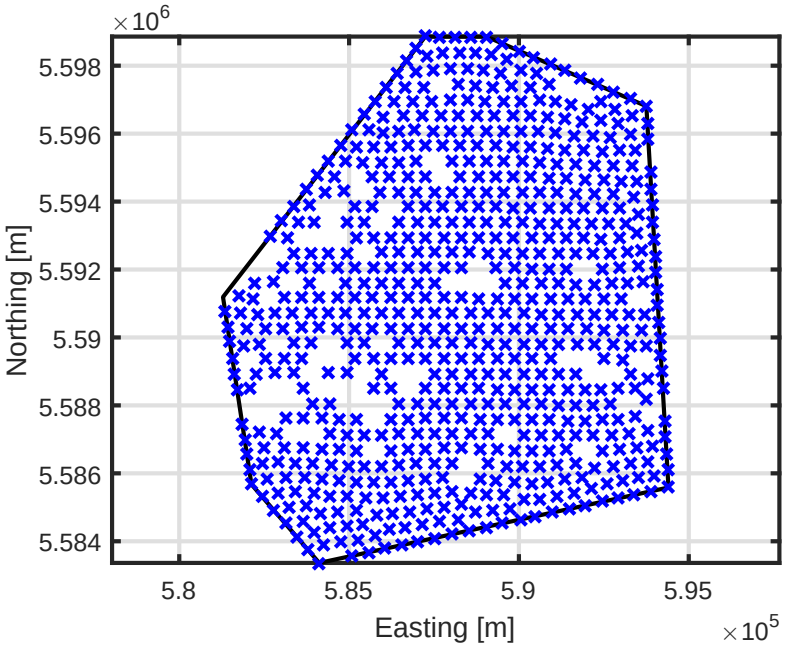

Figure 7.26: UK Round 3 site - allowable points in binary optimization

turbines along regular rows. Although the AEP is greater than many of the other layouts, there are further increases that can be achieved when using the PSO under the same constraint set. This indicates that this final solution is sub-optimal.

Executing the GA with the binary constraint set, therefore limiting the wind turbines to the 638 allowable positions shown in Figure 7.26 produces the wind farm layout shown in Figure 7.28. This wind farm layout produces a layout more in line with traditional layout design trends with a greater number of turbines being pushed to or near the edges of the wind farm thereby increasing the spacing between turbines and the space for wake effects to dissipate. These results are limited by the number and location of the allowable points. Having said that, as the allowable points were uniformly distributed across the wind farm site, the fact that layouts with sparse interiors are preferred indicates that this is a successful strategy for the layout design at this site.

The final mode of the GA, using the continuous constraint set, highlights similar trends to the binary optimizer with many of the wind turbines placed on or near the wind farm boundary thereby increasing the spacing in the interior of the wind farm as shown in Figure 7.29. Compared to the array constraint sets, this solution is very similar with less than 1% increased cost and a 1 percentage point decrease in AEP. These slight variations in cost and AEP produce a layout that has an LCOE approximately £1.20/MWh (1.5%) greater than that of the layout produced by the array optimizer.

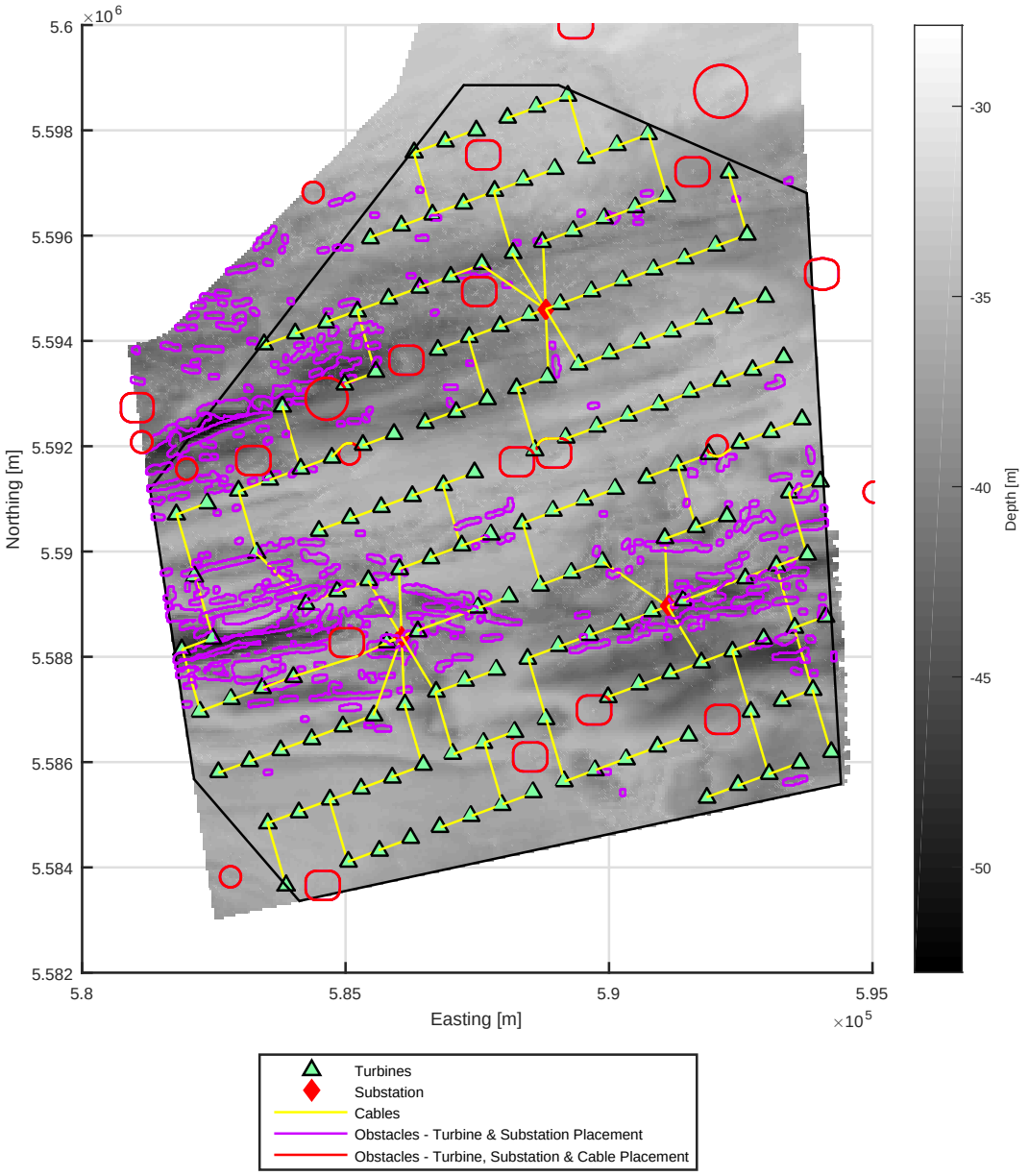

Figure 7.27: UK Round 3 site - optimized layout using array constraint sets and GA optimizer. Darker areas indicate deeper water.

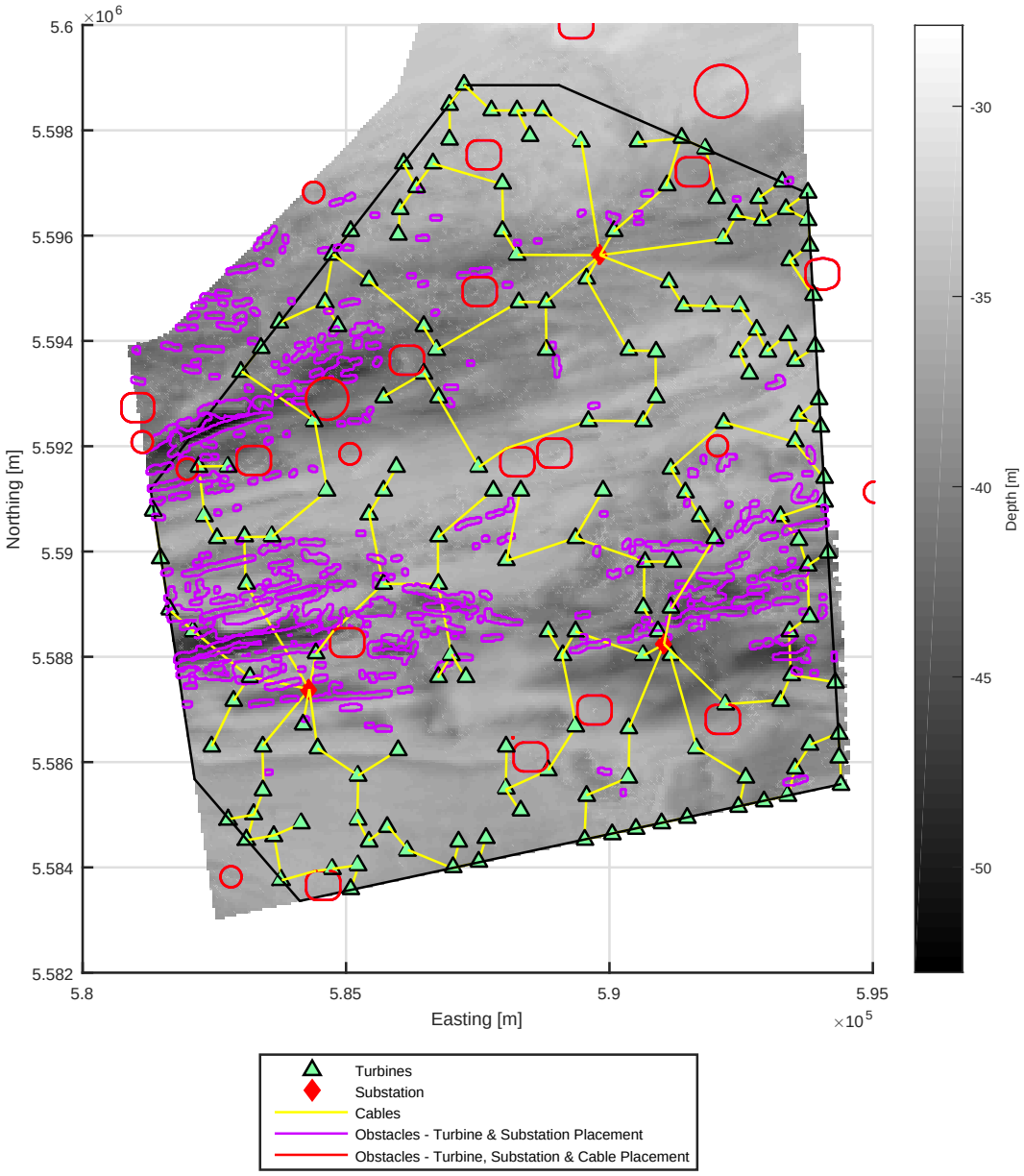

Figure 7.28: UK Round 3 site - optimized layout using binary constraint sets and GA optimizer. Darker areas indicate deeper water.

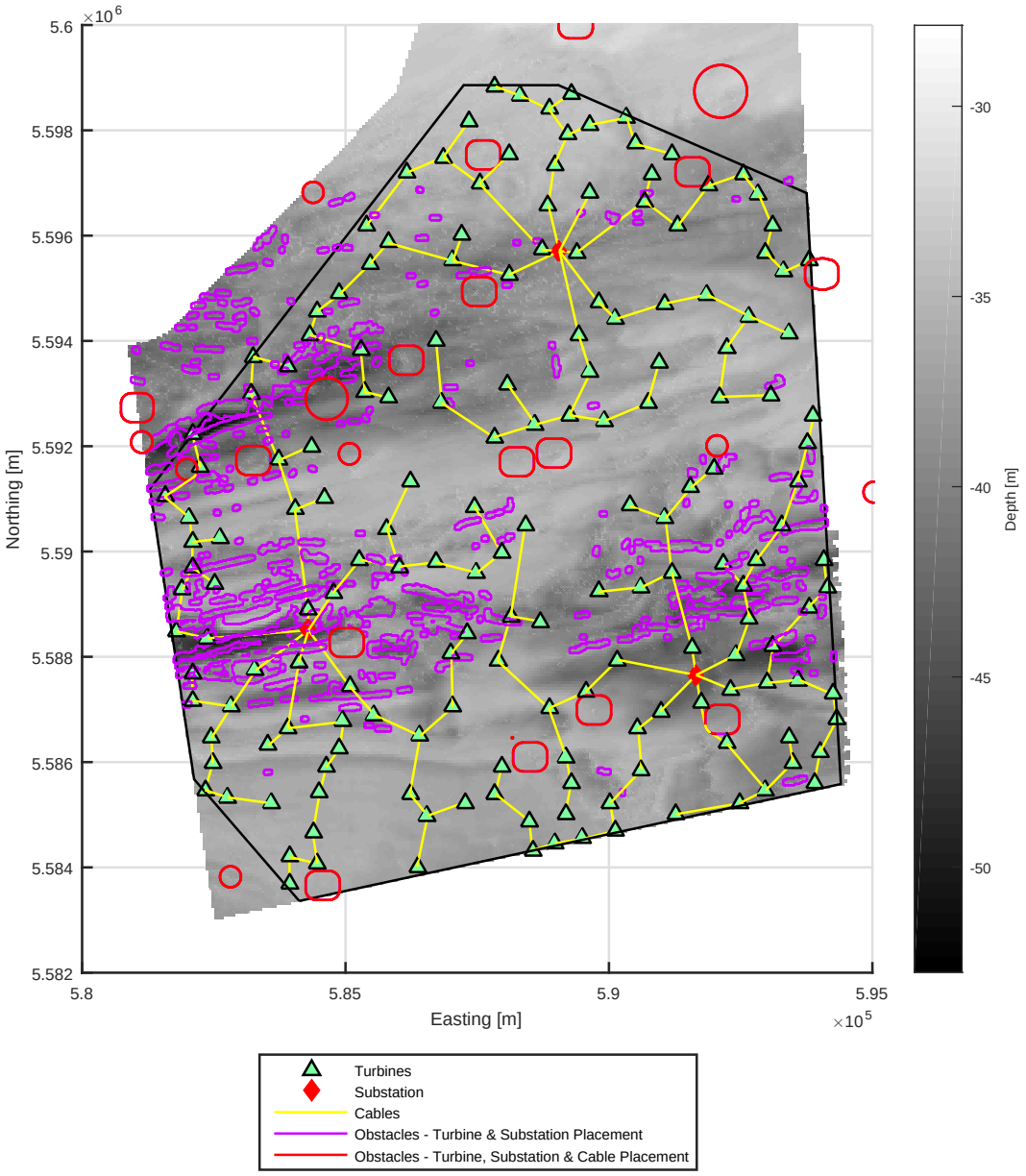

Figure 7.29: UK Round 3 site - optimized layout using continuous constraint sets and GA optimizer. Darker areas indicate deeper water.

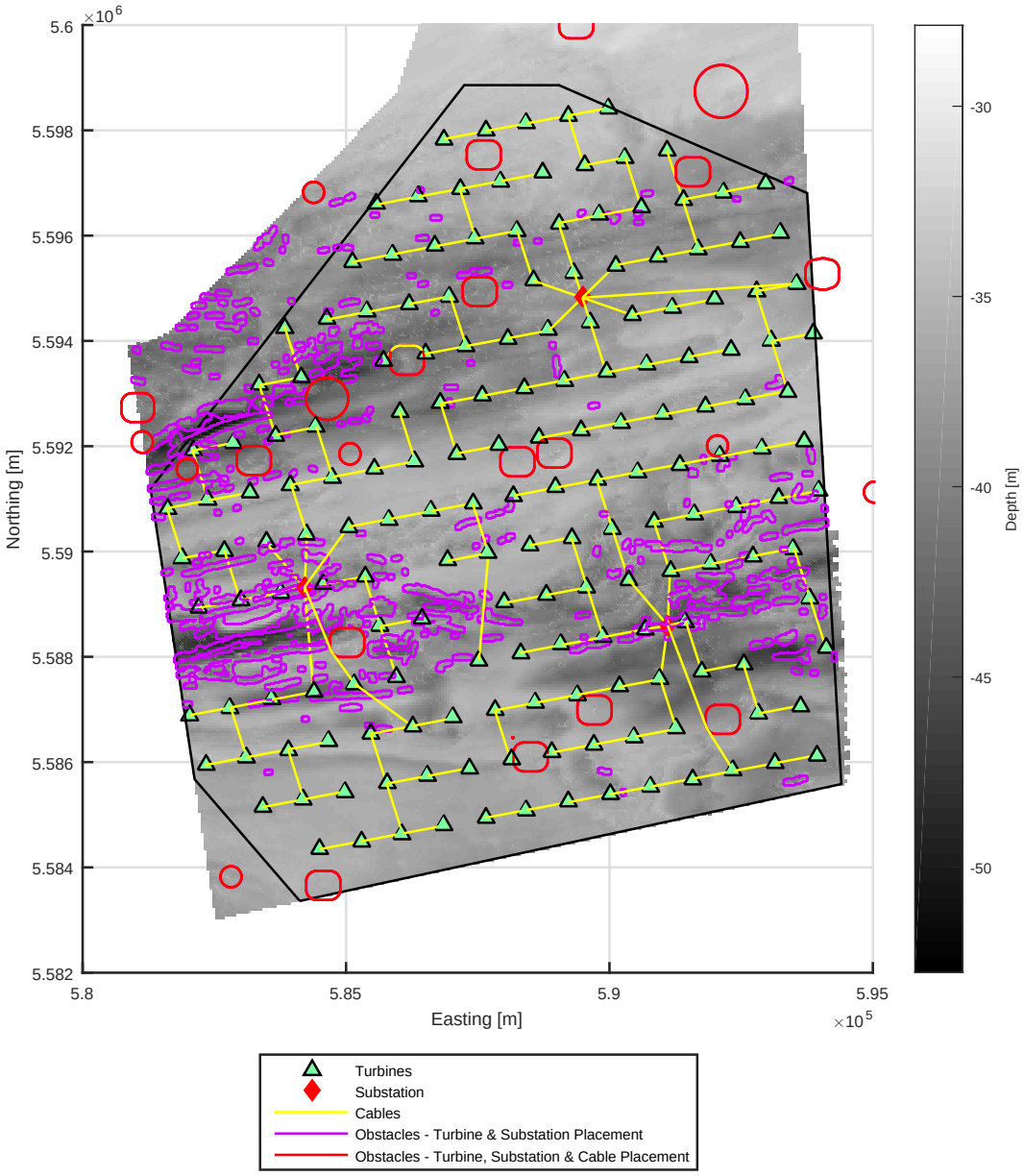

Figure 7.30: UK Round 3 site - optimized layout using array constraint sets and PSO optimizer. Darker areas indicate deeper water.

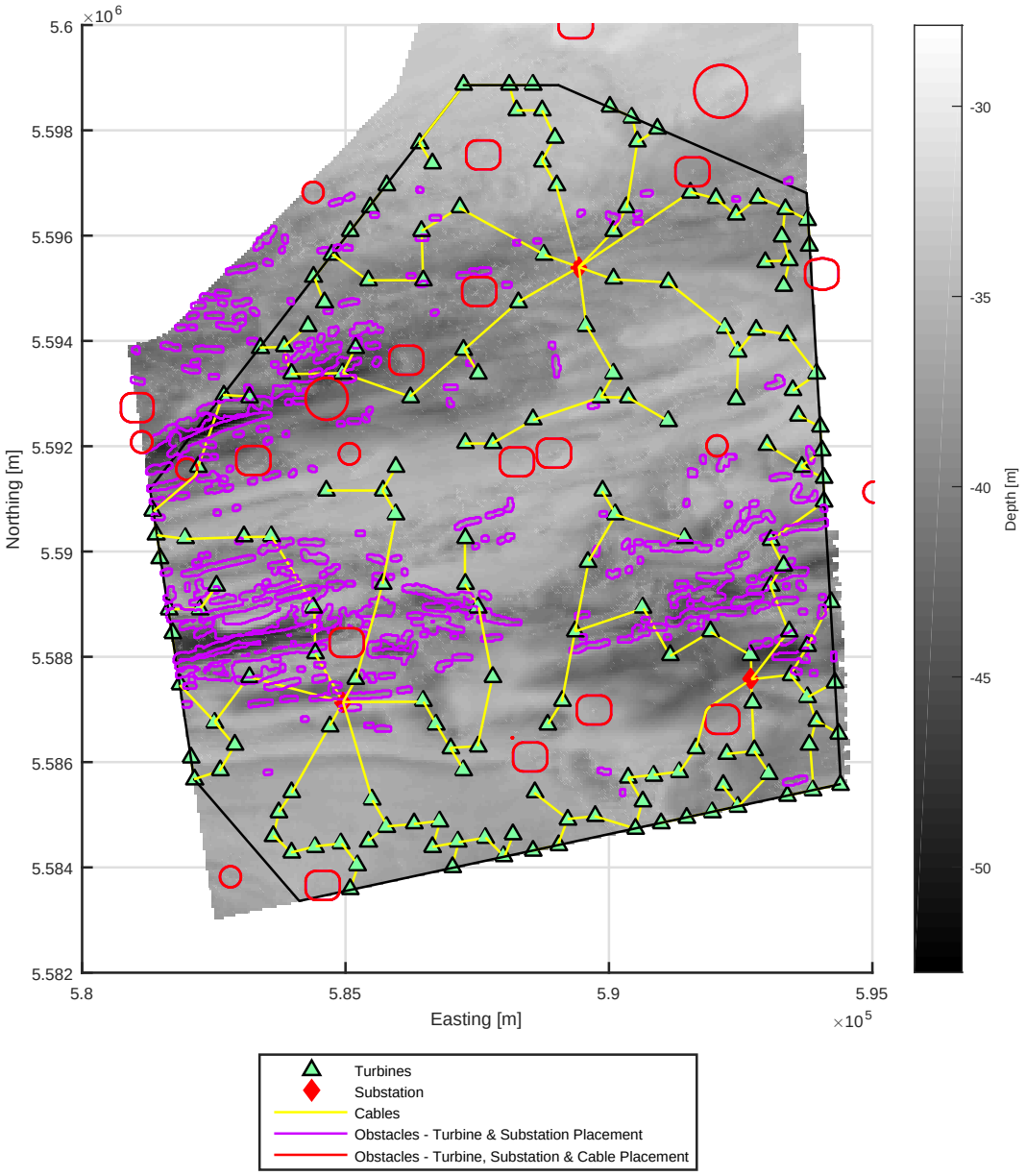

Figure 7.31: UK Round 3 site - optimized layout using binary constraint sets and PSO optimizer. Darker areas indicate deeper water.

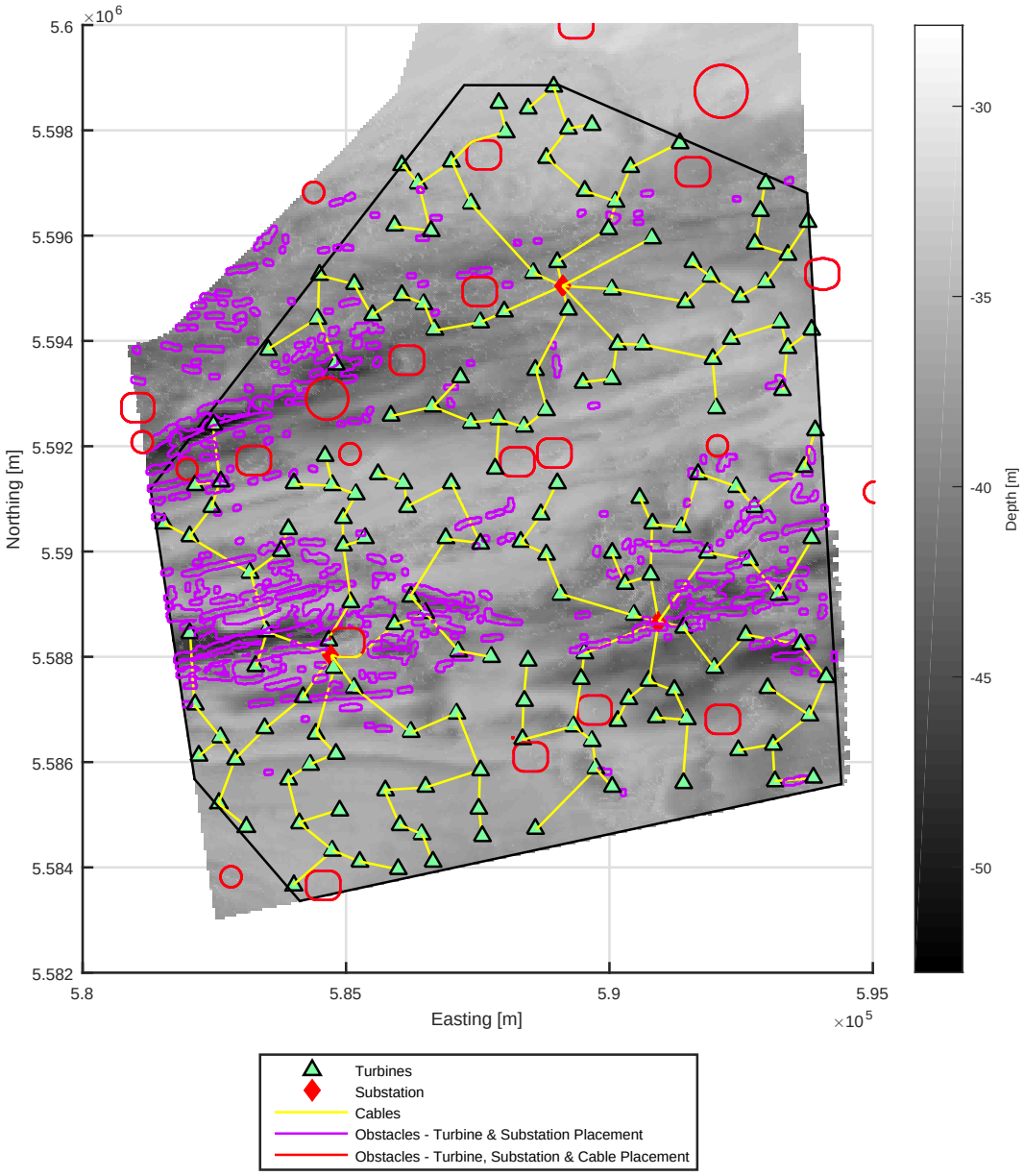

Figure 7.32: UK Round 3 site - optimized layout using continuous constraint sets and PSO optimizer. Darker areas indicate deeper water.

Though these two layouts are very similar in terms of cost, AEP, and LCOE, the layouts themselves are very different as shown in Figure 7.27 and Figure 7.29.

Applying the PSO to the same UK Round 3 site resulted in similar trends being observed as the GA. Applying the PSO using the array constraints is shown in Figure 7.30. This result, contrary to the GA result, makes good use of the wind farm area while still increasing the spacing along the dominant wind direction. Compared to the GA using the same constraint set, the layout produced by the PSO has both increased lifetime cost and AEP, resulting in an overall reduction in the LCOE.

Figure 7.31 shows the results of applying the PSO constrained using the binary constraints. This layout has an LCOE 3.5% lower than the results produced by the GA under the same constraints. Yet it is still significantly higher than the results produced using either of the optimizers and either of the array or continuous constraint sets. As was the case using the GA, the PSO produces a layout with a sparse interior in order to allow the wakes to recover effectively.

Finally, the PSO using the continuous constraint set is shown in Figure 7.32. Interestingly, compared to either the GA or the PSO using the binary constraints, this layout does not appear as sparse in the interior, though at the same time it is not as uniformly designed as the array constrained layouts.

Of the six layouts designed here, all have similar substation positions with one towards the north and two in the south on either side of the wind farm. Given the shape of the wind farm boundary, and the fact that wind farm area narrows towards the north, all the layouts which use the full available space will converge on a similar set of substation positions as these cover the wind farm area efficiently.

7.5 Chapter Summary

This chapter has presented the results from applying the integrated wind farm layout optimization methodology and tool developed as part of this project. By using the electrical infrastructure optimization module, the AEP estimation, the cost assessment, and the implemented metaheuristic algorithms it has been possible to optimize the layouts of offshore wind farms identifying better turbine positions than existing tools. Three case studies have been presented here highlighting the capabilities of this tool and promising initial results. From comparing against the original Mosetti et al. [34] cases it has been possible to compare the performance of this framework to existing frameworks and show that compared to some existing wind farm layout optimization tools the present framework will allow for more detailed sensitivity studies. For each

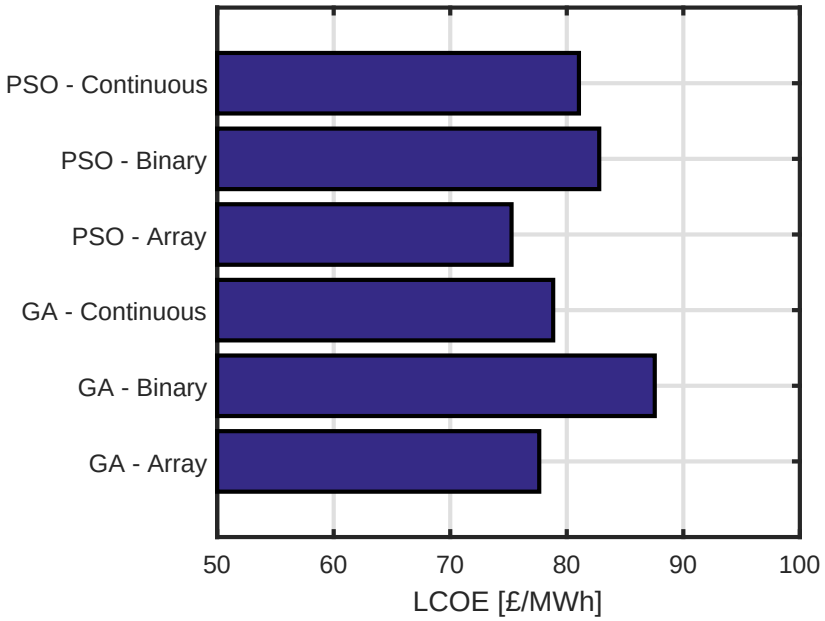

Figure 7.33: LCOE for optimized layouts at the UK Round 3 site

of the Mosetti et al. [34] cases the present tool identified either the same layout as previous tools or improvements in layouts with respect to the LCOE.

This chapter has also applied the methodology to an existing wind farm to highlight how the wind farm could have been better designed had a tool such as this been used during the planning stage of this wind farm. The tool is then applied to a future UK Round 3 wind farm representing a much larger wind farm in order to highlight the scalability of the present approach. The initial results for both the existing wind farm, Middelgrunden, and the UK Round 3 site are promising and lay the groundwork for future studies involving this framework. The present results along with those from the previous chapters are discussed in greater detail in Chapter 8.

Chapter 8

Discussion of Results

8.1 Introduction

In the preceding four chapters the results of applying each of the steps in the evaluation of a wind farm's LCOE has been presented along with the results of applying the full wind farm layout optimization methodology. This chapter describes the implications of the results presented in this project and how these can be used alongside the developed methodology by the offshore wind industry to design wind farms more effectively. Each of the individual modules created, the electrical infrastructure optimization, the annual energy production estimation, and the cost assessment, have helped advance understanding how the layout can impact the feasibility of an offshore wind farm project.

8.2 Electrical Infrastructure Optimization

The electrical infrastructure optimization, a step commonly omitted from the standard formulation of the wind farm layout optimization problem is shown to produce significant reductions in cable length and cost while designing infrastructures which satisfy the constraints faced by a modern offshore wind farm developer. Existing tools for the positioning of substations, design of intra-array cable networks, and export cable path siting do not consider all of the obstacle constraints considered in the present work and are therefore not capable of ensuring that valid infrastructure is designed for the given wind farm layout. This therefore represents a major advancement in computer-aided layout design of wind farms.

This sub-tool, when deployed independently of the full wind farm layout optimization framework, can be used to effectively explore the design options. It can aid in wind farm design by evaluating the impact that design changes such as the location and number of substations, the voltage level of the intra-array network, and the level of redundancy in the intra-array network have on the LCOE. Furthermore, it can also be used to explore the added cost of operating in complex environments with restrictive seabed

constraints. The developed tool in addition to being relevant for offshore wind farm layout optimization will also be useful for future work exploring the sensitivity of the LCOE to the electrical infrastructure. Furthermore, given that this module considers the constraints faced by an offshore renewable energy developer it is likely that this module has relevance when it comes to planning large wave farms or tidal stream deployments which, like wind farms, will need a network to collect and export the power generated.

Leading consultancies in this field therefore make use of manual approaches in the layout design of wind farm collection systems. This incurs significant man-hours and, without a systematic approach, it is often difficult to easily consider changes in the design variables. Compared to these manual approaches, the application of this approach was capable of identifying savings in cables between 3 km and 16 km depending on the turbine layout under consideration and the voltage level of the collection network (see Figure 8.1) corresponding to savings of between £1 million and £8 million [252].

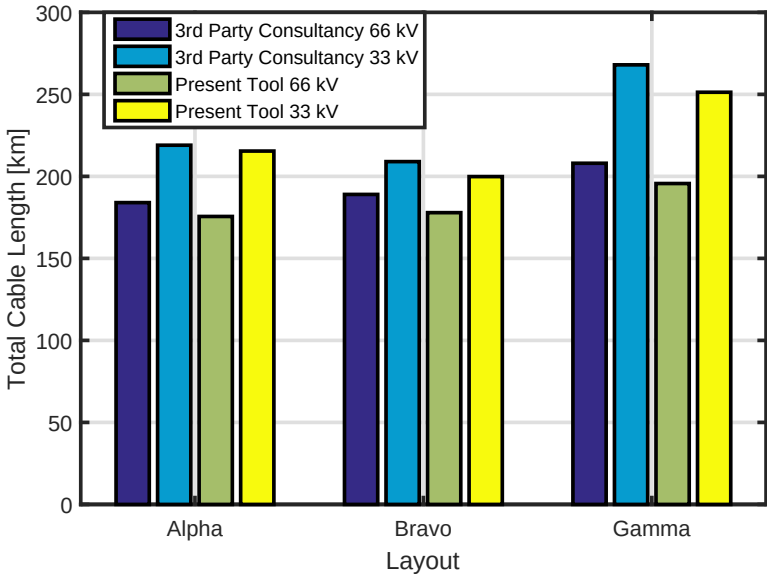

Figure 8.1: Cable length comparison against a 3rd Party Consultancy [252] considering three proposed layouts with complex GIS constraints at both 33 kV and 66 kV. All the layouts made use of the same turbine layout of 184 6 MW turbines, but with varying number and locations of offshore substations.

The application of this tool allows developers to evaluate the differences in collection network voltage. For a range of turbine layouts considered for a UK Round 3 project, it was found that moving from a radial network at 33 kV to a 66 kV network, allowed a reduction in cable length between 15% and 30% depending on the location of the substations and the specific layout under consideration. This reduction in cable length comes principally as a result of having more turbines on each string and therefore reducing the total number of cable strings required. The specific reduction incurred by

a site will be dependent on the turbine layout, the constraints of the site, and the cable cross-sections under consideration.

Simple rules of thumb for estimating the amount of cable required by a wind turbine layout do not consider the site constraints or even the capacity constraints on cables. As a result of this, it was found in Chapter 4 that the supply cost of the cable for an offshore wind farm could be underestimated by approximately £5.7 million in the example case explored. Though this does not represent a significant proportion of total CAPEX, it does represent design work which must be completed prior to construction of the wind farm, and by inclusion here it can aid in the differentiation between the different layouts under consideration. As wind farm projects are often CAPEX-constrained, a small CAPEX reduction in this manner may make the project more bankable and should therefore be taken into account as early as possible.

Using the developed methodology, an analysis was completed in Chapter 4 using a simplified probabilistic approach in order to evaluate the value of including varying degrees of redundancy in the collection network. At the site considered, it was shown that given typical failure rate data commonly used for subsea cables, a single sided ring network could result in a lower lifetime cost when the value of the lost production due to turbine downtime is included. The similarity in cost between the three levels of reliability, however, supports further study using a more detailed stochastic simulation approach taking into account more accurate downtime modelling through the integration of a weather model.

Although the developed approach is capable of identifying valid cable layouts in an efficient manner, there is no guarantee that the optimal design will be found as a combination of metaheuristics are used. While previous studies had identified that substations placed in the interior of a wind farm would generally produce more efficient intra-array cable networks, these studies have not considered the potential complex networks required by offshore wind farms due to the complex seabed constraints [253, 254]. The work done here, has not explored if this is the case or if more cost effective infrastructure could be designed by considering the substation placement, intra-array network, export cable path, and avoidance of cable crossings in one stage rather than in three separate stages as done here. Integrating each of these steps into a single optimization problem would need to take a fundamentally different approach as the possible cable paths will change as a result of decision variables. In the approach taken, the set of paths to consider is dependent on the turbine layout and therefore once these paths are found, the optimizer only needs to select which of these are to be deployed. In order to efficiently design the network considering each of the parameters simultaneously would require the use of a multi-agent pathfinding algorithm coupled with a facility location problem in order for the paths under consideration to be impacted by the

positions of the substations and the other cables. As these problems are classed in computational complexity as PSPACE-hard and NP-hard respectively, the combination of both will produce a problem exponentially more challenging to solve than the present approach [14, 255, 256]. The decision to divide the problem into a series of sub-problems is therefore seen as a pragmatic approach to allow the problem to be solved in reasonable time-scales while identifying sufficiently good quality results to aid in the design of offshore wind farms.

8.3 Estimation of Annual Energy Production

Although past studies have explored the behaviour and characteristics of wind turbine wakes, it was important to evaluate the suitability of wake models and wake modelling tools to wind farm layout optimization. The work completed in this study implemented and applied five wake models to three sites using real site data to validate their performance and assess their suitability. For two of these sites, a variation of the models in which the interaction between the wind farm and the PBL was also implemented and evaluated. The estimation of the AEP not only includes the aerodynamic losses due to wake interactions, but also the electrical losses in the collection network and turbine transformers.

The AEP estimation implemented in this methodology can therefore be considered to be made up of two steps completed in series. In the first step, the wind resource along with a representation of the wind turbine layout is used to determine the AEP taking into account the aerodynamic losses due to wakes. The second step, then uses the specifications of the turbine transformers and intra-array cables as well as the electrical cable layout to estimate the losses through these electrical systems. This corresponds to the AEP metered at the low voltage side of the offshore substations. In the UK, wind farms are metered at the low voltage side of the offshore substation after which the OFTO is responsible for the power. From a project developer perspective, this is the AEP delivered that is relevant for the calculation of the LCOE. For non-UK projects, the losses through the export cable, and any onshore cables may potentially need to be considered depending on the relevant regulatory framework.

The results from the validation of wake models agreed with past studies, identifying the Larsen wake model as a model which balanced accuracy and computational complexity [53, 186]. In fact, the results from the present study showed that more complex models such as the Simplified Ainslie Eddy-Viscosity model did not consistently improve accuracy with both the Larsen and Simplified Ainslie Eddy-Viscosity models yielding results with RMS errors below 3% under specific conditions. The Larsen model, however, reached these results consistently in less than one twelfth the time compared to the

Simplified Ainslie Eddy-Viscosity model. This has highlighted that the simple analytic wake models are the most relevant in the context of wind farm layout optimization.

Of the models implemented, the Jensen, Larsen, and Eddy-Viscosity had consistent errors depending on the wind speed bin and the size of the wind direction sector while the remaining models, the Frandsen and Ishihara models, were at times extremely accurate (under 3.5% error), but in other cases very inaccurate (as high as 50% and 30% error, respectively). Specifically, all the implemented wake models performed poorly when narrow wind direction sectors were considered with the best models still generating at least 7% error for a wind direction with few wake interactions when a 5° sector width used. This performance drops to at least 12% error for Horns Rev and over 40% error at Middelgrunden if the wind direction sector width is reduced to 2°. This performance indicated that the calculation of AEP should be done on larger sectors such as 20°, 30°, or 60° sector widths. Going larger than this, the wind direction is effectively discretized to too few steps to be representative of the wind climate. In fact, one could argue that using only six discrete directions, each with a width of 60°, is sufficiently few sectors that any variation in wind direction is not fully described.

For a site such as Middelgrunden, where the dominant wind direction is perpendicular to the row of turbines, it is unsurprising that using only a few wind directions (i.e. wide wind direction sectors) will still yield satisfactory results as, in aggregate, most wind directions will not result in any relevant wake effects. In a more complex layout such as Horns Rev or Nysted, winds from any incident direction will result in different wakes which grow along different directions and therefore would impact different turbines. It would be expected that for these sites and sites like this with less defined dominant wind directions and more complex turbine layouts that narrower direction sectors would be needed in order to estimate the AEP accurately considering the impact of wakes on all turbines. Unfortunately, given the available data at both of these sites, it is difficult to conclude if this is the case as data was only available at specific wind speed and wind direction sector sizes. At Horns Rev the 30° sector size (the largest available in the data) gave the best results, while at Nysted, data was only available for 5° sectors. It is therefore unclear if the observed trends relating to the size of the wind direction sectors are site specific or hold true for a wide range of sites. From this, it is therefore difficult to suggest that a particular discretization of the wind direction be used for the estimation of the AEP.

The validation study was limited by the availability of data. At both Horns Rev and Nysted wind farms only averaged aggregated data was available and as a result of this, the available data was only suitable for validating the average power produced under the given conditions rather than specific time intervals. It would be expected that a more rigorous study using the time series data such as the study completed

at Middelgrunden would be a useful study in order to better assess the performance of these wake models. A major area of improvement would be to understand the uncertainty on the measured data. From the results at Nysted wind farm, where the standard deviation of the wind speed was provided, it was found that for specific cases, despite the high levels of relative error, the models were still predicting results within the uncertainty bands of the data. This identifies the need for higher quality data measurements with which the modelled results can be compared. This was especially noticeable in the Middelgrunden study where no upstream met mast was present, and the cup anemometers were generally known to be poorly calibrated resulting in erroneously low wind speed measurements [191].

While the data could be improved, the results from this study support the suggestion that the LWC may not be relevant to all large sites, and that the conditions under which it should be applied need to be further explored using additional site data from a wider range of sites. Though it is understood that some interactions with the PBL would need to be considered, it remains to be seen if the simple approaches taken thus far are accurate representations of the interaction [195].

A major output from the application of the wake models at the three sites was that the different wake models had differing performance depending on the free stream wind speed. As shown by studying Middelgrunden wind farm, it was possible to identify that all the wake models under consideration had poor performance at high wind speeds. As most offshore wind farms have average wind speed in the range of 6 m/s to 12 m/s and the turbines are therefore optimized in design for energy extraction at these wind speeds, one would want to select a wake model that performs best in this range. It is within this range, leading up to the rated wind speed, that wind turbines are operating at the steepest points of the power curve and are therefore most sensitive to the wind speed. Future work may find it worth exploring the application of different wake models at different inflow conditions in order to use the models that best describe the behaviour of the wake for those particular inflow conditions.

The transformer losses are based on the manufacturer specifications. The cable losses, however, are based on a calculation from the relevant IEC standards [196, 197]. As the standards are designed for the safe sizing of conductors and insulation, they likely overestimate the losses in order to assume worst case scenarios under which the conductors and insulation are sized correctly with the appropriate safety factors. The losses calculation should therefore be validated against measured cable losses in order to evaluate its accuracy. The approach taken, using the relevant standards should at least consistently correlate to the real losses, however, there may be a systematic overestimation. Assuming that in the development of the standards the calculation has been validated, this should give accurate results. As the present model is applied to

explore the relative AEP of competing layouts, the relative accuracy is more important than the absolute accuracy, and therefore it is not expected that this should significantly impact the results of the optimization tool.

A major area where the AEP estimation could be improved is the inclusion of ageing, component deterioration, and the introduction of turbine-specific availability depending on the layout of the wind farm. The inclusion of these parameters would allow the modelling of each turbine's individual availability. However, without the data with which to validate these relationships, they cannot be included without significantly increasing the uncertainty. Though it is recognized that the wakes impact the loading conditions on turbines, this is a difficult factor to consider when modelling the turbine downtime or component failure rates [160]. If these impacts could be accurately taken into account, then the AEP would be capable of reflecting the impact that the layout has on fatigue loads and therefore turbine component reliability. This would not only give more accurate layout dependent AEP assessments, but would also advise on the layout dependent costs such as operations and maintenance costs.

8.4 Cost Modelling

The final step in the evaluation function is the integration of the parametric cost model. This cost model makes use of generic cost estimation methods; however, it includes some consideration for the impacts of the wind turbine layout. Having said that, the layout impacts are highly dependent on the available site data. For early stage projects where even budget quotes may not be available, simple models such as these will likely be used to estimate the project cost and are therefore frequently used and trusted throughout the industry. As discussed in Chapter 6, the the use of generic cost modelling approaches has been to ensure that the cost estimation methodology is applicable to a wide range of projects that may be considered in the future. In addition to this, the use of cost models using a deterministic calculation approach ensures that the costs can be established without significant time spent on the calculation. As the goal of the cost model has been to capture the layout dependent elements; costs such as development costs, taxes, interest/finance payments, and seabed leasing have been omitted as these costs will be project specific and will not impact the selection of the wind farm layout. As a result of these omissions, the costs estimated by this tool are an underestimation of the real costs that will be incurred by the wind farm developer and are not reflective of real prices that the developer will need to take into account when preparing their subsidy bids.

The model parameters presented in Chapter 6 and validated in Section 7.3.2.1 are project and site specific and will therefore need to be selected depending on the design

and specifications of the project. The principal areas where the layout is seen to impact the cost is in the installation operations, the foundation supply cost, the intra-array cabling, and the operations and maintenance. These cost elements have therefore been designed to account for the correlation between the cost elements and the wind turbine layout. Some cost centres may have high absolute error, or may simplify elements which are not affected by the layout.

By including the depth at each of the turbine locations, the costs of the foundations are modelled as having variation across the site; however, this does not include a consideration for the soil conditions. Realistically, the design of the foundations would be dependent on the turbine loads, the depth, the soil conditions, wind loading on the structure, wave loading on the structure, and loading due to tidal forces. By looking only at the water depth and turbine size, the soil conditions are not considered and averaged environmental conditions are taken into account. This simplification could introduce error if the soil conditions or environmental loading vary across the site and deviate from the assumed conditions for specific regions of the site. For a complex site in which the soil conditions or environmental loading conditions vary across the site, some further development will therefore be required in order to take this into account. Given the design of the framework, however, once the cost function is updated to include this consideration, no further changes are needed for the optimization process to take this into account.

The functions modelling the costs of installation take into account the wind farm design, and assume a specific installation strategy. They therefore do not optimize the installation strategy. The present work could be linked with a more detailed logistics model in order to evaluate different installation strategies and select the most applicable for each layout.

As discussed previously, it remains to be seen what will be done to offshore wind farm installations at the end of life, and therefore the decommissioning phase remains unclear and will likely vary from site to site. The present model assumes the full removal of all turbines and foundations and that cables are cut and left buried. This represents an upper bound on the decommissioning costs as it does not account for any revenue from recycling of any material. Additionally, if due to the development of artificial reefs any foundations will be left in place in the marine environment, this will further reduce the cost of decommissioning by reducing the elements which will need to be removed. Figure 8.2 shows the marine growth on a monopile at Teesside Offshore Wind Farm after 2.5 years of operation.

The end goal of this tool has been to identify optimal layouts. As part of this, the cost is used to help differentiate between different layouts. The priority has therefore been

Figure 8.2: ROV Footage from Teesside Wind Farm showing marine growth on a monopile foundation [257].

on identifying the layout-dependent cost elements and including these within the cost assessment, thereby creating a model which is accurate on a relative basis. Though the costs may carry absolute error, the relative error, using the defined assumptions, will be low.

8.5 Layout Optimization

Applying the full methodology to optimize the layouts of offshore wind farms was done in Chapter 7. When applied to a series of test cases, the tool identified layouts with improved LCOE compared to past studies, identified layouts with improved LCOE compared to existing wind farms, and highlighted the scalability of the methodology applying it to a wind farm consisting of over 100 turbines with an installed capacity of over 1000 MW.

8.5.1 Mosetti Cases

The results for the three Mosetti cases presented insight into the value of specific constraint types. Previously, this problem had been addressed either as a binary decision problem with 100 fixed grid cells where the turbines could be placed or as a continuous problem in which the turbines could be placed anywhere within the domain. In the past, studies have not compared the two constraint sets, nor explored how limiting the turbine positions to a fixed grid limits the solution space and impacts the quality of the solution. Changing the solution encoding from a binary encoding required the optimizers to be changed from binary coded to real coded in order to facilitate the real valued decision variables.

From the results presented here, it was interesting to note that constraining the search space by stipulating that the turbine layout must adhere to a symmetrical array layout produced better solutions using the same optimizers. This points to the fact that the continuous problem is a large search space, even in these small wind farms, and that further constraining the search space can improve the performance of the optimizer. Given this, it is likely that a hybrid optimization algorithm based on combining an evolutionary algorithm with a local search algorithm would be well-suited to addressing the continuous problem [258, 259]. The studies of Elkinton [17] and Réthoré et al. [27] had reached similar results, but had not explored the improvements to solutions that could be identified by further constraining the search space. A combination of constraining the search space and hybrid optimization algorithms will likely need to be implemented in order to identify the best layouts for future projects.

Limiting the turbine positions to 100 possible positions significantly constrained the search space such that the solutions had inferior fitness values compared to the more relaxed constraint sets. This indicates that moving to the binary constraints with a discretized set of turbine positions over-constrains the problem, eliminating high quality, valid solutions. Considering the Mosetti cases, the impact of this on the LCOE varied from £1/MWh to £70/MWh increases, corresponding to 0-16% potential improvements in LCOE from relaxing the constraints. Given some of the assumptions, the percentage difference is smaller than it would be if this were a real site, as there are some fixed costs which are intentionally overestimated. As described in Chapter 6, the port location was defined as far away relative to the size of the wind farm in order to avoid the optimizer clustering turbines close to the installation port. The installation costs are therefore larger than they would be for a real case thereby increasing the LCOE. For these cases, it is therefore more valuable to analyse the absolute difference in LCOE rather than the percentage reduction.

8.5.2 Middelgrunden

The application of the tool at Middelgrunden allowed the AEP and cost estimation modules to be validated prior to the application of the optimization framework.

From the results in Section 7.3.2.1 it can be seen that the AEP estimation for Middelgrunden wind farm is within 1% of the reported values, indicating that for this site the Larsen wake model accurately describes the influence of the wakes on the AEP for all wind speeds and directions. The reported AEP was computed as the sum of the turbine generator outputs, and therefore did not account for any turbine transformer or electrical cable losses. These elements of the AEP estimation were therefore not included in the validation of the AEP module.

On the cost side, however, significant differences were observed between the costs reported by the developer and those estimated in the present model. The lower than anticipated turbine costs have been discussed in previous studies with Middelgrunden consistently coming out as a cheaper than expected project as a result of incurring lower turbine supply costs than models predict. Compared to projects using similar turbines or constructed during a similar time period, Middelgrunden still represents an uncharacteristically cheap project.

In the case of the O&M costs, this difference can be explained by the fact that the reported figure is based on the actual O&M spend from two years of the project while the model estimate is the annual O&M costs anticipated through the life of the project. The modelled values therefore take into account some major repair works which will need to be done during the lifetime of the project. During the two years (2003 and 2004) from which the reported costs are taken, the wind farm maintained high availability (95.9% and 95.6% respectively) indicating that no major repair works were carried out. These two years would therefore be expected to have a lower incurred cost than the modelled values. As the wind farm is now approaching year sixteen of operation it is likely that costs more representative of the wind farm's lifetime would be available.

8.5.3 UK Round 3

The application of the methodology to a UK Round 3 site tested the tool's ability to scale to larger sites involving more turbines. This case study which considered 175 6 MW turbines dwarfs the other case studies in terms of size of the individual turbines, the size of the wind farm, and even the number of substations required. This therefore helps show the capabilities of the tool for future wind farm projects.

For the six optimization runs executed for this site, it was found that the electrical cable optimization results in a CAPEX variation of £12 million. Though this has a relatively small LCOE contribution, a CAPEX reduction of this order might still be important in order to help make the project more bankable. Furthermore, though it is a small contribution to the LCOE, it is still an important way in which the project costs can be reduced and should therefore be taken into account.

The optimization of this larger wind farm, resulted in similar trends to those observed for the smaller cases, with the best layouts for each optimizer coming with the array constraints, then the continuous constraints, and the worst results coming when applying the binary constraints. The binary constraint set considered a fixed set of 638 possible turbine positions approximately 500 m apart. The quality of the results is directly a function of the number of valid turbine positions considered as this describes the degree to which the search space has been discretized and possible positions have

been omitted. The present work did not explore how to effectively design this grid and it is without a doubt that with a grid with more points within the wind farm area a better solution could be reached. The idea of using a binary constraint set like this, is generally to reduce the computational time by limiting the wind turbine positions to a finite set rather than the open-ended continuous problem. As a decision problem the selection of 175 positions from the available 638 still defines over 2.13×10^{161} valid combinations for the layout. This is significantly more than was experienced in the Mosetti binary case (9.01×10^{27} possibilities) and the Middelgrunden binary case (7.11×10^{37} possibilities). Given this, and that the search space for the continuous problem must be *even* larger, it is not surprising that both of the implemented optimizers are prematurely converging to a solution which is inferior to that of the array optimizer.

The present work has shown that simple optimization algorithms with only basic tuning (including a GA and a PSO) are unable to solve the continuous problem without converging prematurely to a non-optimal solution. This is an interesting result as it indicates that work in this field will need to either consider further tuning of the optimization algorithms or more complex optimization algorithms if the true optima is to be located for this problem instance. This is supported by the array optimizer, a more constrained version of the same problem, identifying superior layouts. Having said that, the implemented optimizers deploying the same parameters for all constraint sets were able to find suitable layouts for a range of wind farm types. This indicates that this framework offers a strong starting position for future studies into the design of wind farms. Further tuning will need to consider multiple wind farm sizes and types in order to ensure that the tuning does not become too specific to a given instance of the problem.

In other ways this result regarding the array layouts is an important finding for The UK Crown Estate; The Nautical and Offshore Renewable Energy Liaison (NOREL) Group; and the Maritime and Coastguard Agency (MCA), as it indicates that imposing a requirement for layouts to be regular arrays does not eliminate all good solutions, and in fact high quality solutions can still be identified with this constraint set even for a large 175 turbine wind farm. Given the safety and navigational concerns which are not directly considered in this tool, it is likely that future offshore wind farms will be designed using the array constraints. This will comply with the MCA requirements, but also make it possible to identify navigational channels through through the wind farm if necessary as clear transit corridors can be identified. Given this, the present framework will allow the wind farm developer to assess the "cost" of these additional constraints at their specific site by comparing it against the continuous results.

A common conclusion from existing layout optimization approaches has been to introduce some degree of edge-weighting through which turbines are pushed to the edges of

the wind farm thereby increasing the inter-turbine distance in the interior of the wind farm allowing a greater degree of wake recovery. Although the solutions presented by the continuous optimizer do show greater turbine densities as the edges of the wind farm, the performance of the array optimizer indicates that while edge-weighting will theoretically improve the performance of the wind farm, for a large wind farm, the search space that the continuous optimizer needs to explore may grow to be too large for these improvements to be realized.

From the results shown, it can be said that the optimization of a wind farm layout is highly site specific and rules of thumb for separation distances may not offer the best potential layout for a given site. The use of a methodology such as the present framework will allow the layout of the site to be designed taking advantage of the specific site characteristics in order to minimize the LCOE.

8.6 Optimizer Performance

A constant struggle with the use of metaheuristics such as genetic algorithms or particle swarm optimizers is that these algorithms are only guaranteed to deliver a feasible solution, there is no guarantee that the solution presented will be optimal or near optimal. Although the optimizers identify improvements to the population through the optimization run there is still no guarantee that the converged solution represents an optima. As discussed earlier in this chapter, in the case of the continuous optimizer it is known that the optimal solution is not being found, as the array optimizer, a further constrained version of the problem, was capable of identifying superior solutions. This indicates the continuous optimizer, and likely all optimizers regardless of constraint sets, are prematurely converging. Appendix D shows the convergence plots for the case studies presented in Chapter 7. From the plots presented, it can be observed that a number of the optimization runs reach their final solutions relatively early in the optimization process or, have in fact not converged when the optimization process reaches a termination criteria. This highlights that the optimizers are prematurely converging or terminating. Further tuning could avoid this, however, it is important when tuning the optimizers that a range of wind farm sizes and types are considered in order to ensure that the optimizers are not biased towards wind farms with specific characteristics. The continuous optimizer in particular represents a significantly more complex search space than either the array or binary constraint sets and therefore, more sophisticated optimization algorithms are likely required in order to ensure that these do not converge prematurely. As the goal of this work was to construct and demonstrate this framework, this further tuning has not been completed, although initial tuning of all the implemented optimizers has been done.

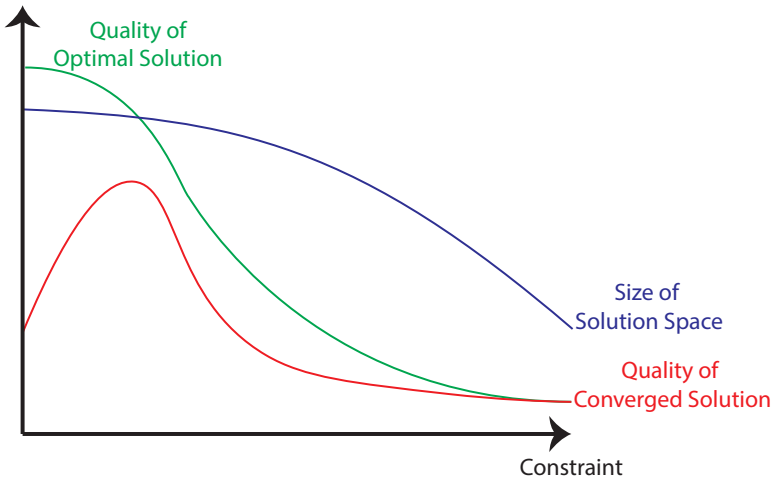

Figure 8.3: Illustrative curves highlighting how the introduction of constraints impacts the size of the solution space, the quality of the optimal solution, and the quality of the converged solution considering the same optimization strategy using the same optimizer parameters

Figure 8.3 shows how as a result of introducing constraints to an optimization problem the search space size reduces, as this happens, the quality of the optimal solution remaining within the search space will generally decrease, slowly at first, but eventually given sufficient constraints this can be quite significant. It is possible that the introduction of further constraints will not impact the quality of the optimal solution as is the case when cutting planes are generated. However, for problems in general where constraints are not generated specifically in order to maintain the optimal solutions, it is believed that the global optima will reduce in quality as further constraints are introduced. At the same time, if the same optimization strategy is used with the same parameters, the "optimizer efficiency" or the relative difference between the converged solution and the optimal solution increases as a result of the smaller search space which still includes high quality solutions. However, as further constraints are introduced and high quality solutions are eliminated from the search space, both the quality of the optimal and converged solutions decrease, slowly converging under sufficient constraint. This highlights the observed phenomena where the continuous constraints, despite being a less constrained problem, was unable to surpass the solution quality of the array constraints.

Furthermore, the size of the search space for the continuous optimizer compared to both the array and binary constraint sets, highlights that a larger population or swarm size may be necessary to address this formulation of the problem. In the results shown in Chapter 7, both the GA and PSO were run with population/swarm sizes of 100 individuals regardless of the constraint sets used. This represents the maximum population

size that could be run on the computer available for this study and does not represent the ideal population size for these problems. Given the performance of the optimizers it would be prudent to recommend the use of greater computing power in order to allow larger population sizes to be used. As implemented, all the optimizers are well suited to parallel computing and deployment on a cluster if such resources are available. The trends shown in Figure 8.3 hold for situations in which the same optimization strategy and parameters are used. If the population/swarm sizes are increased as suggested, this would represent a change in the parameters allowing better solutions for the less constrained case to be realized utilizing the same optimization strategies.

Each of the optimization runs here represents a single execution for each combination of case, optimizer, and constraint set. In order to improve the performance of the optimizers and the confidence in the results not only should further parameter tuning be explored, but additional studies into increasing the size of the population and averaging the results of multiple runs. By including multiple runs, any seeding bias of a particular run will be identified and there should be a greater chance that the search space is effectively explored across the ensemble of runs. Even though only single runs have been completed here, these results are still valuable as they still identify improvements that can be made with the expectation that multiple runs would only further improve the results or at least the confidence in the results. In the present framework, completing multiple runs in parallel can easily be accomplished if the framework has access to additional nodes or a cluster. With the computational power available for this project, a single node, it was not feasible to complete multiple runs in a sensible time scale and in fact was not necessary in order to demonstrate the capabilities of the framework.

Although the approach presented is capable of finding substation placements and intra-array cable layouts which can successfully reduce cost, there is a question as to whether this additional level of detail is necessary for a wind farm layout optimization tool. Compared to the remaining components of the evaluation function, the majority of time is spent computing intra-array cable network as for large wind farms, a number of crossing constraints must be generated. As shown in Table 4.1, a full 175 turbine wind farm with three offshore substations can take close to 2000 s to solve on a multi-core CPU. The AEP and cost calculations on the other hand due to their deterministic approaches are significantly faster and in many ways have a more significant impact on the LCOE. This results in the overall optimization process when including the intra-array cable network step taking up to 20 days for some large wind farm cases.

Comparing the GA and the PSO directly to one another, it was interestingly found that for all the case studies, the PSO gave the best results for the array constraints while the GA gave the best results for the continuous constraints. When examining the results for the binary constraints it was observed that neither optimizer consistently outperformed

the other. This identifies that although both optimizers are capable of addressing this problem regardless of the constraint set, it may be wise to deploy different types of optimizers depending on which constraint set is used.

Chapter 9

Concluding Remarks

9.1 The Approach to the Problem

This thesis presents a methodology and the development of a new tool for the optimization of offshore wind farm layouts including the placement of turbines, substations, and subsea cables. In the literature review, existing tools for the optimization of offshore wind farm layouts are presented, and are analysed to identify the major areas of improvement from a project developer perspective. Previously developed tools have often omitted many real constraints and considerations important to project developers thereby reducing the applicability of the methodology to real projects. The principal aim of this thesis has therefore been to:

> To present a flexible framework for the optimization of offshore wind farm layouts including a greater consideration of the impact the wind farm layout has on the LCOE than existing tools and thereby provide a methodology that can be deployed by wind farm developers to real sites.

Layout optimization of offshore wind farms is an active field with many tools and approaches having been developed specifically to address this problem. These existing methods have identified a need for tools which encapsulate a greater degree of detail and capture the impact the layout has on not only the energy yield of the wind farm, but also the project costs.

The LCOE has been defined to be comprised of two elements: the energy yield of the wind farm and the lifetime costs of the wind farm. The evaluation of the wind farm layouts has therefore divided the the evaluation of a wind farm's layout into three separate steps, each of which contributes to either the AEP, the cost, or a combination of both. The evaluation of a wind farm layout by first estimating the energy yield and then the costs of the project is therefore commonly deployed by wind farm layout optimization approaches and is generally seen to be the standard paradigm. The work here, however, increases the level of detail with which both the energy and the costs are assessed, thereby capturing more accurately the impact the layout can have.

Deploying the integrated framework using two common engineering metaheuristic algorithms to hypothetical, existing, and future wind farms highlights the advantages of this holistic layout optimization framework over the industry standard approaches commonly deployed in offshore wind farm design. Application of the tool to a UK Round 3 site recently under development highlighted how the use of this tool can aid in the development of future regulations by considering various constraints on the placement of wind turbines within the site and exploring how these impact the levelized cost of energy.

9.2 Findings and Contribution to Knowledge

In the development of this layout optimization framework, three separate modules addressing the evaluation of different aspects of a wind farm have been constructed, validated, and then implemented into the layout optimization framework. These three modules, the electrical infrastructure design, the AEP estimation, and the cost assessment modules, have been independently validated prior to integration into the layout optimization framework allowing each module to either be run independently or as part of the full layout optimization process.

The first of the developed sub-models represents a new approach for the design of the electrical infrastructure required by an offshore wind farm. This work expands on existing methodologies taking into account the consideration of exclusion areas where offshore substations and sub-sea cables cannot be placed using a pathfinding heuristic. By including these additional constraints in addition to the electrical constraints of the cables it has been possible to produce collection network layouts which not only represent reduced cable length relative to industry standard approaches, but also consider more complex exclusion areas reducing the amount of manual labour necessary in the design process. Applying this tool to a UK Round 3 recently under development identified significant savings up to £8 million as a result of more optimal cable paths.

In order to highlight the accuracy of the approach, each of these steps has been validated where possible against existing data. Using the production data at Horns Rev I, Nysted, and Middelgrunden, it has been possible to compare a number of leading analytic wake models both in terms of their accuracy and the computational time required to execute the models. From this work, it was found that the Larsen model represented a good balance between accuracy and computational complexity. In addition, it was found that for the validation sites the LWC, a correction factor recommended to account for the interaction between the wind farm and the PBL, did not result in more accurate results. The work from this validation has therefore supported that the use of the Larsen (EWTS II) wake model without the LWC should be used for layout optimization

purposes. Furthermore, an IEC based computation was introduced to account for the electrical losses in the collection network.

The last independent module developed here has been the cost estimation module. This module makes use of industry costs which have been collected and from which empirical correlations have been built. These correlations have been built such that the wind farm layout is considered where relevant and the impact of layout changes is therefore incorporated into the costs. Though many of the cost parameters will be project specific, it is believed that the default values presented here will present a starting point from which layouts can be compared.

The developed optimization process considered three different means of constraining the turbine placement, representing three different sets of constraints that developers may be interested in. By considering these all within a single framework, this increases the flexibility of the framework and the comparison studies which can be completed using the developed framework. Execution of the full optimization methodology indicates that regardless of how the turbine placement is constrained, optimization using this framework is capable of identifying improvements in hypothetical and existing wind farms through both an increase in the project AEP and a reduction in the project costs. At the same time, application of the full methodology to a UK Round 3 site recently under development demonstrates the value that this methodology can present to offshore wind farms currently under development allowing. The full optimization framework has also demonstrated that optimal layouts are highly site specific and the use of rules of thumb by the industry is both over simplifying the problem and resulting in sub-optimal designs.

9.3 Recommendations for Further Work

This thesis has focused on the development of the presented framework and further work will need to explore the application of this framework to further case studies and sensitivity studies in order to understand the relationships between wind farm design and the optimal layouts. With this in mind, further work can both explore improvements to the developed framework and methodology as well as explore the application of this methodology.

Improvements to the electrical infrastructure module that further work can explore include the inclusion of the reliability criterion in the collection network optimization process. Presently, the reliability level is as an input, and different reliability levels can be explored by performing a sensitivity study. As offshore wind farm developers will seek to use this for large offshore wind farms there is value in including this within the

optimization process of this module thereby allowing the collection network layout and reliability level to be simultaneously found. This would require significant changes to the way in which this problem is approached, however, it would increase the capabilities of the tool and meet an industry need.

Within the AEP module it is important that further validation be completed using more wind farms as well as additional wake models. The present study has been unable to conclude under what conditions the LWC should be applied or if it should be applied at all. Further work will therefore need to explore this. As the phenomena is observed at numerous wind farms, it will be important to include this if the tool is to yield reliable results for large offshore wind farms. Along these same lines, it would be beneficial to further validate the full AEP module by acquiring data for losses through subsea cables. As no data was available, these losses have not been directly validated in the present study.

The final module of the tool, the cost module, requires numerous inputs, and it is therefore important to ensure that these inputs are calibrated accurately. The cost model could be further improved by including the soil conditions as this has a bearing not only on the design and therefore costs of specific components, but this also impacts the installation processes by affecting the time and tools required for operations and therefore the cost. More advanced probabilistic logistics models for the installation processes as well as the operations and maintenance processes could be linked to this tool providing more accurate costs for these steps. These types of tools would likely increase the total time for the optimization processes, but it may be possible to produce look-up tables using these stochastic tools to provide baseline values under specific conditions which will help characterize the wind farm layout's impact on these. EDF's ECUME tools which provide more detailed installation and O&M costs by taking into account meteorological data, vessel specifications, and failure data could also potentially be used in conjunction with this tool in order to account for the variation in O&M costs as a result of layout changes and potentially highlight how O&M strategies will need to change as a result of changes to the layout.

For future offshore wind farms in deeper waters, the tool will also need to be redesigned to include considerations of floating turbines which will have different cost functions associated.

Some wind farm optimization projects have explored allowing the turbine size or height vary within the wind farm. Although this would be a challenge to implement for a project developer, it may still be of use to expand the tool to be capable of accommodating these design options as it would improve the developers' understanding of the factors which affect the project LCOE.

With regards to the optimization algorithms, further tuning of the algorithms can be done potentially improving the results. This will need to be done using additional computational power than was available for this study, and using case studies more relevant to the offshore wind community than the Mosetti et al. [34] case studies. An interesting extension will be to explore additional optimization algorithms and specifically hybrid algorithms which attempt to take the strongest elements from two or more optimization algorithms in a single optimization algorithm.

Finally, sensitivity studies can explore how different constraints such as the types and shapes of exclusion areas, the specifications of cables, and the wind farm boundaries impact the wind farm layout. Similarly, given the implementation of the three different modes of operation will allow sensitivity studies to explore the impact of imposing symmetry or limiting the turbine positions to specific pre-defined positions. Given that The Crown Estate is presently considering requiring wind farms to be designed with symmetric layouts it is of great interest to offshore wind farm developers to understand how this will impact their business cases. This tool can also be used to define new case studies which will be relevant to the offshore wind community, allowing them to better benchmark future layout optimization tools and frameworks.

This thesis has focused on the development of a framework for the optimization of offshore wind farm layouts. It is for future work to improve upon this framework and to explore the full characteristics that an offshore wind farm's layout can have on the LCOE. If used effectively at the correct stage in the planning process, the use of tools and methodologies such as these can help further reduce the cost of offshore wind energy.

References

[1] C. Rochlin. Is electricity a right? *Electricity Journal*, 15(2):31–36, 2002. ISSN 10406190. doi: 10.1016/S1040-6190(02)00264-6.

[2] Stephen Tully. The Human Right to Access Electricity. *The Electricity Journal*, 19(3), 2006.

[3] BP. BP Energy Outlook 2016 Edition. Technical report, BP plc, 2016.

[4] Global Wind Energy Council. Global Wind Statistics. Technical report, Global Wind Energy Council, 2016.

[5] Andrew Ho, Ariola Mbistrova, and Giorgia Corbetta. The European offshore wind industry - key trends and statistics 2015. Technical report, European Wind Energy Association, feb 2016.

[6] Nicolas Fichaux, Jos Beurskens, Peter Hjuler Jensen, Justin Wilkes, Sten Frandsen, John Dalsgaard Sørensen, Peter Eecen, Charalambos Malamatenios, Joaquin Arteaga Gomez, Jan Hemmelmann, Gijs van Kuik, Bernard Bulder, Flemming Rasmussen, Bert Janssen, Tim Fischer, Ervin Bossanyi, Mike Courtney, Jochen Giebhardt, Rebecca Barthelmie, Ole Holmstrøm, Dorina Iuga, and Sharon Wokke. UpWind Design limits and solutions for very large wind turbines. EU Sixth Framework Programme, 2011. URL `http://www.upwind.eu/`.

[7] 4C Offshore Limited. 4C Offshore Wind Farm Database, 2016. URL `http://www.4coffshore.com/windfarms/`.

[8] Rabia Ferroukhi, Dolf Gielen, Ghislaine Kieffer, Michael Taylor, Divyam Nagpal, Arslan Khalid, Douglas Cook, Gus Schellekens, Hannes Reinisch, and Mark Turner. *REthinking Energy: Towards a new power system*. IRENA - International Renewable Energy Agency, 2014.

[9] By Sacha Alberici, Sil Boeve, Pieter Van Breevoort, Yvonne Deng, Sonja Förster, Ann Gardiner, Valentijn van Gastel, Katharina Grave, Heleen Groenenberg, David de Jager, Erik Klaassen, Willemijn Pouwels, Matthew Smith, Erika de Visser, Thomas Winkel, and Karlien Wouters. Subsidies and costs of EU energy Final report. Technical report, Ecofys, 2014.

[10] A Tesauro, PE Réthoré, and GC Larsen. State of the art of wind farm optimization. *Proceedings of EWEA 2012*, pages 1–11, 2012.

[11] Pedro Santos Valverde, Antonio J. N. A. Sarmento, and Marco Alves. Offshore Wind farm layout optimization - State of the art. *Journal of Ocean and Wind Energy*, 9(1):157–163, 2013.

[12] José Herbert-Acero, Oliver Probst, Pierre-Elouan Réthoré, Gunner Larsen, and Krystel Castillo-Villar. A Review of Methodological Approaches for the Design and Optimization of Wind Farms. *Energies*, 7(11):6930–7016, oct 2014. ISSN 1996-1073. doi: 10.3390/en7116930.

[13] Silvio Rodrigues, Carlos Restrepo, George Katsouris, Rodrigo Teixeira Pinto, Maryam Soleimanzadeh, Peter Bosman, and Pavol Bauer. A Multi-Objective Optimizaiton Framework for Offshore Wind Farm Layouts and Electric Infrastructures. *Energies*, 9(3):1–42, 2016. doi: 10.3390/en9030216.

[14] Edmund K Burke and Graham Kendall. *Search Methodologies*. Springer US, Boston, MA, second edition, 2013. ISBN 978-0-387-23460-1. doi: 10.1007/0-387-28356-0.

[15] The Interntaional Renewable Energy Agency (IRENA). Renewable Energy Technologies: Cost Analysis Series - Wind Power. Technical Report February, The Interntaional Renewable Energy Agency (IRENA), 2012.

[16] Fernando Borbón Guillén. *Development of a design tool for offshore wind farm layout optimization*. Master of Science Dissertation, Delft University of Technology, 2010.

[17] Christopher Neil Elkinton. *Offshore Wind Farm Layout Optimization*. Doctor of Philosophy Dissertation, University of Massachussetts Amherst, 2007.

[18] Souma Chowdhury, Jie Zhang, Achille Messac, and Luciano Castillo. Unrestricted wind farm layout optimization (UWFLO): Investigating key factors influencing the maximum power generation. *Renewable Energy*, 38(1):16–30, feb 2012. ISSN 09601481. doi: 10.1016/j.renene.2011.06.033.

[19] N.O Jensen. A Note on Wind Generator Interaction. Technical report, Risø DTU, 1983.

[20] I. Katic, J. Højstrup, and N.O. Jensen. A Simple Model for Cluster Efficiency. *Proceedings of European Wind Energy Conference and Exhibition 1986 Rome, Italy*, (October):407–410, 1986.

[21] Gunner C. Larsen. A Simple Wake Calculation Procedure. Technical report, Risø National Laboratory, 1988.

[22] Gunner C Larsen. A simple stationary semi-analytical wake model. Technical Report August, Risø National Laboratory, 2009.

[23] T. Ishihara, a. Yamaguchi, and Y. Fujino. Development of a new wake model based on a wind tunnel experiment. *Global Wind Power*, page 6, 2004.

[24] Sten Frandsen, Rebecca Barthelmie, and Sara Pryor. Analytical modelling of wind speed deficit in large offshore wind farms. *Wind Energy*, (January):39–53, 2006.

[25] Søren Ott, Jacob Berg, and Morten Nielsen. Linearised CFD Models for Wakes. Technical Report December, Risø National Laboratory, 2011.

[26] Søren Ott and Morten Nielsen. Developments of the offshore wind turbine wake model Fuga Wind Energy E Report 2014. Technical Report January, 2014.

[27] Pierre-Elouan Réthoré, Peter Fuglsang, Torben J Larsen, Thomas Buhl, and Gunner C Larsen. *TOPFARM wind farm optimization tool*. Riso DTU National Laboratory for Sustainable Energy, 2011. ISBN 9788755038844.

[28] Anshul Mittal. *Optimization of the Layout of Large Wind Farms Using a Genetic Algorithm*. Master of Science Dissertation, Case Western Reserve University, 2010.

[29] Bryony L. DuPont and Jonathan Cagan. An Extended Pattern Search Approach to Wind Farm Layout Optimization. *Journal of Mechanical Design*, 134(8): 081002, 2012. ISSN 10500472. doi: 10.1115/1.4006997.

[30] Grigorios Marmidis, Stavros Lazarou, and Eleftheria Pyrgioti. Optimal placement of wind turbines in a wind park using Monte Carlo simulation. *Renewable Energy*, 33(7):1455–1460, jul 2008. ISSN 09601481. doi: 10.1016/j.renene.2007.09.004.

[31] Christopher M. O'Reilly. *Offshore Wind Farm Siting Procedures Applied Offshore of Block Island, Rhode Island*. Master of Science Dissertation, University of Rhode Island, 2013.

[32] Patrik Fagerfjäll. *Optimizing wind farm layout - more bang for the buck using mixed integer linear programming*. Master of Science Dissertation, Chalmers University of Technology and Gothenburgh University, 2010.

[33] Rajai Aghabi Rivas. *Optimization of Offshore Wind Farm Layouts*. Master of Science Dissertation, Technical University of Denmark, 2007.

[34] G. Mosetti, C. Poloni, and B. Diviacco. Optimization of wind turbine positioning in large wind-farms by means of a genetic algorithm. *Journal of Wind Engineering and Industrial Aerodynamics*, 51(1):105–116, 1994.

[35] S.A. Grady, M.Y. Hussaini, and M.M. Abdullah. Placement of wind turbines using genetic algorithms. *Renewable Energy*, 30(2):259–270, 2005. ISSN 09601481. doi: 10.1016/j.renene.2004.05.007.

[36] S Tegen, E Lantz, M Hand, B Maples, A Smith, and P Schwabe. 2011 Cost of Wind Energy Review. Technical Report March, National Renewable Energy Laboratory, 2013.

[37] Prof John Foster, Liam Wagner, and Alexandra Bratanova. LCOE models: A comparison of the theoretical frameworks and key assumptions CSIRO Future Grid Flagship Cluster Project 3 : Economic and Investment Models For Future Grids. University of Queensland, 2014.

[38] Singiresu S. Rao. *Engineering Optimization: Theory and Practice*. 2009. ISBN 978-0-470-18352-6. doi: 10.1002/9780470549124.

[39] Christopher N. Elkinton, James F. Manwell, and Jon G. McGowan. Algorithms for offshore wind farm layout optimization. *Wind Engineering*, pages 67–83, 2008.

[40] Souma Chowdhury, Jie Zhang, Achille Messac, and Luciano Castillo. Optimizing the arrangement and the selection of turbines for wind farms subject to varying wind conditions. *Renewable Energy*, 52(315):273–282, apr 2013. ISSN 09601481. doi: 10.1016/j.renene.2012.10.017.

[41] Hou-Sheng Huang. Efficient hybrid distributed genetic algorithms for wind turbine positioning in large wind farms. *IEEE International Symposium on Industrial Electronics*, (ISIE):2196–2201, 2009.

[42] Carlos M. Ituarte-Villarreal and Jose F. Espiritu. Optimization of wind turbine placement using a viral based optimization algorithm. *Procedia Computer Science*, 6:469–474, jan 2011. ISSN 18770509. doi: 10.1016/j.procs.2011.08.087.

[43] Tales G Couto, Bruno Farias, Alberto Carlos G C Diniz, and Marcus Vinicius G De Morais. Optimization of Wind Farm Layout Using Genetic Algorithm. *10th World Congress on Structural and Multidisciplinary Optimization Orlando, USA*, pages 1–10, 2013.

[44] Peter Yun Zhang. *Topics in Wind Farm Layout Optimisation: Analytical Wake Models, Noise Propagation, and Energy Production*. Master of applied science dissertation, University of Toronto, 2013.

[45] Zong Woo Geem and Junhee Hong. Improved Formulation for the Optimization of Wind Turbine Placement in a Wind Farm. *Mathematical Problems in Engineering*, 2013(1):1–5, 2013. ISSN 1024-123X. doi: 10.1155/2013/481364.

[46] Ying Chen, Hua Li, Kai Jin, and Qing Song. Wind farm layout optimization using genetic algorithm with different hub height wind turbines. *Energy Conversion and Management*, 70:56–65, jun 2013. ISSN 01968904. doi: 10.1016/j.enconman.2013.02.007.

[47] Peter Y. Zhang, David A. Romero, J. Christopher Beck, and Cristina H. Amon. Solving wind farm layout optimization with mixed integer programs and constraint programs. *EURO Journal on Computational Optimization*, 2(3):195–219, jul 2014. ISSN 2192-4406. doi: 10.1007/s13675-014-0024-5.

[48] Rabia Shakoor, Mohammad Yusri, Abdur Raheem, and Nadia Rasheed. Wind farm layout optimization using area dimensions and definite point selection techniques. *Renewable Energy*, 88:154–163, 2016. ISSN 0960-1481. doi: 10.1016/j.renene.2015.11.021.

[49] Christopher N. Elkinton, James F. Manwell, and Jon G. McGowan. Offshore Wind Farm Layout Optimization (OWFL) Project: An Introduction. *Proceedings of Offshore Wind Conference & Exhibition Copenhagen 2005*, 2005.

[50] Christopher N. Elkinton, James F. Manwell, and Jon G. McGowan. Offshore wind farm layout optimization (OWFLO) project: an introduction. *Proceedings of Offshore Wind Conference & Exhibition Copenhagen 2005*, 2005.

[51] Christopher N. Elkinton, James F. Manwell, and Jon G. McGowan. Offshore Wind Farm Layout Optimization (OWFLO) Project: Preliminary Results. *44th AIAA Aerospace Sciences Meeting and Exhibit Reno, USA*, pages 1–9, jan 2006. doi: 10.2514/6.2006-998.

[52] Matthew A. Lackner and Christopher N. Elkinton. An Analytical Framework for Offshore Wind Farm Layout Optimization. *Wind Engineering*, 31(1):17–31, 2007.

[53] M Gaumond, PE Rethore, and A Bechmann. Benchmarking of Wind Turbine Wake Models in Large Offshore Windfarms. *Proceedings of the Science of Making Torque from Wind Conference Oldenburg, Germany*, 2012.

[54] R. J. Barthelmie, L. Folkerts, G. C. Larsen, S. T. Frandsen, K. Rados, S. C. Pryor, B. Lange, and G. Schepers. Comparison of Wake Model Simulations with Offshore Wind Turbine Wake Profiles Measured by Sodar. *Journal of Atmospheric and Oceanic Technology*, 23(7):888–901, jul 2006. ISSN 0739-0572. doi: 10.1175/JTECH1886.1.

[55] M. Kühn, W.A.A.M Bierbooms, G.J.W van Bussel, M.C. Ferguson, B. Göransson, T.T. Cockerill, R. Harrison, L.A. Harland, J.H. Vugts, and R. Wiecherink.

Opti-OWECS Final Report Vol. 0: Structural and Economic Optimisation of Bottom-Mounted Offshore Wind Energy Converters - Executive Summary. Technical Report January 1996, The European Commission: Non Nuclear Energy Programme, 1997.

[56] M Kühn, L.A. Harland, W.A.A.M Bierbooms, T.T. Cockerill, M.C. Ferguson, B. Göransson, G.J.W van Bussel, and J.H. Vugts. Opti-OWECS Final Report Vol. 1: Integrated Design Methodology for Offshore Wind Energy Conversion Systems. Technical Report January 1996, The European Commission: Non Nuclear Energy Programme, 1997.

[57] M Kühn, T.T. Cockerill, L.A. Harland, R. Harrison, C. Schöntag, G.J.W van Bussel, and J.H. Vugts. Opti-OWECS Final Report Vol. 2: Methods Assisting the Design of Offshore Wind Energy Conversion Systems. Technical Report January 1996, The European Commission: Non Nuclear Energy Programme, 1997.

[58] T.T. Cockerill, R. Harrison, M. Kühn, and G.J.W van Bussel. Opti-OWECS Final Report Vol. 3: Comparison of Cost of Offshore Wind Energy at European Sites. Technical Report January 1996, The European Commission: Non Nuclear Energy Programme, 1997.

[59] M.C. Ferguson and M. Kühn. Opti-OWECS Final Report Vol. 4: A Typical Design Solution for an OWECS. Technical report, The European Comission: Non Nuclear Energy Programme, 1998.

[60] T.T. Cockerill. Opti-OWECS Final Report Vol. 5 : User Guide OWECS Cost Model. Technical Report January 1996, The European Commission: Non Nuclear Energy Programme, 1997.

[61] SA Herman. DOWEC Cost Model-Implementation. Technical Report April, Energy Research Centre of the Netherlands (ECN), 2002.

[62] SD Wright, AL Rogers, JF Manwell, and Anthony Ellis. Transmission options for offshore wind farms in the United States. *Global Wind Power Conference and Exhibtion 2002 Paris, France*, pages 1–12, 2002.

[63] T Ackermann and NB Negra. Evaluation of Electrical Transmission Concepts for Large Offshore Windfarms. *Proceedings of Offshore Wind Conference & Exhibition Copenhagen 2005*, pages 1–10, 2005.

[64] Gunner C. Larsen, Helge Aa. Madsen, Niels Troldborg, Torben J. Larsen, Pierre-Elouan Réthoré, Peter Fuglsang, Søren Ott, Jakob Mann, Thomas Buhl, Morten Nielsen, Helen Markou, Jens N. Sørensen, Kurt S. Hansen, Robert Mikkelsen,

Valery Okulov, Wen Zhong Shen, Malcolm Heath, John King, Graeme McCann, Wolfgang Schlez, Ingemar Carlén, Hans Ganander, Emilio Migoya, Antonio Crespo, Angel Jiménez, J.L. Prieto, Amy Stidworthy, Davis Carruthers, Julian Hunt, Stephanie Gray, Dick Veldkamp, Ander S. Mouritzen, Leo Jensen, Thomas Krogh, Björn Schmidt, Kimon Argyriadis, and Peter Frohnböse. TOPFARM - Next Generation Desgin Tool for Optimisation of Wind Farm Topology and Operation. Technical Report February, Risø DTU, Roskilde, Denmark, 2011.

[65] Gunner Chr. Larsen and Pierre-Elouan Réthoré. TOPFARM - A Tool for Wind Farm Optimization. *Energy Procedia*, 35:317–324, jan 2013. ISSN 18766102. doi: 10.1016/j.egypro.2013.07.184.

[66] PE Réthoré and Peter Fuglsang. TopFarm: Multi-fidelity optimization of offshore wind farm. *Proceedings of the Twenty-first (2011) International Ocean and Polar Engineering Conference Maui, USA*, 2011.

[67] PE Réthoré, Peter Fuglsang, and GC Larsen. TOPFARM: Multi-fidelity optimization of wind farms. *Wind Energy*, 2013. doi: 10.1002/we.

[68] TJ Larsen, HA Madsen, GC Larsen, and KS Hansen. Validation of the dynamic wake meander model for loads and power production in the Egmond aan Zee wind farm. *Wind Energy*, (16):605–624, 2012. doi: 10.1002/we.

[69] Dirk Schoenmakers. *Optimization of the coupled grid connection of offshore wind farms*. Graduation project at Evelop Netherlands BV, Technical University of Eindhoven, 2008.

[70] S A Herman. Probabilistic Cost Model for Analysis of Offshore Wind Energy Costs and Potential. Technical Report May, Energy Research Centre of the Netherlands (ECN), 2002.

[71] The World Bank. Global Economic Monitor, 2016. URL `http://data.worldbank.org/data-catalog/global-economic-monitor`.

[72] Alireza Emami and Pirooz Noghreh. New approach on optimization in placement of wind turbines within wind farm by genetic algorithms. *Renewable Energy*, 35 (7):1559–1564, jul 2010. ISSN 09601481. doi: 10.1016/j.renene.2009.11.026.

[73] B.P Rašuo and A.Č Bengin. Optimization of wind farm layout. *FME Transactions*, pages 107–114, 2010.

[74] Andrew Kusiak and Zhe Song. Design of wind farm layout for maximum wind energy capture. *Renewable Energy*, 35(3):685–694, mar 2010. ISSN 09601481. doi: 10.1016/j.renene.2009.08.019.

[75] Rabia Shakoor, Mohammad Yusri Hassan, Abdur Raheem, Nadia Rasheed, and Mohamad Na. Wind Farm Layout Optimization by Using Definite Point Selection and Genetic Algorithm. *IEEE International Conference on Power & Energy (PECON) 2014 Kuching, Sarawak, Malaysia*, pages 191–195, 2014.

[76] Rabia Shakoor, Mohammad Yusri Hassan, Abdur Raheem, and Nadia Rasheed. The Modelling of Wind Farm Layout Optimization for the Reduction of Wake Losses. *Indian Journal of Science and Technology*, 8(August), 2015.

[77] K. Chen, M. X. Song, Z. Y. He, and X. Zhang. Wind turbine positioning optimization of wind farm using greedy algorithm. *Journal of Renewable and Sustainable Energy*, 5(2):023128, 2013. ISSN 19417012. doi: 10.1063/1.4800194.

[78] U. Aytun Ozturk and Bryan A. Norman. Heuristic methods for wind energy conversion system positioning. *Electric Power Systems Research*, 70(3):179–185, aug 2004. ISSN 03787796. doi: 10.1016/j.epsr.2003.12.006.

[79] Bryony L DuPont and Jonathan Cagan. Multi-Stage Optimization of Wind Farms with Limiting Factors. *ASME Internation Design Engineering Technical Conferences and Computers and Information in Engineering Conference Portland, USA*, pages 1–12, 2013. doi: 10.1115/DETC2013-12503.

[80] Bryony L DuPont and Jonathan Cagan. Multi-Stage Optimization of Wind Farms with Limiting Factors. *ASME Internation Design Engineering Technical Conferences and Computers and Information in Engineering Conference Portland, USA*, pages 1–12, 2013. doi: 10.1115/DETC2013-12503.

[81] Bistra N. Dilkina, Jayant R. Kalagnanam, and Elena A. Novakovskaia. *Method for Designing the Layout of Turbines in a Windfarm*. US Patent US 2011/0208483 A1, 2010.

[82] Rosalind Archer, Gary Nates, Stuart Donovan, and Hamish Waterer. Wind Turbine Interference in a Wind Farm Layout Optimization Mixed Integer Linear Programming Model. *Wind Engineering*, 35(2):165–175, apr 2011. ISSN 0309-524X. doi: 10.1260/0309-524X.35.2.165.

[83] Maurice Clerc. *Particle Swarm Optimization*. Wiley-ISTE, 2006. ISBN 9781905209040.

[84] Souma Chowdhury, Weiyang Tong, Achille Messac, and Jie Zhang. A mixed-discrete Particle Swarm Optimization algorithm with explicit diversity-preservation. *Structural and Multidisciplinary Optimization*, 47(3):367–388, dec 2012. ISSN 1615-147X. doi: 10.1007/s00158-012-0851-z.

[85] Yunus Eroglu and Serap Ulusam Seçkiner. Design of wind farm layout using ant colony algorithm. *Renewable Energy*, 44:53–62, 2012. ISSN 09601481. doi: 10.1016/j.renene.2011.12.013.

[86] Ju Feng and Wen Zhong Shen. Solving the wind farm layout optimization problem using random search algorithm. *Renewable Energy*, 78:182–192, 2015. ISSN 0960-1481. doi: 10.1016/j.renene.2015.01.005.

[87] Martin Bilbao and Enrique Alba. Simulated Annealing for Optimization of Wind Farm Annual Profit. *2009 2nd International Symposium on Logistics and Industrial Informatics (LINDI), Lintz, Austria*, (2):1–5, sep 2009. doi: 10.1109/LINDI.2009.5258656.

[88] Rajai Aghabi Rivas, Jens Clausen, Kurt S. Hansen, and Leo E. Jensen. Solving the Turbine Positioning Problem for Large Offshore Wind Farms by Simulated Annealing. *Wind Engineering*, 33(3):287–297, may 2009. ISSN 0309-524X. doi: 10.1260/0309-524X.33.3.287.

[89] AWS Truepower. OpenWind Theoretical Basis and Validation. Technical Report April, AWSTruepower LLC, Albany, New York, 2010.

[90] Meagan Krawczyk, Nick Robinson, and Sara Tyler. Testing the Effect of Different Optimization Parameters on Layout Design Using openWind: A GIS Based Wind-Modeling Platform, 2011.

[91] Beatriz Pérez, Roberto Mínguez, and Raúl Guanche. Offshore wind farm layout optimization using mathematical programming techniques. *Renewable Energy*, 53:389–399, may 2013. ISSN 09601481. doi: 10.1016/j.renene.2012.12.007.

[92] Sanjay Saigal. *Optimization for Dummies Gurobi Special Edition*. John Wiley & Sons, Hoboken, New Jersey, 2012. ISBN 978-1-118-17672-6.

[93] JT Linderoth and A Lodi. MILP software. *Wiley Encyclopedia of Operations Research*, pages 1–17, 2011. doi: 10.1002/9780470400531.

[94] Johann Dréo and Caner Candan. Different classifications of metaheuristics. Wikipedia, 2011. URL `https://commons.wikimedia.org/wiki/File:Metaheuristics{_}classification.svg`.

[95] Christian Blum and Andrea Roli. Metaheuristics in Combinatorial Optimization: Overview and Conceptual Comparison. *ACM Computing Surveys*, 35(3):268–308, 2003. ISSN 0360-0300. doi: 10.1145/937503.937505.

[96] Zahra Beheshti and Siti Mariyam Hj. Shamsuddin. A review of population-based meta-heuristic algorithm. *International Journal of Advances in Soft Computing and its Application*, 5(1):1–35, 2013.

[97] David Beasley, DR Bull, and RR Martin. An overview of genetic algorithms: Part 1. Fundamentals. *University Computing*, 15:1–16, 1993.

[98] R. Baños, F. Manzano-Agugliaro, F.G. Montoya, C. Gil, a. Alcayde, and J. Gómez. Optimization methods applied to renewable and sustainable energy: A review. *Renewable and Sustainable Energy Reviews*, 15(4):1753–1766, may 2011. ISSN 13640321. doi: 10.1016/j.rser.2010.12.008.

[99] NOREL Group. Nautical and Offshore Renewable Energy Liaison Group (NOREL) Action Points from the 27th NOREL held on 11 July 2013. Technical Report July, The Crown Estate, 2013.

[100] A Neubert, A Shah, and W Schlez. Maximum yield from symmetrical wind farm layouts. *Proceedings of DEWEK*, pages 3–6, 2010.

[101] Graeme Proctor. Offshore Wind Farm Layout Rules. Private Correspondance, 2014.

[102] NOREL Group. Nautical and Offshore Renewable Energy Liaison Group (NOREL) Minutes and Action Points from the 30th NOREL held on 17 December at DfT, Great Minister House, London SW1P 4DR. (December):1–7, 2014.

[103] John H Holland. *Adaptation In Natural And Artificial Systems. [Electronic Resource] : An Introductory Analysis With Applications To Biology, Control, And Artificial Intelligence*. MIT Press, Cambridge, Mass., second edition, 1992. ISBN 0262082136.

[104] Randy L Haupt and Sue Ellen Haupt. *Practical Genetic Algorithms*. Wiley-Interscience Publication, second edition, 2004. ISBN 9786468600.

[105] Charles Darwin. *The Origin of Species*. P.F. Collier & Sons, New York, NY, sixth edition, 1909. ISBN 978-0674637528.

[106] Kenneth A. De Jong. *Evolutionary Computation*. MIT Press, Cambridge, Mass., 2006. ISBN 0262041944.

[107] Melanie Mitchell. *An Introduction to Genetic Algorithms*. The MIT Press, Cambridge, Mass., first edition, 1999.

[108] Ed Keedwell. NATCOR Evolutionary Algorithm Tutorial. Lecture - NATCOR: Heuristcs and Approximation Algorithms, 2014. URL `http://www.natcor.ac.uk`.

[109] William M Spears and Kenneth A De Jong. On the Virtues of Parameterized Uniform Crossover. Technical report, Naval Research Lab, Washington DC, 1995.

[110] KA De Jong and WM Spears. An analysis of the interacting roles of population size and crossover in genetic algorithms. *Parallel problem solving from nature*, 1991.

[111] M. Srinivas and L.M. Patnaik. Genetic algorithms: a survey. *Computer*, 27(6): 17–26, jun 1994. ISSN 0018-9162. doi: 10.1109/2.294849.

[112] S.N. Sivanandam and S.N. Deepa. *Introduction to Genetic Algorithms*. Springer-Verlag, Berlin, 2008. ISBN 9783540731894.

[113] Robert Hinterding, Z Michalewicz, and A E Eiben. Adaptation in evolutionary computation: A survey. *Transations on Evolutionary Computation*, 3(2):124–141, 1997. ISSN 0780339495. doi: Doi10.1109/Icec.1997.592270.

[114] D. Thierens. Adaptive mutation rate control schemes in genetic algorithms. *Proceedings of the 2002 Congress on Evolutionary Computation. CEC'02 Washington D.C., USA*, 1:2–7, 2002. doi: 10.1109/CEC.2002.1007058.

[115] J Kennedy and R Eberhart. Particle swarm optimization. *IEEE International Conference on Neural Networks, 1995 Perth, Australia*, 4:1942–1948 vol.4, 1995. ISSN 19353812. doi: 10.1109/ICNN.1995.488968.

[116] James Kennedy. Small worlds and mega-minds: Effects of neighborhood topology on particle swarm performance. *Proceedings of the 1999 Congress on Evolutionary Computation (CEC) Washington D.C., USA*, 3:1931–1938, 1999. doi: 10.1109/CEC.1999.785509.

[117] S. Burak Akat and Veysel Gazi. Particle swarm optimization with dynamic neighborhood topology: Three neighborhood strategies and preliminary results. *2008 IEEE Swarm Intelligence Symposium St. Louis, USA*, pages 1–8, 2008. doi: 10.1109/SIS.2008.4668298.

[118] M Clerc. Think locally act locally-a framework for adaptive particle swarm optimizers. *IEEE Journal of Evolutionary Computation*, 29:1951–1957, 2002.

[119] M. Clerc and J. Kennedy. The particle swarm - explosion, stability, and convergence in a multidimensional complex space. *IEEE Transactions on Evolutionary Computation*, 6(1):58–73, 2002. ISSN 1089-778X. doi: 10.1109/4235.985692.

[120] J. Kennedy and R.C. Eberhart. A discrete binary version of the particle swarm algorithm. *IEEE International Conference on Systems, Man, and Cybernetics. Computational Cybernetics and Simulation 1997 Orlando, Florida*, 5:4–8, 1997. ISSN 1062-922X. doi: 10.1109/ICSMC.1997.637339.

[121] E. García-Gonzalo and J. L. Fernández-Martínez. A Brief Historical Review of Particle Swarm Optimization (PSO). *Journal of Bioinformatics and Intelligent Control*, 1(1):3–16, 2012. ISSN 23267496. doi: 10.1166/jbic.2012.1002.

[122] Seyedali Mirjalili and Andrew Lewis. S-shaped versus V-shaped transfer functions for binary Particle Swarm Optimization. *Swarm and Evolutionary Computation*, 9:1–14, 2013. ISSN 2210-6502. doi: 10.1016/j.swevo.2012.09.002.

[123] M. Lindahl, N.C. Fink Bagger, T. Stidsen, S. Frost Ahrenfeldt, and I. Arana. OptiArray from DONG Energy. *Proceedings of the 12th Wind Integration Workshop (International Workshop on Large-Scale Integration of Wind Power into Power Systems as well as on Transmission Networks for Offshore Wind Power Plants) London, UK*, 2013.

[124] Harald G. Svendsen. Planning Tool for Clustering and Optimised Grid Connection of Offshore Wind Farms. *Energy Procedia*, 35:297–306, jan 2013. ISSN 18766102. doi: 10.1016/j.egypro.2013.07.182.

[125] Anita Amberg, Wolfgang Domschke, Stefan Vo, and D Braunschweig. Capacitated minimum spanning trees: Algorithms using intelligent search. *Combinatorial Optimization: Theory and Practice*, 1996.

[126] S Dutta and T Overbye. A clustering based wind farm collector system cable layout design. *2011 IEEE Power and Energy Conference at Illinois (PECI) Urbana-Champaign, USA*, pages 4–9, 2011.

[127] FM González-Longatt and Peter Wall. Optimal electric network design for a large offshore wind farm based on a modified genetic algorithm approach. *IEEE Systems Journal*, 6(1):164–172, 2012.

[128] Adelaide Cerveira and Eduardo J Solteiro Pires. Optimisation Design in Wind Farm Distribution Network. *Proceedings of International Joint Conference SOCO'13-CISIS'13-ICEUTE'13, Advances in Intelligent Systems and Computing Salamanca, Spain*, 239, 2014. doi: 10.1007/978-3-319-01854-6.

[129] DD Li, Chao He, and Yang Fu. Optimization of internal electric connection system of large offshore wind farm with hybrid genetic and immune algorithm. *Proceedings of Third International Conference on Electric Utility Deregulation and Restructuring and Power Technologies (DRPT) 2008 Nanjing, China*, pages 2476–2481, 2008.

[130] M Zhao, Z Chen, and F Blaabjerg. Application of genetic algorithm in electrical system optimization for offshore wind farms. *Proceedings of Third International Conference on Electric Utility Deregulation and Restructuring and Power Technologies (DRPT) 2008 Nanjing, China*, (April):7–12, 2008.

[131] M Zhao, Z Chen, and F Blaabjerg. Optimisation of electrical system for offshore wind farms via genetic algorithm. *IET Renewable Power Generation*, 3(2008): 205–216, 2009. doi: 10.1049/iet-rpg.

[132] Sara Lumbreras and Andres Ramos. Optimal design of the electrical layout of an offshore wind farm applying decomposition strategies. *IEEE Transactions on Power Systems*, 28(2):1434–1441, 2013.

[133] J Bauer and J Lysgaard. The Offshore Wind Farm Array Cable Layout Problem - A Planar Open Vehicle Routing Problem. *Journal of the Operational Research Society*, 66(3):1–16, 2015.

[134] Sudipta Dutta and Thomas Overbye. Design Considering Total Trenching Length. *IEEE Transactions on Sustainable Energy*, 3(3):339–348, 2012.

[135] Sudipta Dutta and Thomas Overbye. A graph-theoretic approach for addressing trenching constraints in wind farm collector system design. *2013 IEEE Power and Energy Conference at Illinois (PECI) Urbana-Champaign, USA*, pages 48–52, feb 2013. doi: 10.1109/PECI.2013.6506033.

[136] T Burton, N Jenkins, D Sharpe, and E Bossanyi. *Wind energy handbook*. John Wiley & Sons, Ltd, second edition, 2011. ISBN 0471489972.

[137] Marcos Negreiros and Augusto Palhano. The capacitated centred clustering problem. *Computers & Operations Research*, 33(6):1639–1663, jun 2006. ISSN 03050548. doi: 10.1016/j.cor.2004.11.011.

[138] S Geetha, G Poonthalir, and PT Vanathi. Improved K-Means Algorithm for Capacitated Clustering Problem. *International INFOCOMP Journal of Computer Science*, 2009.

[139] Antonio Augusto Chaves and Luiz Antonio Nogueira Lorena. Clustering search algorithm for the capacitated centered clustering problem. *Computers & Operations Research*, 37(3):552–558, mar 2010. ISSN 03050548. doi: 10.1016/j.cor.2008.09.011.

[140] David Arthur and Sergei Vassilvitskii. k-means++: The Advantages of Careful Seeding. *Proceedings of the 18th Annual ACM-SIAM symposium on Discrete Algorithms New Orleans, USA*, 8:1–11, 2007.

[141] J MacQueen. Some methods for classification and analysis of multivariate observations. *Proceedings of the Fifth Berkeley Symposium on Mathematical Statistics and Probability Berekeley, USA*, 233(233):281–297, 1967.

[142] SK Ghosh. *Visibility algorithms in the plane*. Cambridge University Press, Cambridge, first edition, 2007. ISBN 9780521875745.

[143] Mark de Berg, Otfried Cheong, Marc van Kreveld, and Marc Overmars. *Computational Geometry*. Springer-Verlag, Berlin, Heidelberg, third edition, 2008. ISBN 9783540779735.

[144] Gene Eu Jan, Wei Chun Tsai, Chi-Chia Sun, and Bor-Shing Lin. A Delaunay triangulation-based shortest path algorithm with O(n log n) time in the Euclidean plane. *2012 IEEE/ASME International Conference on Advanced Intelligent Mechatronics (AIM) Kaohsiung, Taiwan*, pages 186–189, jul 2012. doi: 10.1109/AIM.2012.6266051.

[145] Gene Eu Jan, Chi-chia Sun, Wei Chun Tsai, and Ting-hsiang Lin. An O (n log n) Shortest Path Algorithm Based on Delaunay Triangulation. *IEEE/ASME Transactions on Mechatronics*, 19(2):660–666, 2014.

[146] Gurobi Optimization Inc. Gurobi Optimizer Reference Manual, 2015. URL `http://www.gurobi.com`.

[147] L Gouveia. A comparison of directed formulations for the capacitated minimal spanning tree problem. *Telecommunication Systems*, 1:51–76, 1993.

[148] Luis Gouveia. A 2n Constraint Formulation for the Capacitated Minimal Spanning Tree Problem. *Operations Research*, 43(1):130–141, 1995.

[149] Bezalel Gavish. Formulations and Algorithms for the Capacitated Minimal Directed Tree Problem. *Journal of the ACM*, 30(1):118–132, jan 1983. ISSN 00045411. doi: 10.1145/322358.322367.

[150] Eduardo Uchoa, Ricardo Fukasawa, and Jens Lysgaard. Robust branch-cut-and-price for the capacitated minimum spanning tree problem over a large extended formulation. *Mathematical Programming*, pages 1–30, 2006.

[151] G Quinonez-Varela. Electrical collector system options for large offshore wind farms. *IET Renewable Power Generation*, pages 107–114, 2007. doi: 10.1049/iet-rpg.

[152] N. Barberis Negra, J. Todorovic, and T. Ackermann. Loss evaluation of HVAC and HVDC transmission solutions for large offshore wind farms. *Electric Power Systems Research*, 76(11):916–927, jul 2006. ISSN 03787796. doi: 10.1016/j.epsr.2005.11.004.

[153] Nicola Barberis Negra, Ole Holmstrøm, Birgitte Bak-jensen, and Poul Sorensen. Reliability Assessment. *IEEE Transactions on Energy Conversion*, 22(1):159–166, 2007.

[154] Ambra Sannino, Henrik Breder, and Erik Koldby Nielsen. Reliability of Collection Grids for Large Offshore Wind Parks. *2006 International Conference on Probabilistic Methods Applied to Power Systems Stockholm, Sweden*, pages 1–6, 2006. doi: 10.1109/PMAPS.2006.360415.

[155] A Saltelli, K Chan, and E M Scott. *Sensitivity Analysis*. Wiley, 2009. ISBN 0470743824.

[156] J.F. Manwell, J.G. McGowan, and A.L. Rogers. *Wind Energy Explained*. Wiley & Sons, Chichester, second edition, 2009. ISBN 9780470015001.

[157] R J Barthelmie, K Hansen, S T Frandsen, O Rathmann, J G Schepers, W Schlez, J Phillips, K Rados, A Zervos, E S Politis, and P K Chaviaropoulos. Modelling and measuring flow and wind turbine wakes in large wind farms offshore. *Wind Energy*, 12(5):431–444, jul 2009. ISSN 10954244. doi: 10.1002/we.348.

[158] DNV GL - Energy. WindFarmer Theory Manual. GL Garrad Hassan, 2014. URL `https://www.dnvgl.com/services/windfarmer-3766`.

[159] Michael C Brower, Bruce H Bailey, Philippe Beaucage, Daniel W. Bernadett, James Doane, Matthew J Eberhard, Kurt V Elsholz, Matthew V Filippelli, Erik Hale, Michael J Maruks, Mark A Taylor, and Jeremy C Tensen. *Wind Resource Assessment*. John Wiley & Sons, Hoboken, New Jersey, 2012. ISBN 9781118022320.

[160] S Lee, M Churchfield, and P Moriarty. Atmospheric and Wake Turbulence Impacts on Wind Turbine Fatigue Loading: Preprint. *Proceedings of AIAA Aerospace Sciences Meeting Nashville, USA*, 2011.

[161] Kenneth Thomsen and Poul Sørensen. Fatigue loads for wind turbines operating in wakes. *Journal of Wind Engineering and Industrial Aerodynamics*, 80(1-2): 121–136, mar 1999. ISSN 01676105. doi: 10.1016/S0167-6105(98)00194-9.

[162] L.J. Vermeer, J.N. Sørensen, and A. Crespo. Wind turbine wake aerodynamics. *Progress in Aerospace Sciences*, 39(6-7):467–510, aug 2003. ISSN 03760421. doi: 10.1016/S0376-0421(03)00078-2.

[163] B Sanderse. Aerodynamics of wind turbine wakes. Technical report, Energy Research Centre of the Netherlands, 2009.

[164] Charlotte Hasager, Leif Rasmussen, Alfredo Peña, Leo Jensen, and Pierre-Elouan Réthoré. Wind Farm Wake: The Horns Rev Photo Case. *Energies*, 6(2):696–716, 2013. ISSN 1996-1073. doi: 10.3390/en6020696.

[165] Douwe J Renkema. *Validation of wind turbine wake models*. Master of Science Dissertation, TU Delft, 2007.

[166] Philippe Beaucage and Nick Robinson. Overview of six commerical and research wake models for large offshore wind farms. *Proceedings of EWEA 2012*, 2012.

[167] Giorgio Crasto and Francesco Castellani. Wakes Calculation in a Offshore Wind Farm. *Wind Engineering*, 37(3):269–280, jun 2013. ISSN 0309-524X. doi: 10.1260/0309-524X.37.3.269.

[168] M H M Kloosterman. *Development of the Near Wake behind a Horizontal Axis Wind Turbine: Including the development of a Free Wake Lifting Line Code*. Master of Science Dissertation, TU Delft, 2009.

[169] A Crespo. Turbulence characteristics in wind-turbine wakes. *Journal of Wind Engineering and Industrial Aerodynamics*, 61:71–85, 1996.

[170] JF Ainslie. Calculating the flowfield in the wake of wind turbines. *Journal of Wind Engineering and Industrial Aerodynamics*, 27:213–224, 1988.

[171] DNV GL - Energy. WindFarmer Validation Report. GL Garrad Hassan, 2014. URL `https://www.dnvgl.com/services/windfarmer-3766`.

[172] Morten Lybeech Thøgersen. WindPRO / PARK. EMD International A/S, 2005. URL `www.emd.dk`.

[173] Tuhfe Göçmen, Paul Van Der Laan, Pierre-elouan Réthoré, Alfredo Peña Diaz, Gunner Chr Larsen, and Søren Ott. Wind turbine wake models developed at the technical university of Denmark: A review. *Renewable and Sustainable Energy Reviews*, 60:752–769, 2016. ISSN 1364-0321. doi: 10.1016/j.rser.2016.01.113.

[174] David Luna Molina. *Modeling of Wakes Behind Wind Turbines*. Master of Science Dissertation, Technical University of Denmark, 2008.

[175] J.A.J. Jansen. *Development of a Wind Farm Power Forecast Model*. Master of Science Dissertation, TU Delft, 2012.

[176] Weiyang Tong, Souma Chowdhury, Jie Zhang, and Achille Messac. Impact of Different Wake Models On the Estimation of Wind Farm Power Generation. *Proceedings of AIAA Aviation Technology, Integration, and Operations (ATIO) Indianapolis, USA*, 14, 2012.

[177] Mike Anderson. Simplified Solution to the Eddy-Viscosity Wake Model. Technical report, Renewable Energy Systems Ltd (RES), 2009.

[178] J Crank and P Nicolson. A practical method for numerical evaluation of solutions of partial differential equations of the heat-conduction type. *Mathematical Proceedings of the Cambridge Philosophical Society*, 43(01):50–67, 1947. ISSN 1019-7168. doi: 10.1007/BF02127704.

[179] A Crespo, J Hernandez, and S Frandsen. Survey of modelling methods for wind turbine wakes and wind farms. *Wind Energy*, 24:1–24, 1999.

[180] Alexandros Makridis. *Modelling of wind turbine wakes in complex terrain using Computational Fluid Dynamics*. Doctor of Philosophy Dissertation, The University of Edinburgh, 2010.

[181] J G Schepers. ENDOW: Validation and improvement of ECN's wake model. Technical Report March, ECN, 2003.

[182] Souma Chowdhury, Achille Messac, Jie Zhang, Luciano Castillo, and Jose Lebron. Optimizing the Unrestricted Placement of Turbines of Differing Rotor Diameters in a Wind Farm for Maximum Power Gneration. *Proceedings of the ASME 2010 International Design Engineering Technical Conferences & Computers and Information in Engineering Conference IETC/CIE 2010 Montreal, Canada*, pages 1–16, 2010.

[183] Wolfgang Schlez and Anja Neubert. New developments in large wind farm modelling. *Proceedings of European Wind Energy Conference 2009 Warsaw, Poland*, 2009.

[184] MC Brower and NM Robinson. The openWind deep-array wake model: development and validation. AWSTruepower, 2009. URL `http://www.awstruepower.com`.

[185] J.R. Garratt. *The atmospheric boundary layer*. Cambridge University Press, Cambridge, 1992.

[186] M Gaumond, PE Réthoré, S Ott, A Bechmann, and K.S. Hansen. Evaluation of the wind direction uncertainty and its impact on wake modeling at the Horns Rev offshore wind farm. *Wind Energy*, 2013. doi: 10.1002/we.

[187] RJ Barthelmie, ST Frandsen, MN Nielsen, SC Pryor, PE Rethore, and HE Jørgensen. Modelling and measurements of power losses and turbulence intensity in wind turbine wakes at Middelgrunden offshore wind farm. *Wind Energy*, 10 (July):517–528, 2007. doi: 10.1002/we.238.

[188] RJ Barthelmie and LE Jensen. Evaluation of wind farm efficiency and wind turbine wakes at the Nysted offshore wind farm. *Wind Energy*, (June):573–586, 2010. doi: 10.1002/we.

[189] R.J. Barthelmie and S.C. Pryor. An overview of data for wake model evaluation in the Virtual Wakes Laboratory. *Applied Energy*, 104:834–844, apr 2013. ISSN 03062619. doi: 10.1016/j.apenergy.2012.12.013.

[190] Middelgrundens Vindmøllelaug I/S. Middelgrundens Vindmøllelaug Regnskab og budget. Technical report, Middelgrundens Vindmøllelaug I/S, 2016.

[191] Hans E Jørgensen, Sten Frandsen, and Per Vølund. Wake Effects on Middelgrund Windfarm. Technical Report July, Risø National Laboratory, jul 2003.

[192] D. Medici and P. H. Alfredsson. Measurements behind model wind turbines: further evidence of wake meandering. *Wind Energy*, 11(2):211–217, 2008. ISSN 10954244. doi: 10.1002/we.247.

[193] R J Barthelmie, S T Frandsen, O Rathmann, K Hansen, E S Politis, J Prospathopoulos, J G Schepers, K Rados, Author R J Barthelmie, and E Politis. Flow and wakes in large wind farms : Final report for UpWind WP8 Risø-R-Report. Technical Report February, Risø DTU - UPWIND Project, 2011.

[194] RJ Barthelmie and SC Pryor. Wake Model Evaluation Metrics and The Virtual Wakes Laboratory. *Proceedings of ICOWES 2013 Copenhagen*, pages 173–181, 2013.

[195] T Sorensen and P Nielsen. Recalibrating Wind Turbine Wake Model Parameters – Validating the Wake Model Performance for Large Offshore Wind Farms. *In: European Wind Energy Conference and Exhibition, EWEA, Athens, Greece*, 2006.

[196] IEC. *IEC 60228: Conductors of insulated cables*. International Electrotechnical Commission, Geneva, Switzerland, third edition, 2006.

[197] IEC. *IEC 60287: Electric Cables - Calculation of the current rating - Part 1-1: Current rating equations (100% load factor) and calculation of losses - General*. International Electrotechnical Commission, Geneva, Switzerland, second edition, 2006.

[198] A. Gustafsson, J. Karlstrand, G. Clasen, R. Donaghy, R. Gruntjes, A. Jensen, S. Krüger Olsen, G. Miramonti, T. Nakajima, H. Orton, J. Prieto, and C. Rémy. Technical Brochure 490: Recommendations for Testing of Long AC Submarine Cables with Extruded Insulation for System Voltage above 30 (36) to 500 (550) kV. Technical report, CIGRE, 2012.

[199] Stefan Fassbinder. Application Note Efficiency and Loss Evaluation of Large Power Transformers. European Copper Instititue, 2013. URL `http://www.leonardo-energy.org`.

[200] Stefan Lundberg. Performance comparison of wind park configurations. Technical report, Chalmers University of Technology, 2003.

[201] Raymond Van Schevensteen, Technology Head, Distribution Transformers, Jan Declercq, and C T O Power Systems. The "Life starts at 36" -project : development of wind turbine generator transformers above 36kV. *Proceedings of European Wind Energy Conference & Exhibition 2013 Vienna, Austria*, pages 1–9, 2013.

[202] Brad Rabone and Colin Henvey. JDR Cables. Private Correspondence, 2014.

[203] María Isabel Blanco. The economics of wind energy. *Renewable and Sustainable Energy Reviews*, 13(6-7):1372–1382, aug 2009. ISSN 13640321. doi: 10.1016/j.rser.2008.09.004.

[204] Shiu Hui, Mark Lawson, and Keith Moss. Offshore Wind Industry Cost Assumptions. Private Correspondance, 2014.

[205] L Fingersh, M Hand, and A Laxson. Wind Turbine Design Cost and Scaling Model. Technical Report December, National Renewable Energy Laboratory (NREL), 2006.

[206] European Wind Energy Association. *Wind Energy - The Facts: A Guide to the Technology, Economics, and Future of Wind Power*. Taylor & Francis, 2012. ISBN 9781849773782. doi: 10.1093/isle/ist137.

[207] Erich Hau. *Wind Turbines*. Springer Berlin Heidelberg, Berlin, Heidelberg, 2013. ISBN 978-3-642-27150-2. doi: 10.1007/978-3-642-27151-9.

[208] M. Dicorato, G. Forte, M. Pisani, and M. Trovato. Guidelines for assessment of investment cost for offshore wind generation. *Renewable Energy*, 36(8):2043–2051, aug 2011. ISSN 09601481. doi: 10.1016/j.renene.2011.01.003.

[209] M Junginger and A Faaij. Cost reduction prospects for the offshore wind energy sector. *Proceedings of European Wind Energy Conference & Exhibition Madrid, Spain*, (0):1–12, 2003.

[210] Christopher Mone, Tyler Stehly, Ben Maples, and Edward Settle. 2014 Cost of Wind Energy Review. Technical Report February, National Renewable Energy Laboratory, 2015.

[211] Mark J Kaiser and Brian F Snyder. *Offshore Wind Energy Cost Modeling*. Green Energy and Technology. Springer London, London, 2012. ISBN 978-1-4471-2487-0. doi: 10.1007/978-1-4471-2488-7.

[212] Mark J. Kaiser and Brian Snyder. Offshore wind capital cost estimation in the U.S. Outer Continental ShelfâĂŤA reference class approach. *Marine Policy*, 36 (5):1112–1122, sep 2012. ISSN 0308597X. doi: 10.1016/j.marpol.2012.02.001.

[213] Mark J. Kaiser and Brian F. Snyder. Modeling offshore wind installation costs on the U.S. Outer Continental Shelf. *Renewable Energy*, 50:676–691, 2013. ISSN 09601481. doi: 10.1016/j.renene.2012.07.042.

[214] Douglas Westwood. OWF and WTIV Study. Technical Report May, Douglas Westwood, 2013.

[215] E ter Horst. Principle Power: GL Garrad Hassan Study. Technical report, GL Garrad Hassan, Energy Technologies Insititute, 2011.

[216] MB Zaaijer. Comparison of monopile, tripod, suction bucket and gravity base design for a 6 MW turbine. *OWEMES, ENEA, Naples*, (April), 2003.

[217] Sam Weller, Lars Johanning, Lander Victor, Madjid Karimirad, Jason Heath, John Eddy, Richard Jensen, Jesse Roberts, and Stephen Banfield. DTOcean Tool Deliverable 4.5: Mooring and Foundation Module Framework for DTOcean Tool. Technical report, EU FP7: DTOcean, The University of Exeter, DEME Blue Energy, MARINTEK, Sandia National Laboratories, Tecnalia, University College Cork, WavEC - Offshore Renewables, Tension Technology International Ltd, University of Edinburgh, Aalborg University, 2015.

[218] Casey M. Fontana, Sanjay R. Arwade, Don J. Degroot, Melissa Landon, Andrew T. Myers, and Charles Aubeny. Efficient Multiline Anchor Systems for Floating Offshore Wind. *Proceedings of the ASME 2016 35th International Conference on Ocean, Offshore and Arctic Engineering (OMAE 2016) Busan, South Korea*, pages 1–7, 2016.

[219] EWEA. Wind in our Sails. The European Wind Energy Association, 2011. URL `http://www.ewea.org/fileadmin/files/library/publications/reports/Offshore{_}Report.pdf`.

[220] M B Zaaijer. Properties of Offshore Support Structures for Large Scale Wind Turbines. *Offshore Wind Energy Special Topic Conference Brussels, Belgium*, (December):2–5, 2001.

[221] Bloomberg New Energy Finance. Offshore Wind: Foundations for Growth. Technical report, Rabobank International, 2011.

[222] Sophia von Waldow, Michael Wilshire, Justin Wu, and Fraser Johnston. Offshore Wind Supply Chain: Diving Into Deep Sea Foundations. Technical report, Bloomberg New Energy Finance, 2013.

[223] EDF Energy R&D UK Centre. "Gravity Based Foundations (GBS) EPCI" - Part IV Technical Memorandum. Technical report, EDF Energy R&D UK Centre, 2013.

[224] M Seidel. 6MW Turbines with 150m+ Rotor Diameter - What is the Impact on Substructures? *Proceedings of DEWEK 2012 Bremen, Germany*, pages 1–4, 2012.

[225] Nick Rey and ORJIP Working Group. Offshore Renewables Joint Industry Programme - Strategic Joint Industry Project No.3: Underwater Noise Mitigation technologies for piled foundations in deeper water. Technical Report 3, The Crown Estate, nov 2012.

[226] Max Verhaegh. *Modelling the manufacturing and installation costs of offshore wind farm substructures for a micro siting model.* Master of Science Dissertation, TU Delft, 2014.

[227] Mark J. Kaiser and Brian F. Snyder. Offshore wind structure weight algorithms - technical note. *Ships and Offshore Structures*, (August):1–6, feb 2014. ISSN 1744-5302. doi: 10.1080/17445302.2013.870772.

[228] Martijn van Wijnagaarden. *Concept design of steel bottom founded support structures for offshore wind turbines.* Bachelor thesis, Delft University, 2013.

[229] Hugo Gaillard. *Optimization of export electrical infrastructure in offshore windfarms.* Master of Science Dissertation, KTH Industrial Engineering and Management, 2015.

[230] E. Lozano-Minguez, A.J. Kolios, and F.P. Brennan. Multi-criteria assessment of offshore wind turbine support structures. *Renewable Energy*, 36(11):2831–2837, nov 2011. ISSN 09601481. doi: 10.1016/j.renene.2011.04.020.

[231] Mainstream Renewable Power. Offshore O&M Costs Estimates. Technical report, Mainstream Renewable Power, jul 2009.

[232] Cheng-Ta Chu, Alexandre Meunier, Alan Taylor, and Alban Virlet. *Cost Economics of Offshore Wind.* Master of philosophy dissertation, University of Cambridge, 2011.

[233] Ofgem. OFTO Build : Providing additional flexibility through an extended framework Updated policy proposals. Technical report, Ofgem, 2014.

[234] Mark Lawson and Charles Balderston. OFTO Discussion. Private Correspondence, 2014.

[235] National Grid. COIN Document, 2012. URL `http://www2.nationalgrid.com/`.

[236] Scott Freeland and Sarah Brownie. Ecosse Subsea Systems. Presentation, 2014. URL `http://www.ecosse-subsea.com/`.

[237] Fugro Geoconsulting Limited. Navitus Bay Wind Farm Development, GIS-Based Export Cable Corridor Assessment, 2014.

[238] National Grid. Forecast TNUoS tariffs from 2016/17 to 2019/20. National Grid, jan 2015. URL `http://www2.nationalgrid.com/`.

[239] National Grid. An Introduction to Balancing Services Use of System Charging (BSUOS), 2014.

[240] Feng Wang, Deyou Liu, and Lihua Zeng. Modeling and simulation of optimal wind turbine configurations in wind farms. *2009 World Non-Grid-Connected Wind Power and Energy Conference*, pages 1–5, sep 2009. doi: 10.1109/WNWEC.2009.5335756.

[241] Bryony DuPont, Jonathan Cagan, and Patrick Moriarty. An Advanced Modeling System for Optimization of Wind Farm Layout and Wind Turbine Sizing Using a Multi-Level Extended Pattern Search Algorithm. *Energy*, pages 1–26, 2015. ISSN 03605442. doi: 10.1016/j.energy.2015.12.033.

[242] Javier Serrano González, Angel G. Gonzalez Rodriguez, José Castro Mora, Jesús Riquelme Santos, and Manuel Burgos Payan. Optimization of wind farm turbines layout using an evolutive algorithm. *Renewable Energy*, 35(8):1671–1681, aug 2010. ISSN 09601481. doi: 10.1016/j.renene.2010.01.010.

[243] Wing Yin Kwong, Peter Y Zhang, Michael Morgenroth, David Romero, Cristina Amon, and Joaquin Moran. Wind Farm Layout Optimization Considering Energy Generation and Noise Propagation. In *Proceedings of the ASME 2012 International Design Engineering Technical Conferences & Computers and Information in Engineering Conference IDETC/CIE 2012 Chicago, USA*, pages 1–10, Chicago, 2012.

[244] Sittichoke Pookpunt and Weerakorn Ongsakul. Optimal placement of wind turbines within wind farm using binary particle swarm optimization with time-varying acceleration coefficients. *Renewable Energy*, 55:266–276, jul 2013. ISSN 09601481. doi: 10.1016/j.renene.2012.12.005.

[245] General Bathymetric Chart of the Oceans. The GEBCO_2014 Grid, version 20150318, 2015. URL `http://www.gebco.net`.

[246] Jens H M Larsen, Hans Christian Soerensen, Erik Christiansen, Stefan Naef, and Per Vølund. Experiences from Middelgrunden 40 MW Offshore Wind Farm. *Proceedings of Offshore Wind Conference & Exhibition Copenhagen 2005*, 2005.

[247] SeaZone Solutions Ltd. Tile(s): nw25000020. EDINA Marine Digimap Service, 2013. URL `http://digimap.edina.ac.uk/`.

[248] Met Office. 2011 Zone 7 Navitus Bay, Met Office Zone Wind Analysis. The Crown Estate Marine Data Exchange, 2011. URL `http://www.marinedataexchange.co.uk/`.

[249] FUGRO. 2011 Zone 7 Navitus Bay West Isle of Wight, FUGRO Geophysical Survey. The Crown Estate Marine Data Exchange, 2011. URL `http://www.marinedataexchange.co.uk/`.

[250] Alstom. Power Curve Haliade 150, 2013. URL `www.alstom.com`.

[251] Navitus Bay Development Limited. Navitus Bay Wind Park. National Infrastructure Planning, 2014. URL `https://infrastructure.planninginspectorate.gov.uk/projects/south-east/navitus-bay-wind-park/`.

[252] Joris van Doorn and Her van Doorn. Intra-Array Cable Optimization Discussion. Private Correspondance, 2014.

[253] Oriol Gomis-Bellmunt, Jun Liang, Janaka Ekanayake, Rosemary King, and Nicholas Jenkins. Topologies of multiterminal HVDC-VSC transmission for large offshore wind farms. *Electric Power Systems Research*, 81(2):271–281, feb 2011. ISSN 03787796. doi: 10.1016/j.epsr.2010.09.006.

[254] Mircea Scutariu, Xiao Yi, and Power Transmission. Optimisation of offshore wind farm collection systems. *Proceedings of EWEA Offshore 2015 Copenhagen, Denmark*, pages 1–8, 2015.

[255] KHC Wang and Adi Botea. MAPP: a scalable multi-agent path planning algorithm with tractability and completeness guarantees. *Journal of Artificial Intelligence Research*, 42:55–90, 2011.

[256] Reza Zanjirani Farahani, Nasrin Asgari, Nooshin Heidari, Mahtab Hosseininia, and Mark Goh. Covering problems in facility location: A review. *Computers & Industrial Engineering*, 62(1):368–407, feb 2012. ISSN 03608352. doi: 10.1016/j.cie.2011.08.020.

[257] Paul Falloon. RES Offshore - Teesside OWF Sub-Sea Inspection Report. Technical report, Atlantas Marine, 2015.

[258] T El-Mihoub, Adrian Hopgood, L Nolle, and A Battersby. Hybrid genetic algorithms - a review. *Engineering Letters*, 11(August):124–137, 2006. ISSN 1816-093X.

[259] Sarvesh S Chakradeo. Generalized Theory for Hybridization of Evolutionary Algorithms. *2014 IEEE Conference on Computational Intelligence and Computing Research Coimbatore, India*, 2014.

[260] Tao Han. *The Assessment of Dynamic Wake Effects on Loading*. Master of Science Dissertation, TU Delft, 2011.

[261] C. Elkinton, A. Blatiak, and H. Ameen. Assessment of Ports for Offshore Wind Development in the United States. Technical report, GL Garrad Hassan, 2014.

[262] Anders Myhr, Catho Bjerkseter, Anders Ågotnes, and Tor A Nygaard. Levelised cost of energy for offshore fl oating wind turbines in a life cycle perspective. *Renewable Energy*, 66:714–728, 2014. ISSN 0960-1481. doi: 10.1016/j.renene.2014.01.017.

[263] W.E. de Vries and V.D. Krolis. Effects of Deep Water on Monopile Support Structures for Offshore Wind Turbines. *Proceedings of EWEC 2007 Milan, Italy*, pages 1–10, 2007.

[264] Walney Offshore Wind Farm. Walney Offshore Wind Farm Project, Cumbria , United Kingdom, 2015. URL `http://www.power-technology.com/projects/walneyoffshorewindfa/`.

[265] E.ON. Construction begins on Amrumbank West wind farm in the North Sea, 2015. URL `https://www.eon.com/en/media/news/press-releases/2014/1/15/construction-begins-on-amrumbank-west-wind-farm-in-the-north-sea.html`.

[266] Belwind Offshore Energy. Facts and Figures, 2009. URL `http://www.belwind.eu/en/facts-and-figures/`.

[267] ReNews. First monopile goes in at Baltic, 2015.

[268] Christian Leblanc Thilsted. Vibro-driving monopiles - a feasible installation concept for the future? *Geotechnical Engineering in Offshore Wind, Danish Geotechnical Society Seminar 2014 Lyngby, Denmark*, 2014.

[269] Ballast Nedam. Ballast Nedam Offshore and Vestas designed and built the first wind farm off the dutch coast, on a turnkey basis, West of Egmond aan Zee (The Netherlands) in 2006., 2015. URL http://www.ballast-nedam.com/.

[270] Per Aarsleff A/S. Offshore Wind Farm London Array. Technical report, Per Aarsleff A/S, 2012.

[271] DONG Energy. First foundation successfully installed, 2015. URL http://www.dongenergy.com/en/media/newsroom/news/articles/first-foundation-successfully-installed1.

[272] E.ON Climate & Renewables. E.ON Offshore Wind Energy Factbook. Technical Report December, E.ON Climate & Renewables, dec 2011.

[273] Talisman Energy. The Beatrice Wind Farm Demonstrator - Fact Sheet, 2007. URL http://talismanenergy.mwnewsroom.com/Files/ed/ed64d5f8-763c-4beb-bf7a-1fe6eb5b3f2b.pdf.

[274] Smulders Projects Belgium. Thornton Bank Phase II and III, 2012. URL http://www.smulders-hoboken.com/project-references/thornton-bank-phase-ii-and-iii.

[275] Kabie Intelligence Ltd. Ormonde Offshore Wind Farm, United Kingdom. Power Technology Market & Customer Insight, 2009. URL http://www.power-technology.com/projects/ormonde-offshore-wind-farm/.

[276] Seaway Heavy Lifting. Thanet Substation, 2010. URL https://www.seawayheavylifting.com.cy/projects/thanet-substation.

[277] Christian Bartsch. Fact-Sheet Alpha Ventus, 2012. URL http://www.alpha-ventus.de/fileadmin/user{_}upload/av{_}Factsheet{_}engl{_}Dec2012{_}2.pdf.

[278] ISC Consulting Engineers A/S. Offshore Substations. ISC Consulting Engineers A/S, 2013. URL http://www.isc.dk/wp-content/uploads/2016/09/offshore-substations-2014.pdf.

[279] Heerema Fabrication Group. Projects DolWin alpha HVDC, 2013. URL http://hfg.heerema.com/content/activities/projects/show/project/dolwin-alpha-hvdc-platform/.

[280] Overdick. HVDC Sylwin alpha, 2014. URL http://www.overdick.com/projects/offshore-wind/hvdc{_}sylwin{_}alpha.

[281] Heerema Fabrication Group. Projects BorWin alpha platform. pages 1–2, 2010.

[282] Heerema Fabrication Group. HelWin bèta jacket leaves Heerema Vlissingen yard, 2014. URL http://hfg.heerema.com/content/news-media/news-releases/news-detail/article/helwin-beta-jacket-leaves-heerema-vlissingen-yard/.

[283] Wim Bal. *Iv-Oil & Gas*. Iv-Oil & Gas, Papendrecht, 2015.

[284] Ajit C. Pillai, John Chick, Lars Johanning, Mahdi Khorasanchi, and Vincent de Laleu. Offshore wind farm electrical cable layout optimization. *Engineering Optimization*, 47(12):1689–1708, 2015. ISSN 0305-215X. doi: 10.1080/0305215X.2014.992892.

[285] Ajit C. Pillai, John Chick, Lars Johanning, Mahdi Khorasanchi, and Sebastien Pelissier. Optimisation of Offshore Wind Farms Using a Genetic Algorithm. *International Journal of Ocean and Polar Engineering*, 26(3):225–234, 2016. doi: 10.17736/ijope.2016.mmr16.

[286] Ajit C. Pillai, John Chick, and Vincent de Laleu. Modelling Wind Turbine Wakes at Middelgrunden Wind Farm. In *Proceedings of European Wind Energy Conference & Exhibition 2014 Barcelona, Spain*, pages 1–10. EWEA, 2014.

[287] Ajit C. Pillai, John Chick, Lars Johanning, Mahdi Khorasanchi, and Sebastien Pelissier. Optimisation of Offshore Wind Farms Using a Genetic Algorithm. In *Proceedings of the Twenty-fifth (2015) International Ocean and Polar Engineering Conference Kona, USA*, pages 644–652, 2015. ISBN 9781880653890.

[288] Ajit C. Pillai, John Chick, Lars Johanning, Mahdi Khorasanchi, and Sami Barbouchi. Comparison of Offshore Wind Farm Layout Optimizaiton Using a Genetic Algorithm and a Particle Swarm Optimizer. In *Proceedings of the ASME 2016 35th International Conference on Ocean, Offshore and Arctic Engineering (OMAE 2016) Busan, South Korea*, pages 1–11. ASME, 2016.

Appendix A

Simplification of Ainslie Eddy-Visocisty Model

The original formulation of the thin shear layer Navier-Stokes as given by Ainslie using the eddy-viscosity closure is [170, 177, 260]:

$$U\frac{\partial U}{\partial x}+V\frac{\partial U}{\partial r}=\frac{\varepsilon}{r}\left(\frac{\partial U}{\partial r}+r\frac{\partial^2 U}{\partial r^2}\right) \tag{A.1}$$

$$\frac{\partial U}{\partial x}=-\frac{1}{r}\left(r\frac{\partial V}{\partial r}+V\right) \tag{A.2}$$

Ainslie's model initializes the wake two rotor diameters downwind of the turbine. This is done in order to allow the pressure gradient terms in the Navier-Stokes equation to be ignored. Experimental work by Ainslie showed that the wake profile is self similar at all distances downwind of the turbine. This implies that the Gaussian shape that was assumed is preserved throughout the wake and the only factors that vary with downwind distance are the width and depth of the wake [177].

The initial wake profile at a distance of two rotor diameters was found to be:

$$U=U_0\left(1-D_M e^{-3.56\left(\frac{r}{b}\right)^2}\right) \tag{A.3}$$

where b is the dimensionless wake width parameter that is given by:

$$b=\sqrt{\frac{3.56C_T}{8D_M\left(1-\frac{1}{2}D_M\right)}} \tag{A.4}$$

Differentiating Equation A.3 with respect to the downwind distance x:

$$\begin{aligned}\frac{\partial U}{\partial x}&=0-U_0\frac{\partial\left(D_M e^{-3.56\left(\frac{r}{b}\right)^2}\right)}{\partial x}\\&=-U_0 e^{-3.56\left(\frac{r}{b}\right)^2}\frac{\partial D_M}{\partial x}-D_M U_0\frac{\partial e^{-3.56\left(\frac{r}{b}\right)^2}}{\partial x}\end{aligned} \tag{A.5}$$

Substituting the dimensionless wake width parameter (Equation A.4) gives:

$$\begin{aligned} e^{-3.56\left(\frac{r}{b}\right)^2} &= \exp\left(\frac{-3.56r^2}{\frac{3.56C_T}{8D_m(1-0.5D_M)}}\right) \\ &= \exp\left(\frac{-r^2 \cdot 8D_M(1-0.5D_M)}{C_T}\right) \end{aligned} \tag{A.6}$$

Differentiating this with respect to x gives:

$$\frac{\partial\left(e^{-3.56\left(\frac{r}{b}\right)^2}\right)}{\partial x} = -\frac{8}{C_T} r^2 e^{-3.56\left(\frac{r}{b}\right)^2} \frac{\partial\left(D_M\left(1-0.5D_M\right)\right)}{\partial x} \tag{A.7}$$

Substituting Equation A.7 into Equation A.5 gives:

$$\frac{\partial U}{\partial x} = -\left[1 - \frac{8}{C_T} D_M r^2 \left(1 - D_M\right)\right] U_0 e^{-3.56\left(\frac{r}{b}\right)^2} \left(\frac{\partial D_M}{\partial x}\right) \tag{A.8}$$

Next, Equation A.3 is differentiated with respect to r to give:

$$\begin{aligned} \frac{\partial U}{\partial r} &= U_0 \frac{\partial\left(1 - D_M e^{-3.56\left(\frac{r}{b}\right)^2}\right)}{\partial r} \\ &= -D_M U_0 \frac{\partial\left(e^{-3.56\left(\frac{r}{b}\right)^2}\right)}{\partial r} \\ &= U_0 D_M \frac{2 \cdot r \cdot 3.56 e^{-3.56\left(\frac{r}{b}\right)^2}}{b^2} \end{aligned} \tag{A.9}$$

And differentiating again to get the second derrivitive with respect to r gives:

$$\begin{aligned} \frac{\partial^2 U}{\partial r^2} &= \frac{\partial}{\partial r}\left(U_0 D_M \frac{2 \cdot r \cdot 3.56 e^{-3.56\left(\frac{r}{b}\right)^2}}{b^2}\right) \\ &= U_0 D_M \left[\frac{2 \cdot 3.56 e^{-3.56\left(\frac{r}{b}\right)^2}}{b^2} - \frac{4 \cdot r^2 \cdot 3.56^2 e^{-3.56\left(\frac{r}{b}\right)^2}}{b^4}\right] \end{aligned} \tag{A.10}$$

Next, it is assumed that the flow within the wake is perpendicular to the rotor plane of the upwind turbine. Therefore it can be assumed that at the center-line, $V(r=0) = 0$.

Using this assumption and the above derivations:

$$\frac{U_c}{U_0}\frac{\partial U_c}{\partial x} = 16 \frac{1}{Re_w} \frac{U_c^3 - U_0 U_c^2 - U_0^2 U_c + U_0^3}{U_0^3 C_T} \tag{A.11}$$

Given that all parameters have been non-dimensionalised, $U_0 = 1$ and therefore:

$$\frac{dU_c}{dx} = \frac{16\left(U_c^3 - U_c^2 - U_c + 1\right)}{Re_w U_c C_T} \tag{A.12}$$

Appendix B

UpWind Wake Validation Cases

B.1 Horns Rev

Table B.1: Horns Rev Test Cases [193, 194]

Case	Wind Speed [m/s]	Wind Direction [°]
1.6.7	6	270° ± 15°
1.8.4	8	270° ± 15°
1.10.4	10	270° ± 15°
1.6.6	6	270° ± 10°
1.8.3	8	270° ± 10°
1.10.3	10	270° ± 10°
1.6.4	6	270° ± 5°
1.8.2	8	270° ± 5°
1.10.2	10	270° ± 5°
FC6_270fw	6	270° ± 2.5°
FC8_270fw	8	270° ± 2.5°
FC10_270fw	10	270° ± 2.5°
1.6.1	6	270° ± 1°
1.8.1	8	270° ± 1°
1.10.1	10	270° ± 1°
2.6.7	6	221° ± 15°
2.8.4	8	221° ± 15°
2.10.4	10	221° ± 15°
2.6.2	6	221° ± 1°
2.8.1	8	221° ± 1°
2.10.1	10	221° ± 1°
3.6.7	6	312° ± 15°
3.8.4	8	312° ± 15°
3.10.4	10	312° ± 15°
3.6.2	6	312° ± 1°
3.8.1	8	312° ± 1°
3.10.1	10	312° ± 1°

B.2 Nysted

Table B.2: Nysted Test Cases [193, 194]

Case	Wind Speed [m/s]	Wind Direction [°]
FC6_263	6	$263° \pm 2.5°$
FC6_268	6	$268° \pm 2.5°$
FC6_273	6	$273° \pm 2.5°$
FC6_278	6	$278° \pm 2.5°$
FC6_283	6	$283° \pm 2.5°$
FC6_288	6	$288° \pm 2.5°$
FC6_293	6	$293° \pm 2.5°$
FC8_263	8	$263° \pm 2.5°$
FC8_268	8	$268° \pm 2.5°$
FC8_273	8	$273° \pm 2.5°$
FC8_278	8	$278° \pm 2.5°$
FC8_283	8	$283° \pm 2.5°$
FC8_288	8	$288° \pm 2.5°$
FC8_293	8	$293° \pm 2.5°$
FC10_263	10	$263° \pm 2.5°$
FC10_268	10	$268° \pm 2.5°$
FC10_273	10	$273° \pm 2.5°$
FC10_278	10	$278° \pm 2.5°$
FC10_283	10	$283° \pm 2.5°$
FC10_288	10	$288° \pm 2.5°$
FC10_293	10	$293° \pm 2.5°$

Appendix C

Monopile and Jacket Data

C.1 Monopile Data

Table C.1: Monopile specifications used to construct empirical mass correlation

Water Depth [m]	Power Rating [MW]	Rotor Diameter [m]	Hub Height [m]	Mass [kg]	Source
20	4.0	120	90	500000	[261]
20	5.0	135	93	788000	[261]
20	6.0	150	100	1076000	[261]
30	4.0	120	90	675000	[261]
30	5.0	135	93	1070000	[261]
30	6.0	150	100	1464000	[261]
20	3.6	107	79	502000	[228]
20	6.0	154	102	827000	[228]
20	8.0	164	107	943000	[228]
40	3.6	107	79	897000	[228]
40	6.0	154	102	1566000	[228]
40	8.0	164	107	1912000	[228]
30	5.0	126	88	1000000	[262]
21	6.0	129	90	556000	[216]
20	3.6	120	90	635000	[226]
18	2.3	93	72	410000	[226]
20	3.0	90	70	415000	[263]
25	3.0	90	70	580000	[263]
30	3.0	90	70	620000	[263]
35	3.0	90	70	775000	[263]
40	3.0	90	70	900000	[263]
45	3.0	90	70	1040000	[263]
50	3.0	90	70	1300000	[263]
20	6.0	150	100	500000	[224]

25	6.0	150	100	700000	[224]
30	6.0	150	100	950000	[224]
35	6.0	150	100	1100000	[224]
40	6.0	150	100	1325000	[224]
20	6.0	150	100	550000	[224]
25	6.0	150	100	750000	[224]
30	6.0	150	100	900000	[224]
35	6.0	150	100	1100000	[224]
40	6.0	150	100	1400000	[224]
20	5.0	126	88	450000	[224]
25	5.0	126	88	600000	[224]
30	5.0	126	88	750000	[224]
35	5.0	126	88	900000	[224]
40	5.0	126	88	1100000	[224]
28	3.6	120	90	800000	[264]
23	3.6	120	90	800000	[265]
15	3.0	90	70	300000	[266]
24	3.0	90	70	550000	[266]
32	3.6	120	90	930000	[267]
17	3.6	120	90	277000	[268]
18	3.6	120	90	272000	[268]
20	3.0	90	70	230000	[269]
25	3.6	120	90	650000	[270]
31	6.0	154	102	939000	[271]
8	2.0	66	60	110000	[272]
15	2.0	80	60	200000	[272]
9	3.0	90	80	260000	[272]
17	3.0	112	80	750000	[272]

C.2 Jacket Data

Table C.2: Jacket specifications used to construct empirical mass correlation

Platfrom Type	Water Depth [m]	Topside Mass [kg]	Foundation Mass [kg]	Source
HVAC	30	1030000	990000	[227]
HVAC	30	700000	750000	[227]
HVAC	13	1230000	800000	[227]
HVAC	19	1600000	1200000	[227]
HVAC	24	1800000	1400000	[227]
HVAC	10	2250000	950000	[227]
HVAC	21	1200000	695000	[227]
5 MW Turbine	40	547000	609000	[261]
6 MW Turbine	40	697000	684000	[261]
7 MW Turbine	40	811000	759000	[261]
8 MW Turbine	40	925000	834000	[261]
3.6 MW Turbine	40	565000	216000	[228]
6 MW Turbine	40	760000	468000	[228]
8 MW Turbine	40	905000	646000	[228]
3.6 MW Turbine	60	565000	461000	[228]
6 MW Turbine	60	760000	669000	[228]
8 MW Turbine	60	905000	713000	[228]
5 MW Turbine	30	600000	510000	[262]
5 MW Turbine	40	620000	500000	[262]
5 MW Turbine	45	620000	730000	[273]
5 MW Turbine	25	735000	400000	[274]
5 MW Turbine	21	661000	500000	[275]
HVAC	20	1460000	820000	[276]
5 MW Turbine	30	620000	510000	[277]
HVAC	30	630000	650000	[277]
HVAC	28	1900000	1300000	[278]
HVAC	30	1950000	1750000	[278]
HVAC	33	1950000	1700000	[278]
HVAC	19	1500000	1150000	[278]
HVAC	24	1784000	1435000	[278]
HVAC	21	1030000	994000	[278]
HVAC	24	1030000	995000	[278]
HVAC	13	1238000	798000	[278]

HVDC	27	10000000	4100000	[279]
HVDC	29	15000000	5600000	[280]
HVDC	40	3500000	1500000	[281]
HVDC	24	12000000	4500000	[282]
Oil & Gas	40	1000000	1050000	[283]
Oil & Gas	34	800000	800000	[283]
Oil & Gas	20	2125000	965000	[283]
Oil & Gas	20	285000	180000	[283]
Oil & Gas	30	3200000	1100000	[283]
Oil & Gas	35	1200000	800000	[283]

Appendix D

Optimization Convergence

D.1 Middelgrunden Wind Farm

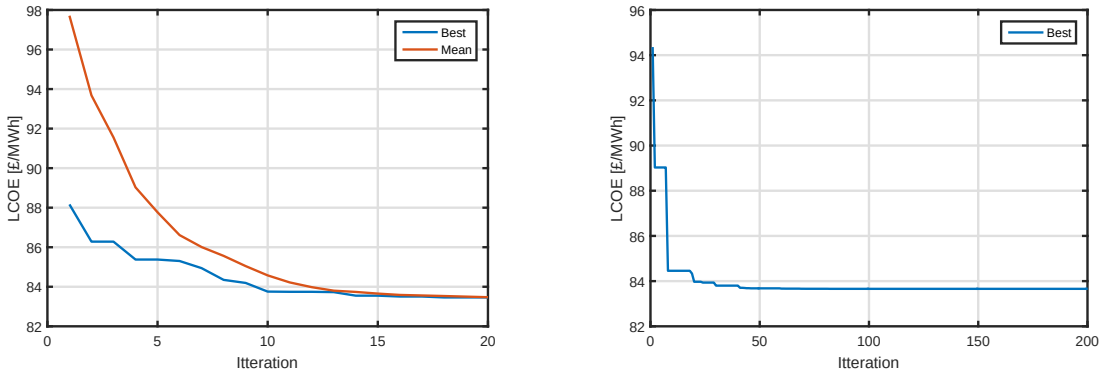

(a) GA **(b)** PSO

Figure D.1: Middelgrunden optimization convergence for array constraints

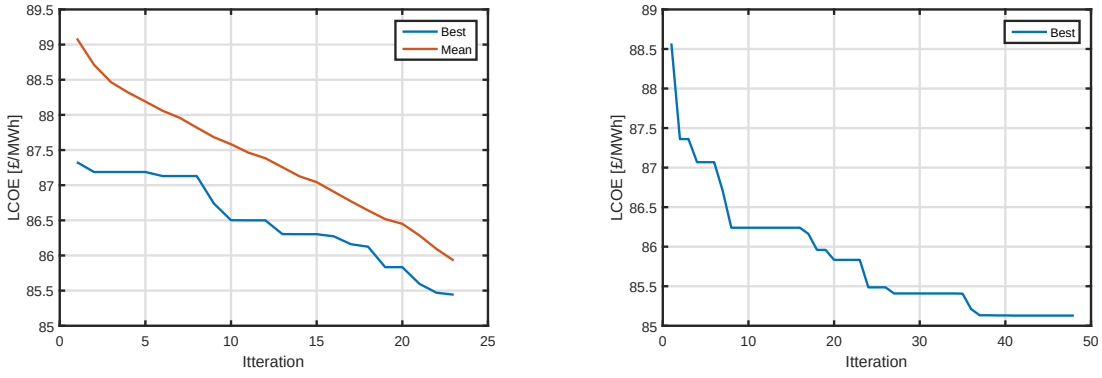

(a) GA **(b)** PSO

Figure D.2: Middelgrunden optimization convergence for binary constraints

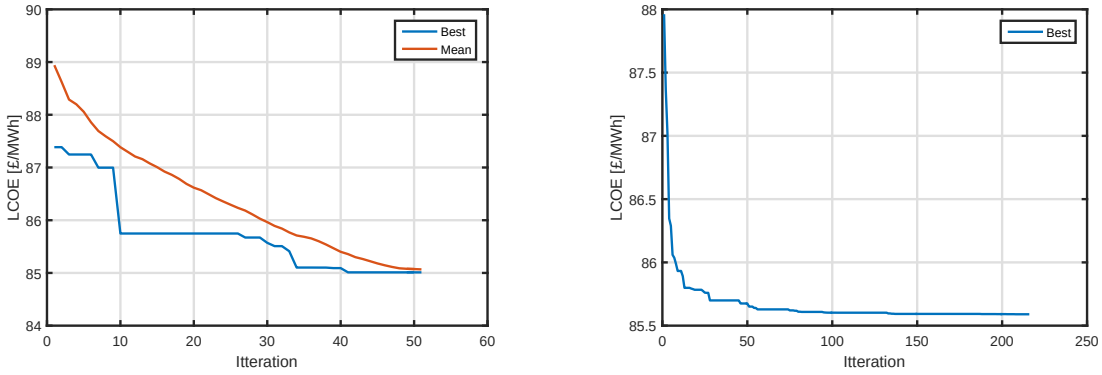

(a) GA **(b)** PSO

Figure D.3: Middelgrunden optimization convergence for continuous constraints

D.2 UK Round 3 Site

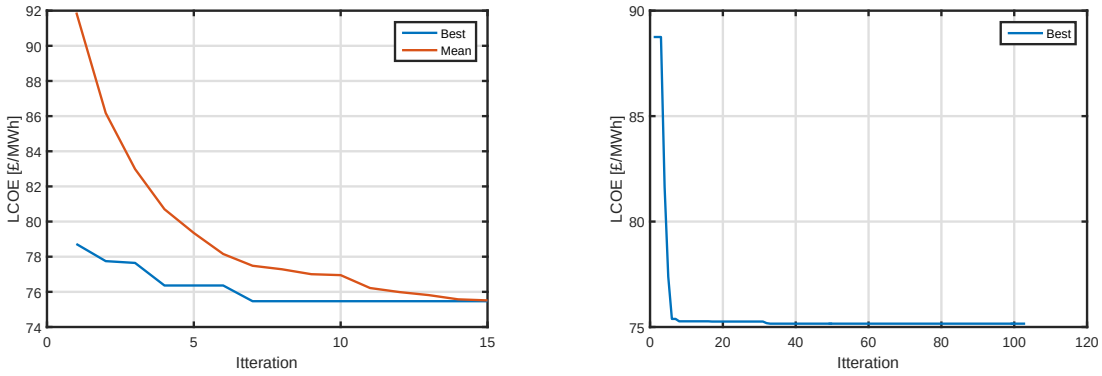

(a) GA **(b)** PSO

Figure D.4: UK Round 3 optimization convergence for array constraints

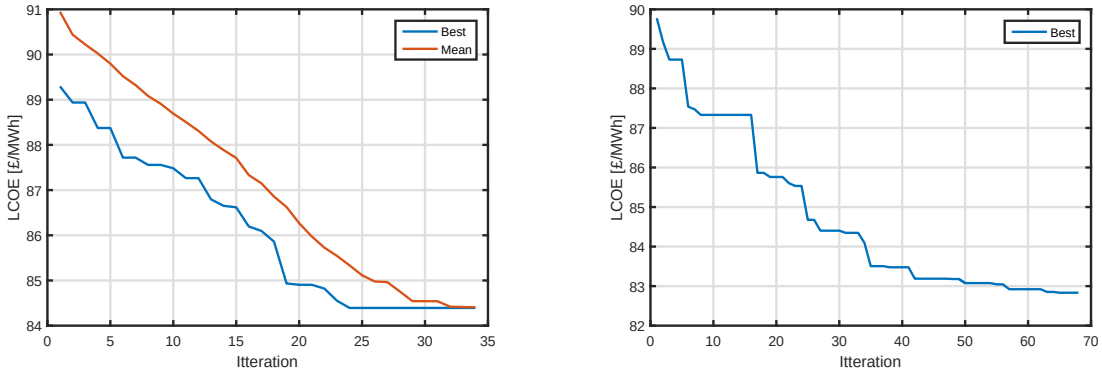

(a) GA **(b)** PSO

Figure D.5: UK Round 3 optimization convergence for binary constraints

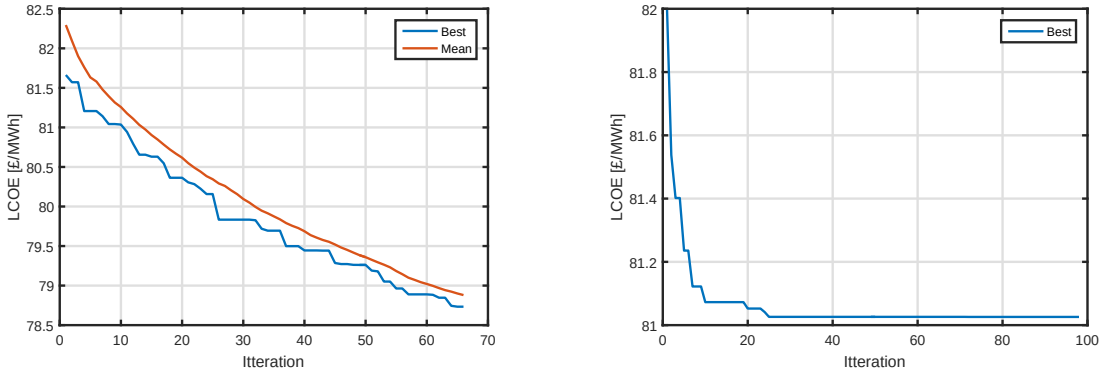

(a) GA **(b)** PSO

Figure D.6: UK Round 3 optimization convergence for continuous constraints

Appendix E

Published Work

E.1 Journal Publications

I Ajit C. Pillai, John Chick, Lars Johanning, Mahdi Khorasanchi, and Vincent de Laleu. Offshore wind farm electrical cable layout optimization. *Engineering Optimization*, 47(12):1689–1708, 2015. ISSN 0305-215X. doi: 10.1080/0305215X.2014.992892

II Ajit C. Pillai, John Chick, Lars Johanning, Mahdi Khorasanchi, and Sebastien Pelissier. Optimisation of Offshore Wind Farms Using a Genetic Algorithm. *International Journal of Ocean and Polar Engineering*, 26(3):225–234, 2016. doi: 10.17736/ijope.2016.mmr16

E.2 Conference Publications

IV Ajit C. Pillai, John Chick, and Vincent de Laleu. Modelling Wind Turbine Wakes at Middelgrunden Wind Farm. In *Proceedings of European Wind Energy Conference & Exhibition 2014 Barcelona, Spain*, pages 1–10. EWEA, 2014

V Ajit C. Pillai, John Chick, Lars Johanning, Mahdi Khorasanchi, and Sebastien Pelissier. Optimisation of Offshore Wind Farms Using a Genetic Algorithm. In *Proceedings of the Twenty-fifth (2015) International Ocean and Polar Engineering Conference Kona, USA*, pages 644–652, 2015. ISBN 9781880653890

VI Ajit C. Pillai, John Chick, Lars Johanning, Mahdi Khorasanchi, and Sami Barbouchi. Comparison of Offshore Wind Farm Layout Optimizaiton Using a Genetic Algorithm and a Particle Swarm Optimizer. In *Proceedings of the ASME 2016 35th International Conference on Ocean, Offshore and Arctic Engineering (OMAE 2016) Busan, South Korea*, pages 1–11. ASME, 2016

Engineering Optimization

ISSN: 0305-215X (Print) 1029-0273 (Online) Journal homepage: http://www.tandfonline.com/loi/geno20

Offshore wind farm electrical cable layout optimization

A.C. Pillai, J. Chick, L. Johanning, M. Khorasanchi & V. de Laleu

To cite this article: A.C. Pillai, J. Chick, L. Johanning, M. Khorasanchi & V. de Laleu (2015) Offshore wind farm electrical cable layout optimization, Engineering Optimization, 47:12, 1689-1708, DOI: 10.1080/0305215X.2014.992892

To link to this article: http://dx.doi.org/10.1080/0305215X.2014.992892

Published online: 13 Jan 2015.

Engineering Optimization, 2015
Vol. 47, No. 12, 1689–1708, http://dx.doi.org/10.1080/0305215X.2014.992892

Offshore wind farm electrical cable layout optimization

A.C. Pillai[ab*], J. Chick[a], L. Johanning[c], M. Khorasanchi[d] and V. de Laleu[b]

[a]*School of Engineering, The University of Edinburgh, Edinburgh, UK;* [b]*EDF Energy R&D UK Centre, London, UK;* [c]*College of Engineering, Mathematics, and Physical Sciences, University of Exeter, Penryn, UK;* [d]*Faculty of Engineering, The University of Strathclyde, Glasgow, UK*

(*Received 9 June 2014; accepted 29 October 2014*)

This article explores an automated approach for the efficient placement of substations and the design of an inter-array electrical collection network for an offshore wind farm through the minimization of the cost. To accomplish this, the problem is represented as a number of sub-problems that are solved in series using a combination of heuristic algorithms. The overall problem is first solved by clustering the turbines to generate valid substation positions. From this, a navigational mesh pathfinding algorithm based on Delaunay triangulation is applied to identify valid cable paths, which are then used in a mixed-integer linear programming problem to solve for a constrained capacitated minimum spanning tree considering all realistic constraints. The final tree that is produced represents the solution to the inter-array cable problem. This method is applied to a planned wind farm to illustrate the suitability of the approach and the resulting layout that is generated.

Keywords: offshore wind farm layout optimization; inter-array cabling; clustering; pathfinding; capacitated minimum spanning tree

1. Introduction

Over the last decade the renewable energy sector has grown substantially and European governments are now targeting high levels of renewable energy penetration in the forthcoming decade. In order to achieve these ambitious targets, many utilities are looking to large offshore wind farms as part of the solution. Optimization of these large wind farms has therefore arisen as a growing field of research for both developers and academics.

The layout optimization problem arises primarily due to the variation of wind speed and therefore wind energy throughout a wind farm site. The variation is further intensified as all wind turbines operating in the wind produce a wake, a region of air directly behind the turbine where the wind speed is reduced and the turbulence intensity is increased. The effect of an upwind turbine's wake decreases the further downwind that a subsequent turbine is placed; however, the effect is still observed up to 20 rotor diameters downwind (Chamorro and Porté-Agel 2010). Further complicating matters, the cables that are needed to export the energy from each turbine have energy losses and costs which are associated with the length of cable and the cross-section of the cable. Also to be taken into consideration are the environmental and social constraints such as the seabed geology, local marine species, visual impact, shipping routes, and fishing areas, to name but a few. The layout optimization problem therefore becomes a problem of balancing the

*Corresponding author. Email: a.pillai@ed.ac.uk

energy extraction from the wind; the system losses; the project costs; and the environmental and social constraints.

Many of the planned offshore wind farms in the UK, the Crown Estate Round 3 Projects, exceed 1 GW in installed capacity and are expected to consist of several hundred individual wind turbines. In existing offshore wind farms, the turbines tend to be connected in strings of 5–10 turbines to a central collection point known as an offshore high voltage substation (OHVS). These substations are in turn connected to grid connection points onshore. As offshore sites offer little as regards complex-terrain (*i.e.* hills, valleys, *etc.*) the turbines have until now generally been placed in straight lines along a regular grid. This, however, has not been optimized and early studies have indicated that optimization of the turbine positions can lead to more efficient use of the wind farm area (Fagerfjäll 2010; Elkinton 2007). Existing tools have approached the optimization of offshore wind farm layouts as a maximization of the energy yield and the minimization of wake losses; however, it can more accurately be characterized from a utility perspective as an optimization of the profitability of the generation asset or a minimization of the levelized cost of energy (LCOE). With regards to this, it therefore becomes important to consider all layout dependent aspects that either affect the energy yield of the wind farm or the lifetime costs.

The electrical infrastructure impacts both the energy yield and the costs and therefore has an important role to play in the optimization of offshore wind farms. The length of cable and therefore the capital costs of the project are directly a function of the positions of the turbines and the length of the cables also affects the energy losses that occur when transmitting through the cables. Similarly, these lengths of cable depend on where the substations are placed relative to both the onshore connection point and the turbines. The optimization of the collection network, the cables and the substations therefore forms an important component of the overall global optimization of an offshore wind farm layout.

In the development of a tool to be used to optimize the layouts of offshore wind farms, the problem of optimizing the electrical collection network for an offshore wind farm has been examined. Considering the future UK Round 3 Projects as a point of reference, the problem has been approached including as many realistic constraints as possible and formulated using a combination of heuristics and mixed-integer linear programming (MILP). As heuristics are used, this method may not reach proven optimality, but rather reaches a good feasible solution in an acceptable run time.

This optimization problem includes the determination of the substation positions given the realistic constraints faced by a developer, and the determination of the cable layout given this substation position. The export cable, a component of the transmission network, is not considered as part of this optimization problem.

Previous work in this field has tended to look at small wind farms, or has omitted some of the necessary constraints needed for the optimization of a real wind farm. Most have elected to work only on a single construction phase of a wind farm with a single OHVS, as subsequent phases and additional OHVSs would follow the same procedure.

Fagerfjäll (2010) implemented an MILP based approach for the electrical cable layout, assuming that all the turbines were connected to a single substation. This approach used a variation on the minimum spanning tree problem, a minimum Steiner tree, in order to solve for the electrical cabling. A minimum Steiner tree is similar to a minimum spanning tree; however, the arcs may branch anywhere along an arc and not only at nodes. By approximating the problem to that of the minimum Steiner tree, the cable length is therefore further minimized. Similar work has also been undertaken by Svendsen (2013) and Lindahl *et al.* (2013) using an MILP implementation to solve for a capacitated minimum spanning tree. Both of these studies, however, correctly identified that the computational time for these problems grows very quickly with the number of turbines. In fact, the capacitated minimum spanning tree (CMST) problem is NP-hard and therefore an optimal solution cannot be found in polynomial time, but rather in exponential time. The

problem therefore becomes exponentially complex as more turbines are added and more possible cable arcs must be considered.

Due to the complexity, a number of studies have opted to use heuristic algorithms such as genetic algorithms in order to optimize the electrical cable layout (Dutta and Overbye 2011; González-Longatt and Wall 2012; Cerveira and Pires 2014; Li, He, and Fu 2008; Zhao, Chen, and Blaabjerg 2008, 2009; Lumbreras and Ramos 2013). These studies have therefore sacrificed finding the proven optimal solution in favour of a good feasible solution in acceptable timescales. Bauer and Lysgaard (2013) simplified the problem to only allowing strings of turbines without any branching, allowing a variation on a vehicle routing problem algorithm to be applied. This too finds solutions in reasonable timescales; however, by not allowing branching, this approach reduces the problem complexity significantly, and eliminates many feasible solutions unnecessarily including, potentially, the optimal solution.

Studies carried out by Dutta and Overbye (2011, 2012, 2013) have looked at using a minimum spanning tree (MST) and applying the capacity constraints by running the MST on clustered turbines representing the capacity constraints of the largest cross-section of cable. This work has also modified the MST to represent a minimum Steiner tree. Dutta and Overbye (2013) also include an algorithm to account for exclusion areas where cables may not be placed, by constructing convex hulls from the obstacle and turbine positions to derive a shortest path.

Given the desire to apply the methodology to real sites, the electrical inter-array cable optimization problem has been approached pragmatically, dividing the overall problem into two sub-problems: the placement of the substations and then the determination of the cable layout. The study at hand intentionally opted to continue on from the work of Fagerfjäll (2010), Svendsen (2013) and Lindahl *et al.* (2013) using an MILP formulation for the electrical cable layout problem and introducing additional constraints to represent the realistic case of UK Round 3 sites. The new constraints introduced in this work take into account complex geographical information systems (GIS) shapes as constraints and the fact that cables may not cross in the offshore environment. Additional constraints have also been explored to aid in reducing the computational time.

2. Process overview

The design of offshore wind farms and the decision regarding the number of substations to build is largely driven by the capital expenditure (CAPEX) associated with building a substation along with the necessary foundation works. Projects tend therefore to minimize the number of substations such that substations are efficiently designed with a minimum surplus capacity. The total number of substations is therefore often predetermined based on the number of construction phases or the total wind farm capacity.

As a result of this, the decision of where to place the substations is effectively a process of selecting the substation positions which will result in the minimum total collection network cable as this will minimize both costs and losses of the collection system. The export cable should also be considered; however, it has been previously shown that given the significant length of cable already required for the export cable when compared to the in-field cables and the high voltage levels used, the costs associated with the export cable are minimally impacted by changes in the substation positions (Fagerfjäll 2010). In order to address this problem it was therefore decided to break the problem into two sub-problems: first the determination of the substation positions and secondly the construction of a CMST representing the cabling for each substation and its assigned turbines.

In the offshore environment, cable junctions require additional switch-gear and power electronics, the installation of which will require some sort of physical structure to house them. Presently, all junction boxes and circuit breakers designed for the offshore wind sector are

designed to be housed in a turbine or placed on a substation platform (Burton *et al.* 2011). This limitation in the offshore environment results in wind farm collection networks only branching at either turbines or substations. Though a minimum Steiner tree or a CMST with Steiner points would reduce the length of cable needed to connect a wind farm as proposed by Fagerfjäll (2010) and Dutta and Overbye (2012, 2013), it is not feasible to implement a Steiner tree in the offshore environment. A CMST without Steiner points was therefore selected for use in this study as this better represents the physical constraints of offshore wind farms.

The CMST formulation requires the costs for each potential cable connection under consideration. In order to assess these, it was first necessary to determine the length of cable required to connect two turbines, and then apply a per metre cost for that cable type. As the costs of cables including the installation costs scale with cable length, it is necessary to determine the lengths of potential cables prior to running the CMST. This effectively introduces another sub-problem. Given the complex GIS constraints, this was addressed through the implementation of a pathfinding algorithm in order to ensure that the cables would not pass through the constrained regions. Additional constraints were also introduced in order to reflect that cables may not cross one another. The overall programme approach is outlined below in Algorithm 1.

Algorithm 1 Offshore wind farm inter-array cable optimization

Require: The turbine positions, the GIS obstacles, and the number of substations
1: Given the number of substations assign each turbine to a substation and compute the substation positions using the *Capacitated kmeans++ Clustering*
2: **for** all substations **do**
3: **for** all turbines assigned to substation **do**
4: Identify the 10 closest turbines
5: Identify the constrained shortest path between the turbine and substation using *Delaunay Triangulation Based Navigational Mesh Pathfinding*
6: **for** 10 closest turbines **do**
7: Identify the constrained shortest path between turbine pair using *Delaunay Triangulation Based Navigational Mesh Pathfinding*
8: **end for**
9: **end for**
10: Formulate MILP for substation and its assigned turbines given the 11 possible arcs for each turbine computed above
11: **repeat**
12: Solve *MILP*
13: **if** any cables in MILP solution cross **then**
14: Add individual crossing constraints
15: **end if**
16: **until** No cables cross
17: **end for**
18: **return** substation positions, cable paths, cable flows, and cable types

As shown in Algorithm 1, there are in fact three optimization sub-problems as part of this overall optimization:

(1) *Capacitated Clustering Problem/Facility Location*;
(2) *Constrained Shortest Path/Pathfinding*;
(3) *Construction of Constrained Capacitated Minimum Spanning Tree*.

Table 1. Notation for automated electrical network design.

Name	Description	Type
A	All traversable points	Set
L	All cable types	Set
N_t	All turbines that can be connected to turbine t	Set
S	All substations	Set
T	All turbines and substations	Set
V	All turbine and substation positions, all vertices of the full graph, $V = T \cup S$	Set
X_l	All cables that intersect cable arc l	Set
$u_{i,j}$	Arc between vertex i and vertex j is active in shortest path	Binary variable
$y_{i,j,l}$	Presence of cable of type l between nodes i and j	Binary variable
$z_{t,s}$	Assign turbine t to substation s	Binary variable
$d_{i,j}$	Arc length between vertex i and vertex j	Variable
$f_{i,j}$	Flow between nodes i and j	Variable
n_s	Number of turbines assigned to substation s	Variable
p_1	Source point	Variable
p_2	Termination point	Variable
x_s	Position in x–y space of substation s	Variable
x_t	Position in x–y space of turbine t	Variable
A_l	Cross-sectional area of cable type l	Parameter
c_f	Price of electricity	Parameter
c_l	Cost of cable type l per metre installed	Parameter
g_j	Power generated at node j	Parameter
I	Current level at peak	Parameter
$Q_{\text{connection}}$	Number of cables that can be connected to a turbine node	Parameter
Q_l	Power flow capacity of cable type l	Parameter
Q_s	Capacity of substation s	Parameter
R	Cable resistivity	Parameter

The *Constrained Shortest Path* problem is executed for each turbine finding the possible connections between it, the ten closest turbines to it, and the substation. These data are used for the MILP CMST problem which is executed for each of the substations. The number of turbines to pathfind to is a parameter, and ten was empirically selected as turbines were found to always be connected either to one of their six closest neighbours or to the substation in all tests conducted. Ten was therefore selected to give additional flexibility; however, the framework is designed to accept any valid integer for this parameter.

3. Substation placement based on *kmeans*++ clustering

3.1. *Problem description*

The substation placement problem can be described as follows: for n_t turbines, k substations must be placed optimally. As the overall problem seeks to design the inter-array cable paths, the logical approach is to try and reduce these path lengths from the outset by efficiently placing the substations. The substation placement problem has therefore been addressed as a capacitated centred clustering problem (CCCP) and facility location problem. Based on the turbine positions and the number of substations desired, the turbines are divided into clusters, each within the capacity of the substations.

3.2. *Problem formulation*

Mathematically, the problem can be expressed as

$$\text{minimize} \quad \sum_{t \in T} \sum_{s \in S} (x_t - x_s)^2 z_{t,s} \tag{1a}$$

$$\text{subject to} \quad \sum_{s \in S} z_{t,s} = 1 \qquad \forall t \in T, \tag{1b}$$

$$\sum_{t \in T} z_{t,s} = n_s \qquad \forall s \in S, \tag{1c}$$

$$\sum_{t \in T} x_t z_{t,s} = n_s x_s \qquad \forall s \in S, \tag{1d}$$

$$\sum_{t \in T} z_{t,s} \leq Q_s \qquad \forall s \in S, \tag{1e}$$

$$z_{t,s} \in \{0, 1\} \tag{1f}$$

$$x_t \in \mathbb{R}^n \quad x_s \in \mathbb{R}^n \quad n_s \in \mathbb{N} \quad \forall t \in T \quad \forall s \in S, \tag{1g}$$

where T is the set of turbines and S is the set of substations.

In the above formulation, Equation (1a) states the objective function of the optimization process which is to minimize the square of the Euclidean distance between the position x_s of each substation, s, and the individual turbine positions x_t if the turbine t is assigned to substation s denoted by the state of $z_{t,s}$. The variable $z_{t,s}$ is defined as one if the turbine t is assigned to substation s; it is zero otherwise. Equation (1b) limits each turbine to being connected to exactly one substation. Equation (1c) defines the number of turbines assigned to substation s to be given by n_s. Equation (1d) defines the geometric centroid of the turbines assigned to substation s to be the position of the substation, and Equation (1e) ensures that each substation satisfies the capacity constraints Q_s.

3.3. *Solution approach*

The CCCP as formulated above is NP-complete and has previously been studied by Negreiros and Palhano (2006), Geetha, Poonthalir, and Vanathi (2009) and Chaves and Lorena (2010). These studies have identified heuristic algorithms to be well suited for solving this problem. Based on the comparative study by Negreiros and Palhano (2006), which compared heuristic approaches for the CCCP, it was decided to build a two-phase heuristic for this problem. The first stage would identify the ideal cluster centres ignoring the capacity and obstacle constraints, and the second phase would apply first the capacity constraints finding a good solution starting from the solution of the first stage, and finally, once the capacity constraints were satisfied, the obstacle constraints would be applied to refine the solution. It is recognized that the implementation of a heuristic algorithm cannot ensure an optimal solution, and the substation positions generated by this algorithm represent only a feasible solution.

For the first phase, a *kmeans*++ algorithm was selected. This is a variation on the well-known *kmeans* clustering methodology which intelligently selects the initial cluster centre positions in order to improve performance (Arthur and Vassilvitskii 2006; MacQueen 1967). Both *kmeans* and *kmeans*++ work by iteratively computing the cluster centre (geometric median) based on what turbines are assigned to the cluster, then, based on the new geometric median, the turbines are each reassigned to the closest cluster centre. This process is repeated until the cluster centres converge. In general, both *kmeans* and *kmeans*++ have been shown to be effective clustering techniques (Negreiros and Palhano 2006).

Using the approach outlined in Algorithm 2, it was possible successfully to partition a wind farm to ensure that substations were in good, feasible positions if not in the optimal position. This process also ensured that the substation capacities and any GIS obstacles were correctly implemented as constraints for the substation positions.

Algorithm 2 Capacitated kmeans++ Clustering

Require: Set of turbines T to be clustered into k clusters while obeying O obstacles

1: Perform kmeans++ Clustering
2: Balance clusters based on capacity
3: Update cluster centres based on assigned turbines
4: Look for elements which can be moved to improve total distance while maintaining capacity constraints.
5: Update cluster centres based on assigned turbines
6: Identify pairs of turbines which can have their substation assignments swapped to yield improved total distance between turbines and substations
7: Update cluster centres based on assigned turbines
8: Shift substations (cluster centres) to nearest allowable position based on obstacles
9: **return** Substation positions and turbine assignments

The proposed method also explored swapping turbine assignments in order to ensure that the identified substation positions accurately minimize the distance to turbines, and each turbine is therefore assigned to the closest substation unless capacity constraints are active in which case the turbines with the lowest global impact on the cost are assigned to a substation farther away. It should be noted that the result of introducing the GIS and capacity constraints has a major impact on the computational time of the clustering, but a very minor effect on the value of the objective function.

4. Cable path creation based on Delaunay triangulation and pathfinding

4.1. *Problem description*

Before constructing the capacitated minimum spanning tree it is necessary to compute the costs of putting a cable between two turbine locations. In order to do this while considering the GIS obstacle constraints, it was necessary to compute a constrained shortest path between the positions. Given the constraints, the construction of the graph of possible cable paths is an NP-complete problem. Dutta and Overbye (2013) addressed exclusion areas by defining a bypassing algorithm. This bypassing algorithm constructs a convex hull of the obstruction and the turbines to be connected. The edge of this convex hull can then be traversed to find the shortest path. This approach, however, is not guaranteed to find the shortest path, and in fact will incorrectly mark areas as impassable if the obstacle is not convex. This bypassing algorithm is therefore only well suited if the exclusion areas can be described as simple convex shapes. As the tool developed here sought to account for realistic seabed constraints that may take on concave shapes it was decided that a convex hull based bypassing algorithm would not be the most efficient approach. As a result, a pathfinding approach was taken. The pathfinding approach was found to account for concave obstacle regions correctly.

Pathfinding can theoretically, depending on the algorithm applied, guarantee a shortest path between two points in a constrained configurational space regardless of if the obstacles are convex or not. Pathfinding problems frequently arise in video games and robot motion problems as it is necessary for a *robot* to move from an origin location to a destination location taking into account obstacles which it cannot pass through. In the case of cable paths, turbines are either connected by a cable to another turbine or the substation and therefore there is a finite set of origin–destination pairs for which a path must be found.

4.2. *Problem formulation*

In general, pathfinding can be described as a specific case of a shortest path tree traversal. The shortest path of a graph can be mathematically formulated as

$$\text{minimize} \sum_{i \in A} \sum_{j \in A} d_{i,j} \cdot u_{i,j} \tag{2a}$$

$$\text{subject to} \sum_{i:(i,k) \in V} u_{i,k} - \sum_{j:(k,j) \in A} u_{k,j} = \begin{cases} -1, & \text{if } k = p_1 \\ 1, & \text{if } k = p_2 \\ 0, & \text{if } (k \in A : k \notin \{p_1, p_2\}) \end{cases} \tag{2b}$$

$$u_{i,j} \in 0, 1 \qquad \forall (i,j) \in A, \tag{2c}$$

where $u_{i,j}$ is a binary variable describing the connectivity between points i and j in space A in the shortest path. This variable is one if i and j are connected in the shortest path and zero otherwise. The points p_1 and p_2 represent the source and termination points, respectively, and are also within the space A. The cost of connecting points i and j (the length of the edge connecting i and j) is given by $d_{i,j}$.

This general formulation, however, represents the optimization problem once a graph representing the configurational space (*i.e.* the traversable space in which cables can be laid) has been constructed. There are a number of different methods to construct this graph depending on what kind of pathfinding algorithm is deployed. For this study, both a grid based pathfinding algorithm and a navigational mesh were implemented. The navigational mesh ultimately proved to be the more appropriate algorithm to implement.

4.3. *Solution approach*

For problems such as this, there are two principle approaches for finding the shortest path, one is to reduce the obstacle data to a *walkability grid* representing on a regular grid where cables can and cannot be placed. The shortest path can then be found using a standard grid search algorithm such as *A* Pathfinding* or *Dijkstra's Algorithm*. However, this simplifies all the constraints to consist of regular rectangles, and given the complexity of real offshore wind sites this was often found to eliminate possible paths, as can be observed in Figure 1. Though this could be avoided by using a finer grid size, other challenges still remained. For example, by creating a grid, the cable paths were limited in having only eight options of where to go from any given grid position (Figure 2), often causing problems with paths overlapping cables near substations and no simple means of avoiding this. Paths based on the grid were also longer than necessary due to being fixed to the grid.

The alternative method uses what is known as a visibility graph and navigational mesh, and is capable of avoiding all of the above problems, but at a significant cost in complexity (Ghosh 2007). The visibility graph is a graph for which an arc exists between any two vertices if they are 'visible' to one another. Visibility is defined as true if the two points can be connected by an arc without the arc passing through an obstacle. It is important to note that, in terms of a visibility graph, points along the obstacle edges are considered to be an open set, *i.e.* that valid arcs can pass along edges. The optimal path is in fact the shortest path between vertices on such a graph. The difficulty in working with visibility graphs is that algorithms for testing visibility are computationally complex. The most efficient algorithms still operate in $O(n \log n + k)$, where n is the number of vertices and k is the number of edges (de Berg *et al.* 2008). Given that the GIS constraints for a typical offshore wind farm will constitute several thousand vertices, this was thought to be too computationally complex.

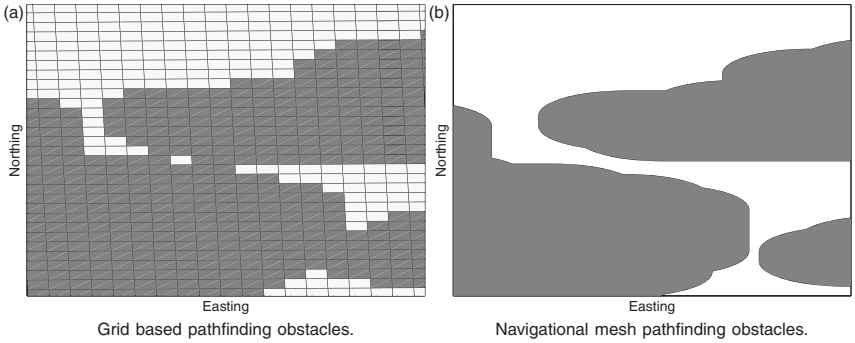

Figure 1. Comparison of obstacle representation in grid based and navigational mesh based pathfinding.

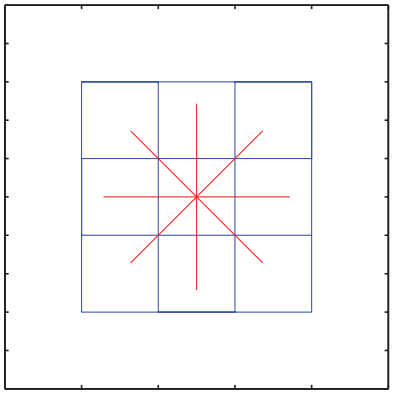

Figure 2. Grid based system allows a path to go to only one of the eight adjacent squares surrounding it.

The proposed methodology, therefore uses a heuristic algorithm which can create a close approximation of the visibility graph in a fraction of the computational time. This approach, known as a navigational mesh based pathfinding algorithm creates a traversable graph which obeys the obstacle constraints. One such algorithm, proposed by Jan *et al.* (2012, 2014), was adopted for this project. This approximation method uses the edges of a constrained 'Delaunay triangulation' to define the graph. A Delaunay triangulation is defined as a triangulation in which no vertex is within the circumcircle of any triangle of the triangulation, and a constrained Delaunay triangulation is defined such that, given the obstacle edges as a constraint, no triangulation edges cross the obstacles. By triangulating the obstacle vertices along with the origin and destination positions, it is possible to create a graph representing the traversable area. In order to improve the performance of the graph and better approach the full visibility graph solution, this method includes the Fermat points of the triangles and connects these to the graph. For triangles for which the largest angle is less than 120°, a Fermat point is defined to be the position internal to the triangle that minimizes the distance to the triangle vertices. For a triangle in which the largest angle is greater than or equal to 120°, the Fermat point is located at one of the vertices.

Once these Fermat points are found, they are then added to the graph and connected to their respective triangle vertices and any adjacent Fermat points (Figures 3(d) and 3(e)).

Algorithm 3 Delaunay triangulation based navigational mesh shortest path

Require: Polygon obstacles, origin point, destination point, and site boundary
1: Construct the configurational space given the obstacle polygons
2: For the configurational map construct a constrained Delaunay triangulation for the vertices making up the obstacles, the origin point, and the destination point. The edges of the obstacles serve as the constraints for the triangulation
3: Create a graph of all vertices and triangle edges of the triangulation
4: Insert Fermat points in triangles that have angles less than 120°
5: Connect the Fermat points to the vertices of their triangles and any adjacent Fermat points
6: Find the shortest path in the graph using Dijkstra's algorithm
7: Apply the path shortening procedure
8: **return** Cable path

As this produces a potentially sub-optimal path, Jan *et al.* (2014) proposed a *path shortening* method which removes redundant Fermat points or vertices from the solution paths therefore reducing the total length to on average within 2% of the optimal path, but in a fraction of the time. The original path shortening algorithm was enhanced by checking all possible shortcuts, constructing a graph, and then running Dijkstra's shortest path algorithm.

Algorithm 4 Path shortening

Require: Polygon obstacles, cable path
1: Compute the length of each segment of the path
2: Compute the length for all possible shortcuts
3: **for** all possible shortcuts **do**
4: **if** shortcut does not intersects an obstacle **then**
5: Add shortcut length to graph adjacency matrix
6: **end if**
7: **end for**
8: Find shortest path along graph using Dijkstra's algorithm
9: **return** Cable path

Figure 3 shows a visual representation of the pathfinding process. Comparing the resulting paths in Figures 3(e) and 3(f) shows the need for including the path shortening subroutine. It is important to note that inclusion of the path-shortening algorithm with the improvement suggested still does not ensure optimality; however, it can lead to significantly reduced path lengths. It should be noted that generally, however, this method does find the optimal path between two points.

5. MILP formulation of offshore wind farm electrical layout optimization

5.1. *Problem description*

Through the preceding sub-problems the substations have been placed and a graph of possible cable connections has been constructed with the path and length of each cable computed. The

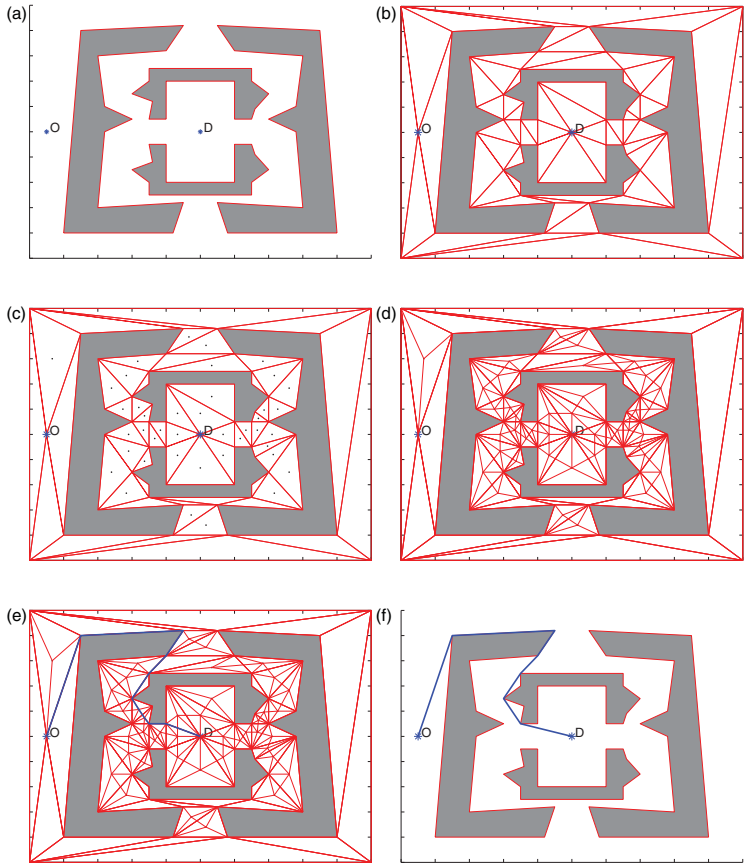

Figure 3. A simplified example of the pathfinding approach. (a) The problem formulation with the origin and destination points marked and obstacles shown in grey. (b) The result after performing a Delaunay triangulation on the configurational space. (c) The Delaunay triangulation with the Fermat points added for the appropriate triangles. (d) The graph formed by the triangle edges and Fermat points connected to the appropriate triangle vertices and adjacent Fermat points. (e) The results from a Dijkstra's shortest path algorithm on the constructed graph. (f) The results after performing the path shortening function.

remaining task is to select which of these cables to use to minimize the total cost of the inter-array cable infrastructure. Given the arc costs between turbines and the constraints described below, this problem could be described as a capacitated minimum spanning tree (CMST) problem with additional constraints. The minimum spanning tree problem (MST) seeks to find the sub-graph of a connected graph which connects all vertices at minimum total cost (Figure 4). The CMST variation on this problem introduces additional constraints to account for maximum capacities on the arcs. The CMST is an NP-complete problem and exact methods are often avoided though easily formulated. Similar to previous studies, the CMST was here implemented as an MILP problem and solved using the Gurobi package through MATLAB®.

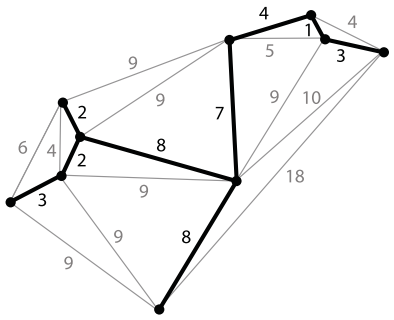

Figure 4. Example of a minimum spanning tree with arc costs shown.

The CMST is not a new problem and the formulation used in this work is based on that of Gouveia (1993, 1995). This work has generalized this formulation to allow for multiple arc types and a simultaneous selection of not only the cable paths, but the cable cross-sectional area.

5.2. *Problem formulation*

Mathematically, the CMST can be formulated as

$$\text{minimize} \quad \sum_{i\in V}\sum_{j\in N}\sum_{l\in L}\left[\left(c_l \cdot d_{i,j} \cdot y_{i,j,l}\right) + \left(f_{i,j} \cdot y_{i,j,l} \cdot d_{i,j} \cdot \frac{R}{A_l} \cdot c_f \cdot I^2\right)\right] \tag{3a}$$

$$\text{subject to} \quad \sum_{i\in V}\sum_{l\in L} y_{j,i,l} \le 1 \qquad \forall j \in V, \tag{3b}$$

$$\sum_{i\in V}\sum_{l\in L} f_{j,i} \cdot y_{j,i,l} - \sum_{i\in N}\sum_{l\in L} f_{i,j} \cdot y_{i,j,l} = g_j \qquad \forall j \in V, \tag{3c}$$

$$f_{i,j} - \sum_{l\in L} Q_l \cdot y_{i,j,l} \le 0 \qquad \forall (i,j) \in V,\ \forall l \in L, \tag{3d}$$

$$\sum_{l\in L} y_{i,j,l} \le 1 \qquad \forall (i,j) \in V, \tag{3e}$$

$$\sum_{l\in L} y_{i,j,l} + y_{q,r,l} \le 1 \qquad \forall (i,j,q,r) \in X, \tag{3f}$$

$$\sum_{i\in V}\sum_{l\in L} y_{i,j,l} + y_{j,i,l} \le Q_{\text{connection}} \qquad \forall j \in T, \tag{3g}$$

$$f_{i,j} \ge 0 \qquad \forall (i,j) \in V, \tag{3h}$$

$$y_{i,j,l} \in \{0,1\} \qquad \forall (i,j) \in V,\ \forall l \in L. \tag{3i}$$

The above formulation represents the minimum constraints to account for a CMST with multiple arc types each with a different capacity rating. In this formulation there are two decision variables: $f_{i,j}$ represents the power flow between nodes i and j and $y_{i,j,l}$ is a binary variable representing the presence of a cable between nodes i and j of cable-type l. Both i and j are turbine or substation elements of the set V and l is a cable-type of the set L. The quantity $Q_{\text{connection}}$ represents the physical constraint on the number of connections at each turbine position.

The objective function is made up of two terms, the first represents the fixed capital cost of the cable and its installation where c_l is the per-length cost of cable-type l, $d_{i,j}$ is the length of cable needed between nodes i and j. The second term represents a factor to account for the peak losses in the cable. In this regard, the CMST is bi-objective and minimizes both the CAPEX costs of the cable and the losses in the cable. The losses are monetized by applying a cost of electricity c_f to represent the forgone revenue due to the loss. The losses are computed using: R, the resistivity of the cable; A_l, the cross-sectional area of cable type l; I, the current level at peak; the cable length; and the flow in the cable. This bi-objective approach ensures that not only is the cable length minimized, but solutions with lower flow levels in cables are preferred in order to reduce Ohmic losses.

The seven constraints listed represent the minimum necessary for this problem including the fact that cables cannot cross one another. General CMST formulations and past wind farm planning tools do not include the constraints given by Equations (3e)–(3g) (Gouveia 1993; Gavish 1983; Uchoa, Fukasawa, and Lysgaard 2006; Fagerfjäll 2010; Svendsen 2013). Constraint (3b) stipulates that each node, or turbine, can have at most one cable exporting power. Constraint (3c) imposes the flow balance constraints such that the difference between all flow out of each node and the flow into each node must be equal to the flow supplied at each node (the power generated by the turbine) denoted by g_j. Constraint (3d) imposes the capacity constraint where Q_l is the capacity of cable-type l. Constraint (3e) ensures that every cable can be of only a single cable-type. Constraint (3f) accounts for the fact that, for an offshore wind farm, inter-array cables may not cross. In order to impose this, X is the set of turbine pairs for which cables cross. Constraint (3g) constrains the number of cables connected to a turbine to be $Q_{\text{connection}}$ to account for the physical space for circuit breakers in a turbine tower. Finally Equations (3h) and (3i) constrain x_{ij} to be a positive flow, and y_{ijl} to be a binary variable as explained earlier.

5.3. *Solution approach*

Although previous work formulated the problem similarly, it identified that a heuristic algorithm would be appropriate given the NP-completeness of the problem (Svendsen 2013; Lindahl *et al.* 2013; Li, He, and Fu 2008). For this reason, it was decided to use Gurobi 5.6, a commercial MILP solver that combines Simplex solving techniques with bespoke cutting plane generation algorithms and heuristic algorithms. Using Gurobi, the MIP gap (the relative difference between the upper and lower bounds) is used as a measure of optimality and a termination criterion. In general, Gurobi attempts to find a true global optimum which has an MIP gap approaching zero. In order to improve the performance, the MIP gap was relaxed to 0.01. This means that once the upper and lower bound of the solutions are within a 1% difference, the solution is considered optimal. This means that, in the worst case, the solution found is 1% away from optimality for the given path lengths.

As stated earlier, crossing constraints were imposed; however, it was found during the development of the methodology that imposing the full set of crossing constraints for all pairs of cables resulted in many inactive constraints. It was also found that for problems with more than 40 turbines significant amounts of memory were required in order to avoid out-of-memory errors. It was instead decided to take an approach similar to the implementation of cutting planes and instead solve the MILP, check if any of the paths in the solution crossed, and if so impose that specific constraint. In this way the MILP solver is called iteratively, slowly increasing the number of constraints until the solution is found. By doing this, the inactive constraints are not formulated unnecessarily and less memory is required. Even in small cases this row generation approach was shown to perform better than the full implementation. Table 2 shows a comparison of the performance using the full constraints and using the row generation approach. Owing to the way

Table 2. Comparison of the full crossing constraint implementation with the row generation method.

		Number of crossing constraints		Time to solve CMST (s)	
	Turbines	Full	Row generation	Full	Row generation
	52	790,804	104	701.47	1867.68
	62	844,914	2	847.94	13.79
	61	405,862	0	1340.13	36.43
Total	175	2,041,580	106	2889.54	1917.90

in which the cable routes were found using the pathfinding algorithm described in Section 4, it was not necessary to impose further constraints representing the regions where cables could not be placed.

Based on previous work by Fagerfjäll (2010) it was decided to explore the introduction of additional constraints in order to improve performance. Two additional constraints were therefore introduced:

$$f_{i,j} - \sum_{l \in L} y_{i,j,l} \geq 0 \quad \forall i,j \in T, \tag{4a}$$

$$\sum_{i \in T} \sum_{l \in L} y_{i,j,l} + y_{j,i,l} \geq 1 \quad \forall j \in T. \tag{4b}$$

Equation (4a) relates the flow and activity of an arc, while Equation (4b) stipulates that there must be at least one active edge connected to each node. Neither of these constraints is necessary in order to solve the problem; however, performance improvements were noted when they were included.

6. Results

6.1. *Study description*

In order to assess the performance of this approach compared with other MILP and simple estimation methodologies, it was applied to a real offshore wind farm. Navitus Bay Windpark, off the south coast of England is a Round 3 wind farm site which will have between 121 and 194 turbines. The site interestingly has a number of GIS constraints that would need to be taken into account during both the siting of turbines and the design of the inter-array cable network. These GIS constraints include unexploded World War II ordnance (UXOs), ship wrecks, and areas where the seabed characteristics are unsuitable for turbines or cables.

As no decision has been made on the layout of the turbines or the turbine size, a realistic turbine layout was designed using WindFarmer 5.2. This layout considers only the overall site boundary and the GIS constraints and has been generated for the explicit purpose of testing this inter-array cable optimization tool; it does not represent a real layout designed by the project developer. The layout studied here consists of 175 6 MW turbines representing 1050 MW installed. This layout is larger than the 968 MW maximum allowed capacity for the wind farm and has been generated for the explicit purpose of demonstrating the capabilities of this optimization tool.

For this layout, the results using this tool are compared to running a simple design tool ignoring the GIS constraints, as well as estimating the total cable length using only the separation distance between turbines in the crosswind direction. The latter two represent methodologies often employed in layout optimization tools and cost models. The estimation based on the

turbine separation considers neither the GIS constraints nor the capacity of cables and therefore represents a theoretical lower bound on the length of cable.

Based on the most recent boundaries shown in Figure 5 along with the GIS data provided by the Navitus Bay Development it was possible to generate turbine layouts using DNV GL WindFarmer 5.2. These turbine positions were then input to the inter-array cable optimization tool.

All MILP optimization problems were run using a gap of 0.01. A solution is also shown using the grid based pathfinding; however, this method required the relaxation of the crossing constraint and the solutions produced by this method therefore do not represent realistic solutions.

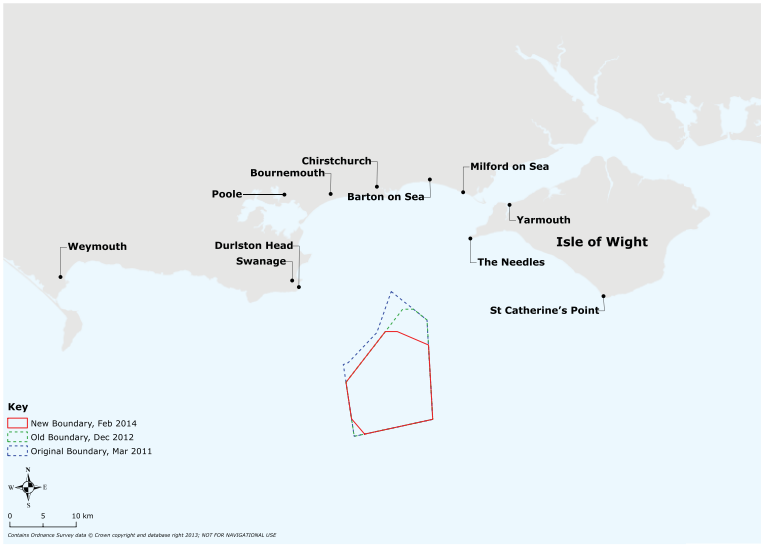

Figure 5. Illustrative map showing the Navitus Bay project site. Image courtesy Navitus Bay Development.

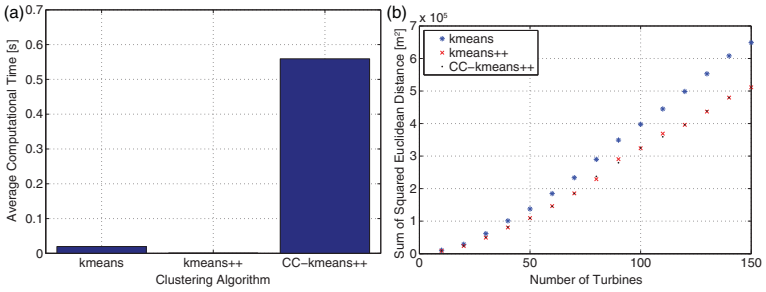

Figure 6. Comparison of the clustering algorithms. In both graphs, lower values indicate better performance.

6.2. *Substation placement*

First running the substation placement component of the tool allowed the new constrained capacitated kmeans++ (CC-kmeans++) algorithm to be benchmarked against common clustering approaches such as traditional kmeans and kmeans++. It should be noted that neither of these algorithms are designed to include capacity constraints or GIS based constraints limiting the area where it is permissible to place the cluster centre.

Comparing the performance for a range of wind farm sizes within the Navitus Bay region it was found that the clustering was relatively inelastic to the number of turbines, and more strongly governed by the number of clusters that the turbines were to be partitioned into. Importantly, the

Table 3. Cable length comparison.

Method	Cable length (km)	Delta (km)
Turbine spacing based	148.75	–
CMST, no GIS	157.66	8.91
CMST with GIS	161.84	13.09

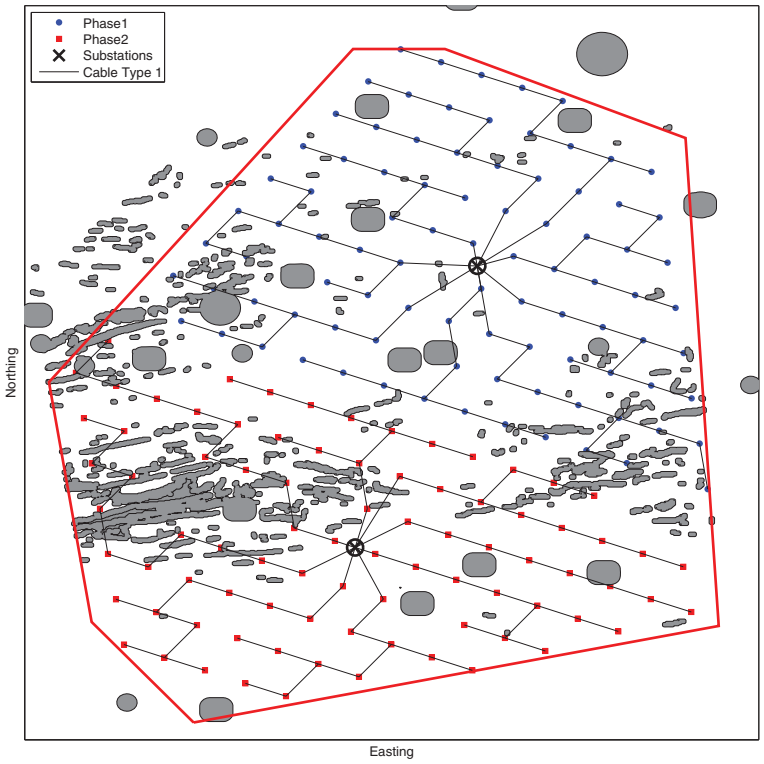

Figure 7. Cable layout, no GIS constraints.

constrained capacitated kmeans++ approach proved to be far slower than traditional clustering approaches; however, even given this it was deemed to have an acceptable performance as 150 turbines were easily partitioned into two clusters in less than a second.

As can be seen in Figure 6, although the performance of the new clustering algorithm is much slower than kmeans++, it gives similar results in terms of total distance between the turbines and the centre location, while at the same time adhering to the GIS and substation capacity constraints. Though the increase in computational time is relatively significant it is still a quick algorithm in absolute terms partitioning 150 turbines into two clusters in under 0.6 seconds.

6.3. *Optimized inter-array cable layout*

The full implementation of both the substation placement and the inter-array cable optimization for a number of wind farms within the Navitus Bay site area gave the cable results shown in Figures 7 and 8. When compared to the solutions of simpler MILP programmes, ignoring GIS constraints, it was found that the total cable length increased by almost 9 km, representing an added capital cost of approximately €4.5 million and, when compared to using an estimation based on the inter-turbine spacing, the total amount of cable is increased by approximately 13 km, representing approximately €6.5 million.

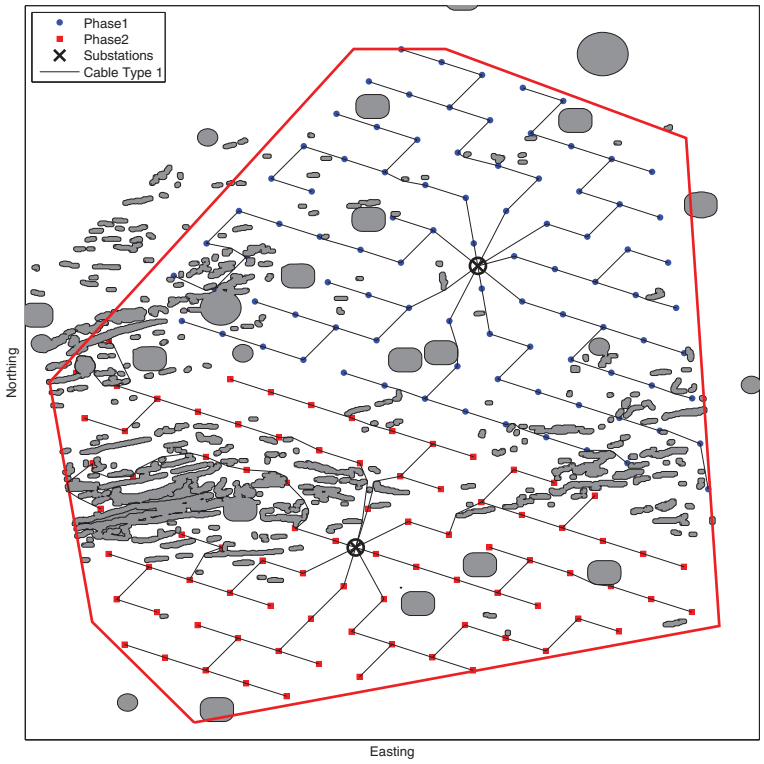

Figure 8. Cable layout, full optimization method.

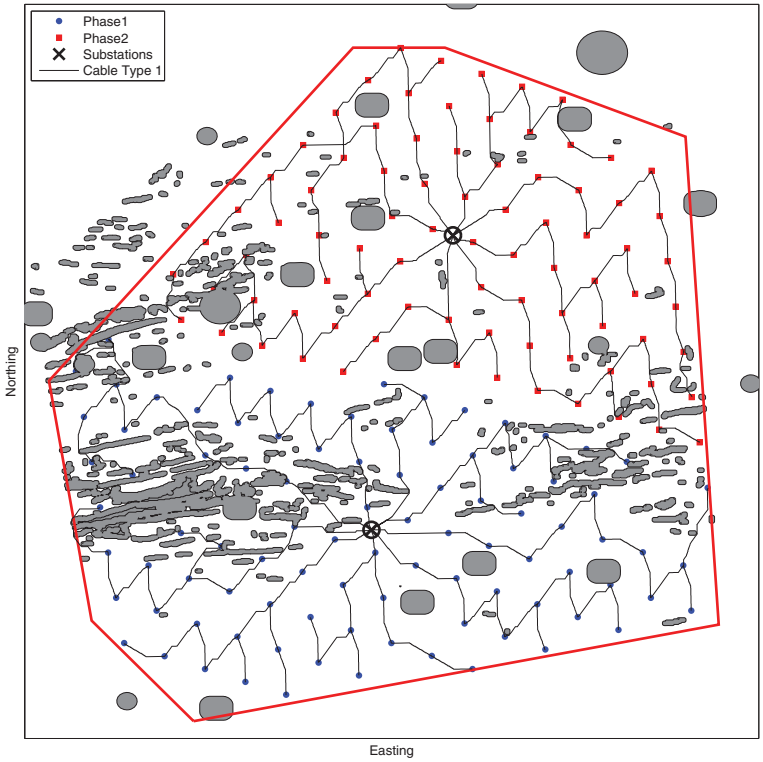

Figure 9. Grid based pathfinding using an A* search algorithm.

From the results, a number of differences can be observed: ignoring the GIS constraints leads to a number of cables crossing the obstacle regions as would be expected. Interestingly, however, running either the A* grid based pathfinding algorithm (Figure 9) or the navigational mesh algorithm both produce solutions to the cable layout problem fundamentally different from the base case. This can be attributed to the optimal solution being more than just re-routing the cables that violate the obstacle constraint.

Looking at the A* solution shown in Figure 9, it can be observed that the grid based system experiences difficulty due to the limitations mentioned previously and in fact was unable to produce solutions without cables crossing. The proposed full methodology does, however, successfully place the substations at acceptable locations and designs an infield cable layout that does not violate any of the constraints, including the GIS based constraints. This is shown in Figure 8.

7. Conclusion

This article has outlined a new approach for the inter-array cable design problem for an offshore wind farm by means of breaking it into several sub-problems. These sub-problems have

included a location-constrained capacitated clustering approach for placing the substations, a navigational mesh based pathfinding algorithm to determine possible cable connections, and an MILP approach to solve for a CMST and select which cable connections should be installed.

The CCCP compares well in performance against traditional clustering methods such as kmeans and kmeans++; though consistently slower than both, it has consistently better cluster centres than kmeans, and very similar results to kmeans++ while respecting the GIS constraints. This implementation represents a novel approach to the positioning of an offshore substation and is one of the first automated approaches used for this application.

This study then opted to implement a navigational mesh pathfinding algorithm to determine possible cable connections based on constructing an approximation of a visibility graph to describe the configurational space where cables can be placed. From the resulting graph that is constructed, a simple shortest path algorithm with a bespoke path shortening heuristic is applied in order to produce good feasible solutions which approach optimality. The lengths of these paths are then used as edge lengths in an MILP implementation of a capacitated minimum spanning tree.

The results of this approach applied to a real offshore wind farm currently in the planning stages have yielded promising results indicating that this approach is not only valid but shows improvements over commonly used approaches based on the turbine separation distance. There are still improvements that can be made, but this approach represents a strong step forward to the efficient automation of the layout design of an offshore wind farm and optimizing all aspects of the layout.

Acknowledgements

The authors would like to acknowledge EDF Energy Renewables and the Navitus Bay Project Development teams for the provision of the Navitus Bay GIS data and maps of the site.

Funding

This work is funded in part by the Energy Technologies Institute (ETI); Research Councils UK (RCUK); Energy programme for the Industrial Doctorate Centre for Offshore Renewable Energy (IDCORE) [grant number EP/J500847/1].

References

Arthur, David, and Sergei Vassilvitskii. 2006. *k-Means ++: The Advantages of Careful Seeding* (Technical Report). Stanford University InfoLab.

Bauer, J., and J. Lysgaard. 2013. "The Offshore Wind Farm Array Cable Layout Problem—A Planar Open Vehicle Routing Problem." Department of Informatics, University of Bergen, Norway, 1–16. http://www.ii.uib.no/~joanna/papers/owfacl.pdf.

Burton, T., N. Jenkins, D. Sharpe, and E. Bossanyi. 2011. *Wind Energy Handbook*. 2nd ed. Chichester: John Wiley & Sons.

Cerveira, Adelaide, and Eduardo J. Solteiro Pires. 2014. "Optimisation Design in Wind Farm Distribution Network." In *Proceedings of the International Joint Conference SOCO'13-CISIS'13-ICEUTE'13*, Vol. 239 of *Advances in Intelligent Systems and Computing*. Springer International Publishing Switzerland. http://link.springer.com/10.1007/978-3-319-01854-6.

Chamorro, Leonardo P., and Fernando Porté-Agel. 2010. "Effects of Thermal Stability and Incoming Boundary-Layer Flow Characteristics on Wind-Turbine Wakes: A Wind-Tunnel Study." *Boundary-Layer Meteorology* 136 (3): 515–533. http://link.springer.com/10.1007/s10546-010-9512-1.

Chaves, Antonio Augusto, and Luiz Antonio Nogueira Lorena. 2010. "Clustering Search Algorithm for the Capacitated Centered Clustering Problem." *Computers & Operations Research* 37 (3): 552–558. http://linkinghub.elsevier.com/retrieve/pii/S0305054808001779.

de Berg, Mark, Otfried Cheong, Marc van Kreveld, and Marc Overmars. 2008. *Computational Geometry*. 3rd ed. Berlin: Springer-Verlag. http://medcontent.metapress.com/index/A65RM03P4874243N.pdf.

Dutta, S., and T. J. Overbye. 2011. "A Clustering Based Wind Farm Collector System Cable Layout Design." In *Proceedings of the Power and Energy Conference at Illinois (PECI)*, 25–26 February 2011, Champaign, IL, 4–9. IEEE. http://ieeexplore.ieee.org/xpls/abs_all.jsp?arnumber=5740480.

Dutta, Sudipta, and Thomas J. Overbye. 2012. "Design Considering Total Trenching Length." *IEEE Transactions on Sustainable Energy* 3 (3): 339–348.

Dutta, Sudipta, and Thomas Overbye. 2013. "A Graph-Theoretic Approach for Addressing Trenching Constraints in Wind Farm Collector System Design." *Proceedings of the IEEE Power and Energy Conference at Illinois (PECI)*, 22–23 February 2013, Champaign, IL, 48–52. IEEE. http://ieeexplore.ieee.org/lpdocs/epic03/wrapper.htm?arnumber=6506033.

Elkinton, Christopher Neil. 2007. "Offshore Wind Farm Layout Optimization." Doctor of Philosophy diss., University of Massachussetts Amherst.

Fagerfjäll, Patrik. 2010. "Optimizing Wind Farm Layout—More Bang for the Buck Using Mixed Integer Linear Programming." Master of Science diss., Chalmers University of Technology and Gothenburgh University.

Gavish, Bezalel. 1983. "Formulations and Algorithms for the Capacitated Minimal Directed Tree Problem." *Journal of the ACM* 30 (1): 118–132. http://portal.acm.org/citation.cfm?doid=322358.322367.

Geetha, S., G. Poonthalir, and P. T. Vanathi. 2009. "Improved *K*-Means Algorithm for Capacitated Clustering Problem." *International INFOCOMP Journal of Computer Science* 8 (4): Article Number 07. http://www.dcc.ufla.br/infocomp/artigos/v8.4/art07.pdf.

Ghosh, S. K. 2007. *Visibility Algorithms in the Plane*. 1st ed. Cambridge, UK: Cambridge University Press.

González-Longatt, F. M., and Peter Wall. 2012. "Optimal Electric Network Design for a Large Offshore Wind Farm Based on a Modified Genetic Algorithm Approach." *IEEE Systems Journal* 6 (1): 164–172. http://ieeexplore.ieee.org/xpls/abs_all.jsp?arnumber=6007042.

Gouveia, L. 1993. "A Comparison of Directed Formulations for the Capacitated Minimal Spanning Tree Problem." *Telecommunication Systems* 1 (1): 51–76. http://link.springer.com/article/10.1007/BF02136155.

Gouveia, Luis. 1995. "A 2*n* Constraint Formulation for the Capacitated Minimal Spanning Tree Problem." *Operations Research* 43 (1): 130–141.

Jan, Gene Eu, Chi-chia Sun, Wei Chun Tsai, and Ting-hsiang Lin. 2014. "An $O(n \log n)$ Shortest Path Algorithm Based on Delaunay Triangulation." *IEEE/ASME Transactions on Mechatronics* 19 (2): 660–666.

Jan, Gene Eu, Wei Chun Tsai, Chi-Chia Sun, and Bor-Shing Lin. 2012. "A Delaunay Triangulation-Based Shortest Path Algorithm with $O(n \log n)$ time in the Euclidean Plane." In *Proceedings of the IEEE/ASME International Conference on Advanced Intelligent Mechatronics (AIM)*, 11–14 July 2012, Kaohsiung, Taiwan, 186–189.: IEEE. http://ieeexplore.ieee.org/lpdocs/epic03/wrapper.htm?arnumber=6266051.

Li, D. D., Chao He, and Yang Fu. 2008. "Optimization of Internal Electric Connection System of Large Offshore Wind Farm with Hybrid Genetic and Immune Algorithm." In *Proceedings of the Third International Conference on Electric Utility Deregulation and Restructuring and Power Technologies (DRPT 2008)*, 6–9 April 2008, Nanjing, PR China, 2476–2481. http://ieeexplore.ieee.org/xpls/abs_all.jsp?arnumber=4523827.

Lindahl, M., N. C. Fink Bagger, T. Stidsen, S. Frost Ahrenfeldt, and I. Arana. 2013. "OptiArray from DONG Energy: An Automated Decision Support Tool for the Design of the Collection Grid in Large Offshore Wind Power Plants." In *Proceedings of the 12th Wind Integration Workshop (International Workshop on Large-Scale Integration of Wind Power into Power Systems as well as on Transmission Networks for Offshore Wind Power Plants)*, 22–24 October 2013, London, edited by Uta Betancourt and Thomas Ackermann. Langen, Germany: Energynautics.

Lumbreras, Sara, and Andres Ramos. 2013. "Optimal Design of the Electrical Layout of an Offshore Wind Farm Applying Decomposition Strategies." *IEEE Transactions on Power Systems* 28 (2): 1434–1441. http://ieeexplore.ieee.org/xpls/abs_all.jsp?arnumber=6263256.

MacQueen, J. 1967. "Some Methods for Classification and Analysis of Multivariate Observations." In *Proceedings of the Fifth Berkeley Symposium on Mathematical Statistics and Probability* 233 (233): 281–297.

Negreiros, Marcos, and Augusto Palhano. 2006. "The Capacitated Centred Clustering Problem." *Computers & Operations Research* 33 (6): 1639–1663. http://linkinghub.elsevier.com/retrieve/pii/S0305054804003120.

Svendsen, Harald G. 2013. "Planning Tool for Clustering and Optimised Grid Connection of Offshore Wind Farms." *Energy Procedia* 35: 297–306. http://linkinghub.elsevier.com/retrieve/pii/S187661021301268X.

Uchoa, Eduardo, Ricardo Fukasawa, and Jens Lysgaard. 2006. "Robust Branch-Cut-and-Price for the Capacitated Minimum Spanning Tree Problem over a Large Extended Formulation." *Mathematical Programming*Volume 112 (2): 443–472. http://link.springer.com/article/10.1007/s10107-006-0043-y.

Zhao, M., Z. Chen, and F. Blaabjerg. 2008. "Application of Genetic Algorithm in Electrical System Optimization for Offshore Wind Farms." In *Proceedings of the Third International Conference on Electric Utility Deregulation and Restructuring and Power Technologies (DRPT 2008)*, 6–9 April 2008, Nanjing, PR China, 7–12. Aalborg, Denmark: VBN.

Zhao, M., Z. Chen, and F. Blaabjerg. 2009. "Optimisation of Electrical System for Offshore Wind Farms via Genetic Algorithm." *IET Renewable Power Generation* 3 (September): 205–216. .

International Journal of Offshore and Polar Engineering (ISSN 1053-5381) http://www.isope.org/publications/publications.htm

Vol. 26, No. 3, September 2016, pp. 225–234; http://dx.doi.org/10.17736/ijope.2016.mmr16

Optimisation of Offshore Wind Farms Using a Genetic Algorithm

Ajit C. Pillai
Industrial Doctorate Centre for Offshore Renewable Energy, The University of Edinburgh
Edinburgh, United Kingdom

John Chick
Institute for Energy Systems, The University of Edinburgh
Edinburgh, United Kingdom

Lars Johanning
College of Engineering, Mathematics, and Physical Sciences, University of Exeter
Penryn, United Kingdom

Mahdi Khorasanchi
Department of Naval Architecture, University of Strathclyde
Glasgow, United Kingdom

Sebastien Pelissier
EDF Energy R&D UK Centre
London, United Kingdom

A modular framework for the optimisation of an offshore wind farm using a discrete genetic algorithm is presented. This approach uses a bespoke grid generation algorithm to define the discrete positions that turbines may occupy, thereby implicitly satisfying navigational and search and rescue constraints through the wind farm. The presented methodology takes a holistic approach, optimising both the turbine placement and intra-array cable network while minimising the levelised cost of energy and satisfying real-world constraints. This tool therefore integrates models for the assessment of the energy production including wake losses, the optimisation of the intra-array cables, and the estimation of the costs of the project over the lifetime. This framework will allow alternate approaches to wake and cost modelling as well as optimisation to be benchmarked in the future.

INTRODUCTION

With the growth of the offshore wind sector and the development of large offshore wind farms in the coming years, it has become an important point to ensure that the wind farms are developed in such a way as to maximise their potential. In order to meet this need, the field of wind farm layout optimisation has been in development since the seminal paper by Mosetti et al. (1994). Though this field has been in development for the past twenty years, there still remains much work before layout optimisation displaces the industry standard rule-of-thumb approach to layout design. This paper presents a new framework that has been developed to address the layout optimisation problem, with the goal of ultimately developing a tool that would be deployed by wind farm site developers.

This framework takes a holistic approach to layout optimisation based on the objectives and constraints that would be faced by an offshore wind farm developer in the UK. This approach introduces a generalised means of discretising the wind farm area in such a way that a grid of potential turbine positions is first generated. The use of this grid ensures that the final turbine positions, which are selected from this grid, satisfy the requirement of having turbines along straight lines.

From the perspective of an offshore wind farm operator, it is important not only to maximise the energy yield from the wind farm but also to optimise the levelised cost of energy (LCOE). The full layout optimisation problem therefore represents striking a balance between maximising the energy yield and minimising the lifetime costs.

To this end, a number of projects have looked at the optimisation of wind farm layouts. This project has addressed this problem through a similar approach to previous schemes by using a genetic algorithm (GA) to minimise the LCOE (Mosetti et al., 1994; Grady et al., 2005; Elkinton, 2007; Fagerfjäll, 2010; Guillen, 2010):

$$LCOE = \frac{\sum_{t=1}^{n} C_t/(1+r)^t}{\sum_{t=1}^{n} AEP_t/(1+r)^t} \quad (1)$$

where C_t are the costs incurred in year t, n is the project lifetime time, AEP_t is the annual energy production (AEP) in year t, and r is the discount rate of the project. The LCOE measured in £/MWh effectively gives a measure of the cost effectiveness of the layout proposed and therefore acts as a means to compare the layouts under consideration on a relative basis.

Existing approaches do not apply tools and methodologies that have considered all the constraints faced by a developer, nor do

Received September 18, 2015; updated and further revised manuscript received by the editors April 27, 2016. The original version (prior to the final updated and revised manuscript) was presented at the Twenty-fifth International Ocean and Polar Engineering Conference (ISOPE-2015), Kona, Hawaii, June 21–26, 2015.
KEY WORDS: Offshore wind farm layout optimisation, genetic algorithm.

they consider the full impact the layout has on the LCOE. Many of the previous studies opted to use simpler cost models, thereby ignoring the effect the layout has on costs (Mosetti et al., 1994; Grady et al., 2005). The studies that have considered detailed cost models, however, have not considered the full set of constraints with which a developer would be faced (Elkinton, 2007; Larsen et al., 2011; Larsen and Réthoré, 2013). A tool has been developed as part of this work that seeks to reconcile these elements by including both detailed models for assessing the layout-dependent elements as well as a full set of constraints in order to generate layouts that would be acceptable from a developer's perspective.

The work presented has developed a flexible framework through which the energy, cost, and electrical infrastructure are assessed independently for each layout. Due to the modularity, alternate wake, cost, or electrical infrastructure, models can easily be implemented in the future for comparison purposes and sensitivity studies. The approach presented has also included constraints for maintaining navigation channels through the sites, a minimum separation between turbines, and seabed restrictions; these constraints are less frequently seen in existing tools. The tool also generates an optimised intra-array electrical configuration, simultaneously satisfying not only seabed constraints but also cable capacity, cable crossing, and junction box capacity constraints.

A GA with bespoke crossover and mutation operators has been developed and applied successfully to this problem. The constructed modular platform would allow other optimisation algorithms, such as particle swarm, ant colony optimisation, or simulated annealing, to be implemented through the use of the same evaluation function and tool approach.

This paper summarises the initial application of this holistic approach to the layout optimisation of offshore wind farms. The optimisation framework is applied to a hypothetical wind farm made up of thirty wind turbines in order to demonstrate the capabilities of the approach. The discussion section explores further improvements that will be made to the framework to increase the relevance to a wind farm developer.

METHODS

As this tool has been developed as part of a larger project that seeks to assess the suitability of different wake models, cost models, optimisation objectives, and optimisation algorithms, it has been intentionally designed to be as flexible as possible while also adhering to the realistic challenges that would be faced by a project developer.

Grid Generation

In the UK, project developers have been urged to use symmetric layouts with turbines placed along a regular grid in order to comply with the navigational safety and search and rescue requirements (NOREL Group, 2013). Rather than navigational channels being defined, this constraint has been proposed that requires the turbines to be placed in straight lines with no deviation from these lines. As a result of this, most optimisation approaches have limited the optimisation process to specifying the regular spacing between turbines. The tool developed here, however, looks instead to give the optimiser greater freedom by designing a grid that has more potential turbine positions than there are turbines to be placed. This allows the optimiser to change the spacing between turbines throughout the wind farm while still keeping the turbines in straight lines. It is believed that even though this creates a regular grid with holes, the final layout will still satisfy the navigational requirements.

The first step in this optimisation approach, therefore, is to produce this grid of potential turbine positions. To do this, the tool first identifies the dominant wind direction on the basis of the wind rose, describing the wind resource at the site and converting this to an energy rose representing the kinetic energy flux of the wind and the relative occurrence of the wind speed and wind direction combination. The dominant wind direction is then defined as the weighted circular mean of the wind direction sector where the wind direction is weighted by the kinetic energy flux. The dominant wind direction, once identified, will act as one of the principal axes along which the grid of points is generated. By aligning the principal axis with the dominant wind direction, the optimiser will be able to align turbines in rows perpendicular to the dominant wind direction, thereby minimising the interaction of wakes. At the same time, having a large grid with more possible positions than turbines to be placed allows the optimiser to introduce space for wakes to recover where necessary. This approach also allows the optimiser to have flexibility in adjusting the spacing relative to each individual turbine rather than for the entire wind farm.

Once the dominant wind direction is identified, the algorithm expands and contracts the spacing as necessary until a grid with the desired number of valid turbine positions is generated. For each spacing, the grid is produced with a fixed ratio between the downwind and crosswind spacing. After this, each point is checked to ensure that it satisfies the geographical information system (GIS) constraints regarding where turbines can be placed. If after this it is found that

a) insufficient grid points are in valid positions, then the spacing is *decreased*, and the process is repeated; or

b) too many grid points exist, then the spacing is *increased*, and the process is repeated.

The desired number of grid positions is treated as a minimum, and a small tolerance of the range of 10% is introduced to ensure that a valid grid can always be generated. In this way, "too many" is defined as more grid points present than the desired range, while "insufficient" refers to grids that have fewer valid turbine positions than desired.

Annual Energy Production

The principal output of a wind farm is the energy produced by the wind farm that is represented in the LCOE by the annual energy production term. In order to accurately assess the impact that the layout has on the LCOE, it is important to characterise the effect that the layout has on the AEP and the lifetime energy yield. The energy yield assessment in turn can be said to be made up of two components, an understanding of the wind resource at the site and the modelling of potential wakes behind each proposed turbine.

Any device that extracts energy from a natural flux, such as the wind, is known to directly impact and alter the natural flux as a result of the energy extraction. In the case of wind turbines, the wake behind a wind turbine is characterised by lower extractable wind speeds but higher levels of turbulence intensity (Barthelmie et al., 2006, 2009; Burton et al., 2011). These wakes are also known to interact with one another, leading to a more significant reduction in available energy as a result of the superposition of multiple upwind wakes (Katic et al., 1986; Schlez and Neubert, 2009).

Wake models can be broadly categorised into two categories: analytic wake models and field models. Analytic wake models are simpler models, while field models are generally based on solving the Navier-Stokes equations. Though the annual energy

production module can be run either independently or as part of the optimisation tool, it was decided that an analytic wake model should be used instead of a field model to predict the wakes as this results in substantially quicker computational times (Renkema, 2007; Sanderse et al., 2011).

Previous work by the authors (Pillai et al., 2014) and other studies (Gaumond et al., 2012) had shown that for existing wind farms, the Larsen model (Larsen, 1988) represents a good balance between accuracy and computational complexity when compared to the Jensen/PARK model (Katic et al., 1986), the Ishihara model (Ishihara et al., 2004; Crasto and Castellani, 2013), and the Ainslie eddy-viscosity model (Ainslie, 1988; Anderson, 2009). The Larsen model is an analytic model based on a closed-form solution of the Reynolds-Averaged Navier Stokes (RANS) equations and Prandtl mixing theory (Larsen, 1988; Renkema, 2007). For this study, the Larsen model has therefore been deployed; however, other wake models can easily be implemented if need be.

In order to assess the AEP, the wind distribution at the site is used to determine the frequency of occurrence for each wind speed/direction combination. For each of these bins, the turbines in the layout are sorted such that the first turbine is the turbine furthest upwind. For each turbine, the free wind speed is then updated to account for the wakes created by any upwind turbines and the superposition of these wakes. The variation in the power generation and thrust coefficient is considered on the basis of the modified wind speed as a result of the wake effect, and bins are generated in relation to speed and directionality. The aggregate power generated for the entire layout for these bins is then multiplied by the frequency of this wind speed and direction combination. The sum of the powers for each bin represents the AEP for the proposed layout. This approach is similar to that taken by other tools and AEP computations (Mosetti et al., 1994; Grady et al., 2005; Elkinton, 2007; Pérez et al., 2013; DNV GL - Energy, 2014).

Electrical Infrastructure Optimisation

Previous layout optimisation tools have generally assumed a constant inter-turbine spacing, and therefore the changes in the total cost due to the intra-array cables are not characterised. However, as the layout changes, the total length of the required infield cable can change quite significantly, thereby affecting the costs. As the turbine layout has a direct impact on the cable layout, it is important for a layout optimisation tool to take this into account. This tool therefore implements an intra-array cable optimisation tool in order to determine the cost of the electrical system for each turbine layout under consideration.

The authors have previously developed an optimisation methodology for optimising the intra-array cable network of an offshore wind farm (Pillai et al., 2015). This approach accounts for real wind farm planning constraints in order to determine the optimal positions for the necessary offshore substations and then designs an intra-array collection network that minimises both the cost and the peak losses.

The optimisation tool first determines the optimal positions of the substations on the basis of a modified kmeans++ algorithm. Kmeans++ is a modified version of the commonly used kmeans clustering algorithm that uses a weighted random approach to seed the initial cluster centres, resulting in both better solutions and quicker runtimes than the original kmeans algorithm (MacQueen, 1967; Arthur and Vassilvitskii, 2006). For this tool, the kmeans++ algorithm is further constrained to account for the capacity constraints of each substation and the fact that within the wind farm area there are regions where substations cannot be placed. A pathfinding algorithm based on Delaunay triangulation is then used to determine possible cable paths for each turbine and the respective cost of these paths. The pathfinding algorithm is used to account for the areas in which cables cannot be laid due to seabed constraints and obstacles. Finally, a capacitated minimum spanning tree (CMST) is constructed on the basis of the cable costs found in the pathfinding step. The CMST represents the optimal network and is solved through the use of Gurobi, a commercial mixed-integer linear programming (MILP) software. An iterative approach is taken in order to eliminate any cable crossings in the solution. This tool has been previously applied to large wind farms and has been found to offer significant reductions in the total cable needed when compared to industry standard approaches (Pillai et al., 2015).

Cost Assessment

Previous works that have included a cost breakdown typically have not been able to validate their cost models and as a result, have introduced significant uncertainty into the optimality of their solutions (Elkinton, 2007; Fagerfjäll, 2010). As this tool has been developed in conjunction with EDF Energy R&D UK Centre, it has been possible to directly develop and validate the cost assessment methodologies. Consequently, this work presents costs that have been parameterised and validated against real costs expected to be incurred by large offshore wind farms deploying wind turbines in the 5–8 MW range in UK waters.

The total cost of the wind farm is broken down into eight major cost elements:

1. Turbine supply
2. Turbine installation
3. Foundation supply
4. Foundation installation
5. Intra-array cables (supply and installation)
6. Decommissioning
7. Operations and maintenance (O&M)
8. Offshore transmission assets

Turbine Supply. The turbine supply costs are determined on the basis of the price per turbine that turbine manufacturers have provided. This cost, therefore, does not vary due to the layout unless the total number of turbines or installed capacity changes.

Turbine Installation. The turbine installation costs are based on the market values for vessel costs and capacities and are modelled by the total amount of time needed to install all the turbines at their specific locations. This includes not only the computation of the travel time between the turbines but also the necessary time to go to and from the construction port. To calculate this, the turbines are clustered on the basis of the capacity of the installation vessel, and for each cluster a shortest path is computed between the port, each turbine in the cluster, and the port again. This approach, therefore, accurately computes the distance that the vessel must travel during the installation process. From this, the total time is computed on the basis of the assumed weather availability, and the costs are computed on the basis of the vessel and equipment day rates. The turbine layout, therefore, has a direct impact on the time needed to travel between turbine positions as well as to and from the port.

Foundation Supply. Foundation costs are found to be highly dependent on the site conditions where the foundation is to be installed. To account for this dependence, previous cost models

have attempted a bottom-up approach based on the soil characteristics at the installation site to model the costs. Unfortunately, this approach has proven to be difficult to validate for all foundation types (Elkinton, 2007). For this tool, therefore, a depth dependency has been developed from discussions with manufacturers, but the specific soil conditions are not included. Larger turbines in the 5–8 MW range are more likely to use jacket foundations that have been found to be less sensitive to the soil conditions than to the depth (Elkinton, 2007). Detailed bathymetry of the site is therefore necessary in order to accurately estimate the variation in foundation supply costs as a function of the turbine layout. For a jacket foundation, the cost from discussions with manufacturers was found to follow empirically the nonlinear relationship given below:

$$C_{\text{foundation}} \propto D^{0.7574} \tag{2}$$

Foundation Installation. The foundation installation process, like the turbine installation module, is based on estimating the time needed to complete the operations and converting this time to a cost. Unlike the turbine installation, however, this is modelled as three distinct phases that each uses a different vessel to complete the operations.

Regardless of the foundation type (gravity-based, monopile, or jacket), some seabed preparation is necessary. For a gravity-based foundation, this might be the necessary dredging and levelling of the seabed, while for monopiles and jackets, this would more likely be pre-pilling works including surveying and drilling. After this step, the foundations will be installed as a separate operation, following which some kind of scour protection will often be added. The installation of scour protection is again modelled as a separate step involving a different vessel from either the site preparation or foundation installation processes. Under some conditions, the scour protection will not be necessary; however, for the time being this model has assumed that all turbines will require scour protection.

Intra-array Cable Costs. The required total horizontal length of intra-array cables is computed from the intra-array cable optimisation tool described earlier. This tool is described in detail in previous work by the authors (Pillai et al., 2015). This tool has the support for optimising the layout for different cable cross-section sizes and therefore can output not only the total length of cable but also the horizontal lengths required for each segment and the required cross-section. From this, the intra-array cable cost module computes the necessary vertical cable and the necessary spare cable before computing the costs.

After the supply cost is calculated, the installation cost is computed in a similar manner to the turbine and foundation installation modules. This is done on the basis of the data available for cable trenching vessels and therefore assumes that all cables are trenched and buried.

Decommissioning. The decommissioning costs include the removal of the turbines and foundations. At the moment, it is unclear what will happen to the transmission and export cables. The model therefore assumes that these cables are not removed at the time of decommissioning but are simply cut at the turbines and substation, so the buried lengths are left as they are. The decommissioning costs are therefore modelled similarly to the installation processes, with the time required by each vessel computed first before it is converted to a cost. Like the installation processes, it is assumed that the vessels have some finite capacity and must return to the decommissioning port during the overall operation. The turbines and foundations are assumed to be decommissioned in separate steps requiring separate vessels. Like the installation phases, this term is therefore dependent on the turbine positions and is affected by the proposed layout.

Cost Element	CAPEX	OPEX	Sensitivity to Layout
Turbine supply	Yes	–	Low
Turbine installation	Yes	–	Medium
Foundation supply	Yes	–	Medium
Foundation installation	Yes	–	Medium
Intra-array cable	Yes	–	High
Decommissioning	Yes[1]	–	Medium
Operations and maintenance	–	Yes	Medium
Offshore transmission assets	Yes	Yes	Low

[1]Though categorised as a CAPEX term, this cost is applied only to the years during which decommissioning occurs at the end of life.

Table 1 Cost element contribution to CAPEX/OPEX

Operations and Maintenance. The operations and maintenance costs are based on a tool developed by EDF Energy R&D UK Centre that models the anticipated operations and maintenance costs of a project so that they vary with the project's distance from the operations and maintenance port and the capacity of the project. As this term is affected by the distance of the wind farm from the operations and maintenance port, this term is also affected by the layout. The operations and maintenance costs are classed as Operational Expenditure (OPEX) as these are incurred during each year of operation as opposed to the preceding cost elements that are incurred only during the construction period and are therefore classed as Capital Expenditure (CAPEX) elements.

Offshore Transmission Assets. The final cost element of this cost model is the inclusion of the offshore transmission assets and the offshore transmission asset transfer fees. In the UK, the offshore substation, export cables, and onshore substation must be owned and operated by a separate company from the wind farm operator. Practically, therefore, most wind farm developers build these assets and then transfer them to a transmission operator before commissioning the wind farm. As a result, only some of the CAPEX is incurred by the project, and the rest is incurred as a component of the transmission fee along with regionally-based costs set by the network operator, which is National Grid in the UK. Both the CAPEX and OPEX components of the Offshore Transmission Owner's assets have been computed in discussion with National Grid and equipment manufacturers on the basis of the capacity of the assets.

Table 1 summarises each of the cost element contributions to both CAPEX and OPEX as well as the relative sensitivity of each of these elements to the wind farm layout.

Constraints

An important step for all optimisation routines is to clearly define the constraints that must be applied and that limit the solution space. In this case, the intra-array cables are optimised as part of the evaluation function for the larger turbine placement problem, and there are a number of constraints to be considered just for this subproblem, which are separate from those that explicitly constrain the turbine placement.

First, the site boundary defines the area in which turbine foundations can be placed. As developers are required to keep the

entire wind turbine within their leased turbine area, the boundary is adjusted through the use of GIS software to include the necessary negative buffer to account for the size of the turbine blades. The boundary used by this tool therefore represents a smaller region than the overall turbine area.

Second, within the site there may be areas containing unexploded ordnance (UXOs) or wrecks. These areas generally cannot contain turbines or cables and are therefore treated as exclusion areas by the optimiser. Similarly, turbines generally cannot be placed in areas where the seabed slope is too steep. Generally, areas over a slope of 5% will be considered to be too steep for turbines and are similarly treated as exclusion areas. All areas also have an additional 50-m buffer area. Through the use of the grid generation method, these placement constraints are implicitly satisfied for the turbines within the wind farm and need to be considered only for the substation and intra-array cables.

Third, the turbines generally need to be a minimum distance away from one another for safety and navigational reasons. These distances are generally given as exclusion circles around each turbine; however, consenting bodies may alternatively give separate downwind and crosswind distances defining an exclusion ellipse. These ellipses will generally require more significant separation in the downwind direction than in the crosswind direction.

Finally, in the case of most UK offshore wind farms, consenting bodies have stipulated that the layout of turbines in offshore wind farms should have some degree of uniformity to ensure safe passage through the farm and not to act as a hindrance to search and rescue operations (NOREL Group, 2013). This constraint is explicitly satisfied by the grid generation approach prior to the execution of the GA. By doing this, a clear grid is defined on which turbines can be placed. As this constraint is already considered, it is not implemented within the framework of the GA.

The intra-array cable optimisation also has a number of constraints unique to its subproblem. These include not only that the cables and substations must be within the turbine area and may not enter the exclusion areas (the seabed slope is not an exclusion area for cables), but also that (1) power cannot be stored at a turbine, and therefore the intra-array cable network must be balanced; (2) turbines have a limited number of connection points, and therefore a maximum number of cables that connect to a turbine exists; (3) cables may not intersect except at the substation or at turbines; and (4) cables have a finite capacity that cannot be exceeded (Pillai et al., 2015).

Genetic Algorithm

GAs are a type of population-based evolutionary algorithm that are well suited to a variety of problem types (Holland, 1992). GAs have previously been deployed for optimising offshore wind farm layouts and have generally been found to offer good solutions to the problem at hand (Elkinton, 2007; Guillen, 2010; Larsen et al., 2011).

GAs are so-named as they borrow from biological evolution and have algorithms analogous to genetic principles. In a GA, the solutions are thought of as genomes with each turbine position thought of as a gene. GAs operate on a population basis, i.e., a population of solutions is considered in which the best solutions have a higher probability of passing on genes to members of the next generation. The flowchart in Fig. 1 outlines the operating principles of a GA and the steps involved. The unique aspect of the GA at hand is that rather than implementing a generic GA and then testing for compliance within the evaluation function, the crossover and mutation steps have been designed specifically to include the constraints. In this case, because a predefined grid has been created during the grid generation step, the genes of the GA are binary and represent the presence of a turbine at the specific grid locations. There is one gene per grid location.

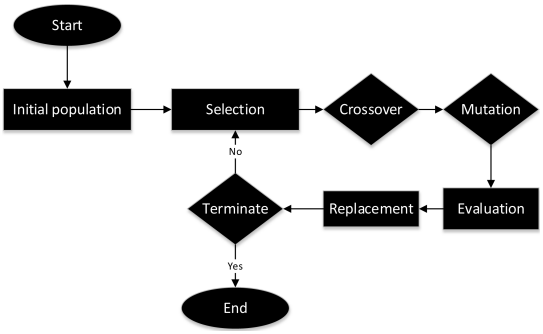

Fig. 1 Layout optimisation approach

For the implementation at hand, the problem was formulated as a minimisation problem in which the fitness of an individual was given by its LCOE. In this case, individuals with lower LCOE values correlate with a higher fitness. For this tool, the fitness values have not been scaled.

The initial population is created through the generation of random strings of 1's and 0's representing potential individuals. The individuals are created in such a way that all have the correct number of turbines and are unique individuals. Each individual is then checked to ensure that the placement satisfies all constraints, and if any individuals are invalid, they are regenerated. This ultimately produces a population containing random, valid individuals from which the evolution can proceed.

Selection. Selection is the process through which two individuals of the population are chosen to contribute genetic material to member(s) of the new population. The selected individuals then act as parents to children (new solutions) of the new generation. Though there are a number of different types of selection approaches, a roulette wheel section algorithm was deployed for this. Roulette selection, also known as fitness proportionate selection, assigns a probability to each member of the population on the basis of each member's fitness value. In this sense, better solutions have a higher probability of selection than worse solutions. The probability of selection is given by

$$P_{s,i} = 1 - \frac{f_i}{\sum_i f_i} \tag{3}$$

where $P_{s,i}$ is the probability that individual i is selected, and f_i is the fitness of individual i. As this problem is structured as a minimisation problem, lower LCOE values will correspond to a higher probability of selection.

Crossover. Crossover is the principal genetic operator that is used to combine the selected parents to create children. In crossover, part of the genetic material from each parent is combined in such a way that it does not violate the constraints in order to create two new individuals who will potentially be added to the population. As a discrete GA has been implemented here, approximately 50% of the genes should come from each of the parents. In order to do this, a uniform crossover or crossover mask approach is applied. In a crossover mask, each gene is randomly assigned to one of the parents. If a gene is assigned to a parent,

then the first child has the same value for this gene as its parent. To generate a second child that is a foil to the first child, the crossover mask is flipped (all 1s become 0s and vice versa). Each of the children is checked against the minimum separation constraint, and in the event of an invalid solution, the mask is regenerated. The crossover mask generation procedure maintains the number of turbines such that this constraint does not need to be checked following crossover. If crossover will occur, it will be a probabilistic event, and there exists a chance that crossover will not occur, and the two children solutions will identically match the parents. This can also happen even if crossover does occur though the probability is very low.

Mutation. The other genetic operator that is applied to solutions is mutation. Mutation randomly changes part of the solution. In this implementation, there is a low probability that a bit gets flipped (i.e., a 1 becomes a 0, and a 0 becomes a 1). Whereas crossover explores solutions similar to the existing solutions, mutation randomly explores the remaining regions of the solution space. The mutation operator is necessary to ensure that the solution does not converge to a local solution but rather finds the global solution. Like crossover, the mutated children are checked against the constraints as well as the number of turbines, and mutation happens repeatedly until a valid solution is generated.

In this tool, adaptive crossover and mutation operators based on the existing literature have been applied (Srinivas and Patnaik, 1994). The adaptive crossover and mutation rates are implemented to allow the algorithm to self-tune and to correctly ensure that bad solutions have a higher probability of changing. Similarly, this adaptive approach to these parameters allows the algorithm to better maintain a diverse population of the solution as the solution converges, thereby allowing the GA to continue to operate effectively without terminating prematurely. These adaptive parameters are given by

$$p_c = \frac{k_1(f_{\max} - f')}{f_{\max} - \bar{f}} \quad \text{for } f' \geq \bar{f} \tag{4}$$

$$p_c = k_3 \quad \text{for } f' < \bar{f} \tag{5}$$

$$p_m = \frac{k_2(f_{\max} - f)}{f_{\max} - \bar{f}} \quad \text{for } f \geq \bar{f} \tag{6}$$

$$p_m = k_4 \quad \text{for } f < \bar{f} \tag{7}$$

where p_c is the probability of crossover, p_m is the probability of mutation, $f_{\max}$ is the fitness of the best individual of the population, f' is the fitness of the best parent, $\bar{f}$ is the mean fitness value of the individuals in the population, and f is the fitness of the individual under consideration. The constants are defined such that $k_1 = k_3 = 1$ and $k_2 = k_4 = \frac{1}{2}$.

Replacement. The final step of a steady-state GA procedure is to introduce the newly generated individuals into the next generation of the population. As an elitism parameter is used, the very best individuals within the population are carried over to the next generation, and the remaining members of the population are replaced by the newly generated individuals. In this routine, a "replace first weakest" approach is taken. In this replacement strategy, child solutions are compared with the worst members in the current generation's population. If the child solution has a superior fitness value compared to the worst member of the population, then the child is marked for inclusion in the next generation, and the worst member is marked for removal. The process continues, each time comparing the child's fitness against the worst member of the population that has not yet been marked for removal. In this specific case, an elitism parameter of 50% is used. The process, therefore, continues until 50% of the population has been replaced by new individuals. This entire GA process is repeated until the solutions converge or the termination criteria are met.

For this study, a test case involving thirty turbines in a 47 km^2 area was considered. For this area, bathymetry and seabed surveys were available for defining the depth, the areas where turbines cannot be placed, and the areas where cables cannot be placed.

The GA was executed with a population size of fifty. Previous work has found that for specific problem instances, a smaller population size of approximately twenty to thirty individuals may work effectively (Haupt and Haupt, 2004; Grefenstette, 2006). For this problem, however, it was found that a population size smaller than fifty led to a loss of diversity after very few generations, resulting in little improvement in the best individual before termination. Diversity in this case was defined as the proportion of the population that was unique solutions. A larger population size was therefore selected in order to ensure that diversity was maintained through the optimisation process. The full parameters of the executed GA are given in Table 2.

For each proposed solution, the energy yield was first assessed, followed by the execution of the intra-array cable optimiser after which the cost for the proposed layout was assessed. From this, the LCOE was evaluated assuming a constant Capital Expenditure (CAPEX) spend profile (50% each over two years), a twenty-year project lifetime prior to decommissioning, and a discount rate of 8%.

A representative wind rose for a UK offshore site is assumed. This wind rose has strong winds principally from the south/southwest direction; therefore, this direction is identified as

Parameter	Value
GA Encoding	Discrete
Population size	50
Maximum generations	100
Probability of crossover	Adaptive
Probability of mutation	Adaptive
Elitism	50%
Stop criteria	Loss of diversity or maximum number of generations reached

Table 2 GA parameters

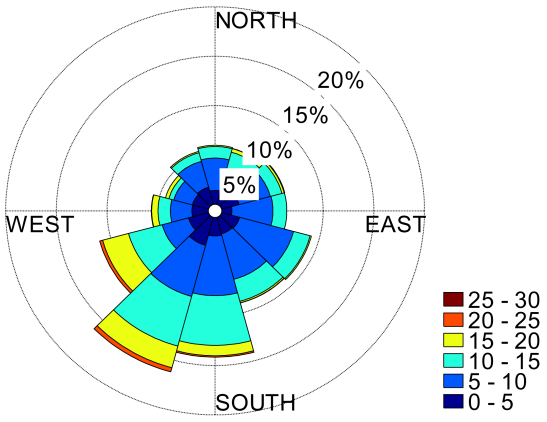

Fig. 2 Wind rose representing the wind resource for the test case

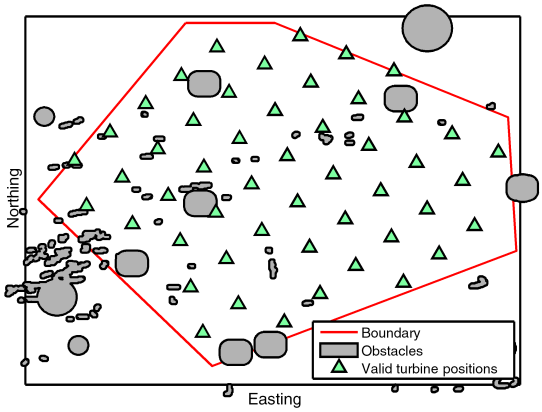

Fig. 3 Generated grid of valid turbine positions from which turbine positions are selected

the principal direction in which turbines should be aligned. This wind rose does not represent any site in particular but is simply used for the demonstration of the capabilities of this tool.

Given the wind rose shown in Fig. 2, the tool next generates a grid of potential turbine positions. This grid contains fifty possible turbine positions aligned roughly perpendicular to the dominant wind direction. The grid generation algorithm removes positions on the grid that are in illegal positions shown in grey in Fig. 3. These illegal positions can be due to wrecks, UXOs, or the seabed slope. Each row of the grid is offset to ensure that the distance between turbines is increased along this dominant wind direction.

RESULTS

Executing the full approach for a wind farm containing thirty turbines resulted in the layout shown in Fig. 4 after thirteen generations. This solution was based on generating a grid made up of fifty potential turbine positions. This grid size was selected to ensure that there were more possible turbine positions than turbines. The solution produced does adhere to the site constraints and produces a solution that conforms to a regular grid, thereby satisfying the necessary navigational and search and rescue constraints. The solution produced also leaves larger gaps between

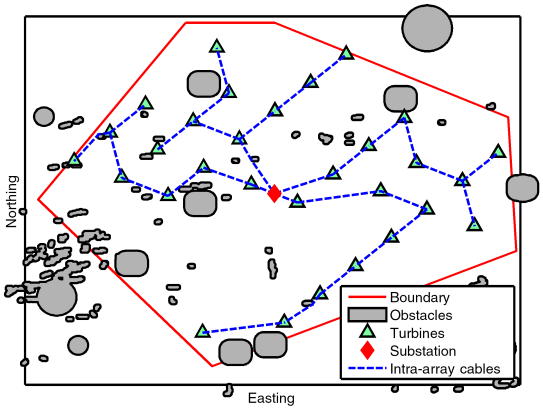

Fig. 4 Optimised turbine placement. LCOE for this layout is £89.51/MWh.

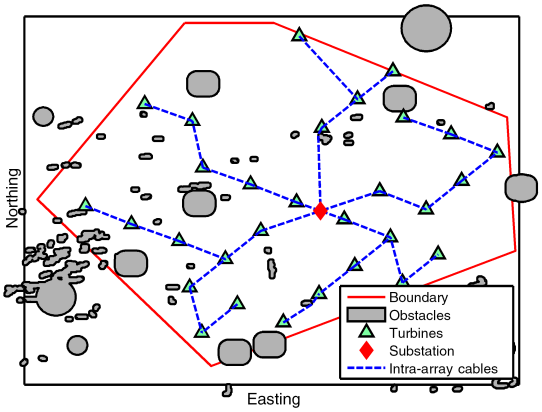

Fig. 5 An inferior layout proposed by the optimiser during the first generation. LCOE for this layout is £92.45/MWh.

turbines in the interior of the wind farm, which is consistent with the relevant theory of wind turbine wakes and allows the wakes to recover before a new turbine is placed. Though significant gaps are left, the optimiser does not eliminate turbines from the centre of the wind farm. This indicates that the AEP can still be increased but likely at a higher cost. The presence of the turbines in the centre of the wind farm indicates the importance of considering not only the wakes but also the cost of the wind farm.

Figure 5 shows an inferior turbine layout proposed during the first generation of the optimisation process, which has a higher LCOE of £92.45/MWh. As can be observed, fewer holes are left at the site, while a few turbines are isolated. The combined effect of this is that wake effects are not effectively minimised and costs are unnecessarily increased to accommodate the inclusion of the isolated turbines.

The approach ensures that all constraints are satisfied while at the same time using a dynamic spacing parameter to minimise the effect of wind turbine wakes and thereby the LCOE.

From the convergence plot in Fig. 6, it can be seen that over the execution of the algorithm, both the best and mean solution scores progressively improved. This indicates that the GA was operating as expected. The final solution identified by the GA has an LCOE of £89.51/MWh.

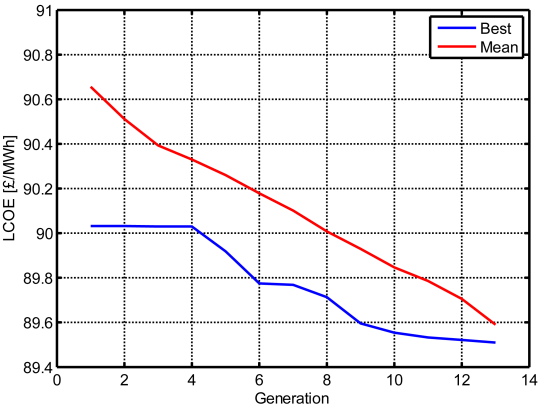

Fig. 6 Minimal and mean LCOE over generations

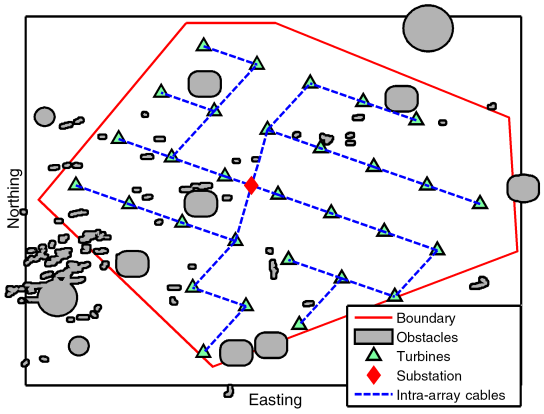

Fig. 7 The layout proposed by the use of DNV-GL WindFarmer's Symmetrical Optimiser. LCOE for this layout is £90.53/MWh.

Running DNV GL WindFarmer's Symmetrical Layout Optimisation as a benchmark on the same site yields a layout optimised for the AEP (see Fig. 7). This layout, which represents the industry standard approach to designing offshore wind farms, produces a layout with an LCOE of £90.53/MWh when evaluated through the use of our evaluation function. This is slightly higher than the solution produced by this tool and, broken down, represents a 0.69% decrease in the discounted AEP and a 0.44% increase in the discounted cost compared to the solution generated by the GA shown in Fig. 4. Though WindFarmer does not allow LCOE optimisation, it does represent the industry standard approach to designing wind farms. Further improvements to the proposed layout through the use of the methodology at hand could likely be found if the GA were run for more generations. Unfortunately, diversity was not maintained in the population, and the optimiser was forced to stop prematurely.

The scatter diagram in Fig. 8 indicates the mean wind speed experienced by all turbines in each wind speed bin for different layouts relative to the mean free wind speed in each directional sector. Through the use of this approach for comparing the layouts, the relative wake loss in the wind direction can be observed.

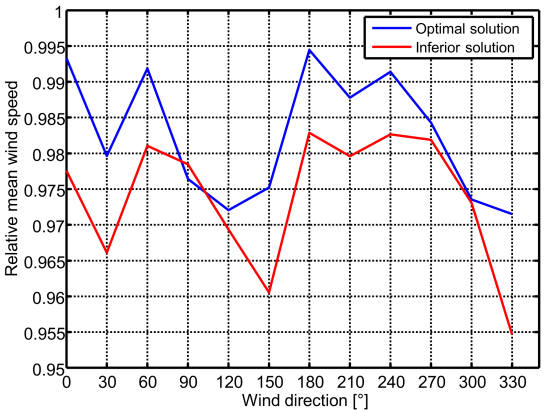

Fig. 8 Scatter diagram showing the mean wind speed experienced through the wind farm for each direction sector for different layouts relative to the mean free wind speed in each direction

From this figure, it can be observed that the inferior layout shown in Fig. 5 leads to more significant reductions in the average wind speed in all wind directions than the more optimal layout shown in Fig. 4. Though the relative decrease in wind speed is small, it is important to note that the power extracted by a wind turbine varies with the cube of the wind speed. Also, this figure does not consider the frequency of the wind directions but is simply used to illustrate one of the key drivers of the LCOE. The overall wake loss is 4.39% for the inferior layout and 3.50% for the more optimal layout, resulting in a change in the AEP of 10,000 MWh per year.

DISCUSSION AND CONCLUSIONS

The present work has highlighted the initial results from the development of a framework for the optimisation of offshore wind farm layouts using an adaptive genetic algorithm. It is believed that this framework will be useful in furthering the field of offshore wind farm layout optimisation and allowing developers to better understand the characteristics of their potential projects. The approach taken has introduced as many realistic constraints as possible in order to maximise the value of the framework while at the same time striving for an accurate assessment of the energy yield of the wind farm, the costs, and the LCOE.

For the test case considered, a fifty-position discrete grid was generated prior to execution of the GA. This grid was oriented such that rows of turbines were perpendicular to the dominant wind direction. From this, the GA selected which thirty of the fifty positions should be used. Interestingly, there is a difference of approximately £2/MWh between the worst result of the first generation and the best result of the last generation, indicating that significant savings can be reached through the application of an optimisation algorithm rather than the random selection of the positions. A comparison of the results of the GA with those of the industry standard approach using DNV-GL WindFarmer also shows a £1/MWh improvement in the LCOE through the optimisation of the layout considering the LCOE using the GA rather than the AEP using WindFarmer's built-in optimisation approach.

The number of valid turbine positions was selected arbitrarily to demonstrate the capabilities of this framework. Future work using this framework should explore the relationship between the number of turbines to be placed and the number of possible turbine positions in the discrete grid. Realistically, it would be expected that as the number of possible turbine positions increases, the solutions should improve in fitness; however, at the same time as the number of possible positions increases, the regularity of the layout decreases, and the search and rescue constraints will not remain satisfied. At the same time, the computational complexity will increase. With a grid including fewer holes than turbines, it was found that the search and rescue and navigational constraints were always satisfied; however, further work should explicitly explore this. Presently, the number of turbines to be positioned is also an input to the tool, and further work should explore allowing the algorithm to select this with a maximum number of turbine constraints.

From the minimal and mean LCOE over generations plot shown in Fig. 6, it can be seen that even though adaptive mutation and crossover rates are used, the GA still has some generations in which the overall population improves, but the best solution does not improve. This indicates that further work could explore tuning of the GA parameters to improve the number of generations it takes to converge. Presently, however, the GA is terminating due to a loss of diversity rather than true convergence, and improvements can be expected if methods for maintaining diversity in the

population are introduced to the GA. Having said this, even without any further tuning, the GA still manages to identify a layout with a lower LCOE compared to the industry standard approach using DNV-GL WindFarmer. This highlights not only the need to optimise for a metric by taking into account both energy yield and cost but also the advantage of introducing holes into a regular layout.

Given this platform, future work will expand on this study and examine not only further tuning the GA parameters to effectively solve this problem but also benchmarking the GA against alternate optimisation algorithms. This platform will also allow alternate objective functions, such as the levelised production cost (LPC) or net present value (NPV), to be explored.

The application of this framework will also allow simplifications of the evaluation function to be explored. Presently, the evaluation function is relatively detailed with the majority of time being spent on evaluating the intra-array cable infrastructure and optimising this for each turbine layout under consideration. Having said this, each evaluation call on an 8-core computer is still completed in under a minute. Future work using this framework will also be capable of comparing the results through the use of alternate evaluation functions and characterising which elements of the layout the objective function is most sensitive to. At the same time, however, it is believed that the tool can scale to larger problems representing realistic offshore wind farms without an unrealistic increase in the computational power required. One iteration of fifty individuals has been run on a multi-cored desktop machine; however, it is expected that for a full-sized wind farm the execution of the tool will be transferred to a cluster, which allows the larger problem to be solved in timescales similar to those in the test case through the utilisation of more cores in parallel. Moving away from a single processor will also allow larger population sizes to be explored, which potentially allows the premature convergence problems to be avoided. Realistically for a full wind farm it would be expected that in lieu of using an extremely large population, multiple runs will be completed using slightly larger populations with random seeding in order to ensure that the search space is effectively explored.

The applicability of this tool to larger offshore wind farms is still limited due to the simplification of the wakes and the omission of the interactions between wind turbines and the atmospheric boundary layer (Frandsen et al., 2006). This large wind farm or deep-array effect has been explored through the addition of corrections to analytic wake models (Barthelmie et al., 2007; Brower and Robinson, 2009). Future work intends to use the constructed framework to validate and tune these correction factors before applying them to the overall layout optimisation approach.

ACKNOWLEDGEMENTS

This work is funded in part by the Energy Technologies Institute (ETI) and Research Councils UK (RCUK) Energy programme for the Industrial Doctorate Centre in Offshore Renewable Technologies (IDCORE) (EP/J500847/1).

REFERENCES

Ainslie, J (1988). "Calculating the Flowfield in the Wake of Wind Turbines," *J Wind Eng Ind Aerodyn*, 27, 213–224. http://dx.doi.org/10.1016/0167-6105(88)90037-2.

Anderson, M (2009). *Simplified Solution to the Eddy-Viscosity Wake Model*, Renewable Energy Systems Ltd, 7 pp.

Arthur, D, and Vassilvitskii, S (2006). "k-means ++?: The Advantages of Careful Seeding," *Proc 18th Annu ACM-SIAM Symp Discrete Algorithms*, New Orleans, LA, USA, 8, 1–11.

Barthelmie, RJ, et al. (2006). "Comparison of Wake Model Simulations with Offshore Wind Turbine Wake Profiles Measured by Sodar," *J Atmos Oceanic Technol*, 23(7), 888–901. http://dx.doi.org/10.1175/JTECH1886.1.

Barthelmie, RJ, et al. (2007). "Modelling and Measurements of Wakes in Large Wind Farms," *J Phys Conf Ser*, 75, 012049. http://dx.doi.org/10.1088/1742-6596/75/1/012049.

Barthelmie, RJ, et al. (2009). "Modelling and Measuring Flow and Wind Turbine Wakes in Large Wind Farms Offshore," *Wind Energy*, 12(5), 431–444. http://dx.doi.org/10.1002/we.348.

Brower, M, and Robinson, N (2009). *The OpenWind Deep-array Wake Model: Development and Validation*, AWS Truepower LLC, 17 pp.

Burton, T, Jenkins, N, Sharpe, D, and Bossanyi, E (2011). *Wind Energy Handbook*, 2nd Ed, John Wiley & Sons, Ltd, 780 pp.

Crasto, G, and Castellani, F (2013). "Wakes Calculation in an Offshore Wind Farm," *Wind Eng*, 37(3), 269–280. http://dx.doi.org/10.1260/0309-524X.37.3.269.

DNV GL - Energy (2014). *WindFarmer Theory Manual*, Høvik, Norway.

Elkinton, CN (2007). *Offshore Wind Farm Layout Optimization*, PhD Thesis, University of Massachussetts, Amherst, MA, USA.

Fagerfjäll, P (2010). *Optimizing Wind Farm Layout – More Bang for the Buck Using Mixed Integer Linear Programming*, Master's Thesis, Chalmers University of Technology and Gothenburgh University, Göteborg, Sweden.

Frandsen, S, Barthelmie, R, and Pryor, S (2006). "Analytical Modelling of Wind Speed Deficit in Large Offshore Wind Farms," *Wind Energy*, 9(1), 39–53. http://dx.doi.org/10.1002/we.189.

Gaumond, M, Rethore, P, and Bechmann, A (2012). "Benchmarking of Wind Turbine Wake Models in Large Offshore Windfarms," Presented at *Sci Making Torque Wind Conf 2012*, Oldenburg, Germany.

Grady, SA, Hussaini, MY, and Abdullah, MM (2005). "Placement of Wind Turbines Using Genetic Algorithms," *Renewable Energy*, 30(2), 259–270. http://dx.doi.org/10.1016/j.renene.2004.05.007.

Grefenstette, JJ (2006). "Optimization of Control Parameters for Genetic Algorithms," *IEEE Trans Syst Man Cybern*, SMC-16(1), 122–128. http://dx.doi.org/10.1109/TSMC.1986.289288.

Guillen, FB (2010). *Development of a Design Tool for Offshore Wind Farm Layout Optimization*, MSc Thesis, Delft University of Technology, Delft, Netherlands.

Haupt, R, and Haupt, SE (2004). *Practical Genetic Algorithms*, 2nd Ed, Wiley-Interscience Publication, 272 pp.

Holland, JH (1992). *Adaptation in Natural and Artificial Systems: An Introductory Analysis with Applications to Biology, Control, and Artificial Intelligence*, 2nd edition, MIT Press, 211 pp.

Ishihara, T, Yamaguchi, A, and Fujino, Y (2004). "Development of a New Wake Model Based on a Wind Tunnel Experiment," In: *Global Wind Power*, 6.

Katic, I, Højstrup, J, and Jensen, NO (1986). "A Simple Model for Cluster Efficiency," *Proc Eur Wind Energy Conf Exhib 1986*, W Palz and E Sesto (Eds), Rome, Italy, 1, 407–410.

Larsen, GC (1988). *A Simple Wake Calculation Procedure*, Risø-M, No 2760, Risø National Laboratory, Technical University of Denmark, Roskilde, Denmark.

Larsen, GC, and Réthoré, PE (2013). *TOPFARM - A Tool For Wind Farm Optimization*, Risø National Laboratory, Technical University of Denmark, Roskilde, Denmark.

Larsen, GC, et al. (2011). *TOPFARM – Next Generation Design Tool for Optimisation of Wind Farm Topology and Operation*, Information Service Department, Risø National Laboratory for Sustainable Energy, Technical University of Denmark, Roskilde, Denmark.

MacQueen, J (1967). "Some Methods for Classification and Analysis of Multivariate Observations," *Proc 5th Berkeley Symp Math Stat Probab*, Berkeley, CA, USA, 1, 281–297. http://projecteuclid.org/euclid.bsmsp/1200512992.

Mosetti, G, Poloni, C, and Diviacco, B (1994). "Optimization of Wind Turbine Positioning in Large Wind-farms by Means of a Genetic Algorithm," *J Wind Eng Ind Aerodyn*, 51(1), 105–116. http://dx.doi.org/10.1016/0167-6105(94)90080-9.

NOREL Group (2013). *Action Points from the 27th NOREL held on 11 July 2013*, Nautical and Offshore Renewable Energy Liaison Group (NOREL), UK.

Pérez, B, Mínguez, R, and Guanche, R (2013). "Offshore Wind Farm Layout Optimization Using Mathematical Programming Techniques," *Renewable Energy*, 53, 389–399. http://dx.doi.org/10.1016/j.renene.2012.12.007.

Pillai, AC, Chick, J, and de Laleu, V (2014). "Modelling Wind Turbine Wakes at Middelgrunden Wind Farm," Presented at *Eur Wind Energy Assoc Annu Conf 2014*, Barcelona, Spain, EWEA.

Pillai, AC, Chick, J, Johanning, L, Khorasanchi, M, and de Laleu, V (2015). "Offshore Wind Farm Electrical Cable Layout Optimization," *Eng Optim*, 47(12), 1689–1708. http://dx.doi.org/10.1080/0305215X.2014.992892.

Renkema, DJ (2007). *Validation of Wind Turbine Wake Models*, MSc Thesis, Delft University of Technology, Delft, Netherlands.

Sanderse, B, Pijl, S, and Koren, B (2011). "Review of Computational Fluid Dynamics for Wind Turbine Wake Aerodynamics," *Wind Energy*, 14(7), 799–819. http://dx.doi.org/10.1002/we.458.

Schlez, W, and Neubert, A (2009). "New Developments in Large Wind Farm Modelling," *Proc Eur Wind Energy Conf Exhib 2009*, Marseille, France, EWEA, 8 pp.

Srinivas, M, and Patnaik, LM (1994). "Adaptive Probabilities of Crossover and Mutation in Genetic Algorithms," *IEEE Trans Syst Man Cybern*, 24(4), 656–667. http://dx.doi.org/10.1109/21.286385.

Modelling Wind Turbine Wakes at Middelgrunden Wind Farm

Ajit C Pillai
IDCORE
The University of Edinburgh
a.pillai@ed.ac.uk

Dr. John Chick
Institute for Energy Systems
The University of Edinburgh
john.chick@ed.ac.uk

Vincent de Laleu
EDF Energy
R&D UK Centre
vincent.delaleu@edfenergy.com

Abstract

As part of the development of an offshore wind farm layout optimisation tool, this paper explores the accuracy and computational time of wake models applied to Middelgrunden Wind Farm outside of Copenhagen, Denmark. In this study, four years of data from 2001 to 2004 are used to test the applicability, accuracy, and computational time of the Jensen, Larsen, Ishihara, and a simplified version of the Ainslie Eddy-Viscosity wake models. This study has shown that the size of the directional sector used in the comparison and if that directional sector is applied to all turbines' incoming wind velocities or just the northernmost greatly affects the results. From this it is found that the Larsen wake model provides the best balance between accuracy and computational time. It also shows that even a simplified version of a field model takes significantly longer to compute than an analytic model. This study has also shown that using directional sectors of $\pm 15^{\circ}$ these models perform similarly to previous studies at Nysted and Horns Rev indicating that the close spacing (2.4D) at Middelgrunden is not too close for the use of these models.

Keywords: Middelgrunden wind farm, wake modelling, layout optimisation

1 Introduction

With continuing growth in the size of offshore wind farms, it has become increasingly more important to optimise the layout of wind farms in order to ensure that the wind farm extracts energy effectively. To this end, it is important to model and understand the turbine interactions offshore. In the development of a layout optimisation tool to be used to aid in the decision making process for future offshore wind farm projects, a comparative study of wind turbine wake models has been completed.

As a layout optimisation tool would be required to evaluate several different layouts, it is important for the wake model implemented as part of this tool to have both high accuracy and low computational time. In order to classify the existing wake models it was decided to use data available for Middelgrunden Wind Farm in Denmark to compare four existing wake models. The analytic models of Jensen, Larsen, and Ishihara were compared in terms of accuracy and computational time to one another and to a simplified representation of the Ainslie Eddy-Viscosity field model. The Middelgrunden site poses a unique opportunity as the turbines are spaced at only 2.4D. Though this close spacing is in a non-dominant wind direction, looking specifically at the time periods when the wind is in this direction allows us to establish how these wake models compare for closely spaced

turbines.

This paper will first outline the approach taken in this analysis in terms of how data was selected, and the impact that the data selection criteria had on the results, as well as the formulation used for each of the wake models. Following this, the results of the study are presented before the conclusions and scope for further work is outlined.

2 Approach

The advantage of the Middelgrunden site over other wind farms is that 10-minute averaged data for four years (2001-2004) is available courtesy of the Virtual Wakes Laboratory and Middelgrunden Windfarm Cooperative. Using this data and subsets of this data, it was possible to apply the wake models and compare the results. The site is, however, not the best suited for a wake study given that the dominant wind direction is perpendicular to the single line of turbines. Therefore the reduction in annual energy production (AEP) due to the wake effect is minimal.

The wake modelling done as part of this study can therefore be further subdivided into two major steps: data selection/filtering and the application of the wake models to the selected data periods.

2.1 Data Selection

Given previous studies of the wakes and modelling the turbulence intensity of the flow at Middelgrunden [1, 2] it was decided to use a similar methodology for the selection of data. The Middelgrunden wind farm is comprised of twenty Bonus B-76/2000 turbines placed along a single arc in a roughly North-South orientation. Wakes are therefore only expected when the wind direction is parallel to the dominant direction of this arc (357°). As wakes are the focus of this study, it was important to filter out the data periods during which the wind was perpendicular to the arc of the turbines resulting in little or no wake effect. Though winds from the South would be expected to result in measurable wake effects it is not considered in this study as due to the proximity to shore and as a result of the shorter fetch a more significant speed-up is observed [1].

It was also important to use time periods where data was available for all twenty turbines, all twenty were grid connected, and all were generating power. In order to do this, the data-set was filtered based on the mean active power for each interval to ensure that they were generating, and based on the generator RPM in order to ensure that they were grid-connected. Any time intervals where any one wind turbine was not operating or was in an error-state was immediately filtered out.

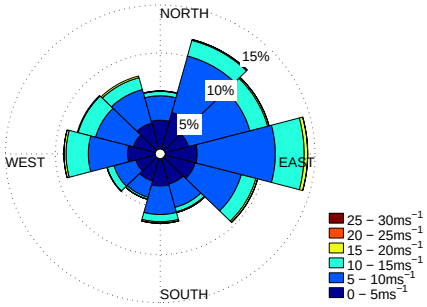

Figure 1: Characteristic wind rose for Middelgrunden Wind Farm based on time-series data from 2001-2004. Data used courtesy of The Middelgrunden Windfarm Cooperative.

Based on these filtering techniques, a number of different sector sizes were considered to observe how this affected the accuracy of the wake models. For each case, the same 357° azimuth was considered. It was also later decided to relax the direction criteria such that turbine 1, the northernmost turbine, was only checked against the incoming wind direction rather than all of the turbines. This is similar to the methodology used in similar studies at Horns Rev [3, 4].

2.2 Wake Models

As this study was completed as part of the development of a layout optimisation tool, it was decided to consider analytic wake models as these would be sufficiently fast to implement as part

Table 1: Data Selection Scenarios

Sector Size	Turbines Checked	Time Intervals
60°	All	1646
30°	All	25
60°	Turbine 1	4701
30°	Turbine 1	2299
20°	Turbine 1	1609
10°	Turbine 1	930
2°	Turbine 1	248

of the optimisation tools. For comparision purposes, a simplification of a field model, the Simplified Ainslie Eddy-Viscosity Model was also implemented. All four of the models under consideration are generally not recommended for use below 4D, though accurate results have been seen for as low as 1.7D. Middelgrunden therefore offers an interesting site to consider as the turbines are spaced at 2.4D [2].

Wake models in general require the thrust curve of the turbine to compute the velocity deficit through conservation of momentum. Some models also take into account the mixing of the air and therefore require a value for the ambient turbulence intensity. For this study, the thrust and power curves for the Bonus B76/2000 were provided in the literature [1]. Previous studies have also identified the ambient turbulence intensity to be approximately 13% which was used in this study [2].

2.2.1 Jensen Model

The simplest of the analytic wake models is the Jensen model which was originally devised in the 1980's. This wake model is based on momentum balance through the rotor plane of a single turbine and assumes that the wake expands linearly behind the rotor [3–6].

As the wake is assumed to expand linearly downstream of the turbine, the wake diameter d_w is given by:

$$d_w = d_r \times (1 + 2ks) \tag{1}$$

where d_r is the rotor diameter, k is the wake decay factor, and s is the non-dimensional distance downwind of the turbine ($s = \frac{x}{d_r}$, where x is the perpendicular distance downwind of the turbine) [6–8].

The wake decay factor, k, describes the relative persistence of the wake downstream of the turbine and can be related to the ambient turbulence intensity (I_a) [8, 9].

$$k = \frac{1}{2} I_a \tag{2}$$

According to this model, the wind velocity deficit experienced by a downstream turbine scales proportionally to the ratio of the rotor area that lies within a wake and is given by:

$$D_{i,j} = \frac{1 - \sqrt{(1 - C_{T_j})}}{(1 + 2ks)^2} \cdot \frac{A_{ij}}{A_i} \tag{3}$$

where C_{T_j} is the thrust coefficient of the upwind turbine j, A_{ij} is the area of intersection between the downstream turbine's rotor plane and the wake of the upstream turbine, and A_i is the rotor swept area of the downwind turbine i [8]. It is important to note that this model assumes that the thrust coefficient C_T does not exceed 1.

The above formulation accounts only for the wake behind a single turbine. However, further development of this model by Katic et al. [10] led to a means of superposing multiple single wakes to compute the total velocity deficit experienced by a turbine due to the combined effect of multiple upwind turbines using a root-sum-square formulation.

Using this updated formulation, the total velocity deficit factor D is given by:

$$D_i = \sqrt{\sum_j (D_{ij})^2} \tag{4}$$

The velocity experienced by the downwind turbine is therefore:

$$u_i = u_\infty \cdot (1 - D_i) \tag{5}$$

where u_∞ is the free stream wind speed.

2.2.2 Larsen Model

A subsequent analytic model that was developed was the Larsen Model which was included as

part of the European Wind Turbine Standards II (EWTS-II) [11]. This model is also an analytic wake model, however, unlike the Jensen model it does not assume a linear expansion, nor does it assume that the deficit is equal in the radial direction [3, 6, 12]. The model is based on a closed-form solution to the Reynolds-Averaged Navier-Stokes (RANS) equations based on Prandtl mixing theory.

Below are the key equations of the Larsen method:

$$u_\infty - u_i = -\frac{u_\infty}{9}\left[C_{T_j}A_i(x + x_0)^{-2}\right]^{\frac{1}{3}}\left[r^{\frac{3}{2}}\left(3c_1^2 C_{T_j}A_i(x + x_0)\right)^{-\frac{1}{2}} - \left(\frac{35}{2\pi}\right)^{\frac{3}{10}}\left(3c_1^2\right)^{-\frac{1}{5}}\right]^2 \tag{6}$$

$$R_w = \left(\frac{35}{2\pi}\right)^{\frac{1}{5}}\left(3c_1^2\right)^{\frac{1}{5}}\left(C_t A x\right)^{\frac{1}{3}} \tag{7}$$

The parameters x_0 and c_1 are given by:

$$x_0 = \frac{9.5d}{\left(\frac{2R_{9.5}}{d_{\text{eff}}}\right)^3 - 1} \tag{8}$$

$$c_1 = \left(\frac{d_{\text{eff}}}{2}\right)^{\frac{5}{2}}\left(\frac{105}{2\pi}\right)^{-\frac{1}{2}}\left(C_{T_j}A_i x_0\right)^{-\frac{5}{6}} \tag{9}$$

where d_{eff} is the effective rotor diameter, and $R_{9.5}$ is the wake radius at a distance of 9.5 rotor diameters downstream of the turbine. This term includes a correction to include the ground effect.

$$d_{\text{eff}} = d\sqrt{\frac{1+\sqrt{1-C_{T_j}}}{2\sqrt{1-C_{T_j}}}} \tag{10}$$

$$R_{9.5} = 0.5(R_{nb} + min(H, R_{nb}) \tag{11}$$

where H is the hub height, and R_{nb} is an empirically found relationship related to the ambient turbulence:

$$R_{nb} = max\left[1.08d, 1.08d + 21.7d(I_a - 0.05)\right] \tag{12}$$

No agreed upon method exists for superposing the single wakes modelled by the Larsen wake model, however, either linear superposition or root-sum-square superposition tend to be used. For this study, a similar root-sum-square superposition as was used in the Jensen model is used similar to eq. (4).

2.2.3 Ishihara Model

The Ishihara model is one of the lesser known analytic wake models which is rarely used in practice. Uniquely this model accounts for not only the ambient turbulence, however, includes a term for the mechanically generated turbulence in the wake recovery zone. This model was originally developed based on wind tunnel experiments, and therefore includes a number of empirical constants. Little work has been done in validation or calibration of this model and it is likely necessary for the empirical constants to be adjusted to better represent real wind farms [4, 13, 14]. Like the other models described, this is a single wake model for which a root-sum-square method has been implemented to account for the superposition of single wakes.

In this model, the wake diameter is given by:

$$d_w = \frac{k_1 C_{T_j}^{\frac{1}{4}}}{0.833} d^{1-\frac{p}{2}} x^{\frac{p}{2}} + d \tag{13}$$

where p is a function of the ambient turbulence I_a and the mechanically generated turbulence I_w.

$$p = k_2\left(I_a + I_w\right) \tag{14}$$

The mechanically generated turbine turbulence is given by:

$$I_w = \frac{k_3 C_T}{max\left(I_a, 0.03\right)}\left(1 - exp\left[-4\left(\frac{x}{10d}\right)^2\right]\right) \tag{15}$$

For a single wake, the velocity experienced by a downstream turbine is given by:

$$u_i = \frac{\sqrt{C_T}u_\infty}{32}\left(\frac{1.666}{k_1}\right)^2\left(\frac{x}{d}\right)^{-p} exp\left(-\frac{r^2}{d_w^2}\right) \tag{16}$$

For this model, the k parameters were empirically found based on the wind tunnel studies to be:

$$k_1 = 0.27 \tag{17a}$$
$$k_2 = 6.00 \tag{17b}$$
$$k_3 = 0.004 \tag{17c}$$

2.2.4 Simplified Ainslie Eddy-Viscosity Model

The final of the wake models used is a simplified version of the Ainslie Eddy-Viscosity field model. The Ainslie Eddy-Viscosity model solves the RANS equations using an eddy-viscosity closure term [15, 16]. This model is widely used in commercial wind resource assessment packages such as WindFarmer, OpenWind, and WindPRO.

The simplified version, developed by Mike Anderson of RES [17] allows the Ainslie Eddy-Viscosity model to be simplified, requiring far less computational time without significantly affecting the result.

Based on the full solution of the eddy-viscosity model it was found that the initial Gaussian shape profile is preserved downstream. Therefore the only parameters of the wake are the centerline velocity profile behind the rotor and the wake width. These assumptions, supported by the full solution to the Navier-Stokes equations, simplify the governing equations to a single ordinary differential equation with the same wake initialization parameters at a distance of two rotor diameters behind the turbine as the original Ainslie Eddy-Viscosity model. The simplified ODE for the center line velocity, u_c, can therefore be given to be:

$$\frac{du_c}{dx} = \frac{16\varepsilon\left(u_c^3 - u_c^2 - u_c + 1\right)}{u_c C_T} \quad (18)$$

As this is a first-order differential equation, a numerical integration scheme using a 4th order Runge-Kutta method is implemented to quickly solve the for the wake effect. It should be noted that in this methodology, all parameters including u_c, u_∞, b, x, and r are non-dimensionalised using the free-stream wind velocity u_∞ and the rotor diameter d as appropriate.

This center line velocity can then be substituted into Ainslie's equation assuming a Gaussian shape profile:

$$1 - \frac{u}{u_\infty} = (u_\infty - u_c)\, exp\left(-3.56\left(\frac{r}{b}\right)^2\right) \quad (19)$$

where the wake width, b, is given by:

$$b = \sqrt{\frac{3.56 C_T}{8 D_m (1 - 0.5 D_m)}} \quad (20)$$

the center line velocity deficit, D_m is given by:

$$D_m = 1 - \frac{u_c}{u_i} \quad (21)$$

The model is initialised two rotor diameters behind the turbine where the initial center line velocity deficit, D_{mi}, is taken to be:

$$D_{mi} = C_T - 0.05 - (16C_T - 0.5)\frac{I_a}{10} \quad (22)$$

This approach has been validated to show that it gives very similar results to the full eddy-viscosity approaches solved using a numerical integration scheme such as Crank-Nicholson [17, 18].

3 Results

For the seven cases outlined in table 1 each of the four wake models described in section 2.2 was run. The total normalised production value for each of the twenty turbines was then computed across the entire data-set while the computational time was measured. The analysis was also repeated for individual wind speed bins to observe the model accuracy at specific wind speed ranges. All wake models were formulated in Matlab 2013a and executed on a Dell PowerEdge R415 with Operton 427HR Processor (2.5 GHz) and 66 GB RAM.

3.1 Computational Time

As would be expected, the computational time for each of the wake models was roughly linear with the number of time intervals for which the wakes needed to be computed.

As can be seen from fig. 2, for each case the Larsen and Ishihara models were consistently the quickest with very little difference between them, while the Simplified Ainslie Eddy-Viscosity model was consistently the slowest.

3.2 Direction Constraint Applied to All Turbines

Following the approach given in section 2, the directional criteria were first imposed on all the turbines. Applying the direction constraint in this

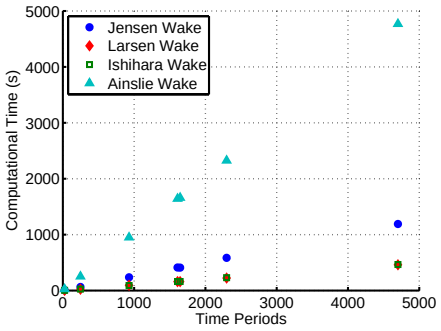

Figure 2: Computational Time

manner lead to fewer valid time periods as is indicated in table 1. In fact, reducing the sector size to 20° led to no valid time periods in the dataset. Therefore the application of the direction constraint to all the turbines is limited to only considering 60° and 30° sectors.

Figures 3a and 3b below show the normalised average power produced from each turbine under the two scenarios. From this it can be observed that all the wake models correctly predict a decrease in the power produced relative to the first turbine in the arc. For the two scenarios considered, the Larsen model was found to be the most accurate for the larger sector size(12.48% RMS error), while the Jensen model was the most accurate for the smaller sector (8.09% RMS error). The smaller sector size was found to have lower RMS errors for each of the models compared to the larger sector size indicating the models are generally more suitable for the smaller sector size. The Jensen and Ishihara models showed the greatest improvement with their RMS errors decreasing 10.62 percentage points and 8.15 percentage points respectively. The Larsen and Ainslie Eddy-Viscosity models, however, only showed a 1.28 percentage point and 3.04 percentage point decrease.

3.3 Direction Constraint Applied to Turbine 1 Only

Relaxation of the directional criteria as described insection 2.1 was similar to the methodology used by Gaumond et al. [3, 13] and Crasto & Castellani [4] in their analyses of wakes at Horns Rev. Relaxation of this directional criteria also allowed for smaller sector sizes to be investigated.

Table 2: RMS Error, Directional Criteria Applied to All Turbines

Sector	Jensen	Larsen	Ishihara	Ainslie
$\pm 15°$	**8.09%**	11.19%	15.10%	10.08%
$\pm 30°$	18.71%	**12.48%**	23.25%	13.13%

Figures 4a and 4b show the normalised power output from each of the turbines for the $\pm 15°$ and $\pm 30°$ sectors respectively. From these it can be observed that as in the previous scenarios a decrease in power output is observed down the line of turbines as would be expected. However, unlike the previous scenarios where the move from a $\pm 30°$ sector to a $\pm 15°$ sector resulted in improvements in the wake models, the application of the directional criteria to only the first turbine appears to increase in error as the directional sectors decrease in size (see table 3). Best performance was in fact observed for all the wake models when the largest sector size was considered. For this method of data selection, the Larsen model proved to be the most accurate for all but the smallest of the sector sizes when the Simplified Ainslie gave marginally better results.

Table 3: RMS Error, Directional Criteria Applied to Turbine 1

Sector	Jensen	Larsen	Ishihara	Ainslie
$\pm 1°$	45.91%	41.76%	61.20%	**41.09%**
$\pm 5°$	38.73%	**33.40%**	53.58%	34.19%
$\pm 10°$	30.97%	**23.77%**	40.20%	26.15%
$\pm 15°$	23.84%	**15.88%**	27.44%	18.67%
$\pm 30°$	15.59%	**8.34%**	13.52%	11.23%

3.4 Model Sensitivity to Wind Speed

As would be expected, the behaviour of the wakes vary with the wind speed and the wake models are therefore more accurate when applied at certain wind speeds at this site. Figures 5a to 5c show the model behaviour at specific wind speeds. As can

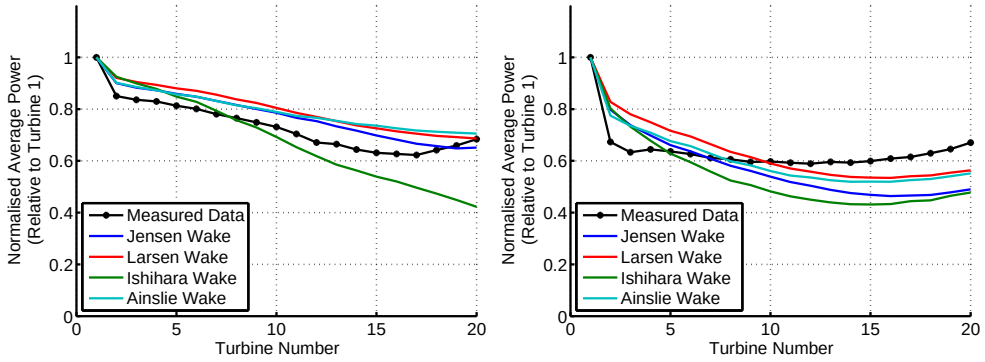

(a) 357°±15° **(b)** 357°±30°

Figure 3: Wake Deficit - Direction Sector Applied to All Turbines

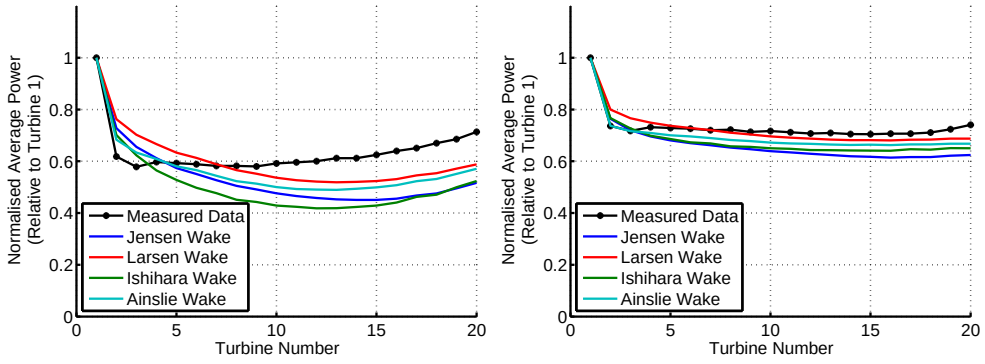

(a) 357°±15° **(b)** 357°±30°

Figure 4: Wake Deficit - Direction Sector Applied to Turbine 1

be seen in this series of figures, the wake models all perform best around $8\,\mathrm{m\,s^{-1}}$. High errors can be observed at both low and high wind speeds.

4 Discussion

The previous similar studies applied to Horns Rev found that the Larsen model best described the power deficit at Horns Rev [3, 4, 13]. These studies also found that decreasing the sector size beyond ±15° led to higher levels of error. Smaller sectors such as ±5° or ±1° therefore led to an over-estimation of the wake effect and the power deficits down a single line of turbines at Horns Rev. Similarly in the present study, smaller sectors such as and ±10° or ±5° lead to higher levels of RMS error. This result did, however, not hold for the analysis in which all turbines were compared against the direction criteria.

Checking all the turbines against the direction criteria lead to difficult results due in part to the amount of data constituting each data-set. The smaller sector size under consideration, ±15°, had only 25 valid time intervals thereby implying high levels of uncertainty. Though this scenario did result in lower RMS error than the case where the direction criteria was only applied to turbine 1, this needs to be further explored with larger data-sets.

In fact checking all the turbines against the di-

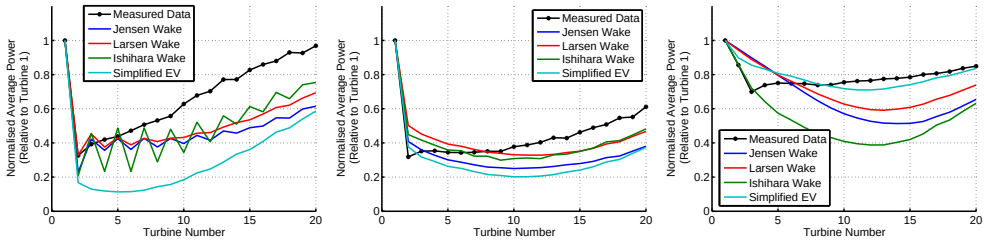

(a) 5 m s^{-1} Free Wind **(b)** 8 m s^{-1} Free Wind **(c)** 15 m s^{-1} Free Wind

Figure 5: Turbine Waked Wind Velocities

rection criteria resulted in lower levels of RMS error for similarly sized sectors. This is in fact as we would expect as comparing all turbines against the directional sector ensures that there is little variation in wind direction through the wind farm. It can be expected that the methodology which is similar to that of studies at Horns Rev, considering the direction only at one turbine, would be more applicable of the end-use in a layout optimisation tool.

Interestingly, the simplified field model was not significantly more accurate than a simpler analytic model and in fact only outperformed the analytic models on one occasion. The Simplified Ainslie Eddy-Viscosity model was, however, consistently the slowest as expected due to the iterative nature required in solving it. The Jensen model, though the simplest in principle requires a relatively complex computation to determine the ratio of the rotor plane area that is within a wake and therefore suffers as a result of this. The Larsen and Ishihara models likely have similar computational times as they are both relatively simple and require the same order of computations in order to compute the waked velocities.

It is important to note that none of the wake models implemented includes any kind of wake drift or wake meandering model. This omission does increase the uncertainty of these wake models, however, it is unclear to what degree [19–21].

The Bonus turbines in question are also known to have anemometers that give erroneously low readings [1]. Looking therefore at the non-normalised values, it can be observed that even at the first turbine the "modelled" power output is under-predicted. The use of these anemometer readings therefore introduces some uncertainty and it is worth exploring a similar study where better data might be available.

The average wind speed measured by the anemometer on turbine 1 over the data period is 6.6 m s^{-1} indicating that the optimal region of the models may in fact be very close to the average condition at the site leading to the low levels of RMS error observed. Had the site had an average condition further from the accurate region of the models we could expect larger levels of error.

5 Conclusion

This study explored modelling the wake effect at Middelgrunden wind farm. The study considered four different wake models, none of which are recommended for turbine spacing below 5D. This study has, however, shown that for turbines spaced at 2.4D all four models can give results on the order of 8-15% RMS error. Likely sources of this error are the error on the anemometer, the use of a global turbulence intensity, and the scarcity of data after the filtering process.

Though each wake model has different errors for each incoming wind velocity, the overall performance of the models was considered here. From this analysis it was found that the lowest RMS errors were on the order of 8% and achieved using either the Jensen or Larsen wake models depending on the data selection criteria. With the

exception of one of the data selection scenarios, the Larsen wake model was consistently the most accurate. The Ainslie Eddy-Viscosity field model had RMS error values close to that of the Larsen model; however, they were consistently higher indicating that for the extra computational time there was no gain in accuracy. These preliminary results suggest that of the four models considered, the Larsen wake model constitutes the best compromise between accuracy and computational time regardless of the data selection criteria, and therefore would be best suited for implementation as part of a layout optimisation tool. Although the Ishihara model was often one of the quickest, it did consistently result in some of the highest errors, consistent with previous work at Horns Rev [3, 4, 13]. It is likely that the Jensen model required additional computational time compared to the other kinematic models due to the fact that it computes the fraction of the rotor plane that is within the wake of another turbine rather than including a radial term. It was also found that the computational time for each model could be approximated as a linear function of the number of 10-minute data points under consideration.

This work has, however, been unable to identify the most appropriate data selection criteria for these models. Further work should validate these models against additional wind farms and explore the data selection criteria at greater depth.

Acknowledgements

The University of Indiana Virtual Wakes Laboratory and Middelgrundens Wind Turbine Cooperative are acknowledged for providing measurement data.

References

[1] H. E. Jørgensen, S. Frandsen, and P. Vølund, “Wake Effects on Middelgrund Windfarm,” Tech. Rep. July, RisøNational Laboratory, July 2003.

[2] R. Barthelmie, S. Frandsen, M. Nielsen, S. Pryor, P. Rethore, and H. Jørgensen, “Modelling and measurements of power losses and turbulence intensity in wind turbine wakes at Middelgrunden offshore wind farm,” *Wind Energy*, vol. 10, no. July, pp. 517–528, 2007.

[3] M. Gaumond, P. Rethore, and A. Bechmann, “Benchmarking of Wind Turbine Wake Models in Large Offshore Windfarms,” *Proceedings of the Science of Making Torque from Wind Conference*, 2012.

[4] G. Crasto and F. Castellani, “Wakes Calculation in a Offshore Wind Farm,” *Wind Engineering*, vol. 37, pp. 269–280, June 2013.

[5] N. Jensen, “A Note on Wind Generator Interaction,” tech. rep., RisøDTU, 1983.

[6] D. J. Renkema, *Validation of wind turbine wake models*. PhD thesis, TU Delft, 2007.

[7] F. Borbon Guillen, *Development of a design tool for offshore wind farm layout optimization*. Master of science in sustainable energy technology, Delft University of Technology, 2010.

[8] B. Pérez, R. Mínguez, and R. Guanche, “Offshore wind farm layout optimization using mathematical programming techniques,” *Renewable Energy*, vol. 53, pp. 389–399, May 2013.

[9] K. Thomsen and P. Sørensen, “Fatigue loads for wind turbines operating in wakes,” *Journal of Wind Engineering and Industrial Aerodynamics*, vol. 80, pp. 121–136, Mar. 1999.

[10] I. Katic, J. Højstrup, and N. Jensen, “A simple model for cluster efficiency,” *Proceedings of EWEC 1986*, vol. 1, pp. 407–410, 1986.

[11] G. C. Larsen, “A Simple Wake Calculation Procedure,” tech. rep., RisøNational Laboratory, 1988.

[12] W. Tong, S. Chowdhury, J. Zhang, and A. Messac, “Impact of Different Wake Models On the Estimation of Wind Farm Power Generation,” *Proceedings of AIAA Aviation Technology, Integration, and Operations (ATIO)*, vol. 14, 2012.

[13] M. Gaumond, P. Réthoré, S. Ott, A. Bechmann, and K. Hansen, “Evaluation of the wind direction uncertainty and its impact on wake modeling at the Horns Rev offshore wind farm,” *Wind Energy*, 2013.

[14] G. Crasto and A. R. Gravdahl, “Validation of wake analytical models of WindSim in neutral conditions in a offshore wind-farm,” 2009.

[15] J. Ainslie, “Calculating the flowfield in the wake of wind turbines,” *Journal of Wind Engineering and Industrial Aerodynamics*, vol. 27, pp. 213–224, 1988.

[16] M. L. Thøgersen, “WindPRO / PARK,” tech. rep., EMD International A/S, 2005.

[17] M. Anderson, “Simplified Solution to the Eddy-Viscosity Wake Model,” tech. rep., Renewable Energy Systems Ltd (RES), 2009.

[18] T. Han, *The Assessment of Dynamic Wake Effects on Loading*. Master of science, TU Delft, 2011.

[19] S. Ott, J. Berg, and M. Nielsen, “Linearised CFD Models for Wakes,” Tech. Rep. December, RisøNational Laboratory, 2011.

[20] D. Medici and P. H. Alfredsson, “Measurements behind model wind turbines: further evidence of wake meandering,” *Wind Energy*, vol. 11, pp. 211–217, Mar. 2008.

[21] T. Larsen, H. Madsen, G. Larsen, and K. Hansen, “Validation of the dynamic wake meander model for loads and power production in the Egmond aan Zee wind farm,” *Wind Energy*, no. 16, pp. 605–624, 2012.

Proceedings of the Twenty-fifth (2015) International Ocean and Polar Engineering Conference **www.isope.org**
Kona, Big Island, Hawaii, USA, June 21-26, 2015

ISBN 978-1-880653-89-0; ISSN 1098-6189

Optimisation of Offshore Wind Farms Using a Genetic Algorithm

Ajit C Pillai
Industrial Doctoral Centre in Offshore Renewable Energy, The University of Edinburgh
Edinburgh, UK

Dr. John Chick
Institute for Energy Systems, The University of Edinburgh
Edinburgh, UK

Dr. Lars Johanning
College of Engineering, Mathematics, and Physical Sciences, University of Exeter
Penryn, UK

Dr. Mahdi Khorasanchi
Department of Naval Architecture, University of Strathclyde
Glasgow, UK

Sebastien Pelissier
EDF Energy R&D UK Centre
London, UK

ABSTRACT

A modular framework for the optimisation of an offshore wind farm using a discrete genetic algorithm is presented. This approach uses a bespoke grid generation algorithm to define the discrete positions that turbines may occupy thereby implicitly satisfying navigational and search and rescue constraints through the wind farm. The presented methodology takes a holistic approach optimising both the turbine placement and inter-array cable network, while minimising the levelised cost of energy and satisfying real world constraints. This tool therefore integrates models for the assessment of the energy production including wake losses; the optimisation of the inter-array cables; and the estimation of costs of the project over the lifetime. This framework will allow alternate approaches to wake and cost modelling as well as optimisation to be benchmarked in the future.

KEY WORDS: offshore wind farm layout optimisation; genetic algorithm

INTRODUCTION

With the growth of the offshore wind sector and the development of large offshore wind farms in the coming years, it has become an important point to ensure that the wind farms are developed in such a way as to maximise their potential. In order to meet this need, the field of wind farm layout optimisation has been in development since the seminal paper by Mosetti, Poloni, and Diviacco (1994). Though this field has been in development for the past twenty years, there still remains much work before layout optimisation displaces the industry standard rules-of-thumb approach to layout design. This paper presents a new framework that has been developed to address the layout optimisation problem with the goal of ultimately developing a tool that would be deployed by wind farm site developers.

This framework takes a holistic approach to layout optimisation based around the objectives and constraints that would be faced by an offshore wind farm developer in the UK. This approach introduces a generalised means of discretising the wind farm area in such a way that a grid of potential turbine positions is first generated. The use of this grid ensures that the final turbine positions which are selected from this grid satisfy the requirement of having turbines along straight lines.

From the perspective of an offshore wind farm operator, it is important not only to maximise the energy yield from the wind farm, but also to optimise the levelised cost of energy (LCOE). The full layout optimisation problem therefore represents striking a balance between maximising the energy yield and minimising the lifetime costs.

To this end, a number of projects have looked at the optimisation of wind farm layouts. This project has addressed this problem in a similar approach to previous schemes by using a genetic algorithm (GA) to minimise the LCOE (Mosetti, Poloni and Diviacco, 1994; Grady, Hussaini and Abdullah, 2005; Elkinton, 2007; Fagerfjäll, 2010; Guillen, 2010).

$$LCOE = \frac{\sum_{t=1}^{n} \frac{C_t}{(1+r)^t}}{\sum_{t=1}^{n} \frac{AEP_t}{(1+r)^t}} \quad (1)$$

where C_t are the costs incurred in year t, n is the project lifetime time, AEP_t is the annual energy production (AEP) in year t, and r is the discount rate of the project. The LCOE measured in £/MWh effectively gives a measure of the cost effectiveness of the layout proposed and therefore acts as a means to compare the layouts under consideration on a relative basis.

Existing approaches do not apply tools and methodologies that have considered all the constraints faced by a developer, nor do they consider the full impact the layout has on the LCOE. Many of the previous studies opted to use simpler cost models thereby ignoring the effect the layout has on costs (Mosetti, Poloni and Diviacco, 1994; Grady, Hussaini and Abdullah, 2005). The studies that have considered detailed cost models however, have not considered the full set of constraints that a developer would be faced with (Elkinton, 2007; Larsen and Réthoré, 2013; Larsen, Madsen, Troldborg, Larsen,

Réthoré, Fuglsang, Ott, Mann, Buhl, Nielsen, Markou, Sørensen, Hansen, Mikkelsen, Okulov, Shen, Heath, King, McCann, Schlez, Carlén, Ganander, Migoya, Crespo, Jiménez, Prieto, Stidworthy, Carruthers, Hunt, Gray, Veldkamp, Mouritzen, Jensen, Krogh, Schmidt, Argyriadis and Frohnböse, 2011). The tool developed as part of this work seeks to reconcile this by including both detailed models for assessing the layout dependent elements as well as a full set of constraints in order to generate layouts which would be acceptable from a developer perspective.

The work presented has developed a flexible framework by which the energy, cost, and electrical infrastructure are assessed independently for each layout. Due to the modularity, alternate wake, cost, or electrical infrastructure models can easily be implemented in the future for comparison purposes and sensitivity studies. The approach presented has also included constraints for maintaining navigation channels through the sites, minimum separation between turbines, and seabed restrictions, constraints that are less frequently seen in existing tools. The tool also generates an optimised inter-array electrical configuration simultaneously satisfying not only seabed constraints, but also cable capacity, cable crossing, and junction box capacity constraints.

A GA with bespoke crossover and mutation operators has been developed and applied successfully to this problem. The modular platform constructed would allow other optimisation algorithms such as particle swarm, ant colony optimisation, or simulated annealing to be implemented using the same evaluation function and tool approach.

This paper summarises the initial application of this holistic approach to layout optimisation of offshore wind farms. The optimisation framework is applied to a hypothetical wind farm made up of 30 wind turbines in order to demonstrate the capabilities of the approach. The discussion section explores further improvements that will be made to the framework to increase the relevance to a wind farm developer.

METHODS

As this tool has been developed as part of a larger project which seeks to assess the suitability of different wake models, cost models, optimisation objectives, and optimisation algorithms, it has intentionally been designed to be as flexible as possible while also adhering to the realistic challenges which would be faced by a project developer.

Grid Generation

In the UK, project developers have been urged to use symmetric layouts with turbines placed along a regular grid in order to comply with the navigational safety and search and rescue requirements (NOREL Group, 2013). Rather than defining navigational channels, this constraint has been proposed as requiring the turbines to be placed in straight lines with no deviation from these lines. As a result of this, most optimisation approaches have limited the optimisation process to specifying the regular spacing between turbines. The tool developed here, however, looks instead to give the optimiser greater freedom by designing a grid which has more potential turbine positions than there are turbines to place. This allows the optimiser to change the spacing between turbines throughout the wind farm while still keeping the turbines in straight lines. It is believed that even though this creates a regular grid with holes, the final layout will still satisfy the navigational requirements.

The first step in this optimisation approach is therefore to produce this grid of potential turbine positions. To do this, the tool first identifies the dominant wind direction based on the wind rose describing the wind resource at the site and converting this to an energy rose representing the kinetic energy flux of the wind and the relative occurrence of the wind speed and wind direction combination. The dominant wind direction is defined as the wind direction sector that has the highest kinetic energy flux over the measurement period. The dominant wind direction, once identified will act as one of the principle axes along which the grid of points is generated. By aligning the principle axis with the dominant wind direction, the optimiser will be able to align turbines in rows perpendicular to the dominant wind direction, thereby minimising the interaction of wakes. At the same time, having a large grid with more possible positions than turbines to be placed allows the optimiser to introduce space for wakes to recover where necessary. This approach also allows the optimiser flexibility in adjusting the spacing relative to each individual turbine rather than for the entire wind farm.

Once the dominant wind direction is identified, the algorithm expands and contracts the spacing as necessary until a grid with the desired number of valid turbine positions is generated. For each spacing, the grid is produced with a fixed ratio between downwind and crosswind spacing. After this each point is checked to ensure that it satisfies the geographical information system (GIS) constraints of where turbines can be placed. If after this, it is found that:

a) insufficient grid points are in valid positions, then the spacing is *decreased*, and the process repeated;

or

b) too many grid points exist, then the spacing is *increased*, and the process is repeated.

Annual Energy Production

The principle output of a wind farm is the energy produced by the wind farm which is represented in the LCOE by the annual energy production term. In order to accurately assess the impact the layout has on LCOE, it is important to characterise the effect that the layout has on the AEP and the lifetime energy yield. The energy yield assessment in turn can be said to be made up of two components, an understanding of the wind resource at the site, and modelling of potential *wakes* behind each proposed turbine.

Any device which extracts energy from a natural flux such as the wind is known to directly impact and alter the natural flux as a result of the energy extraction. In the case of wind turbines, the wake behind a wind turbine is characterised by lower extractable wind speeds, but higher levels of turbulence intensity (Barthelmie, Folkerts, Larsen, Frandsen, Rados, Pryor, Lange and Schepers, 2006; Barthelmie, Hansen, Frandsen, Rathmann, Schepers, Schlez, Phillips, Rados, Zervos, Politis and Chaviaropoulos, 2009; Burton, Jenkins, Sharpe and Bossanyi, 2011). These wakes are also known to interact with one another leading to a more significant reduction in available energy as a result of the superposition of multiple upwind wakes (Katic, Højstrup and Jensen, 1986; Schlez and Neubert, 2009).

Wake models, can broadly be categorised into two categories: analytic wake models and field models. Analytic wake models are simpler models while field models are generally based on solving the Navier-Stokes equations. Though the annual energy production module can either be run independently or as part of the optimisation tool, it was decided to use an analytic wake model as opposed to a field model to predict the wakes, as this results in substantially quicker computational times (Sanderse, Pijl and Koren, 2011; Renkema, 2007).

Previous work by the authors (Pillai, Chick and de Laleu, 2014) as well

as other studies (Gaumond, Rethore and Bechmann, 2012) had shown that for existing wind farms, the Larsen model (Larsen, 1988) represents a good balance between accuracy and computational complexity when compared to a) the Jensen/PARK model (Katic, Højstrup and Jensen, 1986), b) the Ishihara model, and c) the Ainslie eddy-viscosity model (Ainslie, 1988; Anderson, 2009). The Larsen model is an analytic model based on a closed-form solution of the Reynolds-Averaged Navier Stokes (RANS) equations and Prandtl mixing theory (Larsen, 1988; Renkema, 2007). For this study, the Larsen model has therefore been deployed, however, other wake models can easily be implemented if need be.

In order to assess the AEP, the wind distribution at the site is used to determine the frequency of occurrence for each wind speed/direction combination. For each of these bins, the turbines in the layout are sorted such that the first turbine is the turbine furthest upwind. For each turbine, the free wind speed is then updated to account for the wakes created by any upwind turbines and the superposition of these wakes. The variation in power generation and thrust coefficient are considered based on the modified wind speed as a result of the wake effect and bins are generated related to speed and directionality. The aggregate power generated for the entire layout for these bins, are then multiplied by the frequency of this wind speed and direction combination. The sum of each of these powers for the bins represents the AEP for the proposed layout. This approach is similar to that taken by other tools and AEP computations (DNV GL - Energy, 2014; Pérez, Mínguez and Guanche, 2013; Elkinton, 2007; Mosetti, Poloni and Diviacco, 1994; Grady, Hussaini and Abdullah, 2005).

Electrical Infrastructure Optimisation

Previous layout optimisation tools have generally assumed a constant inter-turbine spacing, and therefore the changes in total cost due to the inter-array cables are not characterised. However, as the layout changes, the total length of infield cable required can change quite significantly thereby affecting the costs. As the turbine layout has a direct impact on the cable layout it is important for a layout optimisation tool to take this into account.

This tool therefore implements an inter-array cable optimisation tool in order to determine the cost of the electrical system for each turbine layout under consideration.

The authors have previously developed an optimisation methodology for optimising the inter-array cable network of an offshore wind farm (Pillai, Chick, Johanning, Khorasanchi and de Laleu, 2015). This approach accounts for real wind farm planning constraints in order to determine the optimal positions for the necessary offshore substations and then designs an inter-array collection network which minimises both the cost and the peak losses.

The optimisation tool first determines the optimal positions of the substations based on a modified 'kmeans++' algorithm. Kmeans++ is a modified version of the commonly used kmeans clustering algorithm which uses a weighted-random approach to seed the initial cluster centres resulting in both better solutions and quicker runtimes than the original kmeans algorithm (MacQueen, 1967; Arthur and Vassilvitskii, 2006). For this tool, the kmeans++ algorithm is further constrained to account for the capacity constraints of each substation and the fact that within the wind farm area, there are regions where substations cannot be placed. From here, a pathfinding algorithm based on Delaunay Triangulation is used to determine possible cable paths for each turbine and the respective cost of these paths. The pathfinding algorithm is used to account for the areas in which cables cannot be laid due to seabed constraints and obstacles. Finally, a capacitated minimum spanning tree (CMST) is constructed based on the cable costs found in the pathfinding step. The CMST represents the optimal network and is solved using Gurobi, a commercial mixed-integer linear programming (MILP) software. An iterative approach is taken in order to eliminate any cable crossings in the solution.

This tool has previously been applied to large wind farms and has been found to offer significant reductions in the total cable needed when compared to industry standard approaches (Pillai, Chick, Johanning, Khorasanchi and de Laleu, 2015).

Cost Assessment

Previous works that have included a cost breakdown typically have not been able to validate their cost models and as a result have introduced significant uncertainty into the optimality of their solutions (Elkinton, 2007; Fagerfjäll, 2010). As this tool has been developed in conjunction with EDF Energy R&D UK Centre, it has been possible to directly develop and validate the cost assessment methodologies. Consequently this work presents costs that have been parameterised and validated against real costs expected to be incurred by large offshore wind farms deploying wind turbines in the 5-8 MW range in UK waters.

The total cost of the wind farm is broken down into eight major cost elements:

1. Turbine Supply
2. Turbine Installation
3. Foundation Supply
4. Foundation Installation
5. Inter-array Cables (Supply & Installation)
6. Decommissioning
7. Operations and Maintenance (O&M)
8. Offshore Transmission Assets

Turbine supply. The turbine supply costs are determined based on the price per turbine that turbine manufacturers have provided. This cost therefore does not vary due to the layout unless the total number of turbines or installed capacity changes.

Turbine installation. The turbine installation costs are based on market values for vessel costs and capacities and are modelled by first modelling the total amount of time needed to install all the turbines at their specific locations. This includes not only the computation of the travel time between the turbines, but also the necessary time to go to and from the construction port. To calculate this, the turbines are clustered based on the capacity of the installation vessel, and for each cluster a shortest path is computed between the port, each turbine in the cluster, and the port again. This approach therefore accurately computes the distance that the vessel must travel over the installation process. From this, the total time is computed based on assumed weather availability and the costs computed based on the vessel and equipment day rates. The turbine layout, therefore, has a direct impact on the time needed to travel between turbine positions as well as to and from the port.

Foundation supply. Foundation costs are found to be highly dependent on the site conditions where the foundation is to be installed. To account for this dependence, previous cost models have attempted a bottom up approach based on the soil characteristics at the installation site to model the costs. Unfortunately this approach has proven difficult to validate for all foundation types (Elkinton, 2007). For this tool therefore, a depth dependency has been developed from discussions with manufacturers and the specific soil conditions are not included.

Larger turbines in the 5-8 MW range are more likely to use jacket foundations which have been found to be less sensitive to the soil conditions than to the depth (Elkinton, 2007). Detailed bathymetry of the site is therefore necessary in order to accurately estimate the variation in foundation supply costs as a function of the turbine layout.

Foundation installation. The foundation installation process like the turbine installation module is based on estimating the time needed to complete the operations and converting this time to a cost. Unlike the turbine installation though, this is modelled as three distinct phases which each uses a different vessel to complete.

Regardless of the foundation type (gravity-based, monopile, or jacket), some seabed preparation is necessary. For a gravity-based foundation this might be the necessary dredging and levelling of the seabed, while for monopiles and jackets this would more likely be pre-pilling works including surveying and drilling. After this step, the foundations will be installed as a separate operation following which some kind of scour protection will often be added. The installation of scour protection is again modelled as a separate step involving a different vessel from either the site preparation or foundation installation processes. In some conditions, the scour protection will not be necessary, however, for the time being this model has assumed that all turbines will require scour protection.

Inter-array cable costs. The total horizontal length of inter-array cables required is computed from the inter-array cable optimisation tool described earlier. This tool is described in detail in previous work by the authors (Pillai, Chick, Johanning, Khorasanchi and de Laleu, 2015). This tool has the support for optimising the layout for different cable cross-section sizes and therefore can output not only the total length of cable, but the horizontal lengths required for each segment and the required cross-section. From this, the inter-array cable cost module computes the necessary vertical cable and the necessary spare cable before computing the costs.

Following the calculation of the supply cost, the installation cost is computed in a similar manner to the turbine and foundation installation modules. This is done based on data available for cable trenching vessels and therefore assumes that all cables are trenched and buried.

Decommissioning. The decommissioning costs include the removal of the turbines and foundations. At the moment, it is unclear what will happen to the transmission and export cables. The model therefore assumes that these cables are not removed at the time of decommissioning, but simply cut at the turbines and substation, leaving the buried lengths as they are. The decommissioning costs are therefore modelled similar to the installation processes with the time each vessel is required first computed before this is converted to a cost. Like the installation processes it is assumed that the vessels have some finite capacity and must return to the decommissioning port during the overall operation. The turbines and foundations are assumed to be decommissioned in separate steps requiring separate vessels. Like the installation phases, this term is therefore dependent on the turbine positions and is affected by the proposed layout.

Operations and Maintenance. The operations and maintenance costs are based on a tool developed by EDF Energy R&D UK Centre which models the anticipated operations and maintenance cost of a project to vary with the project's distance from the operations and maintenance port and the capacity of the project. As this term is affected by distance of the wind farm to the operations and maintenance port, this too is affected by the layout. The operations and maintenance costs are classed as operational expenditure (OPEX) as these are incurred each year of operation as opposed to the preceding cost elements which are only incurred during the construction period and are therefore classed as CAPEX elements.

Offshore Transmission Assets. The final cost element of this cost model is the inclusion of the offshore transmission assets and the offshore transmission asset transfer fees. In the UK, the offshore substation, export cables, and onshore substation must be owned and operated by a separate company from the wind farm operator. Practically, therefore, most wind farm developers build these assets, and then transfer them to a transmission operator before commissioning the wind farm. As a result, only some of the CAPEX is incurred by the project, and the rest is incurred as a component of the transmission fee along with regionally based costs set by the network operator, in the UK this is National Grid. Both the CAPEX and OPEX components of the Offshore Transmission Owner's assets have been computed in discussion with National Grid and equipment manufacturers based on the capacity of the assets.

Table 1: Cost Element Contribution to CAPEX/OPEX

Cost Element	CAPEX	OPEX	Sensitivity to Layout
Turbine Supply	Yes	-	Low
Turbine Installation	Yes	-	Medium
Foundation Supply	Yes	-	Medium
Foundation Installation	Yes	-	Medium
Inter-array Cable	Yes	-	High
Decommissioning	Yes[1]	-	Medium
Operations and Maintenance	-	Yes	Medium
Offshore Transmission Assets	Yes	Yes	Low

Constraints

An important step for all optimisation routines is to clearly define the constraints which must be applied and which limit the solution space. In this case, the inter-array cables are optimised as part of the evaluation function for the larger turbine placement problem, and there are a number of constraints to be considered just for this sub-problem separate from those which explicitly constrain the turbine placement.

First, the site boundary defines the area in which turbine foundations can be placed. As developers are required to keep the entire wind turbine within their leased turbine area, the boundary is adjusted using GIS software to include the necessary "negative buffer" to account for the size of the turbine blades. The boundary used by this tool therefore represents a smaller region than the overall turbine area.

Second, within the site there may be areas containing unexploded ordnance (UXOs) or wrecks. These areas generally cannot contain turbines or cables and are therefore treated as exclusion areas by the optimiser. Similarly, turbines can generally not be placed in areas where the seabed slope is too steep. Generally, areas over 5% slope will be considered as too steep for turbines and are similarly treated as exclusion areas. All areas also have an additional 50 m buffer area.

Third, the turbines generally need to be a minimum distance away from one another, for safety and navigational reasons. These are generally given as exclusion circles around each turbine, however, consenting bodies may alternatively give separate downwind and crosswind

[1] Though categorized as a CAPEX term, this cost is only applied to the years during which decommissioning occurs at the end of life.

distances defining an exclusion ellipse. These ellipses will generally require more significant separation in the downwind direction than in the crosswind direction.

Finally, in the case of most UK offshore wind farms, consenting bodies have stipulated that the layout of turbines in offshore wind farms should have some degree of uniformity to ensure safe passage through the farm as well as not act as a hindrance to search and rescue operations (NOREL Group, 2013). This constraint is explicitly satisfied by the grid generation approach prior to execution of the GA. By doing this, a clear grid is defined on which turbines can be placed. As this constraint is already considered, it is not implemented within the framework of the GA.

The inter-array cable optimisation also has a number of constraints unique to its sub-problem. These include not only that the cables and the substations must be within the turbine area and may not enter the exclusion areas (seabed slope is not an exclusion area for cables), but also that power cannot be stored at a turbine and therefore the inter-array cable network must be balanced; turbines have a limited number of connection points and therefore a maximum number of cables that connect to a turbine exists; cables may not intersect except at the substation or at turbines; and cables have a finite capacity which cannot be exceeded (Pillai, Chick, Johanning, Khorasanchi and de Laleu, 2015).

Genetic Algorithm

GAs are a type of population based evolutionary algorithms that are well suited to a variety of problem types (Holland, 1992). GAs have previously been deployed for optimising offshore wind farm layouts and have generally been found to offer good solutions to the problem at hand (Elkinton, 2007; Larsen, Madsen, Troldborg, Larsen, Réthoré, Fuglsang, Ott, Mann, Buhl, Nielsen, Markou, Sørensen, Hansen, Mikkelsen, Okulov, Shen, Heath, King, McCann, Schlez, Carlén, Ganander, Migoya, Crespo, Jiménez, Prieto, Stidworthy, Carruthers, Hunt, Gray, Veldkamp, Mouritzen, Jensen, Krogh, Schmidt, Argyriadis and Frohnböse, 2011; Guillen, 2010).

GAs are so named as they borrow from biological evolution and have analogous algorithms to genetic principles. In a GA, the solutions are thought of as genomes with each turbine position thought of as gene. GAs operate on a population basis that is to say that a population of solutions is considered in which the best solutions have a higher probability of passing on genes to members of the next generation. The flowchart in fig. 1 outlines the operating principles of a GA and the steps involved. The unique aspect of the GA at hand is that rather than implementing a generic GA and then testing for compliance within the evaluation function, the crossover and mutation steps have been designed specifically to include the constraints. In this case, because a predefined grid has been created during the grid generation step, the genes of the GA are binary and represent the presence of a turbine at the specific grid locations; one gene per grid location.

For the implementation at hand, the problem was formulated as a minimisation problem in which the fitness of an individual was given by its LCOE. In this case, individuals with lower LCOE values correlate to a higher fitness. For this tool, the fitness values have not been scaled.

The initial population is created by generating random strings of 1's and 0's representing potential individuals. The individuals are created in such a way that all have the correct number of turbines and are unique individuals. Each individual is then checked to ensure that the placement satisfies all constraints, and if any individuals are invalid they are regenerated. This ultimately produces a population containing random, valid individuals from which the evolution can proceed.

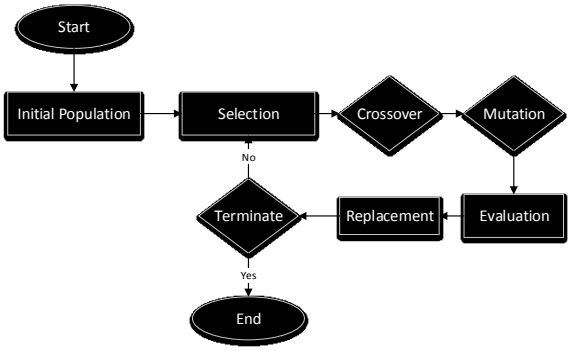

Fig. 1: Layout optimisation approach.

Selection. Selection is the process by which two individuals of the population are chosen to contribute genetic material to member(s) of the new population. The selected individuals then act as parents to children (new solutions) of the new generation. Though there are a number of different types of selection approaches, a roulette wheel section algorithm was deployed for this. Roulette selection, also known as fitness proportionate selection, assigns a probability to each member of the population based on their fitness value. In this sense, better solutions have a higher probability of selection than worse solutions.

Crossover. Crossover is the principle genetic operator that is used to combine the selected parents to create children. In crossover, part of the genetic material from each parent is combined in such a way that does not violate the constraints in order to create two new individuals who will potentially be added to the population. As a discrete GA has been implemented here, approximately 50% of the turbine locations should come from each of the parents. In order to do this, a uniform crossover or crossover mask approach is applied. In a crossover mask, each gene is randomly assigned to one of the parents. If a gene is assigned to a parent, then the first child has the same value for this gene as their parent. To generate a second child that is a foil to the first child, the crossover mask is flipped (all 1s become 0s and vice versa). Each of the children is checked against the constraints, and in the event of an invalid solution, the mask is regenerated. Likewise, the mask is regenerated if the proportion of genes from each parent is not 50%. If crossover will occur is itself a probabilistic event, and there exists a chance that crossover will not occur and that the two children solutions will identically match the parents. This could also happen even if crossover does occur, though the probability is very low.

Mutation. The other genetic operator that is applied to solutions is mutation. Mutation randomly changes part of the solution. In this implementation, there is a low probability that a bit gets flipped (i.e. a 1 becomes a 0, and a 0 becomes a 1). Where crossover explores solutions similar to the existing solutions, mutation randomly explores the remaining regions of the solution space. The mutation operator is necessary to ensure that the solution does not converge to a local solution, but rather finds the global solution. Like crossover, the mutated children are checked against the constraints as well as the number of turbines, and mutation happens repeatedly until a valid solution is generated.

In this tool, adaptive crossover and mutation operators based on

existing literature have been applied (Srinivas and Patnaik, 1994). The adaptive crossover and mutation rates are implemented to allow the algorithm to self-tune and to correctly ensure that bad solutions have higher probability of changing. Similarly, this adaptive approach to these parameters allows the algorithm to better maintain a diverse population of the solution as the solution converges thereby allowing the GA to continue to operate effectively without terminating prematurely. These adaptive parameters are given by:

$$p_c = \frac{k_1(f_{max} - f')}{f_{max} - \bar{f}} \quad \text{for} \quad f' \geq \bar{f} \tag{2}$$

$$p_c = k_3 \quad \text{for} \quad f' < \bar{f} \tag{3}$$

$$p_m = \frac{k_2(f_{max} - f)}{f_{max} - \bar{f}} \quad \text{for} \quad f \geq \bar{f} \tag{4}$$

$$p_m = k_4 \quad \text{for} \quad f < \bar{f} \tag{5}$$

where p_c is the probability of crossover, p_m is the probability of mutation, f_{max} is the fitness of the best individual of the population, f' is the fitness of the best parent, $\bar{f}$ is the mean value of the fitness of the population, and f is the fitness of the individual under consideration. The constants are defined such that $k_1 = k_3 = 1$ and $k_2 = k_4 = \frac{1}{2}$.

Replacement. The final step of a steady-state GA procedure is to replace members of the population with the new children that have been generated. Generally, candidate solutions are replaced by children solutions if the children have a better fitness function. The selection, crossover, and mutation operators are repeated until a target number of children have been created or a target proportion of the population has been replaced by new solutions. Many GA's also include an *elitism* parameter which defines what proportion of the generation should be kept. In this case, an elitism parameter of 50% is used and therefore each generation repeatedly generates children until 50% of the population has been replaced with new individuals.

This entire GA process is repeated until the solutions converges or the termination criteria are met.

For this study, a test case involving 30 turbines in a 47 km^2 area was considered. For this area, bathymetry and seabed surveys were available defining the depth, areas where turbines cannot be placed, and areas where cables cannot be placed.

Table 2: GA Parameters

GA Encoding	Discrete
Population Size	50
Maximum Generations	100
Probability of crossover	Adaptive
Probability of mutation	Adaptive
Elitism	50%
Stop Criteria	Loss of diversity or maximum number of generations reached

The GA was executed with a population size of 50. Previous work has found that for specific problem instances a smaller population size on the order of 20-30 individuals may work effectively (Haupt and Haupt, 2004; Grefenstette, 2006). For this problem, however, it was found that a smaller population size than 50 led to a loss in diversity after very few generations resulting in little improvement in the best individual before termination. A larger population size was therefore selected in order to ensure that diversity was maintained through the optimisation process.

For each proposed solution, the energy yield was first assessed, followed by execution of the inter-array cable optimiser after which the cost for the proposed layout was assessed. From this, the LCOE is evaluated assuming a constant capital expenditure (CAPEX) spend profile (50% each over 2 years) and a 20 year project lifetime prior to decommissioning.

A representative wind rose for a UK offshore site is assumed. This wind rose has strong winds principally from the south/south-west directions identifying this as the principle direction with which turbines should be aligned. This wind rose does not represent any site in particular, but is simply used for the demonstration of the capabilities of this tool.

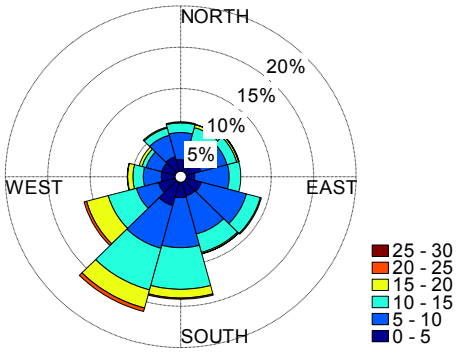

Fig. 2: Wind rose representing the wind resource for the test case.

Given the wind rose shown in fig. 2, the tool next generates a grid of potential turbine positions. This grid contains 50 possible turbine positions aligned roughly perpendicular to the dominant wind direction. The grid generation algorithm removes positions on the grid which are in illegal positions (shown in grey in fig. 3). These illegal positions can be due to wrecks, UXOs, or the seabed slope. Each row of the grid is offset to ensure that the distance between turbines is increased along this dominant wind direction.

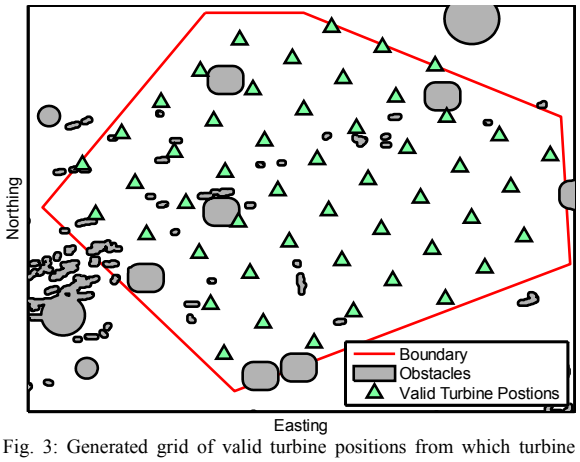

Fig. 3: Generated grid of valid turbine positions from which turbine positions are selected.

RESULTS

Executing the full approach for a wind farm containing 30 turbines resulted in the layout shown in fig. 4 after 13 generations. This solution was based on generating a grid made up of 50 potential turbine positions. This grid size was selected to ensure there were more possible turbine positions than turbines. The solution produced does adhere to the site constraints and produces a solution that conforms to a regular grid thereby satisfying the necessary navigational and search and rescue constraints. The solution produced also leaves larger gaps between turbines in the interior of the wind farm which is consistent with the relevant theory of wind turbine wakes and allows the wakes to recover before a new turbine is placed. Though significant gaps are left, the optimiser does not eliminate turbines from the centre of the wind farm. This indicates that AEP could still be increased, but likely at a higher cost. The presence of the turbines in the centre of the wind farm indicates the importance of not only considering the wakes, but also the cost of the wind farm.

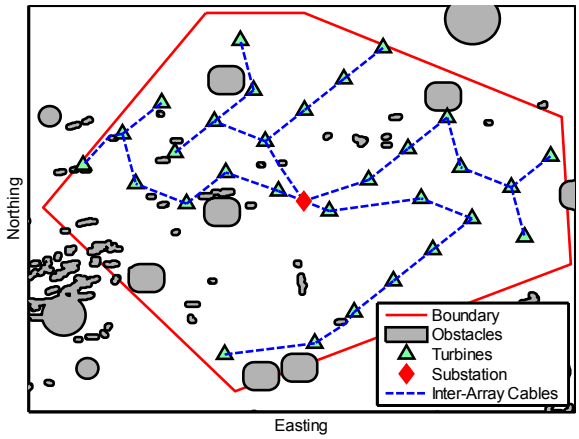

Fig. 4: Optimised turbine placement. LCOE for this layout is £89.51/MWh.

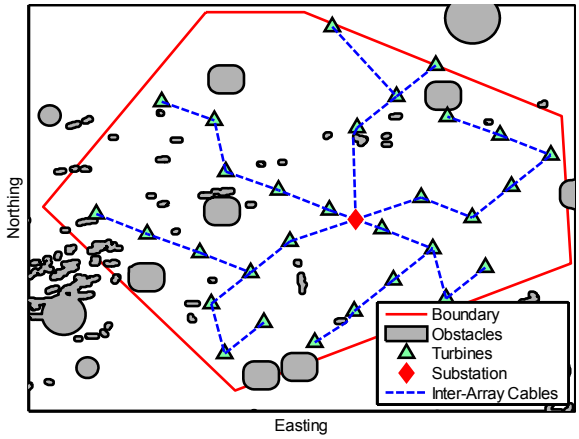

Fig. 5: An inferior layout proposed by the optimiser during the first generation. LCOE for this layout is £92.45/MWh.

Fig. 5 shows an inferior turbine layout which has a higher LCOE of £92.45/MWh. As can be observed, fewer holes are left through the site, while a few turbines are isolated. The combined effect of this is that wake effects are not effectively minimised and costs are unnecessarily increased to accommodate the inclusion of the isolated turbines.

In this way, the approach ensures that all constraints are satisfied while at the same time using a dynamic spacing parameter to minimise the effect of wind turbine wakes and thereby the LCOE.

From the convergence plot (fig. 6) it can be seen that over the execution of the algorithm, both the best and mean solution scores progressively improved. This is indicative that the GA was operating as expected. The final solution identified by the GA has an LCOE of £89.51/MWh.

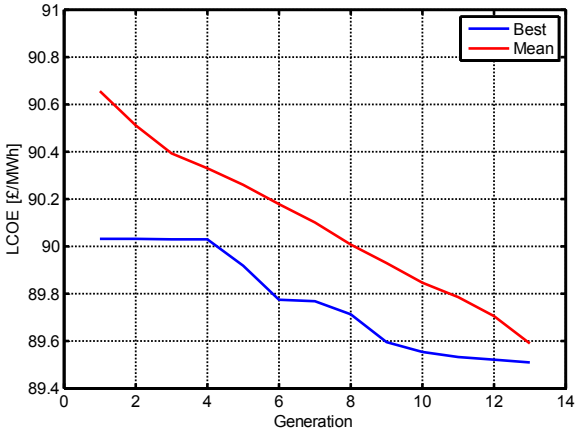

Fig. 6: Minimal and mean LCOE over generations.

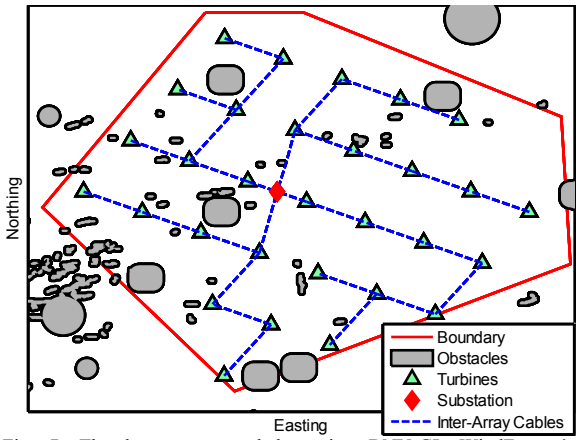

Fig. 7: The layout proposed by using DNV-GL WindFarmer's Symmetrical Optimiser. LCOE for this layout is £90.53/MWh.

Running DNV GL WindFarmer's Symmetrical Layout Optimisation as a benchmark on the same site yields a layout optimised for AEP (fig. 7). This layout which represents the industry standard approach to designing offshore wind farms produces a layout with an LCOE of £90.53/MWh when evaluated using our evaluation function. This is slightly higher than the solution produced by this tool, and broken down represents a 0.69% decrease in discounted AEP and a 0.44%

increase in discounted cost compared to the solution generated by the GA shown in fig. 4. Though WindFarmer does not allow LCOE optimisation, it does represent the industry standard approach to designing wind farms. Further improvements to the proposed layout using the methodology at hand, could likely be found if the GA was run for more generations. Unfortunately, diversity was not maintained in the population and the optimiser was forced to stop prematurely.

The scatter diagram in fig. 8 indicates the mean wind speed experienced by all turbines in each wind speed bin for different layouts relative to the mean free wind speed in each directional sector. Using this approach for comparing the layouts, the relative wake loss by wind direction can be observed. From this figure, it can be observed that the inferior layout considered in fig. 5 leads to more significant reductions in the average wind speed in all wind directions than the more optimal layout shown in fig. 4. Though the relative decrease in wind speed is small, it is important to note that the power extracted by a wind turbine varies with the cube of the wind speed. This figure does also not consider the frequency of the wind directions, but is simply used to illustrate one of the key drivers of the LCOE. The overall wake loss is 4.39% for the inferior layout and 3.50% for the more optimal layout resulting in a change in AEP of 10,000 MWh per year.

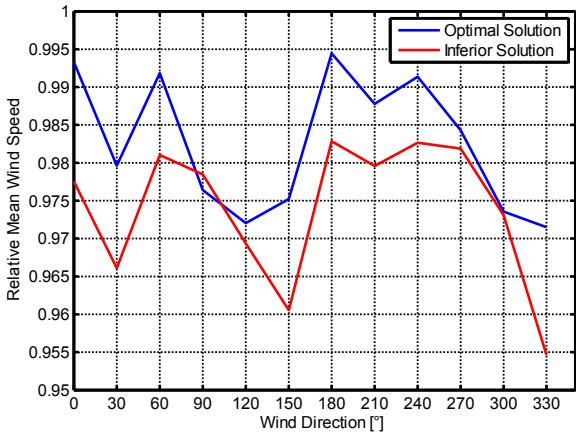

Fig. 8: Scatter diagram showing the mean wind speed experienced through the wind farm for each direction sector for different layouts relative to the mean free wind speed in each direction.

DISCUSSION AND CONCLUSIONS

The present work has highlighted the initial results from the development of a framework for the optimisation of offshore wind farm layouts using an adaptive genetic algorithm. It is believed that this framework will be useful in furthering the field of offshore wind farm layout optimisation as well as allowing developers to better understand the characteristics of their potential projects. The approach taken has introduced as many realistic constraints as possible in order to maximise the value of the framework while at the same time striving for accurate assessment of the energy yield of the wind farm, the costs, and the LCOE.

For the test case considered, a 50 position discrete grid was generated prior to execution of the GA. This grid was oriented such that rows of turbines were perpendicular to the dominant wind direction. From this, the GA selected which 30 of the 50 positions should be used. Interestingly looking at the difference between the worst result of the first generation and the best result of the last generation, there is a difference of approximately £2/MWh indicating that significant savings can be reached by applying an optimisation algorithm rather than randomly selecting the positions. Comparing the results of the GA against the industry standard approach using DNV-GL WindFarmer also shows improvements in LCOE by optimising the layout considering LCOE using the GA rather than AEP using WindFarmer's built in optimisation approach (£1/MWh improvement).

The number of valid turbine positions was selected arbitrarily to demonstrate the capabilities of this framework. Future work using this framework should explore the relationship between the number of turbines to be placed and the number of possible turbine positions in the discrete grid. Realistically, it would be expected that as the number of possible turbine positions increases, the solutions should improve in fitness however, at the same time as the number of possible positions increases, the regularity of the layout decreases and the search and rescue constraints will not remain satisfied. At the same time, the computational complexity will increase. With a grid including fewer holes than turbines, it was found that the search and rescue and navigational constraints were always satisfied, however, further work should explicitly explore this. Presently, the number of turbines to be positioned is also an input to the tool and further work should explore allowing the algorithm to select this as well with a maximum number of turbines constraint.

From the minimal and mean LCOE over generations plot (fig. 6) it can be seen that even though adaptive mutation and crossover rates are used, the GA still has some generations where though the population overall improves, the best solution does not. This indicates that further work could explore tuning of the GA parameters to improve the number of generations it takes to converge. Presently, however, the GA is terminating due to a loss in diversity, rather than true convergence, and improvements can be expected if methods for maintaining diversity in the population are introduced to the GA. Having said that, even without any further tuning, the GA still manages to identify a layout with a lower LCOE than using the industry standard approach with DNV-GL WindFarmer. This highlights the need to not only optimise for a metric taking into account both energy yield and cost, but also the advantage of introducing holes to a regular layout.

Given this platform, future work will expand on this study and look not only at further tuning the GA parameters to effectively solve this problem, but also to benchmark the GA against alternate optimisation algorithms. This platform will also allow alternate objective functions such as levelised production cost (LPC) or net present value (NPV) to be explored.

Application of this framework will also allow simplifications of the evaluation function to be explored. Presently, the evaluation function is relatively detailed with the most time being spent on evaluating the inter-array cable infrastructure and optimising this for each turbine layout under consideration. Future work using this framework will also be capable of comparing the results using alternate evaluation functions and characterising which elements of the layout the objective function is most sensitive to. At the same time, however, it is believed that the tool can scale to larger problems representing realistic offshore wind farms without an unrealistic increase in the computational power required. One iteration of 50 individuals has been run on a multi-cored desktop machine, however, it is expected that for a full-sized wind farm the execution of the tool will be transferred to a cluster allowing the larger problem to be solved in similar timescales as the test case by utilising more cores in parallel. Realistically for a full wind farm it would be expected that in lieu of using an extremely large population,

multiple runs will be completed with random seeding in order to ensure that the search space is effectively explored.

The applicability of this tool to larger offshore wind farms is still limited due to the simplification of the wakes, and the omission of the interactions between wind turbines and the atmospheric boundary layer (Frandsen, Barthelmie and Pryor, 2006). This large wind farm or deep-array effect has been explored by adding corrections to analytic wake models (Barthelmie, Rathmann, Frandsen, Hansen, Politis, Prospathopoulos, Rados, Cabezón, Schlez, Phillips, Neubert, Schepers and Pijl, 2007; Brower and Robinson, 2009). Future work intends on using the constructed framework to validate and tune these correction factors before applying them in the overall layout optimisation approach.

ACKNOWLEDGEMENTS

This work is funded in part by the ETI and RCUK Energy programme for IDCORE (EP/J500847/1).

REFERENCES

Ainslie, J. (1988). Calculating the flowfield in the wake of wind turbines. *Journal of Wind Engineering and Industrial Aerodynamics*, 27, pp.213–224.

Anderson, M. (2009). *Simplified Solution to the Eddy-Viscosity Wake Model*. Renewable Energy Systems Ltd.

Arthur, D. and Vassilvitskii, S. (2006). k-means ++ : The Advantages of Careful Seeding. *Proceedings of the eighteenth annual ACM-SIAM symposium on Discrete Algorithms*, 8, pp.1–11.

Barthelmie, R.J., Folkerts, L., Larsen, G.C., Frandsen, S.T., Rados, K., Pryor, S.C., Lange, B. and Schepers, G. (2006). Comparison of Wake Model Simulations with Offshore Wind Turbine Wake Profiles Measured by Sodar. *Journal of Atmospheric and Oceanic Technology*, 23(7), pp.888–901.

Barthelmie, R.J., Hansen, K., Frandsen, S.T., Rathmann, O., Schepers, J.G., Schlez, W., Phillips, J., Rados, K., Zervos, A., Politis, E.S. and Chaviaropoulos, P.K. (2009). Modelling and Measuring Flow and Wind Turbine Wakes in Large Wind Farms Offshore. *Wind Energy*, 12(June), pp.431–444.

Barthelmie, R.J., Rathmann, O., Frandsen, S.T., Hansen, K.S., Politis, E., Prospathopoulos, J., Rados, K., Cabezón, D., Schlez, W., Phillips, J., Neubert, a, Schepers, J.G. and Pijl, S.P. Van Der (2007). Modelling and measurements of wakes in large wind farms. *Journal of Physics: Conference Series*, 75, p.012049.

Brower, M. and Robinson, N. (2009). *The openWind deep-array wake model: development and validation*. AWS Truepower.

Burton, T., Jenkins, N., Sharpe, D. and Bossanyi, E. (2011). *Wind energy handbook* Second Edi., John Wiley & Sons, Ltd.

DNV GL - Energy (2014). *WindFarmer Theory Manual*. Garrad Hassan & Partners Ltd.

Elkinton, C.N. (2007). *Offshore Wind Farm Layout Optimization*. University of Massachussetts Amherst.

Fagerfjäll, P. (2010). *Optimizing wind farm layout – more bang for the buck using mixed integer linear programming*. Chalmers University of Technology and Gothenburgh University.

Frandsen, S., Barthelmie, R. and Pryor, S. (2006). Analytical modelling of wind speed deficit in large offshore wind farms. *Wind Energy*, (January), pp.39–53.

Gaumond, M., Rethore, P. and Bechmann, A. (2012). Benchmarking of Wind Turbine Wake Models in Large Offshore Windfarms. *Proceedings of the Science of Making Torque from Wind Conference*.

Grady, S.A., Hussaini, M.Y. and Abdullah, M.M. (2005). Placement of wind turbines using genetic algorithms. *Renewable Energy*, 30(2), pp.259–270.

Grefenstette, J.J. (2006). Optimization of Control Parameters for Genetic Algorithms. *IEEE Transactions on Systems, Man, and Cybernetics*, SMC-16(February), pp.122–128.

Guillen, F.B. (2010). *Development of a design tool for offshore wind farm layout optimization*. Delft University of Technology.

Haupt, R.L. and Haupt, S.E. (2004). *Practical Genetic Algorithms* Second Edi., Wiley-Interscience Publication.

Holland, J.H. (1992). *Adaptation In Natural And Artificial Systems. [Electronic Resource] : An Introductory Analysis With Applications To Biology, Control, And Artificial Intelligence* Second Edi., Cambridge, Mass.: MIT Press.

Katic, I., Højstrup, J. and Jensen, N.O. (1986). A Simple Model for Cluster Efficiency. *European Wind Energy Conference and Exhibition 1986*, (October), pp.407–410.

Larsen, G.C. (1988). *A Simple Wake Calculation Procedure*. Risø National Laboratory.

Larsen, G.C., Madsen, H.A., Troldborg, N., Larsen, T.J., Réthoré, P.-E., Fuglsang, P., Ott, S., Mann, J., Buhl, T., Nielsen, M., Markou, H., Sørensen, J.N., Hansen, K.S., Mikkelsen, R., Okulov, V., Shen, W.Z., Heath, M., King, J., McCann, G., Schlez, W., Carlén, I., Ganander, H., Migoya, E., Crespo, A., Jiménez, A., Prieto, J.L., Stidworthy, A., Carruthers, D., Hunt, J., Gray, S., Veldkamp, D., Mouritzen, A.S., Jensen, L., Krogh, T., Schmidt, B., Argyriadis, K. and Frohnböse, P. (2011). *TOPFARM - Next Generation Desgin Tool for Optimisation of Wind Farm Topology and Operation*, Roskilde, Denmark: Information Service Department, Risø National Laboratory for Sustainable Energy Technical University of Denmark.

Larsen, G.C. and Réthoré, P.E. (2013). TOPFARM - A Tool For Wind Farm Optimization. *Energy Procedia,* 35, pp. 317-324.

MacQueen, J. (1967). Some methods for classification and analysis of multivariate observations. *Proceedings of the fifth Berkeley symposium on Mathematical Statistics and Probability*, 233(233), pp.281–297.

Mosetti, G., Poloni, C. and Diviacco, B. (1994). Optimization of wind turbine positioning in large wind-farms by means of a genetic algorithm. *Journal of Wind Engineering and Industrial Aerodynamics*, 51(1), pp.105–116.

NOREL Group (2013). *Nautical and Offshore Renewable Energy Liaison Group (NOREL) Action Points from the 27th NOREL held on 11 July 2013*.

Pérez, B., Mínguez, R. and Guanche, R. (2013). Offshore wind farm layout optimization using mathematical programming techniques. *Renewable Energy*, 53, pp.389–399.

Pillai, A.C., Chick, J., Johanning, L., Khorasanchi, M. and de Laleu, V. (2015). Offshore wind farm electrical cable layout optimization. *Engineering Optimization*, (January), pp.1–20.

Pillai, A.C., Chick, J. and de Laleu, V. (2014). Modelling Wind Turbine Wakes at Middelgrunden Wind Farm. *Proceedings of EWEA 2014*.

Renkema, D.J. (2007). *Validation of wind turbine wake models*. TU Delft.

Sanderse, B., Pijl, S. and Koren, B. (2011). Review of computational fluid dynamics for wind turbine wake aerodynamics. *Wind Energy*, (February), pp.799–819.

Schlez, W. and Neubert, A. (2009). New developments in large wind farm modelling. *Proceedings of EWEC 2009*.

Srinivas, M. and Patnaik, L.M. (1994). Adaptive probabilities of crossover and mutation in genetic algorithms. *IEEE Transactions on Systems, Man, and Cybernetics*, 24(4), pp.656–667.

Proceedings of the ASME 2016 34th International Conference on Ocean, Offshore and Arctic Engineering
OMAE 2016
June 19-24, 2016, Busan, South Korea

OMAE2016-54145

COMPARISON OF OFFSHORE WIND FARM LAYOUT OPTIMIZATION USING A GENETIC ALGORITHM AND A PARTICLE SWARM OPTIMIZER

Ajit C. Pillai*
Industrial Doctorate Centre for
Offshore Renewable Energy
The University of Edinburgh
Edinburgh, United Kingdom
Email: a.pillai@ed.ac.uk

Dr. John Chick
Institute for Energy Systems
The University of Edinburgh
Edinburgh, United Kingdom

Prof. Lars Johanning
College of Engineering,
Mathematics, and Physical Sciences
University of Exeter
Penryn, United Kingdom

Dr. Mahdi Khorasanchi
Department of Naval Architecture,
Ocean and Marine Engineering
University of Strathclyde
Glasgow, United Kingdom

Dr. Sami Barbouchi
EDF Energy R&D UK Centre
London, United Kingdom

ABSTRACT

This article explores the application of a binary genetic algorithm and a binary particle swarm optimizer to the optimization of an offshore wind farm layout. The framework developed as part of this work makes use of a modular design to include a detailed assessment of a wind farm's layout including validated analytic wake modeling, cost assessment, and the design of the necessary electrical infrastructure considering constraints. This study has found that both algorithms are capable of optimizing wind farm layouts with respect to levelized cost of energy when using a detailed, complex evaluation function. Both are also capable of identifying layouts with lower levelized costs of energy than similar studies that have been published in the past and are therefore both applicable to this problem. The performance of both algorithms has highlighted that both should be further tuned and benchmarked in order to better characterize their performance.

*Address all correspondence to this author.

INTRODUCTION

With the development of large offshore wind farms it has become increasingly important to ensure that wind farms are designed such that they use the available space as efficiently as possible.

Wind farm layout optimization tools have grown significantly in recent years from the original tools such as those developed by Mosetti et al. [1] or Grady et al. [2] to include not only the impact the turbine positions have on the energy extracted from the wind, but also to include the impact on the project costs as a result of changes in the layout [3–6]. In recent years, many studies have explored the performance and applicability of different optimization strategies to the wind farm layout optimization problem [7–16]. With the aim of advancing this field further, a layout optimization framework has been developed, including a more detailed approach for assessing wind farm layouts and including as many real world constraints as possible, enabling this framework to be applied to real sites by a project developer.

The levelized cost of energy (LCOE) acts as a single metric which encompasses the annual energy production (AEP) of the wind farm over its lifetime as well as the lifetime project costs.

By using such a metric to evaluate the layouts, it takes into account both the lifetime energy generated by the wind farm and the lifetime costs, allowing a project developer to easily compare the layouts on an economic basis which relates both the energy outputs of the project and the cost inputs. This optimization framework therefore minimizes the LCOE of the wind farm by adjusting the turbine positions, substation positions, and cable routes, ensuring that the effect this has on the AEP and project costs are accurately accounted for.

The LCOE expressed in £/MWh is mathematically given by:

$$LCOE = \frac{\sum_{t=1}^{n} \frac{C_t}{(1+r)^t}}{\sum_{t=1}^{n} \frac{AEP_t}{(1+r)^t}} \quad (1)$$

where C_t is the total costs incurred in year t, n is the project lifetime, AEP_t is the annual energy production in year t, and r is the discount rate of the project.

The present framework has been developed with future UK wind farm sites in mind and therefore includes the consideration of constraints and costs that a future UK offshore wind farm will face. Initial results of this framework previously presented by the authors have shown that it is capable of satisfying real world constraints while at the same time including a validated evaluation function in a manner in which existing work does not [17].

This article deploys this modular framework using two separate optimization algorithms in order to both simultaneously benchmark the framework against existing work, and to identify the differences in performance between the genetic algorithm (GA) and the particle swarm optimization (PSO) algorithm. By deploying these two different optimization algorithms using the same framework, the results can be directly compared advising future work in this field.

APPROACH

The framework deployed for this study is made up of separate modules for the the design of the electrical infrastructure, assessment of the AEP, estimation of the project costs, and for the overall optimization. This approach has allowed alternate wake models, cost functions, and optimization algorithms to be implemented and tested as part of the development. As part of the development, each individual module has been validated independently prior to integrating them into the larger optimization tool. This work, looks specifically at the comparison of two optimization modules for the same case study keeping all other modules in the framework constant. In order to compute the LCOE and thereby get an assessment of each layout, it is necessary for the approach to design the necessary electrical infrastructure, assess the AEP, and estimate the cost in sequence as shown in fig. 1.

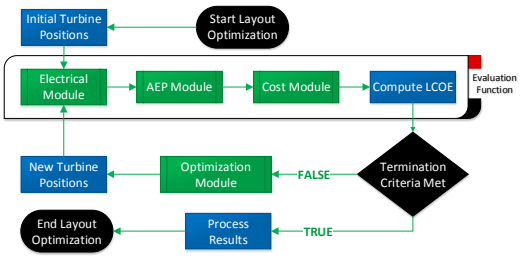

FIGURE 1: MODULAR APPROACH TO WIND FARM LAYOUT OPTIMIZATION

In the case of both optimization algorithms, the assessed LCOE for each layout is an important contributor to how new candidate solutions are generated in subsequent iterations. The LCOE is therefore needed for each layout in order for the optimization algorithms to successfully navigate the search space.

Evaluation of LCOE

As indicated in fig. 1, the assessment of the LCOE is subdivided into three distinct steps. In the first, the electrical infrastructure required for a given turbine layout is determined, then the energy production of the wind farm is assessed, and finally this information is used to estimate the project costs and establish an LCOE for the given layout. The overall approach for the evaluation function is described in greater detail in previous work by the authors [17, 18].

Electrical Infrastructure Optimization. Existing offshore wind farm layout optimization tools generally do not consider any impact on the project cost as a result of changes in the substation positions or intra-array cables [1–5, 7–16]. By including this in the present framework, the accuracy of the cost function is increased and it is easier to differentiate accurately between different layouts. Given that the cost of cables can exceed £500,000 per kilometer installed, it is important that this length be computed accurately [18].

The developed electrical infrastructure optimization tool is unique in its ability to consider not only the electrical constraints of the turbines, substations, and cables, but also the bathymetry, seabed features which define constraint regions, and the physical constraints of the turbines. This therefore, allows the electrical infrastructure optimization tool to propose realistic layouts which satisfy the real constraints of an offshore wind farm developer. It should be noted that as a heuristic approach is used

to define the possible cable paths, the electrical infrastructure is therefore not guaranteed to reach proven optimality, but will find a good feasible solution.

The overall approach further divides the optimization of this infrastructure into three separate stages:

1. Determination of substation positions
2. Determination of possible intra-array cable paths
3. Selection of intra-array cable paths to use

The substation positions and the assignment of turbines to a specific substation are found based on applying a modified version of the *kmeans++* clustering algorithm [19]. It has previously been shown that by placing the substation as close as possible to the center of a wind farm, the intra-array cable costs will be reduced [18,20]. Using the cluster center as the substation position therefore minimizes the distance between the substation and all the turbines assigned to that substation. In this tool, the standard *kmeans++* algorithm is modified to account for the capacity constraints on substations, and the fact that within the wind farm area there may be regions where substations cannot be placed [18].

Once the substation positions are determined and the turbines have been assigned to a specific substation, a pathfinding algorithm is used to identify the possible cable paths and the accurate distance that a cable must cover in order to connect any two turbines, or any of the turbines and the substation. The use of the pathfinding algorithm accounts for the fact that there are regions where cables cannot be placed and must therefore navigate around. From this, a capacitated minimum spanning tree (CMST) is constructed based on the cable costs identified through the use of the pathfinding algorithm. In this case, the CMST represents the optimal intra-array cable network given the possible paths under consideration. The CMST is solved using a standard mixed-integer linear programming (MILP) formulation using the commercial solver Gurobi [21]. As cables in offshore wind farms cannot cross one another, a check is done after solving the MILP problem. If any crossings are found, these individual constraints are introduced to the MILP problem and the problem is resolved. This process has been found to solve the MILP problem more quickly than including all the crossing constraints from the beginning [18].

The electrical infrastructure optimization is run first as part of the evaluation function in order to account for the electrical cable losses in the AEP calculation, and the cable costs in the project cost module.

AEP Estimation. The assessment of the AEP includes considering the local wind conditions, modeling the wakes that develop within the wind farm, as well as modeling any other sources of energy loss that are affected by the wind farm layout.

Any device extracting energy from a natural flux such as winds, is known to directly impact that flux. In the case of wind turbines, the region directly behind an operating wind turbine, known as the wake, is characterized by reduced wind speeds and higher levels of turbulence [22–25]. Wakes of multiple turbines are also known to interact with one another, such that when estimating the AEP for an entire wind farm it is important to account for the impact that the wakes have on one another [26,27]. Though a number of kinematic wake models have been implemented into the framework, the present study uses the G.C. Larsen wake model [28, 29]. This model was selected as previous studies have shown this to be a good balance between accuracy and computational intensity [30, 31].

The AEP is assessed by stepping through each wind speed and direction combination and modeling, using a kinematic wake model, the impact that each turbine has on the free wind speed. Each turbine, therefore, experiences conditions based on how the wakes of the upstream turbines impact the free wind speed. The turbine power curve is then used to assess the energy production from each individual wind turbine using the respective wind speed that they experience. From this, the electrical cable losses for that specific set of conditions is then assessed given the intra-array cable layout previously designed. The total generation for this free wind condition is then scaled by the number of hours during the year that this condition would be expected, and the sum of each of these scaled outputs for all the wind conditions under consideration gives the AEP [17].

$$AEP = 8766 \times \sum_{d_i} \sum_{v_i} P(d_i, v_i) \times [E(d_i, v_i) - L(d_i, v_i)] \quad (2)$$

where d_i is the wind direction; v_i is the wind speed; $P(d_i, v_i)$ is the probability of the combination of d_i and v_i; $E(d_i, v_i)$ is the energy production for the wind farm for that combination of free wind speed and direction; and $L(d_i, v_i)$ is the electrical losses associated with that wind speed and direction.

Cost Assessment. The final step in the assessment of a layout is the determination of the costs incurred by the wind farm. For an offshore wind farm, eight principle cost elements have been identified which all have varying degrees of sensitivity to the layout (table 1). Each of the cost elements outlined in table 1 are estimated using a validated cost model which considers not only the positions of the turbines, but also the water depth. The implemented cost model has been validated where possible using available published data and data supplied by active projects currently under development [17]. By including costs which are relative to the turbines' absolute position and their relative position to one another, more accurate project costs can be computed compared to existing optimization frameworks [7–16].

Though some costs such as the foundation costs, and the cable installation costs would be expected to be impacted by the

TABLE 1: COST ELEMENT CONTRIBUTION TO CAPEX

Cost Element	CAPEX	OPEX	Sensitivity to Layout
Turbine Supply	✓	-	Low
Turbine Installation	✓	-	Medium
Foundation Supply	✓	-	Medium
Foundation Installation	✓	-	Medium
Intra-Array Cables	✓	-	High
Decommissioning	✓	-	Medium
Operations and Maintenance	-	✓	Medium
Offshore Transmission Assets	✓	✓	Low

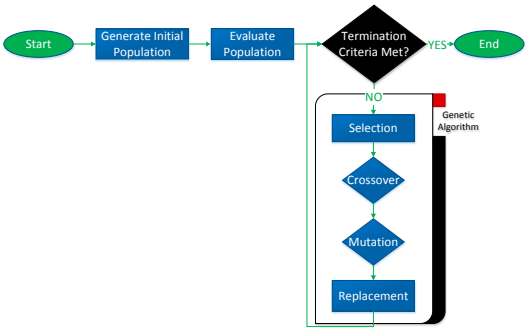

FIGURE 2: FLOWCHART OF THE GENETIC ALGORITHM

soil conditions at the site, previous work has found that even if very detailed geotechnical data is available, a bottom-up cost model tends to validate poorly [3]. Considering this and the fact that the tool would likely be applied at an early stage when geotechnical data would not be available, the present cost relations ignore the geotechnical and soil conditions. Having said that, the modular approach developed would make it straight forward for the optimization process to consider this if the data was available and the cost relationships established.

Genetic Algorithm

The final step of the procedure is to use an optimization algorithm to alter the wind turbine layouts given the LCOE values of already assessed layouts. GAs represent a family of bio-inspired population based heuristic optimization algorithms that borrow ideas from natural evolution as observed in biological systems [32]. GAs are commonly deployed as they represent a family of generic algorithms which can be applied to a wide range of problems of varying degrees of complexity [33]. As such, GAs have commonly been applied to the offshore wind farm layout optimization problem with good quality solutions being found [1–3, 5, 34, 35].

In a GA, the candidate solutions within the population are formulated such that the encoding can be considered a *genome* which defines the individual solutions. The evaluation function is used to determine the *fitness* of each solution. In this case, the fitness of each layout is the LCOE, with small LCOE values considered to be superior in fitness. Under these terms, the GA then tries to use solutions with favorable fitness values to generate new candidate solutions. Solutions with higher fitness values (in this case, layouts with lower LCOE values) have a higher probability of contributing genetic material towards new candidate solutions. The flowchart in fig. 2 shows the principle steps of a GA. After selecting pairs of individuals among the population to reproduce (i.e. to generate new candidate solutions), the pair undergoes what is referred to as *crossover*. During crossover, the two *parent* solutions are combined in such a way that two new solutions are generated, each with 50% of their genome being defined by each parent. In this way, the two candidate child solutions represent a combination of the two parents, hopefully exploiting the good elements of the two parents to create a solution with a superior fitness value. In order to ensure that the GA does not get stuck at a local solution, a *mutation* operator is used to randomly alter the child solutions. This process is repeated until the solutions converge, or there is insufficient diversity within the remaining population for the process to continue effectively. An *elitism factor* is used to define what proportion of the population must be replaced with new solutions in each generation.

In this case, as the wind farm region has been discretized, the problem can be solved using a binary genetic algorithm. A binary genetic algorithm is one in which the genome is represented as a binary string. In this case, each bit of the genome represents the presence of a turbine in a specific cell of the discretized wind farm area. Given the binary GA approach, crossover is implemented using a uniform crossover mask. This is a method in which if crossover occurs, a second binary string the same length as the genome is generated. This string, however, represents which parent the children should inherit each individual bit from (i.e. each bit in the crossover mask represents which parent contributes to that specific bit in the child solution). To generate two complementary children, the crossover mask has every bit flipped to generate a second child. The mutation operator also works on a bitwise basis, cycling through each bit in the child solutions with a low probability that each bit gets flipped.

The key parameters that define a GA are therefore the size of the population; the probabilities associated with mutation and crossover; and the elitism factor. In the present implementa-

tion, adaptive parameters are used for the mutation and crossover rates as this has been shown to improve convergence and foster diversity within the population [36]. The crossover and mutation probabilities are therefore a function of the solution's fitness value (f) compared to the population's mean fitness ($\bar{f}$), the population's best fitness (f_{max}), and the fitness value of the best parent (f').

$$p_c = \frac{k_1 (f_{max} - f')}{f_{max} - \bar{f}} \quad \text{for} \quad f' \geq \bar{f} \tag{3}$$

$$p_c = k_3 \quad \text{for} \quad f' < \bar{f} \tag{4}$$

$$p_m = \frac{k_2 (f_{max} - f)}{f_{max} - \bar{f}} \quad \text{for} \quad f \geq \bar{f} \tag{5}$$

$$p_m = k_4 \quad \text{for} \quad f < \bar{f} \tag{6}$$

where p_c and p_m are respectively the probabilities of crossover and mutation. The population size was kept at 50 individuals, and an elitism factor of 25% was used.

Particle Swarm Optimization

The GA is often thought of as a competitive population based optimization algorithm, as a solution's ability to contribute to the improvement among its peers is based on its own fitness. The PSO on the other hand is considered to be a cooperative population based optimization algorithm in which the candidate solutions (now thought of as particles) explore the search space while aware of their neighbors [33]. Like the GA, this algorithm is also analogous to a biological system, though unlike the GA rather than based on an evolutionary process, it is based on how birds flock or fish school [37]. The general approach is shown in fig. 3.

In a PSO, the particles are randomly seeded in a manner

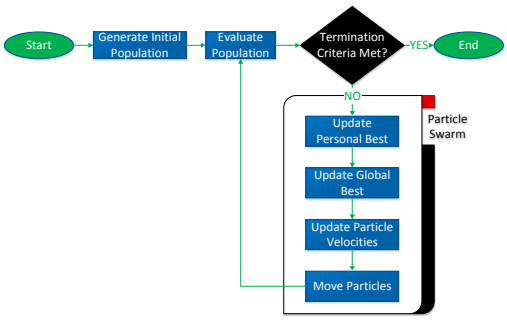

FIGURE 3: FLOWCHART OF THE PARTICLE SWARM OPTIMIZATION ALGORITHM

similar to that of a GA, however, from here the two algorithms differ quite significantly. A PSO treats the candidate solutions and particles exploring the search space. In this analogy, the change from generation to generation is encapsulated in what is thought of as the particle's velocity through the search space. This velocity is partially random to avoid local minima, partially based on the particle's historical best position within the search space, and partially on the population's best position. In this way, by including the particle's previous best position, and the global best positions, the particle tries to exploit the knowledge of the swarm, while the random element helps the particle explore the search space. A major difference between the PSO and the GA is that the PSO allows particles to decline in fitness from generation to generation, recognizing that it may lead to better future positions. In the PSO, each particle's position at any given iteration is related to its past position by:

$$x_i = x_{i-1} + v_{i-1}; \tag{7}$$

where the velocity v_i is given by:

$$v_i = C_1 v_{i-1} + C_2(p - x_i) + C_3(g - x_i) + C_4 \times rand \tag{8}$$

where C_1, C_2, C_3, and C_4 are coefficients representing the weighting of the different contributors determined by tuning the PSO to the problem at hand; p is the best historical position of the particle in question, g is the best historical position of the swarm, and *rand* is a random number between 0 and 1.

Like the GA, the PSO was implemented with a binary encoding. This complicates matters slightly because the position for each bit must be either 0 or 1. The continuous velocity, must therefore be adjusted such that it corresponds to the bit in question changing to either a 0 or a 1. To solve this, a sigmoid transfer function is commonly used to convert the velocity for a given bit to a probability of the bit being a 1 [38–40].

Using this standard transfer function, however, introduces a challenge in satisfying the number of turbines constraint. In order to easily check and satisfy this constraint, the transfer function was redefined such that it represented the probability that a bit is flipped. This then allowed the algorithm to ensure that equal numbers of 1's and 0's were flipped thereby preserving the number of turbines within the wind farm. This, however, required a change in the transfer function as both highly negative and highly positive velocities should correspond to a high probability of the bit flipping. This was done by replacing the s-shaped sigmoid function with a v-shaped function [40]. Figure 4 shows typical s-shaped (sigmoid) and v-shaped transfer functions.

In general, PSO has been found to be suitable for solving similar problems as the GA. However, the PSO tends to require

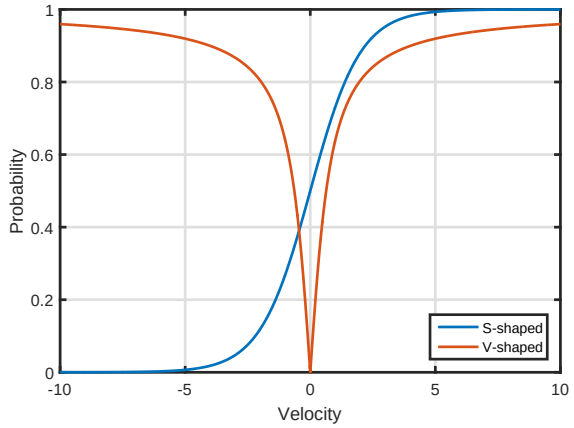

FIGURE 4: TRANSFER FUNCTIONS FOR BINARY PARTICLE SWARM OPTIMIZER

a smaller population to reach similar quality solutions, and as the number of function evaluation calls is related to the size of the population, a smaller population will result in a quicker execution time. PSOs, however, can suffer from premature convergence and sensitivity to local solutions when the population is insufficiently large. For these simulations a population size of 30 was used.

RESULTS

Case Definition

For this comparison of the GA and the PSO it was desirable to use a case which had previously been addressed in other layout optimization projects in order to simultaneously highlight the advantages of including a comprehensive layout evaluation function as well as allowing the optimization algorithms to be benchmarked.

In one of the first works to explore the optimization of wind farm layouts, Mosetti et al. [1] laid out case studies which have been commonly used since. Each of these cases considers a square shaped wind farm area (2 km by 2 km) discretized into 100 possible turbine positions. Given the discretization of the wind farm area, the optimization problem can be implemented as a binary decision problem.

One of these cases, which is under consideration in this study, considers a "case of multiple wind direction with constant intensity" [1]. This wind regime is defined as having a constant wind speed of $12\,\mathrm{m\,s^{-1}}$ with an equal probability that the wind will blow from any direction. For the computation, the wind direction is defined as being discretized into 36 sectors each of 10° width.

The original definition of the cases omitted the water depth, the location of ports to be used relative to the wind farm, or any regions that must be avoided as these were not seen as impacting the layouts. However, all are used by by the present evaluation function in the determination of a layout's LCOE. In order to keep the case as close as possible to the original definition while using the more detailed evaluation function developed here, a constant water depth was assumed, the port was assumed to be very far away relative to the size of the wind farm, and it was assumed that no constraint regions existed within the wind farm area.

As the case study does not define the number of turbines under consideration, the case study was executed for two different wind farm sizes (19 and 39 turbines) corresponding to the results shown in two layout optimization studies using these cases [1,2]. In order to compare fairly, the published optimal layouts for this case study have been re-evaluated using our evaluation function in order to ensure that a direct layout-to-layout comparison can be done for both wind farm sizes.

Though more recent work has explored the same case study, these have on the whole explored the application of more advanced optimization algorithms than the original, making use of the same evaluation function. These studies have also either not used the same number of turbines or the same discretized grid making it difficult to make a fair comparison [7–16]. The work by Mosetti et al. [1] and Grady et al. [2] remain the reference cases which new work is compared against. The present work has focused on the improvement of the evaluation function by adding the detail necessary for the tool to be applied to real sites by a project developer. The results presented here are meant to highlight that even with the increased detail in the evaluation function, these optimization techniques are of interest and can highlight improvements over the original work in the field [1,2].

TABLE 2: ASSESSMENT OF LAYOUTS

	Number of Turbines	AEP [GWh]	Cost [£]	LCOE [£/MWh]
Mosetti et al. [1]	19	81.71	3.770×10^8	540.25
GA-19	19	81.77	3.771×10^8	539.88
PSO-19	19	82.11	3.769×10^8	537.49
Grady et al. [2]	39	156.99	5.620×10^8	419.00
GA-39	39	159.23	5.613×10^8	412.60
PSO-39	39	159.00	5.616×10^8	413.50

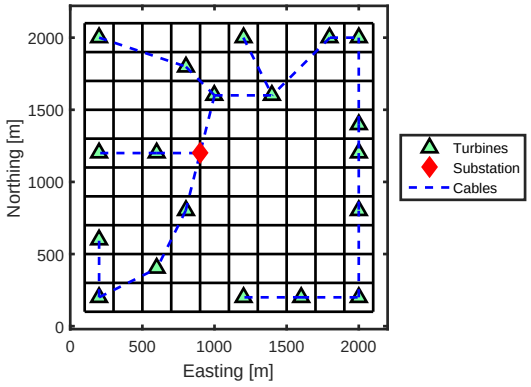

FIGURE 5: LAYOUT PRODUCED BY GA WITH 19 TURBINES

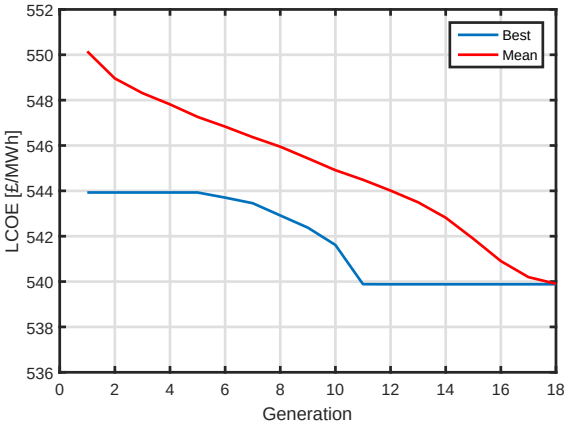

FIGURE 7: CONVERGENCE PLOT FOR GA WITH 19 TURBINES

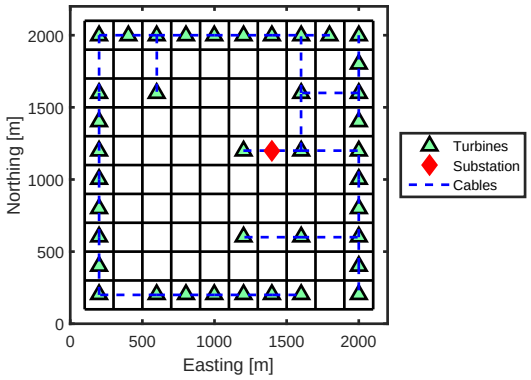

FIGURE 6: LAYOUT PRODUCED BY GA WITH 39 TURBINES

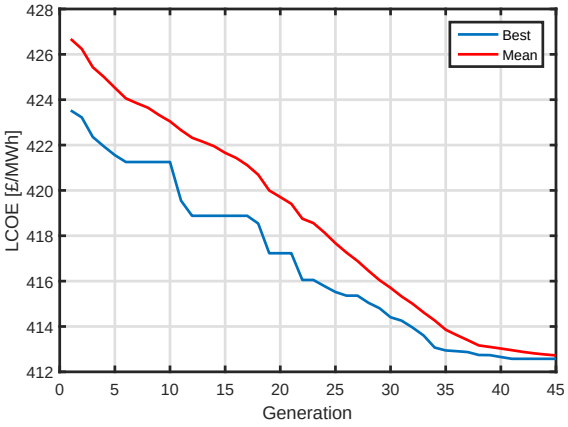

FIGURE 8: CONVERGENCE PLOT FOR GA WITH 39 TURBINES

Genetic Algorithm

Figures 5 and 6 show the layouts produced by the GA. As can be seen, the proposed layouts differ significantly from one another as a result of the additional 20 turbines in the larger wind farm. The plots shown in figs. 7 and 8 show that in both cases the solution converged and the diversity within the population fell below the required threshold terminating the optimization run. Table 2 shows the results attained in this study compared to the layouts proposed by the benchmark studies [1, 2].

Particle Swarm Optimization

Similar to the results of the GA, the PSO was run for both wind farm sizes in order to compare the layouts to both those generated by the adaptive GA and those produced by the previous studies [1, 2]. The layouts produced by the PSO are shown in figs. 9 and 10.

Like the GA, the results in table 2 indicates that the PSO produces layouts for both wind farm sizes that have lower LCOE values than the past studies [1,2]. Interestingly, the PSO does not create the same solutions as the GA.

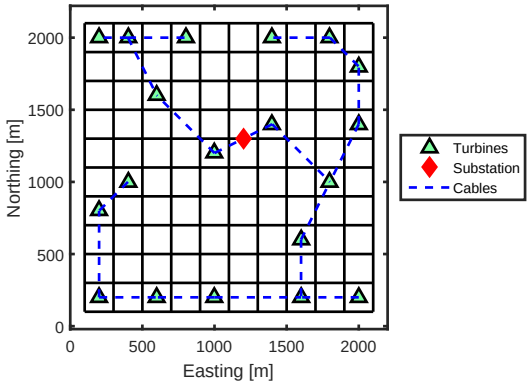

FIGURE 9: LAYOUT PRODUCED BY PSO WITH 19 TURBINES

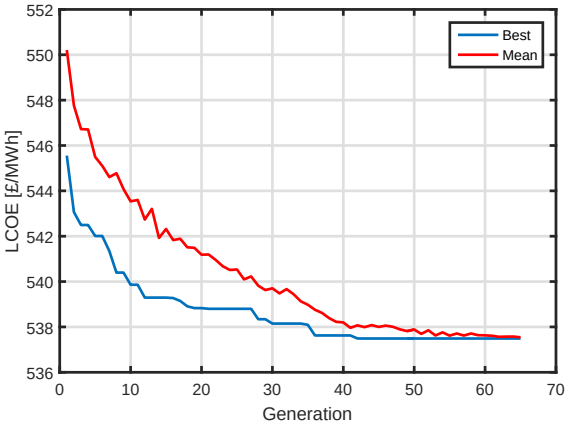

FIGURE 11: CONVERGENCE PLOT FOR PSO WITH 19 TURBINES

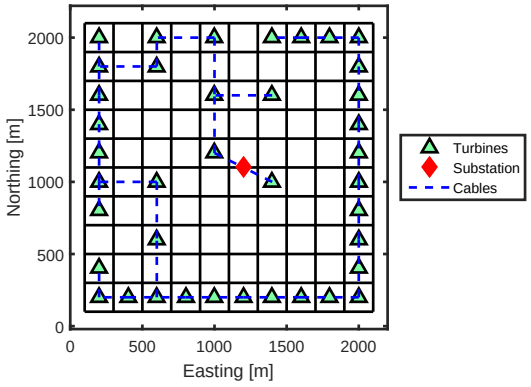

FIGURE 10: LAYOUT PRODUCED BY PSO WITH 39 TURBINES

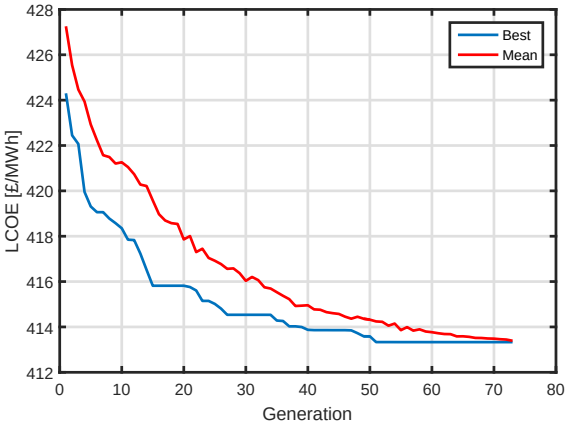

FIGURE 12: CONVERGENCE PLOT FOR PSO WITH 39 TURBINES

DISCUSSION AND CONCLUSIONS

From the four solutions presented here, it can be seen that the new framework shows that given a more accurate evaluation function, both the GA and the PSO are capable of finding better solutions than those found by previous studies [1, 2]. This is an important result as it indicates that even given the increased complexity of the evaluation function, these optimization algorithms are relevant choices.

In general as can be seen in the convergence plots (figs. 7, 8, 11 and 12), all four solutions represent the best solutions found by the solvers prior to convergence. The performance of the GA with the small wind farm, however, showed very quick convergence indicating that the population may have prematurely converged. This suggests that though the solution found is good and in fact better than that found by the literature for the same sized wind farm, it could be further improved by further tuning or executing multiple runs. In fact, comparing it to the PSO results for the same conditions, one can see that the PSO finds a much better solution than both the implemented GA and the results of past studies used as a benchmark [1, 2]. In fact, as heuristic algorithms are deployed, there is no guarantee that proven optimality has been reached and both optimizers could be further tuned to

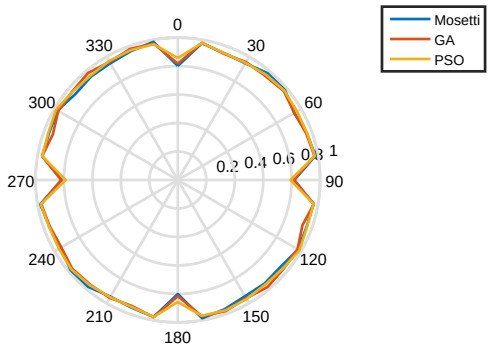

FIGURE 13: WAKE EFFICIENCY BY WIND DIRECTION FOR 19 TURBINE WIND FARM

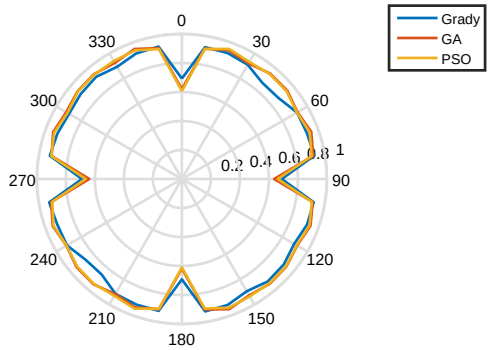

FIGURE 14: WAKE EFFICIENCY BY WIND DIRECTION FOR 39 TURBINE WIND FARM

ensure that they have not prematurely converged.

Both the layouts proposed by this framework for the 39 turbine wind farm (figs. 6 and 10) appear to exploit the symmetry of the wind resource by the majority of the turbines along the edge of the wind farm with the GA slightly outperforming the PSO in this case. For both the proposed layouts, this leads to significant wakes along the four wind direction sectors that are aligned with these edges, however, it also leads to relatively high wake efficiency for the remaining 32 directions (figs. 13 and 14). Taking this idea to the extreme, a case was executed using the GA where three turbines were to be placed in the 64 central cells, and the

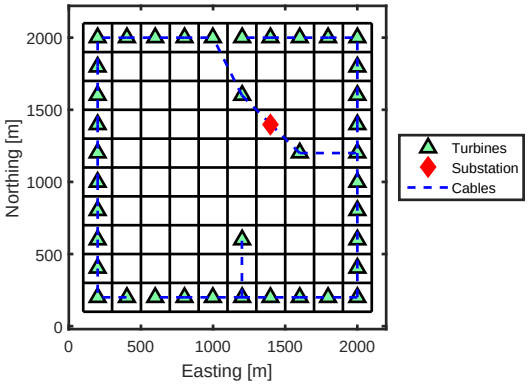

FIGURE 15: LAYOUT PRODUCED BY GA WITH 36 TURBINES FIXED TO EDGE

remaining 36 turbines were locked to the 36 cells along the edges (results shown in fig. 15). For this restricted case, the GA was, however, unable to find a solution that was superior to the layout presented in fig. 6 with the best solution in this restricted case having an LCOE of £412.77/MWh. Though this is very similar to the GA result shown in fig. 6 (LCOE of £412.60/MWh), it is marginally higher, indicating that the optimal solution is likely not symmetrical. It is important to note that though the resource may be symmetrical, the cost functions are not, and we would not therefore expect the optimal layout to be symmetrical.

The wake efficiency plots (figs. 13 and 14) indicate the relative efficiency of the different wind sectors across the different layouts. As can be seen, there is a variation in performance across all sectors, including the inline directions which result in significant reductions in AEP across all the layouts. Interestingly, for the small wind farm it appears to be the slight increase in wake efficiency along these inline wind directions which results in the marginal increase in AEP. For the larger wind farm, however, there are significant increases along the 40°, 50°, 220°, and 230° directions in addition to the North and South inline cases. For both the GA and PSO, however, the East and West wind directions are less efficient than the reference layout.

Given the simplicity of the case at hand, the inclusion of the electrical infrastructure optimization does not significantly affect the layouts produced as it has a very minimal impact on both the AEP and cost. Given the small size of the turbines considered in this case study (659 kW), all the turbines considered could be connected on a single string reducing the sensitivity of the cable cost to the layout. Furthermore, as the site was assumed to be a constant water depth, the cost variation across this site does not represent a realistic case and the very slight improvements

in cost observed come principally from reductions in the installation processes. A real wind farm will be expected to observe a more significant reduction in cost as a result of improvements made to the layout. Given this, the present case is dominated by the AEP term with the electrical infrastructure and cost modules yielding small impacts to the LCOE. However, it can be expected that for large offshore wind farms with real constraints impacting where substations, turbines, and cables can be placed the inclusion of these modules will be necessary in order to ensure that the layouts produced are feasible and to ensure that the LCOE is accurately estimated for the layout.

As the PSO does not require particles to improve in fitness from generation to generation, each iteration of the PSO requires the same number of evaluation calls. The GA, however, looks to replace a specific proportion of the population each generation with superior individuals. The number of layouts that need to be generated and therefore the total number of evaluation calls varies from generation to generation. For the same size population, the PSO would therefore be expected to be faster, as in general fewer evaluation calls will be needed, especially after the results begin to converge. Having said that, PSOs are generally run with a smaller population than their equivalent GA further reducing the total number of evaluation calls required and therefore the execution time.

The initial results shown here have indicated that both the GA and PSO implemented here are capable of finding superior layouts to those that have been identified in previous published studies [1, 2]. At the same time, both the GA and PSO have found solutions of similar quality and as neither optimizer outperforms the other consistently, it has indicated that both are applicable to this problem, though for the reasons stated earlier, the PSO may offer significant time savings when compared to the GA. Future work can explore the application of this framework to additional test cases in order to further benchmark the framework as well as aid in the tuning of both optimization algorithms. A principle output of this work is that though the objective function has increased complexity due to the inclusion of a more detailed cost function and the optimization of the electrical infrastructure, these optimization algorithms are still effective for addressing this problem. While previous studies [7–16] have addressed the problem using a simple evaluation function, this study has advanced the field by including instead a detailed evaluation function representative of what a project developer would use to assess future projects. This demonstrates that the present framework would be of use to a wind farm developer. Future work should also explore the importance of including the electrical infrastructure optimization through the application of the framework to large real offshore wind farms. An important point to note is that the results presented represent only single runs of the optimization algorithm. Given the stochastic nature of the optimization algorithms, future work should explore performing multiple runs and looking at the average results of these ensembles of runs.

ACKNOWLEDGMENT

This work is funded in part by the Energy Technologies Institute (ETI) and RCUK energy program for IDCORE (EP/J500847/1).

REFERENCES

[1] Mosetti, G., Poloni, C., and Diviacco, B., 1994. "Optimization of wind turbine positioning in large wind-farms by means of a genetic algorithm". *Journal of Wind Engineering and Industrial Aerodynamics,* ***51***(1), pp. 105–116.

[2] Grady, S., Hussaini, M., and Abdullah, M., 2005. "Placement of wind turbines using genetic algorithms". *Renewable Energy,* ***30***(2), feb, pp. 259–270.

[3] Elkinton, C. N., 2007. "Offshore Wind Farm Layout Optimization". Doctor of philosophy dissertation, University of Massachussetts Amherst.

[4] Elkinton, C. N., Manwell, J. F., and McGowan, J. G., 2008. "Algorithms for offshore wind farm layout optimization". *Wind Engineering*, pp. 67–83.

[5] Réthoré, P.-E., Fuglsang, P., Larsen, T. J., Buhl, T., and Larsen, G. C., 2011. *TOPFARM wind farm optimization tool*. Riso DTU National Laboratory for Sustainable Energy.

[6] Chowdhury, S., Zhang, J., Messac, A., and Castillo, L., 2013. "Optimizing the arrangement and the selection of turbines for wind farms subject to varying wind conditions". *Renewable Energy,* ***52***(315), apr, pp. 273–282.

[7] Marmidis, G., Lazarou, S., and Pyrgioti, E., 2008. "Optimal placement of wind turbines in a wind park using Monte Carlo simulation". *Renewable Energy,* ***33***(7), jul, pp. 1455–1460.

[8] Huang, H.-S., 2009. "Efficient hybrid distributed genetic algorithms for wind turbine positioning in large wind farms". *IEEE International Symposium on Industrial Electronics*(ISIE), pp. 2196–2201.

[9] Ituarte-Villarreal, C. M., and Espiritu, J. F., 2011. "Optimization of wind turbine placement using a viral based optimization algorithm". *Procedia Computer Science,* ***6***, jan, pp. 469–474.

[10] DuPont, B. L., and Cagan, J., 2012. "An Extended Pattern Search Approach to Wind Farm Layout Optimization". *Journal of Mechanical Design,* ***134***(8), p. 081002.

[11] Couto, T. G., Farias, B., Diniz, A. C. G. C., and Morais, M. V. G. D., 2013. "Optimization of Wind Farm Layout Using Genetic Algorithm". *10th World Congress on Structural and Multidisciplinary Optimization*, pp. 1–10.

[12] Zhang, P. Y., 2013. "Topics in Wind Farm Layout Optimisation: Analytical Wake Models, Noise Propagation, and

Energy Production". Master of applied science dissertation, University of Toronto.

[13] Geem, Z. W., and Hong, J., 2013. "Improved Formulation for the Optimization of Wind Turbine Placement in a Wind Farm". *Mathematical Problems in Engineering,* ***2013***(1), pp. 1–5.

[14] Chen, Y., Li, H., Jin, K., and Song, Q., 2013. "Wind farm layout optimization using genetic algorithm with different hub height wind turbines". *Energy Conversion and Management,* ***70***, jun, pp. 56–65.

[15] Zhang, P. Y., Romero, D. a., Beck, J. C., and Amon, C. H., 2014. "Solving wind farm layout optimization with mixed integer programs and constraint programs". *EURO Journal on Computational Optimization,* ***2***(3), jul, pp. 195–219.

[16] Shakoor, R., Yusri, M., Raheem, A., and Rasheed, N., 2016. "Wind farm layout optimization using area dimensions and definite point selection techniques". *Renewable Energy,* ***88***, pp. 154–163.

[17] Pillai, A. C., Chick, J., Johanning, L., Khorasanchi, M., and Pelissier, S., 2015. "Optimisation of Offshore Wind Farms Using a Genetic Algorithm". In Proceedings of the Twenty-fifth (2015) International Ocean and Polar Engineering Conference, pp. 644–652.

[18] Pillai, A., Chick, J., Johanning, L., Khorasanchi, M., and de Laleu, V., 2015. "Offshore wind farm electrical cable layout optimization". *Engineering Optimization,* ***47***(12), pp. 1689–1708.

[19] Arthur, D., and Vassilvitskii, S., 2006. "k-means ++ : The Advantages of Careful Seeding". *Proceedings of the eighteenth annual ACM-SIAM symposium on Discrete Algorithms,* ***8***, pp. 1–11.

[20] Scutariu, M., Yi, X., and Transmission, P., 2015. "Optimisation of offshore wind farm collection systems". *Proceedings of EWEA Offshore 2015*, pp. 1–8.

[21] Gurobi Optimization Inc., 2015. Gurobi Optimizer Reference Manual.

[22] Barthelmie, R. J., Folkerts, L., Larsen, G. C., Frandsen, S. T., Rados, K., Pryor, S. C., Lange, B., and Schepers, G., 2006. "Comparison of Wake Model Simulations with Offshore Wind Turbine Wake Profiles Measured by Sodar". *Journal of Atmospheric and Oceanic Technology,* ***23***(7), jul, pp. 888–901.

[23] Barthelmie, R. J., Hansen, K., Frandsen, S. T., Rathmann, O., Schepers, J. G., Schlez, W., Phillips, J., Rados, K., Zervos, A., Politis, E. S., and Chaviaropoulos, P. K., 2009. "Modelling and Measuring Flow and Wind Turbine Wakes in Large Wind Farms Offshore". *Wind Energy,* ***12***(June), pp. 431–444.

[24] Renkema, D. J., 2007. "Validation of wind turbine wake models". Master of science dissertation, TU Delft.

[25] Makridis, A., and Chick, J., 2013. "Journal of Wind Engineering Validation of a CFD model of wind turbine wakes with terrain effects". *Jnl. of Wind Engineering and Industrial Aerodynamics,* ***123***, pp. 12–29.

[26] Katic, I., Højstrup, J., and Jensen, N., 1986. "A Simple Model for Cluster Efficiency". *European Wind Energy Conference and Exhibition 1986*(October), pp. 407–410.

[27] Schlez, W., and Neubert, A., 2009. "New developments in large wind farm modelling". *Proceedings of EWEC 2009*.

[28] Larsen, G. C., 1988. A Simple Wake Calculation Procedure. Tech. rep., Risø National Laboratory.

[29] Göçmen, T., Laan, P. V. D., Réthoré, P.-e., Diaz, A. P., Larsen, G. C., and Ott, S., 2016. "Wind turbine wake models developed at the technical university of Denmark: A review". *Renewable and Sustainable Energy Reviews,* ***60***, pp. 752–769.

[30] Pillai, A. C., Chick, J., and de Laleu, V., 2014. "Modelling Wind Turbine Wakes at Middelgrunden Wind Farm". In Proceedings of EWEA 2014.

[31] Gaumond, M., Rethore, P., and Bechmann, A., 2012. "Benchmarking of Wind Turbine Wake Models in Large Offshore Windfarms". *Proceedings of the Science of Making Torque from Wind Conference*.

[32] Holland, J. H., 1992. "Genetic algorithms". *Scientific American,* ***July***.

[33] Burke, E. K., and Kendall, G., 2013. *Search Methodologies*, second ed. Springer US, Boston, MA.

[34] Herbert-Acero, J., Probst, O., Réthoré, P.-E., Larsen, G., and Castillo-Villar, K., 2014. "A Review of Methodological Approaches for the Design and Optimization of Wind Farms". *Energies,* ***7***(11), oct, pp. 6930–7016.

[35] Tesauro, A., Réthoré, P., and Larsen, G., 2012. "State of the art of wind farm optimization". *Proceedings of EWEA 2012*, pp. 1–11.

[36] Srinivas, M., and Patnaik, L. M., 1994. "Adaptive probabilities of crossover and mutation in genetic algorithms". *IEEE Transactions on Systems, Man, and Cybernetics,* ***24***(4), pp. 656–667.

[37] Eberhart, R., and Kennedy, J., 1995. "A new optimizer using particle swarm theory". *MHS'95. Proceedings of the Sixth International Symposium on Micro Machine and Human Science*, pp. 39–43.

[38] Kennedy, J., and Eberhart, R., 1997. "A discrete binary version of the particle swarm algorithm". *1997 IEEE International Conference on Systems, Man, and Cybernetics. Computational Cybernetics and Simulation,* ***5***, pp. 4–8.

[39] García-Gonzalo, E., and Fernández-Martínez, J. L., 2012. "A Brief Historical Review of Particle Swarm Optimization (PSO)". *Journal of Bioinformatics and Intelligent Control,* ***1***(1), pp. 3–16.

[40] Mirjalili, S., and Lewis, A., 2013. "S-shaped versus V-shaped transfer functions for binary Particle Swarm Optimization". *Swarm and Evolutionary Computation,* ***9***, pp. 1–14.